THE GEOCHRONOLOGY AND GEOCHEMISTRY OF KAROO VOLCANICS IN THE LEBOMBO AND ADJACENT AREAS

by

J.W. BRISTOW

Department of Geochemistry,
University of Cape Town.

September, 1980

Thesis submitted in fulfilment of the requirements
for the degree of Ph.D. at the
University of Cape Town.

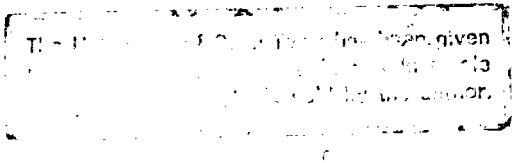

"This is not the end;
It is not even the beginning of the end;
But it is perhaps, the end of the beginning! "

Churchill, Sir Winston L.S.
10 November 1942

ABSTRACT

Karoo volcanics of Jurassic to Cretaceous age crop out in the eastern areas of southern Africa. These volcanics are well preserved in the Lebombo monocline which straddles the borders of South Africa, Swaziland and Mozambique, and in the Nuanetsi and Tuli synclines and Sabi monocline of south-east Zimbabwe. Geochronological and geochemical data have been used to evaluate the geochemistry of the rock types found in the above areas, particularly with respect to the mafic volcanics of the Lebombo.

In the eastwardly dipping Lebombo monocline, nephelinites overlain by picrite basalts occur in the northern part of the volcanic succession whereas over the remaining area olivine-poor basalts are dominant. Rhyolitic volcanics in the form of massive flows overlie the basaltic rocks and attain their maximum thickness in Swaziland and the southern Lebombo. The rhyolites are notably thinner to the north of Swaziland and are overlain by an upper sequence of olivine-poor lavas with interdigitated rhyolite flows. Basic dykes are ubiquitous in the Lebombo whereas acid dykes, though present, tend to be localised. In Nuanetsi, picrite basalts, olivine-poor basalts and rhyolite flows with interbedded basic lavas crop out in a major synclinal structure. Dyke rocks are common and late Karoo intrusive complexes cut the lavas. Volcanic rocks in the Tuli syncline consist predominantly of picrite basalts and olivine poor lavas, whereas nephelinites, picrite basalts and olivine-poor lavas crop out in the Sabi Monocline.

Volcanism in the eastern Karoo was initiated by the emplacement of carbonatite complexes at about 205 my. Thereafter the locus of volcanism migrated southwards through Nuanetsi and the adjoining Sabi and Tuli areas and into the Lebombo area. Nuanetsi volcanism commenced prior to about 192 my and continued until at least 173 my. Lebombo volcanism spans a period

of approximately 70 my from early mafic volcanism at about 190 my to late stage rhyolite emplacement at 133 my. Disconformities between the main volcanic lithologies indicate that volcanism was not a continuous process and age relationships of rhyolitic rocks from the southern Lebombo show that acid volcanism was episodic with three periods of activity at about 177 my, 146 my and 133 my.

Major and trace element modelling of the nephelinite lava and dyke suites indicates that nephelinites in the northern Lebombo and Sabi areas appear to have crystallised from parental magmas which differed slightly in composition due to different degrees of partial melting. Subsequent low-pressure fractional crystallisation appears to have led to the overall geochemical variation shown by the individual nephelinite suites. Geochronological and geochemical data imply that the nephelinite volcanism was associated with the carbonatites emplaced at the onset of the Karoo volcanic cycle. The carbonatites possibly developed in response to localised concentrations of CO_2 in the mantle underlying south-east Zimbabwe in pre-Karoo times and it is inferred that this gas species played a role in the petrogenesis of the undersaturated nephelinite lavas and dykes.

Picrite basalts of the northern Lebombo, Nuanetsi and Tuli are a unique set of porphyritic high-MgO lavas characterised by tholeiitic major element chemistry but abnormally high abundances of incompatible minor and trace elements. Detailed petrographic, mineralogical and geochemical studies of the northern Lebombo picrite basalts indicate that the lavas may have crystallised from magnesian parental magmas with up to 18% MgO. Major element variations within the lavas can be explained in terms of high-pressure crystal fractionation, but the relationships shown by the incompatible elements invalidate such a model unless a series of complicated coincidences are invoked. Crystallisation from a series of partial melts

derived from enriched (possibly metasomatised) mantle domains would, however, appear to offer a plausible explanation of the geochemical relationships shown by the picrite basalts. Other processes such as zone refining and wall rock reaction might also have been involved.

The geochemical relationships of the low-MgO volcanics appear to reflect rather complex petrogenetic processes. In the case of the southern Lebombo low-MgO volcanics it is necessary to consider at least two models to explain the petrogenetic history of the lavas and dykes. Crustal contamination of relatively "depleted" basic magmas similar to those represented by the Rooi Rand dolerite dyke swarm is one possible process, but the lack of a systematic relationships between initial $^{87}Sr/^{86}Sr$ ratio and chemical parameters such as SiO_2 and Fe_2O_3 suggests that this process cannot alone be responsible for the observed data. It is therefore necessary to invoke an additional process which involves melting of a mantle with chemically and isotopically enriched domains to produce a suite of magmas of which some members subsequently suffered crustal contamination.

The low-MgO lavas and dykes of the central and northern Lebombo may, broadly speaking, be grouped into a high-K shoshonitic suite and a low-K normal suite. Rocks of the shoshonitic suite occur to the north of the Komati River and generally crop out above the evolved picrite basalts found at the top of the high-MgO lava succession. Geochemical data for the shoshonitic suite suggests that these rocks may have formed by low-pressure crystal fractionation from magmas similar in composition to some of the relatively evolved picrite basalts. Low-MgO lavas found to the south of the Komati River are characterised by relatively low levels of K and incompatible elements though similar rock types were occasionally found overlying the shoshonitic suite. The low-K rocks appear to have been derived from different source regions to the picrite basalts and shoshonites.

In addition these rocks display chemical characteristics that are more typical of the Swaziland and southern Lebombo low-MgO volcanics and it is therefore proposed that the Lebombo belt can be subdivided into a northern province characterised by incompatible element enriched basalts and a southern province characterised by much lower abundances of incompatible elements.

If one ignores the obvious effects of crustal contamination, then Sr isotope data suggest that mantle heterogeneity played a significant role in the petrogenesis of the mafic volcanics from the Lebombo and the adjoining areas of south-east Zimbabwe. Data from the picrite basalts in the northern Lebombo suggest that the formation of the heterogeneities may have been relatively close in time to the Karoo volcanic event, but in the case of the southern Lebombo volcanics there are indications that the postulated mantle heterogeneity may be a reflection of a much older event. However, the relationships shown by some of the Rb-Sr and Sr-isotope data are conflicting and studies based on alternative isotopic systems such as U/Pb and Sm/Nd are needed to resolve this problem.

Volcanism in the eastern Karoo can be related to a volcano-tectonic process involving initial rupturing of the eastern Gondwanaland crust along pre-existing lines of weakness. It is postulated that initial fracturing promoted volatile release from the mantle which, in conjunction with continued tensional stresses, led to the formation of a proto-rift. Small degrees of melting in the presence of CO_2 also led to the formation of nephelinites and carbonatites at the proto-rift stage of the development of the eastern Karoo volcanic province. Subsequently, increased rifting and associated pressure release led to high degrees of melting and the formation of picritic rocks. Low-MgO volcanics followed at a stage where there was insufficient heat to either promote high degrees of melting or

prevent olivine from crystallising and being fractionated by gravitative settling. Rhyolites which overlie the basaltic rocks are considered to represent partial melts of basic magmas which were underplated onto the base of the crust (Betton and Cox, 1979). However, study of the rhyolites has not formed an essential component of this thesis.

TABLE OF CONTENTS

APPENDICES

LIST OF PLATES

PLATE

1 INTRODUCTION

The Karoo lavas that today cover substantial areas of southern Africa represent remnants of a Mesozoic (Jurassic to Cretaceous) magmatic event that followed the extensive and prolonged sedimentation of the Karoo succession of southern Africa. The area presently underlain by eroded remnants of that volcanic event amounts to at least 140 000 km^2, with outcrops occurring in practically every southern African state (Fig. 1.1).

The southernmost outcrops of Karoo lavas cover substantial areas of Transkei, Lesotho and South Africa and to the north, outcrops of lavas are found in Botswana, Zimbabwe, Zambia and Malawi. To the east, Jurassic and younger volcanics are exposed along the Lebombo monocline, straddling the Mozambique border; in the Tuli, Nuanetsi and Sabi areas of south-eastern Zimbabwe; in the Lupata Gorge of the Zambezi River, and along the north-eastern coast of Mozambique. To the west, in Namibia, Jurassic volcanics crop out in the southern part of the country whereas younger Cretaceous lavas and dykes form extensive outcrops in the Etendeka Plateau (Kaoko region) and extend to the Namibian coast, as well as further north.

Contemporaneous Karoo dolerite intrusives, mostly dykes and sills, are even more widespread than the lavas and are found throughout southern Africa with the possible exception of the Cape fold belt. However, several dolerites are found to the south of the most intensely folded portion of the fold belt in the Cape Peninsula. Dykes are the most common form of Karoo intrusive and are found in nearly all the geological formations of southern Africa whereas sills are less frequent and are

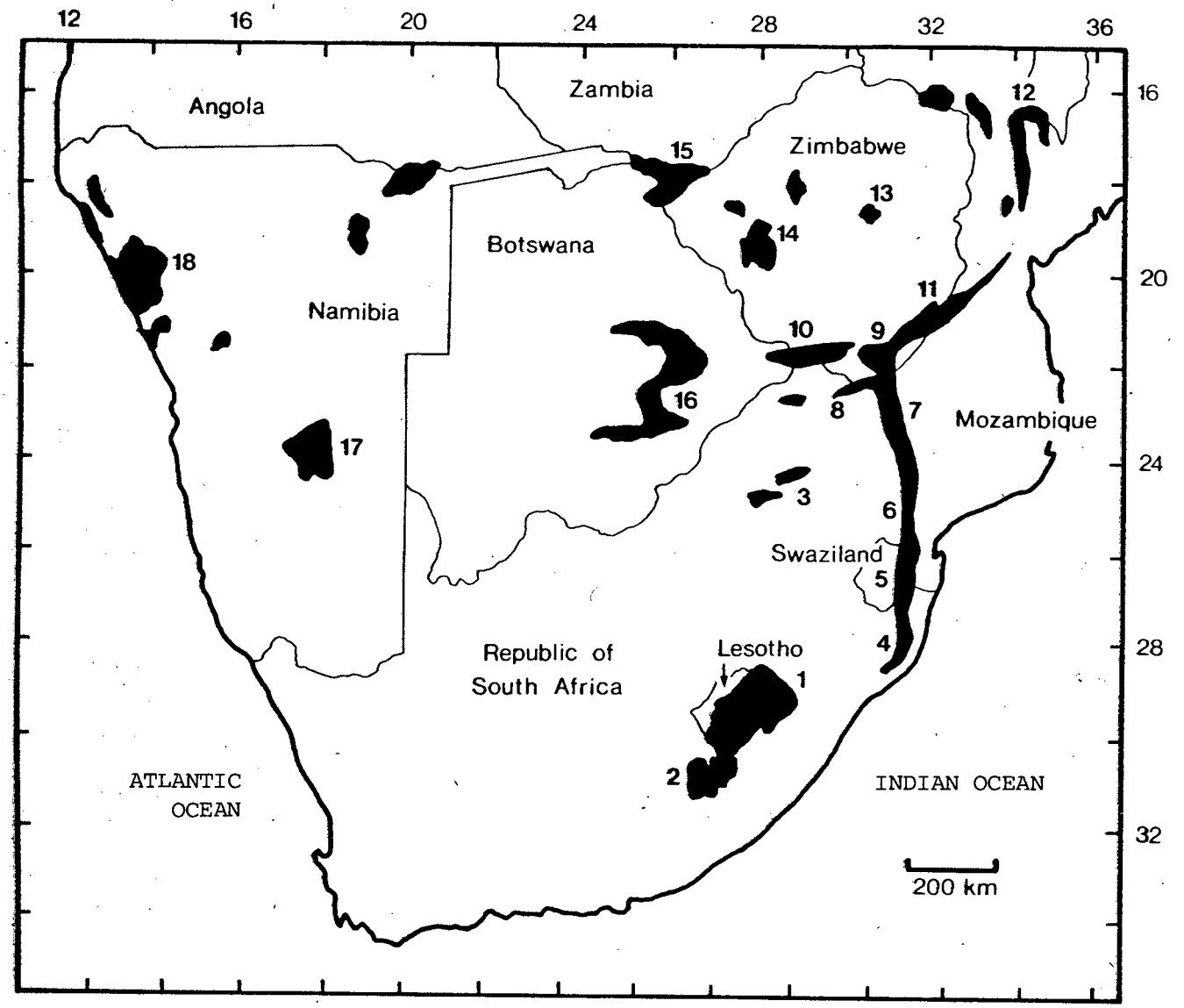

Fig. 1.1 Distribution of Karoo lava outcrops in southern Africa

1. Lesotho
2. Stormberg
3. Springbok Flats
4. Southern Lebombo
5. Swaziland
6. Central Lebombo
7. Northern Lebombo
8. Soutpansberg Extension
9. Nuanetsi
10. Tuli
11. Sabi
12. Lupata
13. Featherstone
14. Nyamandhlovu
15. Victoria Falls - Wankie
16. Botswana
17. Mariental
18. Kaokoveld

generally restricted to the flat-lying Karoo sediments. The Karoo intrusives are generally more resistant to erosion than the country rock and consequently much of the southern African countryside is characterised by narrow criss-crossing ridges constructed by dolerite dykes and flat-topped kopjes capped by sills. Less common are gap or trench dykes, formed where dolerites have weathered more rapidly than the country rock.

The area of Karoo lava sub-outcrop is in turn probably far greater than the sub-aerial remnants. Extensive sub-outcrops occur beneath the Kalahari basin of Botswana (Poldervaart, 1952; Green, 1966), and in Zambia, Drysdall and Weller (1966) have suggested that the greater part of the extensive Barotseland basin of western Zambia may be underlain by Karoo sediments and lavas. In the south-east parts of southern Africa the easterly tilted monoclinal flexures of the Lebombo and Sabi areas and the plunging Nuanetsi syncline carry Karoo volcanics beneath a cover of Cretaceous-Tertiary sediments. Geophysical data (Darracott and Kleywegt, 1974), and the fact that volcanics have been intersected in deep boreholes near the Mozambique coast between latitudes of 22° and 25°S at depths of 1 800 - 3 300 metres (Flores, 1970) indicate that the lavas probably extend up to 300 km to the east of the Lebombo outcrops.

The widespread distribution of dolerite dykes and sills as well as layered complexes such as Ingeli (Maske, 1966) and Insizwa (Bruynzeel, 1957) also imply that the Karoo lava fields were far more extensive than their current outcrop area. It has been found that little difference exits between the chemistry of the dykes, sills and lavas so that it is generally agreed that many of the dykes represent feeders to lava flows. Consequently many of those areas, eg. the eastern Cape and northern Natal, noted for their vast networks of dykes and sills may well have

been overlain by lava sheets in Jurassic times. In central Zimbabwe present day outcrops of Karoo lavas are restricted to small outliers south of Salisbury, but here too Worst (1962) has presented evidence to suggest that the greater part of Zimbabwe was once covered by volcanics.

That the lavas originally covered a far greater area before erosion, is also demonstrated by the existence of abundant basalt xenoliths within kimberlite pipes exposed in areas hundreds of kilometres distant from Karoo lava outcrops. Kimberlites bearing lava fragments occur at Postmasburg and Prieska in the northern Cape (Du Toit, 1954) and at Kolonkwanen near the Cape-Botswana border (Gurney, pers. comm.). These occurrences suggest that the Lesotho lava fields might well have been continuous with the Kalahari lavas, a proposal that is strongly supported by the similarity in composition of the two sets of lavas.

It therefore seems reasonable to accept that even the considerable thickness (~ 1 500m) of basaltic lavas that remain in the Lesotho plateau represent only a remnant of an originally much thicker and more extensive lava pile. The original thickness of the lavas overlying the stable central cratonic regions of southern Africa will probably remain unknown, but it is unlikely to have approached the estimated 6 000 - 10 000m (Cox et al., 1965; Bristow, 1976; Cleverly and Bristow, 1979) of volcanics preserved in the Lebombo and Nuanetsi regions where volcanism was contemporaneous with monoclinal flexuring and crustal depression during the fragmentation of Gondwanaland.

Karoo lavas and dykes found in the central areas of southern Africa are primarily basaltic in composition though minor developments of andesite occur in the eastern Cape in South Africa (Gevers, 1928; Rumble, 1979) and the Quthing district of Basutoland (now Lesotho)

(Stockley, 1947). In contrast, Karoo volcanics found close to the continental margins (Kaoko, Lebombo, Nuanetsi) consist of basaltic and rhyolitic flows. Rocks of intermediate composition are found in the Kaoko region but are almost totally absent from the marginal Lebombo and Nuanetsi areas. In terms of major element chemistry, the Karoo volcanics found in the Lebombo and Nuanetsi areas represent excellent examples of an acid-basic association in which SiO_2 shows a strongly bimodal distribution with maxima corresponding to basalts and rhyolites (sensu lato).

Considerable compositional variations, particularly with respect to minor and trace element composition, are present within the basaltic and rhyolitic rocks of the Karoo. These variations, coupled with many unusual petrographic and geological relationships, have in the past prompted a considerable amount of research in Karoo volcanism and consequently a substantial volume of literature has been generated on the lavas and intrusives. However, the advent of modern analytical techniques, eg. X-Ray Fluorescence and Mass-spectrometry have led to an extensive revision of previous concepts relating to the petrogenesis of volcanic rock suites. With this in mind an intensive program of research, the Karoo Geodynamics Project, was initiated in 1974 in an attempt to gain a better understanding of the geochemical and geodynamic processes that led to the vast Karoo volcanic episode. Some of the data, petrogenetic modelling and ideas generated in the course of the project are presented in this thesis.

1.1 The Karoo Geodynamics Project

Under sponsorship from the South African Council for Scientific and Industrial Research, a project on the Geochemistry of the Karoo volcanics, which forms part of South Africa's contribution to the

International Geodynamics Project, has followed on the pioneering works of Walker and Poldervaart, Du Toit and others, and the subsequent studies of Cox and his co-workers. Workers from several universities in South Africa and abroad (Oxford and Leeds) have been involved in the project and attention has been focussed on the three main areas of preserved Karoo volcanics. The three areas are represented by: (i) the Lebombo and adjoining areas of Nuanetsi, Sabi and Tuli; (ii) the central Karoo, in particular the Stormberg area; and (iii) north-western Namibia. Lavas and dyke rocks in the intervening areas have been studied and data from Karoo volcanics found further afield, eg. Malawi, have been incorporated in an attempt to formulate a plausible overall reconstruction of the Karoo volcano-tectonic and geochemical processes.

1.2 Scope of the Present Study

This thesis is primarily concerned with the mafic volcanics (nephelinites, picrite basalts, basalts) of the Lebombo. However, mafic volcanics of south-east Zimbabwe are in most respects similar to the Lebombo rocks and consequently this study incorporates data from the nephelinites and picrite basalts of Nuanetsi and Tuli. In addition, isotopic data obtained from the Lebombo rhyolites has been used to establish the geochronological development of the volcanic succession. Much additional work has been done on the acid volcanics from the south, central and north Lebombo but is not discussed in this thesis, other than in summary form. It will, however, be presented in a special Karoo Geodynamics Volume to be published in the early part of 1981. Work presented in this dissertation is complementary to the studies which have already been done in south-east Zimbabwe (Norry, 1977), Swaziland (Cleverly, 1977; Betton, 1978) and the southern Lebombo (Bristow, 1976; Armstrong, 1978) as part of the Geodynamics Project. Aims of the present

study were as follows:

(i) To sample the central and northern Lebombo volcanics in detail.

(ii) Establish the geochronological development of the Karoo volcanics in the Lebombo and adjoining areas using both published data and new ages derived by radio-isotope studies.

(iii) Investigate the petrographic and mineralogical characteristics of the mafic volcanics.

(iv) Evaluate possible petrogenetic models which may explain the observed petrographic and geochemical variations within the nephelinitic, picritic ($MgO > 9\%$) and basaltic ($MgO < 9\%$) extrusive and intrusive suites.

(v) Augment major and trace element compositional data with Sr isotope analyses and thereby provide additional constraints on the petrogenetic models.

(vi) Reconstruct a plausible model for the volcano-tectonic development of the Lebombo and adjacent volcanics.

2 PREVIOUS WORK ON LEBOMBO AND KAROO VOLCANICS

The history of geological investigation in the Lebombo dates back over one hundred years. From about 1873 to 1970 numerous papers and reports have been written on various topics concerning the volcanic belt, many of which not only make interesting reading but give an accurate account of the various geological and geomorphological features of the area. However, it is apparent that little geochemical work was done in the Lebombo prior to about 1970 and it is only since the inception of the Karoo Geodynamics Project that an attempt has been made to unravel the complex geochemical problems of the monocline. Early accounts of the Lebombo rocks were presented by, amongst others, Cohen (1874), Wilson Moore (1897), Molengraaf (1898), Kynaston (1907), Henderson (1909) and Young (1920). Though Prior (1910) reported some petrographic data on dolerite and rhyolite collected in the Lebombo, perhaps the most important contribution to the geology of the area during this period were the reports, maps and geochemical analyses relating to the southern Lebombo completed by Anderson (1901, 1904, 1907), the first Natal Government Geologist.

Du Toit (1929) was the first to recognise the geological and structural complexity of the Lebombo belt, describing it as a monocline formed along a line of weakness in a region subjected to tensional stresses. He referred to the petrography of the volcanics and stated that the acid lavas were differentiates of the magma from which the basalts were derived. He also paid particular attention to the intrusive rocks and reached two important conclusions, viz. (a) that the large intrusive granophyres represented consolidated feeders to the rhyolite flows and, (b) that the dolerites represented feeders to the basalts. Du Toit (1929) interpreted the dyke swarm in the south (Rooi Rand) as the

axis of the monocline and made a detailed assessment of the structural configuration of the monocline in relation to the dips of the dykes and lavas (basic and acid), finally concluding that (p.209) :

> "The crustal bending began during about the middle of the lower and ended before the middle of the Upper Basalt phase; its optimum could therefore have fallen within the Middle rhyolitic period of volcanicity."

His statement concerning the relationships between monocline formation and magma extrusion have been quoted extensively by other authors.

Du Toit's classic study of the Lebombo was followed several years later by the work of Lombaard (1952) who presented a petrographic and geochemical account of the volcanics from both the central Karoo and Lebombo areas. However, apart from a regional mapping program in the Soutpansberg extension of the Lebombo (van Eeden et al., 1955) no further work was done in the Lebombo until Urie and Hunter (1963), Stratten (1965, 1970), Van der Schijf (1968) and Saggerson and Logan (1970) completed regional mapping projects, and petrographic and preliminary geochemical studies in Swaziland, the southern Lebombo and central and northern Lebombo. During this period Manton (1968) also analysed rhyolites and basalts from the southern Lebombo, Swaziland and Nuanetsi areas for Sr isotopes. He found that rhyolites from both areas defined isochron ages of approximately 190 my with initial ratios of 0.704 and 0.708, respectively. These ratios were similar to those obtained from basalts in the two areas and Manton (1968) concluded that the rhyolites had evolved from a mantle source. A similar study was also conducted on the Effingham dolerites of the southern Lebombo-Natal area by Frankel (1969). On the basis of their high SiO_2 and K_2O abundances and $^{87}Sr/^{86}Sr$ ratios Frankel (1969) concluded that the intermediate character of the dykes was due to assimilation of crustal material.

Following the earlier geological and geochemical studies of the Lebombo volcanics, attempts were made to establish the structural relationships of the monocline and interpretations of geophysical investigations were published by several authors (Burley et al., 1970; Darracott, 1974; Darracott and Kleywegt, 1974). However, the interpretations were on the whole based on inadequate or insufficient data and consequently several models appear to be compatible with the information obtained. Though recent studies conducted under the auspices of the Karoo Geodynamics Project have provided some new structural information they have also shown that there is a need for an extensive and detailed geophysical study of the Lebombo.

The advent of the International Geodynamics Project in 1974, "an international programme of research on the dynamics and dynamic history of the earth with emphasis on deep seated foundations of geological phenomena" (The Geodynamics Project in South Africa, 1975, p.1) brought about a renewed interest in the Lebombo volcanics and Karoo volcanism as a whole. Intensive research programs were initiated in the main areas of Karoo outcrop with a view to establishing, in detail, the petrological, geochemical and tectonic relationships of the Karoo volcanics. Consequently a wealth of new geological and analytical data have been collected in the Lebombo, and other Karoo localities.

Studies of the southern Lebombo and Swaziland volcanics have been completed by Bristow (1976), Cleverly (1977), Armstrong (1978) and Betton (1978) whereas data collected from the central and northern Lebombo is presented in this thesis. Much emphasis has been placed on the unusual volcanological relationships of the Lebombo rhyolite flows (Bristow, 1976; Cleverly, 1977) and a model of flow emplacement has been proposed

(Bristow and Cleverly, 1979). In Swaziland, chemical and isotope studies have shown that there are considerable differences within the acid volcanics, unlike the rhyolites of the south and central Lebombo which tend to be relatively uniform in character. Possible reasons for the chemical and isotopic variations noted in the Swaziland rhyolites have been discussed by Cleverly and Betton (1979), Betton and Cox (1979) and Betton (1979). In addition, the extensive field mapping and sampling has led to Cleverly and Bristow (1979) being able to formalise volcano-stratigraphic nomenclature for the Lebombo volcanic succession. Work on the Lebombo is continuing, and a detailed geochronological study of the major rock units is nearing completion. Other interesting aspects of the monocline are also being examined eg. Sr and Pb isotopes, and several publications relating to the Lebombo are to be presented in the near future.

In south-east Zimbabwe there is a more continuous record of geological research in the Karoo volcanics and related rocks. The first reference to the Karoo basalts and granitic rocks of the area are found in works by Mennell (1930, 1938). Mennell's work was followed by the investigations of Lightfoot (1938), Tyndale-Biscoe (1949, 1956), Swift et al. (1953) and Swift (1962). These early studies were primarily of a reconnaissance nature and largely concerned with the intrusive granites, granophyres, and alkaline ring complexes.

However, the greatest impact on the understanding of Karoo volcanism undoubtedly resulted from work done on the Pre-Karoo and Karoo rocks of the Nuanetsi syncline by the Research Institute of African Geology, University of Leeds. In the early 1960's the Nuanetsi area was systematically mapped and sampled and a series of papers were presented on the granitic and alkaline ring complexes (Stillman, 1959; Cox, 1964; Johnson, 1961, 1966; Vail, 1962, 1970) basic volcanics (Jamieson, 1966, 1969),

rhyolitic volcanics (Monkman, 1961), and regional geology (Cox et al., 1961; Cox et al., 1965). These studies, and the synthesis presented by Cox et al. (1965), demonstrated that pre-existing Precambrian basement structures played a major role in the development of the Karoo volcano-tectonic provinces, that the rhyolites were in all probability emplaced as ignimbrites and represented primary acid magmas, and that the temporal relationships of the volcanic rocks could be explained in terms of a volcanic cycle.

More important, however, was that the work of Cox and his co-workers provided the basis for further detailed geochemical studies of the Karoo volcanics of south-east Zimbabwe, in particular, the basic volcanics of Tuli (Vail, et al., 1969) and Nuanetsi (Cox, 1972a; Jamieson, 1969, 1970; Jamieson and Clarke, 1970). Though covering a broad range of problems these studies have centered mainly on the olivine-rich picrite basalts (originally referred to as limburgites by Mennell, 1938) which, though tholeiitic in terms of major element chemistry, are anomolously enriched in the incompatible elements Ti, K, P, Sr, Rb, Zr. Subsequent papers and theses (Cox and Jamieson, 1974; Norry, 1977) have outlined processes to account for the enrichment of the above elements but the problem has not yet been entirely resolved.

The atypical geochemical character of the Nuanetsi basic volcanics also prompted a regional study of the Karoo volcanics (Cox and Hornung, 1966; Cox et al., 1967). The petrographic and analytical data obtained showed that the Karoo volcanics could be subdivided into two distinctive provinces (MacDonald, 1967; Cox et al., 1967) though a paucity of data prevented the fitting of the central and northern Lebombo volcanics into a provincial scheme.

> "A northern province included all the Rhodesian basalt localities and is characterised by values of K, Ti, P, Ba, Sr and Zr which are abnormally high for tholeiitic rocks. The southern provinces include the basalts of Basutoland and Swaziland, and the Karoo dolerites of South Africa, all of which have a normal tholeiitic geochemistry." (Cox et al., 1967).

A series of papers discussing the implications of the regional geochemical variations followed (Cox, 1970,1972a; Rhodes and Krohn, 1972) and the concept of a Karoo volcanic cycle was proposed to explain the temporal variation of the Karoo lavas and dykes (Cox, 1972b).

The relationships between the tectonism and volcanism of the Karoo period and the fragmentation of Gondwanaland was also examined with particular emphasis being placed on the Nuanetsi, Sabi and Lebombo localities (Cox, 1970; Flores, 1970; Rhodes, 1972; Burke and Dewey, 1973). Rhodes (1972) postulated that a hotspot had existed beneath Nuanetsi during the emplacement of the volcanics whereas Burke and Dewey (1973) specifically identified the intersection of the Lebombo and Sabi monoclines with the Limpopo fault zone as a triple junction and suggested that it represented the site of a mantle plume. Subsequently Dingle and Scrutton (1974) proposed that the separation between east and west Gondwanaland took place along the line of the Lebombo monocline and its north-eastern extension, the Sabi Monocline.

Geochronological relationships of the volcanics of south-east Zimbabwe have also not been entirely ignored. The earliest age study to be completed provided an age for the Shawa carbonatite (Nicolaysen et al., 1962) which is considered to be an important part of the Karoo volcanic event (Johnson, 1966) and is located to the north-west of the Sabi monocline. Thereafter, several of the volcanic rock units in the Nuanetsi syncline were dated (Vail, 1966; Manton, 1968, 1973; Foland

and Henderson, 1976). The results show that volcanism probably commenced at about 200 my and continued until at least 173 my.

The Karoo Geodynamics Project has ensured the continuation of work in south-east Zimbabwe. Some aspects of the Tuli and Nuanetsi picrite-basalt geochemistry have been re-examined by Norry (1977) and recently a considerable number of rock samples collected in Nuanetsi in the 1960's by the Leeds Institute of African Geology have been analysed for major and trace elements. Some of the data is presented in this thesis whereas the total data set will be incorporated in papers to be presented in the special Karoo Geodynamics volume mentioned in the introduction.

Studies of the central Karoo volcanics, particularly the intrusive rocks, have in general taken precedence over the Karoo volcanics of the Lebombo and south-east Zimbabwe and resulted in numerous publications. The best known works are those of Walker and Poldervaart (1949) on Karoo dolerites, and Stockley's (1947) account of the Basutoland (now Lesotho) lavas and dykes. These pioneering works were followed by a regional study conducted by Lombaard (1952) who attempted to unravel some of the petrographic and geochemical intracacies of the Karoo volcanic province (including the Lebombo).

The intrusive doleritic rocks were undoubtedly the subject of more thorough investigations because of the advanced differentiation effects they exhibited in many exposures (Bruynzeel, 1957; Maske, 1966), their reactivity towards host sediments (Mountain, 1960; Ackermann and Walker, 1960; Frankel, 1950, 1969), the rare occurrence of marginally economic concentrations of Fe-Ni-Cu sulphides (Scholtz, 1937; Dowsett and Reid, 1967), and their importance in creating reservoirs and aquifers (Frommurze,

1937; Meijs, 1960). The wealth of data published prior to 1949 has been comprehensively reviewed by Walker and Poldervaart (1949) and subsequent contributions relating to the mineralogy, petrology and geochemistry of these rocks can be found in the above sources, and in papers by Nockolds and Allen (1956), Moore (1965), Erlank and Hofmeyr (1966, 1968), and Eales (1974).

With the emphasis on the intrusive rocks little work was done on the central Karoo lavas until Cox and co-workers became interested in the geochemical variability of the volcanic province (Cox and Hornung, 1966; MacDonald, 1967; Cox et al., 1967). At much the same time the importance of accurately establishing the geochronology of the volcanic succession was realised and several independant age studies were published, some of which included data obtained from correlatives in Antarctica, South America and Tasmania (McDougall, 1963; Compston et al., 1968; Fitch and Miller, 1971). The data shows that emplacement of the central Karoo lavas commenced at approximately 190 my and continued until about 160 my whereas dykes and sills were intruded from about 190 my to 130 my.

The initiation of the Karoo Geodynamics Project has resulted in even greater interest in the central Karoo volcanics and a considerable amount of new information has been published, or is still to be published. Particular emphasis has been placed on the Stormberg region, though important new data has also been derived from the Lesotho volcanics. Groundwork in the Stormberg area was originally completed by Lock et al. (1974) who subdivided the volcanic sequence in the Barclay East area into a number of lithostratigraphic units. Subsequent geochemical studies (Pemberton, 1978; Mitchell, 1979; Rumble, 1979; Eales and Marsh, 1979) have demonstrated that considerable compositional variation exists in the lavas. In addition, newly acquired data have made it possible to

re-examine the petrogenetic significance of the andesites which crop out at the base of the Karoo succession in the Stormberg region (Rumble, 1979). These rocks were originally described by Du Toit (1904, 1911) and Gevers (1928). Recent controversy concerning the evolution of basaltic melts from picritic precursors has prompted Eales and Marsh (1979) to use Fe-Mg and Ni-Mg distribution coefficients to test the hypothesis for the central Karoo volcanics. Though Eales and Marsh (1979) conclude that the basaltic rocks were not derived from high-Mg liquids their evidence is equivocal and has been disputed by Cawthorn (In press).

Several new studies of the central Karoo intrusive rocks were also initiated within the framework of the Geodynamics Project. The strongly differentiated Birds River Complex, an intrusive body found in the Dordrecht district (eastern Cape) was investigated (Eales and Booth, 1974; Eales and Robey, 1976) and an extensive geochemical study of the Karoo dolerite dykes and sills of the eastern Cape was completed (Robey, 1976). Mineralogical studies of the intrusive rocks have been undertaken and resulted in the identification of anomolous spinels in the Karoo rocks (Eales, 1979; Eales and Snowden, 1979). Further afield in the north-western Cape and southern Namibia, mineralogical and geochemical studies of dolerites have resulted in the formulation of important new ideas concerning flow and gravity differentiation in sills (Le Roex and Reid, 1978; Richardson, 1980).

Interest in Namibian volcanism has been largely confined to studies of the age relationships of the lavas and dykes (Siedner and Mitchell, 1968, 1976), and petrological and geochemical studies of the alkaline complexes of Damaraland (Korn and Martin, 1954; Mathias, 1956, 1957; Verwoerd, 1967; Linning, 1968; Hodgson and Botha, 1974; Prins, 1978)

and Luderitz (Marsh, 1975, 1976). Geochronological studies of the lavas and dykes have shown that there is a close correlation between the youngest phases of emplacement and the period of continental rifting and separation of Africa and South America. As a consequence Gidkeslang et al. (1975) and Marsh et al. (1978) have expressed the view that the Cretaceous volcanics of the Etendeka plateau and younger basic dykes which extend inland from the western seaboard represent magmatism coincident with, or even subsequent to rifting and separation. Much additional geochronological and geochemical data has been obtained recently and will be published in the forthcoming Karoo Geodynamics volume.

Some work has been done in the Karoo volcanics located beyond the borders of South Africa, Namibia and Zimbabwe though there is undoubtedly a need for a detailed reassessment of the geochemical relationships of many of these areas. The upper volcanics of the Lebombo belt which crop out in Mozambique have been mapped by Assuncao et al. (1962) and Wachendorf (1971). Geochemical data are provided by the former and the results indicate that some of the basic lavas are more alkaline than those found lower in the succession. Wachendorf (1971, 1973) concentrated on the interbedded rhyolite flows and concluded that they were differentiates from a basic magma, and were emplaced as lava flows.

Further north in eastern Zimbabwe, Mozambique and Malawi, Karoo volcanics of the Lupata region (Lower Zambezi Valley) and Chilwa Province have been studied by Dixey (1929), Flores (1964) and Wooley and Garson (1970). Bloomfield (1961) and Vail (1966) have provided a summary of the geochronological relationships of the above volcanics. Recently Wooley et al. (1979) have completed a petrographic and geochemical study of the Karoo dolerite dyke swarm in Malawi. Their analytical data shows that

the dolerites are similar to the central Karoo volcanics and they concluded that regional variations in the geochemistry of the Karoo basalts probably reflects mantle heterogeneity. Karoo lavas also occur in Botswana and southwest Zambia though they are mostly covered by Cainozoic Kalahari Sands (Poldervaart, 1952). However, accumulation of borehole data (Green, 1966; Drysdall and Weller, 1966) has shown that the lavas are in most respects similar to those of the central Karoo Province.

Interpretation and subsequent publication of results obtained during the course of the Karoo Geodynamics Project will lead to a far better understanding of the processes and problems associated with the Karoo volcanic event. Results of a preliminary geochemical data synthesis (Duncan and Erlank, 1979) and a more detailed Sr-isotope study (Erlank, et al., 1980) have already shown that mantle inhomogeneities played a major role in Karoo magma genesis and many other important concepts will no doubt emerge from these studies.

3 GENERAL GEOLOGY AND STRUCTURE

3.1 The Lebombo Monocline

The Lebombo monocline is a major flexure of Karoo age (Upper Carboniferous - Lower Cretaceous) which stretches from Empangeni in Natal (South Africa) to the Limpopo River in the north (Fig. 3.1) a distance of 760 km. It straddles the borders of South Africa, Swaziland and Mozambique and forms the south-eastern outcrop margin of the Karoo sedimentary and volcanic province. The monocline consists of a thick (~ 10 km) sequence of mafic and acid volcanics overlying a thin succession of Karoo sediments deposited on Precambrian rocks of the Kaapvaal craton. The Karoo sediments and volcanics display a strong easterly dip and are overstepped from the east by marine sediments of Cretaceous age.

In the extreme south the Lebombo strikes northeast and terminates in a series of fault-blocks which are down-thrown against granitic basement by a series of arcuate faults. Over the remaining areas the volcanic belt as a whole trends north-northwesterly though the majority of individual faults, dykes and joints strike north-south. North of the Limpopo the monocline rotates into the northeast-trending Sabi monocline which can be followed into the Lupata area of the East African Rift system. The Tuli and Nuanetsi synclines are located at the 'hinge' or re-entrant formed by the two monoclines, along the line of the Limpopo Belt.

The Precambrian rocks on which the Karoo succession of the Lebombo rests consist mainly of granitoid rocks of the Kaapvaal Craton (age: ~ 3000 my; Allsopp et al., 1968) though rocks of the Limpopo Mobile Belt (age: ~ 2 500 my; Barton et al., 1979) are encountered in the northern Soutpansberg region. A thin sequence of Karoo sedimentary rocks, occasionally superseded by reworked volcaniclastic deposits (Plate 3.1),

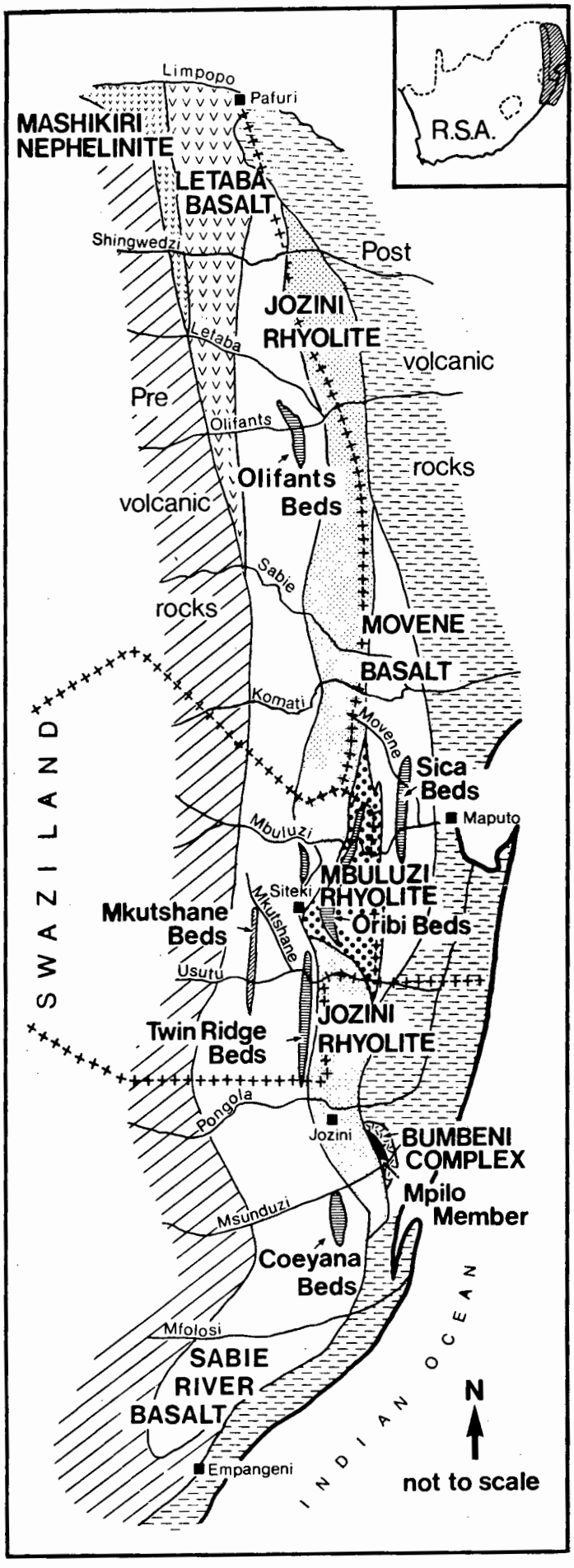

Fig. 3.1 Generalized geological map of the Lebombo.

overlies the older granitoid basement. The Karoo sediments are disconformable on the basement rocks and form a narrow, belt-like outcrop to the west of the volcanics.

A major succession of mafic lavas which consists of nephelinites, picrite basalts, and olivine-poor basalts crops out above the Karoo sediments. The mafic lavas are, in total, approximately 5 km thick and form the lower part of the Lebombo volcanic succession. They are deeply weathered and underlie the flat plain of the Lebombo Lowveld. Thin rhyolite flows or elongate domes are found interdigitated with the mafic lavas in the northern Lebombo, Swaziland and southern Lebombo, and give rise to localised topographic expression within the Lowveld.

A 5 km thick succession of rhyolitic flows overlies the mafic lavas. The rhyolites are resistant to erosion and form the Lebombo Mountain Range which is separated from the Lowveld by an impressive escarpment (Plate 3.2). The rhyolite flows show many unusual volcanological features and have been described in detail by Bristow (1976), Cleverly (1977) and Bristow and Cleverly (1979 - Appendix C). A further succession of basaltic and alkaline lavas with interbedded rhyolite flows (Assuncao et al., 1962; Wachendorf 1971, 1973) overlies the rhyolitic volcanics of the Lebombo Mountain Range. The uppermost volcanics crop out mainly in Mozambique and are of lower Cretaceous age. Basic and acid volcanics of lower Cretaceous age are also found at the southern end of the Lebombo mountains in the Bumbeni Complex. The Complex is clearly disconformable to the main succession of Lebombo rhyolites and consists of a variety of rock types, including one of the few classic examples of an air-fall tuff (Plate 3.3) known in southern Africa.

Plate 3.1 Horizontally bedded, reworked volcanoclastics at the base of the northern Lebombo volcanic succession; Olifants River area. The well bedded tuffaceous sediments are underlain by massive sandstones and overlain by fine grained nephelinite lavas of the Mashikiri Formation. Small north-south trending normal faults have led to a repetition of the volcanic and sedimentary strata in this portion of the Lebombo.

Plate 3.2 The Lebombo escarpment in the vicinity of Mkuze; southern Lebombo. The flat lying topography in the foreground is typical of the Lebombo lowveld which is underlain by deeply weathered basalt lava flows. (View looking south-east with Tshaneni Mountain at the extreme right of the photograph.)

Dyke rocks are ubiquitous, particularly in the lower sequence of mafic lavas and underlying Karoo sediments. Dolerite dykes are dominant and form a major dyke swarm, referred to as the Rooi Rand, in Swaziland and the southern Lebombo whereas less prominent dolerite dyke swarms occur in the Olifants River and Pafuri areas. Rhyolitic dykes occur in the Olifants River area (Plate 3.4) and the southern Lebombo. A series of large rhyolitic domes also crop out in the southern portion of the Mountain range. The domes are younger than the acid volcanics which form the Lebombo Mountains but are older than the volcanics of the Bumbeni Complex. Granophyre dykes are common in Swaziland and the central Lebombo; in addition a number of impressive granophyre bodies crop out along the basalt-rhyolite contact in Swaziland and in the central and northern Lebombo. A conformable, primarily gabbroic, intrusive complex occurs in the Komatipoort area (Saggerson and Logan, 1970) and two thick dolerite sills intrude the lower basaltic succession in the Olifants River area.

The greater part of the Lebombo mafic lava succession consists of olivine-rich and olivine-poor tholeiites. Nephelinites, glassy olivine-bearing lavas (similar rock types are found in Nuanetsi in Zimbabwe and were originally called limburgites by Mennell, 1938) and olivine-rich basalts are found at the base of the succession in the northern Lebombo. The olivine-poor lavas extend throughout the Lebombo and consist largely of basaltic tholeiites and tholeiitic-andesites, with rarer absarokites and shoshonites; more strongly alkaline basalts are present in Mozambique (Assuncao et al., 1962). The acid rocks range from dacitic to rhyolitic in composition though the majority are rhyodacites with relatively uniform compositions and porphyritic textures. Rocks with intermediate composition, eg. andesites and trachybasalts, do occur but are volumetrically insignificant. The main rock types generally form

Plate 3.3 The Nxwala air-fall tuff; Bumbeni Complex, Southern Lebombo. The tuff consists of thin (1 - 4 cm) and thick (20 - 40 cm) ash bands containing unsorted fragments of rhyolite pumice, rhyolite, pitchstone and basalt. Note the classic drape structure of the tuff. (View looking north.)

Plate 3.4 Rhyolite dyke cross cutting basalts of the Sabie River Formation in the northern Lebombo. This north-south trending dyke crops out on the banks of the Letaba River, west of the confluence between the Letaba and Olifants Rivers.

mappable units and the volcano-stratigraphic nomenclature which has been adopted for the Lebombo volcanic succession (Cleverly and Bristow, 1979, Appendix B) is presented in Table 3.1.

The structure of the Lebombo succession is that of a faulted monocline. Faulting and warping appears to have taken place primarily during the emplacement of the lower succession of basalts since the overlying rhyolites and upper volcanics are clearly less strongly affected (Bristow, 1976). Flexuring took place along a north-south trending axis which can be traced in Swaziland and the southern Lebombo. However, since the volcanic belt trends north-northwesterly northwards from Zululand, the north-south trending axial zone is hidden under the upper volcanics and Cretaceous sediments over much of the belt.

Structural elements in the Lebombo volcanics, eg. fault and joint patterns, dyke orientations etc., indicate that the volcano-tectonic development of the belt was strongly controlled by the interaction of pre-Karoo basement trends and lateral tectonic stresses. Over much of the Lebombo, structural elements are aligned predominantly north-south. It is inferred that these trends reflect basement control in the form of a north-south trending contact zone between the Kaapvaal craton and southerly extension of the Mozambique Mobile belt, coupled with tectonic control in the form of tensional east-west stresses (Saggerson and Logan, 1970; Cox, 1970). Basement, and to a lesser extent tectonic control, are also apparent in the extreme south where the volcanics occur in a north-east trending zone of recurring Palaezoic subsidence (Natal embayment and Natal trough - Ryan, 1968; Taverner-Smith, 1979) associated with the contact zone of the Kaapvaal Craton and Natal-Namaqua mobile belt. However, the influence of pre-Karoo basement trends on the Lebombo

TABLE 3.1 Generalised volcano-stratigraphy of the Lebombo Monocline.

GROUP	FORMATION	BEDS	LITHOLOGY
CRETACEOUS			Fossiliferous conglomerates and sandstones
	unconformity		
	Movene Basalt		Basaltic and alkaline lavas
		Sica	Rhyolites
	Bumbeni Complex		Acid extrusives and intrusives
		Mpilo	Trachy-basalt and trachy-andesite
	Mbuluzi Rhyolite		Quartz-phyric rhyolites
		Oribi	Quartz-rich rhyolites
LEBOMBO	Jozini Rhyolite		Plagioclase-phyric rhyolites
		Olifants	Plagioclase-phyric rhyolites
		Twin Ridge	Plagioclase-phyric rhyolites
		Coeyana	Quartz-phyric rhyolites
	Sabie River Basalt		Tholeiitic andesites, basalts, shoshonites and absarokites
		Mkutshane	Plagioclase-phyric rhyolites
	Letaba Basalt		Picritic lavas
	Mashikiri Nephelinite		Nephelinite lavas
	unconformity		
	KAROO SEDIMENTS		Reworked volcanoclastics, massive sandstones, siltstones and shales
	unconformity		
	BASEMENT COMPLEX		Granites, gneisses, greenstones and gabbros

province is most clearly seen in the Soutpansberg section where structural elements within the volcanics follow the trends of the Limpopo mobile belt. Lateral tension is also considered to have played a major part in the alignment of the volcanics found in the Limpopo area (Cox, 1970; Reeves, 1978).

3.2 Karoo Volcanics in South-east Zimbabwe

Karoo volcanics crop out north of the Limpopo River in Zimbabwe in the Tuli and Nuanetsi synclines, and Sabi-Lundi monocline (Fig. 1.1). They have been described by Swift et al. (1953), Swift (1962), Cox et al. (1965), Vail et al. (1969), Jamieson (1969), Cox and Jamieson (1974) and Norry, (1977).

The Tuli and Nuanetsi synclines jointly form an approximately east-west structure lying on the north side of the Messina Block and meeting the Lebombo at its northern end. The Tuli volcanics consist of a succession of olivine-rich and olivine-poor basalts overlying Pre-cambrian rocks of the Limpopo Mobile belt whereas the Nuanetsi volcanics consist of approximately 7 620 m of picrite basalts, basalts and rhyolites which overlie Karoo sediments and are cut by late-Karoo granite and alkaline ring complexes (Cox et al., 1965). The Sabi-Lundi monocline represents a northeasterly extension of the Lebombo flexure and can be followed into the Lupata area of the East African Rift System (Fig. 1.1). Nephelinites, olivine-rich and olivine-poor basalts are found in the Sabi-Lundi monocline (Swift et al., 1953).

The volcanic rocks of the Tuli, Nuanetsi and Sabi areas are in most respects very similar to those found in the northern and central Lebombo and for this reason most of the formational names adopted for the Lebombo volcanics have also been applied to the Zimbabwe rocks (Table 3.2). The

TABLE 3.2 Generalised volcano-stratigraphy of the Nuanetsi Syncline - Sabi syncline area. (The Tuli volcanic succession consists of basalts of the Letaba and Sabie River Formations which overlie granitoid rocks of the Basement Complex.)

GROUP	FORMATION	BEDS	LITHOLOGY
CRETACEOUS (MALVERNIA)			Fossiliferous conglomerates and sandstones
	unconformity		
		Interbedded Basalts	Basaltic lavas
	Nuanetsi Rhyolite		Aphyric rhyolite flows
LEBOMBO			
	Sabie River Basalt		Olivine-poor basic lavas
	Letaba River Basalt		Picritic lavas
	Mashikiri* Nephelinite		Nephelinite lavas
	unconformity		
KAROO SEDIMENTS			Massive sandstones, siltstones and shales.
	unconformity		
BASEMENT COMPLEX			Granites, gneisses, greenstones and gabbros

*Nephelinites crop out at the base of the volcanic succession in the Sabi monocline but have not been reported from Nuanetsi and Tuli.

Nuanetsi rhyolites are an exception since they are invariably aphyric and show compositional and isotopic differences from the Jozini Formation rhyolites of the Lebombo range. Other minor differences are apparent between the Zimbabwe and Lebombo successions. For example, nepheline-bearing dykes appear to be more common in the Karoo volcanics of Zimbabwe, eg. in the Lundi area (see Swift et al., 1953), than is the case in the Lebombo. Thick sequences of basic lavas are also found interdigitated with the Nuanetsi rhyolites and are referred to as the Interbedded Basalts (Cox et al., 1965). No comparable sequence is present in the Lebombo.

Pre-Karoo basement trends and tectonic control clearly played a part in the Karoo volcanism of south-east Zimbabwe. According to Cox et al. (1965) the Tuli syncline owes its location to the zonal structure of the Limpopo mobile belt. The Nuanetsi syncline, by comparison trends somewhat obliquely to the basement structure. However, the syncline lies on the margin of the uplifted shield area of southern Africa at a point where a re-entrant is formed by the north-south trending Lebombo monocline and north-east trending Sabi-Lundi monocline. The axis of the Nuanetsi syncline almost bisects the re-entrant angle and is filled with volcanic rocks which were erupted from fissures parallel to the syncline axis (Cox et al., 1965). Consequently the syncline is envisaged as a tensional feature formed in response to the concentration of lateral tectonic stresses at the point of re-entrancy on the shield margin (Cox et al., 1965).

A series of carbonatite-nephelinite complexes, eg. Chishanya, Dorowa and Shawa (Swift, et al., 1953; Johnson, 1961, 1966; Verwoerd, 1966; Bowen, 1979) crop out to the north-west of the Sabi monocline. Picrite intrusions are found associated with the complexes. Geochronological

studies of the Shawa complex (Nicolaysen et al., 1962) suggest that the carbonatites represent the earliest phase of Jurassic volcanism in south-east Zimbabwe and Johnson (1966) has proposed that the complexes represent an important part of the Karoo volcanic cycle.

TABLE 4.1 Fe_2O_3/FeO ratios of selected Lebombo, central Karoo and Namibian volcanics.

SAMPLE NUMBER	Fe_2O_3	FeO	$\frac{Fe_2O_3}{FeO}$	Rock Type	Locality
L9	6.01	7.49	0.80	Basalt	S. Lebombo
L18	3.95	6.76	0.58	Basalt	S. Lebombo
L29	2.32	8.40	0.28	Basalt	S. Lebombo
L36	2.44	7.72	0.32	Basalt	S. Lebombo
L94	3.04	9.40	0.32	Dolerite Dyke	S. Lebombo
L249	3.91	10.75	0.36	Dolerite Dyke	S. Lebombo
L485a	4.14	10.46	0.40	Dolerite Dyke	S. Lebombo
S8a	7.93	6.33	1.25	Basalt	S. Lebombo
S11	1.39	8.48	0.16	Basalt	S. Lebombo
S14	1.85	8.12	0.23	Basalt	S. Lebombo
J3	6.03	8.59	0.70	Basalt	S. Lebombo
J55	4.54	10.40	0.44	Dolerite Dyke	S. Lebombo
KA25	3.28	7.08	0.46	Basalt	C. Lebombo
KA34	3.01	7.68	0.39	Basalt	C. Lebombo
KA52a	3.99	8.43	9.47	Dolerite Sill	C. Lebombo
KA52b	3.46	8.74	0.40	Dolerite Sill	C. Lebombo
KS3	1.45	9.93	0.15	Picrite Basalt	N. Lebombo
KS47	2.16	8.55	0.25	Picrite Basalt	N. Lebombo
KS53	3.70	9.20	0.40	Picrite	N. Lebombo
KP87	6.18	6.89	0.90	Nephelinite	N. Lebombo
KP89	2.80	8.80	0.32	Dolerite Dyke	N. Lebombo
KP134	6.28	7.02	0.89	Nephelinite	N. Lebombo
SKR	2.12	9.94	0.21	Dolerite Dyke	C. Karoo
KLS38	1.60	9.86	0.16	Dolerite Dyke	Namibia
KLS43	1.25	8.12	0.15	Dolerite Dyke	Namibia

(Abbreviations: S. - South; C. - Central; N. - North)

the literature has been carefully screened and in most cases trace element data has been excluded because it appears as approximate values only, or alternatively, there are clear indications of inter-laboratory differences. Similarly, analyses of highly altered rocks, eg. Swaziland basalts (Urie and Hunter, 1963) have been excluded from the compilation.

To facilitate easy retrieval of material from the data storage system, a series of coded subdivisions were established (Table F 0, Appendix F). These subdivisions relate to geographical area, formation name, petrographic characteristics and rock type, and are arranged in a hierarchial order that was found to be the most suitable arrangement for the handling of the data set. Brief descriptions and locality details are provided for individual samples and in most cases the latitude and longitude of the locality is reported. A reference section is also included in the compilation and provides details of the year in which the analyses were completed, the laboratory in which they were done, the analysts, and the techniques used.

4.4 Mineral Analyses

Mineral compositions were determined by means of a Cambridge Microscan-5 Microanalyser (Electron microprobe). All analytical data has been reduced by on-line data reduction procedures using the method of Bence and Albee (1968) and Albee and Ray (1970) but with appropriate alpha factors for the Cambridge microprobe (Chodos, pers. comm.). Operating conditions, standards used and analytical errors are listed in Appendix A2. Because of the large number of mineral analyses made in the course of this study only selected analyses are presented in tables within the text. The complete set of mineral analyses are, however, included in Appendix E.

4.5 Variation Diagrams

Simple bi-variate scatter diagrams of the various elements or ratios versus MgO have been used throughout this thesis for the interpretation of geochemical trends. MgO is used as a differentiation index since it shows the largest range in the volcanic suites. However, a characteristic feature of Karoo geochemical data is that when plotted on variation diagrams it rarely shows well constrained trends. Instead the data tends to be highly scattered, though it is usually possible to establish overall trends within the scatter. Causes of the scatter include, (i) alteration and leaching of some of the more mobile elements eg. the alkali earths, (ii) possible contamination of the parental magmas by crustal material, (iii) phenocryst redistribution, (iv) inherent variations in the mantle source area, (v) complex fractionation processes such as mantle metasomatism or zone refining, (vi) low pressure crystal fractionation, and are discussed in the text of this thesis.

In order to quantify the apparent trends and thereby model the fractionation processes responsible for the overall variation in the various rock suites trend lines have been fitted to the data points plotted on variation diagrams and estimated liquid compositions have been read off at pre-determined MgO intervals. In variation diagrams where trends are well constrained all data have been used for the computation of regression lines. However, the presence of aberrant points coupled with the extremely diffuse distribution of the data in most of the diagrams has necessitated the construction of best-fit lines by eye. In general the latter method has been adopted throughout this thesis. To calculate liquid compositions, eg. 'parent' and ''daughter', abundances of SiO_2, TiO_2, Al_2O_3, etc. were estimated graphically for the best-fit trend lines at particular MgO values (eg. 9%, 12%, 15% and 18% in the case of the

picrite basalts). Nominal concentrations determined by this method were subsequently normalised to 100% and are referred to as average, or model 'parent' and 'daughter' compositions in this thesis. A similar technique was also used to estimate average trace element concentrations though no normalisation process was applied to the data.

4.6 Petrological Modelling of Major Elements

In order to evaluate the role of high and low pressure fractional crystallisation in the evolution of the lava sequences studied, quantitative tests were made using a least squares mixing program modified by Dr A.R. Duncan from the original of Bryan et al. (1969). The mixing program provides a means of establishing whether or not postulated 'parent' and 'daughter' compositions can be related by addition or subtraction of various mineral phases and is based on the solution of linear mass balance calculations in an overdetermined major element data matrix which may be weighted or unweighted. (The latter option has been used throughout this study.) Calculated solutions are not constrained with respect to sign (ie. may be positive or negative) and to maintain an overdetermined matrix the maximum number of fractionating phases plus parent and daughter compositions, ie. matrix vectors, must be at least one less than the number of elements in the matrix. The mixing calculations can be approached as either fractional crystallisation processes (ie. parent - mineral assemblage = daughter) or crystal accummulation processes (ie. parent + mineral assemblage = daughter) and since both are solved by linear mass balance calculations either may be run in reverse. Consequently fractional crystallisation may be regarded as 'daughter' + mineral assemblage = 'parent'. The advantage of this method is that the proportions of residual magma (F) and fractionating minerals are directly presented in the program output and it is

the approximated 'parent' and 'daughter' compositions generally used in this thesis. Where the range was extremely large (between parent and daughter compositions), compositions of mineral species intermediate to those noted in the end members were used in the mixing calculations. However, this procedure was modified in the case of the picrite basalts (Chapter 8).

The terms 'mixing calculations', 'mixing models', 'least squares approximation' and 'mix' will be used synonomously throughout this thesis when referring to the computer generated models outlined above.

5 GEOCHEMICAL CLASSIFICATION AND PETROGRAPHIC NOMENCLATURE

5.1 Introduction

Geological, petrographic and geochemical studies of the Lebombo, Tuli, Nuanetsi and Sabi volcanics have established the presence of a wide variety of rock types, including nephelinites, picrite basalts, basalts, shoshonites and absarokites. In addition to these basic and alkaline rock types, thick sequences of acid volcanics occur in the Lebombo and Nuanetsi areas. The basic and alkaline volcanics have previously (Cox, 1972a) been subdivided into three groups, namely nephelinites, olivine-rich basalts and olivine-poor basalts with intrusive rocks considered as a separate, but related group (Cox, 1972a). Subsequently, the nephelinites, olivine-rich and olivine poor basalts of the Lebombo have been designated as the Mashikiri Formation, Letaba Formation and Sabie River Formation respectively (Cleverly and Bristow, 1979) and it has been proposed (Chapter 3, section 3.2) that these names should also be applied to the corresponding rock types in the Nuanetsi, Tuli and Sabi areas of south-east Zimbabwe.

In the course of this study all unaltered alkaline, basaltic and rhyolitic samples were analysed for 5 elements (Sr, Rb, Fe_2O_3, K_2O, SiO_2) by means of a rapid "Slab-Analysis" technique (Appendix A 3). From data obtained by this method it became apparent that considerable chemical variation existed within each of the individual groups that could be distinguished petrographically eg. within the olivine-rich and the olivine-poor groups. In the preliminary stages of this study slab data was therefore used to further sub-divide different rock types on the basis of their chemistry and to ensure that a suitably representative suite of rocks was chosen for comprehensive whole rock analysis.

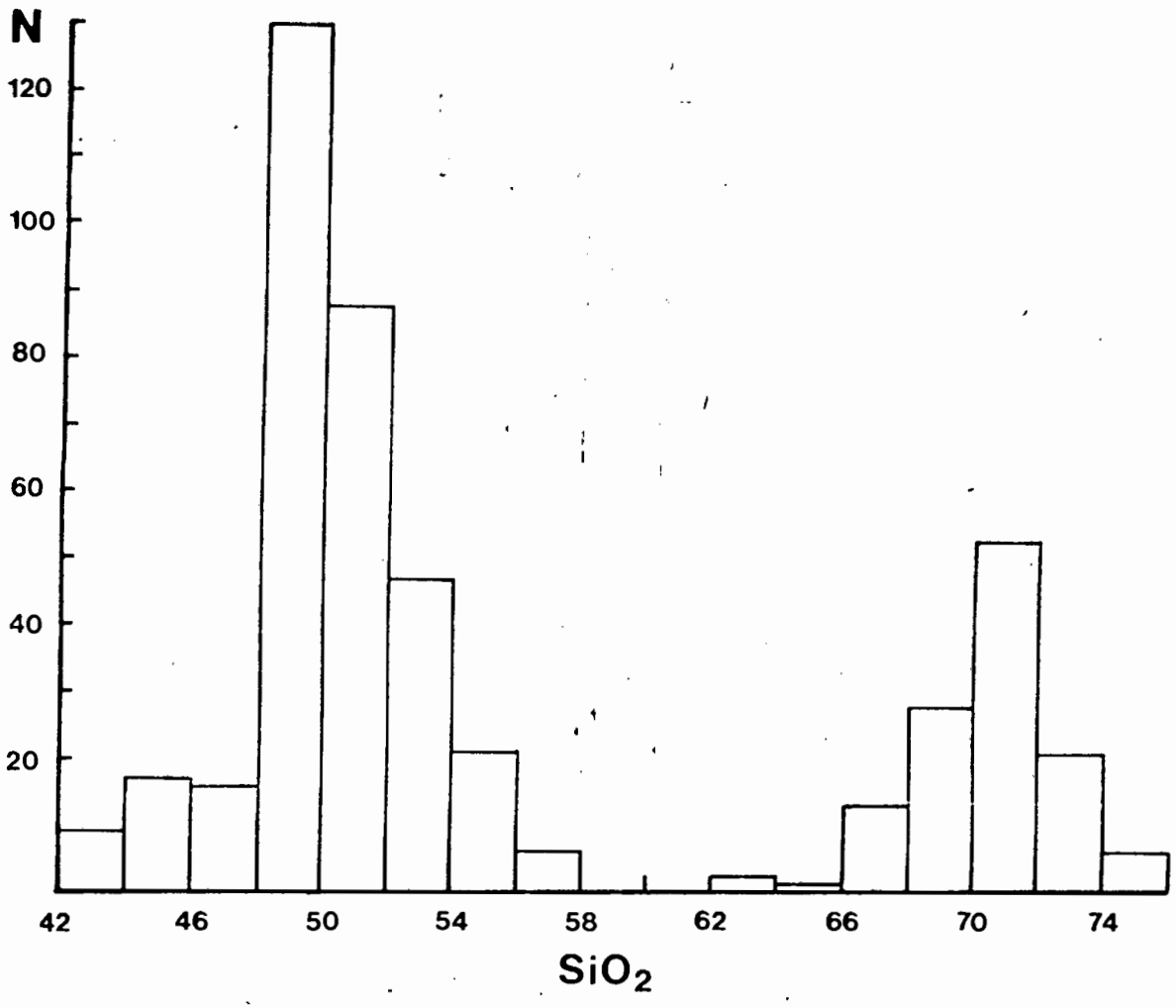

Fig. 5.1 Histogram showing the distribution of silica (weight %) in Karoo nephelinites, basalts and rhyolites from the Lebombo, Nuanetsi-Sabi and Tuli areas of southern Africa. (N = 458; analyses are from the data compilation in Appendix F).

nepheline in the norm whereas nearly all the remaining basic rocks range from quartz-normative through olivine-hypersthene normative (Fig. 5.2). The two groups are therefore easily separable on the basis of their normative character. A few basic rocks contain very small amounts of nepheline in the norm (Fig. 5.2), and the dividing line between basic rocks and nephelinites has thus been chosen as 5% normative nepheline.

iii) MgO weight percent

MgO has been chosen as a primary classification parameter for the basic rocks, firstly because it provides a rough guide to the eruptive temperature of the volcanics and secondly because it provides a measure of the degree of evolution of the basic rocks in terms of their major element composition. It has been used to subdivide basic rocks into three main suites by Cox et al. (In prep.) and a similar scheme has been adopted in this thesis. The suites are referred to as evolved (MgO = 2 - 5%), basaltic (MgO = 5 - 9%) and picritic (MgO > 9%). Distinction between the basaltic and picritic suite is a natural division since it is clear from Figure 5.3 that a strong population minimum exists in the range 8 - 10% MgO. The division at 5% is an arbitrary, but nevertheless useful division, and 2% represents a lower limit for the basic rocks. Very few rocks with a basic affinity were found in the range 2 - 3% MgO and the acid volcanics typically contain less than 1% MgO (Fig. 5.3) with only a few of the more basic dacites exceeding this value.

iv) K_2O weight percent

Potassium has been chosen as a classification parameter because of the large "primary" variations it shows in the volcanic suites. These variations are considered to be "primary" since they are not apparently due to simple crystal fractionation processes, particularly low pressure processes (see Chapters 8, 9). Instead as will be shown, they can be

ascribed to compositional variations in the mantle source materials caused by complex fractionation processes such as mantle metasomatism or zone refining. Contamination by crustal materials may also have contributed to some of the K_2O variation. The "primary" factors have led to the formation of parental magmas with gross variations in K_2O content. These variations existed before the magmas entered the low pressure (crustal) regime where they may have been further modified by crystal fractionation and contamination to give rise to various related rock types.

In view of the large variation in the "primary" K_2O content the basic and alkaline rocks have been subdivided into high-K, intermediate-K and low-K lineages (Fig. 5.3). Boundary lines between the three lineages reflect estimates of the way in which K_2O content varies with MgO during fractionation of olivine from liquids with MgO > 9% and fractionation of plagioclase + clinopyroxene $\pm$ olivine $\pm$ magnetite from liquids with MgO < 9%.

5.3 Classification Scheme

The combined classification scheme for the basic rocks is based on a K_2O versus MgO diagram (Fig. 5.3) thereby facilitating the representation of both lineages (based on K_2O) and suites (based on MgO) on the same diagram. Several authors (eg. Joplin, 1968; Mackenzie and Chappell, 1972; Peccorillo and Taylor, 1976) have used SiO_2 contents as the basis for classification of basic rocks but in the case of the Lebombo and south-east Zimbabwe basic volcanics it is clear that MgO is a much more effective discriminant.

The MgO limits chosen above approximately coincide with the MgO ranges previously adopted in the literature. For example, Joplin (1968) has suggested ranges of 2.75 - 4% MgO for shoshonites, and 5 - 10% MgO

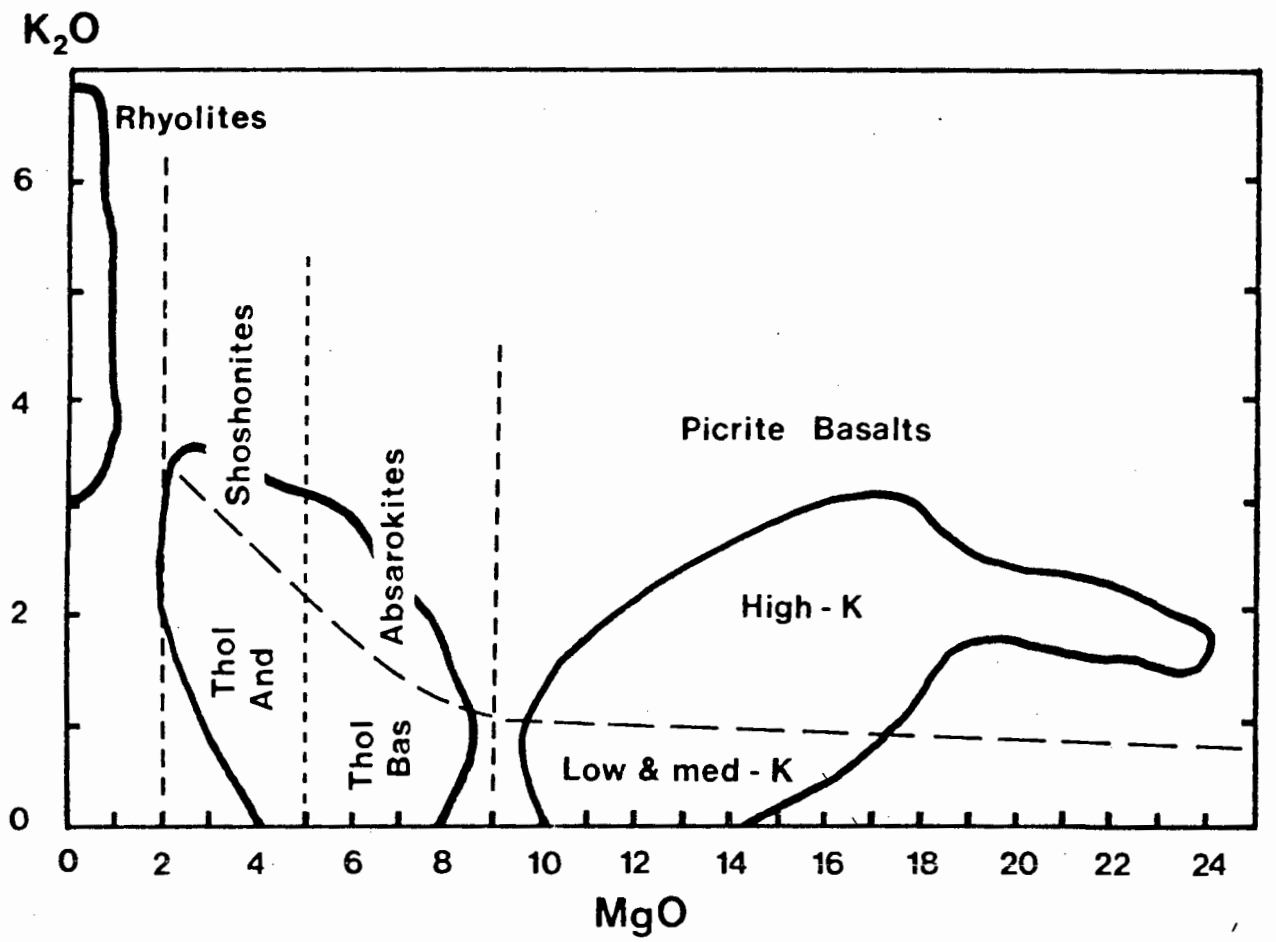

Fig. 5.3 Schematic MgO versus K_2O diagram showing the classification scheme and nomenclature adopted for the basaltic and rhyolitic rocks of the Lebombo, Nuanetsi and Tuli areas. (MgO and K_2O in weight %.)

TABLE 5.1 Classification adopted for the Lebombo, Tuli, Nuanetsi and Sabi volcanics on the basis of geochemical parameters (after Cox et al., 1980).

	2%MgO	5%MgO	9%MgO	
	EVOLVED SUITE	BASALTIC SUITE	PICRITE SUITE	
A	Shoshonites	Absarokites	High-K Picrite Basalts	High-K Lineage
	Tholeiitic Andesites	Basalts	Int-K Picrite Basalts	Int-K Lineage
	Tholeiitic Andesites	Basalts	Low-K Picrite Basalts	Low-K Lineage
B	Nephelinites		Olivine-Nephelinites	Low-Si Lineage

A Silica saturated and oversaturated magma type

B Silica undersaturated magma types

(Int - Intermediate)

TABLE 5.2 Selected analyses of Lebombo, Nuanetsi-Sabi and Tuli mafic volcanics normalised to 100% volatile free.

	N225	N84	N149	KP111	KP97	L12	S14	CL100	Ø183
%SiO_2	48.61	50.79	48.37	51.14	49.61	51.68	53.94	54.72	51.20
TiO_2	2.22	1.83	2.71	3.29	3.25	1.26	1.01	3.19	3.21
Al_2O_3	9.42	11.59	8.87	8.30	7.15	14.53	14.86	12.57	11.42
Fe_2O_3*	15.10	12.78	13.39	11.00	11.82	12.29	10.94	11.16	12.75
MnO	.18	.16	.13	.15	.14	.17	.15	.15	.17
MgO	13.70	11.19	15.29	14.45	16.77	6.61	6.08	5.04	7.67
CaO	8.69	8.70	8.39	6.97	6.34	10.53	8.79	7.79	10.14
Na_2O	1.64	2.21	1.60	1.57	.28	2.35	3.03	2.23	1.44
K_2O	.20	.52	.90	2.56	4.10	.40	.95	2.63	1.57
P_2O_5	.23	.24	.34	.57	.54	.17	.25	.52	.44
ppm Rb	6.1	18.2	21.7	105	84	8.5	22.6	55	19.2
Ba	177	304	511	1201	860	734	290	972	708
Sr	359	358	610	1216	891	751	291	1120	902
Zr	142	132	270	469	425	110	114	403	320
Nb			14.9	28.2	20.3	2.2	3.0	19.5	15.6
Cr	690	790	879	824	879	279	239	175	525
V			216	209	205	265	214	204	273
Sc				20.9	21.5			23.5	
Ni	714	395	744	738	942	67	69	69	238
Co			77	69	79	52	43	45	64
Zn			105	103	113	90	80	108	110
Cu			102	95	86	110	42	114	99
Y			25.7	28.1	27.1	26.5	22.7	32	31

KEY TO TABLE 5.2

N225	Low-K Picrite Basalt : Nuanetsi (311110)
N84	Int-K Picrite Basalt : Nuanetsi (311120)
N149	Int-K Picrite Basalt : Nuanetsi (311120)
KP111	High-K Picrite Basalt : Northern Lebombo (311130)
KP97	High-K Picrite Basalt : Northern Lebombo (311130)
L12	Low-K Basalt : Southern Lebombo (311210)
S14	Int-K Basalt : Southern Lebombo (311220)
CL100	Absarokite : Central Lebombo (311230)
Ø183	Absarokite : Central Lebombo (311230)
CL372	Low-K Tholeiitic Andesite : Central Lebombo (311310)
CL156	Int-K Tholeiitic Andesite : Central Lebombo (311320)
Ø169	Shoshonite : Northern Lebombo (311330)
N436	Shoshonite : Nuanetsi (311330)
KP82	Nephelinite : Northern Lebombo (321300)
KP83	Nephelinite : Northern Lebombo (321300)
KP87	Nephelinite : Northern Lebombo (321300)
NTS12	Nephelinite : Sabi (321300)
N207	Nephelinite : Sabi (321300)

(Number in brackets represents the rock-type code used in the data compilation, Appendix F.)

for absarokites. Similarly most of the average analyses considered by Wilkinson and Binns (1977) to represent tholeiitic andesites are characterised by MgO contents of 4 - 5% whereas the average basalt of Le Maitre (1976) has MgO = 6.73%. Consequently in the intermediate- and low-K lineages, it is now possible to make a distinction between tholeiitic andesites and basalts whereas previously all the rocks within these two groups were referred to as olivine-poor or olivine-free tholeiites (Cox, 1972a), or simply basalts (Bristow, 1976). Names applied to the main rock groups on the basis of the above MgO - K_2O divisions are presented in Table 5.1; many of the names, eg. shoshonite and absarokite have already been used in the Karoo literature (eg. see Vail et al., 1969). Representative analyses of the various rock groups are listed in Table 5.2.

5.4 Petrographic Nomenclature

Each of the main volcanic rock groups of the Lebombo and south-east Zimbabwe regions incorporates rocks which show considerable variations in petrographic type. In previous accounts a variety of petrographic terms have been used to describe the individual rock types which has led to some confusion in the literature, particularly with respect to the olivine-rich volcanics. More useful and consistent petrographic nomenclature, which is compatible with the geochemical classification scheme outlined in the previous section, is presented here.

5.4.1 Nephelinites

The nephelinite lavas present relatively few problems with respect to nomenclature. They are volumetrically insignificant in comparison to the overlying basaltic lavas and are distinctive in terms of their petrography and geochemistry. Furthermore, the mineral assemblages found

be used to distinguish different rock types within either of the two main divisions.

Olivine phyric lavas with modal olivine > 9% and a predominantly glassy or fine grained matrix are referred to as 'picrite-basalts' whereas the predominantly holocrystalline intrusive varieties are referred to as 'picrites' (cf. Cox and Jamieson, 1974). Furthermore, rocks with phenocrysts of olivine + clinopyroxene and olivine + clinopyroxene + plagioclase are referred to as picrite basalts with 'respective phenocrysts' and this may or may not be abbreviated to 2P-picrite basalt or 3P-picrite basalt respectively (lavas with olivine phenocrysts alone, will where necessary, be designated as 1P-picrite basalts). Where orthopyroxene occurs as a phenocryst phase it will be indicated as such. The petrography and mineral chemistry of these rocks will be dealt with in much greater detail in Chapter 8.

In contrast to the lavas with abundant modal olivine and MgO > 9%, lavas and intrusives with no olivine or modal olivine < 9% are referred to simply as basalts and dolerites respectively, whereas rocks that are visibly more evolved are designated as tholeiitic andesites, though the latter are mostly distinguished chemically. In rare instances shoshonites and absarokites can be recognised by their petrographic properties but these too, are mostly classified according to their distinctive chemical characteristics. The nomenclature discussed above is outlined in Table 5.3.

5.4.3 Rhyolites

Rhyolite flows and dykes found in the Lebombo consist of fine grained or glassy rocks which are seldom without phenocrysts and are therefore generally referred to as porphyritic rhyolites. In contrast, acid volcanics in Nuanetsi rarely contain phenocrysts and are referred

TABLE 5.3 Petrographic nomenclature for the Karoo basaltic rocks of the Lebombo, Nuanetsi and Tuli.

> 9% MODAL OLIVINE

a) Extrusive Rocks

Picrite Basalts

Prefix	Phenocrysts	Groundmass Textures
1P	Olivine	Glassy or microcrystalline
2P*	Olivine + clinopyroxene	Fine grained, rarely glassy.
3P*	Olivine + clinopyroxene + plagioclase	Fine grained

b) Intrusive Rocks

Picrites	Olivine + clinopyroxene ± orthopyroxene	Medium to coarse, rare interstitial glass

< 9% MODAL OLIVINE

a) Extrusive Rocks

Basalts (Lavas)	Plagioclase > clinopyroxene > olivine (or aphyric)	Glassy to medium grained

b) Intrusive Rocks

Dolerites (Dykes)	Plagioclase > clinopyroxene > olivine (or aphyric)	Fine to coarse grained

*Orthopyroxene phenocrysts are commonly found in 2P- and 3P-Picrite Basalts.

to as aphyric rhyolites. Phenocrysts in the Lebombo rhyolites may include plagioclase, clinopyroxene, titanomagnetite, sanidine, apatite, zircon and olivine with quartz being found in some Swaziland and southern Lebombo rocks. Plagioclase is invariably the dominant phenocryst phase in the Lebombo rhyolites and it is therefore possible to subdivide these rocks into plagioclase-phyric or quartz-phyric types.

6 GEOCHRONOLOGY

6.1 Introduction

The geochronology of the Lebombo volcanics was first investigated by Manton (1968) who obtained a Rb-Sr isochron relationship with a low initial $^{87}Sr/^{86}Sr$ ratio (0.7042) for the acid volcanics of Swaziland and the southern Lebombo. Manton (1968) reported a Rb-Sr age of 202 $\pm$ 13 my for the rhyolites on the basis of $\lambda^{87}Rb = 1.39 \times 10^{-11} y^{-1}$ and application of York's (1966) regression method. Recalculation of the above age using Manton's (1968) data yields an age of 193 $\pm$ 7 my ($\lambda^{87}Rb = 1.39 \times 10^{-11} y^{-1}$) or 189 $\pm$ 7 my ($\lambda^{87}Rb = 1.42 \times 10^{-11} y^{-1}$) which suggests that Manton (1968) erred slightly in his regression treatment. However, the prime objective of Manton's study was to investigate the Sr-isotope relationships of the basic and acid lavas of the Lebombo (and Nuanetsi) with a view to establishing whether the rhyolites originated from mantle or crustal sources and the slight error in age determination in no way affects his overall conclusions.

A more detailed knowledge of the geology and geochemistry of the Lebombo volcanics (Bristow, 1976; Cleverly, 1977; Armstrong, 1978; Betton, 1978; this thesis), and the greater precision inherent in modern mass spectrometry, has afforded the opportunity to re-examine the geochronology of the volcanics with a view to establishing the age relationships between the different rock groups recognised in the field. Furthermore, in the light of the age data available from the Jurassic and Cretaceous volcanics of Mozambique and Malawi, Zimbabwe, the central area of southern Africa and Namibia it has been possible to evaluate the geochronological development of the Karoo lavas and dykes in southern Africa.

This chapter presents all the Rb-Sr isotopic data completed for dating purposes during the course of the Lebombo Geodynamics Project (Table 6.1). In addition U-Pb and Rb-Sr data extracted from the literature and unpublished sources are discussed briefly. Rb-Sr data have been plotted on conventional isochron diagrams and best fit straight lines were computed using the regression method of York (1966). Isochron ages and initial $^{87}Sr/^{86}Sr$ ratios (abbreviated to Ro or initial-Sr) are reported together with an estimate of their uncertainties. The uncertainties listed for each data point are 1σ values whereas uncertainty intervals reported for all ages and initial-Sr ratios represent 2σ values. Overall precision as determined from the analytical data corresponds to $\pm$ 0.00006 (1σ) and 1.5% for $^{87}Sr/^{86}Sr$ and $^{87}Rb/^{86}Sr$ ratios respectively (see Appendix A4). These values have been used as "blanket" errors (cf. Brooks et al., 1972) in the York (1966) regression treatment except where the 1σ uncertainty for the $^{87}Sr/^{86}Sr$ ratio exceeds $\pm$ 0.00006 in which case the higher value has been used.

Following Brooks et al. (1972) a distinction is made between isochrons and errochrons. This is achieved by computing the mean sum of the residuals (MSUM, York, 1966; MSUM = SUMS / n-2, Allsopp et al., 1979) and comparing it to the F-variate appropriate for a given number of samples and degrees of freedom (20*in this case). If the MSUM is less than the F-variate, then the data points are considered to define an isochron, whereas the reverse applies for an errochron. In the case of errochrons the scatter of data points is considered to be a function of geological factors, eg. alteration, and for such cases the quoted uncertainties do not reflect the real uncertainties (Allsopp, et al., 1979).

*Footnote: This number is based on duplicate analyses run by the writer (Appendix A4) and Prof. H.L. Allsopp of the B.P.I.

TABLE 6.1 Rb and Sr concentrations(ppm), Rb/Sr ratios and atomic ratios in Lebombo acid volcanics.
[x] - Analyst
(y) - 1σ Uncertainty

NAME	Rb	Sr	Rb/Sr	87Rb/86Sr	87Sr/86Sr	FORMATION or BEDS
a. NORTHERN AND CENTRAL LEBOMBO						
KS16[3]	111	500	0.222	0.642	.70648(6)	Joz. Fm.
KS19[3]	133	226	0.588	1.703	.70914(3)	Joz. Fm.
KA6B[3]	119	189	0.630	1.822	.70928(2)	Joz. Fm.
KA78[3]	111	179	0.620	1.794	.70933(6)	Joz. Fm.
KA13[1]	132	284	0.465	1.345	.70834(10)	Dyke
CL209[3]	122	208	0.587	1.697	.70925(4)	Joz. Fm.
b. SWAZILAND						
RC36[3]	127	193	0.658	1.904	.70914(4)	Twn. Bd.
RC40[3]	117	174	0.672	1.945	.70938(6)	Twn. Bd.
RC66[3]	121	168	0.720	2.084	.70951(4)	Joz. Fm.
RC74[4]	144	105	1.371	3.969	.71460(9)	Orb. Bd.
RC128[3]	88	245	0.359	1.039	.70705(2)	Twn. Bd.
RC131[4]	144	124	1.161	3.362	.71276(8)	Mbz. Fm.
SK138[4]	143	191	0.749	2.167	.70953(6)	Mbz. Fm.
SK153[4]	125	131	0.954	2.762	.71142(8)	Mbz. Fm.
c. SOUTHERN LEBOMBO						
L333[1]	119	143	0.832	2.408	.71033(2)	Joz. Fm.
L335[1]	121	151	0.801	2.318	.71004(7)	Joz. Fm.
L336[1]	122	139	0.878	2.540	.71042(4)	Joz. Fm.
L431[1]	128	172	0.744	2.153	.70984(7)	Joz. Fm.
L467[1]	111	201	0.552	1.598	.70834(5)	Joz. Fm.
J5[1]	131	133	0.985	2.851	.71165(5)	Joz. Fm.
J11[1]	131	134	0.978	2.830	.71151(7)	Joz. Fm.
J16[1]	113	204	0.554	1.603	.70844(6)	Joz. Fm.
J18[1]	116	197	0.589	1.704	.70850(3)	Joz. Fm.
J66[1]	129	147	0.878	2.540	.71066(6)	Joz. Fm.
Kuleni Rhyolites (Rb as 87Rb, Sr as 86Sr)						
78-5[3]	73.49	.5810		125.04	.9695(25)	
78-40[3]	75.70	.2137		350.17	1.4317(15)	
78-40b[1]	79.81	.2082		378.94	1.4962(30)	
BK-6[1]	79.56	.2143		367.00	1.4672(10)	
BK-7[1]	77.60	.2344		327.26	1.3963(30)	

Details of analytical methods, data processing, regression procedures and interlaboratory comparisons are summarised in Appendix A.4. Because Rb-Sr and Sr-isotope data have been obtained from different laboratories during the Karoo Geodynamics Project, viz. the Department of Geochemistry, UCT, Bernard Price Institute for Geophysical Research, Witwatersrand University, the Department of Geology and Mineralogy, Oxford University, care has been taken to ensure that no interlaboratory bias exists in the data presented here. The decay constant used is $\lambda^{87}Rb = 1.42 \times 10^{-11} y^{-1}$ which is in keeping with the proposals of the Subcommission on Geochronology (Steiger and Jager, 1977). All previously published ages calculated on the basis of $\lambda^{87}Rb = 1.39 \times 10^{-11} y^{-1}$ have been recalculated using the new decay constant.

6.2 Mafic Lavas and Dykes : K-Ar data

The lower mafic lavas of the Lebombo and south east Zimbabwe do not define an isochron on a conventional $^{87}Rb/^{86}Sr$ versus $^{87}Sr/^{86}Sr$ plot and would therefore have to be dated by K-Ar techniques. (Reasons for the absence of an isochron relationship will be discussed in Chapter 10). An attempt has been made by other workers to obtain K-Ar ages on the basaltic rocks from the Lebombo area for the Geodynamics Project. However, discussion of their ages is beyond the scope of this thesis in view of the large spread in the data that has been obtained by K-Ar dating methods (Fitch and Miller, pers. comm.).

It is commonly found that K-Ar dating of continental volcanics eg. Parana Basalts (Amaral et al., 1966), Mesozoic basalts of Antarctica(McDougall, 1963; Compston et al., 1968) yield discordant age spectra and/or ages which on the basis of other geological evidence, eg. stratigraphic relationships, are clearly too young. The disruption

of the age patterns are usually reconciled with Ar-loss and/or Ar-redistribution during alteration and devitrification of the volcanics (Amaral et al., 1966; Fleck et al., 1977). It is therefore probable that many of the anomolously young ages obtained for Lebombo lavas (Fitch and Miller, pers. comm.) reflect Ar loss due to alteration.

In comparison to the lavas, the dyke rocks of the Lebombo (and Karoo in general) are generally less prone to alteration and as a result K-Ar dating of these rocks usually results in ages which are reproducible and concordant (eg. see Sauvan, 1975). Several Swaziland dolerite dykes (Cleverly, 1977) and a single northern Lebombo basic dyke (Fitch and Miller, unpubl. data) have been dated by K-Ar methods. The Swaziland dykes yield an average age of 188 $\pm$ 5 my (Cleverly, 1977). They are intrusive into the basalts of the Sabie River Formation and are considered to represent a northerly extension of the Rooi Rand Swarm (Cleverly, 1980) which is particularly well exposed in the southern Lebombo. The northern Lebombo dyke intrudes the picrite basalts of the Letaba Formation and yields an age of 159 $\pm$ 2 my. The dyke represents part of a major swarm of dolerites which trend north-west and on the basis of the young age (relative to the 175 $\pm$ 12 my age for the northern Lebombo rhyolites) obtained for this intrusion, it is possible that it may represent a feeder to some of the lavas of the upper Movene Formation which crop out in Mozambique.

6.3 Whole Rock Rb-Sr Data

6.3.1 The Main Succession of Lebombo Acid Volcanics

Though the Swaziland and southern Lebombo rhyolites were originally dated by Manton (1968) by means of Rb-Sr isotope techniques his data has not been used in this study because of i) the uncertainties

associated with the precision of his data, and ii) the availability of a large amount of new high quality data from Swaziland and the southern Lebombo.

Rb-Sr data obtained in the course of this study for the main succession of Lebombo acid volcanics, viz. the Jozini and Mbuluzi Formations, Twin Ridge, Olifants and Oribi beds and rhyolite dykes and granophyres from the central and northern Lebombo, are listed in Table 6.1 and plotted in Figure 6.1. Broadly speaking the data define two reasonably colinear trends which are represented by, a) northern and central Lebombo data points, and b) Swaziland and southern Lebombo data points, respectively. The two sets of data have been regressed separately and the results are shown in Table 6.2. Both regression lines are incorporated on the isochron diagram (Fig. 6.1). Rb-Sr data from Swaziland and the southern Lebombo have also been regressed separately and the results of these computations are included in Table 6.2.

The regression computations for the main succession of Lebombo rhyolites yield isochron ages which indicate that emplacement of the acid volcanics occurred approximately 177 my ago (Table 6.2, 1-4). Rhyolites from the northern and central Lebombo may be slightly younger than those to the south though additional analyses are needed to verify the younger age which has been calculated from only 6 analyses (Table 6.1). Data points lying at the extremities of an isochron fitted to a small number of analyses eg. 5 or less, are capable of causing significant changes in the computed ages unless the regression line is very tightly constrained, ie. 2σ errors are less than a few million years. For example, it was found that in the case of the Swaziland rhyolites Cleverly (1977) originally obtained a 4 point isochron age of 189 $\pm$ 18 my for the rhyolites

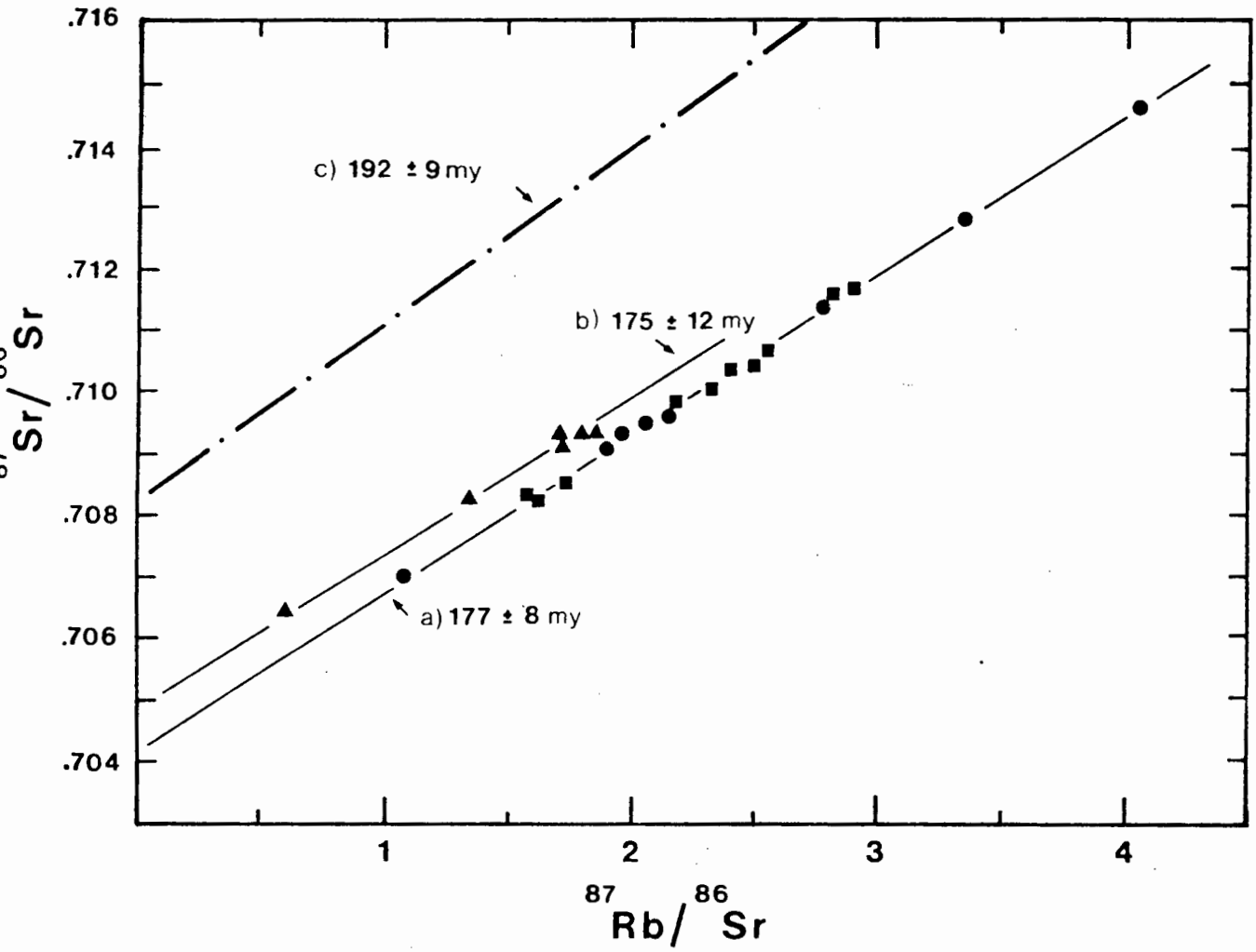

Fig. 6.1 Rb-Sr isochron diagram for the main sequence of Lebombo rhyolites. The isochron obtained for the Nuanetsi rhyolites (c) (Manton, unpubl. data) is included for comparison.

a) Southern Lebombo and Swaziland

- ■ Southern Lebombo
- ● Swaziland

b) Central and Northern Lebombo (▲)

c) Nuanetsi

TABLE 6.2 Summary of whole rock Rb-Sr ages calculated for the acid volcanics in different sections of the Lebombo.

AREA	AGE & ERROR 2σ	R_o & ERROR 2σ	NO. ANALYSES	COMMENTS
1) Northern and Central	175 ± 12	.70490 ± 24	6	Isochron MSUM = 1.48 F = 2.87
2) Southern and Swaziland	177 ± 8	.70434 ± 23	18	Isochron MSUM = 1.82 F = 2.20
3) Swaziland	177 ± 10	.70436 ± 32	8	Isochron MSUM = 2.42 F = 2.60
4) Southern	177 ± 12	.70431 ± 40	10	Isochron MSUM = 1.63 F = 2.45
5) Kuleni	146 ± 2	.71043 ± 72	6	Isochron MSUM = 0.23 F = 2.87
6) Bumbeni	133 ± 5	.70546 ± 28	4	Isochron MSUM = 1.48 F = 3.49

NOTE: 1) - 4) Constitute the main succession of Lebombo acid volcanics and include rocks of the Twin Ridge Beds, Jozini Formation, Mbuluzi Formation, Oribi Beds and rhyolite dykes from the northern Lebombo.

whereas an age of 177 ± 10 my was obtained following the completion of additional Rb-Sr analyses (Table 6.2).

6.3.2 Bumbeni Complex

Four rhyolite and syenite samples from the Bumbeni Complex (Cleverly and Bristow, 1979) have been analysed for their Sr isotopic compositions; the data are shown in Table 6.2 and plotted in Figure 6.3. Regression of the 4 analyses yields an isochron age of 133 ± 5 my (MSUM = 1.48; F = 3.49) with an initial ratio of .70546 ± 28. The Complex is located on the eastern flank of the Lebombo mountains at the southern end of the Lebombo and the significant difference in age between the Jozini rhyolites and Bumbeni rocks is reflected by a very distinct angular disconformity.

6.3.3 Kuleni Rhyolites

Six samples of rhyolite collected from the Kuleni domes and dykes of the southern Lebombo (Bristow, 1976; Cleverly and Bristow, 1979) were analysed. The resulting data are listed in Table 6.1 and plotted in Figure 6.2. The data points define an isochron which yields an age of 146 ± 2 my and an initial ratio of .71043 (MSUM = 0.22; F = 2.87).

6.4 U-Pb Ages of Rhyolite Zircon Separates

A U-Pb study conducted on zircons extracted from a Jozini Formation rhyolite (van Niekerk, 1968; Sample H1) yielded a Pb-Pb age of about 950 my suggesting that older (crustal) zircons may be present in the rhyolites. Morphological characteristics of the zircons also suggest that more than one population of zircons are present in the rhyolites (Bristow, 1976). The positive identification of older zircons could have important implications with respect to the role (and age) of crustal

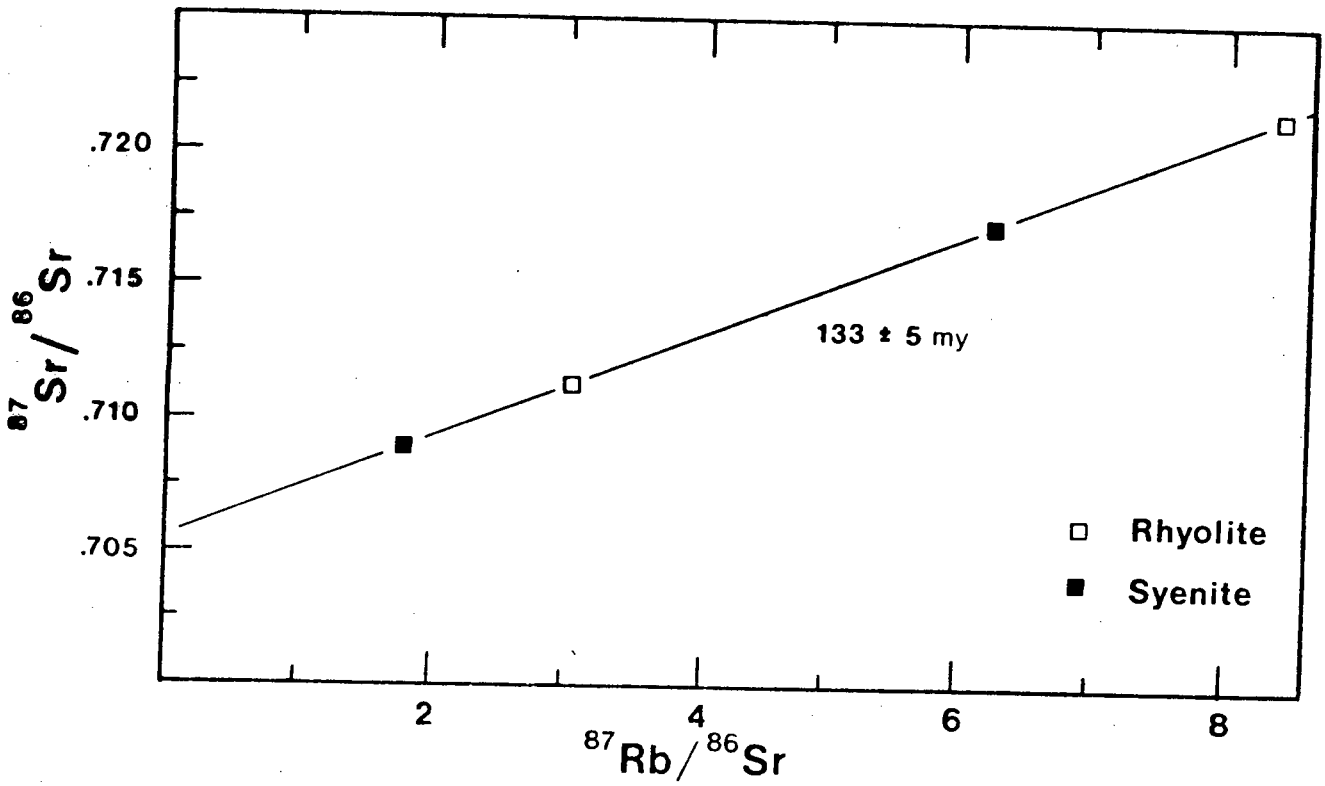

Fig. 6.2 Rb-Sr isochron for the Bumbeni Complex rhyolites and syenites.

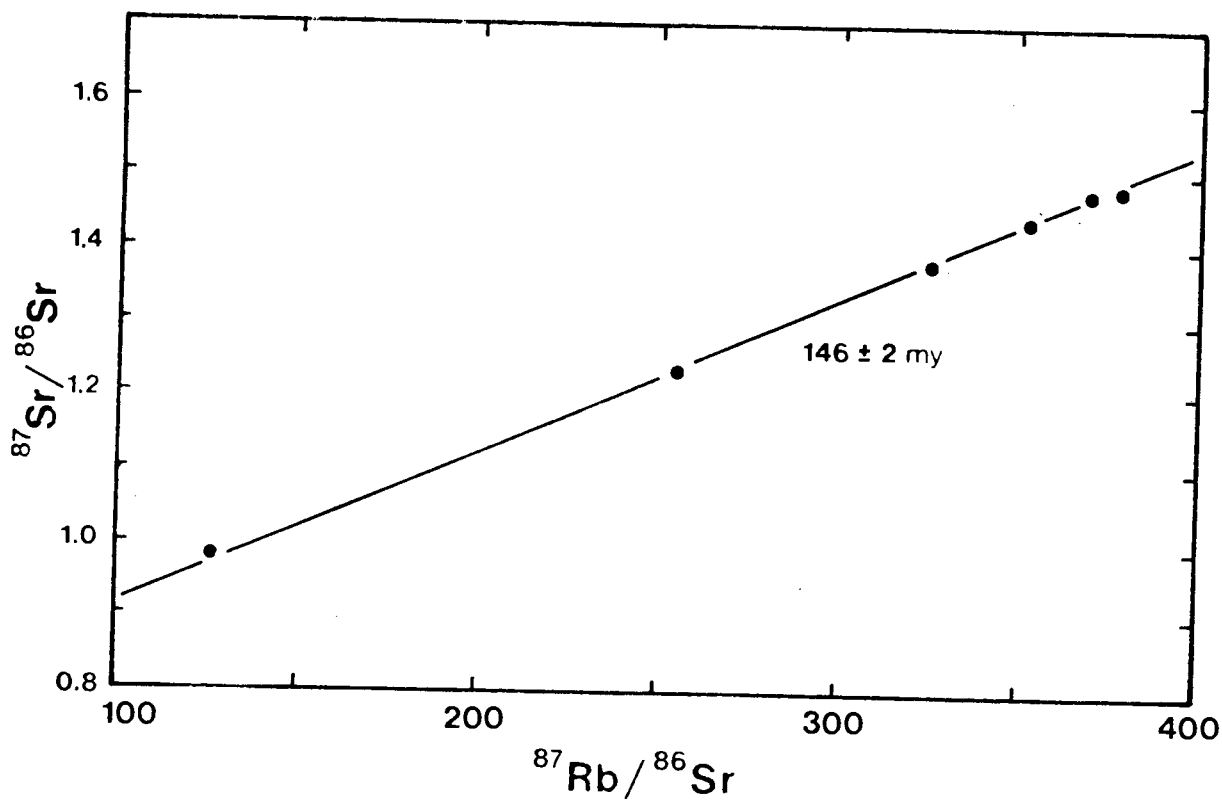

Fig. 6.3 Rb-Sr isochron for the Kuleni rhyolites.

material in the genesis of the acid volcanics. Consequently further U-Pb work on zircon separates is being undertaken by Allsopp (pers.comm.) in the geochronology laboratory at B.P.I. (University of the Witwatersrand).

6.5 K-Ar Dating of the Lebombo Acid Volcanics

An attempt was made by Cleverly (1977) to date both rhyolites and granophyres by conventional K-Ar techniques. According to Cleverly (1977) the data obtained conformed to an errochron which yielded very low ages (121 - 174 my) due to Ar loss. The argon loss was attributed to spherulite formation and recrystallisation within the rhyolite flows and the ages were considered to have no geological significance.

6.6 Geochronology of the Karoo Volcanics

The ages obtained for Karoo volcanics during the course of this study, and in previous studies are summarised in Table 6.3 and are also incorporated on a map showing the main distribution of Karoo volcanic rocks in southern Africa (Fig. 6.4).

In the eastern Karoo areas volcanism appears to have been initiated by the emplacement of a series of carbonatite complexes, eg. Shawa (age: 205 $\pm$ 16 my; Nicolaysen et al., 1962) in south-east Zimbabwe. This early period of alkaline volcanism was subsequently followed by the formation of the voluminous Nuanetsi, Tuli and Lebombo volcanic successions.

The onset of the mafic volcanism in the Nuanetsi area must have taken place approximately 200 my ago since the rhyolites which overlie the basaltic succession have been dated at 192 $\pm$ 9 my (Manton, pers. comm.) though just how long volcanism continued is difficult to establish since the volcanics plunge below a cover of Cretaceous sediments. Nevertheless, the ages obtained from the intrusive Masukwe and Dembe Divula complexes (Manton, 1968) indicate the volcanism in the Nuanetsi region continued

TABLE 6.3 Radiometric ages of Karoo volcanics in southern Africa. (Data from this study as well as published and unpublished sources)

AREA	AGE & ERROR my	METHOD	REF. & COMMENTS
I. EASTERN KAROO			
A. NUANETSI REGIONS			
1. Intrusive Complexes			
Shawa Carbonatite Complex	205 (16)	Rb-Sr	[1] Ijolite
	198 (15)	K-Ar	[2] Biotite ijolite
Marangudzi Complex	200	Rb-Sr	[2] Intrusives
	190 (10)	K-Ar	[3] Ave. of 6 analyses.
	190 (3)	Rb-Sr	[4]
Masukwe & Dembe Divula Complexes	173 (7)	Rb-Sr	[5]
2. Extrusive Rocks			
Jozini Fm.	192 (9)	Rb-Sr	[6]
B. LEBOMBO REGION			
Jozini Fm.	175 (12)	Rb-Sr	[7] N,C Lebombo
	177 (10)	Rb-Sr	[8] Swaziland
	177 (12)	Rb-Sr	[7] South Lebombo
Kuleni Rhyolites	146 (2)	Rb-Sr	[7] South Lebombo
Bumbeni Complex	138 (3)	K-Ar	[9] Syenite
	141	Ar-Ar	[9] Syenite
	133 (5)	Rb-Sr	[7] Syenites & Lavas
Artonvilla Picrite Dykes (Messina)	184 (7)	K-Ar	[10] Ave. of 3 analyses.
Dolerite (Pafuri)	159 (2)	K-Ar	[11] KP89 Cross-cuts L.R.F.
Dolerites (Rooi Rand) (Swaziland)	188 (5)	K-Ar	[12] Ave. of 3 analyses.
C. ZAMBEZI VALLEY - MALAWI			

Lupata Rhyolites	110.5	K-Ar	[3] Anorthoclase
	106	K-Ar	[3] Anorthoclase
	166	K-Ar	[13] Whole Rock
	115	K-Ar	[13] Whole Rock
Chilwa Alkaline Volcanics	130	K-Ar	[14]
D. COASTAL MOZAMBIQUE			
Rhyolites	169 (3)-164 (3)	K-Ar	[15]
Tholeiites	177 (3)-121 (2)	K-Ar	[15]
II. CENTRAL KAROO			
Lavas	189 (7)-160 (6)	K-Ar	[16]
Dykes + Sills	190 - 151	K-Ar	[17]
	187 (7)-137 (3)	K-Ar	[16]
	182 - 158	K-Ar	[18]
III. NAMIBIA			
A. SOUTHERN AREA			
Dolerite Dyke	182 (2)	Rb-Sr	[19] Int. isochr.
Dykes + Sills	184 (3)	K-Ar	[20]
B. NORTHERN AREA			
Kaoka Lavas + Dykes	121 (1)	K-Ar	[20]
Dykes	134 (1)	K-Ar	[20]

REFERENCES: [1] Nicolaysen et al. (1962)
[2] Vail (1966)
[3] Miller, in Gough et al. (1964)
[4] Foland & Henderson (1976)
[5] Manton (1968)
[6] Manton (unpubl. data)
[7] Allsopp & Bristow (unpubl. data)
[8] Bristow & Cleverly (unpubl. data)

[9] Burger & Coertze (1973)
[10] Jacobsen et al. (1975)
[11] Fitch & Miller (unpubl. data)
[12] Cleverly (1977)
[13] Flores (1964)
[14] Wooley & Garson (1970)
[15] Jaritz et al. (1977)
[16] Fitch & Miller (1971)
[17] Mcdougall (1963)
[18] Sauvan et al. (1975)
[19] Richardson (unpubl. data)
[20] Siedner + Miller (1976)

ABBREVIATIONS: L.R.F.- Letaba River Formation
N - Northern
C - Central
Int. isochr. - Internal isochron

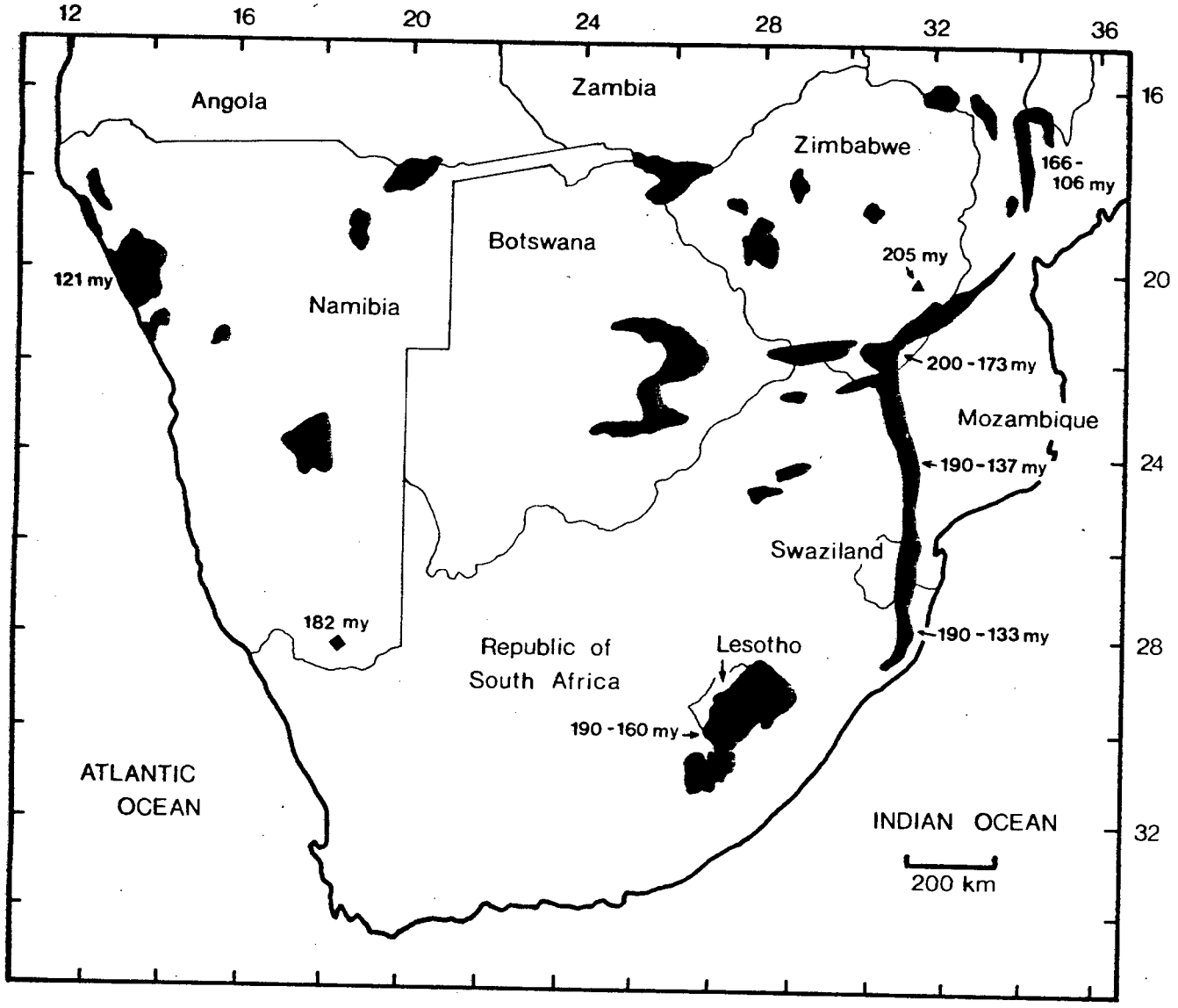

Fig. 6.4 Outline map showing the ages of Karoo volcanics in southern Africa.

until at least 173 my (Table 6.3) and in the light of data from the Lebombo it is probable that younger lavas overlie the Nuanetsi rocks but are covered by the Cretaceous overlap.

In the Lebombo, mafic volcanism clearly began prior to about 177 my (age of emplacement of the rhyolites). The northern Lebombo picrite basalts are contiguous with the Nuanetsi picrite basalts and as such initial emplacement probably took place prior to 200 my, the inferred minimum age of the Nuanetsi mafic volcanics. Olivine bearing dykes with an average K-Ar age of 184 my (Jacobsen et al., 1975) are present near Messina in the Soutpansberg extension of the Lebombo and suggests that emplacement of olivine bearing lavas and dykes may have continued for longer in the northern Lebombo than was the case in Nuanetsi. Further south, Rb-Sr data from the Dokolwayo kimberlite pipe (Hawthorne et al., 1979) indicates that basaltic volcanism in Swaziland and the southern Lebombo was initiated nearer 190 my. The pipe has been dated at approximately 197 my (Allsopp, pers. comm.) and kimberlitic minerals derived from the intrusion have been found in the Karoo sediments (Red Beds, Cave Sandstone) to the east of the pipe. The basalts overlie these sediments and must therefore have been emplaced slightly later than the kimberlite.

Volcanism in the Lebombo continued until about 133 my as is shown by the age of acid volcanics from the Bumbeni Complex (133 $\pm$ 5 my; Table 6.3). Cessation of the Lebombo volcanic activity in the Cretaceous is also implied by the young age (~ 135 my) obtained from a basalt of the Movene Formation in Mozambique (Vail, 1966). However, this age may be unreliable due to the problems of Ar-loss in altered lavas (see section 6.2). The presence of a slight disconformity at the contact between the Sabie River and Jozini Formation indicates that volcanism was not always continuous during the construction of the Lebombo. This disconformity is most noticeable in the southern Lebombo, but less distinct in the

Swaziland, central and northern Lebombo. Rb-Sr data from the Twin Ridge Beds (Cleverly and Bristow, 1979), which are interbedded with the upper basalts of the Sabie River Formation in Swaziland, plot on the same isochron as the main succession of Jozini and Mbuluzi Formation rhyolites (Fig. 6.1). Consequently the time gap between cessation of the mafic volcanism and the first phase of emplacement of the Jozini Formation must have been very small. In the southern Lebombo there is a marked angular disconformity between the Jozini rhyolites (~ 177 my) and the acid volcanics of the Bumbeni Complex (~ 133 my) which is clearly demonstrated by the age difference between the two formations. The Kuleni rhyolite lavas and dykes (~ 146 my) were emplaced during the intervening time gap and it is apparent that rhyolite volcanism was of an episodic nature. The trachybasalts of the Mpilo Member which occur at the base of the Bumbeni Complex may well represent a southern continuation of the Movene Formation (~ 137 my) though at present data available from the Mozambique lavas precludes a detailed comparison and possible correlation of the two sets of mafic volcanics.

To the northeast of the Nuanetsi-Lebombo province much younger K-Ar ages are yielded by the acid volcanics of the Lupata region in the lower Zambezi Valley (166 - 106 my; Flores, 1964; McDougall, in Gough et al., 1964) and basalts of the Chilwa alkaline province south of Lake Malawi (~ 130 my; Vail, 1966; Wooley and Garson, 1970). These volcanics are located in zones of faulting and rifting and on the basis of K-Ar data represent the youngest eastern Karoo lavas recorded thus far. However, in the light of K-Ar data obtained for Lebombo acid volcanics by Cleverly (1977) (see section 6.4.2, this thesis) and mafic lavas from Nuanetsi (unpubl. data) it is possible that the very young ages reported for the Lupata and Chilwa volcanics may not reflect the original age of emplacement of the lavas.

K-Ar studies of rhyolitic and tholeiitic (basalts) volcanics from the coastal areas of northeastern Mozambique indicate that volcanics previously assumed to be Tertiary in age are in fact of Karoo age (Jaritz, et al., 1977). The Mozambique rhyolites range in age from 169 ± 3 to 163.5 ± 2.5 my (Jaritz et al., 1977) and in terms of major element chemistry are broadly similar to the Lebombo rhyolites. The tholeiites show a series of age groupings corresponding to specific localities with an overall range from 177 ± 3 to 120.5 ± 2 my. Field and petrographic descriptions of the rocks (Jaritz, et al., 1977) indicate that they have suffered extensive alteration and as noted previously, it is possible that the reported K-Ar data are minimum ages. However, the range in ages shown by the northeastern Mozambique samples are broadly speaking similar to that found in the Lebombo which suggests that the volcanics from the coastal areas of Mozambique may represent a north easterly extension of the Lebombo belt.

The central Karoo lavas and dykes appear to be broadly contemporaneous with the Swaziland and southern Lebombo volcanics. Age determinations by McDougall (1963), Compston et al. (1968), and Fitch and Miller (1971) indicate that the main period of central Karoo volcanism commenced between 185 - 190 my (Table 6.3). However, evidence of preceeding localised and relatively minor volcanism is found in several Stormberg localities. For example, a basalt flow is found interbedded with sediments of the Elliot Formation on the farm Siberia between Barclay East and Dordrecht (Lock et al., 1974). Furthermore, the large proportion of volcanoclastic material (eg. glass shards) found in the underlying Karoo sedimentary strata (see Stockely, 1947; Botha and Theron, 1967; Elliot and Watts, 1974; Martini, 1974; Ho-Tun, 1979) suggests that the main period of Karoo lava and dyke emplacement was preceeded by periods of highly

explosive activity. Published K-Ar data indicate that the youngest central Karoo lavas were emplaced approximately 160 my ago whereas dyke intrusion may have continued until 140 my (Table 6.3) though the few younger ages reported may reflect Ar loss. The establishment of an accurate upper limit is, however, difficult because it would appear that erosion has removed the uppermost part of the lava succession. Had volcanism continued for much longer periods it is probable that younger dolerite dykes, which are generally considered to represent feeders to the lava flows, would have been found cutting the underlying Karoo sediments.

Age data obtained from Namibia show a bimodal distribution. An internal Rb-Sr isochron obtained from dolerites in southern Namibia yieldsan age of 182 ± 2 my (Richardson, pers. comm.) whereas lavas and dykes which crop out in the north western areas of the country have been dated at about 121 my (Siedner and Mitchell, 1976) by K-Ar methods. Though considerably younger than the typically 'Jurassic' Karoo lavas of the central area the volcanics encountered in northwest Namibia are nevertheless considered to represent an integral part of the Karoo volcanic episode.

6.7 Conclusion

Karoo volcanism appears to have been initiated around 200 my in Upper Triassic times in south-east Zimbabwe. Thereafter the focus of volcanism spread to the Nuanetsi-Tuli areas and down the Lebombo belt. The event appears to have reached its culmination between 190 my and 177 my with outpourings of extensive basaltic lavas and more localised rhyolitic flows. Waning activity through to the Cretaceous in the Lebombo region saw the emplacement of further localised rhyolitic rocks, eg. Kuleni and Bumbeni, and an upper succession of basaltic rocks represented

by the Movene Formation. In the central area volcanism appears to have ceased prior to the Cretaceous. However, with the waning of activity in the Lebombo and central Karoo areas the focus of volcanism appears to have shifted to the north eastern areas of Mozambique, Lupata and Malawi and northwestern areas of Namibia. Rocks of tholeiitic, alkaline (Lupata and Malawi only) and rhyolitic affinity were emplaced during the early-middle Cretaceous in these areas, though some of the ages may not reflect the original age of emplacement.

Overall the Karoo event covered a time span of approximately 100 my from the late Triassic to mid Cretaceous times. However, the errors and uncertainty associated with much of the published data prevents a detailed and precise reconstruction of volcanic history of the magmatic episode. Much of the early (pre-1968) Rb-Sr data was obtained prior to the advent of high precision mass spectrometry whereas K-Ar dating of volcanic rocks is invariably beset with problems related to alteration and associated Ar loss. Nevertheless, the data do provide an overall picture of the timing of the Karoo magmatic event though subsequent age studies may well lead to refinement and/or alteration of the geochronological history as ascertained from the data presently available.

7 THE NEPHELINITES

7.1 Introduction

The nephelinites represent the earliest lavas seen in the volcanic succession of the northern Lebombo and also crop out in the northern Soutpansberg and at the base of the Karoo succession in the Sabi area of south-east Zimbabwe (Rogers, 1925; Swift et al., 1953; Cox, 1972a). They are volumetrically insignificant in comparison to the high- and low-MgO basic volcanics but nevertheless represent an important part of the Karoo volcanics of eastern southern Africa since they contrast strongly with the overlying picrite and MgO-poor basalts.

Previous studies of the nephelinites have been dependant on a relatively small amount of geochemical data. In this chapter new mineralogical and geochemical data are presented and the petrogenesis of these rocks is considered in the light of this new data. The mineralogical data has been obtained exclusively from the northern Lebombo nephelinites though it is apparent from the brief petrographic descriptions of the Sabi lavas and dykes (Swift et al., 1953, Jamieson, 1969 - Appendix D) that no major petrographic differences exist between the nephelinite lavas of South Africa and south-east Zimbabwe. The new bulk geochemical data have been derived from both the Lebombo and Sabi volcanics.

7.2 Petrography and Mineralogy

7.2.1 General Statement

General petrographic relationships of nephelinites from the Sabi-Nuanetsi and northern Lebombo-Limpopo areas have been described by Rogers (1925), Lombaard (1952), Swift et al. (1953) and Cox (1972a). They are a most distinctive group of rocks and though they show a certain amount of

interflow variation they are invariably characterised by the presence of large clinopyroxene phenocrysts, frequently arranged in stellate (glomeroporphyritic) aggregates, set in a dark crystaline or glassy matrix. Small phenocrysts of altered olivine and nepheline are also recognisable in some lava flows and many flows are studded with large spherical amygdales. These features allow easy recognition of the nephelinite rock types in the field and makes them readily distinguishable from the overlying olivine-rich lavas.

In thin section, the majority of the lava samples are porphyritic, often seriate (Plate 7.1.A), with phenocrysts of clinopyroxene (two generations in the seriate rocks), small subhedral or subrounded olivines (Plates 7.1. E,F), rare subhedral nepheline crystals, titanomagnetite phenocrysts (Plate 7.1.G), and small biotite tablets set in a fine grained or cryptocrystalline matrix. The pyroxenes (titaniferous augites) are often found in clusters (Plate 7.1.A) and are frequently overgrown by aegerine-augite. Nepheline and clinopyroxene are the predominant groundmass minerals, with minor amounts of aegerine-augite, disseminated opaque-oxide and more rarely intergranular biotite and sodic amphibole. Apatite occurs as both a phenocryst phase, included in the pyroxene phenocrysts, and as a groundmass constituent. Euhedral grains of titanomagnetite are included in some olivine and pyroxene crystals.

Some of the lavas are characterised by relative coarse, equi-granular groundmass textures. Biotite, aegerine-augite and sodic amphibole are invariably present as groundmass phases in these rocks. Nepheline is nearly always more strongly altered than the other mineral constitutents and many of the rocks with large amounts of nepheline are found to be pitted and oxidised. Since the Lebombo samples were collected

PLATE 7.1

A - Photomicrograph of nephelinite KP92 showing well developed seriate texture exhibited by clinopyroxene phenocrysts and microphenocrysts. Crossed polars.

B - Portion of a euhedral clinopyroxene phenocryst showing fine oscillatory zoning; nephelinite KP92. Crossed polars.

C - Photomicrograph showing clinopyroxene phenocryst with bisegmental twinning in nephelinite KP92.

D - 'Cored' clinopyroxene phenocryst in nephelinite KP83. The light coloured core is much less titaniferous than the surrounding clinopyroxene. Note also that the clinopyroxene surrounding the central unpigmented core has a well developed sieve texture. Patches of carbonate, infilling irregular shaped vesicles are apparent to the right hand side of the photomicrograph. Crossed polars.

E - Photomicrograph of a subrounded olivine phenocryst (centre) associated with clinopyroxene crystals in nephelinite KP87. Crossed polars.

F - Pseudomorphed olivine phenocrysts in nephelinite KP83. Portion of a clinopyroxene macrophenocryst is apparent in the lower right corner of the photomicrograph. Irregular patches of light coloured calcite and zeolite are also seen in the photograph. Crossed polars.

G - Subhedral titanomagnetite phenocrysts associated with clinopyroxene crystals in nephelinite KP92. Plane polarised light.

PLATE 8.1

Picrite basalt characterised by olivine phenocrysts (euhedral, subhedral and rounded) and skeletal clinopyroxene (needle-like crystals with clothes peg structures or small equant and hollow-ended prisms) set in a glassy groundmass. Rocks such as these are typical of the lower portion of the Letaba River Formation in the Northern Lebombo, particularly in the Pafuri and Shingwedzi River areas. Note fairly intensive alteration of some olivines. (Sample KP108, Crossed polars : Pafuri River area, Kruger National Park).

PLATE 7.1

A

2.4mm

B

1.2mm

C

1mm

D

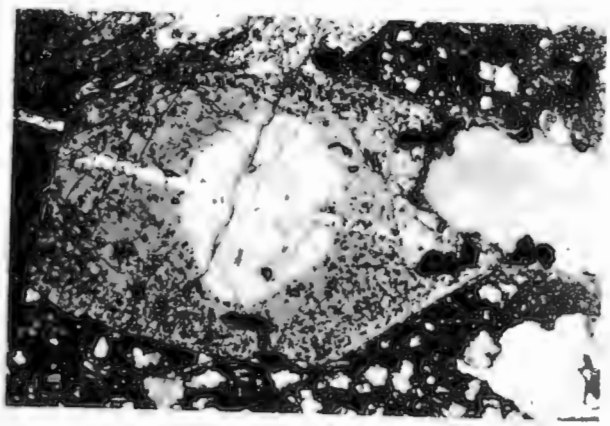

1.2mm

E

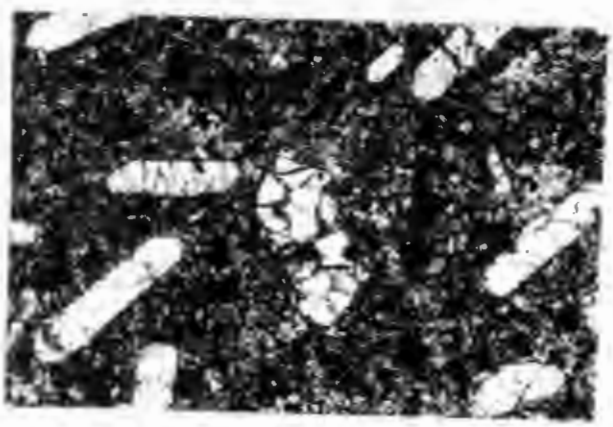

1.3mm

F

1.5mm

G

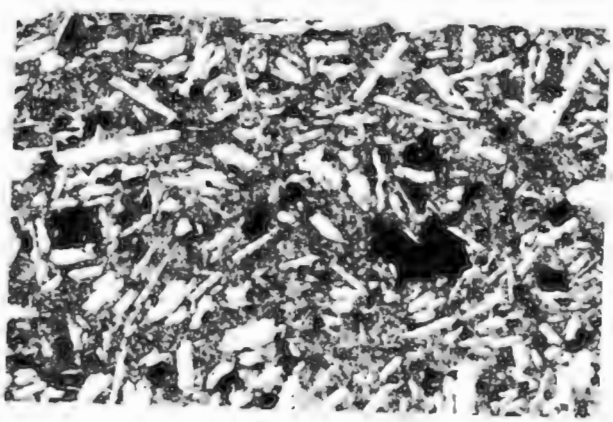

1mm

Its tendency to be overgrown by clinopyroxene was first noted by Rogers (1925) in the northern Lebombo rocks and by Cox et al. (1965) in Nuanetsi lavas. The term mantled is used to describe these orthopyroxenes. Plagioclase phenocrysts are notably scarce and are found in only the most evolved lavas of the group as is the case in the Nuanetsi olivine-rich sequence (Cox and Jamieson, 1974).

The groundmass textures of the picrite-basalts vary from glassy through microcrystalline to fine or medium grained. The glassy lavas (Plate 8.1) are characterised by the presence of numerous skeletal crystals of opaque-oxide, abundant microlitic or skeletal clinopyroxene and apatite needles, in addition to olivine phenocrysts. In rocks with a microcrystalline groundmass, plagioclase appears as sheaves of quenched microlites accompanying acicular and equant euhedra of clinopyroxene and needles of apatite. Coarser lavas are characterised by well formed laths of plagioclase, subhedral and rounded clinopyroxene, spicular and lath shaped opaque oxide and ubiquitous apatite.

The picrite basalts are rarely amygdaloidal. Vesicles, if present, are generally extremely angular in outline and invariably infilled with chloritic material. Small angular amygdales are very often found within or closely associated with glomeroporphyritic aggregates of olivine and mantled orthopyroxene.

8.2.2 Olivine

Three main groups of olivine crystals are recognised in the picrite basalts on the basis of crystal morphology, viz. macrophenocrysts, phenocrysts and microphenocrysts.

primarily for geochemical work, weathered outcrops were mostly avoided. Even so, many of the lavas were subsequently found to be highly altered and as such unsuitable for petrographic or geochemical work. Replacement of nepheline by calcite and zeolite is particularly common. Partial calcitisation of pyroxene was also noted and olivines are either strongly altered or pseudomorphed. According to Cox (pers. comm.) nepheline phyric lavas are common on the Lundi River (Sabi area) in south-east Zimbabwe. Few nepheline-phyric rocks were obtained from the northern Lebombo though this may be a function of sampling bias.

Several thin sections display petrographic evidence of the production of late crystallisation residua composed of variable amounts of nepheline, analcite and traces of alkali feldspar. These assemblages occur as irregular patches intimately associated with the matrix and appear to be similar to the 'trachytic' segregations described in volcanic rocks (Bryan 1967; Wright, 1967). Amygdales, containing both zeolite and calcite, are distinguished from the segregation patches by the presence of a well developed rim that separates the vesicle infilling from the matrix; many of the amygdales are also spherical.

Rapidly cooled lavas contain variable amounts of intersertal pale-brown glass or patches of irresolvable microcrystalline mesostasis, and habits of clinopyroxene and opaque oxides found in these rocks are often indicative of skeletal growth (cf. Coombs and Wilkinson, 1969). These features are particularly well displayed by the series of thin nephelinite lava flows found at the base of the Olifants River section. Some fine grained rocks also contain abundant isotropic material, thought to be analcite, and a large amount of opaque dust.

7.2.2 Clinopyroxene

Clinopyroxene is the dominant phenocryst phase in the nephelinitic lavas. The crystals show a great complexity in morphology, zoning and twinning and an irregular variation in certain chemical parameters. In this respect they are typical of pyroxene phenocrysts found in other alkaline lavas e.g. Mt. Selale basalts, Ethiopia (Augustithus, 1978).

The modal concentration of clinopyroxene (see Table 7.1) is extremely variable (range 17-47%) though concentrations of greater than about 20% probably reflect phenocryst accumulation. Most lavas contain abundant phenocrysts which vary in length from about 1.0 - 2.5 mm. Macrophenocrysts up to 7.0 mm are also common and microphenocrysts in lavas with a seriate texture are mostly less than 0.5 mm in length. Crystals have a flattened prismatic habit and are predominantly euhedral or subhedral. They commonly assume a needle like shape and may attain length to breadth ratios of 15 : 1. Tabular and needle shaped phenocrysts and macrophenocrysts with hollow interiors filled with groundmass material and/or inclusions of subhedral titanomagnetite were found in some rocks.

The pyroxenes range in colour from neutral, through pale-yellow to light-brown due to increasing degrees of Ti-pigmentation. Fine oscillatory zoning is common (Plate 7.1.B) and strong hour glass zoning is apparent in some phenocrysts. Twinning is less common and is mostly of a polysynthetic or bi-segmental type (Plate 7.1.C) developed subsequent to zoning. Several phenocrysts and macrophenocrysts are 'cored' by augite essentially free of Ti-pigmentation and zoning (Plate 7.1.D) whereas the surrounding pyroxene is strongly pigmented and zoned. Some of the cores show apparently corroded outlines.

TABLE 7.1 Modal analyses of representative nephelinite lavas

	KP82*	KP83*	KP84	KP87	KP92*	KP131
PHENOCRYSTS						
Olivine°°	3.3	8.4	3.4	6.8		4.3
Clinopyroxene	29.9	16.7	17.1	16.8	46.9	14.6
Titanomagnetite	3.7	5.8	4.7	5.4	10.4	4.7
Nepheline$^{\phi}$		10.5				
MATRIX						
Nepheline Clinopyroxene }	58.2	49.8	62.6	59.2	42.7	71.4
Biotite				7.2		
Opaques	1.0	1.5	4.6	4.6		2.8
Zeolite, Calcite	3.9	7.3	7.7			2.2

* Rocks have well developed seriate textures

°° Olivine is mostly pseudomorphed

ϕ Present as partially altered microphenocrysts

Abundant inclusions of opaque oxide and groundmass material often impart a sieve-like appearance to the clinopyroxenes (Plate 7.1.D). These inclusions are frequently located in bands within the pyroxenes and the following sequence is typical:- massive core, sieved zone, massive rim. Large patches of devitrified glass and crystalline material e.g. sheaves of nepheline, occur in other crystals. Fine canals of glassy material usually extend into the cavities filled with crystalline or fine grained matrix and re-entrants indicative of corrosion or rapid growth are common.

Small patches and blebs of carbonate were noted in a few of the clinopyroxene phenocrysts though it is uncertain as to whether or not the carbonate represents a primary phase. Many of the lavas contain vesicles filled with calcite and consequently carbonate material contained in the phenocrysts could have originated from the same source as that in the amygdales. Narrow rims of aegerine-augite occur as overgrowths on some clinopyroxenes, particularly in those rocks with a relatively coarse matrix in which intergranular aegerine-augite is apparent. Blebs and rods of apatite are also found in pyroxene phenocrysts of some, but not all rocks.

Groundmass pyroxenes assume various crystalline shapes, depending on the degree of crystallinity of the matrix. Pyroxenes in lavas with relatively coarse textures assume anhedral, rarely subhedral, lath shapes and are strongly intergrown with other matrix minerals. Irregular micro-crystals and prisms characterise the fine grained rocks and prominent clinopyroxene needles are common in the very fine grained, almost glassy lavas.

In terms of their chemistry, the pyroxenes (macrophenocrysts, phenocrysts and microphenocrysts) are strongly titaniferous, plot in the Ca-rich

portion of the pyroxene diagram (Fig. 7.1) and show a relatively small range in composition: $Wo_{42}En_{49}Fs_9$ to $Wo_{47}En_{40}Fs_{13}$. Representative analyses are given in Table 7.2, and individual analyses in Microfiche Table E.1. Individual crystals in any given rock display an extremely small but irregular variation in composition from core to margin (Fig. 7.2) though in general core analyses, particularly unpigmented cores, represent the most basic composition in terms of MgO content whereas the rims are slightly more iron rich. Overall, the pyroxene analyses define a weak trend of Ca- and Fe-enrichment typical of alkali lavas (cf. Baker et al., 1977), Al_2O_3 shows a slight overall increase with increasing ferrosilite content, and MnO and NaO remain relatively constant; TiO_2 is extremely irregular in its behaviour.

The irregular variations in terms of Wo-En-Fs found between the core and margin of individual crystals are magnified by several of the minor and trace element contents. Variations in the concentrations of TiO_2, Al_2O_3 and Fe/Mg ratio between core and margin of an oscillatory-zoned macrophenocryst, as determined by EMP analysis, are shown in Fig. 7.2. In the main portion of the phenocryst, the Fe/Mg ratio shows a series of reversals whereas, TiO_2 and Al_2O_3 are more variable in their behaviour. Both the Fe/Mg ratio and absolute levels of TiO_2 and Al_2O_3 show a sharp increase near the rim and though not shown, there is also a close correspondence between the fine zonal patterns displayed by the pyroxene and the oscillation in percentage content in each of these elements.

Wass (1979) has shown that with decreasing pressure, pyroxenes in alkali basalts show an increase in Al^{iv}/Al^{vi}, a linear increase of atomic proportions of Ti and Al with decreasing Si, and an increase in the Ti : (100 Mg/Mg + Fe) ratio. Similar relationships are demonstrated by a

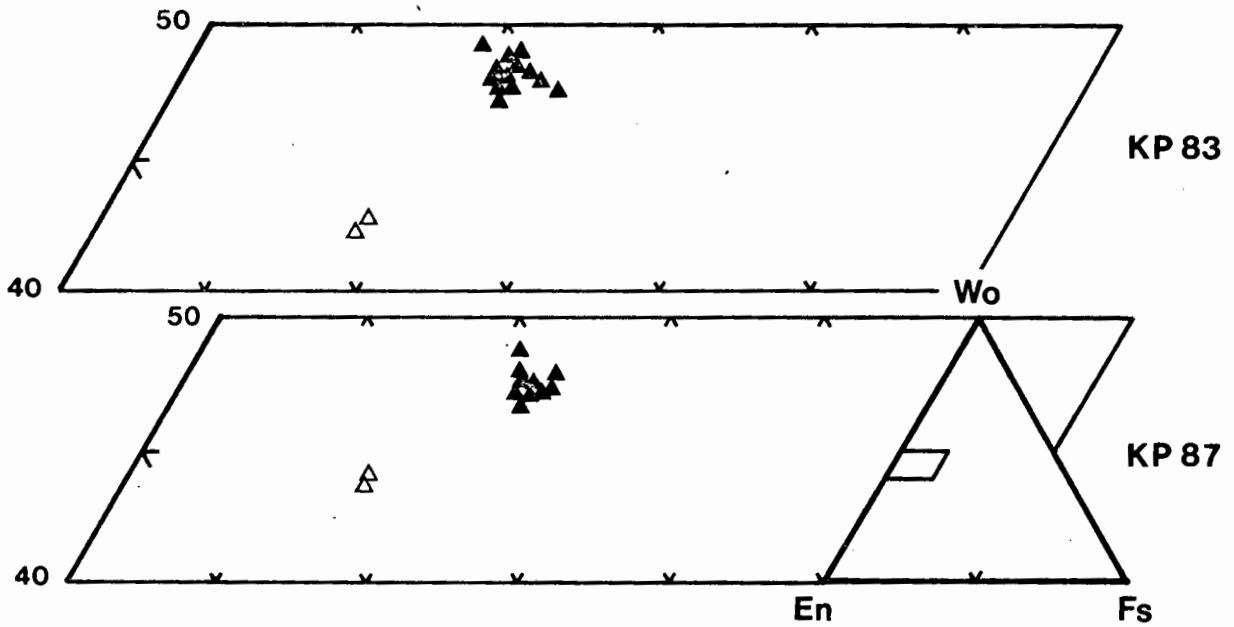

△ Unpigmented cores

▲ Cpx enclosing unpigm. cores, phenocrysts, macrophenocrysts

Fig. 7.1 Compositional range of clinopyroxenes analysed in the northern Lebombo nephelinite lavas expressed in terms of Wo-En-Fs.

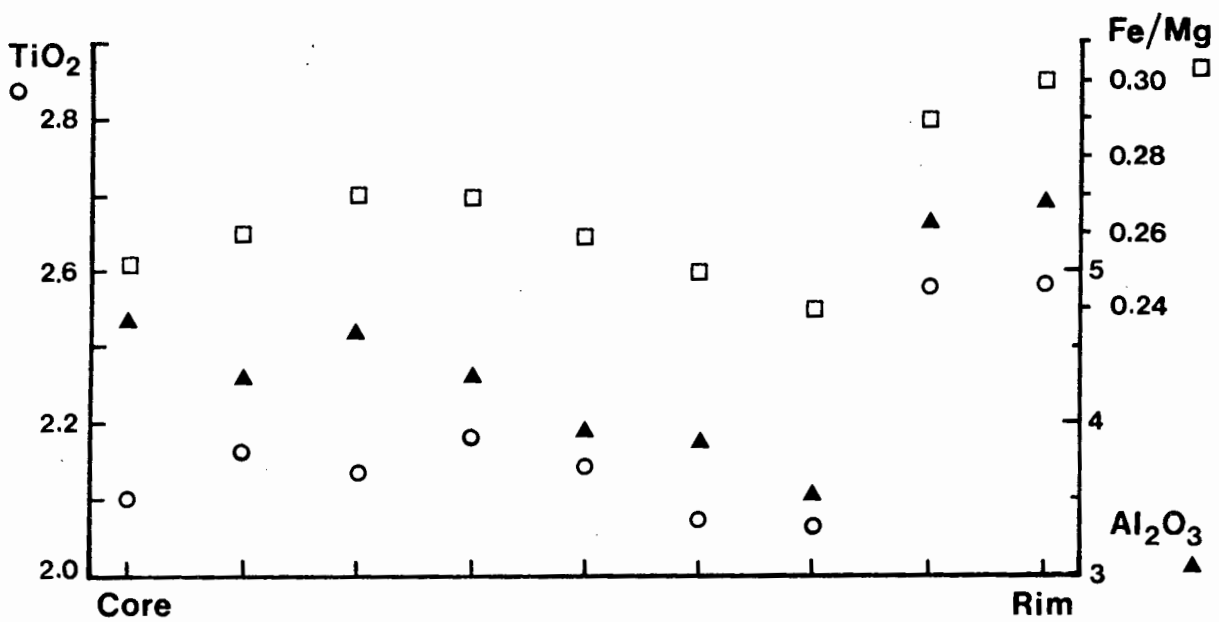

Fig. 7.2 Compositional variations shown between core and margin by an oscillatory zoned clinopyroxenes macrophenocryst.

TABLE 7.2

NEPHELINITES : REPRFSENTATIVE ANALYSES OF CLINOPYROXENES

	1	2	3	4	5	6	7	8	9	10
SIO2	48.72	48.80	50.74	50.30	50.42	49.72	50.16	50.52	50.51	50.40
TIO2	2.79	2.73	2.02	2.16	1.61	2.32	2.45	2.31	2.47	1.40
AL203	4.99	4.89	3.30	3.36	2.95	3.94	3.71	3.80	3.51	4.81
CR203	-	-	-	-	-	-	-	-	-	-
FEO	6.97	6.73	6.17	6.35	6.58	6.51	6.59	6.52	6.30	7.28
MNO	.10	.10	.09	.11	.12	.10	.10	.10	.13	.11
MGO	13.24	13.17	14.22	14.07	14.28	13.60	13.76	14.08	14.07	12.66
CAO	22.01	21.90	22.63	22.39	23.42	22.70	22.38	22.82	22.48	20.86
NA2O	1.15	1.24	.89	.92	.93	.95	.90	.97	.89	1.59
K2O	-	-	-	-	-	-	-	-	-	-
TOTAL	99.97	99.56	100.06	99.66	100.31	99.84	100.05	101.12	100.36	99.11

* * ATOMIC PROPORTIONS BASED ON SELECTED NO. OF OXYGENS * *

OXYGEN	6	6	6	6	6	6	6	6	6	6
SI	1.818	1.826	1.881	1.874	1.875	1.854	1.863	1.858	1.868	1.886
ALIV	.182	.174	.119	.126	.125	.146	.137	.142	.132	.114
ALVI	.037	.042	.025	.022	.004	.027	.026	.023	.021	.098
TI	.078	.077	.056	.061	.045	.065	.068	.064	.069	.039
CR	-	-	-	-	-	-	-	-	-	-
FE2+	.218	.211	.191	.198	.205	.203	.205	.201	.195	.228
MN	.003	.003	.003	.003	.004	.003	.003	.003	.004	.003
MG	.736	.734	.785	.781	.791	.756	.762	.772	.775	.706
CA	.880	.878	.899	.894	.933	.907	.891	.899	.891	.836
NA	.083	.090	.064	.066	.067	.069	.065	.069	.064	.115
K	-	-	-	-	-	-	-	-	-	-
SUM	4.036	4.034	4.023	4.025	4.049	4.029	4.019	4.030	4.019	4.026
	WO 47.99	WO 48.16	WO 47.92	WO 47.72	WO 48.37	WO 48.61	WO 47.96	WO 48.05	WO 47.86	WO 47.25
	EN 40.15	EN 40.28	EN 41.88	EN 41.71	EN 41.02	EN 40.51	EN 41.01	EN 41.23	EN 41.67	EN 39.88
	FS 11.86	FS 11.55	FS 10.20	FS 10.56	FS 10.61	FS 10.88	FS 11.02	FS 10.72	FS 10.47	FS 12.87

* * * SAMPLE DIRECTORY * * *

ANALYSIS NO.	DESCRIPTION
1	MACROPHENOCRYST CORE - 1A (KP83)
2	MACROPHENOCRYST - 1B (KP83)
3	MACROPHENOCRYST - 1C (KP83)
4	MACROPHENOCRYST - 1D (KP83)
5	MACROPHENOCRYST - 1E (KP83)
6	MACROPHENOCRYST - 1F (KP83)
7	MACROPHENOCRYST - 1G (KP83)
8	MACROPHENOCRYST - 1H (KP83)
9	MACROPHENOCRYST RIM - 1I (KP83)
10	PHENOCRYST (KP83)

TABLE 7.2 (CONTINUED)

NEPHELINITES : REPRESENTATIVE ANALYSES OF CLINOPYROXENES

	11	12	13	14	15	16	17
SIO2	53.14	53.02	50.83	50.35	50.82	50.46	50.28
TIO2	.49	.52	1.55	1.79	1.61	1.58	1.44
AL2O3	2.48	2.46	2.87	3.28	2.95	3.42	2.75
CR2O3	-	-	-	-	-	-	-
FEO	4.86	4.92	6.67	6.90	6.58	7.09	6.56
MNO	.10	.10	.11	.12	.12	.13	.11
MGO	16.70	16.61	14.19	13.96	14.28	13.97	14.38
CAO	20.75	20.79	22.94	22.63	23.42	22.57	23.47
NA2O	1.01	.97	.92	.94	.93	1.07	.83
K2O	-	-	-	-	-	-	-
TOTAL	99.53	99.39	100.08	99.97	100.71	100.29	99.82

* * ATOMIC PROPORTIONS BASED ON SELECTED NO. OF OXYGENS * *

OXYGEN	6	6	6	6	6	6	6
SI	1.948	1.948	1.890	1.876	1.880	1.876	1.879
ALIV	.052	.052	.110	.124	.120	.124	.121
ALVI	.055	.054	.016	.020	.009	.025	.000
TI	.014	.014	.043	.050	.045	.044	.040
CR	-	-	-	-	-	-	-
FE2+	.149	.151	.207	.215	.204	.220	.205
MN	.003	.003	.003	.004	.004	.004	.003
MG	.912	.909	.786	.775	.787	.774	.801
CA	.815	.818	.914	.903	.929	.899	.940
NA	.072	.069	.066	.068	.067	.077	.060
K	-	-	-	-	-	-	-
SUM	4.021	4.019	4.037	4.036	4.044	4.044	4.050
	WO 43.44	WO 43.56	WO 47.91	WO 47.71	WO 48.37	WO 47.48	WO 48.30
	EN 48.62	EN 48.40	EN 41.22	EN 40.94	EN 41.02	EN 40.88	EN 41.16
	FS 7.94	FS 8.05	FS 10.87	FS 11.35	FS 10.61	FS 11.64	FS 10.54

* * * S A M P L E D I R E C T O R Y * * *

ANALYSIS NO.	DESCRIPTION
11	HIGH PRESS CPX CORE - 1A (KP87)
12	HIGH PRESS CPX CORE - 1B (KP87)
13	CORED MACROPHENOCRYST - 1C (KP87)
14	CORED MACROPHENOCRYST - 1D (KP87)
15	CORED MACROPHENO - 1E (KP87)
16	MACROPHENO RIM - 1F (KP87)
17	PHENOCRYST (KP87)

'cored' pyroxene macrophenocryst from nephelinite KP87 (Table 7.2; analyses 11-16). The central unpigmented core of the phenocryst has a particularly low Al^{iv}/Al^{vi} ratio compared to the outer, pigmented part, suggesting that it represents a high pressure relict which formed a nucleus for later pyroxene growth under lower pressure conditions. In addition to showing chemical relationships considered to be typical of high pressure clinopyroxenes by Wass (1979), interpretation of the unpigmented cores as high pressure relicts is also supported by comparison of the Lebombo analyses (Table 7.2, analyses 11-16) with electron microprobe analyses of clinopyroxenes considered to contain high pressure relicts presented by Gibb and Henderson (1978). Both sets of analyses show that the proposed high pressure relicts are lower in TiO_2 and Al_2O_3, but generally higher in SiO_2 than the surrounding supposedly low pressure pyroxene. In the case of the Lebombo rocks the high pressure cores are also lower in CaO and more magnesian than the overgrowths. High pressure clinopyroxene-bearing megacrysts and phenocrysts, and relicts thereof, are commonly reported from rocks of silica undersaturated alkaline affinity (Binns et al., 1970; Aoki and Kameyame, 1970; Thompson, 1974; Ellis, 1976; Wass, 1979).

Crystallisation of the clinopyroxene surrounding the high pressure cores, though continuing at an apparently lower pressure, appears to have taken place in a rapidly changing pressure environment since the Al^{iv}/Al^{vi} ratio changes continuously from core to margin; other parameters considered by Wass (1979) to reflect changing pressure conditions also vary considerably. Consequently the small but significant chemical variations found within the clinopyroxenes and reflected by oscillatory zoning are considered to reflect crystal growth within a rapidly changing physico-chemical environment, due probably to movement of the crystals within a magma chamber as proposed by Augustithus (1978).

7.2.3 Olivine

Small euhedral and subrounded olivine phenocrysts, less than 0.5 mm in diameter occur in some northern Lebombo nephelinite lava flows (Plate 7.1.E); in several cases olivines were found to be poikilitically enclosed in large clinopyroxene macrophenocrysts or phenocrysts. Modal contents of this mineral are generally in the range of 1-8% though it is often difficult to recognise olivine in thin section because it is invariably altered or pseudomorphed (Plate 7.1.G). An opaque oxide, serpentinite and light green saponite are the most common replacement minerals.

Composition of the few olivines it was possible to analyse range from Fo_{75} to Fo_{77}; representative analyses are included in Table 7.3 and individual analyses are listed in Microfiche Table E1, Appendix E. The phenocrysts are strongly magnesian (average = Fo_{77}) and show very slight zoning near the rims to a more iron rich composition ($\sim Fo_{75}$). The average composition of the nephelinite olivines is about the same as that of the more evolved olivines found in the picrite-basalts of the Letaba River Formation (range: Fo_{73} - Fo_{89}). However, olivines from the nephelinites are notably depleted in nickel and strongly enriched in Mn in comparison to the olivines analysed in the picrite basalts.

7.2.4. Nepheline

Few examples of nephelinite lavas with visible nepheline phenocrysts were noted in the northern Lebombo; where present, nepheline phenocrysts were almost entirely replaced by zeolite and calcite. Pseudomorphs do, however, indicate that the original phenocryst crystallised as laths up to 1 mm in length and were often arranged in glomeroporphyritic aggregates.

Though scarce as a phenocryst phase, nepheline constitutes the major portion of the groundmass in the lavas. In relatively coarse grained

TABLE 7.3

NEPHELINITES : ANALYSES OF OLIVINES, FE-TI OXIDES AND ACCESSORY MINERALS

	1	2	3	4	5	6	7	8	9	10
SIO2	38.16	39.12	38.76	.04	.41	.36	.44	50.35	49.73	36.42
TIO2	-	-	-	24.79	20.46	24.82	13.23	2.44	3.93	7.40
AL203	-	-	-	1.06	.28	.90	4.12	2.74	2.46	11.80
CR203	-	-	-	-	.22	.16	.19	-	-	-
FE203	-	-	-	19.85	28.09	19.48	39.91	-	-	-
FEO	22.31	21.80	20.76	52.95	49.91	53.15	35.53	12.00	14.80	13.93
MNO	.36	.35	.27	.86	.80	1.27	.02	.18	.21	.11
MGO	38.22	38.83	39.28	.30	-	.30	5.75	15.23	12.80	15.88
CAO	.50	.47	.34	-	-	-	-	7.16	5.79	.05
NA2O	-	-	-	-	-	-	-	5.55	6.28	.87
K2O	-	-	-	-	-	-	-	1.52	1.74	8.37
NIO	.09	.10	.12	-	-	-	-	-	-	-
TOTAL	99.64	100.67	99.53	99.85	100.16	100.44	99.19	97.17	97.74	94.83

* * ATOMIC PROPORTIONS BASED ON SELECTED NO. OF OXYGENS * *

OXYGEN	4	4	4	4	4	4	4	23	23	22
SI	.999	1.008	1.006	.001	.015	.013	.016	7.418	7.391	5.470
ALIV	-	-	-	.047	.012	.039	.174	.476	.431	2.089
ALVI	-	-	-	-	-	-	-	-	-	-
TI	-	-	-	.696	.578	.693	.356	.270	.439	.836
CR	-	-	-	-	.007	.005	.005	-	-	-
FE3+	-	-	-	.558	.794	.544	1.076	-	-	-
FE2+	.488	.470	.451	1.654	1.568	1.649	1.065	1.478	1.840	1.750
MN	.008	.008	.006	.027	.025	.040	.001	.022	.026	.014
MG	1.491	1.491	1.519	.017	-	.017	.307	3.344	2.835	3.554
CA	.014	.013	.009	-	-	-	-	1.130	.922	.008
NA	-	-	-	-	-	-	-	1.585	1.810	.253
K	-	-	-	-	-	-	-	.286	.330	1.604
NI	.002	.002	.003	-	-	-	-	-	-	-
SUM	3.001	2.992	2.994	3.000	3.000	3.000	3.000	16.010	16.024	15.578
	FO 75.33 FA 24.67	FO 76.04 FA 23.96	FO 77.13 FA 22.87	US 71.40 MT 28.60	US 59.28 MT 40.72	US 71.81 MT 28.19	US 39.85 MT 60.15			

* * * S A M P L E D I R E C T O R Y * * *

ANALYSIS NO.	DESCRIPTION
1	OLIVINE PHENOCRYST (KP87)
2	OLIVINE PHENOCRYST (KP87)
3	OLIVINE PHENOCRYST (KP87)
4	TI-MAGNETITE PHENOCRYST (KP87)
5	TI-MAGNETITE PHENOCRYST (KP87)
6	TI-MAGNETITE PHENOCRYST (KP87)
7	EUH TI-MAG IN CPX (KP87)
8	NA-AMPHIBOLE GRAIN (KP87)
9	NA-AMPHIBOLE GRAIN (KP87)
10	BIOTITE GRAIN (KP87)

porphyritic rocks it is apparent as a rectangular or hexagonal crystals (depending on which crystallographic axis the crystal is cut across) intimately associated with groundmass pyroxene (and biotite if present) whereas in fine grained lavas it occurs as small prisms and fan-like aggregates (sheaves) of microcrystals.

7.2.5 Fe-Ti Oxides

Titanomagnetite occurs as discrete subhedral and anhedral phenocrysts, typically less than 0.7 mm in diameter (Plate 7.1.G). It commonly forms small glomeroporphyritic aggregates with one or two other opaque crystals and/or clinopyroxene phenocrysts. In addition, phenocrysts are found as inclusions in some clinopyroxene phenocrysts, particularly in those pyroxene crystals which have a sieve texture. Representative analyses of the titanomagnetite phenocrysts are listed in Table 7.3.

Euhedral titanomagnetite microphenocrysts occur as minute inclusions in some clinopyroxene phenocrysts. Because of their extremely small size they are exceedingly difficult to probe. However, analyses were obtained from two microphenocrysts and the results indicate that they are more strongly magnesian than the titanomagnetite phenocrysts (see Table 7.3, analysis 7), though it is possible that the high MgO value may be an analytical artifact due to proximity to the clinopyroxene matrix.

7.2.6 Accessory Minerals

Apatite is an important constituent of the nephelinite lavas. It is most common as abundant needles in the groundmass, but a few rocks, (e.g. KP84, KP131) were found to contain blebs and needles of apatite enclosed within clinopyroxene phenocrysts.

Biotite, sodic-amphibole and aegerine-augite represent the remaining accessory minerals. Flakes and rare phenocrysts or microphenocrysts of foxy

red biotite commonly occur in rocks with crystalline groundmasses. A sodic amphibole, pleochroic from pinkish-brown, pale-grey to yellow-green usually accompanies the biotite. Aegerine-augite is found as subhedral microprisms in some of the lavas, in addition to forming overgrowths on clinopyroxene phenocrysts. Analyses of the biotite and amphibole are included in Table 7.3 (analyses 8, 9, 10).

7.3 Geochemistry

7.3.1 General Statement

Representative and average analyses of the northern Lebombo and Sabi nephelinite suites are presented in Table 7.4. Overall, the lavas and dykes show a range of approximately 10% MgO and in general the northern Lebombo lavas are more magnesian than the Sabi suite. The most magnesian analysis contains 12.2% MgO but since the sample was obtained from a sill in the Sabi area (Swift et al., 1953) it is possible that the high MgO content reflects low pressure cumulus enrichment of olivine $\pm$ clinopyroxene during solidification of the intrusion.

Analyses of nephelinites and ijolites from the Zwibi Plug which is associated with the Dorowa Carbonatite Complex (Johnson, 1966) are included in Table 7.4. The carbonatite complexes of south-east Zimbabwe (Dorowa, Shawa, Chishanya) and the northern Lebombo (Messina) are considered to have played an important role in the Karoo volcanic event (cf. Johnson, 1966) and the reasons for including the Zwibi data will become apparent later.

The analytical data obtained for the nephelinite rocks in both this study and from published and unpublished sources are listed in full in Microfiche Tables F16, F21, Appendix F. The data included in the Microfiche tables have been used to construct major and trace element variation

TABLE 7.4 Selected and average analyses of Lebombo, Sabi and Dorowa Complex nephelinite rocks.

	KP82	KP92	KP127	KA16	BR8	NTS12	N222	NEPH	IJOLITE	AVE.
%SiO_2	44.54	42.80	42.96	42.94	46.11	41.30	44.20	42.81	42.40	44.19
TiO_2	2.94	3.51	2.65	2.48	2.35	4.18	3.06	1.28	1.00	3.04
Al_2O_3	7.56	7.66	12.10	12.31	8.95	12.47	16.30	18.91	20.82	13.59
Fe_2O_3*	15.02	16.28	13.84	13.57	13.42	15.26	10.30	10.40	7.40	13.33
MnO	.18	.15	.19	.19	.17	.22	.21	.18	.14	.21
MgO	8.05	7.92	7.36	6.60	12.01	5.84	2.59	4.10	3.30	6.40
CaO	10.79	11.77	8.95	9.96	12.25	8.13	3.83	8.31	6.45	9.05
Na_2O	5.68	4.11	5.90	5.88	2.43	6.74	10.90	9.59	11.69	7.13
K_2O	.80	1.18	1.84	1.54	.70	2.67	2.04	3.02	3.40	2.13
P_2O_5	.88	1.21	.93	.88	.27	1.14	1.24	1.38	1.00	.95
H_2O^+	2.55	2.66	2.91	3.67	2.06	1.82	4.23	.41	1.57	
H_2O^-	.57	.62	.38	.09	.49	.18		.15	.04	
CO_2	.39	.05	.07						.74	
TOTAL	99.85	99.92	100.08	100.11	101.21	99.95	98.90	100.54	99.95	
ppm Rb	28.7	51	63	39		63	75			58
Ba	655	2501	1274	1329		1713	2240			1679
Sr	1039	769	1338	1319		1663	2020			1353
Zr	195	165	157	112		271	320			216
Nb	109	101	84	83		187				125
Cr	135	57	97	59		86	65			80
V	208	431	305	298		338				320.
Sc	20	24.4	16	13.9						
Ni	62	39	71	83		53				53
Co	55	62	48	51		55				52
Zn	145	130	109	116		137				125
Cu	217	246	232	264		429				294
Y	23.8	12.7	25.7	17.4		22.6				23

TABLE 7.4 Continued

	KP82	KP92	KP127	KA16	BR8	NTS12	N222	NEPH	IJOLITE	AVE.
Zr/Nb	1.79	1.63	1.87	1.35		1.45				
Zr/Y	8.19	13.0	6.11	6.44		12.0				
K/Rb	231	192	242	328		352	226			
K/Ba	10.1	3.92	12.0	9.62		12.9	7.56			
K/Sr	6.39	12.70	11.4	9.69		13.3	8.38			
K/Zr	34.1	59.4	97.3	114		81.1	52.9			
K/Nb	60.9	97	182	154		119				
K/Y	279	771	594	735		981				
Ba/Rb	22.8	49	20.2	34.1		27.2	29.9			
Ba/Sr	.630	3.25	.952	1.01		1.03	1.11			
Ba/Zr	3.36	15.2	8.11	11.9		6.32	7.00			
Rb/Sr	.028	.066	.047	.029		.038	.037			
Mg //	56.0	53.5	55.6	53.3	66.8	47.3	37.0	47.9	50.9	
				- C.I.P.W. NORMS -						
Ne	12.16	13.11	23.10	23.37	3.93	26.69	29.47	43.58	47.76	
Lc						6.57		13.88	15.75	
Or	4.73	6.97	10.87	9.10	4.20	7.40	12.05	.14	-	
Pl	11.48	8.63	8.38	9.26	25.41	-	18.08	-	-	
Di	37.28	41.26	30.19	33.78	39.22	27.27	9.16	26.83	17.12	
Hy	-	-	-	-	-	-	-	-	-	
Ol	13.67	11.67	13.07	10.36	18.96	12.22	9.00	6.86	6.70	
Mt	-	2.28	2.63	2.54	2.53	-	-	1.53	-	
Il	5.58	6.67	5.03	4.71	4.56	7.94	5.81	2.43	1.90	
Ap	2.08	2.87	2.20	2.08	.66	2.70	2.94	3.27	2.37	
Cc	.89	.11	.16	-	-	-	-	-	1.68	

KEY TO TABLE 7.4

KP82	-	Nephelinite lava : Mashikiri, Northern Lebombo.
KP92	-	Nephelinite lava : Kloppersfontein Dam, Northern Lebombo.
KP127	-	Nephelinite lava : Mutale Road, Northern Lebombo.
KA16	-	Nephelinite lava : Olifants River, Northern Lebombo
BR8	-	Nephelinite sill : Chiredzi River, Sabi.
NTS12	-	Nephelinite lava : Lundi River area, Sabi.
N222	-	Nephelinite lava : Lundi River area, Sabi.
NEPH	-	Nephelinite intrusive : Zwibi Plug, Dorowa Complex.
IJOLITE	-	Intrusive rock : Zwibi Plug, Dorowa Complex.
AVE.	-	Average Nephelinitic rock from the northern Lebombo, Sabi and Dorowa (N = 24 for major elements but is generally less than 16 for trace elements).

diagrams for the nephelinites which are presented in Figures 7.3 a-j and Figures 7.5 a-e respectively.

7.3.2 Parental or Primary Magma Problems

The most notable conclusions to be drawn from the major element variation diagrams presented in Figure 7.3 a-i is that the northern Lebombo and Sabi nephelinite suites appear to show separate, but roughly parallel trends for the critical elements SiO_2, TiO_2 and Fe_2O_3 thereby suggesting that the individual lava and dyke suites crystallised from slightly different parental or primary magmas. In the case of SiO_2 versus MgO (Fig. 7.3a) rocks from the northern Lebombo are generally enriched in SiO_2 relative to the Sabi nephelinites whereas the reverse applies for TiO_2, (Fig. 7.3b) and Fe_2O_3 (Fig. 7.3d). Clearly there are some data points which show overlap between the two apparent trends though it is probable that these points may have been displaced from the inferred 'primary' trends by either (i) phenocryst accumulation or removal in different proportions to the assemblage controlling the main fractionation trend or (ii) alteration, particularly in the case of mobile elements such as K_2O, Rb and Sr.

With respect to point (i) above, modal analyses of the Lebombo nephelinites (Table 7.1) have shown that there are considerable variations in phenocryst abundance from lava to lava and this probably holds true for the Sabi lavas as well. For example northern Lebombo sample KP92 contains a higher modal abundance of titanomagnetite than other Lebombo nephelinites (Table 7.1) and this is reflected by slight displacement of KP92 (along titanomagnetite control) from the overall northern Lebombo fractionation trend. However, sample KP92 is even more strongly enriched in clinopyroxene (see Table 7.1) and as a result is displaced from the main field of Lebombo data (along clinopyroxene control) in almost all the major and trace element diagrams presented in Figures 7.3 and 7.5 respectively, though the overall

Fig. 7.3 Major element variation diagrams for the northern Lebombo and Sabi nephelinites.

Northern Lebombo:

□ Lavas

◩ Lavas enriched in cumulus clinopyroxene (KP82)
◪ or clinopyroxene + magnetite (KP92).

Sabi:

○ Lavas

◒ Lavas enriched in cumulus olivine

● Intrusive rock (sill) enriched in cumulus olivine.

△ Zwibi (Dorowa Carbonatite) nephelinites and ijolites.

Vector Plots: A series of vector diagrams are included on the right hand side of Figures 7.3 a-j. The vectors represent the trends which would be followed by compositions of the residual liquid during removal of the minerals olivine (ol), clinopyroxene (cpx) and titanomagnetite (timg) from a parental magma represented by composition B. The lengths of the control lines represent removal of 78% clinopyroxene, 20% titanomagnetite and 2% olivine from B. The implications of this assemblage will be discussed in section 7.3.4.

(Data from Microfiche Tables F16, F21, Appendix F)

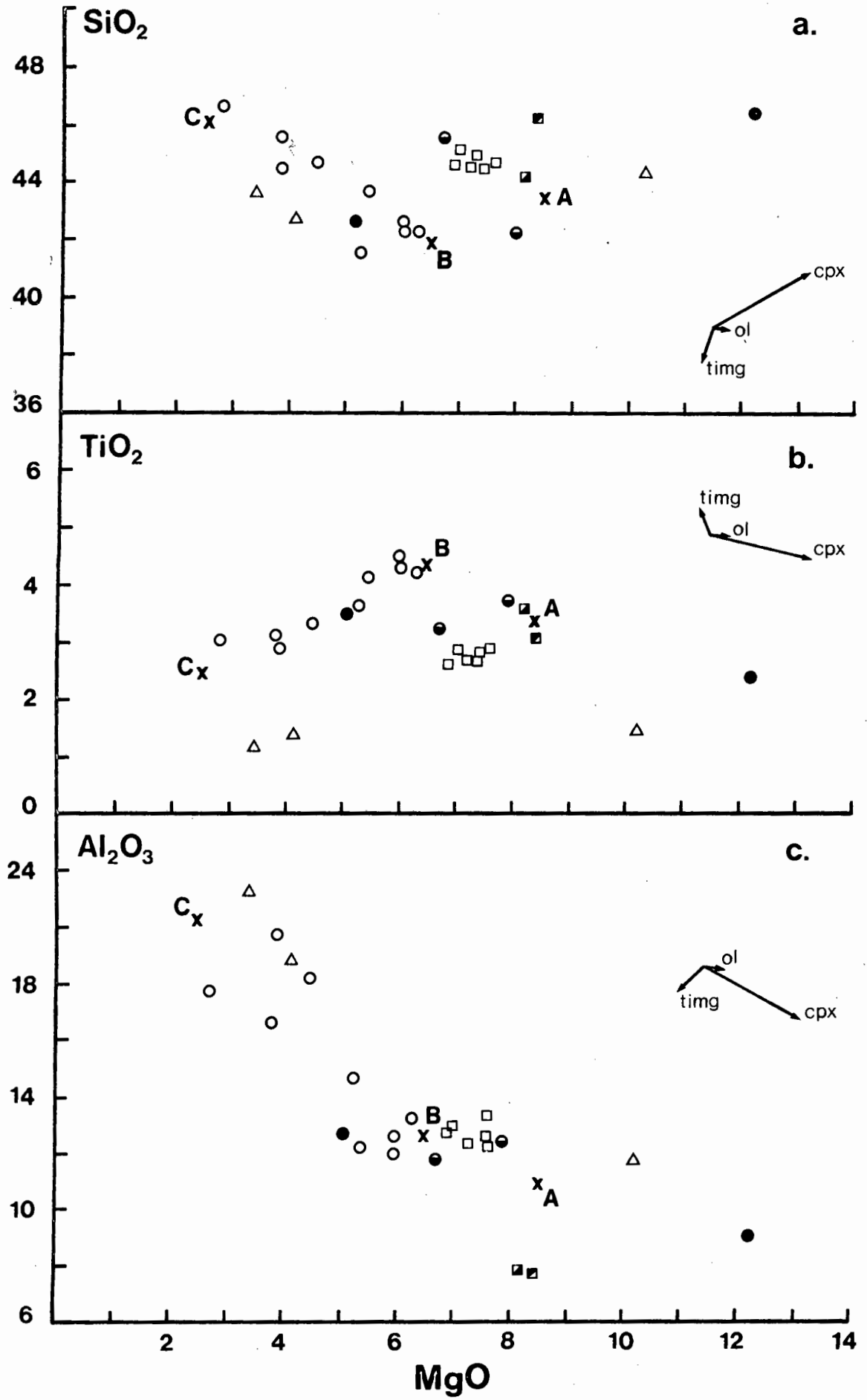
SiO2
a.
48
44
40
36
Cx
xA
xB
cpx
ol
timg
TiO2
b.
6
4
2
0
timg
ol
cpx
xB
xA
Cx
Al2O3
c.
24
18
14
10
6
Cx
ol
timg
cpx
xB
xA
2
4
6
8
10
12
14
MgO

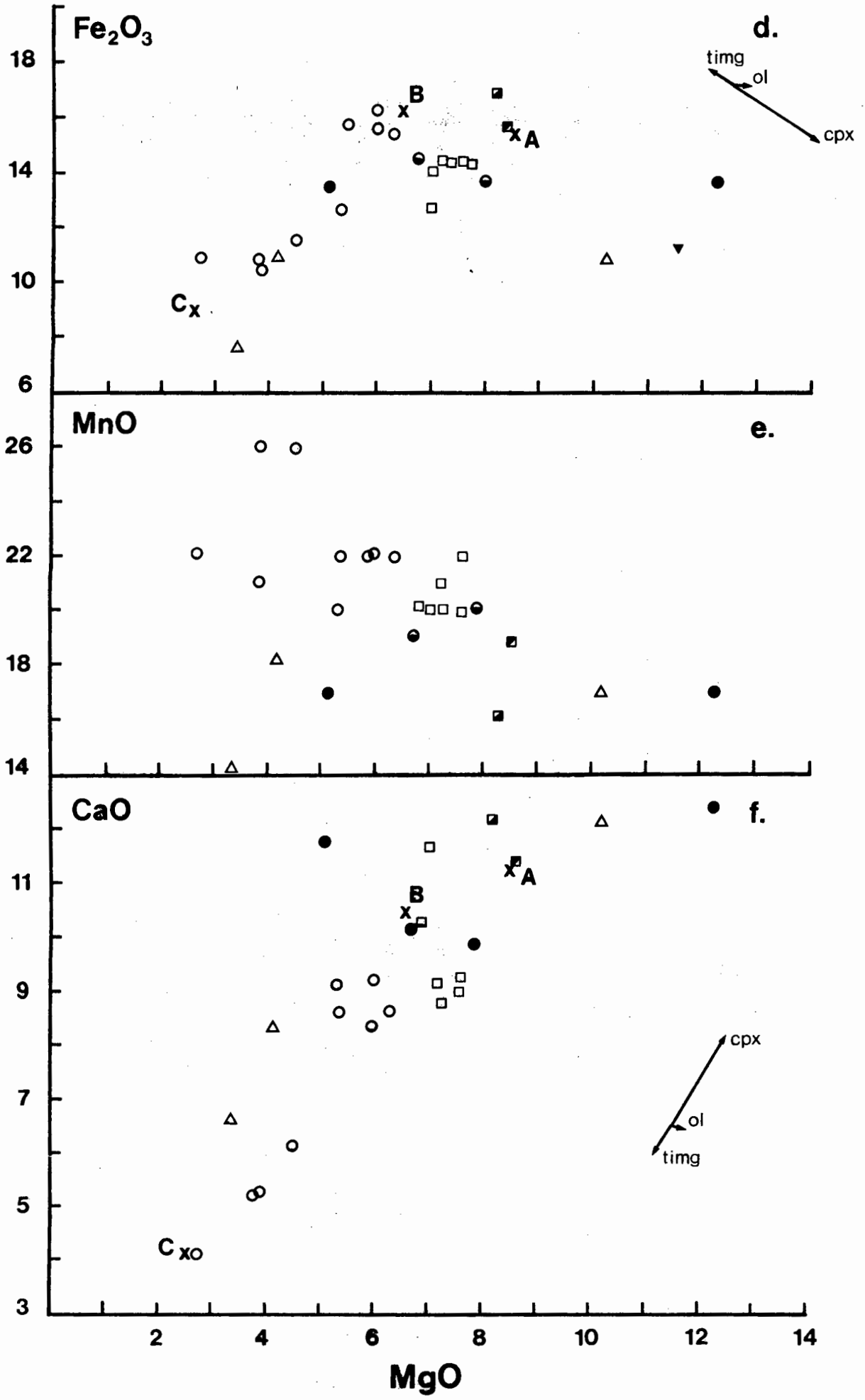
Fe2O3
d.
timg
ol
cpx
18
14
10
6
B
A
Cx
MnO
e.
26
22
18
14
CaO
f.
11
9
7
5
3
cpx
ol
timg
Cxo
2
4
6
8
10
12
14
MgO

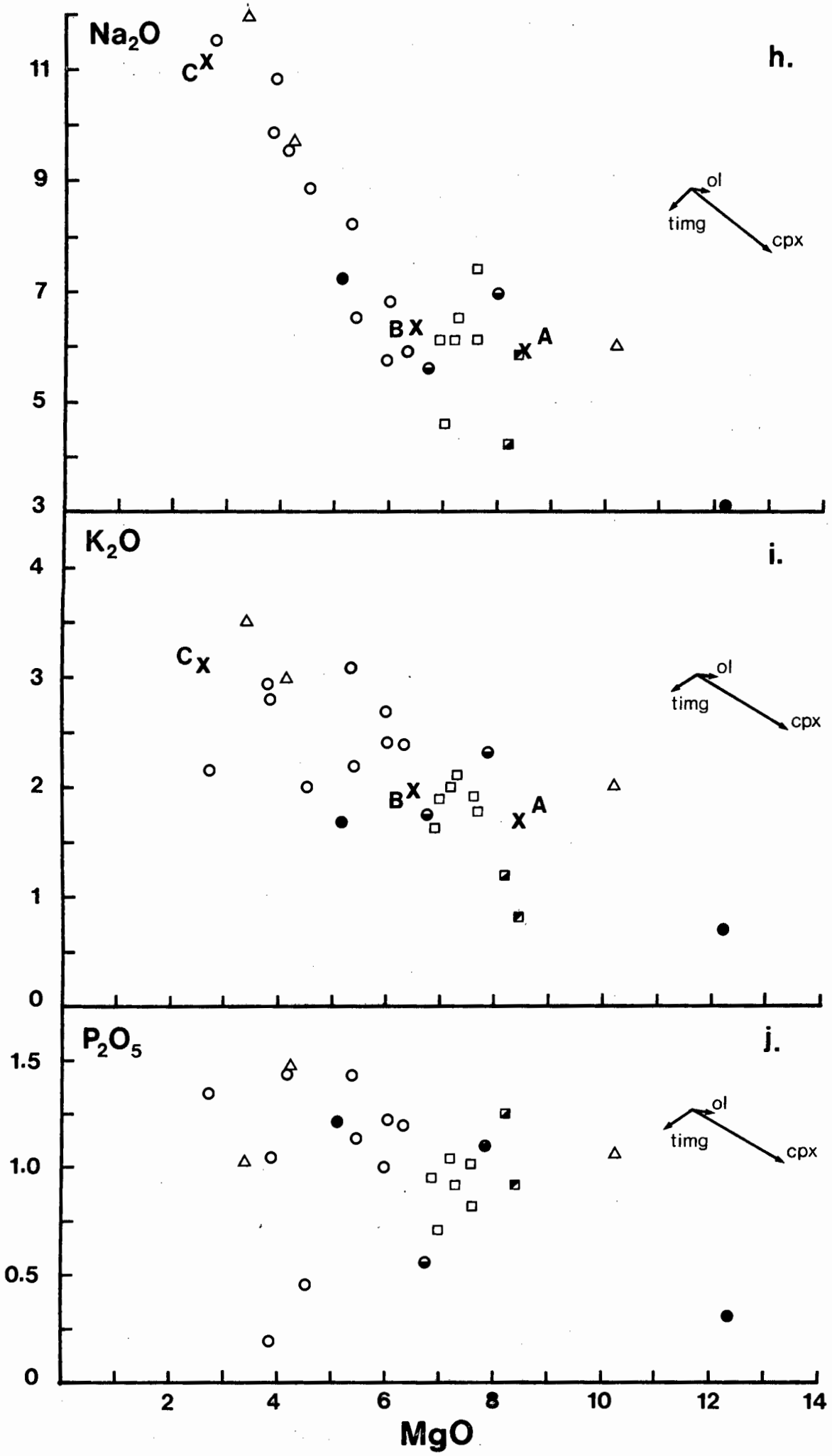
Na2O
h.
11
9
7
5
3
C
B
A
ol
timg
cpx
K2O
i.
4
3
2
1
0
P2O5
j.
1.5
1.0
0.5
0
2
4
6
8
10
12
14
MgO

displacement probably reflects the combined effects of cumulus enrichment in titanomagnetite + clinopyroxene. Sample KP82 is also enriched in cumulus clinopyroxene and it too is generally displaced from the main Lebombo fractionation trend.

Displacement of certain Sabi data from the inferred 'primary' fractionation trends is also explicable in terms of crystal accumulation. Two Sabi analyses which generally conform with the northern Lebombo data represent analyses of olivine-phyric rocks suggesting that they have been displaced from the inferred Sabi trend by cumulus enrichment in olivine. Similarly, sample BR8 is described as an olivine nephelinite (Swift et al., 1953) and since it was obtained from a sill its exceptionally high MgO content (12.2%) is probably a function of low-pressure cumulus enrichment of olivine during emplacement and crystallisation of the intrusive body. Those nephelinite samples which may therefore have suffered cumulus enrichment are represented by different symbols in Figures 7.3 a-j and 7.5 a-l as are one or two samples which appear to be strongly altered. For example northern Lebombo nephelinite KP83 is characterised by a high loss on ignition and is clearly altered in thin section which may explain its somewhat depleted abundances of Rb (Fig. 7.5a) and Sr (Fig. 7.5c) relative to the other Lebombo nephelinites. Similarly the more altered appearance of sample KA16 may account for its apprently depleted Rb content in Figure 7.5a.

If less attention is then paid to rocks which may have suffered cumulus enrichment or excessive alteration it is apparent that the inferred subparallel trends for the Lebombo and Sabi nephelinites are reasonably well defined on plots of SiO_2, TiO_2 and Fe_2O_3 versus MgO. Furthermore, by recourse to a certain degree of subjectivity it is possible to envisage that the two suites of nephelinites show somewhat different (semi-parallel?) trends in some of the other major element, and to a lesser extent trace element, variation diagrams.

The premise that the Sabi and northern Lebombo nephelinite suites crystallised from two slightly different parental magmas would therefore appear to be a reasonable conclusion on the basis of the data presented in Figures 7.3 a-j. Nevertheless it is possible that the two suites of rocks are related to each other, particularly since these rocks occupy similar stratigraphic positions in the Lebombo and Sabi volcanic successions and are characterised by similar mineralogical assemblages.

Critical geological and geochemical criteria that can be used to indicate genetic relationships between effusive igneous rocks include: i) close association in space and time; ii) provenance from the same volcanic pile; iii) similar mineralogical and petrographic features; iv) smooth compositional and mineralogical variations; v) covariation of incompatible elements and similar incompatible element ratios; vi) conformity to a clearly defined and rigorously tested petrogenetic model. In general the two nephelinite suites considered here pass the first three tests though northern Lebombo lavas are separated from those of the Sabi area by approximately 100 km. In contrast, application of the remaining criteria, suggests that the two suites of nephelinites are not comagmatic though some of the data are conflicting. For instance it has been shown that Zr/Nb ratios are relatively constant between comagmatic suites but may vary between different suites (Erlank and Kable, 1976; Weaver et al., 1972). In the case of the rocks considered here the Zr/Nb ratios are reasonably consistent for both suites of lavas and dykes (Fig. 7.4) implying that they could have been derived from similar source types. Sr-isotope data have been obtained for the nephelinites and initial-Sr ratios are presented in Table 7.7. Initial-Sr ratios for two northern Lebombo rocks (KP82, KP127; Pafuri area) are higher than the initial ratios obtained for a nephelinite from the Olifants River (KA16; northern Lebombo) and Sabi nephelinites (NTS7, NTS8, NTS12) suggesting that the nephelinites

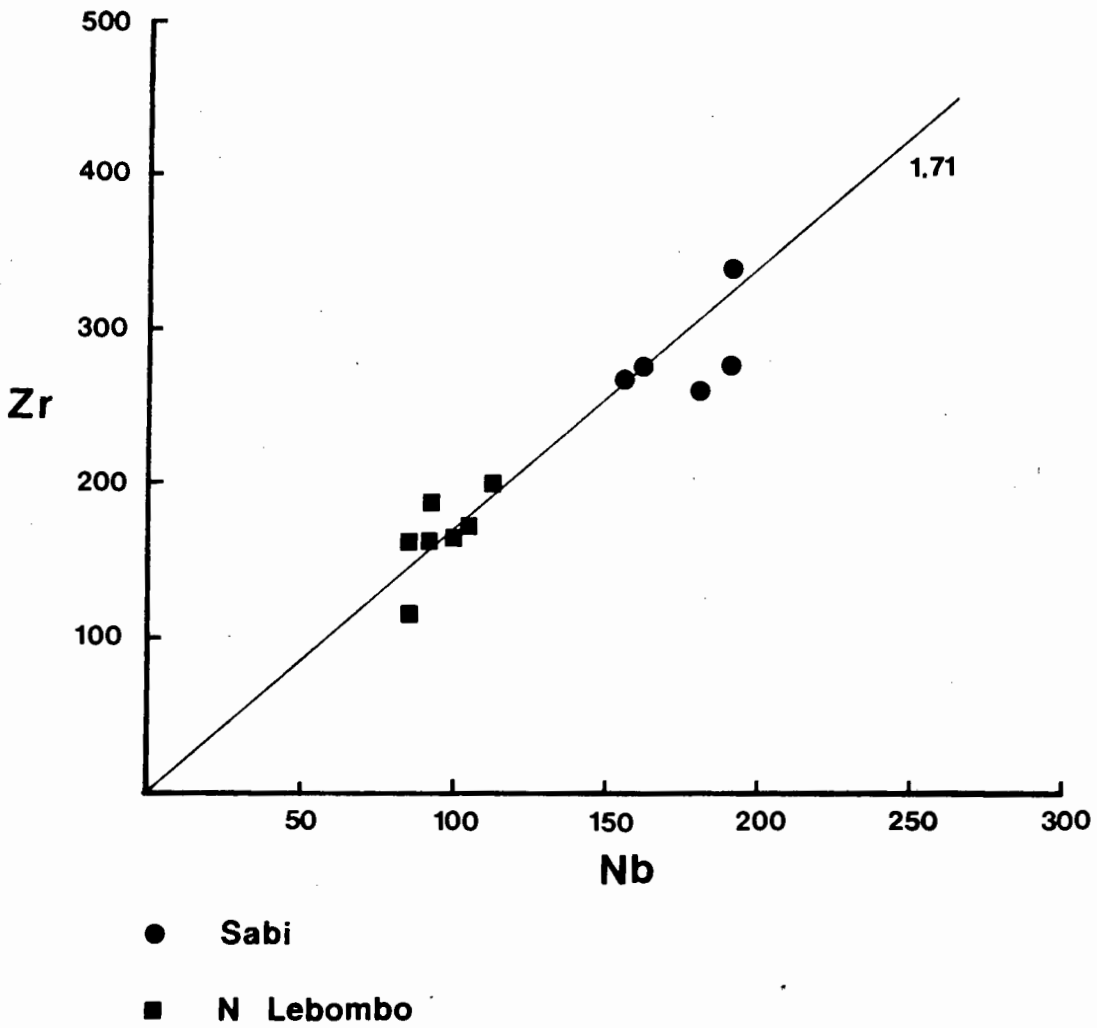

Fig. 7.4 Plot of Zr versus Nb for the northern Lebombo and Sabi nephelinite lavas and dykes.

were derived from a source which was heterogeneous with respect to Sr isotopes. However, the isotopic data do not disprove a comagmatic origin for the nephelintes and additional Sr-isotope data are needed to confirm the existence of the inferred isotopic heterogeneities.

TABLE 7.5 Initial Sr ratios for northern Lebombo and Sabi nephelinites (Ro calculated for 190 my).

	Sample	$^{87}Sr/^{86}Sr_o$
Northern Lebombo	KP82	.70675
	KP127	.70687
	KA16	.70520
Sabi	NTS7	.70529
	NTS8	.70551
	NTS12	.70510

One means of overcoming the apparent problem presented by the geochemical data for the nephelinite suites is to invoke a mechanism whereby the primary nephelinite magmas were derived from broadly similar source areas and account for the apparent differences in the compositions of the parental magmas by different degrees of high pressure fractionation. One of the most significant pieces of evidence in support of a high-pressure fractionation model is that unpigmented clinopyroxene cores, considered to represent high pressure relicts, have been identified in the northern Lebombo nephelinites (section 7.2.2). The cores are characterised by much higher SiO_2 and lower TiO_2 and CaO abundances than the low-pressure clinopyroxene overgrowths and phenocrysts with which they are associated and show similar properties to clinopyroxenes considered to be of high pressure origin by Gibb and Henderson (1978). Unfortunately there is little detailed petrographic data available from the Sabi nephelinites and consequently it has not been possible to verify the presence of high pressure

clinopyroxenes in these rocks. However, the high pressure relicts are exceptionally rare in the Lebombo rocks and may not occur at all in the Sabi nephelinites. As noted in section 7.2.2 the cores found in the Lebombo pyroxenes show evidence of resorption and it is probable that they were almost totally resorbed into the parental magmas at lower pressures, only being preserved in exceptional cases.

The validity of the above hypothesis, viz. that the northern Lebombo and Sabi nephelinite parental magmas may be linked by high pressure fractionaction processes, has been tested by least squares linear regression techniques. (It should be noted here that the overall fractionation trends shown by the nephelinites will be discussed in the following section). The method applied involved the compilation of two hypothetical parental magmas for each nephelinite suite and a series of mixing calculations were then carried out to establish whether the two parental compositions (A, B, Figs. 7.3 a-j) could be related by crystal fractionation of possible high pressure phases e.g. unpigmented clinopyroxene and olivine. The parental magma compositions (A, B, Table 7.6) were derived from the major element variation diagrams by drawing 'trend lines' through the data and estimating the elemental abundances at MgO values of 6.5 and 8.6%. P_2O_5 was not included because of the extreme scatter it shows when plotted against MgO. Several mixing models were tested using slightly different mineral compositions and the solution of the best model is presented in Table 7.6. The results indicate that it is possible to generate parental magma B by fractionation crystallisation of approximately 11% of high pressure clinopyroxene and 3% magnesian olivine from parental magma A. Equally, however, the results could be interpreted in terms of a partial melting model whereby the parental magma to the northern Lebombo nephelinite suite (A) formed by a slightly larger degree of melting than the Sabi parent magma (B). In this case extended

TABLE 7.6 Least squares approximation relating the postulated parental magmas of the northern Lebombo (A) and Sabi (B) nephelinite suites by high pressure fractionation. (HPCPX represents average of analyses 11 and 12, Table 7.2; olivine is from Table 7.3, analysis 3).

Input Data

	A	HPCPX	OLIVINE	B
SiO_2	43.73	53.35	38.95	42.38
TiO_2	3.45	.50	.01	4.14
Al_2O_3	11.06	2.48	.01	12.82
FeO*	14.11	4.92	20.86	14.71
MnO	.20	.10	.27	.22
MgO	8.63	16.74	39.48	6.66
CaO	11.37	20.87	.34	10.60
Na_2O	5.72	1.01	.01	6.46
K_2O	1.73	.01	.01	2.02
		Wo 48.51		
		En 43.49	Fo 77.13	
		Fs 8.00	Fa 22.87	

Least Squares Approximation

	A			MIX		
	OBS	CALC	DIFF	COMP.	Wt%	S.D.
SiO_2	43.73	43.65	-0.08	B	86.47	0.99
TiO_2	3.45	3.63	0.18	HPCPX	10.83	0.87
Al_2O_3	11.06	11.35	0.29	OLIVINE	3.15	0.53
FeO*	14.11	13.91	-0.20			
MnO	.20	.21	0.01	TOTAL	100.45	1.42
MgO	8.63	8.81	0.18			
CaO	11.37	11.44	0.07			
Na_2O	5.72	5.70	-0.02			
K_2O	1.73	1.75	0.02			

Sum of Squares of residuals = 0.21

melting of clinopyroxene and olivine in the source area would account for the major element variations between the two parental magmas and the high pressure pyroxene cores found in the Lebombo lavas would represent xenocrysts derived from the source region.

It should be possible to use trace element data to test the validity of the major element model relating to the two parental magma compositions (A,B). However, although this has been done, the results obtained are largely subjective in view of the extreme scatter in most of the trace element data (Figs. 7.5 a-1). Attempts have been made to define parental magma compositions with respect to Rb, Ba, Sr, Zr, Nb and some of the compatible elements, though even these elements show poorly defined trends when plotted against MgO thereby making it exceedingly difficult to arrive at realistic estimates of the parental magma compositions. For those elements where an approximation of the two parental magma compositions has been made, fractional crystallisation equations have been used to establish whether parent 'B' can be derived from parent 'A' by crystallisation of clinopyroxene and olivine in the proportions depicted in Table 7.6. Expressions describing the behaviour of a trace element during surface-equilibrium crystallisation (ie. Rayleigh Fractionation) have been proposed by Gast (1968) and Greenland (1970). Following Gast's (1968) formulation, the concentration of a trace element a in a residual magma is given by the equation:

$$C_a^{\ell} / C_a^{o} = F^{\bar{D}-1} \quad \ldots\ldots\ldots\ldots\ldots\ldots\ldots\ldots\ldots\ldots \quad (1)$$

where F = weight fractionation of residual liquid (derived from the major element modelling).

C_a^{ℓ} = concentration of trace element a in the residual liquid.

C_a^{o} = concentration of trace element a in the initial liquid.

$\bar{D}_a$ = bulk distribution coefficient for element a in the initial liquid.

The bulk distribution coefficient $\bar{D}$ is a function of all the phases crystallising from the initial liquid and is expressed as follows:

$$\bar{D}_a = \sum_{i=1}^{i=n} D_i^a \cdot x_i$$

where D_i^a = the distribution coefficient for element a in mineral i.

x_i = weight fraction of mineral i (derived from major element model.)

In those cases where distribution coefficients are very small (e.g. incompatible elements) equation (1) may be expressed as:

$$C_a^{\ell} / C_a^{o} = 1/F \quad \ldots\ldots\ldots\ldots\ldots\ldots\ldots\ldots\ldots\ldots\ldots\ldots \quad (2)$$

Equations (1) or (2) have therefore been used to establish whether the trace element data provide additional support for relating the possible parental nephelinite magmas A and B. Results of the crystal fractionation calculations are presented in Table 7.7 along with a tabulation of D values used to compute the bulk distribution coefficient for the fractionating assemblage. Data presented in Table 7.7 do not show a particularly good match between the observed and calculated data. However, considering the limited number of trace element analyses and the inherent difficulties associated with estimating the compositions of the two parental magmas the results are considered to be satisfactory and in accord with the major element model. Because the composition of the original fractionation assemblage is not accurately known it is also possible that the F value derived from the major element model is not that precise. For example a smaller F value would result in a closer agreement between observed and predicted values for most of the elements listed in Table 7.7. However, regardless of the poor trace element match in Table 7.7, the overall enrichment shown by elements such as Zr and Nb in the Sabi nephelinites relative to the northern Lebombo nephelinites, coupled with the uniformity of Zr/Nb

TABLE 7.7 Predicted and observed trace element contents of parental magma B using results of the least squares approximation given in Table 7.6 and distribution coefficients listed below.

Trace Element Match (Data in ppm)

	A	B	
	OBS	CALC	OBS
Rb	50	58	60
Ba	1250	1443	1500
Sr	1200	1371	1420
Zr	210	237	250
Nb	125	143	160
Cr	185	49	45
Ni	95	53	55

Distribution Coefficients

	OLIVINE	CLINOPYROXENE	TITANOMAGNETITE$^{\phi}$
Rb	0.0[1]	0.053[3]	-
Ba	0.007[1]	0.013[1]	-
Sr	0.0002[2]	0.11[1]	
Zr	0.03[1]	0.22[1]	
Nb	0.05[1]	0.09	
Cr	0.72[1]	12.98[1]	100 - 620[4]
Ni	15.63*	1.77[1]	20 - 77[4]

* D^{Ni}_{ol} calculated from $D^{Ni}_{ol} = 124 / MgO - 0.9$ (Hart and Davis, 1979) where MgO = 7.50.

ϕ Titanomagnetite distribution coefficients are included here for use in subsequent modelling calculations.

References:

1 Le Roex (1980)
2 Hart and Brooks (1974)
3 Frey et al. (1978)
4 Lindstrom (1976)
5 Baker et al. (1977)

ratios for both suites, strongly supports a model involving different degrees of fractionation from the same source area.

On the basis of the present major and trace element data it is therefore concluded that high pressure clinopyroxene + olivine fractionation provides a plausible method of accounting for the variation in parental magma compositions between the Lebombo and Sabi nephelinite suites. Furthermore in the light of the results obtained from extensive studies of silica undersaturated alkalic lavas (e.g. see Bultitude and Green, 1968; Knutson and Green, 1975; Wass, 1979) there appears to be no reason why fractionation dominated by clinopyroxene should not have played a role in the petrogenesis of the Lebombo and Zimbabwe nephelinites, and there does not appear to be any compelling reason for investigating alternative mechanisms.

7.3.3 Major and Trace Element Variations within the Lebombo and Sabi Nephelinite Suites

In the previous section it was shown that the Lebombo and Sabi nephelinite suites may have been derived from parental magmas with slightly different compositions. Furthermore on the basis of major element and limited trace element modelling it was found that the parental compositions could be linked by different degrees of high pressure fractionation. In this section variations within the nephelinite suites are discussed.

Assuming that the Sabie and northern Lebombo nephelinite suites evolved from immediately parental compositions B (6.5%) and A (8.5% MgO) respectively, inspection of the bivariate plots suggest that the variations in major element composition within the individual suites were largely controlled by the subtraction of clinopyroxene and lesser amounts of olivine and titanomagnetite, ie. the low pressure phenocryst assemblage. In order to visualise the mineralogical controls imposed by fractionation of the low pressure assemblage, a series of vector diagrams depicting clinopyroxene

+ olivine + titanomagnetite fractionation from a parental magma of composition B are included in the variation diagrams. For reasons that will become apparent later the vector diagrams have been constructed to represent fractionation of the low pressure assemblage in the following porportions: $cpx_{0.78}$* $timt_{0.20}$ $ol_{0.02}$. Particular emphasis has been placed on the Sabi lavas and dykes since they display the greatest relative degree of low-pressure fractionation. However, the qualitative results and conclusions arrived at for the Sabi rocks appear to be applicable for the Lebombo lavas though the latter suite appear to have undergone far less low-pressure fractionation; this may, however, be a function of sampling.

As noted in the previous section, data points occur which are clearly displaced from the main fractionation trends. However, it was suggested that these points could be overlooked with respect to the petrogenesis of the nephelinite suites since in most cases the points are offset towards one or other of the phenocryst phases which occur in the lavas and dykes indicating that crystal accumulation or removal in different proportions to those controlling the main trends have been responsible for deviations from the general fractionation trends. Furthermore, since apatite has been observed as needles and blebs in some of the clinopyroxenes from the northern Lebombo and as a phenocryst phase in the Sabi lavas (Jamieson, 1969) scatter in the P_2O_5 versus MgO diagram may also be due to minor amounts of apatite fractionation. In addition alteration will also cause increased scatter amongst the more mobile elements e.g. K_2O.

Selected trace elements are plotted against MgO in Figures 7.5 a-l Unfortunately a comprehensive interpretation of the intra-suite variation is prevented by the limited amount of trace element data available for the

*Footnote: 0.78 = weight fraction of cpx etc.

Fig. 7.5 Trace element variation diagrams for the northern Lebombo and Nuanetsi nephelinites. (Note: many of the nephelinite analyses obtained from the literature and other laboratories have incomplete or no trace element data such that there are far fewer points plotted in Figure 7.5 compared to the major element plots in Figure 7.3)

Symbols as in Figure 7.3.

(Data from Microfiche Tables F16, F21, Appendix F)

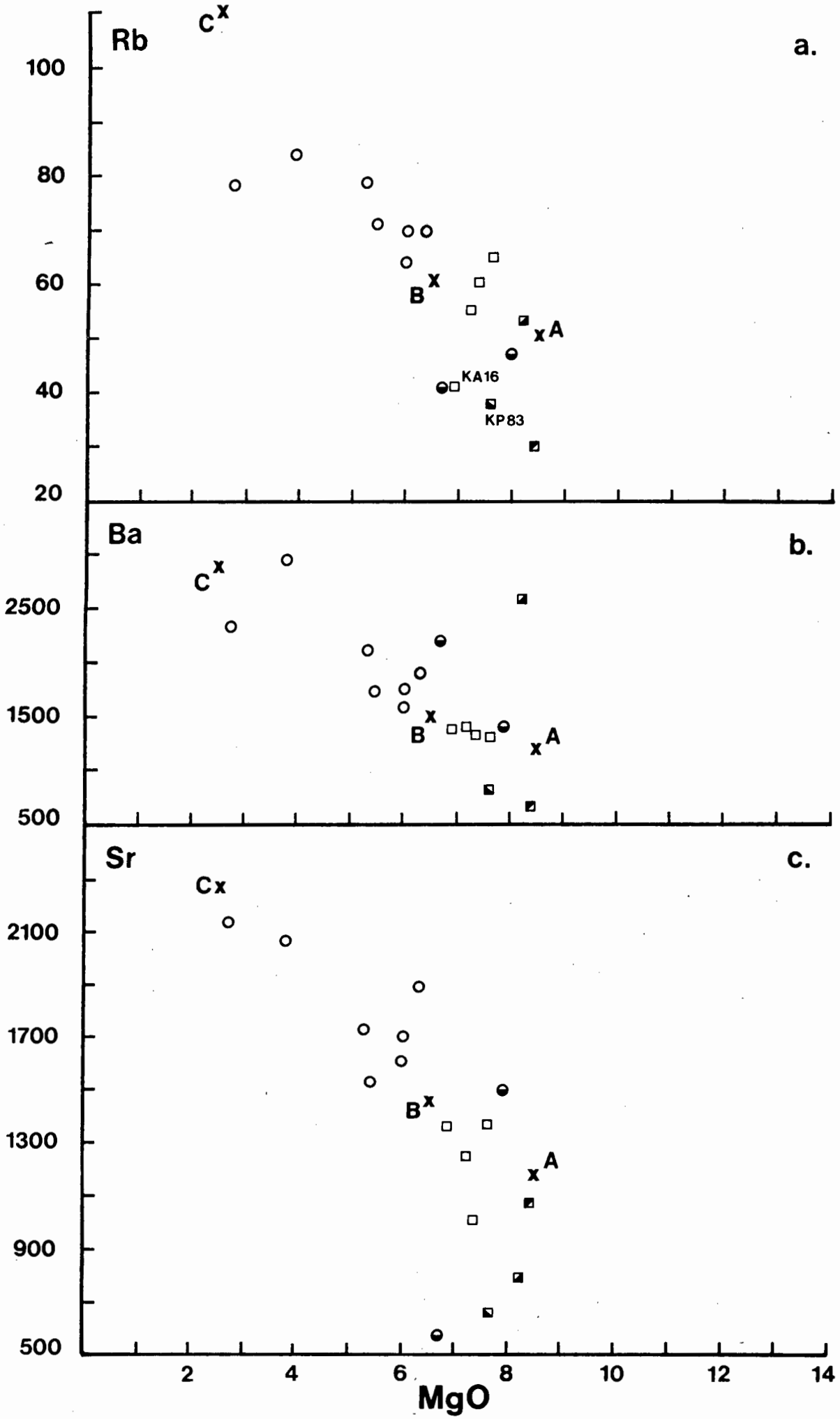
Rb
a.
100
80
60
40
20
C
B
A
KA16
KP83
Ba
b.
2500
1500
500
C
B
A
Sr
c.
2100
1700
1300
900
500
Cx
B
A
2
4
6
8
10
12
14
MgO

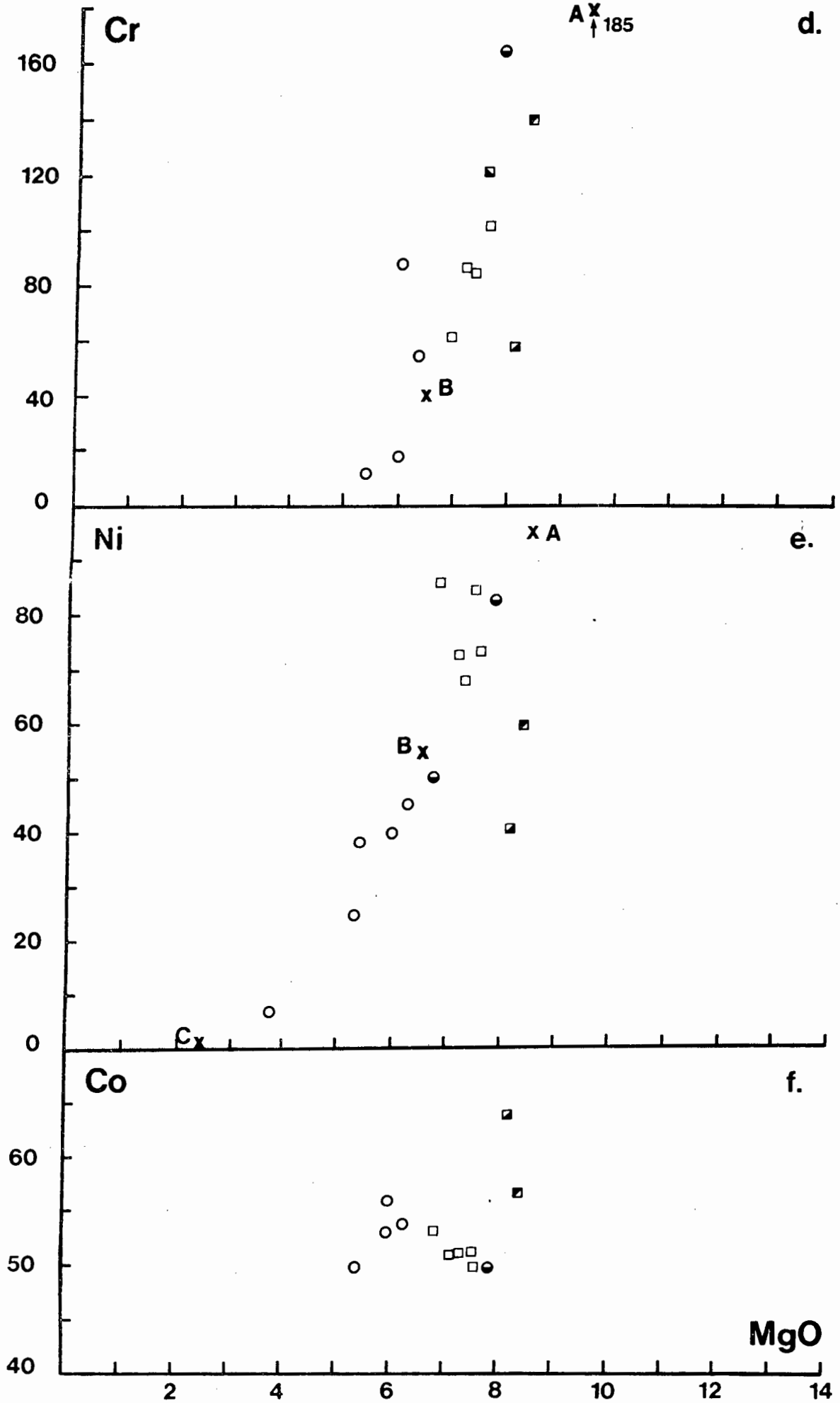
Cr
d.
A
185
160
120
80
40
0
B
Ni
e.
A
80
60
40
20
0
B
C
Co
f.
60
50
40
MgO
2
4
6
8
10
12
14

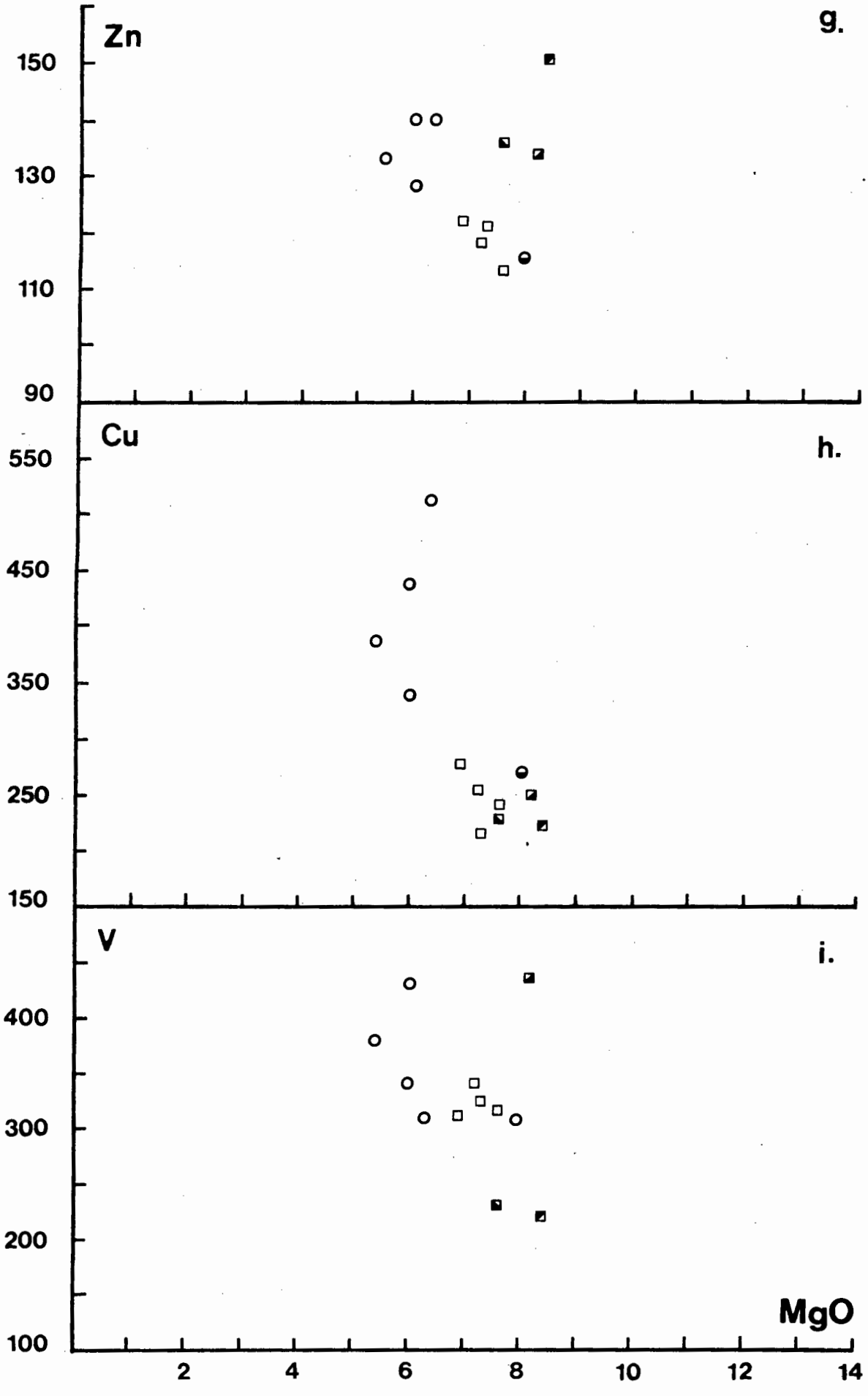
Zn
g.
150
130
110
90
Cu
h.
550
450
350
250
150
V
i.
400
300
200
100
MgO
2
4
6
8
10
12
14

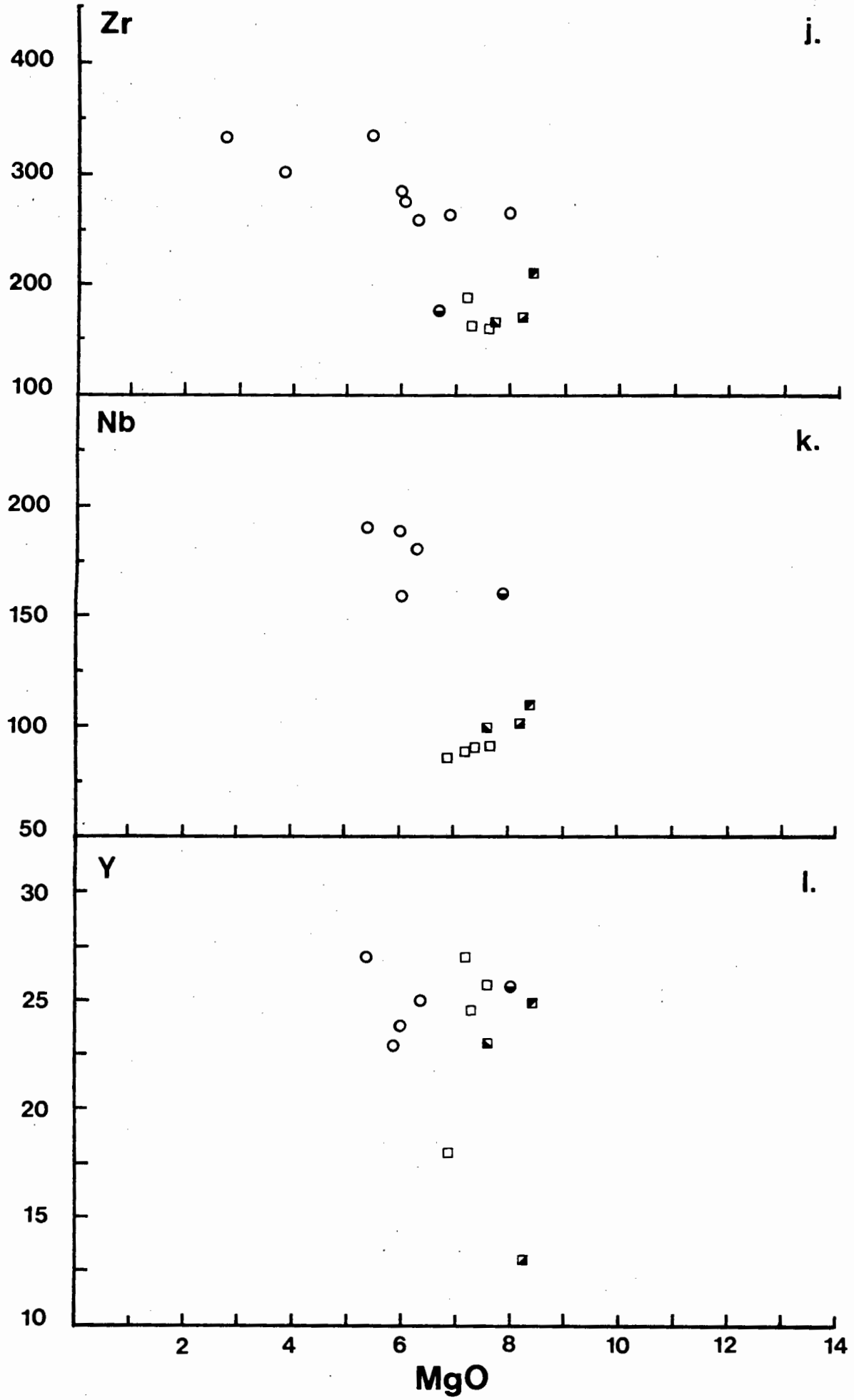
Zr
j.
400
300
200
100
Nb
k.
200
150
100
50
Y
l.
30
25
20
15
10
2
4
6
8
10
12
14
MgO

nephelinites, particularly the more evolved Sabi nephelinites. In general, however, the trace element data are broadly compatible with low pressure crystal fractionation from two parental magmas of slightly different composition.

Rb, Ba and Sr are plotted against MgO in Figures 7.5 a-c. If rocks which show signs of excessive alteration and cumulus enrichment are ignored overall trends of enrichment with decreasing MgO can be inferred for both nephelinite suites. The Sabi rocks do in fact show reasonably well developed trends for Rb, Ba and Sr which are compatible with low-pressure fractionation of clinopyroxene, titanomagnetite and olivine from a parental magma with about 6.5% MgO.

Cr (Fig. 7.5d) and Ni (Fig. 7.5e) both show reasonably systematic differentiation trends which are compatible with fractionation of clinopyroxene + titanomagnetite + olivine from the nephelinite parental magmas. Again there are data points which are displaced from the main trends though in the case of the Lebombo data these points generally represent analyses of rocks which appear to be enriched in cumulus clinopyroxene and are therefore displaced towards more magnesian-rich compositions. Interpretation of Co, Zn, Cu and V data (Figs. 7.5 f,g,h,i) is practically impossible due to the paucity of analytical data for these elements and the scatter shown by the few analyses that have been plotted, particularly in the case of Co and V. Cu does, however, appear to show a trend of enrichment with decreasing MgO which is in accord with crystal fractionation of clinopyroxene, titanomagnetite and olivine since these minerals are characterised by low D values for Cu (e.g. see Le Roex, 1980).

Zr, Nb and Y are plotted against MgO in Figures 7.5 j, k and l respectively. Y data are particularly scattered for both nephelinite

suites and it is therefore impossible to ascertain the overall fractionation trends. It is notable however, that the northern Lebombo lava (KP92) which is characterised by cumulus enrichment in clinopyroxene and titanomagnetite is strongly depleted in Y suggesting that both these phases were characterised by low abundances of Y. Zr data show no apparent trend in the Lebombo nephelinites. Conversely Nb shows a relatively well constrained trend of deplenishment in the Lebombo nephelinites which is in accord with low-pressure crystal fractionation of clinopyroxene, titanomagnetite and olivine, whereas the scatter and limited number of Zr and Nb data for the Sabi nephelinites, particularly the evolved rocks for which major element data are available, precludes any detailed assessment of Zr and Nb fractionation trends in these rocks. However, as noted previously the Sabi and northern Lebombo Zr and Nb data form two indistinct but separate groups when plotted against MgO (Figs. 7.5 j,k) which is compatible with a model involving crystallisation from two slightly different parental magmas.

7.3.4 Major and Trace Element Modelling of the Sabi Nephelinite Suite

Least squares mixing models (section 4.6) have been used to quantify a crystal fractionation model for the compositional variation shown by the Sabi nephelinite suite. The parental magma was taken to be that represented by composition B (Table 7.6) and a daughter composition C (Table 7.8) was determined graphically at an MgO value of 2.5%. Several mixing models were tested using slightly different mineral compositions selected from the mineral analyses obtained from the northern Lebombo nephelinites. Though the use of northern Lebombo mineral analyses detracts slightly from the overall value of the mixing model presented in Table 7.8, the results nevertheless imply that compositions of clinopyroxene, olivine and titanomagnetite found in the Sabi rocks were much the same as the phenocrysts from the

TABLE 7.8 Least squares approximation relating the Sabi nephelinite parental magma B to the evolved end member composition C. (Mineral data from Tables 7.2, 7.3 and Table E1b, Appendix E)

Input Data

	B	CPX	TIMG	OLIVINE	C
SiO_2	42.38	48.75	.44	38.55	46.38
TiO_2	4.14	2.79	20.92	.01	2.55
Al_2O_3	12.82	4.99	.29	.02	21.68
FeO	14.71	6.79	78.29	21.87	8.27
MnO	.22	.10	.01	.29	.20
MgO	6.66	13.24	.01	38.70	2.55
CaO	10.60	22.01	.01	.52	4.08
Na_2O	6.46	1.15	.01	.01	11.22
K_2O	2.02	.01	.01	.01	3.07
		Wo 47.99	Us 39.85	Fo 75.93	
		En 40.15	Mt 60.15	Fa 24.07	
		Fs 11.86			

Least Squares Approximation

	A			MIX		
	OBS	CALC	DIFF	COMP	Wt%	S.D.
SiO_2	42.38	42.45	0.07	C	50.80	1.09
TiO_2	4.14	4.39	0.25	CPX	38.03	1.28
Al_2O_3	12.82	12.94	0.12	TIMG	9.73	0.40
FeO*	14.71	14.64	-0.07	OLIVINE	1.00	0.87
MnO	.22	.14	-0.08			
MgO	6.66	6.64	-0.02	TOTAL	99.56	1.93
CaO	10.60	10.45	-0.15			
Na_2O	6.46	6.14	-0.32			
K_2O	2.02	1.56	-0.46			

Sum of squares of residuals = 0.43

Assuming that the estimated trace element abundances of the daughter 'C' are realistic then the agreement between the observed and calculated data for Rb and Ba is good. Sr data are not compatible with fractionation of

TABLE 7.9 Predicted and observed trace element contents of evolved Sabi nephelinite C using results of the least squares approximation given in Table 7.8 and distribution coefficients listed in Table 7.7.

Trace Element Match (Data in ppm)

	B	C		
	OBS	CALC.	CALC.(1)	OBS
Rb	60	115		110
Ba	1500	2893	2844	2800
Sr	1420	2638	2464	2300
Ni	55	2		3

(1) includes 2% apatite in the fractionating assemblage.

only clinopyroxene, olivine and titanomagnetite, that is providing the estimated parental (B) and daughter (C) compositions are realistic and distribution coefficients used in calculating the theoretical Sr composition of C are applicable to nephelinitic rocks. On the basis of clinopyroxene + olivine + titanomagnetite fractionation and using the distribution coefficients for Sr presented in Table 7.7 a differences of approximately 340 ppm Sr is present between the observed and calculated composition of Sr for end member C. However, the presence of 1 - 2% of apatite (D_{ap}^{Sr} = 5; Baker et al., 1977) in the fractionating assemblage partly overcomes the Sr discrepancy and is supported by petrographic data (see section 7.2.6, and petrographic descriptions of Sabi nephelinties, Table 6, Appendix D). Published distribution coefficients for Ba in apatite are extremely low (D_{ap}^{Ba} = 0.1; Baker et al., 1977) and consequently small amounts of apatite fractionation would be indistinguishable with respect to the present Ba

data. It is also unlikely that apatite fractionation would have any affect on the Rb data. Ni data also provides a reasonable fit in terms of a fractionational crystallsation model relating the Sabi parental magma composition to the more evolved end member C. However, the remaining trace elements have not been modelled in terms of crystal fractionation because of excessive scatter coupled with insufficient data.

7.3.5 Summary

From the preceeding arguments and modelling calculations it is apparent that the limited amount of whole rock chemical data coupled with the lack of mineralogical data for the Sabi nephelinites makes it difficult to reconstruct well constrained models to explain the geochemical relationships of the Lebombo and Sabi nephelinitic suites. Nevertheless, a model involving the formation of two slightly different parental magma compositions due to different degrees of high-pressure fractionation, followed by low pressure crystal fractionation appears to be plausible in terms of explaining most of the geochemical variations apparent in the nephelinitic volcanics. However, the model outlined above is based largely on major element data. A rigorous assessment of this model must therefore await more detailed petrographic and mineralogical studies of the Sabi nephelinites and additional whole rock major and trace element data for both suites of nephelinites.

7.4 Carbonatites, Nephelinites and Experimental Studies

Problems relating to the petrogenesis of nephelinite rock suites (and alkali volcanics in general) are many since, firstly, their major element chemistry poses severe problems for any process of differentiation from basaltic parents (e.g. see Bultitude and Green, 1971) and secondly, the abnormal abundances of alkali elements such as Ti, K, Rb and Ba found in these rocks present problems with respect to mechanisms of trace element

enrichment in either the primary mantle source region or during the genesis of nephelinite suites. In the past the petrogenesis of the alkali-basalt, basanite, nephelinite spectrum has been attributed to high pressure fractionation (Green and Ringwood, 1967; Bultitude and Green, 1968; Ito and Kennedy, 1968), differences in partial melting regimes (Gast, 1968; Green 1971) or combinations of the above processes plus low pressure fractionation (O'Hara, 1968a). However, the inherent problem associated with almost all these models is that abundances of incompatible elements in nephelinites and associated alkali volcanics relative to those in tholeiites, have been largely inexplicable in terms of the major processes proposed.

Though studies of the distribution of trace elements (e.g. Gast, 1968) have led to the conclusion that alkali basalts could be derived by very small degrees of partial melting ($< 7\%$) rather than fractional crystallisation, recent studies (Kesson and Price, 1972; Kesson, 1973; Sun and Hanson, 1975; Frey et al., 1978; Boettcher et al., 1979) have shown that some degree of pre-enrichment of the mantle source area is necessary prior to or during the melting event giving rise to nephelinitic and alkaline suites. For example, Frey et al. (1978) have shown that though it is possible to derive basanites, olivine-nephelinites and olivine-melilitites from a lherzolitic source composition by small degrees of melting, it is a prerequisite that the source be enriched with respect to LREE's and incompatible elements.

Average trace element abundance data (Table 7.10) indicates that the Karoo nephelinites are enriched in incompatible element contents relative to the reported average tholeiitic basalt (Wedepohl and Muramatsu, 1979), average Lebombo tholeiitic basalt, and slightly enriched relative to the 'average nephelinite' though this may be a function of fractionation since

TABLE 7.10 Average abundances of major and trace elements in Karoo nephelinites, Low-MgO lavas, picrite basalts and related rock types. (Data in columns 3-7 from Wedepohl and Muramatsu, 1979.)

	1 Karoo Nephelinite	2 Karoo Low-MgO Basalts	3 Karoo Picrite Basalts	4 Nephelinite	5 Kimberlite	6 Alkali Olivine Basalt	7 Tholeiitic Basalt	8 U/Mafics
% MgO	6.40	5.38	15.14	11.80	26.53	7.50	6.12	41.03
ppm P	4146	2313	1877	3800	3880	2090	960	220
K	17682	16354	14611	12200	10400	13280	6970	390
Ti	18225	19424	16906	16800	11800	14390	9710	780
Ba	1679	839	817	1046	1000	528	246	20
Rb	58	41	39	39	65	32	22	1.2
Sr	1353	847	913	1350	740	530	328	22
Y	23	37	27	36	22	33	28	2.88
Zr	216	349	338	205	250	189	137	16
Nb	125	21	22	103	110	69	13	1.3
Zr/Nb	1.71	16.6	15.36	1.99	2.27	2.74	10.5	
	N = 24	N = 17	N = 77	N 148	N 670			

2 : Average central and northern Lebombo low-MgO lava.

the 'average nephelinite' contains 11.80% MgO in comparison to 6.53% MgO in the average Karoo nephelinite. Most significant, however, is that data presented in Table 7.10 for the Lebombo-Sabi nephelinites and low-MgO basalts (both of which have MgO contents which differ by ~ 1% absolute) indicates that the alkali and tholeiitic suites cannot be derived from the same source by either simple fractional crystallisation or partial melting processes (relationships between the nephelinites and overlying picrite basalts will be discussed in the following chapter). On the basis of data presented in Table 7.10 it is therefore possible to speculate that the parental magmas from which the Karoo nephelinites crystallised were derived from an enriched source area. In this respect rare earth element patterns of the Karoo nephelinites are closely comparable to those of nephelinites from Australia (Fig. 7.6) which according to Frey et al. (1978) were derived by small degrees of partial melting from a source region enriched in both LREE and other incompatible elements. The similarity of both sets of rare earth data thus provides additional support for enrichment of the Karoo nephelinite source though it is by no means conclusive.

Much petrochemical evidence now exists in the literature which suggests that pervasive metasomatism giving rise to enrichment in LREE and incompatible elements of mantle material preceeds or accompanies the genesis of deep seated alkali-basaltic magmas. For example, ultramafic mantle xenoliths sampled by alkali-lavas commonly exhibit evidence of metasomatic enrichment (see Varne and Graham, 1971; Best, 1974; Frey and Green, 1974; Lloyd and Bailey, 1975; Francis, 1976; Basu and Murthy, 1977) as do many xenoliths contained in kimberlites. Evidence of metasomatism in mantle derived nodules from the latter rocks is particularly well displayed by the development of phlogopite and potassic-richterite in peridotite xenoliths

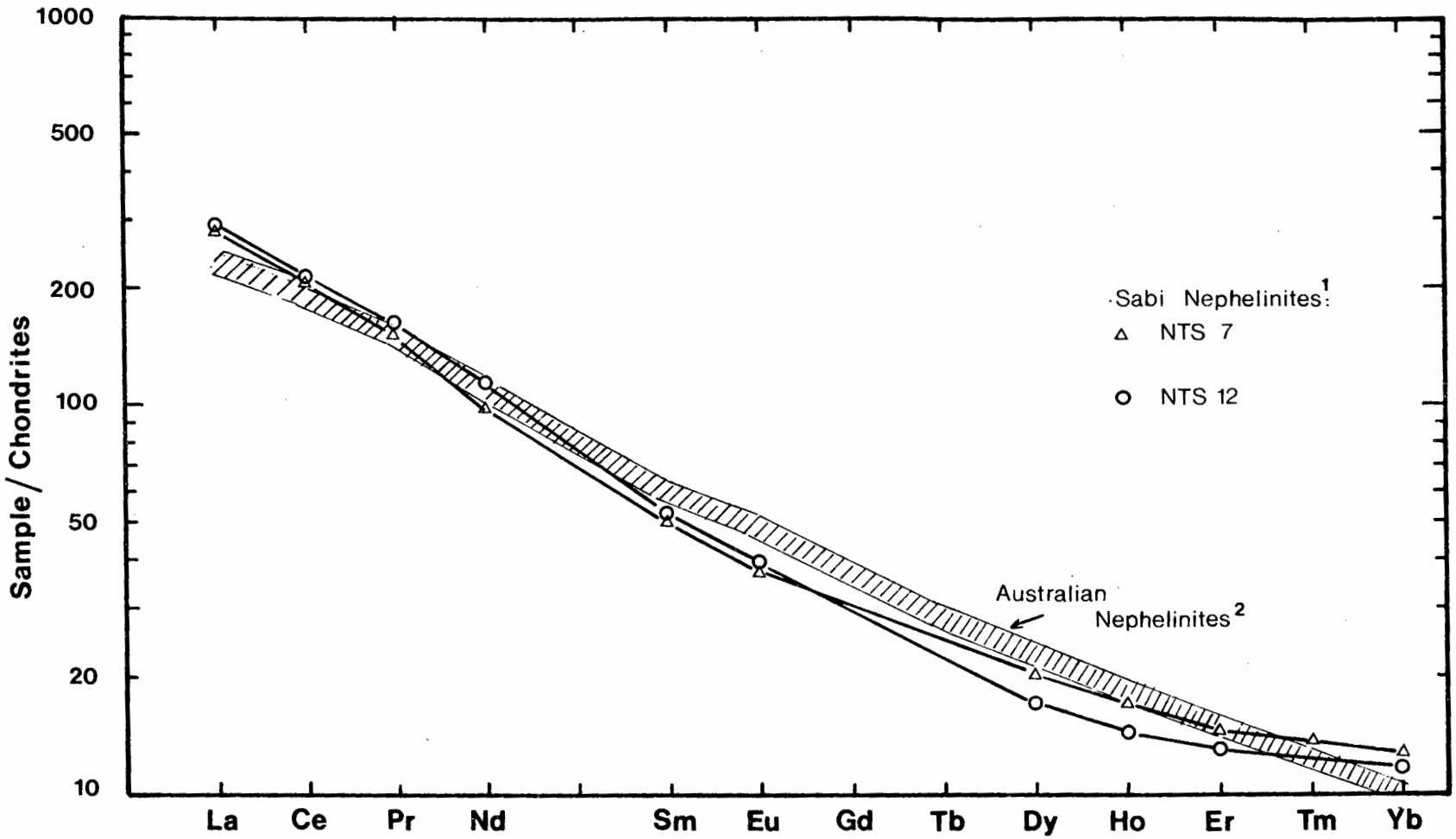

Fig. 7.6 REE/Chondrite normalised plot for Karoo (Sabi) and Australian nephelinite rocks (1 - Duncan, unpublished data; 2 - Frey et al., 1978).

obtained from southern African kimberlites (see Erlank, 1976; Erlank and Rickard, 1977; Boettcher et al., 1979). Considerable emphasis has been placed on the role played by metasomatism in mantle enrichment since it provides a means of eliminating the need for very small degrees of partial melting during the petrogenesis of nephelinitc and related alkali volcanics. Furthermore, apart from enriching portions of the mantle it may also promote melting in the mantle by providing a source of: i) CO_2, H_2O and other volatiles, ii) low temperature melting componenets, e.g. alkali element rich phases such as phlogopite and amphibole, iii) additional heat from the breakdown of radioactive elements such as K^{40}. Furthermore, volatile activity associated with metasomatic fluids may account for the updoming which appears to preceed many rift-volcanism events (see Bailey, 1974, 1977).

Though it can be inferred that the Karoo nephelinites were derived from a metasomatically enriched source, there remains the problem of producing highly silica undersaturated parental magmas at the onset of the volcanic episode. However, this problem can be overcome by postulating that a carbonate phase, e.g. CO_2, played a role during melting of the mantle source from which the Karoo nephelinites were derived. In view of the often noted association of carbonatites and nephelinites, a classic example of which is found in the East African Rift province (see Bailey, 1977), it is now widely accepted that carbonate species play a major role in the petrogenesis of these rock types. More significant, however, is that experimental studies have shown that it is possible to produce silica-undersaturated compositions by melting peridotitic material in the presence of CO_2.

Early studies of the fluid inclusions in peridotite xenoliths (Roedder, 1965; Green, 1972) showed that carbon dioxide was the dominant volatile species of the entrapped phases and prompted several investigations

into the role of CO_2 in peridotite melting (e.g. Eggler, 1974, 1978; Boettcher et al., 1975; Mysen and Boettcher, 1975 a,b). During investigations of the synthetic system $Mg_2SiO_4 - SiO_2 - H_2O - CO_2$ (Eggler, 1974) and natural peridotites (e.g. Mysen and Boettcher, 1975 a,b) it was found that the effect of CO_2 on melting was the opposite of that of H_2O such that melting in the presence of CO_2 (low H_2O) produced silica undersaturated liquids whereas liquids melting in H_2O (low CO_2) systems produced more silica saturated liquids. Results obtained from the experimental studies showed that CO_2 was not an inert compound during melting but that it dissolved in silicate melts thereby causing distinct changes in melt structure. The most notable of these changes was that the orthopyroxene field, and to a lesser extent, the clinopyroxene field were found to expand in the presence of CO_2 such that compositions of melts derived from CO_2 bearing peridotitic sources would be silica undersaturated (Eggler, 1974).

Two experimental studies at intermediate pressures (15 - 20 kb) on the compositions of glasses quenched from liquids with $CO_2 + H_2O$ have an important bearing on the Karoo nephelinitic and carbonatitic volcanics. Eggler (1975) studied a synthetic forsterite-enstatite system at 20 kbar, and Mysen and Boettcher (1975 a,b) studied four peridotites from 10 - 20 kbar. Their results indicate that near-solidus liquids are quartz-normative for vapours up to about $X^V (CO_2) = 0.5$ between 10 and 20 kbar. However, in the presence of vapours with greater $X^V (CO_2)$, Mysen and Boettcher (1975b) reported glasses that were nepheline normative and even larnite normative at 10 and 15 kbar.

Compositions of Mysen and Boettcher's starting material and selected daughter products are listed in Table 7.12 which also includes the estimated composition of Karoo nephelinite parent magma A. The experimental daughter composition (column 2, Table 7.12) is clearly nephelinitic in

TABLE 7.12 Partial melt composition produced from a spinel lherzolite + CO_2 + H_2O by Mysen and Boettcher (1975 a,b).

	1	2	3	4
$X^v_{H_2O}$		0.50	0.20	
T(°C)		1100	1150	
P(kb)		10	15	
SiO_2	43.70	45.6	43.5	43.73
TiO_2	0.20	1.0	0.5	3.45
Al_2O_3	4.00	18.9	10.5	11.06
FeO*	8.89	6.0	13.0	14.11
MnO	0.12	0.2	0.3	.20
MgO	37.4	5.9	10.7	8.63
CaO	3.5	18.5	13.8	11.37
Na_2O	0.38	3.8	7.6	5.72
K_2O	0.01	0.1	0.4	1.73

1. Spinel lherzolite starting composition.

2, 3. Composition of partial melts formed from 1 in a CO_2 + H_2O system at various temperatures, pressures and values of $X^v_{H_2O}$.

4. Estimated composition of the northern Lebombo parental nephelinite magma.

respect of most of its major element constitutents but is low in K_2O and TiO_2, though Mysen and Boettcher (1975b) suggest that the TiO_2, K_2O problem could be alleviated by melting of a phlogopite-bearing peridotite. Comparison of the experimental daughter composition and Lebombo parental magma (columns 2,3,4, Table 7.12) indicates that there is a broad similarity between the two rock types with the exception of TiO_2 and K_2O. However, if a metasomatic event similar to that which is inferred to have enriched the source area from which the Karoo nephelinites were derived had enriched the spinel peridotite from which Mysen and Boettcher (1975b) generated their nephelinite, it may well have shown even greater similarity to the Karoo parental magma.

The close association of the Sabi and northern Lebombo nephelinites with a series of carbonatite complexes which are either the same age or marginally older than the nephelinite volcanics suggest that CO_2 may well have played a part in the petrogenesis of the Karoo nephelinites and related rocks. In Zimbabwe a series of carbonatites (Dorowa, Shawa, Chishanya) and associated alkaline and picrite plugs and dykes are found to the northwest of the Sabi nephelinite outcrops (Swift et al., 1953; Swift, 1962; Nicolaysen et al., 1962; Johnson, 1966; Bowen, 1979) whereas a carbonatite-type intrusion has been described from the Messina area (Jacobsen and Mc Carthy, 1975) which adjoins nephelinite lava outcrops in the Soutpansberg extension of the Lebombo.

Age relations and a brief summary of the rock types found in these complexes are summarised in Table 7.11. The Dorowa Complex is undoubtedly the most important since not only has it been shown to be an unequivocal carbonatite but also contains intrusive dunites nephelinites and ijolites in a subsidiary centre known as the Zwibi Plug (Johnson, 1966). Data for the latter rocks (major elements only) have been plotted on the variation

TABLE 7.11 Age relationships of Karoo carbonatite complexes and nephelinite lavas in south-east Zimbabwe and the northern Lebombo.

	ROCK TYPES PRESENT	AGE	REF'S.
Dorowa Carbonatite Complex	Carbonatite, fenite, ijolite nephelinite	~ 205 my	1
Shawa Carbonatite Complex	Fenite, carbonatite, dunite, ijolite, nephelinite	205 ± 16 my	1,2,3
Chishanya Carbonatite Complex	Fenite, carbonatite, foyaite, ijolite, nephelinite	~ 205 my	4
Messina Carbonatite	Carbonatite	~ 200 my	5
Mashikiri Formation	Lebombo and Sabi Nephelinite lavas and intrusives	~ 200 my	6

References:

1 Johnson (1966)
2 Swift (1962)
3 Nicolaysen et al. (1962)
4 Bowen (1979)
5 Jacobsen and McCarthy (1975)
6 This study

diagrams (Figs. 7.3 a-i) and it is apparent that, with the exception of TiO_2, the nephelinitic and ijolitic rocks from Zwibi conform to the major element trends defined by the Sabi nephelinite suite. On a TiO_2 versus MgO diagram the Zwibi nephelinites and ijolites are strongly displaced from the fractionation trend shown by Sabi lavas and dykes and lie on a possible extension of the trend shown by the Lebombo data. No reason can be given for the apparent discrepancy shown by the Zwibi TiO_2 data though it is possible that inter-laboratory analytical error may be reponsible, bearing in mind that the Zwibi analyses were completed some years ago using conventional wet-chemical analytical techniques. The Chishanya Complex is also characterised by the presence of ijolite and nepheline bearing dykes in addition to carbonatites, foyaites and fenites (Bowen, 1979) whereas rock types reported from Shawa include dunites, ijolites, nephelinites and nepheline basalts (Swift, 1962; Johnson, 1966). In contrast to the Zimbabwe carbonatites, the Messina intrusive shows an almost monomineralic character and is also smaller than the complexes encountered to the north (Jacobsen and McCarthy, 1975).

The geochronological and field relationships (Table 7.11) and geochemical compatibility shown between the rocks of the carbonatite complexes and the nephelinite lava and dyke suites are considered here to provide evidence of an intimate association of carbonate rich and nephelinitic magmatism at the onset of Karoo volcanism in the Lebombo-Sabi area. Since the petrogenesis of the carbonatite complexes is compatible with melting of the same peridotite source from which the nephelinites were derived it is therefore concluded that the Karoo nephelinitic parental magmas may represent partial melts of a vapour rich (CO_2 + H_2O) peridotite. At high pressures ($\sim$ 30 kb), the range in composition between CO_2 vapour saturated and H_2O vapour saturated liquid in equilibrium with peridotite minerals is more

extreme than at lower pressures, varying from kimberlitic or carbonatitic in the presence of CO_2 (Eggler, 1978; Wyllie and Huang, 1975) to olivine tholeiitic in the presence of H_2O (for the system K_2O - CaO - MgO - Al_2O_3 - SiO_2 - H_2O; Bravo and O'Hara, 1975). Melting at increased pressures, coupled with localised concentrations of CO_2 rich volatiles in the mantle below the Sabi-Lebombo areas could therefore account for the carbonatite complexes located in the south-eastern areas of Zimbabwe and Messina area of South Africa. Conversely, melting of a CO_2 and H_2O rich peridotite at lower pressures (15 - 20 kbar) could explain the presence of the nephelinite lavas which crop out at the base of the Karoo volcanic sequence in the northern Lebombo and Sabi areas.

7.5 Summary and Conclusions

The following conclusions may be reached from the data and models presented above. However, a point that should be borne in mind is that the models are primarily based on major element data since there are insufficient trace element data to adequately test the proposed fractionation processes.

1. Modelling calculations indicate that nephelinites in the northern Lebombo and Sabi areas appear to have crystallised from parental magmas which differed slightly in composition due to different degrees of high pressure fractionation.

2. Low pressure fractional crystallisation appears to have led to the overall geochemical variation shown by the individual nephelinite suites.

3. Geochronological and geochemical data imply that the nephelinite volcanism was associated with the carbonatites emplaced at the onset of the Karoo volcanic cycle.

4. The carbonatites possibly developed in response to localised concentrations of CO_2 in the mantle underlying south-east Zimbabwe in pre-Karoo times and it is inferred that this gas species played a role in the petrogenesis of the undersaturated nephelinite lavas and dykes.

8 THE PICRITE BASALTS

8.1 Introduction

Olivine rich lavas and intrusives of the central and northern Lebombo are referred to as picrite basalts and picrites respectively. These rocks dominate the volcanic succession north of the Olifants River area and are also abundant in the Tuli (Vail et al., 1969) and Nuanetsi (Cox et al., 1965; Jamieson, 1969) areas of Zimbabwe. Chemically these rocks show unusual features for though they are hypersthene normative (see Table 8.10) and may therefore be termed tholeiites they are characterised by unusually high abundances of K, Ti, P, Ba, Sr and Zr (Cox and Jamieson, 1974).

The chemistry and petrogenesis of the Tuli and Nuanetsi olivine rich lavas and dykes have been considered in some detail by Vail et al. (1969), Jamieson (1966, 1969) and Cox and Jamieson (1974) whereas no detailed work has been done on the Lebombo picrite basalts prior to the present study. However, the compilation of a particularly large picrite-basalt data set which, in addition to Tuli and Nuanetsi rocks, incorporates many new analyses from the northern Lebombo has allowed a more comprehensive study of the petrogenesis of the high magnesian lavas than has previously been possible.

A detailed assessment of the petrography, mineralogy and geochemistry of these olivine-rich rocks is presented in this chapter. In addition the petrogenesis of the lavas is considered in relation to high pressure crystal fractionation and/or melting processes and an attempt is made to elucidate criteria which imply that some of the lavas, though porphyritic, may represent high-magnesium basalt magmas. Mechanisms whereby the precursive magmas could be enriched in K and related elements are also examined.

8.2 Petrography: Picrite Basalts

8.2.1 General Statement

The picrite basalts are characterised by an abundance of olivine phenocrysts which are commonly visible in hand specimen. In thin section they display porphyritic or glomeroporphyritic textures and show a broad spectrum of textural and petrographic features, most of which are reflected by variations in the chemistry of the lavas. Principal mineralogical differences result from variations in the amount of plagioclase, clinopyroxene, orthopyroxene and fine grained or glassy mesostasis contained in the lavas, bearing in mind that olivine is always present as a phenocryst phase. Modal analyses (Table 8.1) demonstrate the variability of the mineral content of the picrite basalts.

Phenocrysts present, other than olivine, may include orthopyroxene, clinopyroxene and occasionally plagioclase. Olivine, in particular, demonstrates a remarkable range in modal abundance (range 6.5 - 46.1%) and crystal habit, though it is most commonly found as phenocrysts and microphenocrysts with euhedral, subhedral and rounded shapes often modified by re-entrants (Plate 8.1). In rocks with a highly chilled appearance the olivines may show skeletal crystal forms similar to those described from other localities by Drever and Johnston (1957) and Bryan (1972), and in experimental charges by Donaldson (1976). Olivine macrophenocrysts are also found in many of the lavas. Clinopyroxene is present as skeletal crystals, microphenocrysts and phenocrysts with subhedral or rounded shapes, and more rarely as macrophenocrysts with euhedral or subhedral outlines. Some of the clinopyroxene phenocrysts contain cores of orthopyroxene and occasionally olivine.

Orthopyroxene is predominantly found as small (<1mm), resorbed crystals overgrown by clinopyroxene and rarely as discrete phenocrysts.

TABLE 8.1 Modal analyses of Picrite basalts

(Volume %)	KS47	KS3	KA24	KP111*	KA98*	KP121	KP101*	KA29	KP108*	KP112*
Olivine	6.5	10.9	16.3	17.7	20.6	21.8	23.0	29.1	32.6	46.1
Orthopyroxene	13.6	2.1	10.3	-	-	1.9	tr	tr		
Clinopyroxene	29.3	21.0	27.0	34.7	27.3	23.7	27.5	27.0	25.5	20.3
Plagioclase	20.0	36.0	20.3			21.0		17.4		
Opaques	13.4	10.3	7.9	12.8	16.0	10.4	8.4	4.7	9.8	5.3
Groundmass°°	14.5	28.7	14.9	30.2	32.2	18.0	37.7	20.2	28.6	25.3
Accessories ø	2.7	1.0	3.3	4.6	3.9	8.2	3.4	1.6	3.5	3.0
WR % MgO	12.0	10.72	14.68	14.45		14.59	16.37	17.69	21.04	24.03

ø - Mostly chlorite and zeolite filling small vesicles.

°° - Incorporates apatite which varies from less than 1% to approximately 2%.

* - Glassy or microcrystalline lavas. Clinopyroxene in KP108 and KP111 is predominantly skeletal.

WR - Whole Rock

PLATE 8.1

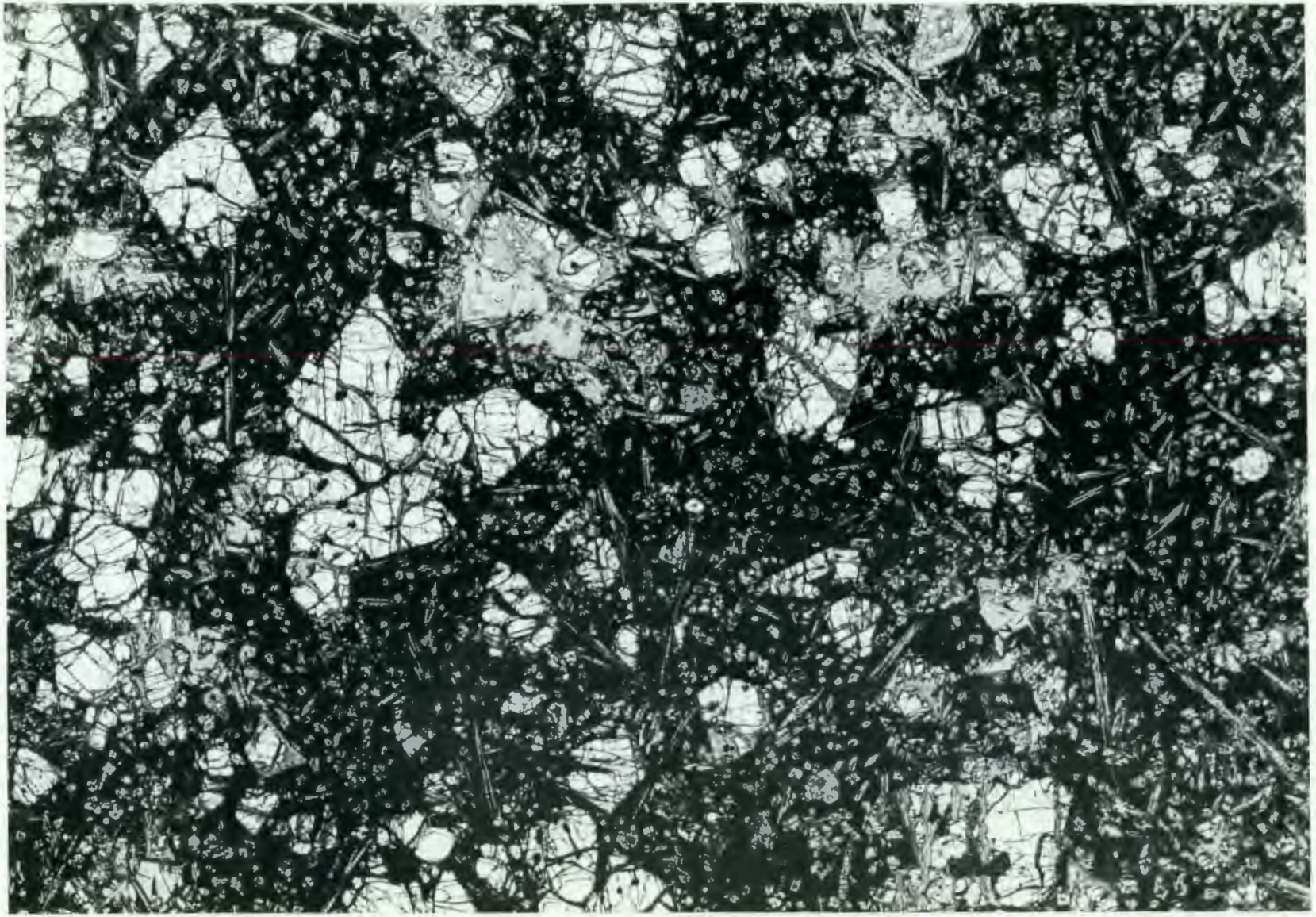

i) Macrophenocrysts (Plates 8.2 A,B)

Crystals with a diameter greater than about 3.0 mm are referred to as macrophenocrysts. The largest macrophenocrysts are 6 - 7 mm in diameter. They may be euhedral, subhedral or rounded in habit. Re-entrants and irregular shaped cavities filled with groundmass material occur in some of the crystals, as do near spherical brown glass inclusions. (The glass is usually slightly devitrified). They are commonly pseudomorphed by a light green mineral similar to that found in the Nuanetsi picrite-basalts and identified as saponite (Cox et al., 1967) or else strongly altered around the edges and along cracks traversing the crystals.

Cox and Jamieson (1974) referred to crystals of similar dimensions found in the Nuanetsi lavas as megacrysts and proposed that they represented high pressure relicts whereas the ordinary phenocrysts formed at lower pressures. Data collected during this study and presented in section 8.3.1 shows that there are no noticeable differences in chemistry between the above two groups and 'macrophenocryst' is therefore used in preference to 'megacryst'.

ii) Phenocrysts (Plates 8.2 E,F)

Crystals falling in the size range 0.5 - 2.75 mm are designated as phenocrysts. Two groups of phenocrysts are recognised on the basis of different morphologies, viz. euhedral or subhedral phenocrysts, and rounded phenocrysts.

The euhedral and subhedral phenocrysts are most commonly found in the very glassy lP* picrite-basalts and may be accompanied by skeletal pyroxenes; they very rarely occur in the evolved or cumulate, plagioclase bearing lavas. They are typically equant or tabular (Plates 8.2 C,D) and either have well formed crystal faces or else show a

*Footnote: For explanation of petrographic nomenclature see section 5.4.2.

PLATE 8.2

A - Photomicrograph of an olivine macrophenocryst with well formed re-entrants in picrite basalt KP106. Crossed polars.

B - Olivine macrophenocryst in picrite basalt KP108. Plane polarised light.

C - Photomicrograph of picrite basalt KP108 showing euhedral olivine phenocryst characterised by re-entrants, and slightly curvo-linear lobes. Note skeletal clinopyroxenes with either needle or hollow-ended crystal habits. Crossed polars.

D - Olivine phenocryst containing rounded glass inclusions set in a glassy groundmass. Skeletal clinopyroxenes, including a micro-crystal with a hollow belt buckle form, are seen abutting the olivine. Picrite basalt KP111. Crossed polars.

E - Photomicrograph of picrite basalt KP97 showing nodular aggregate of olivine. Crossed polars.

F - Nodular aggregate of olivine crystals in picrite basalt KS65. Note curvolinear margins of some of the olivines. Crossed polars.

G - Photomicrograph of picrite basalt KP111 showing skeletal crystals of clinopyroxene set in a glassy matrix. Crossed polars.

PLATE 8.2

A

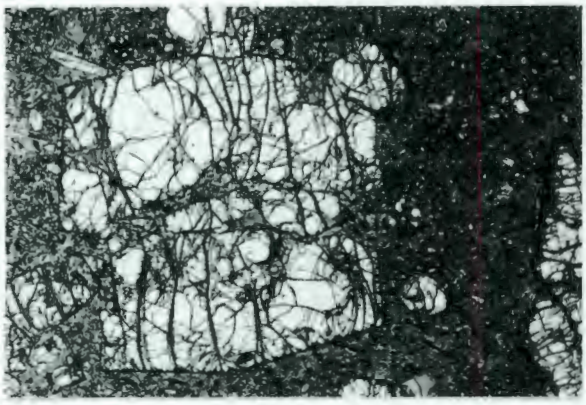

3 mm

B

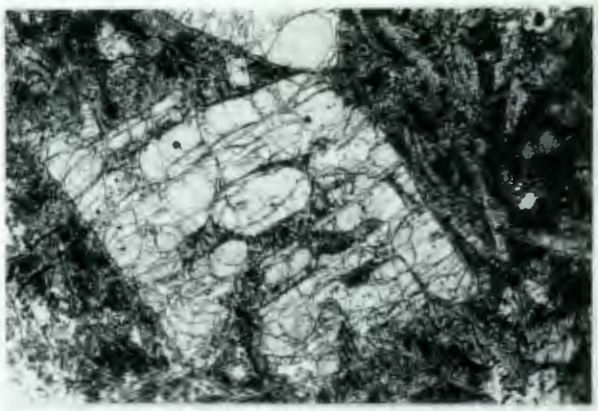

1.2 mm

C

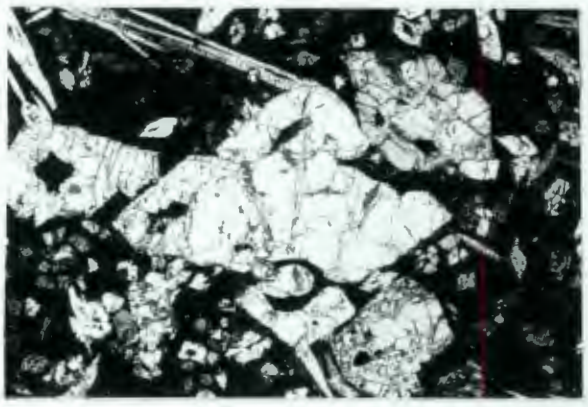

0.9 mm

D

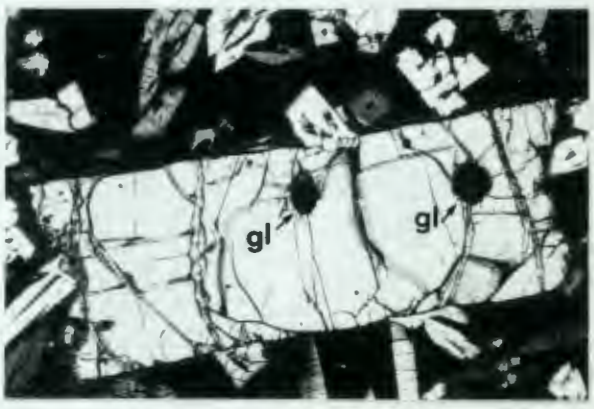

0.5 mm

E

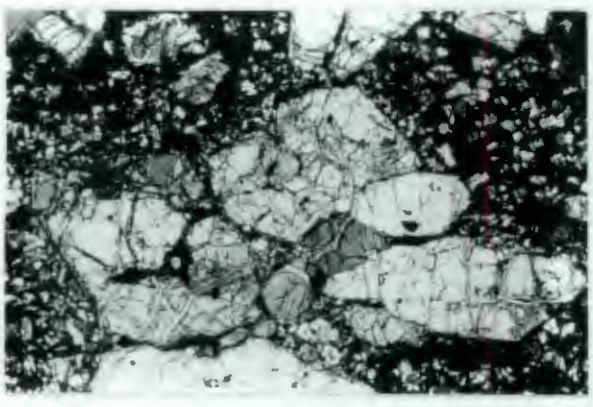

1.5 mm

F

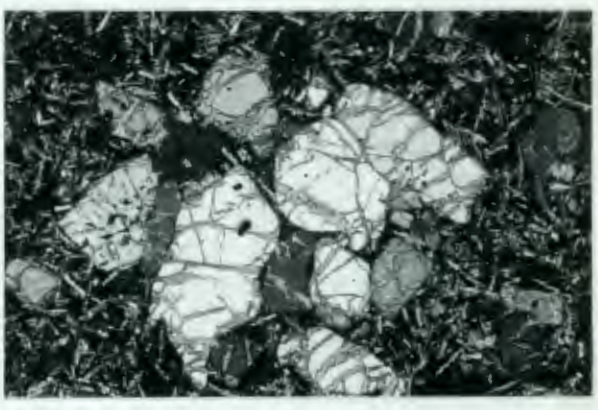

1.5 mm

G

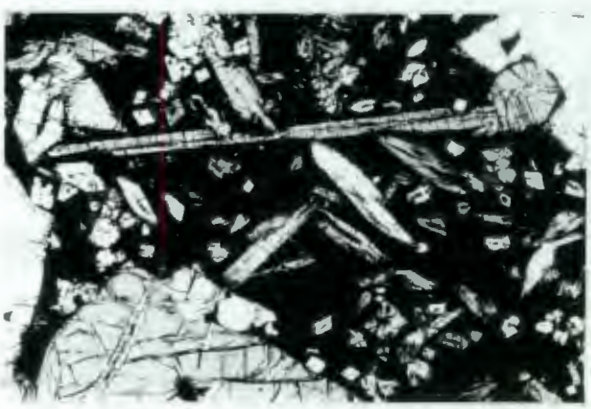

0.9 mm

combination of planar faces, curvolinear lobes and re-entrants (Plate 8.2 C). They may contain round or oval inclusions of glass and groundmass material (Plate 8.2 D).

The rounded phenocrysts, by comparison, are ubiquitous in the 2P and 3P picrite basalts but seldom found in 1P-lavas. They are generally slightly smaller than the euhedral or subhedral phenocrysts and may also contain rounded or oval inclusions of glass and groundmass material. Re-entrants are found in some of the rounded phenocrysts but are far less common than in the euhedral and subhedral phenocrysts.

Clots of phenocrysts with unusual curvolinear boundaries occur in many of the lavas. They commonly have a nodular appearance (Plate 8.2 E,F) and may be up to 4mm in diameter. In view of their monomineralic character it is possible that they represent fragments of either olivine cumulates or a dunitic rock.

iii) Microphenocrysts

Rounded and skeletal olivines less than 0.5mm in diameter are referred to as microphenocrysts. Skeletal forms are only found in the very glassy rocks and resemble the morphologies of chain olivines described by Bryan (1972) in ocean floor pillow basalts and by Donaldson (1976) in experimental charges. Needle shaped olivines and 'limited parallel growth phenocrysts' (Donaldson, 1976) were also found in a few samples.

Microphenocrysts with rounded and subhedral outlines occur in many of the picrite basalts. They are commonly as forsteritic in composition as the larger crystals and as such appear to represent remnants of corroded and resorbed phenocrysts or macrophenocrysts. Small rounded or subhedral olivines that are more fayalitic in composition than the

macrophenocrysts and phenocrysts are found in the evolved picrite basalts.

8.2.3 Orthopyroxene

Orthopyroxene occurs as a phenocryst in approximately 55 percent of the picrite basalts examined. It is almost invariably mantled or jacketed by clinopyroxene (cf. Cox and Jamieson, 1974) and is present as discrete phenocrysts in only three lavas (samples KA24, Ø248, KS47). It is generally found in trace amounts ($<1\%$) though an exceptional specimen (sample KS47) contains 13.6% orthopyroxene (by volume)(Table 8.1).

Crystal habits of the mantled orthopyroxenes vary considerably. Many of them exhibit undulose extinction and are distinctly rounded or 'spidery' in appearance suggesting that the orthopyroxene crystals were strongly resorbed prior to crystallisation of the clinopyroxene mantle. In contrast, some rocks contain small altered blebs and patches of orthopyroxene ($\sim$ 0.5mm) which are barely discernable within large clinopyroxene phenocrysts. Others however, contain large mantled orthopyroxene crystals (up to 3mm) with intensely pitted and corroded margins and clinopyroxene overgrowths that tend to be highly irregular or else discontinuous (Plate 8.3.A). Less common, are large phenocrysts of orthopyroxene (up to 3.5mm) that have retained their overall crystal shape and are mantled by narrow rims of clinopyroxene (Plate 8.3.B). These narrow mantles may not always be continuous and in the case of rectangular crystals are commonly only found on prism faces.

Unmantled orthopyroxene phenocrysts are characterised by well formed (euhedral-subhedral) or slightly rounded crystal habit. Sample KS47 contains a number of unmantled crystals in addition to rectangular phenocrysts that display clinopyroxene overgrowths on prism faces only. The unmantled crystals in sample KS47 are notably smaller than the mantled crystals and are also very slightly zoned, particularly towards the rim.

PLATE 8.3

A

Photomicrograph of orthopyroxene crystals mantled by clinopyroxene in picrite basalt KS3. Note the relatively well formed clinopyroxene rim on the large central orthopyroxene crystal; a strongly altered olivine grain is present in the centre of this crystal. Crossed polars.

B

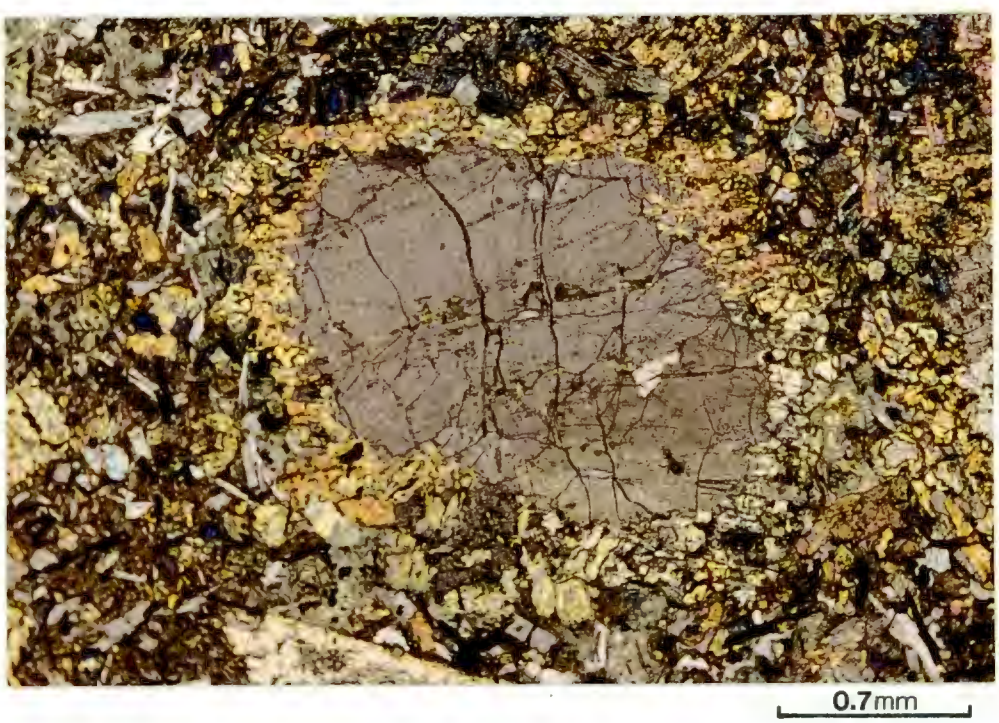

Rounded aggregate of orthopyroxene mantled by an irregular overgrowth of clinopyroxene in picrite basalt KA24. Crossed polars.

8.2.4 Clinopyroxene

Clinopyroxene is found in nearly all the picrite basalts with the exception of a few very glassy lavas. It shows a wide range in modal abundance (Table 8.1) and a diversity of crystal shapes. It is most commonly found as phenocrysts (0.5 - 2.0mm) in the 2P and 3P picrite-basalts or as skeletal crystallites in glassy and cryptocrystalline lavas. However, it may also occur as large rectangular and anhedral phenocrysts (1 - 2.0mm) with small cores of orthopyroxene, as narrow overgrowths on orthopyroxene phenocrysts (Plate 8.3 A,B) and less commonly as substantial macrophenocrysts (up to 4mm).

Clinopyroxene appears as a skeletal phase in the glassy and crypto-crystalline picrite basalts (Plates 8.1, 8.4 C,D,G). Its appearance in the first stages of skeletal crystallisation is characterised by needle-shaped microcrystalline or radial feather-like intergrowths with feldspar, and more rarely, as fine dendritic growth forms. With slightly more advanced crystallisation it assumes a complex acicular or needle-like habit characterised by ragged and hollow ends and chain structures. Viewed in a direction parallel to the c-axis, the crystals tend to have a double swallow-tailed or clothes-peg appearance (Plates 8.4 C,G) whereas sections viewed perpendicular to the c-axis are represented by equant euhedra and subhedra which are mostly hollow (Plate 8.4 G). Skeletal crystals are also frequently found arranged in a radial fashion about olivine microphenocrysts suggesting that nucleation of the clino-pyroxene was assisted by the presence of the olivine crystals. Occasionally skeletal crystals may be moderately large.

Phenocrysts of clinopyroxene are abundant in the evolved picrite basalts. They are either subhedral or rounded in habit and occur as

PLATE 8.4

A - Photomicrograph of picrite basalt KS65 showing a cluster of clinopyroxene microphenocrysts set in groundmass consisting of plagioclase laths and intersertal glass. Crossed polars.

B - Clinopyroxene macrophenocryst with complex twinning in picrite basalt KS65. Crossed polars.

C - Photomicrograph of picrite basalt KS65 showing a clinopyroxene macrophenocryst that is cored by an irregular shaped olivine crystal. Crossed polars.

D - Plagioclase phenocrysts (lath shaped) associated with a nodular aggregate of clinopyroxene and minor olivine in picrite basalt KS3. Crossed polars.

E - Photomicrograph of spicular ilmenites in picrite basalt KP123. Part of an orthopyroxene crystal mantled by clinopyroxene is present in the lower portion of the photomicrograph. Crossed polars.

F - Picrite basalt KP123 showing stubby and needle-like ilmenite crystals set in a glassy groundmass. Crossed polars.

G - Photomicrograph of a coarse grained picrite dyke KS7. Subhedral and rounded olivine crystals are the dominant minerals in this rock with the lesser amounts of clinopyroxene and intergranular plagioclase. Crossed polars.

H - Clinopyroxene macrophenocryst in coarse grained picrite dyke KS53. Subrounded olivines, spicular ilmenite and plagioclase, occasionally overgrown with rims of K-feldspar, constitute the remaining mineral species found in this rock. Crossed polars.

PLATE 8.4

A

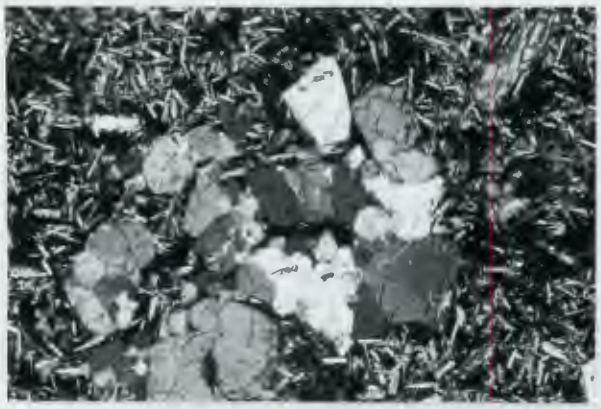

1.2mm

B

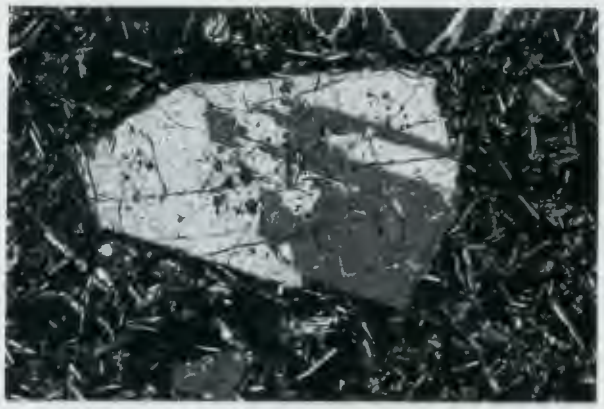

0.9mm

C

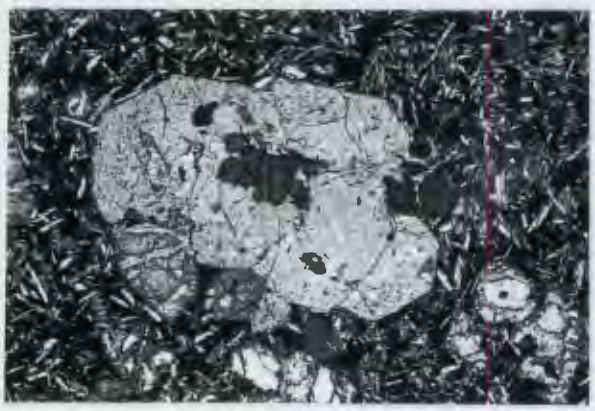

1.2mm

D

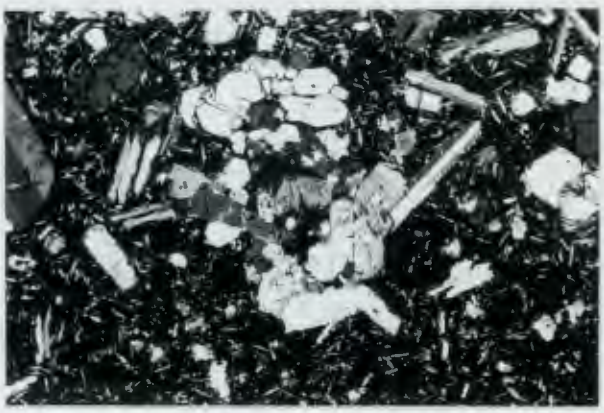

1.3mm

E

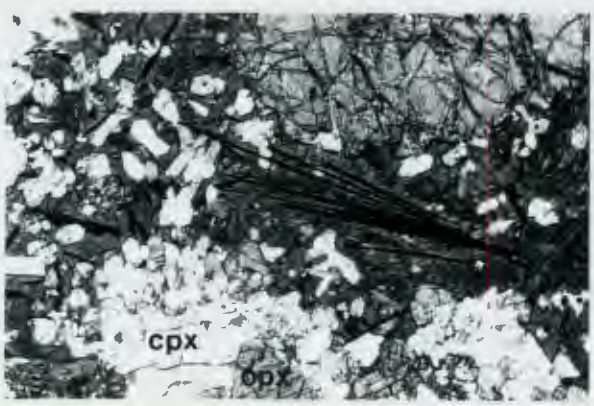

0.9mm

F

1.2mm

G

3mm

H

3mm

discrete crystals in the groundmass and in nodular aggregates up to 2.5mm across (Plate 8.4 A,D). The aggregates generally consist of tightly packed clinopyroxene crystals which may exhibit irregular or curvolinear internal contacts. They resemble the olivine nodules described in a previous section (8.2.2) but are generally smaller. They may occasionally include a grain or two of olivine and patches of microcrystalline groundmass.

Macrophenocrysts of clinopyroxene are found in several 2P and 3P picrite basalts (Plates 8.4 B,C). They are characterised by a euhedral or subhedral crystal habit and are inclined to show complex twinning (Plate 8.4 B). They may be slightly resorbed and occasionally enclose small olivine crystals. Clinopyoroxene overgrowths or mantles on orthopyroxene have been discussed in section 8.2.3. It should be noted, however, that where the orthopyroxene remains as small irregular blebs and patchy crystals, the surrounding clinopyroxene tends to attain dimensions and crystal outlines characteristic of macrophenocrysts.

Clinopyroxene is present as a groundmass phase in all of the evolved, fine grained picritic basalts. It forms subhedral and anhedral laths and grains intergrown with plagioclase, apatite, opaque oxide and more rarely, olivine microphenocrysts.

8.2.5 Plagioclase Feldspar

Plagioclase feldspar rarely occurs as a phenocryst phase in the northern Lebombo picrite basalts. Similarly, in Nuanetsi Cox and Jamieson (1974) found phenocrysts of plagioclase in only two picritic lavas. Plagioclase is, however, found as rare skeletal crystals in the glassy rocks and is a common groundmass phase in the evolved picrite basalts.

The skeletal plagioclases show a variety of microcrystalline forms, the most common being feather-like crypto-crystalline intergrowths of plagioclase and pyroxene, which are similar to those described by Bryan (1972) in ocean floor basalts, and acicular prism shapes. The acicular crystals are strongly elongated in the a-axis direction with hollow cores parallel to this axis filled with glass or cryptocrystalline material. Sections cut perpendicular to the a-axis show a characteristic hollow-rectangular 'belt-buckle' (Bryan, 1972) form. The acicular plagioclases also grow in sheaf-like clusters and these are often arranged in radial forms.

Groundmass plagioclases in the evolved, fine to medium grained picrite basalts typically occur as anhedral laths or subrounded grains intergrown with clinopyroxene. Rare phenocrysts or microphenocrysts of plagioclase are found in the most evolved picrite basalts. Both phenocrysts and microphenocrysts occur as subhedral prisms (Plate 8.4 D) which may be present as discrete crystals in the groundmass or glomeroporphyritic clusters associated with olivine and clinopyroxene grains. The phenocrysts rarely exceed 1mm and commonly display albite or carlsbad twinning. They may also be very slightly zoned.

8.2.6 Potassium Feldspar

Potassium feldspar in the form of sanidine is found as overgrowths on plagioclase laths and as highly irregular grains in some of the lavas with coarser matrix textures. Rocks with visible K-feldspar are generally characterised by exceptionally high K_2O contents (weight %) and fall in the high-K picrite basalt field (section 5.3). Similar rock types occur in the Tuli and Nuanetsi areas and were described as absarokites by Vail et al. (1969) and Cox (1972) respectively. They are, however, relatively scarce and since it is invariably necessary to

resort to the use of EMP scans to identify the presence of K-feldspar it has been considered expedient to simply refer to these lavas as picrite basalts.

8.2.7 Fe-Ti Oxides

Fe-Ti oxides are a ubiquitous constituent of the picrite basalts. In the very glassy lavas Fe-Ti oxides appear as fine needles (Plate 8.4 E) and fragile dendritic growths. In the remaining glassy and microcrystalline rocks the opaque oxides occur as skeletal needles or blades (Plate 8.4 F), commonly several millimetres long, and rectangular laths with rather ragged terminations. By comparison Fe-Ti oxides found in the more evolved crystalline lavas, are usually stubbier and subhedral or anhedral in habit.

The oxide minerals are generally opaque, though some of the blades and needles are translucent and characterised by a dark orange-brown colour. Similar translucent oxide minerals have been described in the Nuanetsi lavas and were identified as a new mineral (Kennedyite) in the pseudobrookite series (Von Knorring and Cox, 1961).

8.2.8 Apatite

Apart from alteration products and rare amygdales, apatite represents the only additional mineral species found in the picrite basalts. The apatites are almost always confined to the groundmass and are invariably needle shaped. They are strongly elongated parallel to the c-axis with length to breadth ratios of 60 : 1 or more being common. The crystals are frequently hollow and crystal ends are commonly slightly flared or ragged in appearance. Broken needles are also found in some lavas. Apatites in the Nuanetsi volcanics show identical characteristics to those in the Lebombo lavas (see Cox et al., 1965; Wyllie et al., 1962).

TABLE 8.2 Modal analyses of Lebombo and Nuanetsi Picrites

(Volume %)	KS7	KS53	N15	N26	N41	N95
Olivine	34.2	55.2	19	21	33	36
Orthopyroxene	6.5			1	tr	tr
Clinopyroxene	20.7	14.3	31	25	25	27
Plagioclase	32.4	24.9	34		22	25
Opaques	4.5	2.9	2	7	5	3
Groundmass*			14	46	14	8
Accessories	1.7	2.7				
WR - MgO~	20.78	27.72	13.46	15.41	17.66	17.22

KS7, KS53 - N. Lebombo

N15, N26, N41, N95 - Nuanetsi (Data from Jamieson, 1969)

* - Includes apatite and alkali-feldspar

WR - Whole Rock

According to Wyllie et al. (1962) the apatite forms noted in the Nuanetsi picrite basalts are similar to those shown by synthetic quench apatites.

8.2.9 Picrites

In comparison to the fine grained and glassy textures of the lavas, the picrites are typically coarse grained or holocrystalline (Plates 8.4 G,H). They consist of olivine, clinopyroxene, ore minerals including both ilmenite and kennedyite (von Knorring and Cox, 1961), and plagioclase accompanied by unmantled orthopyroxene and alkali feldspar; apatite needles are also ubiquitous. Mantled orthopyroxenes were not found in the Lebombo picrites though they are reported from the Nuanetsi intrusives (Cox and Jamieson, 1974). Modal analyses of these rocks are listed in Table 8.2.

8.3 Mineral Chemistry

8.3.1 Olivine

Olivine phenocrysts have been analysed in 10 picrite-basalts. The rocks chosen represent a selection of picrite basalts from glassy 1P lavas through to the more evolved and generally crystalline 3P lavas and range from 10.72 - 24.93% MgO (weight percent). Selected olivine analyses are listed in Table 8.3 and the complete data set is to be found in Microfiche Table E.2. Ranges in composition, the amount of zoning shown by individual crystals and the morphological characteristics are listed in Table 8.4; whole-rock MgO values (weight percent) are included in this table.

The olivine show a significant range in composition (range: $Fo_{76.5}$-$Fo_{89.3}$) and broadly speaking Fo content decreases from the most basic to more evolved lavas. Zoning is generally normal and continuous with the

TABLE 8.3

PICRITE-BASALTS : REPRESENTATIVE OLIVINE ANALYSES

	1	2	3	4	5	6	7	8	9	10
SIO2	38.90	37.79	37.93	38.58	38.97	38.60	40.04	39.21	39.76	40.09
TIO2	.05	.06	.05	.05	.05	.04	.04	.05	-	-
AL2O3	-	-	-	-	.03	.04	-	.04	.04	-
CR2O3	.04	.04	-	-	-	.05	-	-	.11	.11
FEO	19.22	24.11	21.27	19.28	19.55	19.25	12.46	13.60	10.76	10.39
MNO	.21	.25	.22	.22	.23	.22	.20	.19	.08	.14
MGO	40.73	36.61	39.59	41.84	40.58	41.23	46.93	46.63	47.92	48.63
CAO	.27	.27	.29	.31	.27	.26	.23	.26	.23	.22
NA2O	-	-	-	-	-	-	-	-	-	-
K2O	-	-	-	-	-	-	-	-	-	-
NIO	-	-	.29	.32	.32	.35	-	-	.50	.50
TOTAL	99.42	99.13	99.64	100.60	100.00	100.04	99.90	99.98	99.40	100.08

* * ATOMIC PROPORTIONS BASED ON SELECTED NO. OF OXYGENS * *

OXYGEN	4	4	4	4	4	4	4	4	4	4
SI	1.003	1.001	.989	.986	1.002	.992	.995	.981	.989	.988
AL	-	-	-	-	.001	.001	-	.001	.001	-
TI	.001	.001	.001	.001	.001	.001	.001	.001	-	-
CR	.001	.001	-	-	-	.001	-	-	.002	.002
FE2+	.414	.534	.464	.412	.420	.414	.259	.285	.224	.214
MN	.005	.006	.005	.005	.005	.005	.004	.004	.002	.003
MG	1.565	1.446	1.538	1.594	1.554	1.579	1.739	1.739	1.776	1.787
CA	.007	.008	.008	.008	.007	.007	.006	.007	.006	.006
NA	-	-	-	-	-	-	-	-	-	-
K	-	-	-	-	-	-	-	-	-	-
NI	-	-	.006	.007	.007	.007	-	-	.010	.010
SUM	2.996	2.997	3.010	3.013	2.997	3.006	3.004	3.017	3.010	3.010
	FO 79.06 FA 20.94	FO 73.02 FA 26.98	FO 76.83 FA 23.17	FO 79.45 FA 20.55	FO 78.72 FA 21.28	FO 79.24 FA 20.76	FO 87.03 FA 12.97	FO 85.94 FA 14.06	FO 88.81 FA 11.19	FO 89.29 FA 10.71

* * * S A M P L E D I R E C T O R Y * * *

ANALYSIS NO.	DESCRIPTION
1	PHENOCRYST CORE - 1A (KA29)
2	PHENOCRYST RIM - 1B (KA29)
3	MICROPHENOCRYST (KS3)
4	MICROPHENOCRYST (KS3)
5	MACROPHENOCRYST (KP121)
6	MACROPHENOCRYST (KP121)
7	MACROPHENOCRYST (KP112)
8	MACROPHENOCRYST (KP112)
9	PHENOCRYST (KP111)
10	PHENOCRYST (KP111)

T A B L E 8.3 (CONTINUED)

PICRITE-BASALTS : REPRESENTATIVE OLIVINE ANALYSES

	11	12	13	14	15	16	17	18	19	20
SIO2	39.56	39.89	39.80	39.51	39.22	39.24	39.23	39.52	39.26	39.38
TIO2	-	-	-	-	-	-	-	-	-	-
AL2O3	-	-	-	-	-	-	-	-	-	-
CR2O3	-	-	-	-	-	-	-	-	-	-
FEO	14.63	13.56	13.08	15.46	18.98	11.52	11.51	11.43	13.02	14.27
MNO	.18	.15	.14	.16	.21	.15	.15	.14	.16	.19
MGO	44.80	45.81	46.00	44.36	41.64	48.64	48.64	48.72	46.40	45.46
CAO	.29	.25	.24	.24	.30	-	-	-	-	-
NA2O	-	-	-	-	-	-	-	-	-	-
K2O	-	-	-	-	-	-	-	-	-	-
NIO	-	-	-	-	-	.43	.45	.43	.35	.29
TOTAL	99.46	99.66	99.26	99.73	100.35	99.98	99.98	100.24	99.19	99.59

* * ATOMIC PROPORTIONS BASED ON SELECTED NO. OF OXYGENS * *

OXYGEN	4	4	4	4	4	4	4	4	4	4
SI	.998	.999	.998	.997	1.000	.974	.974	.978	.988	.992
AL	-	-	-	-	-	-	-	-	-	-
TI	-	-	-	-	-	-	-	-	-	-
CR	-	-	-	-	-	-	-	-	-	-
FE2+	.309	.284	.274	.326	.405	.239	.239	.237	.274	.301
MN	.004	.003	.003	.003	.005	.003	.003	.003	.003	.004
MG	1.684	1.709	1.720	1.669	1.582	1.800	1.800	1.796	1.740	1.706
CA	.008	.007	.006	.006	.008	-	-	-	-	-
NA	-	-	-	-	-	-	-	-	-	-
K	-	-	-	-	-	-	-	-	-	-
NI	-	-	-	-	-	.009	.009	.009	.007	.006
SUM	3.002	3.001	3.002	3.003	3.000	3.026	3.026	3.022	3.012	3.008
	FO 84.51 FA 15.49	FO 85.76 FA 14.24	FO 86.24 FA 13.76	FO 83.64 FA 16.36	FO 79.63 FA 20.37	FO 88.27 FA 11.73	FO 88.28 FA 11.72	FO 88.37 FA 11.63	FO 86.40 FA 13.60	FO 85.02 FA 14.98

* * * S A M P L E D I R E C T O R Y * * *

ANALYSIS NO.	DESCRIPTION
11	MACROPHENOCRYST CORE - 1A (KS47)
12	MACROPHENOCRYST - 1B (KS47)
13	MACROPHENOCRYST - 1C (KS47)
14	MACROPHENOCRYST - 1D (KS47)
15	MACROPHENOCRYST RIM - 1E (KS47)
16	PHENOCRYST CORE - 2A (KP111)
17	PHENOCRYST - 2B (KP111)
18	PHENOCRYST - 2C (KP111)
19	PHENOCRYST - 2D (KP111)
20	PHENOCRYST RIM - 2E (KP111)

TABLE 8.4 Morphological and compositional characteristics of olivines analysed in picrite basalts. Value in brackets indicates total number of EMP analyses completed.

Sample Numbers		Olivine Morphology	Compositional Range (moles Fo)	Degree of Zoning* (moles Fo)	Whole Rock MgO (wt%)	Modal Olivine (vol %)
KS3	(16)	□ △	76.5 - 79.5	2	10.72	10.9
KS47	(7)	▣ □	79.6 - 86.2	6.61	12.00	6.5
KP111	(27)	□	77.8 - 89.3	3.3	14.45	17.7
KP121	(10)	▣ □	78.0 - 80.0	1	14.59	21.8
KA24	(13)	▣ □ △	73.5 - 79.4	6.5	14.68	16.3
KP101	(6)	□ △	83.9 - 87.6	2.2	16.37	23.0
KA29	(13)	▣ □ △	73.0 - 80.9	6.7	17.69	29.0
KP108	(4)	□ △	86.0 - 87.7	1	21.04	32.6
KP112	(6)	▣ □	82.4 - 87.0	4.2	24.03	46.1
KP98	(12)	□ △	79.5 - 84.7	2		20.6

* - Represents maximum amount of zoning shown by any single olivine crystal in each sample.

▣ - macrophenocrysts

□ - phenocrysts

△ - microphenocrysts and groundmass olivines

exception of a single macrophenocryst in sample KS47 (analyses 11-15, Table 8.3) which shows a slight increase in Fo content away from the core followed by a decrease nearer the rim. The zonation range shown by the olivines is about 2 - 7 percent Fo (Table 8.4) and is most extreme in the macrophenocrysts. Zoning in the high-magnesian phenocrysts is commonly very slight ($\backsim$ 2 percent Fo) suggesting some degree of equilibrium crystallisation.

Composition of olivine cores are plotted in Figure 8.1b. The core analyses exhibit almost the same range as the total olivine variation in Fig 8.1a, but show a strong bimodal distribution with a gap in the range $Fo_{81 - 83}$. Group I ($Fo_{83 - 90}$) values (Fig. 8.1a) are almost exclusively analyses of euhedral and subhedral olivine phenocrysts and to a lesser degree olivine macrophenocrysts (section 8.2.2); the most magnesian core analyses ($Fo_{88 - 90}$) are representative of slightly altered euhedral and subhedral phenocrysts (occasionally with re-entrants) set in a glassy to cryptocrystalline matrix (sample KP111; Plate 8.2.D). By comparison, Group II analyses ($Fo_{76 - 81}$) (Fig. 8.1.a) are mostly representative of groundmass crystals, microphenocrysts and rounded phenocrysts (section 8.2.2), as well as several macrophenocrysts.

In Nuanetsi Cox and Jamieson (1974) found that megacrysts (macrophenocrysts in this study; see section 8.2.2) were generally more magnesian ($Fo_{78 - 92}$) than phenocrysts and groundmass crystals ($Fo_{71 - 81}$). Though the compositional ranges and groupings of olivines in the Zimbabwe lavas are practically the same as those found in the northern Lebombo there is an apparent variance in the 'crystal type - Fo content' correlation between the two localities since in the Lebombo the most magnesian olivines are represented by phenocrysts rather than macrophenocrysts. It is probable, however, that this apparent discrepancy

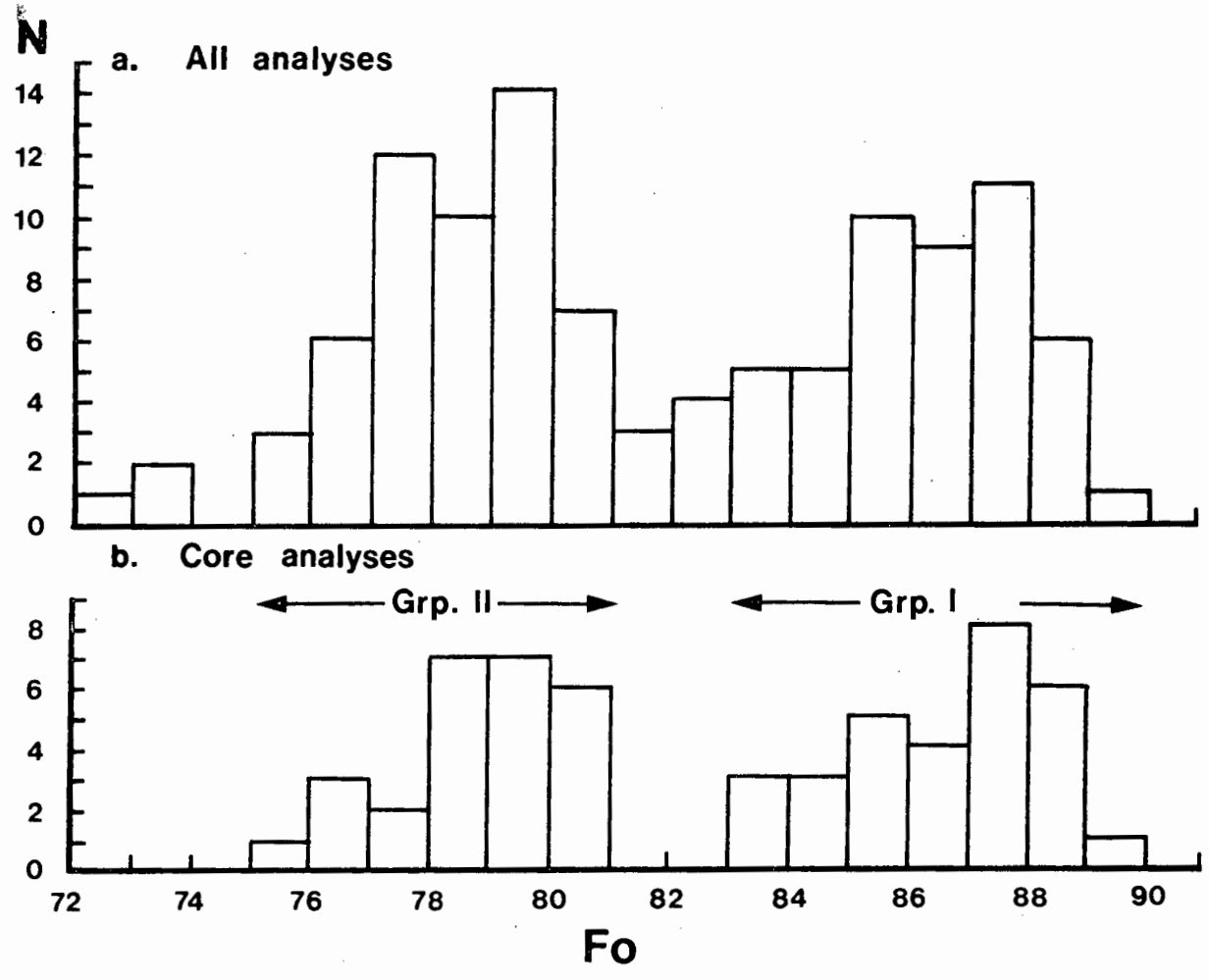

Fig. 8.1 Histogram showing the variation in the Forsterite (Fo) content of olivines analysed in the northern Lebombo picrite basalts.

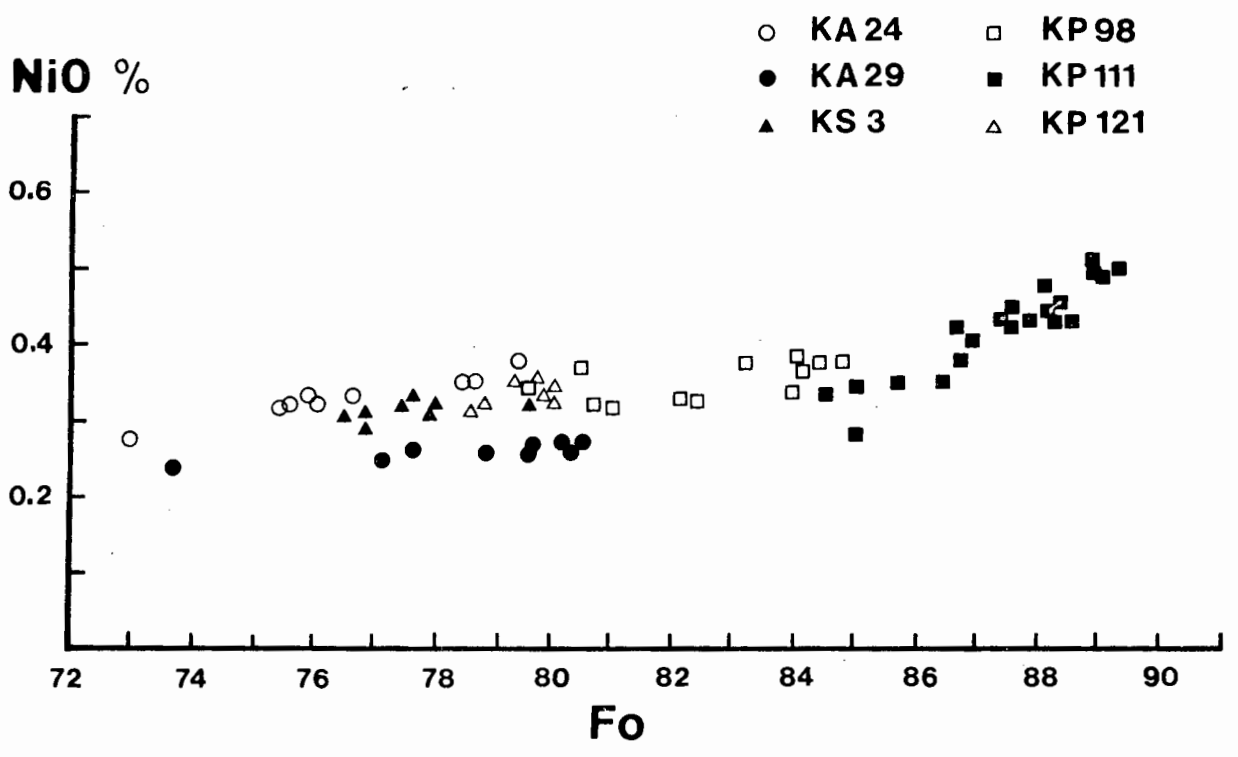

Fig. 8.2 Plot of NiO (weight %) versus Forsterite content (Fo) for olivines analysed in the northern Lebombo picrite basalts.

is related to the use of different interpretative criteria coupled with the fact that fewer olivine analyses are available from the Nuanetsi lavas.

The nickel content of olivines from the northern Lebombo picrite basalts is shown in Table 8.3 (Microfiche Table E.2) and the variation of NiO in relation to Fo content is shown in Figure 8.2. Nickel shows an overall decrease with falling Fo content (Fig. 8.2) and ranges from 0.24%-0.50% NiO in the range Fo_{73} - Fo_{85}. NiO is most enriched in the olivine phenocrysts of sample KP111 which shows a compositional trend from 0.50% (Fo_{89}) to 0.29% (Fo_{85}). Different samples may show distinctly different NiO values at a particular Fo content such as those displayed by olivines from samples KA24 and KA29 in Figure 8.2. Nickel data for these two samples plots on two well constrained lines separated by approximately 0.1% NiO at $Fo_{79.5}$. Experimental data (eg. Arndt, 1977 ; Hart and Davis, 1978) shows that D_{Ol}^{Ni} decreases with increasing MgO in the liquid such that the differences apparent between nickel contents of olivines in samples KA29 and KA24 may be due to the more magnesian character of KA29 (MgO = 17.69) relative to KA24 (14.68). Other experimental work (Mysen, 1976 a,b, 1978; Mysen and Kushiro, 1979) has shown that D_{Ol}^{Ni} decreases with increasing pressure. An alternative explanation for the olivines with higher nickel contents in KA24 could therefore be that they have crystallised at slightly lower pressures than those in KA29.

Compositions of the cores of the most magnesian olivines Fo_{88} - Fo_{89} are within the range of the assumed compositions of mantle olivine (Irving 1971; O'Hara, 1973) and similar to those found in alpine harzburgites and peridotites (Himmelberg and Loney, 1971; Menzies, 1977). However, the broad range in compositions of olivine cores in Group I is more typical of the compositional range found in stratiform intrusions and suggests that olivine fractionation has taken place in the magma from

which the lavas were derived (cf. Frey et al., 1974). Alternatively the olivines may have crystallised from a temperature zoned magma chamber characterised by compositions with higher Fe/Mg ratios at lower temperatures.

8.3.2 Orthopyroxene

Representative analyses of mantled and unmantled orthopyroxenes are given in Table 8.5. Ranges in composition of analysed phenocrysts are shown in Fig. 8.3. Individual analyses are listed in Microfiche Table E2.

The orthopyroxenes define a trend of strong Fe-enrichment and slight Ca-enrichment and show a fairly large compositional range (Fig. 8.3). Mantled orthopyroxenes vary between En_{82} and $En_{89.6}$ (includes Nuanetsi data) whereas the unmantled phenocrysts vary between $En_{78.1}$ and $En_{83.9}$. Compositions of the most basic phenocrysts are, with the exception of TiO_2 and Al_2O_3, similar to those found in alpine peridotites (lherzolites) (see Menzies, 1977) and ultramafic inclusions (see Frey and Prinz, 1978); Lebombo and Nuanetsi orthopyroxenes are notably enriched in TiO_2 and depleted in Al_2O_3 relative to orthopyroxenes from alpine peridotites and ultramafic inclusions.

Zoning was seldom noted in the mantled orthopyroxene crystals. However, because these orthopyroxene crystals are only found as partly resorbed relicts surrounded by clinopyroxene, analyses were seldom obtained from what appeared to be the original core and margin of a crystal. Zoning is present in the unmantled orthopyroxene crystals and was found to be rather variable. In three separate phenocrysts analysed in sample KS47 (see analyses 9-17, Microfiche Table E2-d) zoning was found to be normal, weakly reversed and oscillatory.

TABLE 8.5

PICRITE-BASALTS : REPRESENTATIVE ORTHOPYROXENE ANALYSES

	1	2	3	4	5	6	7	8	9	10
SIO2	56.11	55.80	56.22	56.20	55.62	55.38	54.31	55.50	55.24	55.80
TIO2	.26	.26	.35	.25	.37	.38	.50	.26	.35	.37
AL2O3	.79	.80	.79	.69	1.08	.63	1.01	.61	.36	.81
CR2O3	.29	.30	.31	.32	.37	.25	.45	.39	.32	.52
FEO	7.20	8.40	8.58	8.97	7.87	11.23	11.39	8.88	10.49	8.87
MNO	.08	.10	.13	.11	.11	.18	.17	.11	.10	.10
MGO	34.05	33.24	32.76	32.77	32.80	30.18	30.16	32.88	30.34	32.26
CAO	1.27	1.34	1.83	1.81	1.52	2.39	2.61	1.72	2.31	1.68
NA2O	-	.06	.04	-	.07	.04	.05	-	.04	.07
K2O	-	-	-	-	-	-	-	-	-	-
TOTAL	100.05	100.30	101.01	101.12	99.81	100.66	100.65	100.35	99.55	100.48

* * ATOMIC PROPORTIONS BASED ON SELECTED NO. OF OXYGENS * *

OXYGEN	6	6	6	6	6	6	6	6	6	6
SI	1.951	1.948	1.952	1.952	1.947	1.956	1.926	1.944	1.966	1.950
ALIV	.032	.033	.032	.028	.045	.026	.042	.025	.015	.033
ALVI	-	-	-	-	-	-	-	-	-	-
TI	.007	.007	.009	.007	.010	.010	.013	.007	.009	.010
CR	.008	.008	.009	.009	.010	.007	.013	.011	.009	.014
FE2+	.209	.245	.249	.261	.230	.332	.338	.260	.312	.259
MN	.002	.003	.004	.003	.003	.005	.005	.003	.003	.003
MG	1.765	1.729	1.695	1.696	1.711	1.589	1.594	1.716	1.609	1.681
CA	.047	.050	.068	.067	.057	.090	.099	.065	.088	.063
NA	-	.004	.003	-	.005	.003	.003	-	.003	.005
K	-	-	-	-	-	-	-	-	-	-
SUM	4.022	4.027	4.020	4.023	4.018	4.019	4.035	4.031	4.014	4.018
	WO 2.34	WO 2.48	WO 3.38	WO 3.33	WO 2.85	WO 4.50	WO 4.88	WO 3.16	WO 4.38	WO 3.14
	EN 87.30	EN 85.41	EN 84.24	EN 83.80	EN 85.62	EN 79.00	EN 78.48	EN 84.09	EN 80.08	EN 83.91
	FS 10.36	FS 12.11	FS 12.38	FS 12.87	FS 11.53	FS 16.50	FS 16.63	FS 12.74	FS 15.54	FS 12.95

* * * S A M P L E D I R E C T O R Y * * *

ANALYSIS NO.	DESCRIPTION
1	MANTLED PHENOCRYST (KA24)
2	MANTLED PHENOCRYST (KA24)
3	MANTLED PHENOCRYST (KA24)
4	MANTLED PHENOCRYST (KA24)
5	MANTLED MACROPHENOCRYST (KA24)
6	UNMANT PHENO (KS47)
7	UNMANT PHENO CORE - 1A (KS47)
8	UNMANT PHENO RIM - 1B (KS47)
9	UNMANT PHENO CORE - 2A (KS47)
10	UNMANT PHENO RIM - 2B (KS47)

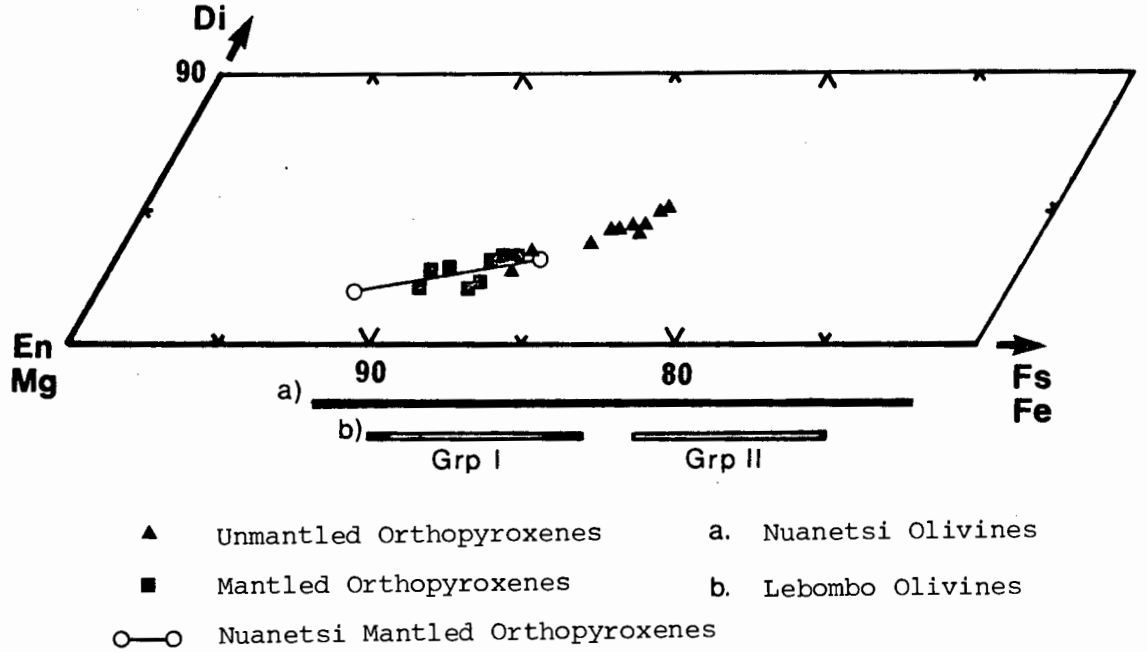

Fig. 8.3 Compositional variation of orthopyroxenes and olivines analysed in the northern Lebombo picrite basalts. Nuanetsi data from Cox and Jamieson (1974) are shown for comparison.

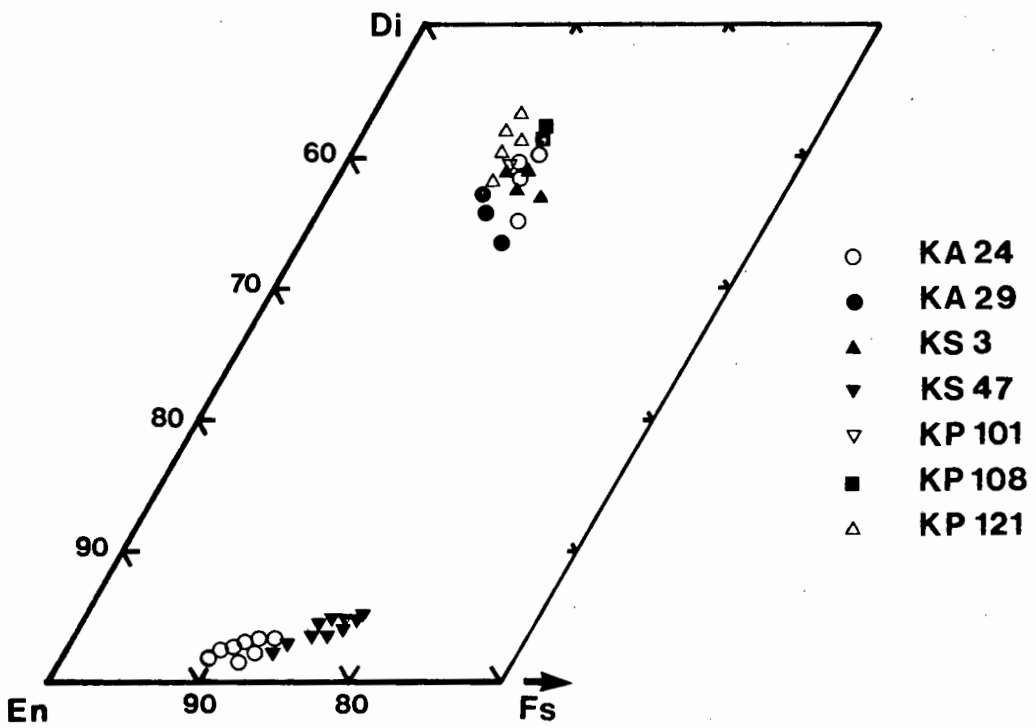

Fig. 8.4 Compositional variation of clinopyroxenes and orthopyroxenes analysed in the northern Lebombo picrite basalts.

8.3.3 Clinopyroxene

Compositions of the clinopyroxenes analysed in the picrite basalts are plotted in Figure 8.4 and representative analyses are listed in Table 8.6. Individual analyses are tabulated in Microfiche Table E2.

The overall compositional variation in the clinopyroxenes is rather small with a range from approximately $En_{53}Wo_{37}Fs_{10}$ to $En_{46}Wo_{44}Fs_{10}$. The most magnesian compositions are represented by clinopyroxene rims on orthopyroxenes and by phenocrysts. Skeletal quench crystals typical of the glassy lavas tend to be slightly enriched in TiO_2 and lower in SiO_2 than the other pyroxenes. Slight normal zoning is present in most of the phenocrysts.

8.3.4 Fe-Ti Oxides

Two oxide minerals were identified on the basis of petrographic criteria (section 8.2.7) and this is confirmed by EMP analysis. Analyses of the distinctly opaque ore prisms and needles indicate that they are ilmenites whereas compositions of the translucent microcrystals correspond to the pseudobrookite mineral, kennedyite, which was originally identified in the Nuanetsi picrite basalts and picrites by Von Knorring and Cox (1961).

Selected analyses of the ilmenites and kennedyites are included in Table 8.7; an analysis of kennedyite from the Nuanetsi volcanics is included for comparison. (Individual analyses of both ore phases are present in Microfiche Table E2). The ilmenites are somewhat unusual in that they are characterised by very high MgO abundances. Similarly, the kennedyites also contain very high contents of MgO as well as high levels of Al_2O_3. The high levels of magnesium present in the oxide minerals implies that they crystallised from high-MgO liquids.

T A B L E 8.7

PICRITE-BASALTS : REPRESENTATIVE FE-TI OXIDE ANALYSES

	1	2	3	4	5	6	7	8	9	10
SIO2	-	-	.10	.31	.04	.04	.05	.05	.04	-
TIO2	42.98	46.38	50.02	59.74	53.05	51.89	52.00	63.57	62.10	60.33
AL2O3	.53	.13	.29	1.86	.19	.18	.26	1.58	1.74	2.15
CR2O3	.18	.16	.26	1.16	-	-	-	-	-	.37
FE2O3	21.28	15.65	7.24	21.34	3.35	4.70	2.88	12.64	14.73	23.76
FEO	30.78	32.90	36.77	7.87	36.53	37.36	40.33	15.48	15.61	9.19
MNO	.29	.36	.38	.15	.28	.38	.94	.20	.10	.07
MGO	4.25	4.74	4.46	7.46	6.14	5.03	3.11	5.35	4.66	6.55
CAO	-	-	-	-	-	-	-	-	-	-
NA2O	-	-	-	-	-	-	-	-	-	-
K2O	-	-	-	-	-	-	-	-	-	-
TOTAL	100.29	100.32	99.52	99.89	99.58	99.58	99.57	98.87	98.99	102.42

* * ATOMIC PROPORTIONS BASED ON SELECTED NO. OF OXYGENS * *

OXYGEN	3	3	3	5	3	3	3	5	5	5
SI	-	-	.002	.011	.001	.001	.001	.002	.002	-
AL	.015	.004	.008	.080	.005	.005	.008	.070	.077	.091
TI	.794	.853	.924	1.639	.966	.953	.968	1.786	1.752	1.628
CR	.003	.003	.005	.033	-	-	-	-	-	.010
FE3+	.393	.288	.134	.586	.061	.086	.054	.355	.416	.642
FE2+	.632	.672	.755	.240	.740	.763	.835	.483	.490	.276
MN	.006	.007	.008	.005	.006	.008	.020	.006	.003	.002
MG	.156	.173	.163	.406	.222	.183	.115	.298	.261	.350
CA	-	-	-	-	-	-	-	-	-	-
NA	-	-	-	-	-	-	-	-	-	-
K	-	-	-	-	-	-	-	-	-	-
SUM	2.000	2.000	2.000	3.000	2.000	2.000	2.000	3.000	3.000	3.000
	IL 64.44	IL 68.23	IL 76.77		IL 74.71	IL 77.29	IL 85.77			
	GK 15.70	GK 17.33	GK 16.48		GK 22.23	GK 18.38	GK 11.53			
	HM 19.85	HM 14.45	HM 6.75		HM 3.06	HM 4.33	HM 2.70			

* * * S A M P L E D I R E C T O R Y * * *

ANALYSIS NO.	DESCRIPTION	ANALYSIS NO.	DESCRIPTION
1	ILMENITE MICROPHENOCRYST (KA24)	6	ILMENITE MICROPHENO (KA29)
2	ILMENITE MICROPHENOCRYST (KA24)	7	ILMENITE MICROPHENO (KA29)
3	ILMENITE MICROPHENOCRYST (KA24)	8	KENNEDYITE MICROPHENO (KA29)
4	KENNEDYITE MICROPHENOCRYST (KA24)	9	KENNEDYITE MICROPHENO (KA29)
5	ILMENITE MICROPHENOCRYST (KA29)	10	KENNEDYITE (VON K & COX,1961)

8.3.5 Plagioclase Feldspar

Representative analyses of plagioclase microphenocrysts and groundmass glass are presented in Table 8.8. Individual analyses are tabulated in Microfiche Table E2.

The plagioclase show a small compositional range, varying from about $An_{67}Ab_{30}Or_3$ to $An_{56}Ab_{40}Or_4$. Zoning, though not particularly strong, is normal and, as noted previously, alkali feldspar overgrowths can be identified on some plagioclase phenocrysts. An additional feature of the plagioclases is their enriched K_2O content which is notably higher than plagioclases of similar anorthite content found in other picrite basalt suites, eg. the Deccan Traps (Krishnamurthy and Cox, 1977).

8.3.6 Olivine, Orthopyroxene, Clinopyroxene Assemblages

In view of the fact that there appear to be distinct populations of mineral phases, eg. Group I and II olivines and mantled and unmantled orthopyroxenes, it is important to know which assemblages are in equilibrium and which are not.

Studies of co-existing olivine : orthopyroxene pairs (eg. Ramberg and De Vore, 1951; O'Hara 1963) in magnesian assemblages indicate that both minerals generally have similar Mg : Fe ratios or that the olivine is relatively more magnesian. On this basis the olivines of Group I (Mg : Fe = 49 - 90) could well have been in equilibrium with both the mantled and the unmantled orthopyroxenes (Mg : Fe = 65 - 84 and 47 - 53 respectively) since both sets of minerals have similar ranges of Mg : Fe ratios. However, the olivine phenocrysts of Group II (Mg : Fe = 30 - 43) are unlikely to have been in equilibrium with the mantled orthopyroxene, but may have been in equilibrium with the unmantled orthopyroxene.

TABLE 8.8

PICRITE-BASALTS : REPRESENTATIVE PLAGIOCLASE ANALYSES

	1	2	3	4	5	6	7	8
SIO2	52.82	52.82	53.21	54.31	53.51	54.33	51.92	53.66
TIO2	.13	.13	.15	.14	.15	.12	.17	.16
AL2O3	30.02	30.02	28.85	28.98	28.83	28.41	29.78	28.52
CR2O3	-	-	-	-	-	-	-	-
FEO	.52	.52	.57	.65	.57	.65	.78	.77
MNO	-	-	-	-	-	-	-	-
MGO	.19	.19	.18	.10	.16	.15	.17	.15
CAO	13.10	13.10	12.43	11.77	12.31	11.82	13.01	11.55
NA2O	3.37	3.37	3.75	4.11	4.23	4.33	3.75	4.80
K2O	.44	.44	.55	.70	.76	.88	.50	.70
TOTAL	100.59	100.59	99.69	100.76	100.52	100.69	100.08	100.31

* * ATOMIC PROPORTIONS BASED ON SELECTED NO. OF OXYGENS * *

OXYGEN	8	8	8	8	8	8	8	8
SI	2.384	2.384	2.423	2.444	2.423	2.452	2.366	2.435
AL	1.597	1.597	1.548	1.537	1.538	1.511	1.600	1.525
TI	.004	.004	.005	.005	.005	.004	.006	.005
CR	-	-	-	-	-	-	-	-
FE2+	.020	.020	.022	.024	.022	.025	.030	.029
MN	-	-	-	-	-	-	-	-
MG	.013	.013	.012	.007	.011	.010	.012	.010
CA	.634	.634	.606	.567	.597	.572	.635	.561
NA	.295	.295	.331	.359	.371	.379	.331	.422
K	.025	.025	.032	.040	.044	.051	.029	.041
SUM	4.973	4.973	4.980	4.983	5.011	5.003	5.009	5.029
	AN 66.42	AN 66.42	AN 62.55	AN 58.73	AN 58.99	AN 57.09	AN 63.80	AN 54.82
	AB 30.92	AB 30.92	AB 34.15	AB 37.11	AB 36.68	AB 37.85	AB 33.28	AB 41.23
	OR 2.66	OR 2.66	OR 3.30	OR 4.16	OR 4.34	OR 5.06	OR 2.92	OR 3.96

* * * SAMPLE DIRECTORY * * *

ANALYSIS NO.	DESCRIPTION
1	MICROPHENOCRYST CORE - 1A (KS3)
2	MICROPHENOCRYST - 1B (KS3)
3	MICROPHENOCRYST RIM - 1C (KS3)
4	MICROPHENOCRYST (KS3)
5	MICROPHENOCRYST (KP121)
6	MICROPHENOCRYST (KP121)
7	MICROPHENOCRYST (KS47)
8	MICROPHENOCRYST (KS47)

Comparison of Mg : Fe ratios of the mantled orthopyroxenes and their clinopyroxene rims (Table 8.9) also indicate that these two minerals are not in equilibrium; this relationship is substantiated by Fe : Mg K_D calculations. The distribution of Mg and Fe between co-existing orthopyroxenes and clinopyroxenes has been discussed by Mueller (1960, 1961) Kretz (1961, 1963), O'Hara and Mercy (1963) and Bunch et al. (1970). These studies indicate that the mineral pair orthopyroxene : clinopyroxene generally behaves as an ideal solid solution and despite limitations imposed by non-ideal mixing of Mg and Fe, variations in temperature and/or pressure and compositional variations, the K_D (Mg:Fe) has been used as a possible indicator of equilibrium and non-equilibrium pyroxene assemblages (eg. see Bunch et al., 1970). Kretz (1961, 1963) originally recorded K_D (Mg:Fe) values in the range 0.65 - 0.86 for pyroxene pairs in igneous environments. Subsequent studies of pyroxene pairs in continental volcanics and meteorites (Bunch et al., 1970; K_D (Mg:Fe) = 0.50 - 1.0) and ultramafic inclusions (Frey and Prinz, 1978; K_D (Mg:Fe) = 0.80 - 1.10) have extended the above range slightly. K_D (Mg:Fe) values for the mantled orthopyroxene : clinopyroxene pairs in the northern Lebombo picrite basalts are consistently outside the range of K_D's calculated for equilibrium assemblages (Table 8.9) indicating a probable lack of equilibrium between these two minerals. Conversely K_D (Mg:Fe) values for most of the unmantled orthopyroxene : clinopyroxene pairs fall in the range considered to be representative of equilibrium conditions (Table 8.9).

Consequently, on the basis of Mg : Fe distribution between the olivine, orthopyroxene and clinopyroxene assemblages found in the picrite basalts it is apparent that the Group I olivines and mantled orthopyroxenes crystallised in a different environment to the Group II olivines, unmantled orthopyroxenes and clinopyroxenes. As noted previously,

TABLE 8.9 Analyses and Fe/Mg relationships of mantled orthopyroxenes and clinopyroxene rims.

	OPX 1	CPX 2	CPX 3	OPX 4
SiO_2	56.11	49.42	50.82	55.34
TiO_2	.26	.85	1.68	.29
Al_2O_3	.79	2.02	1.83	.69
Cr_2O_3	.29	-		.34
FeO	7.20	8.85	7.76	10.39
MnO	.08	.13	.11	.14
MgO	34.05	19.89	17.19	30.58
CaO	1.27	19.00	20.06	2.04
K_2O	.02	.22	.23	.05
Wo	2.34	35.47	40.10	3.87
En	87.30	51.64	47.79	80.73
Fs	10.36	12.89	12.11	15.39
Mg/Fe	84	40	39	53
K_D 1:2		0.47		
1:3			0.47	
4:3				0.75

$$K_D = \frac{(Fe/Mg)\ opx}{(Fe/Mg)\ cpx}$$

1 Mantled orthopyroxene (Sample KA24, analysis 14, Microfiche Table E2-a).

2,3 Clinopyroxene rim on orthopyroxene grain 1. (Sample KA24, analyses 15,16, Microfiche Table E2-a).

4 Unmantled orthopyroxene (Sample KS47, analysis 8, Microfiche Table E2-d).

the olivines of Group I and mantled orthopyroxenes are broadly similar in composition to mantle olivines and orthopyroxenes implying that a possible high-pressure fractionation process may have been involved in the generation of the lavas. Conversely the assemblage: olivine (Grp II) + clinopyroxene (+ unmantled orthopyroxene) is typically that observed as a low-pressure fractionation assemblage in basaltic rocks (Thompson and Flower, 1971; Thompson, 1972; Cox and Jamieson, 1974).

Similar relationships to those described above were previously noted in the Nuanetsi picrite basalts (Cox and Jamieson, 1974). High pressure melting experiments were carried out on a number of Nuanetsi rocks by the above authors and it was found that in the absence of volatiles, pressures of between 7 and 10 Kb at temperatures of 1270°C and 1400°C were necessary to stabilise both olivine and orthopyroxene at the liquidus. Accordingly the magnesian olivine + mantled orthopyroxene assemblages were considered to represent high pressure (6 - 12 Kb) relicts whereas the remaining olivines and all the clinopyroxenes were considered to have crystallised at low pressures shortly before solidification of the lavas (Cox and Jamieson, 1974).

8.4 Whole Rock Chemistry and Petrogenesis

8.4.1 General Statement

A representative suite of northern Lebombo picrite basalts has been analysed and incorporated into a data set (Appendix F, Microfiche Tables F17, F22 and F28) which includes analyses of picrite basalts from Nuanetsi (Jamieson, 1969; UCT unpublished data) and Tuli (Vail et al., 1969). Selected major and trace element analyses as well as CIPW norms and inter-element ratios of basalts from the above areas are presented in Tables 8.10. The rocks are all hypersthene normative tholeiites and are characterised by a large range (approximately 9 - 24%) in MgO content. Average analyses of

TABLE 8.10 Selected analyses of picrite basalts from the northern Lebombo and Nuanetsi areas of southern Africa

	KP112	KP108	KP106	KP97	KP101	KP144	KP111	KS47	KS3	N245
%SiO_2	45.17	47.20	47.71	48.65	47.89	49.16	49.26	51.48	49.77	49.80
TiO_2	2.23	2.51	2.75	3.19	3.39	3.17	3.17	2.76	3.18	1.62
Al_2O_3	5.64	6.54	6.05	7.01	7.19	8.10	8.00	9.27	10.50	13.30
Fe_2O_3	11.52	11.59	11.46	11.59	10.58	10.60	10.60	11.66	12.49	12.24
MnO	.13	.14	.14	.14	.13	.13	.14	.17	.15	.16
MgO	23.02	20.52	20.17	16.44	15.69	14.53	13.92	11.80	10.60	9.65
CaO	4.68	5.62	5.38	6.22	6.27	6.40	6.71	8.70	8.39	9.36
Na_2O	.50	1.98	.59	.27	1.36	1.31	1.51	1.54	2.27	2.59
K_2O	2.52	.97	2.96	4.02	2.75	2.69	2.47	1.19	1.10	.76
P_2O_5	.38	.46	.43	.53	.58	.48	.55	.40	.45	.29
H_2O^+	3.63	3.29	2.08	1.91	3.22	2.12	3.14	1.22	1.32	1.36
H_2O^-	.90	.33	.60	.45	.43	.55	.81	.74	.54	
CO_2	.11								.08	
TOTAL	100.43	101.15	100.32	100.42	99.48	99.24	100.28	100.30	100.84	101.13
ppm Rb	61	67	65	82	90	53	101	28.8	58	11.0
Ba	967	1076	977	840	1084	1320	1154	627	588	656
Sr	795	956	934	870	1101	1417	1168	843	842	676
Zr	349	390	392	415	491	474	451	300	368	148
Nb	17.8	21.9	23.3	19.8	22.7	34	27.1	10.2	16.5	
Cr	931	861	954	858	796	700	792	731	503	730
V	143	155	174	200	194	180	201	213	240	
Sc	14.4	16.3	17.7	21	19	18.9	20.1	23.2	23.8	
Ni	1435	1306	1177	920	832	779	709	455	470	296
Co	95	105	88	77	71	70	66	63	64	
Zn	105	106	111	110	99	99	99	107	120	
Cu	54	74	72	84	75	84	91	85	107	
Y	20.8	22.6	22.9	26.5	27.6	27.5	27	27.9	35	

TABLE 8.10 Continued

	KP112	KP108	KP106	KP97	KP101	KP144	KP111	KS47	KS3	N245
Zr/Nb	19.6	17.8	16.8	21.0	21.6	13.9	16.6	29.4	22.3	
Zr/Y	16.8	17.3	17.1	15.7	17.8	17.2	16.7	10.8	10.5	
K/Rb	343	120	378	4070	254	421	203	343	157	574
K/Ba	21.6	7.48	25.2	398	21.1	16.9	17.8	15.8	15.5	9.62
K/Sr	26.3	8.42	26.3	384	20.7	15.8	17.6	11.7	10.8	9.33
K/Zr	59.9	20.6	62.7	804	46.5	47.1	45.5	32.9	24.8	42.6
K/Nb	1175	368	1055	16850	1006	657	757	969	553	
K/Y	1006	356	1073	12959	827	812	759	354	261	
Ba/Rb	15.9	16.1	15	10.2	12.0	24.9	11.4	21.8	10.1	59.6
Ba/Sr	1.22	1.13	1.05	.964	.985	.932	.988	.744	.698	.970
Ba/Zr	2.77	2.76	2.49	2.02	2.21	2.78	2.56	2.09	1.60	4.43
Rb/Sr	.077	.070	.070	.094	.082	.037	.087	.034	.069	.016
Mg //	82.6	80.7	80.6	76.9	77.7	76.2	75.3	70.0	66.1	64.3
				- C.I.P.W. NORMS -						
Qz	-	-	-	-	-	-	-	3.81		
Ne	-	-	-	-	-	-	-	-		
Or	14.89	5.73	17.49	23.76	16.25	15.90	14.60	7.03	6.50	4.49
Pl	9.93	22.85	10.11	8.33	16.90	19.36	20.53	27.90	34.42	44.34
Di	11.38	14.93	14.91	17.01	17.43	16.21	17.50	18.15	18.55	18.00
Hy	19.79	18.72	24.93	26.48	22.12	28.64	28.40	32.25	27.80	16.56
Ol	31.29	26.23	20.81	12.01	12.47	6.48	5.20	-	1.24	9.52
Mt	2.25	2.23	2.18	2.17	1.95	1.93	1.88	2.01	2.10	2.03
Il	4.24	4.77	5.22	6.06	6.44	6.02	6.02	5.24	6.04	3.08
Ap	.90	1.09	1.02	1.26	1.37	1.14	1.30	.95	1.07	.69
Cc	.25									

KEY TO TABLE 8.10

KP112	-	Picrite basalt : Pafuri area, Northern Lebombo
KP108	-	Picrite basalt : Pafuri area, Northern Lebombo
KP106	-	Picrite basalt : Pafuri area, Northern Lebombo
KP97	-	Picrite basalt : Pafuri area, Northern Lebombo
KP101	-	Picrite basalt : Pafuri area, Northern Lebombo
KP144	-	Picrite basalt : Pafuri area, Northern Lebombo
KP111	-	Picrite basalt : Pafuri area, Northern Lebombo
KS47	-	Picrite basalt : Shingwedzi River, Northern Lebombo
KS3	-	Picrite basalt : Shingwedzi River, Northern Lebombo
N245	-	Picrite basalt : Nuanetsi

the Lebombo, Nuanetsi and Tuli picrite basalts are presented in Table 8.11 along with a selection of average analyses calculated for picritic rocks from localities outside southern Africa, viz. India, Iceland and Greenland. Inspection of Table 8.11 shows that the Karoo picrite basalts have an average MgO content of about 15% and are slightly depleted in Al_2O_3 and CaO relative to picritic rocks with similar abundances of MgO, eg. picrite basalts from India. Most significant however, is that data presented in Table 8.11 (and Table 8.10) shows that the picrite basalts are extremely enriched in K_2O (up to 4%) TiO_2, P_2O_5, Rb, Ba, Sr and Zr relative to other picrite lava sequences characterised by more or less the same spread in MgO contents, e.g. picritic lavas from India (Krishnamurthy and Cox, 1977), Iceland (Jakobsson et al., 1978) and Greenland (Clarke, 1970). The enrichment with respect to K and associated elements in the Karoo picrite basalts has in the past drawn considerable comment from, amongst others, Jamieson (1969), Jamieson and Clarke (1970), Cox (1972b) and Cox and Jamieson (1974) and will be discussed later.

Inspection of Table 8.11 also shows that the picrite basalts derived from the different Karoo localities (viz. northern Lebombo, Nuanetsi and Tuli) are characterised by variable degrees of enrichment with respect to K_2O and other elements listed above. Average MgO values are much the same for rocks from all three localities which suggests that variable degrees of ferromagnesian mineral fractionation is an unlikely explanation for the apparent differences in enrichment. It is therefore more likely that the variations reflect a primary feature of the parental magmas from which the different lava successions crystallised. Interlaboratory bias could also account for the apparent differences in the geochemistry of the individual provinces. However, reruns of samples from the Nuanetsi area in the UCT analytical laboratory have shown that the older Nuanetsi and Tuli data which

TABLE 8.11 Average analyses of picrite basalts from the Karoo (Lebombo, Nuanetsi, Tuli), India, Iceland and Greenland.

	1	2	3	4	5	6	7	8	9	10
$\%SiO_2$	49.97	49.49	49.25	49.58	49.79	46.91	47.12	44.27	45.86	48.26
TiO_2	3.07	2.70	3.02	2.83	2.88	2.03	1.05	.58	.77	.99
Al_2O_3	8.22	8.82	8.57	8.64	9.01	9.61	14.40	8.35	10.98	14.02
Fe_2O_3*	12.02	12.34	13.62	12.42	12.44	11.92	11.00	12.05	11.59	10.92
MnO	.16	.15	.15	.15	.15	.17	.17	.19	.18	.17
MgO	15.52	15.20	14.78	15.22	14.23	15.11	12.71	26.16	20.03	11.99
CaO	7.07	7.54	6.76	7.33	7.61	11.62	11.74	7.35	9.35	11.89
Na_2O	1.43	1.63	1.65	1.58	1.68	1.54	1.64	.91	1.06	1.55
K_2O	2.10	1.70	1.82	1.82	1.79	.80	.08	.06	.08	.10
P_2O_5	.45	.43	.38	.43	.43	.29	.09	.07	.09	.10
ppm Rb	51	34	41	39	38	24		1	2	2
Ba	871	793	914	829	810	320		44	55	56
Sr	955	856	1024	904	899	275		87	186	161
Zr	379	308	435	343	340	135		45	52	66
Nb	18	19	22	19	19	35				
Cr	758	941		889	838					
V	204	191		197	208					
Sc	20	21		20	21					
Ni	777	761		766	674					
Co	77	88	58	75	71					
Zn	104	103	115	106	105			60	58	57
Cu	78	72		75	80			81	109	133
Y	26	25		26	27	22		13	18	21

KEY TO TABLE 8.11

1. Average northern Lebombo picrite basalt (N = 19).
2. Average Nuanetsi picrite basalt (N = 48).
3. Averate Tuli picrite basalt (N = 10).
4. Average of all Lebombo, Nuanetsi and Tuli picrite basalts (N = 77).
5. Average of all Lebombo, Nuanetsi and Tuli picrite basalts with 9-18% MgO (N = 65).
6. Average of 5 Deccan Traps picrite basalts (Analyses 1-5, Table 5; Krishnamurthy and Cox, 1977).
7. Average of 14 olivine and picrite basalts from the Reykjanes Peninsula, Iceland (Analyses 1-14, Table 3; Jakobsson, et al., 1978).
8. Average of 12 Group I picrite basalts from Baffin Island (Analysis 1, Group I picrite basalts; Clarke, 1970).
9. Average of 4 Group II olivine basalts from Baffin Island (Analysis 3, Table 1; Clarke, 1970).
10. Average of 21 Group III olivine-poor basalts from Baffin Island (Analysis 5, Table 1; Clarke, 1970).

was obtained from different sources is reliable for most elements. As noted previously (section 4.3) those elements which do show interlaboratory bias were excluded from the data compilation used in this thesis.

Temporal geochemical relationships shown by the northern Lebombo picrite basalts are also relevant to the present discussion. Analytical data derived from a considerable number of slab analyses (see section 5.1 and Appendix A3) show that the most incompatible enriched picrite basalts crop out at the base of the high-MgO lava succession. This relationship is also shown by conventional major and trace element analyses presented in Table 8.10 since the most K-rich picrite basalts, viz. samples KP106 (K_2O = 2.96%) and KP97 (K_2O = 4.02%), both crop out just above the nephelinite-picrite basalt contact. In contrast the less enriched northern Lebombo basalts presented in Table 8.10, e.g. KP111 (K_2O = 2.47%) and KS3 (K_2O = 1.10%), were collected from the uppermost portion of the Letaba River Formation. Furthermore, it was also found that the lowermost outcrops of picrite basalts were, in general, characterised by a greater proportion of very high MgO (~ 14 - 20%) glassy and fine grained lavas, whereas lavas higher in the succession were generally more evolved with respect to MgO (9 - 14%) and were invariably fine to medium grained. The few lavas found to contain well formed plagioclase phenocrysts or microphenocrysts, e.g. KS3, KS47, were sampled in the upper portion of the picritic lava succession and it is notable that they are both characterised by relatively low-MgO abundances, 11.80% and 10.60% respectively. The implications of both the spatial and temporal geochemical relationships noted above will be discussed in a later part of this chapter.

8.4.2 Major and Trace Element Variations

Major and trace element concentrations are plotted against MgO in Figures 8.5, 8.6 and 8.7. Initial examination of the plots show several

Figs. 8.5 a-e Major element variation diagrams for the northern Lebombo, Nuanetsi and Tuli picrite basalts. Average mineral compositions are indicated on the diagrams where possible.

Average mineral compositions:

1. Olivine $Fo_{86}\ Fa_{14}$
2. Olivine $Fo_{78}\ Fa_{22}$
3. Mantled Orthopyroxene $Wo_3\ En_{85}\ Fs_{12}$
4. Unmantled Orthopyroxene $Wo_5\ En_{79}\ Fs_{16}$
5. Clinopyroxene $Wo_{40}\ En_{49}\ Fs_{11}$

   (Note: On the SiO_2 versus MgO diagram this clinopyroxene composition plots at 52% MgO and 17% MgO).

(Data from Microfiche Tables F17, F22, F28, Appendix F)

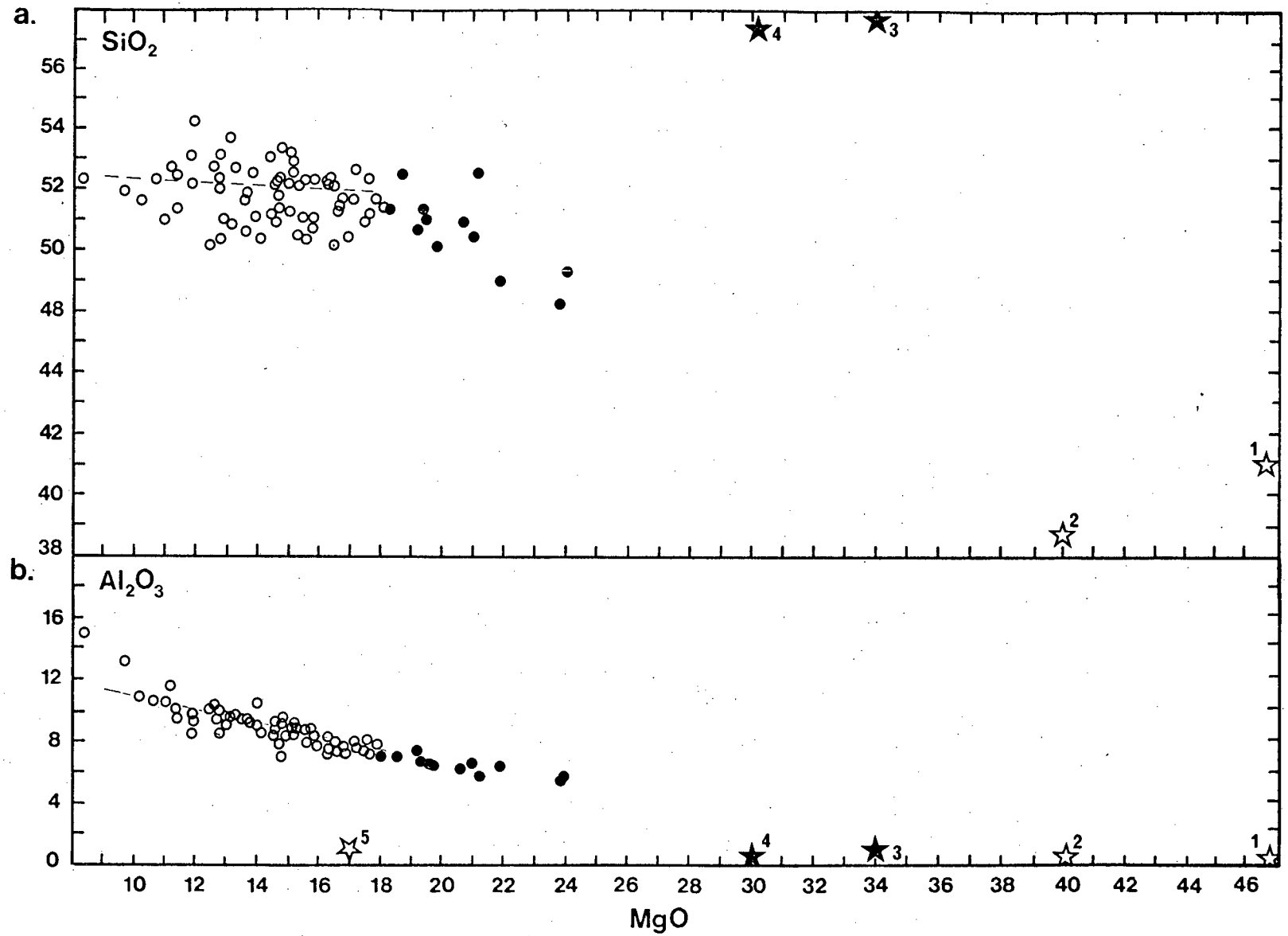
a.
SiO2
56
54
52
50
48
44
42
40
38
1
2
3
4
b.
Al2O3
16
12
8
4
0
5
10
12
14
16
18
20
22
24
26
28
30
32
34
36
38
40
42
44
46
MgO

Fig. 8.5

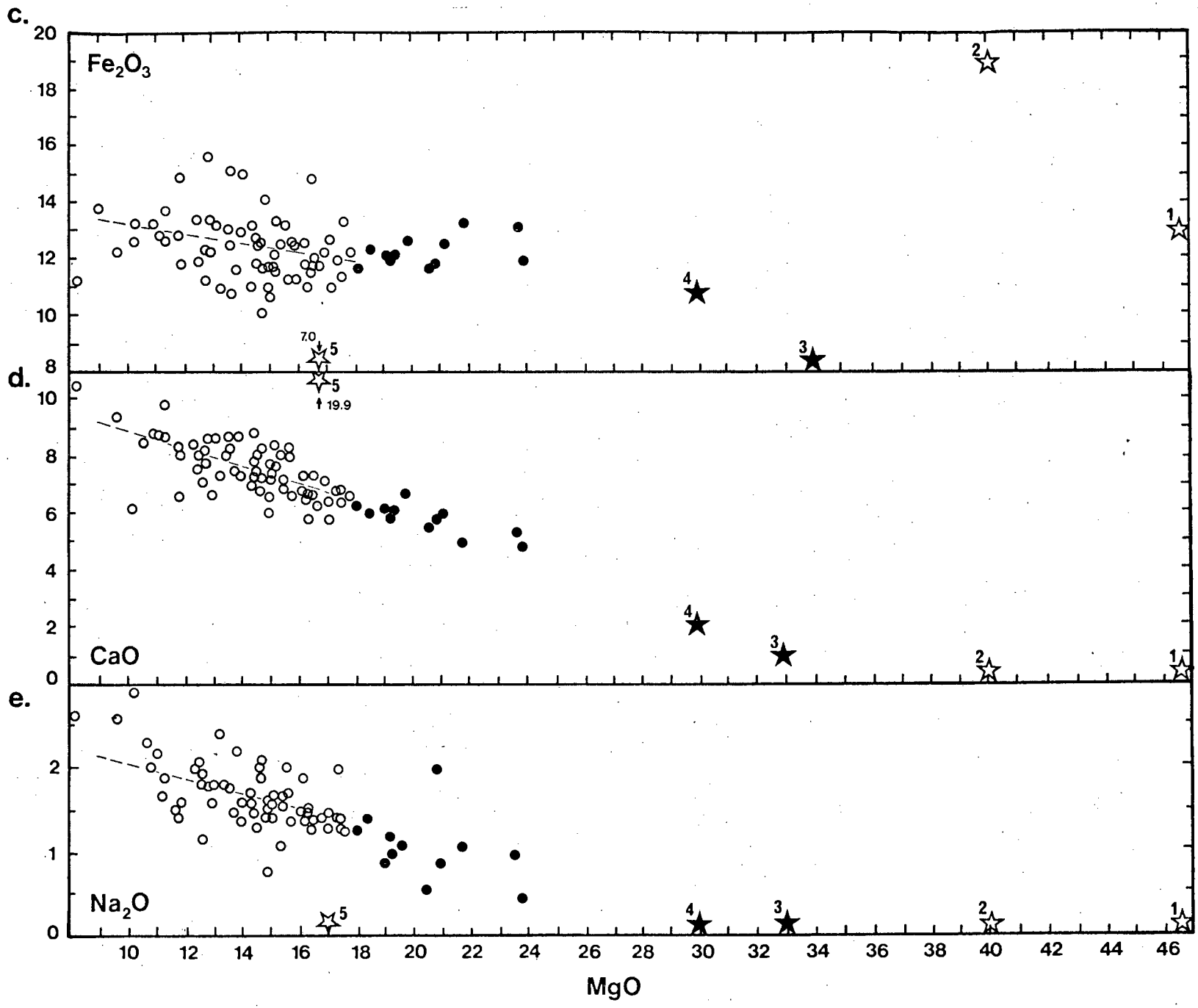
c.
Fe_2O_3
d.
CaO
e.
Na_2O
MgO
7.0
19.9
1
2
3
4
5

important points; (i) though a relatively large amount of scatter is apparent in the diagrams, the lavas do nevertheless show a reasonably coherent serial variation; (ii) the majority of the data plots show a 'kink' or change in trend direction in the vicinity of 18% MgO and trend lines have therefore only been fitted to the data between 9 - 18% MgO; (iii) in the range 9 - 18% MgO the major and minor elements K_2O, P_2O_5 and TiO_2 and trace elements Ba, Sr, Rb, Zr and Nb, collectively referred to as K and related elements (Jamieson and Clarke, 1970; Cox and Jamieson, 1974) and hereafter referred to as the KAR elements, are aberrant in their behaviour and do not show the trend lines that would be expected of a suite of mafic lavas generated by fractional crystallisation of ferromagnesian minerals from a basic liquid. Within this range all six elements show slight positive correlations with MgO (Table 8.12) whereas in normal circumstances, e.g. picrite basalts of the Deccan Traps (Krishnamurthy and Cox, 1977), they would typically show strong negative correlations with MgO. The petrogenetic aspects of this problem will be dealt with in a subsequent section.

With the exception of KAR elements the major element plots (Fig. 8.5) show that the main variation in the picrite-basalts within the range 9 - 18% MgO can be explained in terms of extraction of olivine and orthopyroxene from a melt(s) which probably contained 18% or less MgO. Figures 8.5 a-e show that in all cases the trend lines fitted to the data in the range 9 - 18% MgO back project towards the olivine-orthopyroxene join. (Where possible, the positions of the average compositions of Group I and Group II olivines, mantled and unmantled orthopyroxenes and clinopyroxene phenocrysts encountered in the northern Lebombo picrite basalts are indicated on the major element variation diagrams, Figure 8.5).

TABLE 8.12 Correlation coefficients for picrite-basalts with 9 - 18% MgO

Rb	+.62										
Ba	+.76	+.58									
Sr	+.73	+.65	+.88								
Nb	+.30	+.37	+.36	+.46							
Zr	+.71	+.69	+.74	+.83	+.02						
P	+.63	+.62	+.57	+.65	+.63	+.51					
Ti	+.55	+.57	+.53	+.69	+.27	+.71	+.66				
Y	+.06	+.28	+.07	+.14	+.19	+.11	+.09	+.41			
Zn	-.15	+.00	1.04	+.02	-.32	+.21	-.08	+.24	+.25		
Cu	-.17	-.01	-.16	-.13	+.14	-.09	-.12	+.00	+.38	-.15	
Si	+.20	+.28	+.30	+.30	+.01	+.21	+.24	+.10	+.08	-.25	-.05
Fe	-.44	-.34	-.48	-.34	-.15	-.13	-.45	-.16	-.23	+.46	+.24
Na	-.42	-.23	-.12	-.12	+.26	-.32	-.09	-.32	+.36	-.03	+.30
Al	-.42	-.41	-.34	-.35	+.11	-.50	-.31	-.45	+.64	-.25	+.45
Ca	-.65	-.52	-.59	-.55	-.15	-.66	-.35	-.30	+.49	-.08	+.24
Mg	+.25	+.20	+.20	+.09	-.14	+.29	+.08	+.06	-.76	+.03	-.38
Ni	+.46	+.41	+.33	+.33	-.04	+.43	+.27	+.25	-.73	-.05	-.30
Cr	+.27	+.28	+.31	-.27	+.03	+.24	+.32	+.02	-.79	-.09	-.56
Co	-.17	+.04	-.46	-.33	-.65	-.05	-.21	-.31	-.32	-.07	-.50
Sc	+.01	+.03	+.02	+.17	+.13	-.13	+.26	+.42	+.61	-.25	+.45
	K	Rb	Ba	Sr	Nb	Zr	P	Ti	Y	Zn	Cu

Confidence limits: 1% - .283, 5% - .217

The behaviour of SiO_2, Al_2O_3 and MnO (not shown) clearly indicate that both olivine and orthopyroxene should be included in the fractionating assemblage whereas CaO and Fe_2O_3* also fit the pattern but do not distinguish between the two ferromagnesian phases. In general the position of the intersection of the 'trend line - ferromagnesian mineral join' indicates a slightly greater degree of orthopyroxene extraction relative to olivine. In addition it is apparent that the position of clinopyroxene in the Al_2O_3 - MgO and CaO - MgO diagrams (Figs. 8.5 a and b respectively) lie at almost right angles to the main compositional trend of the lavas and thus show that this phase was unlikely to have constituted any significant proportion of the fractionating assemblage. This relationship is also borne out to a lesser extent by the Fe_2O_3 - MgO and Na_2O - MgO diagrams.

Rocks with MgO contents exceeding 18% clearly do not lie on the general fractionation trend defined by lavas in the range 9 - 18% MgO. Instead, variations within lavas in the range 18 - 25%MgO appear to be more closely related to olivine control alone. This relationship is probably best shown amongst the major elements on plots of MgO versus SiO_2 (Fig. 8.5a) and Fe_2O_3* (Fig. 8.5c). In particular, the SiO_2 versus MgO diagram shows that orthopyroxene played at most, a very minor role as a fractionating phase in rocks with greater than 18% MgO and in both plots the trends shown by the data lying above 18% MgO back projects towards an extract consisting predominantly of an evolved olivine $\pm$ minor amounts of orthopyroxene. KAR elements also show a change in the slope of the general variation trend above 18% MgO (Figs. 8.7 a-h) and it is notable that the positive correlation found between MgO and KAR elements in the range 9 - 18% MgO is reversed in the lavas with MgO > 18%; in most cases the previously positive trend becomes weakly negative.

Petrographic studies have shown that in general rocks with MgO > 18% are characterised by high modal contents of olivine (see Table 8.1) and are

seldom glassy such that on the basis of petrographic data lavas with greater than 18% MgO would appear to represent picrite basalts that have been strongly enriched in cumulus olivine (± minor orthopyroxene). Consequently the major element relationships shown by lavas with greater than 18% MgO appear to be compatible with the incorporation of excessive amounts of olivine into magmas with approximately 18% or less MgO. Similarly, the change in slope from positive to flat or slightly negative shown by the KAR elements in the range 18 - 24% MgO can best be explained as a dilution effect caused by the addition of olivine (± minor orthopyroxene) to magmas with initially higher incompatible element concentrations, but lower (less than 18%) MgO contents. On the basis of the petrographic and geochemical variations shown by the picrite lavas, it is therefore possible that the olivine rich basalts of the Karoo may have crytallised from parental picritic magmas with up to 18% MgO. This point will be reiterated later.

The development of lavas with MgO values in excess of the parental liquid composition (assumed for the present to be 18% MgO or less) may occur in several ways. Gravitative settling and accumulation of olivine crystals in a magma chamber and crystal settling in a lava flow are probably the two most important mechanisms whereby parental liquid compositions may be significantly changed. For example investigation of a picrite-basalt flow in Iceland (Jakobsson et al., 1978) has shown that the variation within a single flow may be as much as 10.7 - 28.8% MgO. Though this would appear to represent an extreme case since variations in other Icelandic flows have been found to be much less, it is nevertheless an important aspect and should be taken into account when interpreting analyses of randomly collected olivine-rich lava samples. Because of the extremely poor exposure in the northern Lebombo it was impossible to establish where, in relation to the flow boundaries, samples were collected from and the

possibility that some samples represent cumulate enriched flow bases cannot be excluded. The effects of crystal accumulation in a magma chamber are no doubt equally important and will be discussed later.

In addition to those samples which may have been enriched in cumulus olivine (+ minor orthopyroxene) some picritic lavas which are strongly enriched in cumulus orthopyroxene are also found in both the northern Lebombo and Nuanetsi (see Cox and Jamieson, 1974). Northern Lebombo sample KS47 represents a good example of a lava enriched in orthopyroxene. It is characterised by an unusually high content of modal orthopyroxene (13.6%, Table 8.1) and is displaced along orthopyroxene control in plots such as SiO_2 versus MgO (Fig. 8.6a). However, the effect of orthopyroxene is not as distinctive as that shown by rocks enriched in olivine.

8.4.3 Other Trace Elements

Elements referred to as the 'other trace elements' include Cr, Y, Ga, Sc, V, Zn, Cu and Co. Cr and Y are plotted against MgO in Figure 8.6 whereas plots of the remaining elements have been omitted because fewer analyses have been obtained for these elements. However, the available data do in general show variations which are in agreement with olivine and orthopyroxene fractionation from high magnesian liquids to form the observed range of picrite basalts. V shows a slight overall enrichment with increasing differentiation compatible with olivine and orthopyroxene fractionation whereas Zn and Cu show rather scattered and relatively flat trends when plotted against MgO. Co on the other hand shows a relatively well defined decrease with decreasing MgO which is compatible with the relatively high distribution coefficients shown by both olivine (D^{Co}_{ol} = 2.75 - 4.44; Dale and Henderson, 1972) and orthopyroxene (D^{Co}_{opx} = 1.61 - 6.43; Le Roex, 1980). Cr is plotted against MgO in Figure 8.6a. The data is relatively scattered but does nevertheless show a

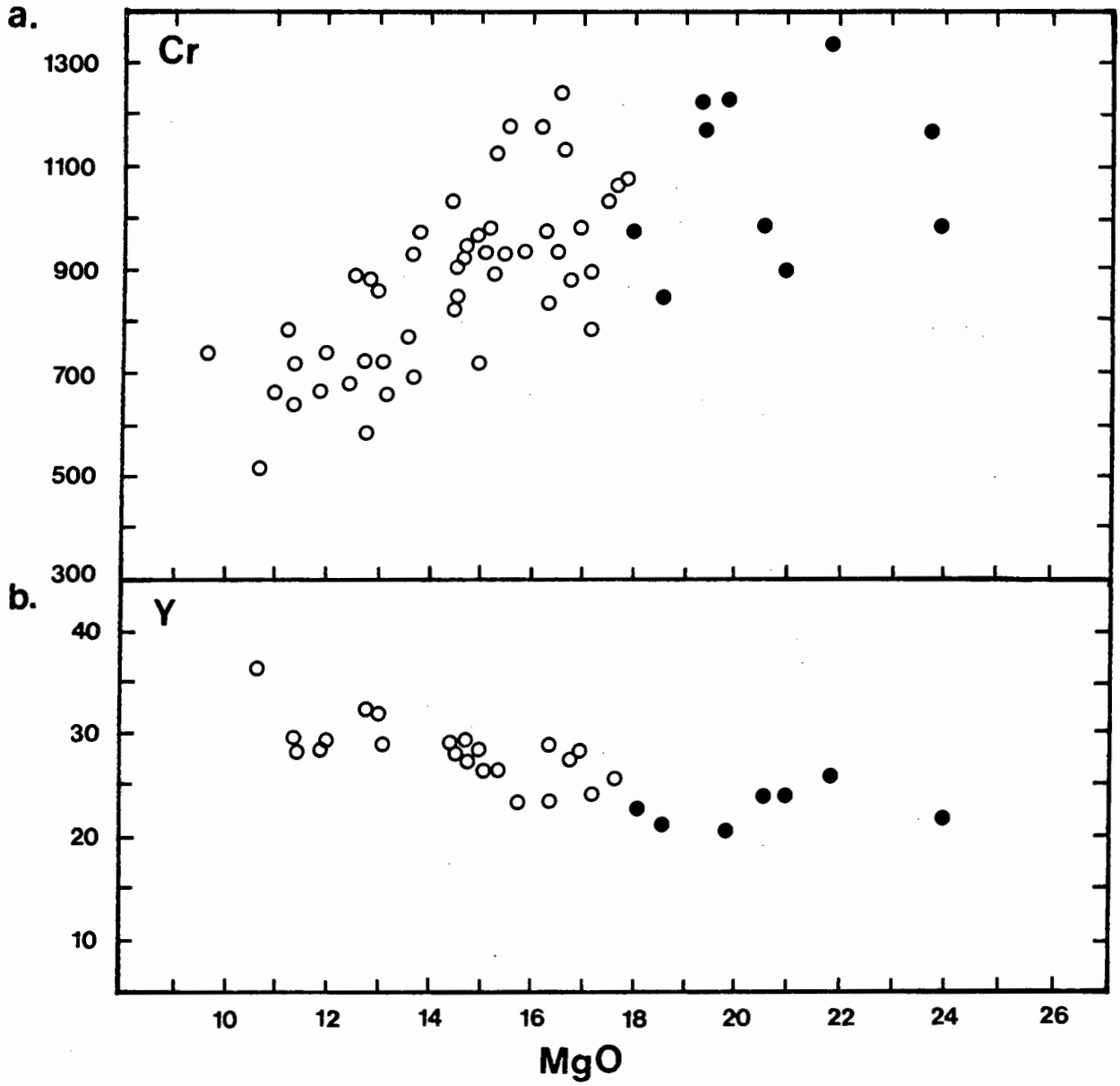

Fig. 8.6 Plots of Cr and Y versus MgO for the picrite basalts of the Lebombo, Nuanetsi and Tuli areas. (Symbols as in Figures 8.5.)

reasonably well defined trend of decreasing Cr with increasing differentiation that may be explained in terms of fractionation of olivine and orthopyroxene from a parental magma with a relatively high MgO content. Ni shows a similar relationship (see Fig. 8.9) but will be discussed in more detail in section 8.5.5.

Y is the only member of the normal group of incompatible elements (e.g. Zr, Nb, Y) which behaves as expected in the picrite basalts. It is plotted against MgO in Figure 8.6b and shows an overall increase with decreasing MgO though there is a fair amount of scatter in the data plotted on the variation diagram. In this respect Y appears to have been decoupled from the elements Zr and Nb since both Zr and Nb show considerable scatter and poorly defined positive trends when plotted against MgO (Fig. 8.7). In addition Zr shows an unusually high level of enrichment in the Karoo picritic rocks (see Table 8.11) whereas the average value obtained for Y is only marginally higher than Y abundances in picritic rocks from other localities, e.g. India.

8.4.4 KAR Elements

As noted previously plots of KAR elements (Figs. 8.7 a-h) indicate that there is generally a crude trend of enrichment with increasing MgO in the range 9 - 18% MgO which is reflected by the weak positive correlations in the correlation data listed in Table 8.11. The data plotted in Figures 8.7 a-h also indicate that the KAR elements show different rates of enrichment with respect to MgO. K_2O would appear to show the largest degree of enrichment whereas P_2O_5 and TiO_2 are characterised by very samll degrees of enrichment as MgO increases. This is to some extent reflected by the higher positive correlation coefficients between K_2O and MgO. However, in the case of elements such as TiO_2 and P_2O_5 the presence of positive trends is a somewhat subjective issue such that the point to be stressed is that

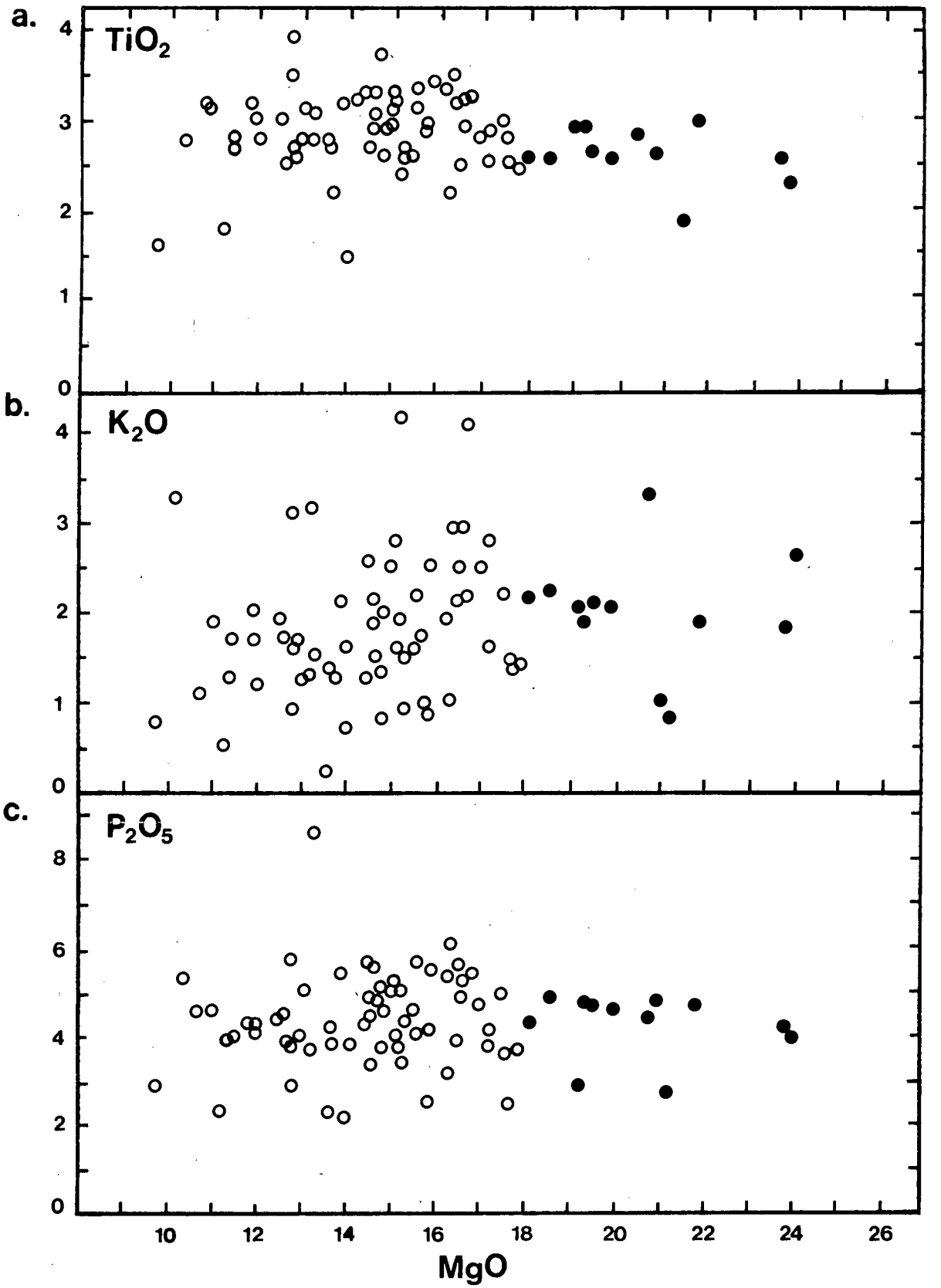

Fig. 8.7 KAR element variation diagrams for the Lebombo, Nuanetsi and Tuli picrite basalts. (Symbols as in Figures 8.5.)

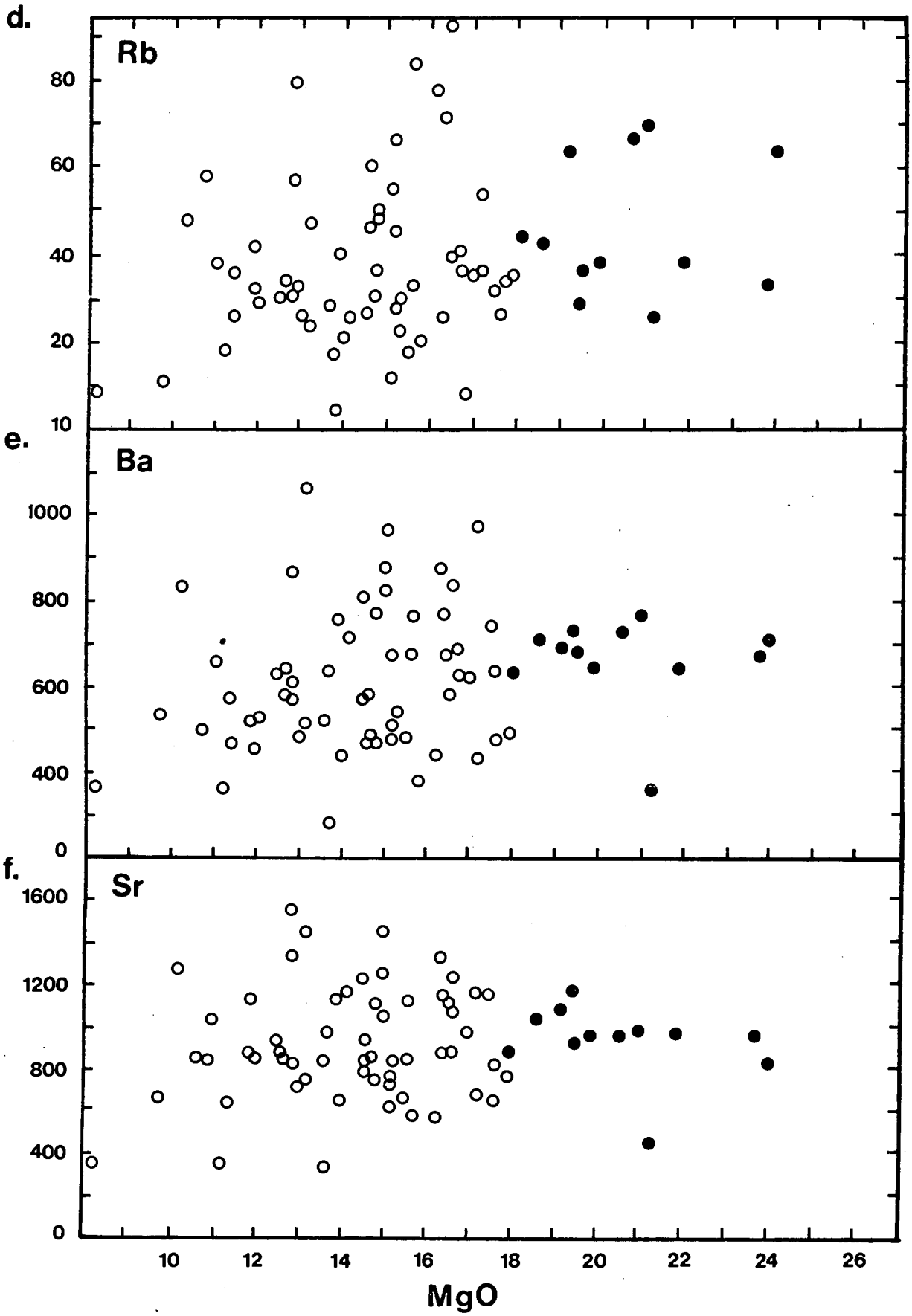
d.
Rb
80
60
40
20
10
e.
Ba
1000
800
600
400
0
f.
Sr
1600
1200
800
400
0
10
12
14
16
18
20
22
24
26
MgO

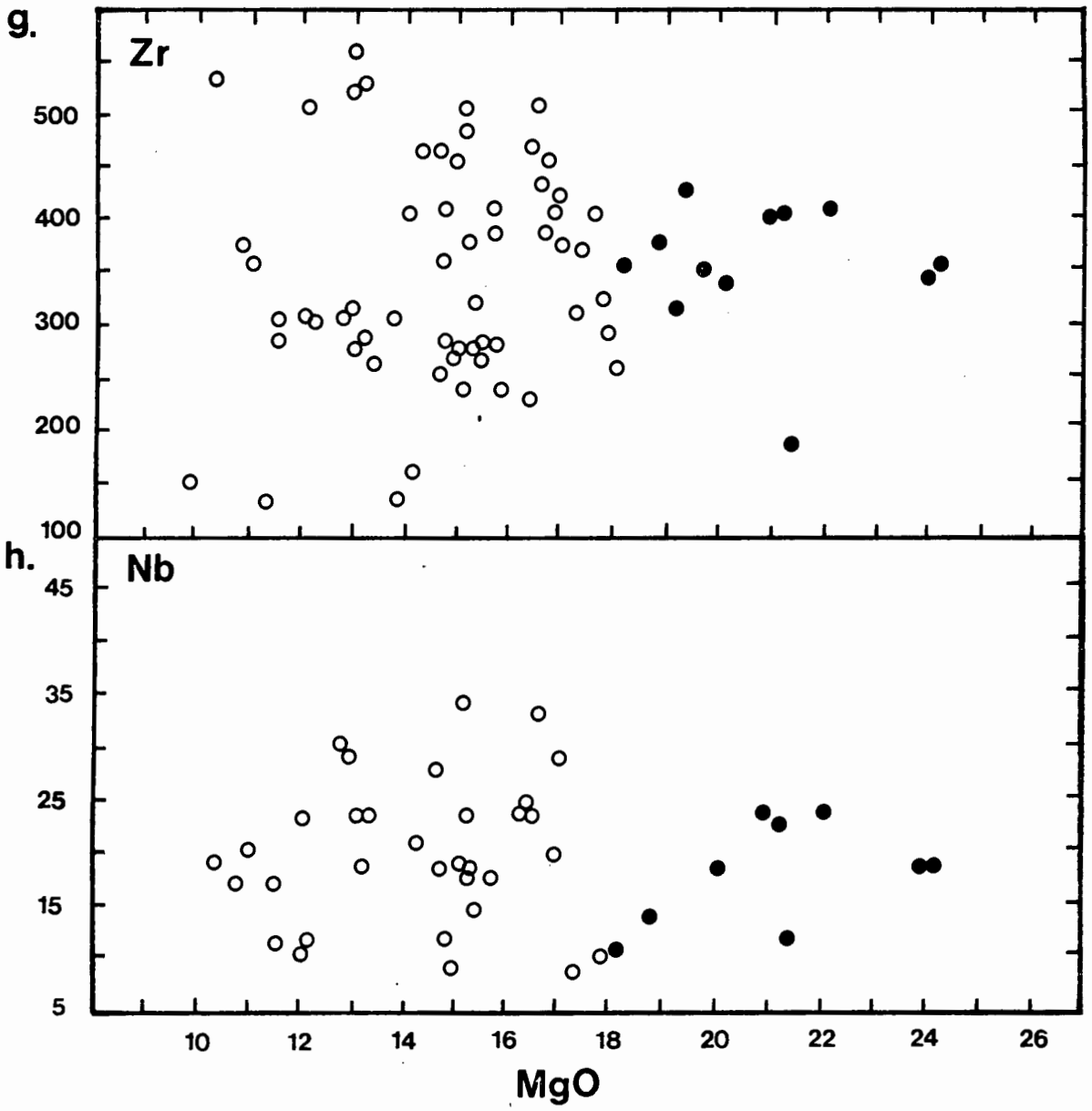
g.
Zr
500
400
300
200
100
h.
Nb
45
35
25
15
5
10
12
14
16
18
20
22
24
26
MgO

in all the variation diagrams (Figs. 8.7 a-h) the usually expected inverse correlation between MgO and the KAR elements is not developed.

Correlations between individual KAR elements are strong for rocks with 9 - 18% MgO and values of as high as 0.90 are apparent for some pairs of elements, eg. Sr and Zr (Table 8.12). Most of the incompatible element pairs have correlations of about 0.50 with the exception of those involving Nb which are generally lower. The relatively poor correlations apparent between some element pairs can be partly explained in relation to enrichment rates shown by the individual elements. Clearly, correlations between those elements such as K_2O and Rb which show reasonably well constrained enrichment trends when plotted against MgO will be good, whereas correlations between data which are less tightly constrained when plotted against the fractionation index will be poor.

The considerable scatter shown by the incompatible element data on the variation diagrams (Figs. 8.7 a-h) warrants comment. Some of the scatter may reflect primary variations in the magma from which the lavas were derived. However, within the overall positive trends shown by KAR elements and MgO there are sub-sets of data which show relatively well defined negative trends suggesting that fractionation of olivine $\pm$ orthopyroxene has modified the original positive trend by either enriching (by olivine $\pm$ orthopyroxene removal) or diluting KAR elements (by olivine $\pm$ orthopyroxene addition). Control lines (not shown) drawn through these trends back project to relatively evolved olivine-orthopyroxene compositions (in terms of Fe and Mg) implying that crystal fractionation at relatively low-pressures (see following section) may have been responsible for some of the scatter apparent in the variation diagrams.

8.4.5 Summary

In summary it is apparent that the chemical variation (excluding KAR elements) within the picrite basalts with 9 - 18% MgO can be explained in terms of fractionation of relatively magnesian olivines and orthopyroxenes (ie. Group I olivines and mantled orthopyroxenes). Furthermore Cox and Jamieson (1974) were able to show by means of high pressure melting experiments that in the absence of volatiles, pressures of 7 to 10 Kbars and temperatures of 1 275° to 1 400°C were necessary to stabilise both olivine and orthopyroxene on the liquidus in the Nuanetsi picrite basalts and postulated a high-pressure fractionation mechanism. Mineral liquidus temperatures calculated for a series of northern Lebombo picrite basalts yield similar temperatures for olivine and orthopyroxene (Table 8.13) and since the Lebombo and Tuli picrite basalts show the same compositional trends and mineralogical characteristics as the Nuanetsi rocks it is assumed that the evolution of the high-MgO lavas from all three areas was controlled by similar processes, viz. high pressure fractionation of magnesian olivine and orthopyroxene.

Fractionation of olivine with evolved compositions e.g. Group II olivines, and clinopyroxene clearly played no (or very little) part in generating the overall major element variation shown by the suite of lavas with 9 - 18% MgO though may be responsible for variations noted in lavas with more than 18% MgO. Similarly some of the scatter apparent in data with less than 18% MgO may reflect localised fractionation of the low pressure olivine + clinopyroxene assemblage. Even though plagioclase was noted as phenocrysts in a few lavas, the existence of an extract incorporating significant amounts of this mineral can be discounted on the basis of the MgO-Al_2O_3 and MgO - CaO relationships shown by the picritic lavas. The relationship shown by K_2O when plotted against MgO (Fig. 8.7a) suggests that a phlogopite-bearing extract should perhaps be considered. However, Al_2O_3 -

TABLE 8.13 Liquidus temperatures calculated for a series of northern Lebombo picrite basalts.

Sample	MgO%	Mineral Liquidus Temperatures and Compositions	
		Olivine	Orthopyroxene
KS3	10.72	1237^{o} (Fo_{87})	1288^{o} (En_{89})
KP111	14.45	1291^{o} (Fo_{91})	1268^{o} (En_{93})
KP121	14.59	1297^{o} (Fo_{90})	1265^{o} (En_{92})
KP101	16.37	1317^{o} (Fo_{92})	1278^{o} (En_{93})
KP97	16.77	1335^{o} (Fo_{92})	1281^{o} (En_{93})
KP106	20.66	1384^{o} (Fo_{93})	1320^{o} (En_{94})

(Temperatures in °C)

NOTE: Results presented in this table were derived from a Liquidus Temperature Computer Program (XTALS) written by Dr A.R. Duncan of the Department of Geochemistry, U.C.T. The program uses Nathan and Van Kirk (1978) distribution coefficients and liquidus mineral data to calculate the temperatures of the liquidus mineral assemblage in equilibrium with a particular magma composition.

MgO relationships (Fig. 8.5b) are quite incompatible with the large proportion of phlogopite (an Al-rich phase) which would be required to satisfy the K_2O - MgO relationship (cf. Cox and Jamieson, 1974). As such, the behaviour of the K_2O and for that matter, the remaining KAR elements does not tally with an olivine and orthopyroxene fractionation process. This problem is therefore treated independantly in a subsequent section.

8.5 Choice of Parental Composition and the Existence of High-MgO Liquids in the Eastern Karoo

8.5.1 General Statement

A problem in the evaluation of fractional crystallisation and partial melting processes for the picrite basalts from the Lebombo, Nuanetsi and Tuli is the extent to which postulated parental magmas represent liquid compositions. Chill margins on intrusive bodies, fresh aphyric lavas and quenched glass rinds on pillow basalts can in general, be taken to represent liquid compositions. In contrast, lavas with varying proportions of phenocrysts pose a problem since crystal accumulation (or removal) may significantly alter the composition of the parental liquid. Even more problematical are those lavas which though highly porphyritic, have maintained their original chemistry due to processes of compensated crystal settling (Cox and Bell, 1972; Krishnamurthy and Cox, 1977).

The recognition of liquid compositions amongst porphyritic lavas has raised considerable comment and controversy in past and present years, particularly with respect to the existence of high-MgO picritic or ultrabasic liquids (e.g. see Clarke and O'Hara, 1979). Rocks within this category which were entirely liquid at the time of eruption are exceptionally rare and most picrite basalt lava successions are characterised by olivine phenocrysts or microphenocrysts. Nevertheless on the basis of field, petrographic and experimental studies many petrologists (e.g.

Clarke, 1970; Cox, 1978; Elthon, 1979; Clarke and O'Hara, 1979; Duncan and Green, 1980) now firmly believe that high-MgO, picritic or ultrabasic liquids exist in nature. In addition a large proportion of these people (e.g. Elthon, 1979; Clark and O'Hara, 1979; Duncan and Green, 1980) adhere to the belief that the high-MgO liquids represent parental magmas to most of the observed low-MgO basaltic succession. However, some geochemists, in particular geochemists involved in trace element studies (e.g. Hart and Davis, 1978) maintain that the low-MgO basalts which are so preponderant on the earth's surface (continental and oceanic) represent primary magmas and that the picritic volcanics are in general derived by olivine accumulation.

Bowen (1928) was probably the first petrologist to comment on the problem of porphyritic, high-MgO lavas. He noted that all the highly magnesian lavas he examined were olivine-phyric and concluded that basaltic liquids with normative olivine greater than approximately 10% could not exist in nature. However, Bowen's (1928) views were not supported by Drever (Drever and Johnston, 1957) who was one of the earliest advocates of high magnesian liquids. Drever proposed that high-MgO lavas characterised by rapidly grown crystals, usually olivines with embayed and skeletal habit could be regarded as liquids whereas lavas with larger unembayed crystals had probably been enriched in MgO due to accumulation of phenocrysts.

The subsequent discovery of komatiites (Viljoen and Viljoen, 1969) with spinifex textures which were considered to represent skeletal growths from quenched liquids, provided additional evidence for the existence of high-MgO primary liquids. Furthermore, Donaldson (1976) was able to reproduce a wide range of skeletal olivine growth forms in experimental charges by quenching melts of natural and synthetic high-MgO liquids. Examples of

skeletal crystallisation forms found in nature are well illustrated in the literature (e.g. Bryan, 1972; Nesbitt, 1971; Pyke et al., 1973; Bickle et al., 1975) though the presence of skeletal crystals need not necessarily imply that the lavas represent original liquid compositions since it has been shown (Pyke et al., 1973) that spinifex olivines can themselves sink after the extrusion of the lavas and form olivine-enriched cumulate layers.

Studies of oceanic and oceanic island basalts have focused much attention on the problem of high-MgO basaltic precursors (e.g. see O'Hara, 1965, 1968b; Green and Ringwood, 1967; Donaldson and Brown, 1977; Jakobsson et al., 1978; Maaløe, 1979; Duncan and Green, 1980). Though no high-MgO glasses have been found (MgO = 9.15% in average glass from the Famous area (Bryan and Moore, 1977) and 7.72% in average oceanic tholeiite glass (ref. in Elthon, 1979)) in the oceanic environment, highly magnesian aphyric lavas have been described from Baffin Island and Svartenhuk (Clarke 1970; O'Nions and Clarke, 1972), and Chile (Elthon, 1979) while high magnesian porphyritic rocks are reported from the Solomon Islands (Stanton and Bell, 1969; Cox and Bell, 1972) and Reykjanes Peninsula (Jakobsson et al., 1978). On the basis of the petrography, mineralogy and general chemical relationships of these high-MgO rocks several authors (e.g. Clarke, 1970; Cox and Bell, 1972; Jakobsson et al., 1978; Elthon, 1979) have concluded that they either represent primary magmas or else crystallised from high- MgO liquids.

Porphyritic high-MgO lavas (excluding komatiites) are found in continental environments though they are less common than in oceanic provinces. Examples of high-MgO continental lavas are found in the western part of the Deccan Traps (Krishnamurthy and Cox, 1977) and in the Nuanetsi (Cox et al., 1965; Jamieson, 1969), Tuli (Vail et al., 1969) and northern Lebombo (this thesis) areas of the Karoo province. Papers discussing the

petrographic and geochemical relationships of the Deccan and Karoo picritic rocks have been published by Krishnamurthy and Cox (1977), Cox (1978) and others and in the light of these studies, Cox (1978) has proposed that at least some of the porphyritic picrite lavas found in the Deccan and Karoo crystallised from high-MgO liquids.

From the above discussions it is apparent that though high-MgO lavas are relatively abundant in nature, there is often doubt as to whether or not they crystallised from high-MgO liquids. Porphyritic rocks undoubtedly pose the greatest problems though Cox (1978) has introduced the term 'primitive porphyritic magma' to describe the magmas from which such rocks may have crystallised. In the following sections a detailed assessment is made of the field and petrographic relationships, and mineral and whole rock chemistry (specifically the Fe-Mg-Ni distribution between olivines and co-existing liquids) of the Karoo picrite basalts with a view to providing further evidence to show that the northern Lebombo (and Nuanetsi and Tuli) lavas may have crystallised from high-MgO magmas, as has been suggested by Cox (1978).

8.5.2 Field Relationships

Cox (1978) has demonstrated that field relationships provide important clues as to whether porphyritic high-MgO lava suites represent liquids enriched in cumulus olivine or not. In the northern Lebombo, Nuanetsi (Cox et al., 1965) and Tuli (Vail et al., 1969) areas the picrite basalts crop out near or at the base of the Karoo volcanic succession and in all cases are overlain by exceptionally thick sequences of low-MgO basalts.

In the case where lavas are erupted from a magma chamber undergoing simple gravitative differentiation it would be expected that evolved, low-MgO liquids, would be emplaced first and would be followed by lavas enriched

in cumulus olivine (and possibly pyroxene). Though it is possible that some low-MgO magmas solidify before reaching the surface it would be expected (see Cox, 1978) that early lavas would be characterised by relatively low-MgO abundances whereas subsequent lavas would be relatively enriched in MgO by virtue of having accumulated olivine phenocrysts. AS such the nature of the Lebombo, Nuanetsi and Tuli volcanic successions which contain substantial amounts of high-MgO lavas emplaced at or near the beginning of the volcanic episode implies that the picritic basalts were not formed by cumulus enrichment of olivine in less magnesian liquids.

8.5.3 Petrographic and Geochemical Relationships

In the northern Lebombo, rocks with 14 - 18% MgO commonly contain abundant glass (e.g. see Plate 8.1) and in many samples a large proportion of the crystals present, invariably olivine and lesser amounts of clinopyroxene, occur as skeletal blades and prisms, and euhedral phenocrysts. Similarly in Nuanetsi, Cox (1978) noted that picrite basalts with up to 18% MgO were characterised by large amounts of glass and skeletal olivines, and inspection of the petrographic descriptions and modal analyses of the Tuli high-MgO lavas (Vail et al., 1969) show that picritic rocks with 14 - 18% MgO are also invariably glassy. The glassy nature of these rocks indicates that they have undergone rapid cooling from relatively high temperatures. More important though is that the morphological habits shown by the skeletal crystals are similar to the crystal forms produced experimentally (Donaldson, 1976) by quenching of magnesian rich melts.

The results achieved by Donaldson (1976) provide important proof for the existence of high-MgO lavas since previously crystal habits characterised by re-entrants and incomplete crystal faces were attributed to resorption. However, Donaldson (1976) was able to produce a complete spectrum of skeletal crystal shapes, ranging from delicate "feather" forms to

relatively large granular olivines by super-cooling molten charges. The most significant relationship he noted, however, was that the skeletal olivines did not necessarily reflect rapid cooling rate, but rapid growth rate caused by the high normative olivine content of the magmas and "probably also by the very high eruption temperatures". Donaldson's (1976) data are therefore consistent with the interpretation that picritic lavas characterised by skeletal olivines set in a glassy matrix, e.g. Karoo picrite basalts with 14 - 18% MgO, may have crystallised from high temperature MgO-rich magmas.

In comparison to the glassy nature of the lavas with 14 - 18% MgO, northern Lebombo picritic lavas with MgO in excess of 18% are predominantly crystalline, often fine to medium grained, and are characterised by large olivine phenocrysts, nodular aggregates of olivine and occasional olivine macrophenocrysts. As noted in section 8.4.2 the majority of these rocks are characterised by high contents of modal olivine and show compositional trends consistent with olivine control implying that they may have formed from magmas with 18% MgO (or less) by olivine accumulation. Furthermore, it was noted (section 8.4.2) that the generally positive correlations between MgO and KAR elements in the range 9 - 18% MgO became negative in the range 18 - 24% and this was attributed to dilution of the original trace element contents of parental magmas with 18% (or less) MgO by olivine addition. Consequently 18% MgO is considered to represent an approximate upper limit for the original parental magma compositions. There are exceptions to this, the most notable being northern Lebombo samples KP108 and KP112. Both contain skeletal clinopyroxenes and olivine phenocrysts (skeletal, euhedral and rounded) set in glass but have whole rock compositions characterised by MgO > 20% suggesting that there may have been parental magmas that were more magnesian than 18% MgO. However, both

samples are enriched in modal olivine in comparison to other glassy lavas (Table 8.1) making it difficult to prove that they represent primary magmas with greater than 18% MgO.

Northern Lebombo picrite basalts with less than 14% MgO are typically fine grained and commonly contain numerous small clinopyroxene phenocrysts (often arranged in nodular-like aggregates, e.g. see Plate 8.4A) and plagioclase laths. Olivine compositions in these rocks are generally evolved and the phenocrysts are typically rounded. As such petrographic relationships imply that some of the evolved rocks formed by crystal fractionation from more magnesian (e.g. 14 - 18% MgO) parental magmas. However, a few rocks with less than 14% were also found to be extremely glassy, e.g. sample KS3, suggesting that they crystallised directly from strongly olivine normative liquids.

To summarise, petrographic criteria viz. skeletal olivines and glassy textures, coupled with geochemical relationships suggest that the picrite basalts may well have crystallised from a range of high to intermediate-magnesian parental melts, ie. magmas with approximately 9 - 18% MgO. However, even some of the very glassy lavas appear to be enriched in cumulus olivine e.g. samples KP108, KP112, thus showing that it is exceedingly difficult to establish primary magma (liquid) compositions in the case of porphyritic, high-MgO lavas.

8.5.4 Olivine : Fe-Mg Distribution

A study of the Fe-Mg distribution between olivines and coexisting liquids should provide some idea of the composition of the liquids from which the picrite basalts formed. The distribution of magnesium and ferrous iron between olivine and coexisting liquids can be represented by the following equation:

$$\tfrac{1}{2}(Mg_2SiO_4)_{ol} + \tfrac{1}{2}(Fe_2SiO_4)_{liq} = \tfrac{1}{2}(Mg_2SiO_4)_{liq} + \tfrac{1}{2}(Fe_2SiO_4)_{ol} \quad \ldots\ldots\ldots(1)$$

The distribution coefficient for this equation can be written as follows:

$$K_D = (x^{ol}_{Fe0} / x^{ol}_{Mg0}) \cdot (x^{liq}_{Mg0} / x^{liq}_{Fe0}) \quad \ldots\ldots\ldots\ldots\ldots\ldots\ldots\ldots(2)$$

where x^{ol}_{Fe0} = the mole fraction in olivine etc.

Roeder and Emslie (1970) have made a detailed investigation of the above relationship. They found that for a variety of basaltic compositions and a wide range of temperatures (1 150 to 1 300^{o}C) and oxygen fugacities ($10^{-0.68}$ to 10^{-12} atm) the K_D was equal to 0.30 $\pm$ 0.03 at one atmosphere pressure, and was independant of temperature and oxygen fugacity. Subsequent studies (Roeder, 1974; Duke, 1976; Longhi et al., 1978) confirmed the value of K_D = 0.30 $\pm$ 0.03 though Cawthorn et al. (1974), Thompson (1975) and O'Hara (1977) predicted slightly higher average K_D's ($\sim$0.33) for high-MgO liquids. Estimates of K_D between olivine and ultramafic komatiite liquids suggest even higher values for picritic liquids, eg. 0.34 - 0.37 (Green et al., 1975; Bickle et al., 1977; Nisbet et al., 1977). However, komatiitic rock types typically contain much higher abundances of MgO (weight %) than the Lebombo picrite basalts such that an Fe : Mg K_D of approximately 0.33 is regarded as representing equilibrium conditions in the present study.

Additional studies have investigated the role of bulk composition and pressure effects in relation to the Fe : Mg K_D for olivine. Roeder (1974) suggested that the K_D was relatively insensitive to change in the bulk compositions of the liquid. However, Longhi et al. (1978) found a small but significant compositional effect on the distribution of FeO and MgO which was ascribed to variations in silica concentration. Pressure effects were investigated by Mysen (1975) and it was found that K_D's increased with

pressure. In addition, Longhi et al. (1978) found a notable increase in K_D above 5 kbar.

Fe : Mg $K_D^{oliv-liq}$ values calculated for the Lebombo picrite basalts are listed in Table 8.14. The K_D's were calculated using the most Mg-rich olivines analysed in the individual samples (EMP analyses) and the whole rock FeO/MgO on the assumption that cores of the most magnesian olivine should represent the equilibrium composition that crystallised from a liquid with the FeO/MgO ratio of the host rock. (Since the Fe^{3+} content of the lavas was not determined Fe_2O_3/FeO ratio of 0.15 has been assumed - see section 4.1. A slightly lower Fe_2O_3/FeO ratio of 0.10 was also used to calculate a second set of K_D's in Table 8.14).

Compared to the experimentally determined value ($\sim$ 0.33) disequilibrium is indicated between the olivine - "liquid" pairs presented in Table 8.14, possible exceptions being samples KP111 and KS47. Both these rocks have K_D values which approach 0.33 and if the lower Fe_2O_3/FeO ratio of the whole rock is used (0.10) then the K_D value for KP111 = 0.33. However, the majority of the calculated K_D's are greater than 0.33 and even if higher equilibrium values are used (0.34 - 0.37) then samples KP111 and KS47 are still the only possible 'magma' compositions. On the basis of Fe : Mg K_D relationships the picritic rocks do not therefore appear to represent 'liquid' compositions, possible exceptions being KP111 and KS47.

Inherent in the above calculations is the assumption that the most Mg-rich olivine cores closely represent liquidus compositions. The fact, therefore, that some olivines are only very slightly zoned (see Table 8.4) could be taken to imply that a certain degree of equilibrium crystallisation took place, in which case the above assumption is invalid and the calculation of K_D's meaningless. If the possibility of equilibrium crystallisation is disregarded then high Fe : Mg K_D values can be explained in terms of either

TABLE 8.14 Calculated Fe-Mg K_D values (Roeder and Emslie, 1970) for the northern Lebombo picrite basalts.

	K_D^1	K_D^2	WR MgO	Fo content of olivine
KS3	0.49	0.47	10.72	$Fo_{79.5}$
KS47	0.36	0.34	12.00	$Fo_{86.2}$
KP111	0.35	0.33	14.45	$Fo_{89.3}$
KP121	0.70	0.67	14.59	$Fo_{80.0}$
KA24	0.68	0.65	14.68	$Fo_{79.4}$
KP101	0.49	0.47	16.37	$Fo_{87.6}$
KP29	0.71	0.68	17.69	$Fo_{80.9}$
KP108	0.56	0.54	21.00	$Fo_{87.7}$
KP112	0.68	0.65	24.03	$Fo_{87.0}$

1 - Calculated assuming whole rock Fe_2O_3 / FeO = 0.15

2 - Calculated assuming whole rock Fe_2O_3 / FeO = 0.10

WR - Whole Rock

(i) incorporation of more Fe-rich olivines into parental magmas by crystal settling, (ii) increase in the MgO content of the original liquid by the addition of olivine. Either of these mechanisms may operate in a magma chamber and could also occur in a magma conduit during emplacement or possibly even within a lava flow. In the general case it would be expected that magmas at the base of a magma column would be enriched in olivines whereas material nearer the top would loose olivine due to crystal settling. However, it would be expected that as the liquid at the top of a magma column became more iron rich, olivines crystallising from the liquid would also become more iron rich so as to maintain a K_D of approximately 0.33. It is therefore possible that rocks such as KP111 and KS47 which have K_D's approaching 0.33 may represent magmas tapped from near the top of a compositionally (temperature) zoned magma column whereas lavas such as KP108 and KP112 which are characterised by glassy textures and high abundances of modal olivine could represent magmas tapped from near the bottom of the column.

A crystal settling mechanism that could explain the Fe : Mg K_D relationships of the picrite basalts is shown in Fig. 8.8. The model indicates how lavas derived from near the base of a temperature zoned magma column would be enriched in olivine and hence more magnesian whereas magmas from the upper portion would have lost olivine by crystal settling and hence would be more evolved. Furthermore it is possible that crystal compensation type processes (Cox and Bell, 1972) could act in the situation depicted in Figure 8.8 in which case many of the porphyritic lavas would closely represent original liquid compositions. However, crystal settling models similar to that depicted in Figure 8.8 must have been of relatively minor importance during the petrogenesis of the picrite basalts since it has been demonstrated that the overall geochemical variation apparent in the lavas (excluding KAR elements) developed in response to fractionation of

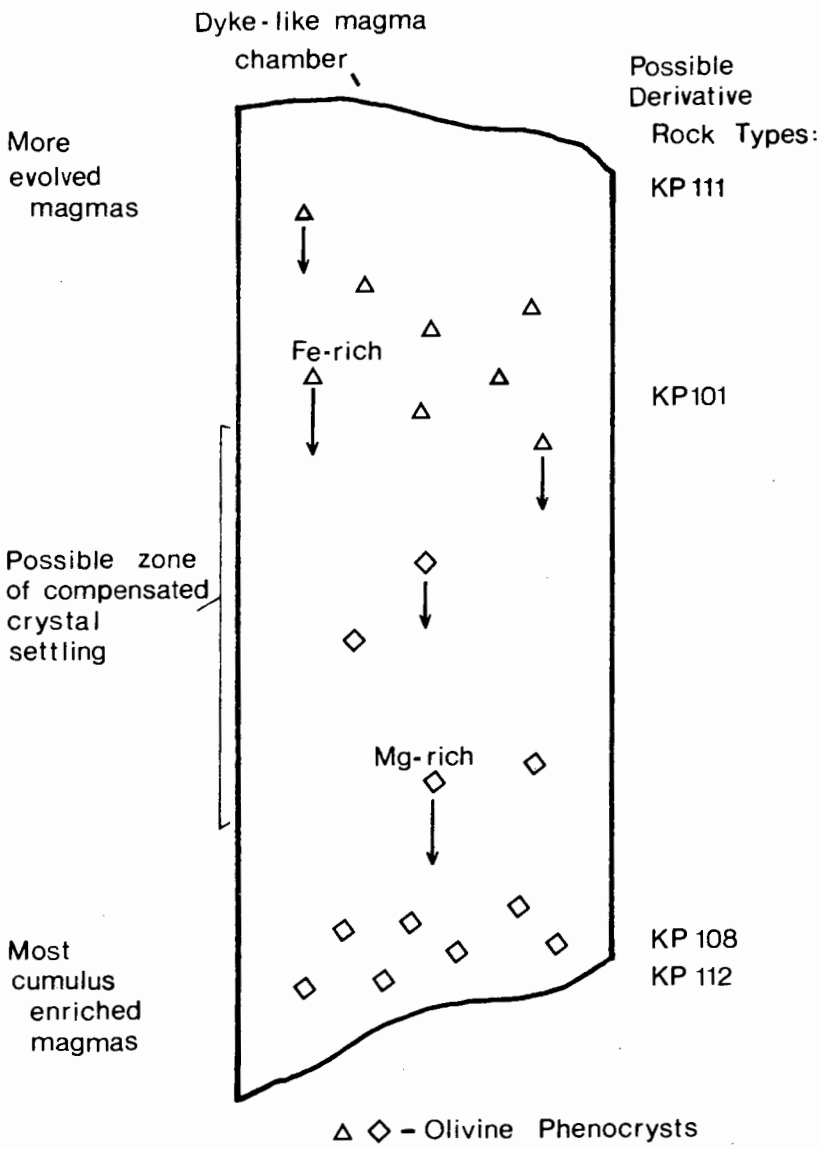

Fig. 8.8 Simplified crystal settling model which could possibly account for the petrographic and compositional characteristics of northern Lebombo picrite basalts characterised by glassy textures and Fe:Mg K_D's$^{oliv:liq}$ which are greater than 0.33.

olivine + orthopyroxene at high pressures (see section 8.4, and Cox and Jamieson, 1974). Consequently the model presented in Figure 8.8 is considered to represent a secondary process superimposed on magmas formed at high pressures in response to olivine + orthopyroxene fractionation.

The significance of the above model is that it provides a means of explaining the large amount of scatter which is apparent in major element plots such as SiO_2 and Fe_2O_3 versus MgO (Figs. 8.5 a,c) and many of the trace element variation diagrams (Figs. 8.6, 8.7). This scatter was commented upon earlier and it was suggested that olivine accumulation or removal by crystal settling from Mg-rich magmas was responsible. Furthermore it was noted that 'control lines' which projected towards relatively evolved olivine compositions could be drawn through sub-sets of data suggesting that the secondary process of olivine redistribution was a relatively low pressure (low temperature) effect. This relationship is particularly well borne out by rocks with greater than 18% MgO since these lavas appear to lie on a control line joining a magma composition with about 18% MgO and olivine composition of about Fo_{78}.

The compositions of the Group I olivines (see Fig. 8.1) and most magnesium rich Nuanetsi olivines may provide an insight into the compositions of the original picritic magmas prior to modification by olivine redistribution. These olivines are considered to have played a role in the high pressure fractionation processes which account for the overall major element variations in rocks with less than 18% MgO (see sections 8.4 and 8.6) and are broadly similar in composition to mantle olivines. They have therefore been used to delimit the possible compositions of the magmas prior to modification by olivine accumulation and/or removal. The most magnesian olivines found in the Lebombo rocks have compositions of about Fo_{89} whereas in Nuanetsi compositions of Fo_{92} were noted by Cox and Jamieson (1974).

Assuming an Fe : Mg $K_D^{oliv-liq}$ of 0.33 and an average olivine composition of Fo_{91} it is possible to calculate the FeO/MgO ratio of the liquid in equilibrium with this olivine. Using the olivine composition Fo_{91} in Table 8.15b, a liquid FeO/MgO ratio of 0.52 can be calculated which is similar to the FeO/MgO ratio of composition P18 (Table 8.15a). If one envisages magma genesis as taking place in a temperature zoned environment, the olivines would reflect a range in compositions in accord with their temperature of crystallisation and composition of the liquid from which they crystallised. The least forsteritic compositions of Group I have a composition of about Fo_{82} which on the basis of a Fe : Mg K_D of 0.33 must have been in equilibrium with a liquid which had an FeO/MgO ratio of 1.17. Inspection of the Table 8.15a shows that the above ratio is similar to that of model composition P9.

On the basis of Fe : Mg K_D's and crystal settling processes discussed above it is therefore concluded that the picrite basalts do not represent true liquid compositions. Instead it would appear that the lavas crystallised from Mg-rich parental magmas whose primary compositions were modified by olivine redistribution at low pressures. Primary melts may have been in the range 9 - 18% MgO and developed in response to high pressure olivine + orthopyroxene fractionation. As suggested previously orthopyroxene and perhaps clinopyroxene crystal fractionation at low pressures may have contributed to some extent towards the modified (parental) compositions since phenocrysts of both these minerals are found in the picritic basalts. However, petrographic and geochemical data imply that olivine redistribution played a more dominant role than did orthopyroxene and clinopyroxene.

8.5.5 Olivines : Mg-Ni Distribution

Mg-Ni distribution relationships between olivine and coexisting liquids have been widely used as a criterion for identifying primary magmas (e.g. Sato, 1977; Arndt, 1977). Sato (1977) suggested that the Mg - Ni

K_D falls in the range 2.0 - 2.6 for the following exchange reaction:

$$\tfrac{1}{2}(Mg_2SiO_4)_{liq} + \tfrac{1}{2}(Ni_2SiO_4)_{ol} = \tfrac{1}{2}(Ni_2SiO_4)_{liq} + \tfrac{1}{2}(Mg_2SiO_4)ol$$

where $K_D = (MgO/NiO)^{liq} / (MgO/NiO)^{ol}$

However, Sato's K_D values were based on data obtained from low MgO (< 9%) Hawaiian basalts by Hakli and Wright (1967) and since it has been shown (Arndt, 1977; Irvine and Kushiro, 1976; Hart and Davis, 1978) that composition, pressure, and temperature, affect the K_D (Mg-Ni), Sato's (1977) values are probably inappropriate for higher MgO liquids.

To monitor Mg : Ni K_D's at higher MgO levels the data of Arndt (1977b), Hart and Davis (1978) and Takahashi (1978) have been investigated. The data from Arndt (1977) indicate that K_D decreases substantially with increasing MgO (K_D = 1.65 at 21% MgO, 2.22 at 12% MgO, 2.57 at 10% MgO). In addition experimental data of Takahashi (1978) indicates a variation in K_D from 1.4 to 3.5 with decreasing MgO content. This relationship has been illustrated by Le Roex (1980) using the data from Hart and Davis (1978). Le Roex (1980) found that K_D shows an exponential decrease with increasing MgO and only falls in the range 2.0 - 2.6 for lavas with between 6 and 12% MgO.

K_D values obtained for the northern Lebombo picrite basalts are, with the exception of KP111 (K_D = 1.58, MgO = 14.45), lower than the values derived at high MgO levels from the experimental work of Arndt (1977) and Takahashi (1978) and, taken together with the Fe - Mg data, tend to support the suggestion that the lavas may be cumulus enriched in olivine. However, the fact that the Mg-Ni K_D varies as a function of composition severely limits its applicability to determining crystal-liquid equilibrium at high MgO levels. Consequently, though the K_D levels in the lavas are generally low, this need not necessarily imply that they have in fact suffered cumulus-enrichment.

The equations of Hart and Davis (1978) and Smith et al. (in press) relating D_{ol}^{Ni} to the composition of the magma are potentially useful since they can be used to model the MgO-Ni fractionation crystallisation paths within the lava suites. According to Hart and Davis (1978) fractionation paths involving batch crystallisation or fractional crystallisation of olivine from a starting liquid with nearly 20% MgO will be curved. However, the majority of high-MgO lava suites investigated by Hart and Davis (1978) show crudely linear trends on a MgO-Ni plot in the higher ranges of MgO composition (approximately 10 - 29% MgO). As such Hart and Davis argue that the roughly linear MgO-Ni trends commonly found in high-MgO lava suites cannot be produced by olivine fractionation from a highly magnesian parent liquid and suggest that the parental liquids lie in the range 6 - 13% MgO with high-MgO lavas being derived by accumulative processes.

A plot of MgO versus Ni for the Lebombo and Nuanetsi picrite basalts is shown in Figure 8.9. Inspection of this figure shows that the data defines a crudely linear array which according to Hart and Davis (1978) would be indicative of olivine accumulation. However, in the case of the Karoo picrite basalts, orthopyroxene must also be considered as a fractionating phase (see sections 8.4 and 8.6). A series of fractionation models have therefore been constructed to test whether the MgO-Ni relationships place constraints on the compositions of the liquids from which the picrite basalts crystallised. Since the lavas are characterised by phenocrysts which are zoned and show a wide range of compositions, Rayleigh fractionation has been used for modelling purposes.

The models have been constructed by assuming that the parental magma had an MgO content of approximately 18% and fractionated olivine and orthopyroxene. A four-stage model has been tested whereby a series of successively lower MgO liquids with 15%, 12% and 9% MgO are produced. The

major element compositions of these liquids were assumed to be the same as the model compositions which are used in the mixing models (section 8.6) and the porportions of olivine and orthopyroxene removed in each step have been obtained from the model results (Table 8.16).

The D_{ol}^{Ni} was calculated using the equation derived by Smith et al. (in press):

$$D_{ol}^{Ni} = 111.3/MgO - 1.71 \quad \ldots\ldots\ldots\ldots\ldots\ldots\ldots\ldots\ldots\ldots (1)$$

This equation has been suggested (Smith et al., in press) to be more applicable than the relationships of Hart and Davis (1978) to lavas with high MgO contents. However, obtaining values of D_{opx}^{Ni} presents a problem in that little work has been done on Ni distribution between orthopyroxene coexisting with high-MgO liquids. At present a wide range of D_{opx}^{Ni} values are reported or used in the literature. For example, Frey et al. (1978) used D_{opx}^{Ni} values of 3 - 5 for modelling purposes in dominantly alkaline lava suites, whereas Le Roex (1980) calculated D_{opx}^{Ni} values ranging from 3.15 to 18.1 in orthopyroxene mineral separates and Ewart and Taylor (1969) measured values of 4.6 - 6.5 in basaltic andesites and andesites. Conversely lower D_{opx}^{Ni} values were obtained in high pressure (10 - 20 kb, D_{opx}^{Ni} = 1.10, 0.60; Mysen, 1976a, 1978) and high temperature (D_{opx}^{Ni} 3.03, 2.47, 1.10, 1 300°C, 1 350°C, 1 400°C; 1 atm; Bird, 1971) experimental studies on pseudobasalt systems thereby implying that D_{opx}^{Ni} varies as a function of pressure. Furthermore, since experimental results indicate that the magnitude of D for a large number of mineral : liquid pairs is dependant on composition (e.g. Henderson, 1977; Takahashi, 1978; Glassley and Piper, 1978; Hart and Davis, 1978) and temperature (e.g. Leeman, 1974; Lindstrom, 1976; Leeman and Lindstrom, 1978; Arndt, 1977) it seems plausible to expect D_{opx}^{Ni} to vary in a similar fashion to D_{ol}^{Ni}.

On the basis of the criteria noted above a simple empirical equation, which effectively relates D^{Ni}_{opx} values to composition (in terms of MgO) was established (Fig. 8.10). The equation may be expressed as follows

$$D^{Ni}_{opx} = -.2448 \cdot MgO + 6.406 \quad \ldots\ldots\ldots\ldots\ldots\ldots\ldots\ldots (2)$$

and reproduces the range of distribution coefficients reported in the literature, yielding higher D's at low MgO values and lower D's at more magnesian (high temperature) compositions. D^{Ni}_{opx} values obtained from the above equation (2) and D^{Ni}_{ol} values calculated from the equation (1) derived by Smith et al. (in press) were then used to calculate the bulk Ni distribution coefficients used in modelling and MgO - Ni variation terms of crystal fractionation.

The results of the modelling calculations are represented graphically in Figure 8.9 and show several interesting relationships. Data generated by fractionation crystallisation from an assumed parental magma with 18% MgO defines an almost straight line (A) passing through the main envelope of data points, provided that compositionally dependant D^{Ni}_{opx} values obtained from equation (2) were used in conjunction with D^{Ni}_{ol} values obtained from the equation of Smith et al. (in press). By comparison, fractional crystallisation data generated using constant values for D^{Ni}_{opx} but compositionally variable D^{Ni}_{ol} values define curved lines (B,C) which encompass very few of the actual data points. The conclusion that is tentatively suggested is that model data derived on the assumption that D^{Ni}_{opx} varies as a function of temperature, pressure and composition (line A, Fig. 8.9) indicates that the Karoo picrite basalts may have been derived from a high-MgO parental magma(s) by fractional crystallisation. However, until the variation in D^{Ni}_{opx} with composition is better documented no unequivocal conclusions can be drawn from Ni-Mg modelling.

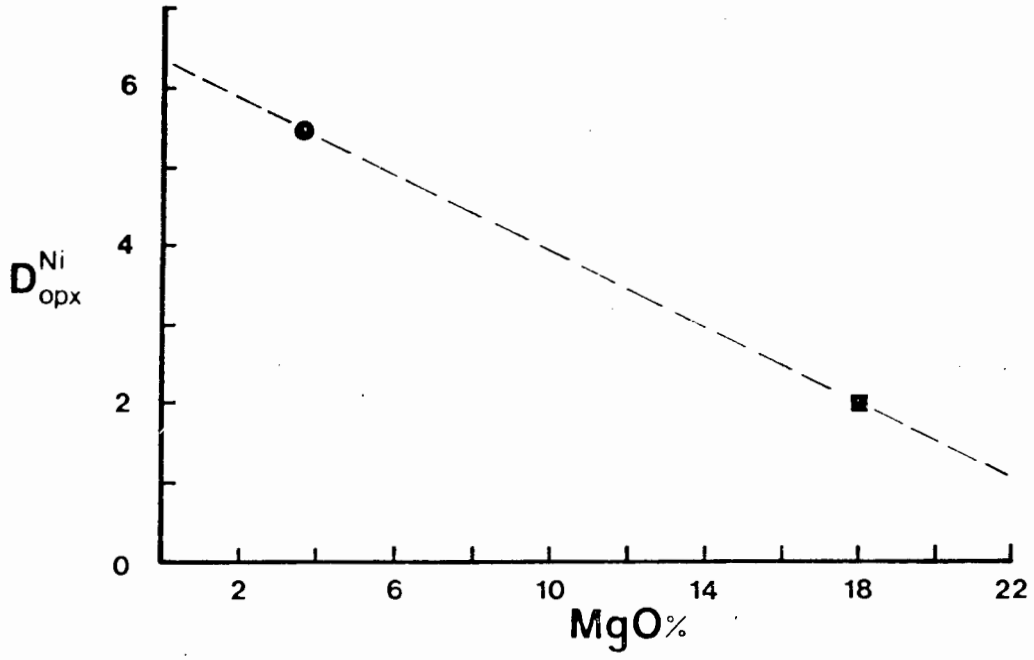

Fig. 8.10 Plot of D^{Ni}_{Opx} versus MgO for average data from experimental work and mineral separates.

(D^{Ni}_{Opx} = -.2448* MgO + 6.406)

● - Average of D^{Ni}_{Opx} measured in basaltic andesites with an approximate MgO content of 3.7% (Ewart and Taylor, 1969; Ewart et al., 1968).

■ - Estimated D^{Ni}_{Opx} for basaltic systems with high MgO compositions based on data that has either been determined experimentally (Bird, 1971 - D^{Ni}_{Opx} ~ 1.91 - 3.03; Mysen, 1976a- D^{Ni}_{Opx} ~ 0.6 - 1.4; Mysen, 1978 - D^{Ni}_{Opx} ~ 1.10; Lindstrom, 1976 - D^{Ni}_{Opx} ~ 3.1) or found to provide well constrained solutions in modelling calculations (e.g. Frey et al., 1978).

NOTE: The relationship which has been inferred from the above data is undoubtedly both imprecise and a gross over-simplification of the real system. It should therefore only be looked upon as a simple empirical relationship which has been used as a 'semiquantitative' tool to assess the effect that variable D^{Ni}_{Opx} values (with respect to compositions) would have on a basaltic system undergoing large amounts of olivine + orthopyroxene fractionation. The establishment of a precise relationship between D^{Ni}_{Opx} and MgO is not feasible at present due to the paucity of orthopyroxene/liquid distribution data from natural basaltic systems and in particular high MgO systems.

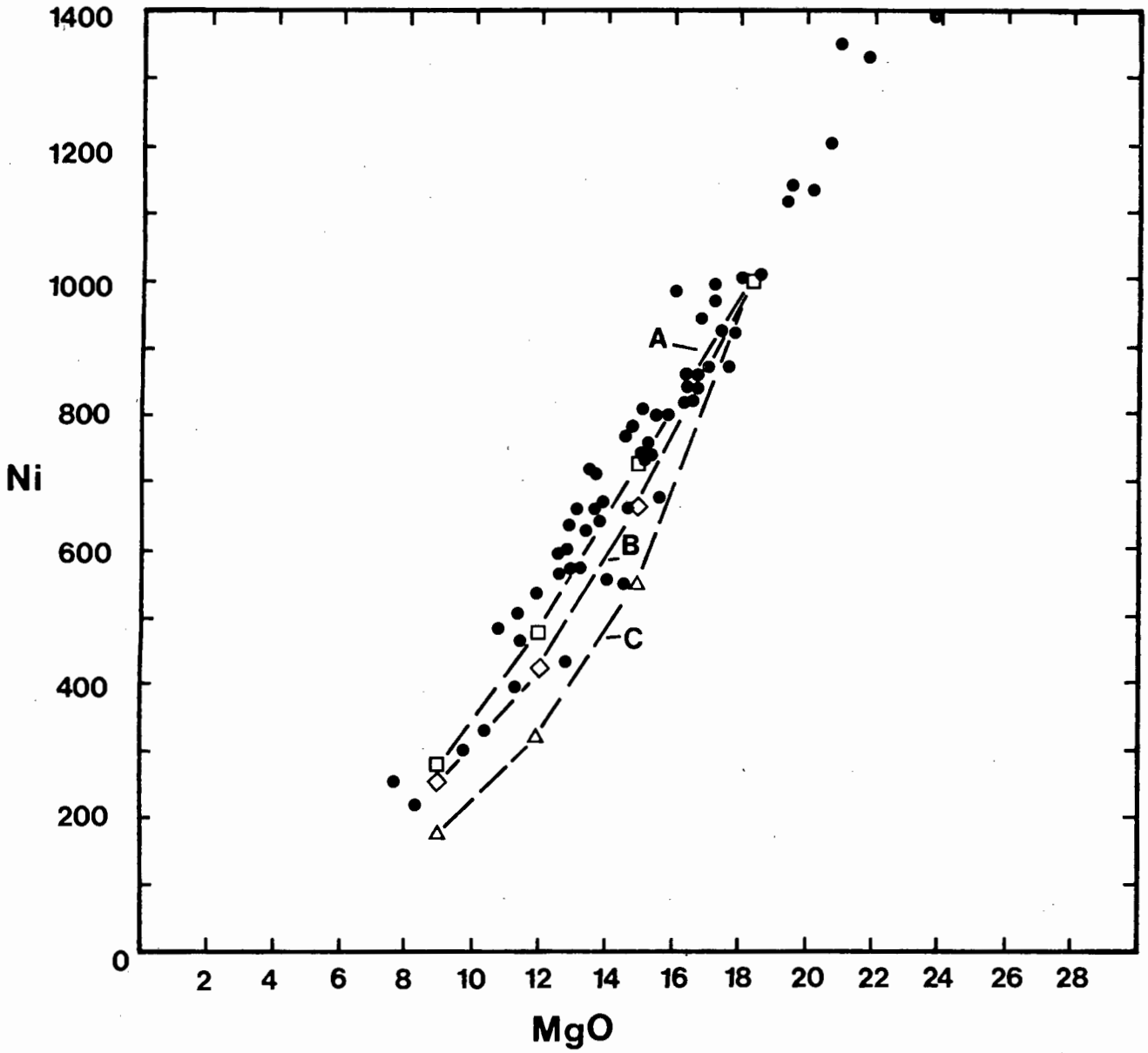

Fig. 8.9 Plot of Ni versus MgO for the Lebombo, Nuanetsi and Tuli picrite basalts. Fractional crystallisation curves are superimposed on the diagram and were modelled on the basis that the parental magma had approximately 18% MgO and 1 000 ppm Ni and fractionated olivine and orthopyroxene in the proportions obtained in Table 8.16.

For curve A: $D^{Ni}_{ol} = 111.31/MgO - 1.71$; $D^{Ni}_{opx} = -.2448.MgO+6.406$

B: D^{Ni}_{ol} as in A; $D^{Ni}_{opx} = 3$

C: D^{Ni}_{ol} as in A; $D^{Ni}_{opx} = 5$

(where MgO = average value for each step)

8.5.6 Summary

Petrographic, geochemical and mineralogical criteria presented above are consistent with the derivation of the northern Lebombo, Nuanetsi and Tuli picrite basalts from high-MgO magmas. The lavas do not represent 'true liquid' compositions due to the effects of olivine phenocryst redistribution in primary magmas which formed by high pressure olivine + orthopyroxene fractionation.

The fact that the lavas contain olivine phenocrysts raises a problem since it is generally assumed that olivines are rapidly removed from magmas due to gravitative settling. However, this problem can be overcome if the structural setting of the picritic lavas of the Lebombo and south-east Zimbabwe are considered (see Cox, 1970). The outcrops of high-MgO lavas found in the northern Lebombo, Nuanetsi and Tuli appear to have been emplaced along zones of major crustal dilation and fracturing associated with the fragmentation of Gondwanaland (see Cox et al., 1965; Cox, 1970; Saggerson and Logan, 1970). The strongly fractured crust would have ensured the existence of numerous intrusive pathways and facilitated the rapid movement of the magmas to the surface, thereby restricting heat loss and excessive crystallisation followed by gravitative settling. The high normative olivine-content of the magmas would have also led to rapid nucleation of olivine in the parental magmas (see Donaldson, 1976) and it is therefore likely that the magmas assumed a 'porphyritic' character soon after melting. In this respect the magmas may be described as primitive porphyritic magmas (Cox, 1978) and did not necessarily acquire their high-MgO chemistry by low pressure cumulus enrichment of olivine in basaltic magmas with less than 9% MgO. A generalised scheme of magma genesis and emplacement for the picritic rocks is outlined below:

1. Formation of high-MgO primary magmas by high pressure olivine + orthopyroxene fractionation.

2. Rapid nucleation of olivine during initial movement in magma conduits.

3. Modification of primary magma compositions by crystal settling of olivine (± minor orthopyroxene and clinopyroxene) at lower pressures.

4. Emplacement of porphyritic picrite magmas.

8.6 Major Element Modelling

Least squares approximation calculations (see section 4.6 and Chapter 7) have been used to assess the role high pressure fractional crystallisation may have played in the petrogenesis of the picrite basalts. As was the case in previous quantitative modelling (Chapter 7) average parent and daughter compositions for the picritic lavas were derived from the trend lines fitted to the major element variation diagrams (Figs. 8.5 and 8.6). Average compositions (Table 8.15a) were calculated at MgO values of 9%, 12%, 15% and 18% and normalised to 100% K_2O free. (These compositions are referred to as P9, P12, P15 and P18). An MgO value of 18% has been chosen as an upper limit on the basis of the criteria noted in the previous section (8.5) and K_2O was excluded because of its abnormally high level of enrichment in the picrite basalts and positive correlation with MgO. TiO_2 and P_2O_5, though showing similar relationships to K_2O, have been included in the model calculation because they are present in low concentrations and have little overall effect on the end result.

In the initial model computations mineral compositions observed in individual picrite basalts (ie. phenocryst compositions as determined by EMP analysis) were used. However, though the sum of squares of the residuals

in oxide abundances between the observed and calculated parental compositions were generally < 1.0 for models using the average liquids and observed phenocryst compositions it was found that F values varied substantially in relation to the mineral compositions used. To overcome this problem and attain a more precise estimate of F, average compositions of olivines and orthopyroxenes in equilibrium with the average liquid compositions (with respect to postulated Fe : Mg distribution coefficients) were used in the calculated fractionation models (see Tables 8.15 a-c and 8.16). These mineral compositions were obtained graphically from the mineralogical data obtained in this thesis by adopting the same computational procedures that were used to calculate the parental magma compositions (see Table 8.15b for further explanation). Average mineral assemblages used in the least squares approximation calculations were then selected assuming Fe-Mg K_D's (ol : liq) = 0.30 (Roeder and Emslie, 1970) and 0.33 (O'Hara, 1977) for olivines, whereas Nathan and Van Kirk (1978) Fe-Mg K_D coefficients (Enstatite : liq) were used to select orthopryoxene.

Compositions of olivines and orthopyroxenes in equilibrium with the parental melts assuming the Fe : Mg K_D's listed above are listed in Table 8.15 a,b. The olivines (Table 8.15a) correspond closely to the range in compositions shown by the Group I olivines. However, orthopyroxene compositions (Table 8.15b) selected assuming a Fe : Mg K_D of 4.15 (Nathan and Van Kirk, 1978) appear to be excessively magnesium whereas those selected assuming a ratio of 2.73 (Nathan and Van Kirk, 1978) show similar Fe : Mg ratios to those orthopyroxenes found in the lavas. Orthopyroxenes with compositions of En 90 have not been found in the Lebombo (this study) or Nuanetsi (Cox and Jamieson, 1974) rocks and least squares linear regression calculations attempted with the highly-magnesium orthopyroxenes provided very poor results. Conversely, good results (ie. low sum of squares of

TABLE 8.15a Average parental and daughter compositions for the picrite basalts determined at 9% (P9), 12% (P12), 15% (P15), and 18% (P18) MgO from the major element variation diagrams. (Figs. 8.5 and 8.6).

	P9	P12	P15	P18	
SiO_2	51.86	51.64	51.20	50.86	
TiO_2	2.77	2.89	2.99	3.08	
Al_2O_3	11.35	10.14	8.96	7.79	
FeO*	12.38	11.18	11.50	10.98	
(FeO)	(10.91)	(10.41)	(10.13)	(9.67)	
MnO	.16	.15	.15	.14	
MgO	9.30	12.40	15.46	18.45	
CaO	9.50	8.58	7.36	6.68	
Na_2O	2.26	1.96	1.65	1.54	
P_2O_5	.42	.44	.45	.48	
FeO/MgO	1.17	0.84	.66	.52	
Mg/Fe^{2+}	1.52	2.12	2.72	3.40	
Ol^1	Fo_{82}	Fo_{86}	Fo_{89}	Fo_{91}	(K_D 0.33)
Ol^2	Fo_{84}	Fo_{88}	Fo_{90}	Fo_{92}	(K_D 0.30)
Opx^1	En_{84}	En_{88}	En_{91}	En_{93}	(K 4.15)
Opx^2	En_{76}	En_{82}	En_{86}	En_{89}	(K 2.73)

Computational Procedure : SiO_2, TiO_2, Al_2O_3 etc. were estimated graphically at particular MgO values and nominal compositions were then nomralised to 100% (see section 4.6)

Ol^1, Ol^2 : Olivines (Table 8.15b) in equilibrium with the parental magmas assuming Ol : liq K_D's of 0.33 (O'Hara, 1977) and 0.30 (Roeder and Emslie, 1970) respectively.

Opx^1, Opx^2 : Orthopyroxenes (Table 8.15c) in equilibrium with the parental magmas assuming Opx : liq K_D's (Fe : Mg) of 4.15 and 2.73 (Nathan and Van Kirk, 1978) respectively.

FeO* : Total Fe

FeO : Calculated assuming Fe_2O_3 / FeO = 0.15

TABLE 8.15b Hypothetical olivine compositions determined from mineral chemistry data. A graphical procedure which is described on the reverse side of this page was used to determine these compositions.

	Fo_{92}	Fo_{91}	Fo_{90}	Fo_{89}	Fo_{88}	Fo_{86}	Fo_{84}	Fo_{82}
SiO_2	40.33	40.23	40.04	40.00	39.90	39.81	39.35	39.19
Ti	.02	.02	.02	.03	.03	.03	.04	.04
Al	.01	.01	.01	.01	.01	.01	.01	.01
FeO	8.09	8.79	9.98	10.82	11.62	13.07	15.42	16.87
MnO	.12	.13	.14	.15	.16	.17	.18	.19
MgO	51.13	50.52	49.49	48.78	47.97	46.60	44.67	43.37
CaO	.27	.28	.28	.28	.28	.28	.30	.30
Na_2O	.01	.01	.01	.01	.01	.01	.01	.01
K_2O	.01	.01	.01	.01	.01	.01	.01	.01
P_2O_5	.01	.01	.01	.01	.01	.01	.01	.01
FeO/MgO	.16	.17	.20	.22	.24	.28	.35	.39

TABLE 8.15c Hypothetical orthopyroxene compositions determined from mineral chemistry data. A graphical procedure similar to that outlined on the reverse side of this page was used to determine the orthopyroxene compositions listed below.

	En_{76}	En_{82}	En_{84}	En_{86}	En_{88}	En_{89}	En_{91}	En_{93}
SiO_2	55.12	55.63	55.74	55.97	56.18	56.42	56.77	57.0
TiO_2	.40	.33	.31	.29	.26	.25	.22	.18
Al_2O_3	.58	.74	.80	.85	.90	.93	.98	1.00
FeO	12.36	9.72	9.09	7.98	6.97	6.64	5.7	4.64
MnO	.16	.15	.14	.12	.09	.07	.05	.04
MgO	28.58	31.47	32.16	33.32	34.30	34.61	35.5	36.76
CaO	2.74	1.90	1.70	1.40	1.14	.99	.70	.30
Na_2O	.04	.04	.04	.05	.05	.06	.06	.06
K_2O	.01	.01	.01	.01	.01	.01	.01	.01
P_2O_5	.01	.01	.01	.01	.01	.01	.01	.01
Ca	5	4	3	2	2	2	2	1
Fe	19	14	13	12	10	9	8	6
Mg	76	82	84	86	88	89	90	93
Mg/Fe^{2+}	4.12	5.77	6.30	7.44	8.77	9.29	11.10	14.12

TABLE 8.16 Mixing calculations for the picrite basalts. Input data are presented in Tables 8.15 a, b and c.

I

	P18			MIX		
	OBS	CALC	DIFF	COMP	Wt%	S.D.
SiO_2	50.86	50.86	-	P15	87.38	1.57
TiO_2	3.08	2.62	-0.46	Fo_{91}	4.64	1.30
Al_2O_3	7.79	7.90	0.11	En_{89}	7.58	2.30
Fe_2O_3	10.98	10.98	-			
MnO	.14	.14	-	TOTAL	99.59	3.08
MgO	18.45	18.45	-			
CaO	6.68	6.77	0.09	Sum of squares of residuals =		0.24
Na_2O	1.54	1.45	-0.09			
P_2O_5	.48	.39	-0.09			

II

	P15			MIX		
	OBS	CALC	DIFF	COMP	Wt%	S.D.
SiO_2	51.20	51.20	-	P12	88.48	1.24
TiO_2	2.98	2.58	-0.40	Fo_{89}	4.87	1.19
Al_2O_3	8.96	9.03	0.07	En_{86}	6.36	1.94
Fe_2O_3	11.50	11.48	-0.02			
MnO	.15	.15	-	TOTAL	99.71	2.59
MgO	15.46	15.46	-			
CaO	7.63	7.69	0.06	Sum of squares of residuals =		0.18
Na_2O	1.65	1.74	0.09			
P_2O_5	0.45	0.38				

III

	P12			MIX		
	OBS	CALC	DIFF	COMP	Wt%	S.D.
SiO_2	51.64	51.64	-	P9	87.77	1.49
TiO_2	2.89	2.46	-0.43	Fo_{86}	2.85	1.58
Al_2O_3	10.14	10.03	-0.11	En_{82}	8.97	2.47
Fe_2O_3	11.81	12.11	0.30			
MnO	.15	.16	0.01	TOTAL	99.59	
MgO	12.40	12.31	-0.09			
CaO	8.58	8.52	-0.06	Sum of squares of residuals =		0.30
Na_2O	1.96	1.99	0.03			
P_2O_5	.44	.37	-0.07			

residuals) were obtained using equilibrium orthopyroxenes selected on the basis of K = 2.73 (value obtained by Nathan and van Kirk (1978) for a simple binary system) and in view of the limited amount of work which has been done on the distribution of Fe and Mg between liquid and orthopyroxene (Bowen and Schairer, 1935; Medaris, 1969), compositions determined using a Nathan and Van Kirk (1978) K_D value of 2.73 are considered to be more realistic.

Results of the mixing calculations are presented in Table 8.16. The models show that the range of selected parent and daughter compositions with 9 - 18% MgO can be generated by the removal of olivine and orthopyroxene from a series of liquids which become progressively depleted in MgO. The rate of extraction of orthopyroxene is clearly greater than olivine, particularly in the final fractionation step. This is in some respects compatible with the petrographic data since the modal abundance of orthopyroxene is generally greatest in rocks with MgO abundances of less than about 16% MgO, though there are exceptions to this e.g. N88 which has 21% modal orthopyroxene and MgO = 21.18% (Cox and Jamieson, 1974). However, rocks such as N88 appear to be enriched in cumulus orthopyroxene and olivine.

In conclusion it may be stated that the overall major element variation (excluding KAR elements) shown by the picrite basalts can be accounted for by high-pressure fractionation of olivine and orthopyroxene from high-MgO primary magmas. Petrographic and geochemical data suggested that the lavas may have evolved from a range of liquids with varying MgO values which would be compatible with results obtained from the modelling calculations. However, the major element models discussed do not take into account KAR elements and as will be shown in the following section it is necessary to invoke more complex petrogenetic models to explain the behaviour of these elements.

8.7 Petrogenetic Model and KAR Element Relationships

8.7.1 General Statement

Any petrogenetic model that is formulated to explain the geochemical relationships of the northern Lebombo, Nuanetsi and Tuli picrite basalts must explain the following relationships:

(i) The presence of glassy- and fine-grained picrite lavas with olivines that commonly show skeletal crystallisation forms (section 8.2.3).

(ii) The high MgO content of the lavas and high liquidus temperatures of olivines and orthopyroxenes found in the lava flows (Cox and Jamieson, 1974; and Table 8.13).

(iii) Abnormally high levels of KAR elements in the lavas and the weak positive correlations found between these elements and MgO (section 8.4).

(iv) The general decrease in enrichment levels with time shown by the KAR elements in the northern Lebombo picrite lavas (section 8.4).

(v) The apparent equilibration of the lavas with harzburgite at 6 - 12 kb (Cox and Jamieson, 1974).

8.7.2 Crystal Fractionation Models

Though the evolution of the lavas has been discussed in terms of a down-temperature process (section 8.6) severe problems are presented by such a mechanism when trying to explain the positive correlation between MgO and the KAR elements. Had the lavas been derived from a single batch of parental-magmas with 18% MgO and approximately 3% K_2O the subsequent fractionation of olivine and orthopyroxene to produce more evolved lavas (9 - 14% MgO) would have led to a significant increase in K_2O and a strong negative MgO - K_2O correlation would have resulted.

As has been previously argued (Cox, 1972b; Cox and Jamieson, 1974) a single parental-magma hypothesis of any sort is therefore untenable. Instead it is necessary to postulate an earlier event which involves enrichment in KAR elements. This process(es) would have to give rise to a series

of liquids with variable incompatible element abundances which would then undergo olivine + orthopyroxene fractionation. However, it is also necessary that the K-enrichment processes be linked to the subsequent ferromagnesian mineral fractionation process if the positive correlation between MgO and KAR elements is to be observed. This implies that K-rich starting materials must fractionate considerably less olivine and orthopyroxene than the K-poor starting materials (Cox and Jamieson, 1974). Such a mechanism clearly involves a series of complex fractionation events coupled with a number of rather unusual coincidences and on these grounds is considered to be implausible. As Cox and Jamieson (1974) noted: "How such a linked process might work is not outside the bounds of petrological imagination, nevertheless the crustal fractionation model must be regarded as complicated and possibly lacking in certain plausibility."

8.7.3 Wall Rock and Zone Refining Processes

Cox and Jamieson (1974) and Norry (1977) have proposed alternate models to account for the unusual relationships found in the picrite basalts. Broadly speaking the models invoke zone refining type processes to account for the compositional relationships noted between the KAR elements and MgO contents of the basalts though the model devised by Cox and Jamieson (1974) appears to provide a more plausible solution to the petrogenetic problems associated with the picrite basalts.

Cox and Jamieson (1974) proposed a wall rock equilibration model which can be summarised as follows. A magma body, or series of magma bodies are assumed to rise from depths within the mantle and to become enriched and compositionally zoned in KAR elements by processes such as wall rock reaction and zone refining. Equilibration with peridotite in the depth range 18 - 35 km is then considered to have led to the liquids being constrained into their observed major element composition by the buffering

action of the wall rocks. Subsequently, sudden fracturing of the crustal rocks above the partially molten mantle is considered to have led to rapid eruption of the magmas without further fractionation.

8.7.4 Mantle Metasomatism: An Alternative Model

In the following section a partial melting model involving derivation of the picrite basalts from magmas generated in an upper mantle source containing domains enriched in KAR elements by a metasomatic process is outlined. The model is in essence simpler than zone refining and wall rock reaction models (Cox and Jamieson, 1974; Norry, 1977) though the end products may well be the same in all cases.

The metasomatic model presupposes that the mantle source from which the picrite basalt magmas were derived underwent a metasomatic event (prior to melting) which led to the creation of mantle domains enriched in KAR elements by formation of mantle phases such as those reported from metasomatised peridotites e.g. phlogopite, the amphibole K-richterite, LIL enriched opaques (e.g. see Erlank and Rickard, 1977). In the subsequent melting event which gave rise to the picrite basalts it is envisaged that these phases contributed to the magmas from which the picrite basalts crystallised, thereby leading to the enrichment of KAR elements in the picritic lavas of the northern Lebombo, Nuanetsi and Tuli areas.

In the early stages of melting of the metasomatically enriched source relatively low-temperature constituents, e.g. phlogopite and amphibole would undergo rapid decomposition such that early formed melts would be enriched in KAR elements. Early formed melts are also likely to have equilibrated with mantle material at greater depths (ie. higher pressures) whereas later magmas would have equilibrated with mantle assemblages at lower pressures during the fragmentation of eastern Gondwanaland. This relationship is shown schematically in Figure 8.11. Continental rifts appear to

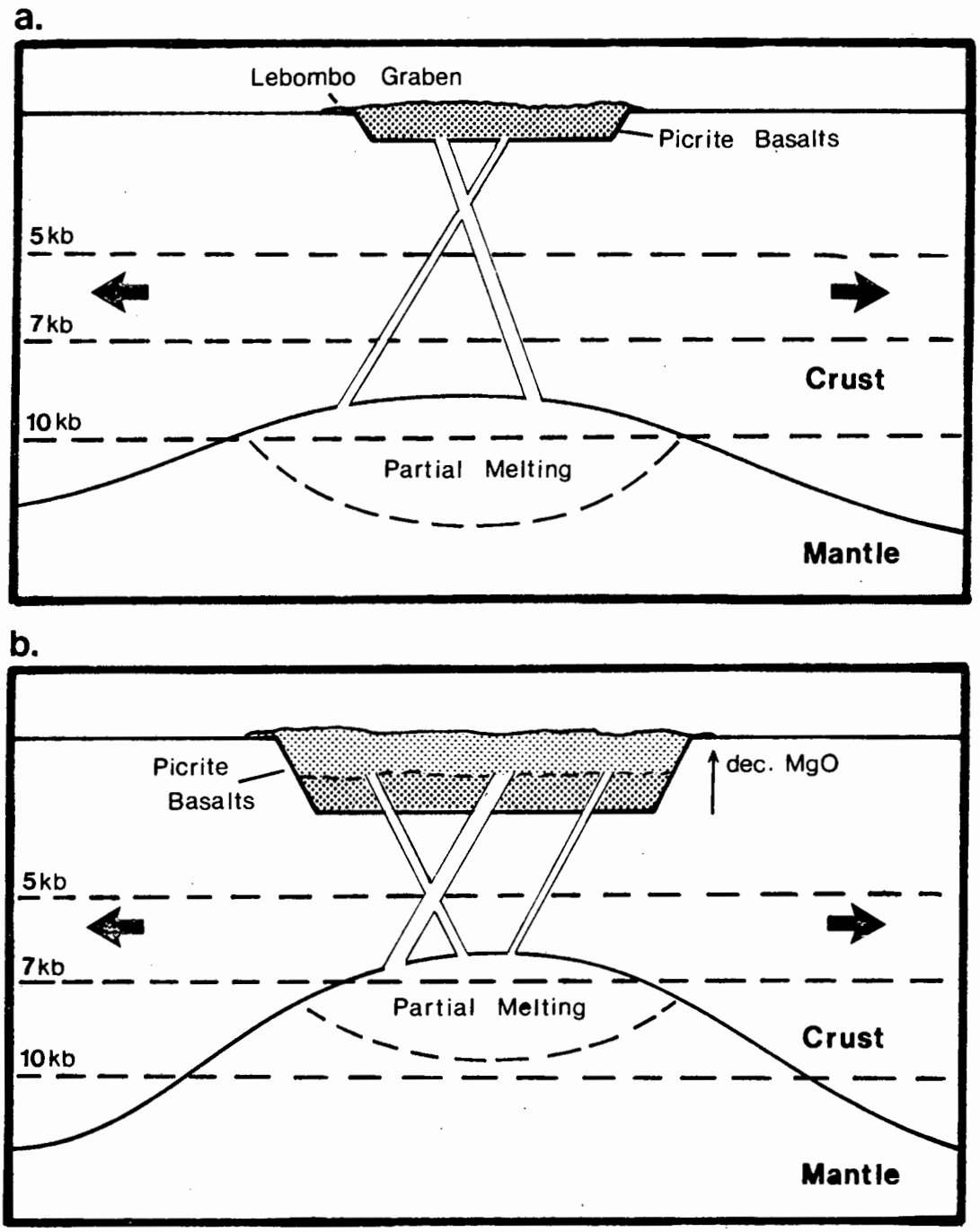

Fig. 8.11 A schematic diagram to show how early formed picritic magmas would equilibrate with mantle phases (viz. olivine and orthopyroxene) at higher pressures than those magmas formed later in the volcanic event which led to the emplacement of the picrite basalts. In continental environments the crust-mantle interface is normally considered to lie at a depth of about 30 km (~ 10 kb) e.g. see Lloyd and Bailey, 1975. The crustal necking model depicted here has been discussed in more detail by Cox (1970), Betton (1978) and Betton and Cox (1979).

develop in response to the action of lateral extensional stresses such that necking of the crust occurs as is shown in Figure 8.11. Cox (1970) and Betton and Cox (1979) have outlined crustal necking models for the Lebombo and adjoining areas. During necking it has been shown (e.g. see Betton and Cox, 1979) that the crust/mantle boundary is upwarped such that mantle material is effectively raised into lower pressure regimes (Fig. 8.11). Magmas formed early in the volcanic cycle will therefore equilibrate at higher pressures (Fig. 8.11a) than later formed magmas (Fig. 8.11b).

Experimental studies of basaltic systems (Green and Ringwood, 1967; Bultitude and Green, 1971; Kushiro, 1973) have shown that increasing pressure reduces the olivine volume stability field in relation to the pyroxenes such that anhydrous liquids produced at higher pressures are richer in normative olivine than low pressure equivalents. In the model presented above (see Fig. 8.11) it is proposed that the early formed picritic magmas equilibrated with olivine and orthopyroxene at higher pressures than later formed magmas. Initial magmas were therefore more strongly olivine normative relative to subsequent magmas and would have also incorporated greater abundances of KAR elements derived from the breakdown of metasomatic phases. With continued melting in the source region the enriched mantle domains would have become progressively or totally depleted in KAR elements. Lavas emplaced high in the volcanic succession would therefore have been derived from magmas with lower abundances of KAR elements. In addition these magmas would have equilibrated with mantle assemblages at lower pressures and on the basis of experimental studies would therefore be less olivine normative (ie. less MgO rich) than the earlier magmas which equilibrated at higher pressures. The overall effect of this model would therefore be to produce high-MgO, high-KAR element lavas early in the volcanic cycle whereas later lavas would be less enriched in MgO and KAR elements. This model would, therefore explain the positive correlation noted between

MgO and KAR elements and also account for the temporal relationships (point iv., section 8.7) shown by the northern Lebombo picrite basalts.

A similar pressure dependant model was proposed by Cox and Jamieson (1974) to explain the geochemical relationships of the Nuanetsi picrite basalts. On the basis of experimental results Cox and Jamieson (1974) concluded that equilibration with olivine and orthopyroxene through a pressure range of 6 - 12 kbar (18 - 36 km) would account for the major element chemistry of the picrite basalts. In most respects the model proposed here is broadly compatible with that model proposed by Cox and Jamieson (1974) though instead of invoking magma genesis from a range of depths (ie. low to high pressures) a model based on mantle updoming into lower pressure regimes is preferred.

The unknown factor in the model proposed above is the effect volatile constituents derived from the breakdown of metasomatic minerals (e.g. phlogopite and amphibole) will have on the melting processes. On the credit side volatiles such as H_2O would have the effect of progressively lowering the solidus and accelerating the increase in MgO with ascent. Under near surface conditions volatiles will escape from the magma and thus raise its liquidus thereby promoting the development of skeletal olivine crystals and causing rapid crystallisation of the magmas as fine grained or glassy lavas. Conversely later lavas derived from drier magmas (ie. magmas derived from source areas depleted in metasomatic constituents) would not have suffered the same effect, thereby explaining the paucity of glassy lavas with skeletal crystals higher in the succession. However, several authors (e.g. Kushiro, 1972; Eggler, 1974) have shown that the effects of H_2O and CO_2 in silicate liquids respectively oppose and reinforce the effects of pressure. Obviously the effect would depend on the H_2O/CO_2 ratio though in the case of the breakdown of metasomatic minerals such as phlogopite and

amphibole it would be expected that H_2O would be the dominant volatile species. The precise effects volatiles have on melting relationships are, however, difficult to establish. Burnham (1975) and Mysen et al. (1976) have shown that the solubility of H_2O and CO_2 in melts decreases with a decrease in pressure. Consequently these components will approach their solubility limits during magma ascent, eventually forming a gas phase which will escape at low pressures. Primary volatile abundances and compositions in magmas will therefore be difficult to analyse and accordingly adjustments to phase volume boundaries in systems such as CMAS will not be possible. Melting experiments with natural or synthetic rock systems are faced with similar problems and may fail to reproduce high-pressure equilibria attained in the mantle. However, though H_2O may cause the olivine stability field to expand relative to the pyroxenes it is unlikely that the effects of melting at pressures of 10 - 12 kbars will be substantially affected by the presence of volatiles in the magma. A model involving melting of a metasomatically enriched source at progressively lower pressures is therefore considered to be capable of producing the relationships observed between the KAR elements and MgO content in the picrite basalts.

8.7.5 Metasomatism : the Petrographic and Geochemical Evidence from Mantle Xenoliths

Metasomatism of mantle nodules has been noted in peridotite xenoliths from a large number of kimberlite pipes in southern Africa (see Aoki, 1975; Harte and Gurney, 1975; Harte et al., 1975; Erlank, 1976; Erlank and Rickard, 1977) as well as in xenoliths derived from alkaline rocks in other parts of Africa, e.g. Uganda (Lloyd and Bailey, 1975). In addition phlogopite which is generally considered to have formed in response to the action of metasomatic fluids (Erlank and Rickard, 1977; Boettcher et al., 1979) is found in xenoliths from kimberlitic-type rocks in Tanzania (Reid et al., 1975 a,b) and also occurs in peridotite xenoliths from the Precambrian Premier

Kimberlite (Erlank, pers. comm.). It would therefore appear that the scale of mantle metasomatic processes is indeed extensive. Furthermore, though the metasomatism described by Erlank and Shimizu (1977) for xenoliths containing K-richterite is apparently of recent (~150 my) age, there is intrinsically no reason why similar processes could not have occurred at earlier times as is suggested by the presence of phlogopite in xenoliths from the Premier kimberlite. In this respect, additional evidence for the existence of considerably older mantle heterogeneities which perhaps reflect previous episodes of mantle metasomatism (?) in the mantle underlying southern Africa has been suggested by Erlank et al. (1980). Two well documented studies relating to metasomatic minerals and processes in peridotite xenoliths from southern African kimberlites, viz. Matsoku and Bultfontein, are discussed below.

Metasomatic minerals that appear to have been introduced into peridotite xenoliths found in the Matsoku kimberlite include phlogopite, ilmenite, rutile and less commonly sulphide minerals (Harte et al., 1975). These minerals show variable grainsize and have been petrographically described as being of primary metasomatic origin. In those portions of the xenoliths which have undergone metasomatism the lherzolite phases are frequently recrystallised, reduced in grainsize or become poikilitic or cloudy. For example Harte et al. (1975) have described a 1 cm wide vein in a xenolith from the Matsoku kimberlite where recrystallised olivine, orthopyroxene, garnet, phlogopite, rutile and sulphides form a roughly polygonal texture whereas the rest of the xenolith has a flasar texture and is free of metasomatic veining.

In the Matsoku xenolith described by Harte et al. (1975) it was also found that the composition of the olivine, orthopyroxene and garnet from the vein are identical to those in the main body of rock. This indicates

that metasomatism must have been confined to the introduction of components such as TiO_2, K_2O, H_2O etc. required to form the metasomatic minerals but did not introduce significant amounts of Fe and Mg. The polygonal texture of the vein filling also suggests slow cooling under stress free conditions late in the structural history of the xenolith. These conditions are unlikely to have been attained within a kimberlite magma and it may be concluded that the introduction of the metasomatic minerals was unrelated to the kimberlite event. In addition the chemical relationships noted by Harte et al. (1975) show that it is possible to enrich mantle source areas without causing significant changes in the major element chemistry of the source.

The process of mantle metasomatism described by Erlank (1976), Aoki (1975) and Erlank and Rickard (1977) from the Bultfontein kimberlite is chemically characterised by the introduction of K (Rb, Ba) and may provide important clues with respect to the type of metasomatic process which could have accounted for the unusual chemical relationships of the picrite basalts found in the Lebombo and adjoining areas of south-east Zimbabwe. Erlank and Rickard (1977) note that the introduction of K and associated elements normally leads to the development of phlogopite but where metasomatism is more extensive, e.g. in Bultfontein peridotites, the rare amphibole potassic richterite forms. Introduction of variable amounts of Ti, Sr, Zr and Nb also occurs and the development of an unidentified opaque phase in a few nodules with Ba, Sr and Zr at the percent level is also reported by Erlank and Rickard (1977).

According to Kushiro and Erlank (1970) K-richterite is not stable in the presence of garnet such that aluminous phases, viz. garnet and aluminous spinels, could not have been present at the time of K-richterite formation. Consequently Erlank and Rickard (1977) note that metasomatic processes

leading to the development of this mineral must occur in or else produce Al-deficient environments and propose that K-richterite is produced by the reaction of olivine, enstatite, diopside (and even phlogopite) with a fluid phase containing K and other elements. The rarity of K-richterite in metasomatised nodules is therefore ascribed to the fact that either too much Al (garnet) is present in the original nodules or not enough K and associated incompatible elements were supplied by most metasomatic processes.

The data presented by authors such as Harte et al. (1975), Erlank and Rickard (1977) and others indicate that mantle metasomatism is indeed an important process and capable of causing high levels of enrichment in incompatible elements in typical mantle assemblages. Consequently it can be speculated that if metasomatic enrichment processes had occured in pre-Karoo times they would have given rise to mantle heterogeneity. More critically, however, under extreme conditions, e.g. similar to those noted by Erlank and Rickard (1977) in the Bultfontein peridotites, it is possible that metasomatic enrichment in K and other incompatible elements could have produced the mantle source required for the generation of the northern Lebombo, Nuanetsi and Tuli picrite basalts. This point will be reiterated in the following section. In addition the development of a mineral such as K-richterite could possibly account for the apparent depletion in Al_2O_3 in the picrite basalts (see section 8.4, Table 8.11)

8.7.6 REE Patterns and Incompatible Inter-element Ratios

Changes in the chemistry of the Lebombo volcanics are well demonstrated by REE data (Erlank et al., 1980). South of the Sabie River the basalts have REE contents and patterns (see Fig. 8.12) similar to those of the Moshesh's Ford Formation of the central Karoo province. Such patterns are not exceptional as far as continental tholeiitic basalts are concerned and do not provide any evidence which might explain the high Sr isotope ratios

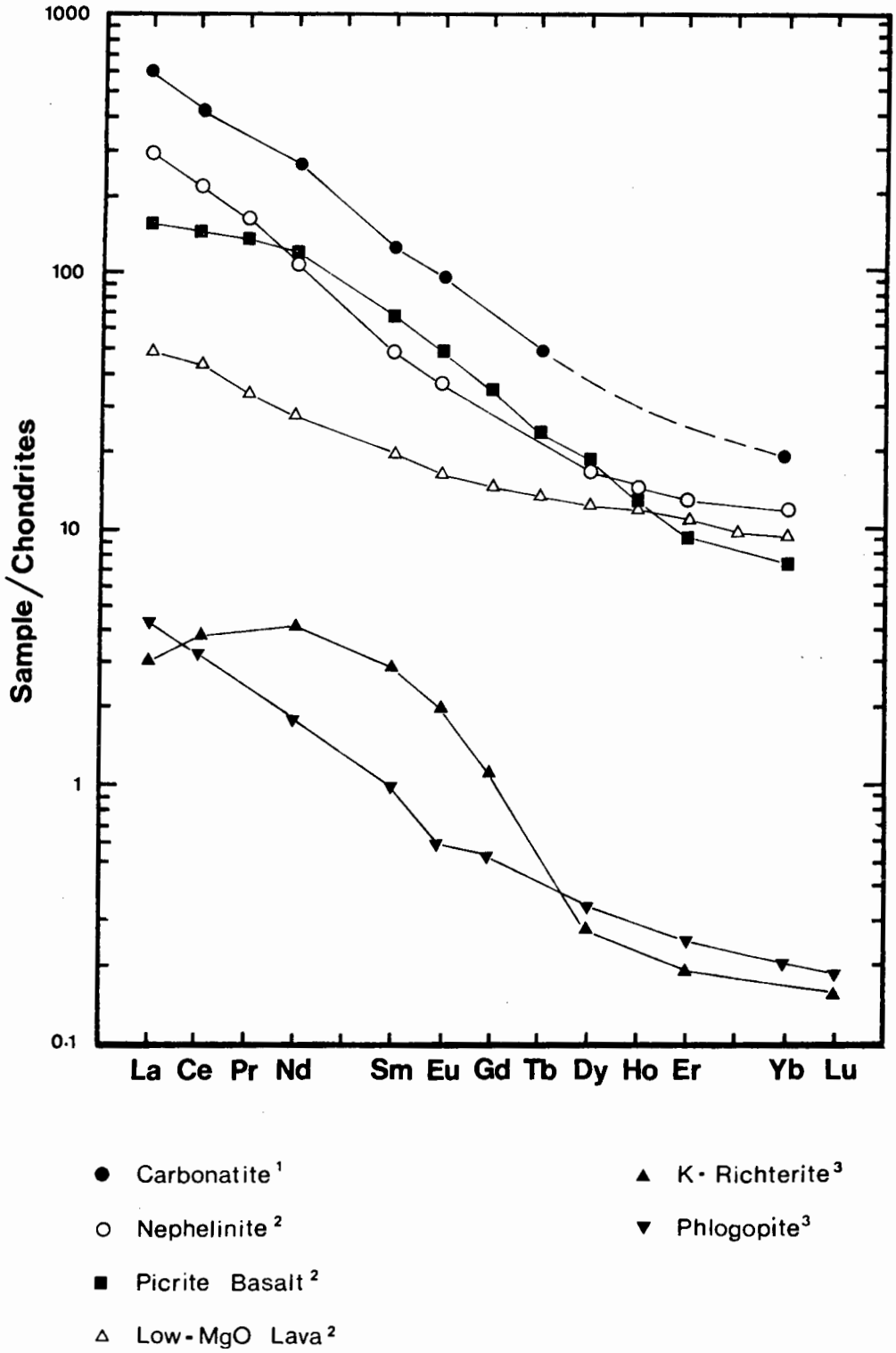

Fig. 8.12 REE/Chondrite normalised plot for Lebombo lavas (2 - Duncan, unpublished data), separated minerals from a peridotite nodule from the Bultfontein mine (3 - Aoki pers. comm. to Erlank) and a carbonatite (1 - Möller, et al., 1980.)

of these low-MgO basalts (see Chapters 9 and 10). However, northwards from the Sabie River greater levels of enrichment are apparent in the basalts, and REE patterns for nephelinite and picrite basalts (Fig. 8.13) are exceptionally steep. More important, however, is the level of REE enrichment and the shape of the REE patterns obtained for the picrite basalts.

The high magnesian picritic rocks are considered to represent liquid compositions that have been only partially modified by olivine accumulation (section 8.5) such that the REE pattern is probably indicative of the source involved. These rocks are also considered to have been unaffected by crustal contamination processes and the REE data and patterns are therefore representative of a source area substantially enriched in REE, correlating with the enrichment noted in KAR elements. Reference to Figure 8.12 also indicates that the picrite basalt has an unusual 'Z shape' REE pattern which is flattened at both ends. This pattern appears to be somewhat unique among basaltic systems and cannot, on the basis of published partition coefficient data (e.g. see Arth, 1976) be produced by combinations of "normal" mantle mineral assemblages (Erlank et al., 1980). Thus both an enriched and unusual mantle source is implied.

REE data for phlogopite and K-richterite have also been superimposed on Figure 8.12. The absolute contents of REE in the minerals are too low to produce the REE contents in the picrite basalts since both minerals would be expected to melt totally during the large degrees of melting required to produce the picrite basalts. More important, however, is the shape of the REE patterns of the two minerals. Combination of the phlogopite and K-richterite data results in a REE pattern which shows a remarkable similarity to the picrite basalts and thus provides clues as to the possible mineralogy of the source region from which the picrite basalts were derived. Also of possible relevance to the present discussion are REE patterns obtained for

carbonatites. These rocks typically show very steep REE patterns and in some instances they also show a tendency to flatten at both ends (see Möller et al., 1980). A REE pattern for a carbonatite is included on Figure 8.12. The pattern shows a strong enrichment relative to the picrite basalt for most of the rare earths. Pervasive metasomatism by carbonate rich metasomatic fluids leading to the formation of phases such as phlogopite and K-richterite could therefore account for apparent enrichment in the source area from which the picrite basalts were derived. In addition, carbonatites are typically highly enriched in Sr and Ba (see Möller et al., 1980) implying that these elements have a strong affinity for carbonate rich solutions. Both elements show unusually high abundances in the picrite basalts thereby providing additional support for heterogeneous upper mantle enrichment in response to the migration of carbonate rich fluids.

Incompatible inter-element ratios provide the most convincing support for heterogeneity in the source area from which the picrite basalts were derived though they do not necessarily provide unequivocal proof of metasomatic enrichment. For example Zr/Nb, K/Rb and TiO_2/Zr ratios vary substantially in the picrite basalts (Fig. 8.13). Since these rocks are considered to be comagmatic and since any fractionation would probably only have involved olivine and orthopyroxene, it would be expected that incompatible inter-lement ratios would be relatively uniform (e.g. see Weaver et al., 1972; Erlank and Kable, 1976). However, this is clearly not the case and since the rocks are considered to have formed by high degrees of partial melting it can be inferred that the ratios are representative of the source. Hence the range of values apparent in Figure 8.13 is most simply explained in terms of melting of a source(s) heterogeneous with respect to incompatible elements, a situation that is most likely to develop in response to pervasive metasomatism on a large scale.

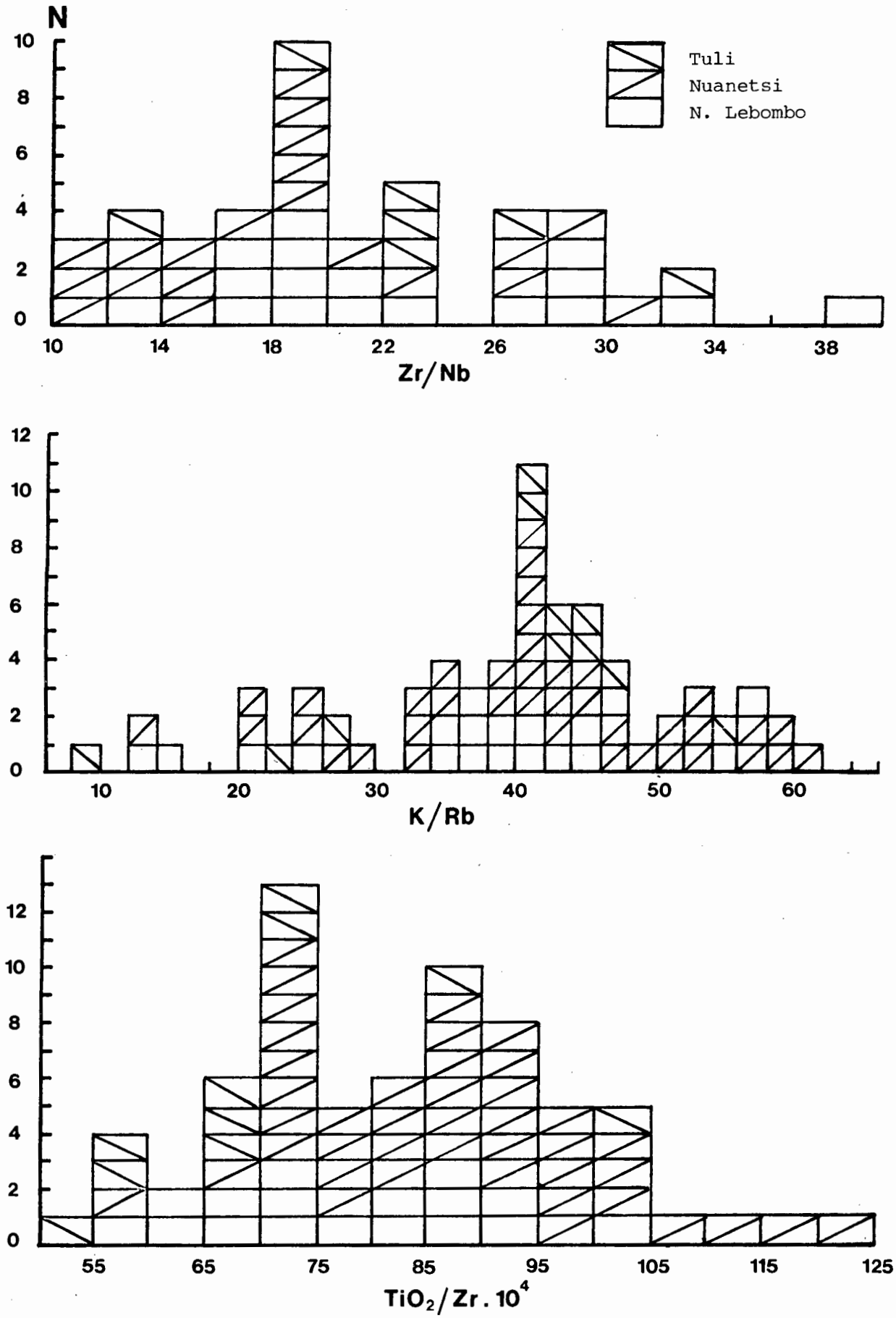

Fig. 8.13 Histograms of inter-incompatible element ratios for the Lebombo, Nuanetsi and Tuli picrite basalts.

Zr/Nb ratios warrant further comment. Though showing considerable spread, inspection of picrite basalt analyses for the Lebombo, Nuanetsi and Tuli (Microfiche Tables F17, 22, 28) shows that most of the variation is due to Zr whereas Nb is relatively constant. This implies that the inferred heterogeneous enrichment of Zr was much stronger than the overall enrichment in Nb. Correlation coefficients support this inference (Table 8.12) since Zr shows strong correlations with all the KAR elements (except Nb) whereas Nb shows very weak correlations with all the incompatible elements. In addition some of the very low K/Rb ratios apparent in Figure 8.13 imply that the enrichment process was not always uniform and that some of the metasomatic fluids carried higher abundances of Rb than K.

Overall, it is apparent that the inferred metasomatic process(es) which led to the formation of the source area from which the picrite basalts were derived were indeed complex. Nevertheless it may be concluded on the basis of the REE and incompatible element data presented above that upper mantle metasomatism caused by K-rich carbonate fluids will not only lead to mantle heterogeneity on a large scale but could have produced the type of enriched mantle that was necessary to generate the unique Mg-rich - KAR element enriched lavas which crop out in the northern Lebombo and adjoining areas of Zimbabwe. Furthermore, Sr-isotope relationships which will be discussed in Chapter 10 suggest that the inferred metasomatic enrichment processes could have occurred relatively close in time to the emplacement of the picrite lavas.

8.7.7 Relationships between the Picrite Basalts and Nephelinites

Figure 8.12 includes a REE pattern obtained for a northern Lebombo nephelinite. The nephelinite (5% MgO) has a concave upwards pattern which contrasts strongly with the REE pattern obtained for the picrite basalt. However, unlike the picrite basalts which appear to have been generated by

large degrees of partial melting the nephelinites have probably been produced by small degrees of partial melting such that their REE patterns may not be reflective of the source area involved. Similar patterns have be observed in kimberlites which are also believed to be produced by small degrees of partial melting (Mitchell and Brunfelt, 1975) though since it is generally concluded that nephelinites (and alkaline rocks, including kimberlites) are derived from source areas that are enriched in incompatible and LREE elements (e.g. see Frey et al., 1978) their REE patterns probably represent an interplay between small degrees of melting superimposed upon an enriched source.

More critical, however, is that the REE patterns for the picrite basalt and nephelinite cannot be related to the same source by conventional partial melting or fractional crystallisation models, bearing in mind the very different bulk chemistry of these two rock types. This conclusion is substantiated by a comparison of Zr and Nb data and ratios for the two suites. Absolute abundances of these elements vary considerably between the two suites with the picrite basalts showing higher Zr but much lower Nb abundances than the nephelinites. Comparison of the ratios also shows that Zr/Nb ratios are considerably higher and more variable in the picrite basalts ($\sim$ 10-34). To change the Zr/Nb ratio from about 10 (minimum for the picrite basalts) to 6 would require over 98% clinopyroxene ($D^{Zr}_{cpx} = 0.1$; $D^{Nb}_{cpx} = 0.03$; Table 9.8) crystallisation so that a change from 10 to 1.71 is clearly impossible in terms of low-pressure fractional crystallisation processes. Partial melting of a source composition incorporating garnet ($D^{Zr}_{gt} = 1.2$; $D^{Nb}_{gt} = 0.01$; Le Roex, 1980) as a residual phase does offer a mechanism whereby incompatible inter-element ratios may be fractionated (see Le Roex, 1980) but even assuming the most extreme conditions e.g. the presence of large amounts (> 10%) of residual garnet in the source it is still not

possible to relate the picrite basalts and nephelinites in terms of partial melting of the same source. Furthermore, the average Zr/Nb ratio (18.1) for the picrite basalts is considerably higher than the ratio of 10 discussed above such that fractionation of a Zr/Nb ratio from 18.1 to 1.71 (for the nephelinites) is almost certainly beyond the bounds of normal crystal fractionation or partial melting processes.

The simplest interpretation of the data presented above is that the nephelinite and picrite basalt, while closely related in the field are derived from different sources. This conclusion can only be avoided if special circumstances are invoked. For example if the bulk REE partition coefficients in the (same) source were close to unity, or if the metasomatic enrichment processes discussed in the previous section served to selectively enrich those segments of the source area from which the picrite basalts were derived it may be possible to overcome these problems. In the case of the latter arguments it could be speculated that the nephelinite and associated carbonatitic volcanics (see Chapter 7) led to a depletion in Nb in the source though it is exceedingly difficult to conceive how it would enrich Zr bearing in mind that the formation of nephelinites is attributed to small degrees of partial melting which would rapidly deplenish the source in Zr. Other models involving the participation or non-participation of opaque phases such as ilmenite which are characterised by low Zr/Nb ratios (e.g. average Zr/Nb ratio in 9 magnesian ilmenites from Lesotho kimberlites = 0.82; Mitchell et al., 1973, Table 65) due to the melting of the same source at different pressures could also be formulated though such models are even more speculative than the processes discussed above.

Given these facts it is suggested here that the nephelinites and picrites were not derived from the same source. Instead it is suggested that the nephelinites were derived from a different source and were formed

by small degrees of partial melting in a CO_2 rich environment during the initial (proto-rift) stage of the fragmentation of eastern Gondwanaland. A model outlining the proposed sequence of events which led to the formation of the nephelinites and overlying picrite basalts is presented in the synthesis in Chapter 11.

8.8 Summary and Conclusions

By invoking the metasomatic and melting processes outlined above it should therefore be possible to create the observed geochemical relationships noted in the picrite basalts, in particular the enrichment in KAR elements and the atypical (positive) correlation between these elements and MgO. Furthermore, a metasomatic process provides a number of advantages in comparison to the zone refining and wall rock reaction models outlined by Cox and Jamieson (1974) and Norry (1977).

Firstly, as noted previously, a mantle metasomatism model is in essence simpler than either wall rock reaction or zone refining. Secondly, introduction of elements such as K and Rb would enrich the upper mantle in radiogenic elements and it is possible, though speculative, that an increase in heat flow associated with the radioactive decay of these elements may have played a role in the initiation of volcanism in the Lebombo and adjoining areas. Thirdly, metasomatism is considered to be a viable mechanism to account for (a) the heterogeneity, both chemical (this chapter) and isotopic (Chapter 10) which appears to have existed in the source area from which the picritic rocks were derived and (b) the enrichment in REE and unusual 'Z shaped' REE pattern obtained for the picrite basalts.

In conclusion, the sequence of events postulated for a metasomatic enrichment model giving rise to the unique picrite basalts of the eastern Karoo are presented here:-

1. Pre-Karoo metasomatism giving rise to mantle domains enriched in KAR elements.

2. Extensional tectonism in eastern Gondwanaland leading to stress release and melting in the upper mantle.

3. Dilation of the eastern Gondwanaland crust along lines of weakness giving rise to an upwarp of the crust/mantle interface such that melting of mantle material is initiated by the lower pressures encountered during up-doming into the lower crustal regime. This would account for the relatively low olivine-orthopyroxene-liquid equilibration pressures (7 - 10 kbar) obtained by Cox and Jamieson (1974) from experimental studies.

4. A range of porphyritic parental melts with up to 18% MgO formed in response to melting. Initial magmas were derived from KAR element enriched domains and equilibrated with olivines and orthopyroxenes at higher pressures such that they were also enriched in normative olivine. The high normative olivine content of these lavas coupled with volatile release at low pressures would have promoted the formation of skeletal olivines and very glassy or microcrystalline groundmasses, textural characteristics that are typically found in the lower portions of the northern Lebombo picrite basalt sequence.

5. Later magmas were derived from source areas which were depleted in KAR elements. In addition these magmas equilibrated at lower pressures than earlier magmas and were therefore less olivine normative. Basalts derived from these magmas were therefore depleted in KAR elements and less magnesian than earlier lavas.

The overall process described above could therefore account for the positive correlations between some of the KAR elements and MgO. Major element variations also indicate that the source composition was rich in olivine and orthopyroxene and the mantle orthopyroxenes and magnesian olivines represent fractionating phases which were brought to the surface in small amounts during the emplacement of the lavas.

9 OLIVINE POOR LAVAS AND DYKES OF THE LEBOMBO

9.1 Introduction

Olivine-poor lavas and dykes with less than 9% modal olivine are the most voluminous of the mafic rock types found in the Lebombo and occur in great thicknesses in the Tuli, Nuanetsi and Sabi areas of Zimbabwe. In terms of the classification scheme outlined in Chapter 5 they fall in the range 3-9% MgO (weight percent) and may be classified as tholeiitic-basalts, shoshonites or absarokites (collectively referred to as low-MgO volcanics) on the basis of the relationship between their MgO and K_2O contents (weight percent).

The olivine-poor lavas are represented primarily by the Sabie River Formation (Cleverly and Bristow, 1979) though basic volcanics found interbedded with rhyolite flows in Nuanetsi (Cox et al., 1965) and in the Movene Formation of Mozambique and northern Natal (Cleverly and Bristow, 1979) fall into this category. The majority of Lebombo intrusive rocks, including the Rooi Rand dyke swarm (Bristow, 1976; Armstrong, 1978) and Effingham dolerites (Frankel, 1969) are also characterised by olivine-poor mineral assemblages and are therefore included in this category. The low-MgO volcanics (lavas and dykes) which crop out in the Lebombo, viz. the Sabie River Formation and Rooi Rand dykes, are discussed below. Unfortunately detailed studies of the olivine-poor lavas of the Movene Formation have been prevented by political 'problems' whereas the petrogenesis of the Nuanetsi low-MgO volcanics has been discussed elsewhere (Cox, 1972a; Cox et al., 1980).

In general the olivine-poor lavas and dykes of the Lebombo are remarkably uniform with respect to their petrography and variations that do exist are mainly of a textural nature. However, significant geochemical

variations are present within the group. An assessment of the petrography mineralogy and geochemistry of these rocks is presented in this chapter and processes which may account for the geochemical variation, eg. crustal contamination, fractional crystallisation, are discussed and modelled.

9.2 Petrography and Mineralogy

9.2.1 General Statement

The petrography of the Lebombo olivine-poor volcanics, and in particular the olivine-poor lavas and dolerites of Swaziland and the southern Lebombo, has been extensively described by Lombaard (1952), Urie and Hunter (1963), Bristow (1976), Armstrong (1978), and Betton (1978). For this reason only the more salient petrographic features of these rocks are presented in this chapter.

New microprobe analyses of the mineral phases found in the olivine-poor lavas and intrusives have been carried out. These data, together with analyses of mineral phases from the Rooi Rand dolerites (Armstrong, 1978) and a lava from Swaziland (Sample EH8; Betton, 1978) have been used to investigate mineralogical variations within these rocks. Representative analyses of mineral phases found in the olivine-poor volcanics are incorporated in the text whereas the complete compilation of electron microprobe data can be found in Microfiche Table E.3, Appendix E.

The olivine-poor lavas and dykes consist predominantly of plagioclase and clinopyroxene (Table 9.1) with lesser amounts of olivine, opaque oxide, apatite, K-feldspar and quartz. They show a range of textures from fine to coarse grained aphyric (Plates 9.1 A,C) through intersertal (Plates 9.1 E,G) to sparsely or strongly porphyritic and glomeroporphyritic (Plates 9.1 B,D). The mesostasis of the very fine grained rocks typically consists of glassy or microcrystalline material (Plates 9.1 D,E,G,H,) which often has a felted texture (Plates 9.1 E,H) due to the presence of

PLATE 9.1

A - Photomicrograph of fine-grained southern Lebombo aphyric dolerite L267. Note the relatively fresh appearance of plagioclase crystals. Crossed polars.

B - Plagioclase phyric dolerite dyke L188 from the southern Lebombo. As in the case of plate 9.1.A the feldspars do not show any noticeable alteration effects. Crossed polars.

C - Photomicrograph of an aphyric low-MgO lava (L202b) from the southern Lebombo. Note the altered appearance of the feldspars in this rock in contrast to the fresh appearance of feldspars in the dolerites depicted in plates A and B. Crossed polars.

D - Plagioclase-phyric low-MgO lava CL372 from the central Lebombo. Feldspars, though reasonably unaltered, do not have the pristine appearance of feldspar crystals in dolerite L188 (Plate 9.1.B). Crossed polars.

E - Photomicrograph of an intersertal textured dolerite sill from the northern Lebombo (KA52b). Microcrystalline mesostasis apparent in the rock consists of tightly appressed feldspar crystallites. Crossed polars.

F - Glomeroporphyritic aggregate of clinopyroxene microphenocryst olivine-poor lava KA25 from the northern Lebombo. Crossed polars.

G - Photomicrograph of spicular ilmenites in a very fine grained intersertal lava from the northern Lebombo (Sample CL100). Plane polarised light.

H - Subhedral ilmenite microphenocrysts in a fine grained dolerite sill from the northern Lebombo. A subrounded olivine crystal is present slightly to the left of centre in the photomicrograph (Sample KA52b). Crossed polars.

PLATE 9.1

A

1.5mm

B

2mm

C

1mm

D

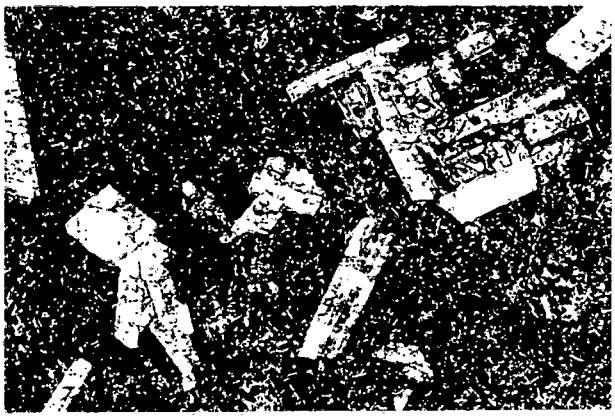

3mm

E

2mm

F

1.6mm

G

1.2mm

H

1mm

tightly appressed feldspar microlites whereas the groundmass in coarser grained rocks often assumes an intergranular appearance. The lavas are invariably altered (Plate 9.1C) and are commonly green or reddish in hand specimen; olivine and plagioclase are particularly prone to alteration. In contrast intrusive rocks are far less susceptible to alteration (Plate 9.1.A) and are therefore more suitable for analytical work. Brief petrographic descriptions of individual rocks are incorporated in Appendix D, Tables 1 - 5.

9.2.2 Olivine

Rounded or subhedral olivine phenocrysts or microphenocrysts are occasionally found in these rocks. They are invariably altered or pseudomorphed and seldom constitute more than 5% by volume of the rocks they are found in (Table 9.1).

Selected olivine analyses are presented in Table 9.2 whereas the compositional range in olivines from the low MgO lavas and dykes is included on Figure 9.1. Microphenocryst olivine relicts in the Rooi Rand dolerites (analyses 1-3, Table 9.2) have magnesian cores ($\sim Fo_{75}$) and show zoning towards their rims to slightly more Fe-rich compositions ($\sim Fo_{73}$). Olivine phenocrysts in the intrusive tholeiitic andesite sills from the Olifants River area (e.g. sample KA52b) are distinctly more Fe rich (analyses 4-5, Table 9.2) with an average composition of about Fo_{49}. Olivine analyses have not been obtained from the lavas because of the paucity of fresh phenocrysts.

9.2.3 Pyroxene

Clinopyroxene occurs in all the rocks of this suite. It is present as phenocrysts in glomeroporphyritic clusters or microphenocrysts in

TABLE 9.2

LEBOMBO LOW-MGO LAVAS + DYKES : MINERAL ANALYSES

	1	2	3	4	5	6	7	8	9	10
SIO2	37.99	37.77	37.51	35.30	35.10	50.62	49.11	51.90	52.57	50.46
TIO2	.05	.06	.05	.07	.07	1.21	.99	1.34	1.04	1.21
AL2O3	.14	.06	.07	.06	.05	3.17	1.56	2.10	1.56	1.93
CR2O3	-	-	-	-	-	-	-	-	-	-
FEO	22.49	24.22	24.98	37.98	43.43	11.05	23.82	8.99	8.77	14.69
MNO	.27	.27	.28	.44	.45	.23	.39	.16	.15	.82
MGO	37.80	37.63	37.12	24.00	21.38	15.50	7.50	15.86	16.56	13.61
CAO	.48	.38	.37	.31	.32	17.09	16.47	18.90	18.21	17.70
NA2O	-	-	-	-	-	.22	.23	.24	.22	.26
K2O	-	-	-	-	-	-	-	-	-	-
TOTAL	99.22	100.39	100.38	98.16	100.80	99.09	100.07	99.49	99.08	100.68

* * ATOMIC PROPORTIONS BASED ON SELECTED NO. OF OXYGENS * *

OXYGEN	4	4	4	4	4	6	6	6	6	6
SI	.998	.989	.987	1.015	1.008	1.902	1.942	1.931	1.955	1.909
ALIV	.004	.002	.002	.002	.002	.098	.058	.069	.045	.086
ALVI	-	-	-	-	-	.042	.014	.023	.024	-
TI	.001	.001	.001	.002	.002	.034	.029	.037	.029	.034
CR	-	-	-	-	-	-	-	-	-	-
FE2+	.494	.531	.550	.914	1.043	.347	.788	.280	.273	.465
MN	.006	.006	.006	.011	.011	.007	.013	.005	.005	.026
MG	1.481	1.469	1.455	1.029	.915	.868	.442	.879	.918	.767
CA	.014	.011	.010	.010	.010	.688	.698	.753	.726	.717
NA	-	-	-	-	-	.016	.018	.017	.016	.019
K	-	-	-	-	-	-	-	-	-	-
SUM	2.998	3.009	3.011	2.982	2.990	4.002	4.002	3.995	3.990	4.024
	FO 74.97	FO 73.47	FO 72.59	FO 52.96	FO 46.73	WO 36.15	WO 36.20	WO 39.39	WO 37.87	WO 36.80
	FA 25.03	FA 26.53	FA 27.41	FA 47.04	FA 53.27	EN 45.60	EN 22.93	EN 45.98	EN 47.90	EN 39.36
						FS 18.24	FS 40.87	FS 14.63	FS 14.23	FS 23.84

* * * S A M P L E D I R E C T O R Y * * *

ANALYSIS NO.	DESCRIPTION
1	OLIVINE PHENO (A186)
2	OLIVINE PHENO (A186)
3	OLIVINE PHENO (A186)
4	OLIVINE PHENO (KA52B)
5	OLIVINE PHENO (KA52B)
6	CPX PHENO CORE (EH8)
7	CPX GRAIN RIM (EH8)
8	CPX GRAIN (CL100)
9	CPX GRAIN (CL100)
10	CPX MICROPHENO (KA52B)

TABLE 9.2 (CONTINUED)

LEBOMBO LOW-MGO LAVAS + DYKES : MINERAL ANALYSES

	11	12	13	14	15	16	17	18	19	20
SIO2	53.16	53.52	51.18	50.90	51.41	51.65	58.80	52.58	65.69	67.36
TIO2	.25	.28	.57	.57	.58	.34	.13	.09	-	-
AL2O3	2.10	1.47	3.13	3.07	2.77	2.72	25.72	28.88	24.23	21.24
CR2O3	-	-	-	-	-	-	-	-	-	-
FEO	7.16	9.82	9.21	8.51	8.40	7.44	.82	.54	.11	.06
MNO	.15	.23	.11	.17	.16	.21	-	-	-	-
MGO	19.54	19.79	16.12	16.72	16.49	17.43	.06	.17	-	-
CAO	17.59	14.71	18.72	18.69	19.26	18.45	8.39	12.98	3.15	1.29
NA2O	.19	.14	.25	.24	.19	.24	6.51	3.94	7.27	10.59
K2O	-	-	-	-	-	-	.52	.18	.22	.20
TOTAL	100.14	99.96	99.29	98.87	99.26	98.48	100.95	99.36	100.67	100.74

* * ATOMIC PROPORTIONS BASED ON SELECTED NO. OF OXYGENS * *

OXYGEN	6	6	6	6	6	6	8	8	8	8
SI	1.937	1.960	1.909	1.903	1.914	1.925	2.618	2.405	2.843	2.927
ALIV	.063	.040	.091	.097	.086	.075	1.350	1.557	1.236	1.088
ALVI	.027	.023	.046	.038	.036	.044	-	-	-	-
TI	.007	.008	.016	.016	.016	.010	.004	.003	-	-
CR	-	-	-	-	-	-	-	-	-	-
FE2+	.218	.301	.287	.266	.262	.232	.031	.021	.004	.002
MN	.005	.007	.003	.005	.005	.007	-	-	-	-
MG	1.061	1.080	.896	.931	.915	.968	.004	.012	-	-
CA	.687	.577	.748	.749	.768	.737	.400	.636	.146	.060
NA	.013	.010	.018	.017	.014	.017	.562	.349	.610	.892
K	-	-	-	-	-	-	.030	.011	.012	.011
SUM	4.018	4.006	4.015	4.023	4.016	4.015	4.999	4.993	4.851	4.981
	WO 34.93	WO 29.48	WO 38.73	WO 38.47	WO 39.51	WO 38.04	AN 40.36	AN 63.86	AN 19.01	AN 6.23
	EN 53.97	EN 55.16	EN 46.39	EN 47.86	EN 47.05	EN 49.99	AB 56.67	AB 35.08	AB 79.41	AB 92.61
	FS 11.10	FS 15.36	FS 14.87	FS 13.67	FS 13.45	FS 11.97	OR 2.98	OR 1.05	OR 1.58	OR 1.15

* * * S A M P L E D I R E C T O R Y * * *

ANALYSIS NO.	DESCRIPTION
11	CPX PHENO (A49)
12	CPX MICROPHENO (A49)
13	CPX GRAIN (A170)
14	CPX GRAIN CORE (A186)
15	CPX SUBOPH WITH PLAG (A186)
16	REP. CEN. KAROO CPX
17	PLAG GRAIN CORE (EH8)
18	PLAG PHENO RIM (EH8)
19	PLAG MICROPHENO (CL100)
20	PLAG MICROPHENO RIM (CL100)

TABLE 9.2 (CONTINUED)

LEBOMBO LOW-MGO LAVAS + DYKES : MINERAL ANALYSES

	21	22	23	24	25	26	27	28	29	30
SIO2	52.21	52.97	54.74	55.65	46.31	50.71	.34	.39	-	67.35
TIO2	.04	.05	-	-	.04	.07	22.10	12.54	50.39	.98
AL2O3	30.14	29.58	28.38	27.73	33.45	30.30	.87	1.21	.23	12.07
CR2O3	-	-	-	-	-	-	-	-	-	-
FE2O3	-	-	-	-	-	-	24.38	42.12	5.45	-
FEO	.66	.62	.62	.61	.40	.68	50.03	42.00	41.77	6.65
MNO	.10	.12	.02	.02	-	-	.75	.49	.32	-
MGO	-	-	.10	.09	.21	.26	.26	.24	1.79	1.85
CAO	12.99	12.72	11.43	10.50	17.40	14.12	.69	.28	.02	.52
NA2O	3.94	4.29	4.65	4.74	1.63	3.46	-	-	-	1.92
K2O	.13	.21	.56	.57	.02	.05	-	-	-	7.05
TOTAL	100.21	100.56	100.50	99.91	99.46	99.65	99.42	99.27	99.98	98.39

* * ATOMIC PROPORTIONS BASED ON SELECTED NO. OF OXYGENS * *

OXYGEN	8	8	8	8	8	8	4	4	3	
SI	2.370	2.396	2.468	2.512	2.145	2.324	.013	.015	-	-
AL	1.613	1.577	1.508	1.476	1.826	1.637	.038	.054	.007	-
TI	.001	.002	-	-	.001	.002	.624	.357	.945	-
CR	-	-	-	-	-	-	-	-	-	-
FE3+	-	-	-	-	-	-	.688	1.201	.102	-
FE2+	.025	.023	.023	.023	.015	.026	1.570	1.332	.872	.000
MN	.004	.005	.001	.001	-	-	.024	.016	.007	-
MG	-	-	.007	.006	.014	.018	.015	.014	.067	.000
CA	.632	.617	.552	.508	.864	.693	.028	.011	.001	-
NA	.347	.376	.406	.415	.146	.307	-	-	-	.000
K	.008	.012	.032	.033	.001	.003	-	-	-	-
SUM	4.999	5.008	4.998	4.974	5.014	5.011	3.000	3.000	2.000	.000
	AN 64.07	AN 61.35	AN 55.72	AN 53.15	AN 85.41	AN 69.08	US 64.44	US 37.31	IL 88.19	
	AB 35.17	AB 37.44	AB 41.02	AB 43.42	AB 14.48	AB 30.63	MT 35.56	MT 62.69	GK 6.68	
	OR .76	OR 1.21	OR 3.25	OR 3.44	OR .12	OR .29			HM 5.14	

* * * SAMPLE DIRECTORY * * *

ANALYSIS NO.	DESCRIPTION
21	PLAG PHENO CORE-A (CL372)
22	PLAG PHENO RIM -B (CL372)
23	PLAG PHENO CORE-A (KA52B)
24	PLAG PHENO RIM -B (KA52B)
25	PLAG PHENO CORE-A (A49)
26	PLAG PHENO RIM -B (A49)
27	TI-MAG GRAIN (A129)
28	TI-MAG GRAIN (A170)
29	ILMENITE MICROPHENO (KA52B)
30	GLASS GROUNDMASS (KA52B)

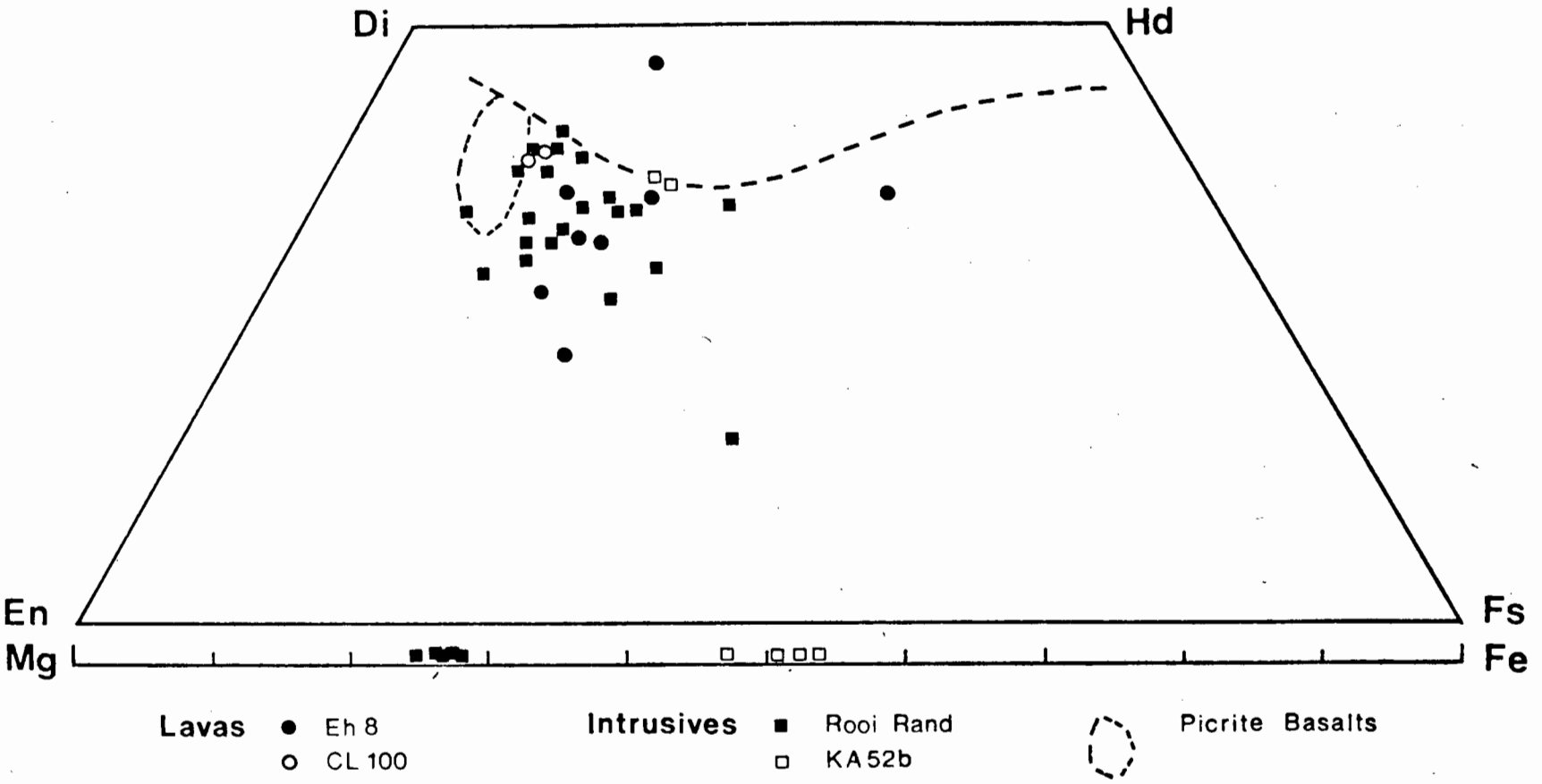

Fig. 9.1 Compositions of pyroxenes and olivines from the Lebombo low-MgO lavas and dykes.

nodular aggregates (Plate 9.1.F) in some of the rocks, but more typically as granules and narrow elongated prisms in the groundmass. It is commonly altered to chlorite. Rare lath shaped relicts and small grains of orthopyroxene have been noted in the Rooi Rand dolerites (Cox pers. comm.) and Swaziland lavas (Betton, 1978; Sample EH8).

Nodular aggregates of clinopyroxene up to 3 or 4mm across (Plate 9.1.F) are only found in the central and northern Lebombo lavas. They are particularly common in the intermediate-K tholeiitic andesite intrusives, absarokites and shoshonites, though they are also found in tholeiitic basalts characterised by relatively high abundances of incompatible elements. Similar aggregates are found in the picrite basalts and are discussed in section 8.2.4.

The compositional trends of the clinopyroxenes are shown in Figure 9.1 and representative analyses are presented in Table 9.2 (analyses 6-15). (Also included on Figure 9.1 is the compositional field of clinopyroxenes found in the picrite-basalts). The clinopyroxenes define a crude Fe-enrichment trend and are generally Ca-rich though a few analyses plot nearer the field of Ca-poor pyoxenes. Phenocrysts are generally more magnesian than the groundmass clinopyroxenes (see analyses from sample A186, Table 9.2) and they tend to be enriched in TiO_2 (weight %) relative to clinopyroxenes from the central Karoo olivine-poor rocks (analysis 16; Table 9.2).

9.2.4 Plagioclase

Plagioclase is the most abundant mineral of the olivine-poor rocks (Table 9.1). Individual grains are present in the form of phenocrysts and microphenocrysts, not uncommonly arranged in glomeroporphyritic aggregates, laths and needles in the groundmass, as well as incipient

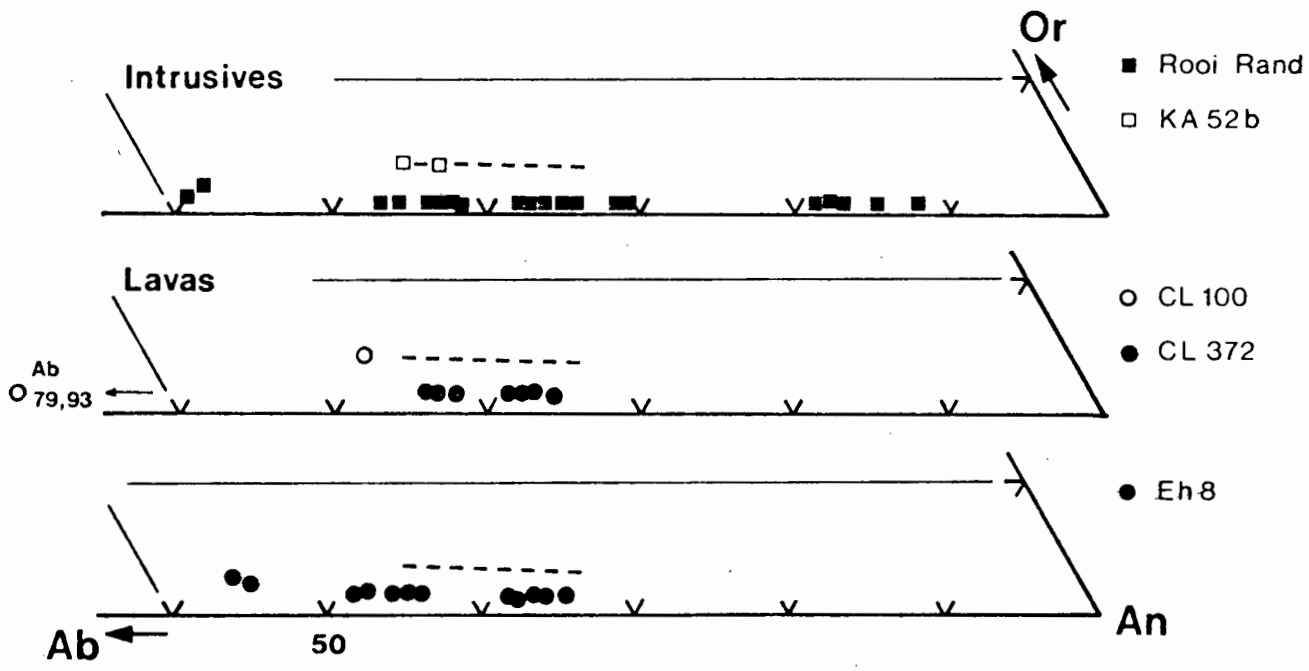

---- Compositional trend of feldspars in the Picrite Basalts.

Fig. 9.2 Compositions of feldspars from the Lebombo low-MgO lavas and dykes.

and skeletal crystals in intersertal glass. A highly plagphyric lava flow from the Letaba River contains plagioclase macrophenocrysts up to 5cm in length.

Crystals are twinned principally on the Carlsbad, pericline and albite laws and zoning is common in phenocrysts, microphenocrysts and groundmass plagioclase. Slight oscillatory zoning has been noted in some phenocrysts. The plagioclases are rarely found in a fresh state in the lavas and are generally altered to sericite and calcite.

Ranges in composition of the analysed plagioclase are shown in Figure 9.2 and representative analyses are presented in Table 9.2 (analyses 17-26); additional analyses can be found in microfiche Tables E.3 a-c. The phenocrysts are strongly zoned, eg. An_{63} - An_{55} (sample CL372), and generally have rather variable rim compositions which may be similar to groundmass analyses in the same rock. Plagioclases in the tholeiitic basalts and andesitic tholeiites (lavas and intrusives) range in composition from An_{85} to An_{40} with most of the analyses falling in the range An_{70} to An_{40}. The most basic plagioclase compositions An_{85} - An_{79} are found in the most primitive Rooi Rand dolerite (MgO = 7.1%).

Plagioclase laths in the aphyric shoshonites (Sample CL100) are strongly albitic in composition (An_{19}; An_{6}) and a single microlath has a composition of An_{49} $Or_{4.5}$. The more potassic nature of the latter suggests that it is a late stage crystallisation product. Plagioclase phenocryst and microphenocryst compositions of the K-rich tholeiitic andesite dolerites (Sample KA52; An_{56} - An_{53}) from the northern Lebombo are notably enriched in the orthoclase molecule ($Or_{3.4}$) and in this respect are similar to feldspars found in the picrite basalts (Fig. 9.2).

Plagioclase rim analyses are commonly enriched in potassium and thin sanidine overgrowths are apparent on some plagioclase phenocrysts and microphenocrysts. Intersertal sanidine is also found in the groundmass of some of these rocks, in particular the shoshonites and absarokites. The increased content of K_2O at phenocryst margins and appearance of sanidine in the matrix reflects the very high potassium content of many of the lavas and intrusives. Since none of the constituent mineral phases, besides sanidine, incorporate K_2O into their lattices it must be partitioned into the matrix and this has been affirmed by the high K_2O content of glass analyses (eg. analysis 30; Table 9.2).

9.2.5 Fe-Ti Oxides

Fe-Ti oxides are generally confined to the groundmass, apart from scarce phenocrysts and microphenocrysts seen in some of the lavas, Rooi Rand dolerites and intrusives of the Olifants River section.

The oxide minerals found in most of the southern Lebombo and Swaziland lavas and dolerites (including Rooi Rand) have a crude octahedral shape and are invariably titanomagnetites (analyses 27,28; Table 9.2). Skeletal crystals are found in some rocks, particularly the fine-grained or glassy intrusives, and 'comb-like' structures occur in the very fine-grained Rooi Rand intrusives.

Opaque minerals found in the majority of the central and northern Lebombo lavas and intrusives are generally spicular in habit (Plate 9.1.G). This is especially true of the fine grained, generally aphyric, shoshonites, absarokites and intermediate-K lavas and intrusives which are dominant in the central and northern part of the volcanic belt. In the fresh rocks compositions of the spicular opaques are ilmenitic though since most of the lavas are altered and oxidised, the opaque

minerals are rarely homogeneous, exsolution of rutile being particularly prevalent in many of the ore spicules. However, octahedral-type microphenocrysts are found in some central and northern Lebombo volcanics, particularly in those lavas and intrusives with relatively normal geochemistry, ie. low contents of K and incompatible elements.

Ilmenite phenocrysts (up to 0.8mm) and microphenocrysts occur in the intermediate-K tholeiitic andesitic intrusives of the Olifants River area. They occur as discrete crystals in the groundmass and also form glomeroporphyritic aggregates with clinopryoxene and plagioclase feldspars (Plate 9.1.H). Analyses of these crystals are included in Table 9.2 (Analysis 29) and it is apparent that they are enriched in magnesium even though the whole rock chemistry of these rocks, eg. Sampe KA52b, is relatively evolved (MgO = 3.71).

9.2.6 Accessory Minerals

Occasional flakes of biotite have been noted in some of the rocks whereas needles of apatite occur in all the lavas and intrusives. Apatite is particularly abundant in those low MgO volcanics rich in K and incompatible elements and appears as prominent microphenocrysts in many of the medium to coarse grained intrusive rocks found in the Olifants River area of the northern Lebombo. Granophyric intergrowths of quartz and feldspar are present in some medium to coarse grained intrusives and both these minerals may occur in lavas. Interstitial glass is a common accessory in lavas and intrusives.

A variety of secondary hydrothermal minerals infilling macro- and micro-vesicles occur in the lavas but rarely in the intrusives. The most common secondary minerals are chlorites, calcite, chalcedoney, quartz and zeolites. The remaining accessory minerals consist of alteration

products. Feldspars typically alter to sericite and saussurite, olivines are mostly serpentinised and pyroxenes are either calcitised or chloritised. Many of the lavas are strongly chloritised and silicified and therefore unsuitable for any form of geochemical study.

9.3 General Geochemistry

Representative analyses of low-MgO lavas and dykes found in the Lebombo are presented in Table 9.3, whereas average analyses are listed in Table 9.4. Inspection of these data indicates that there are considerable areal variations, particularly amongst the minor and trace elements K_2O, P_2O_5, Rb, Sr, Ba, Zr and Nb, within the lavas and dykes. Rooi Rand dolerites* (analyses 1-3, Table 9.3; 1-2, Table 9.4) are undoubtedly the most depleted with respect to these elements and in general tend to be more primitive than the lavas. In view of the relatively depleted nature of the Rooi Rand dykes it is possible that they may have been derived from a source area which had undergone partial depletion by previous magmatic or related processes, a point that will be reiterated later in this thesis in Chapter 10. The dyke swarm cuts the lowermost lavas of the southern Lebombo volcanic succession whereas in Swaziland it crops out within the basaltic lava succession. On the basis of field relationships, the dyke swarm is therefore younger than most of the Swaziland and lower southern Lebombo lavas.

In contrast to the Rooi Rand dykes, lavas which form the surrounding countryrock in Swaziland and the southern Lebombo tend to be more evolved and also show higher levels of incompatible elements (analyses 4-6,

*Footnote: The Rooi Rand dolerite dykes are so named throughout this thesis and specifically referred to as such. In all other cases the use of the term dyke or dykes refers to intrusives other than those of the Rooi Rand Swarm.

TABLE 9.3 Whole rock analyses, inter-element ratios and C.I.P.W. norms for selected Lebombo low-MgO volcanics.

	1 A135	2 A41	3 A117	4 L348	5 J3	6 L418	7 CL376	8 CL100	9 KA34	10 KA52b
%SiO_2	48.27	48.54	51.10	54.64	46.85	57.37	52.75	54.06	50.17	52.09
TiO_2	2.15	2.57	2.74	1.05	2.66	2.46	1.98	3.15	3.36	3.08
Al_2O_3	14.03	13.67	12.67	14.76	12.77	12.00	13.17	12.42	12.01	13.32
Fe_2O_3*	14.19	16.16	14.62	10.32	15.73	13.43	13.52	11.03	11.54	13.17
MnO	.19	.23	.21	.14	.21	.21	.17	.15	.14	.15
MgO	7.20	5.42	4.20	6.20	5.66	2.49	4.92	4.98	6.58	3.66
CaO	9.99	9.71	8.36	9.08	8.79	4.68	8.50	7.70	8.86	6.84
Na_2O	2.17	2.48	2.64	2.09	3.39	3.84	2.41	2.20	2.48	2.95
K_2O	.35	.62	1.02	1.01	.29	2.12	.93	2.60	1.60	2.45
P_2O_5	.22	.29	.51	.13	.31	.46	.19	.51	.50	.94
H_2O^+	.22		.80	.81	.82	.88	1.16	1.43	.88	.32
H_2O^-	.16	.11	.13	.33	3.00	.53	.19	.36	1.56	.70
CO_2					.12				.85	.08
TOTAL	99.14	99.80	99.00	100.56	100.60	100.47	99.89	100.59	100.53	99.75
ppm Rb	7.9	18.8	26.3	41	8.8	49	21.2	54	21.3	50
Ba	80	195	366	159	146	360	179	955	756	881
Sr	224	209	267	166	235	257	318	1100	973	953
Zr	135	162	275	97	163	329	150	396	385	584
Nb	3.6	6.7	17.5	4.5	6.5	15.8	7.4	19.2	21.3	32
Cr	316	104	44	288	82	8.0	55	172	255	39
V	334	347	309	169	348	171	286	200	228	188
Sc	28.7	33	30	22.7	35	30	22.2	23.1	23.9	16.2
Ni	170	57	35	136	48	6.3	83	68	155	54
Co	58	52	45	44	45	23	55	44	45	37
Zn	91	106	132	94	107	126	110	106	115	140
Cu	259	343	335	66	270	568	132	112	102	153
Y	32	39	48	24.9	41	59	28.4	31	35	57

TABLE 9.3 continued

	1 A135	2 A41	3 A117	4 L348	5 J3	6 L418	7 CL376	8 CL100	9 KA34	10 KA52b
Zr/Nb	37.5	24.2	15.7	21.6	25.0	20.8	20.3	20.6	18.1	18.2
Zr/Y	4.22	4.15	5.73	3.90	3.98	5.58	5.28	12.8	11.0	10.2
K/Rb	365	274	322	205	273	359	364	400	624	407
K/Ba	36.3	26.4	23.1	52.7	16.5	48.9	43.1	22.6	17.6	23.1
K/Sr	13.0	24.6	31.7	50.5	10.2	68.5	24.3	19.6	13.7	21.3
K/Zr	21.5	31.8	30.8	86.4	14.8	53.5	51.5	54.5	34.5	34.8
K/Nb	807	768	484	1863	370	1114	1043	1124	624	636
K/Y	90.8	132	176	337	58.7	298	272	696	379	357
Ba/Rb	10.1	10.4	13.9	3.88	16.6	7.35	8.44	17.7	35.5	17.6
Ba/Sr	.357	.933	1.37	.958	.621	1.40	.563	.868	.777	.924
Ba/Zr	.593	1.20	1.33	1.64	.896	1.09	1.19	2.41	1.96	1.51
Rb/Sr	.035	.090	.099	.247	.038	.191	.067	.049	.022	.052
Mg //	51.4	41.3	37.5	56.6	43.7	28.6	41.9	47.2	53.0	35.5
				- C.I.P.W. NORMS -						
Qz	-	-	4.66	7.53	-	9.44	5.34	6.77	2.26	3.06
Ne	-	-	-	-	-	-	-	-	-	-
Or	2.07	3.66	6.03	5.97	1.71	12.53	5.50	15.36	9.45	14.48
Pl	45.87	45.32	42.05	45.59	47.46	41.74	42.76	34.95	37.90	40.83
Di	17.08	18.43	15.55	13.42	18.44	9.36	15.59	15.37	15.14	9.65
Hy	23.23	20.64	21.12	22.59	8.29	17.68	23.79	18.07	22.71	21.19
Ol	3.70	3.50	-	-	11.48	-	-	-	-	-
Mt	.85	1.04	.88	1.05	1.52	1.32	-	-	-	-
Il	4.08	4.88	5.20	1.99	5.05	4.67	3.76	5.98	6.38	5.85
Ap	.52	.69	1.21	.31	.73	1.09	.45	1.21	1.18	2.23
Cc					.27				1.93	.18

KEY TO TABLE 9.3

A135 - Rooi Rand dyke (basaltic) : Southern Lebombo

A41 - Rooi Rand dyke (basaltic) : Southern Lebombo

A117 - Rooi Rand dyke (tholeiitic andesite) : Southern Lebombo

L348 - Basaltic lava : Southern Lebombo

J3 - Basaltic lava : Southern Lebombo

L418 - Tholeiitic andesite lava : Southern Lebombo

CL376 - Tholeiitic andesite lava : Central Lebombo

CL100 - Absarokitic lava : Central Lebombo

KA34 - Absarokitic lava : Northern Lebombo

KA52b - Tholeiitic andesite sill : Northern Lebombo

Table 9.3; 3-4, Table 9.4). Dyke rocks which are clearly dissimilar to the Rooi Rand intrusives are also found in the southern Lebombo and show similar geochemical relationships to the lavas. Many of the lavas and dykes are strongly enriched in Sr (Ave. = 297 ppm) and characterised by high initial-Sr ratios (Ave. = .70795, S.D. = 0.0026) whereas the Rooi Rand dykes have an average $^{87}Sr/^{86}Sr_o$ ratio of .7039 (S.D. = 0.00002) and an average Sr content of 191 ppm (see Table 9.4).

Lavas and dykes from north of Swaziland (ie. central and northern Lebombo: analyses 7-10, Table 9.3; 5-7, Table 9.4) in general show degrees of enrichment in incompatible elements, particularly elements such as K_2O and Rb, which are very much greater than is the case in any of the low-MgO volcanics found to the south. Most of the central and northern lavas can be classified as shoshonites, high-K basaltic andesites or absarokites on the basis of their MgO and K_2O contents, and it is noticeable that the most enriched rocks are generally found towards the base of the succession. Lavas with low contents of K_2O and other incompatible elements are found in the central and northern Lebombo but are invariably high up in the succession and become less frequent to the north. However, all the low-MgO lavas (lower and upper) from the Komati River at the southern end of the central Lebombo are characterised by low abundances of K_2O and other incompatible elements and are in most respects similar to the low-MgO basalts of Swaziland and the southern Lebombo.

A considerable amount of new major and trace element data has been obtained from the southern Lebombo and this has been used, along with data obtained by Armstrong (1978) from the Rooi Rand dolerites, to investigate the rather complex compositional trends shown by the Swaziland and southern Lebombo basaltic lavas and intrusives. Fewer data are available

TABLE 9.4 Average analyses of low-MgO lavas from the Lebombo. Average data for central Karoo lavas, dolerites and 'continental basalts' are included for comparison.

	[1] RRAPHY	[2] RRPOPHY	[3] SLAPHYR	[4] SLPORPH	[5] KMTR	[6] SRAPHYR	[7] OLFR	[8] AVECKB	[9] AVECKD	[10] AVEBAS
%SiO_2	49.69	49.21	53.00	51.00	50.98	51.67	51.00	51.45	51.91	49.9
TiO_2	2.20	2.04	1.60	1.40	2.16	3.12	3.42	.98	.99	1.6
Al_2O_3	13.21	14.32	14.20	15.60	14.11	13.13	13.84	15.57	15.20	16.23
Fe_2O_3*	15.65	14.60	12.70	12.20	13.98	13.56	12.44	11.11	11.29	11.69
MnO	.23	.21	.20	.20	.19	.18	.15	.18	.19	.17
MgO	5.70	6.11	5.70	5.50	5.49	5.32	5.47	6.98	6.82	6.31
CaO	10.16	10.59	9.10	9.90	9.93	8.17	8.94	10.70	10.55	9.82
Na_2O	2.48	2.33	2.60	2.70	2.32	2.43	2.17	2.14	2.31	2.80
K_2O	.45	.38	.74	.59	.59	1.95	2.01	.72	.56	1.10
P_2O_5	.24	.20	.25	.19	.21	.49	.57	.17	.17	.30
ppm Rb	11.0	10.6	18.0	17.0	13.1	42	38	11.5	12.4	
Ba	147	101	286	245	206	790	909	175	205	
Sr	191	189	297	329	323	785	936	186	209	
Zr	156	128	142	111	148	339	364	92	98	
Nb	7.0	5.0	6.0	4.0	9.1	19	23	4.3	6.2	
Cr	99	158	160	137	96	81	218	263	276	
V	351	328	267	245	306	261	253	233	240	
Sc	37	33	30	29	31	26		31		
Ni	57	79	79	100	93	80	124	86	85	
Co	50	53	48	50	54	49	48	46	45	
Zn	111	108	100	92	111	121	118	83	86	
Cu	300	270	142	117	227	142	152	90	87	
Y	38	33	31	25	33	38	37	23.9	25.7	

KEY TO TABLE 9.4

RRAPHY	-	Average aphyric Rooi Rand dolerite (N = 22)
RRPORPH	-	Average porphyritic Rooi Rand dolerite (N = 16)
SLAPHYR	-	Average southern Lebombo-Swaziland aphyric lava (N = 26)
SLPORPH	-	Average southern Lebomob-Swaziland porphyritic lava (N = 16)
KMTR	-	Average Komati River lava (N = 5)
SRAPHY	-	Average Sabie River aphyric lava (N = 10)
OLFR	-	Average Olifants River lava (N = 7)
AVECKB	-	Average Lesotho Formation basalt, central Karoo (N = 53)
AVECKD	-	Average central Karoo chilled dolerite (N = 22) (Marsh, unpubl. data)
AVEBAS	-	Average continental basalt (N = 1513) (Manson, 1967)

from the central and northern Lebombo rocks and they are therefore only dealt with briefly. A further reason for concentrating on the rocks from the southern area is that a large amount of Sr-isotope data is available for the southern Lebombo lavas and dykes, including the Rooi Rand intrusives, and it has therefore been possible to place additional constraints (see Chapter 10) on petrogenetic models based on major and trace element data.

9.4 Rooi Rand Dolerites

9.4.1 Compositional Variation

The Rooi Rand dolerites are of particular importance amongst the basaltic rocks of the Lebombo because their compositional variation is comparatively rational. Trends on variation diagrams show less scatter than those of most Lebombo lava suites (see Figs. 9.3 a-f, 9.4 a-j) and many inter-element correlations have high levels of significance (see Table 9.5). Major element trends are typical of gabbro fractionation, showing strong enrichment in Fe_2O_3 and TiO_2, and depletion in CaO and Al_2O_3 with decreasing MgO. As is typical of basaltic suites SiO_2 shows comparitively little variation though there is a slight tendency for it to rise in the samples most depleted in MgO and CaO and most enriched in Fe_2O_3. Minor and trace elements are clearly divisible into those which are enriched strongly with falling MgO (eg. K_2O, P_2O_5, Rb, Ba, Zr, Nb; see Figs. 9.3, 9.4), those which are enriched at lesser rates (eg. Sr, Y, Zn, Cu), those which show little variation (V, Co), and those which are depleted (Sc, Cr, Ni) with falling MgO. Details of the behaviour of individual elements may be obtained from Table 9.5 and analyses 1 and 2 in Table 9.6 which shows average analyses for the evolved and primitive ends of the Rooi Rand aphyric trend.

TABLE 9.5 Selection of interelement correlation coefficients for 23 samples of aphyric Rooi Rand dolerites

	K	Rb	Ba	Sr	Nb	Zr	P	Ti	Y	Zn	Cu
Rb	+.97										
Ba	+.92	+.94									
Sr	+.88	+.89	+.89								
Nb	+.89	+.92	+.90	+.82							
Zr	+.84	+.86	+.81	+.69	+.94						
P	+.77	+.79	+.72	+.61	+.85	+.93					
Ti	+.57	+.40	+.29	+.17	+.53	+.70	+.81				
Y	+.56	+.58	+.50	+.29	+.71	+.88	+.86	+.83			
Zn	+.35	+.40	+.31	+.27	+.57	+.65	+.58	+.84	+.71		
Cu	+.35	+.36	+.22	+.09	+.47	+.70	+.71	+.81	+.91	+.71	
Si	+.52	+.52	+.68	+.65	+.41	+.21	+.18	-.30	-.14	-.17	-.43
Fe	+.21	+.21	+.08	+.06	+.48	+.48	+.57	+.84	+.80	+.76	+.83
Na	+.38	+.36	+.36	+.38	+.30	+.30	+.13	+.14	+.14	+.17	+.43
Al	-.41	-.40	-.28	-.17	-.55	-.70	-.59	-.86	-.83	-.84	-.80
Ca	-.86	-.88	-.86	-.69	-.92	-.95	-.85	-.75	-.82	-.63	-.60
Mg	-.78	-.80	-.76	-.62	-.85	-.90	-.79	-.78	-.81	-.74	-.62
Ni	-.66	-.68	-.72	-.61	-.69	-.67	-.50	-.47	-.53	-.56	-.30
Cr	-.67	-.66	-.72	-.50	-.63	-.65	-.56	-.45	-.58	-.35	-.33
Co	-.34	-.31	-.45	-.26	-.00	-.16	-.26	-.25	-.16	+.17	-.03
Sc	-.76	-.73	-.67	-.74	-.67	-.56	-.48	-.38	-.22	-.32	-.09

Confidence limits: 1% - .505, 5% - .396

Figs. 9.3 and 9.4 Variation diagrams for major, minor and trace elements in the Rooi Rand dolerites. Only aphyric rocks are included except in the Al_2O_3 diagram (C) where porphyritic rocks are shown by closed circles. This is the only diagram in which porphyritic and aphyric rocks occupy significantly different fields.

O - Aphyric rocks

● - Porphyritic rocks

(Data from Microfiche Table F4, Appendix F)

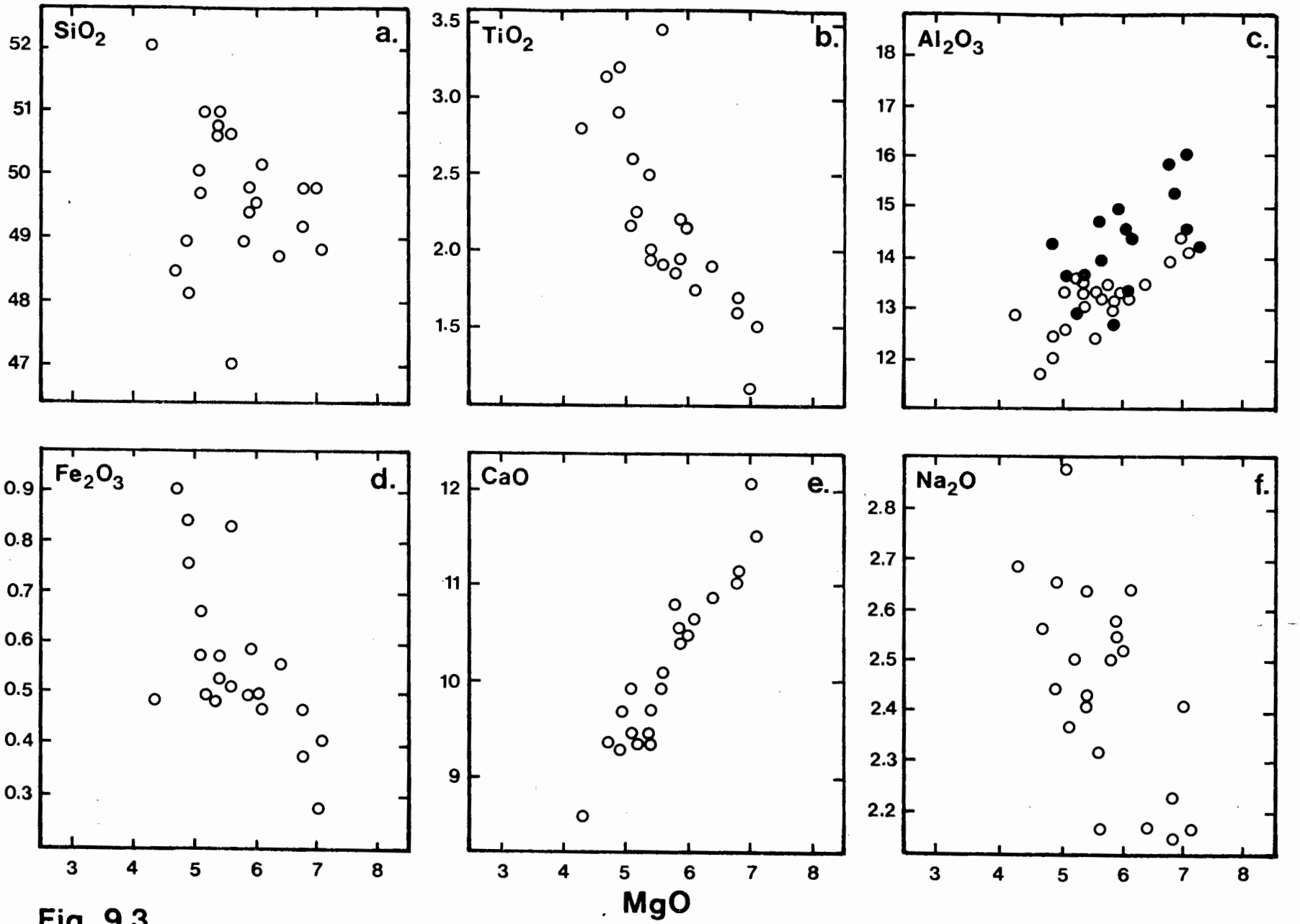
SiO2
a.
52
51
50
49
48
47
TiO2
b.
3.5
3.0
2.5
2.0
1.5
Al2O3
c.
18
17
16
15
14
13
12
Fe2O3
d.
0.9
0.8
0.7
0.6
0.5
0.4
0.3
CaO
e.
12
11
10
9
Na2O
f.
2.8
2.7
2.6
2.5
2.4
2.3
2.2
3
4
5
6
7
8
MgO

Fig. 9.3

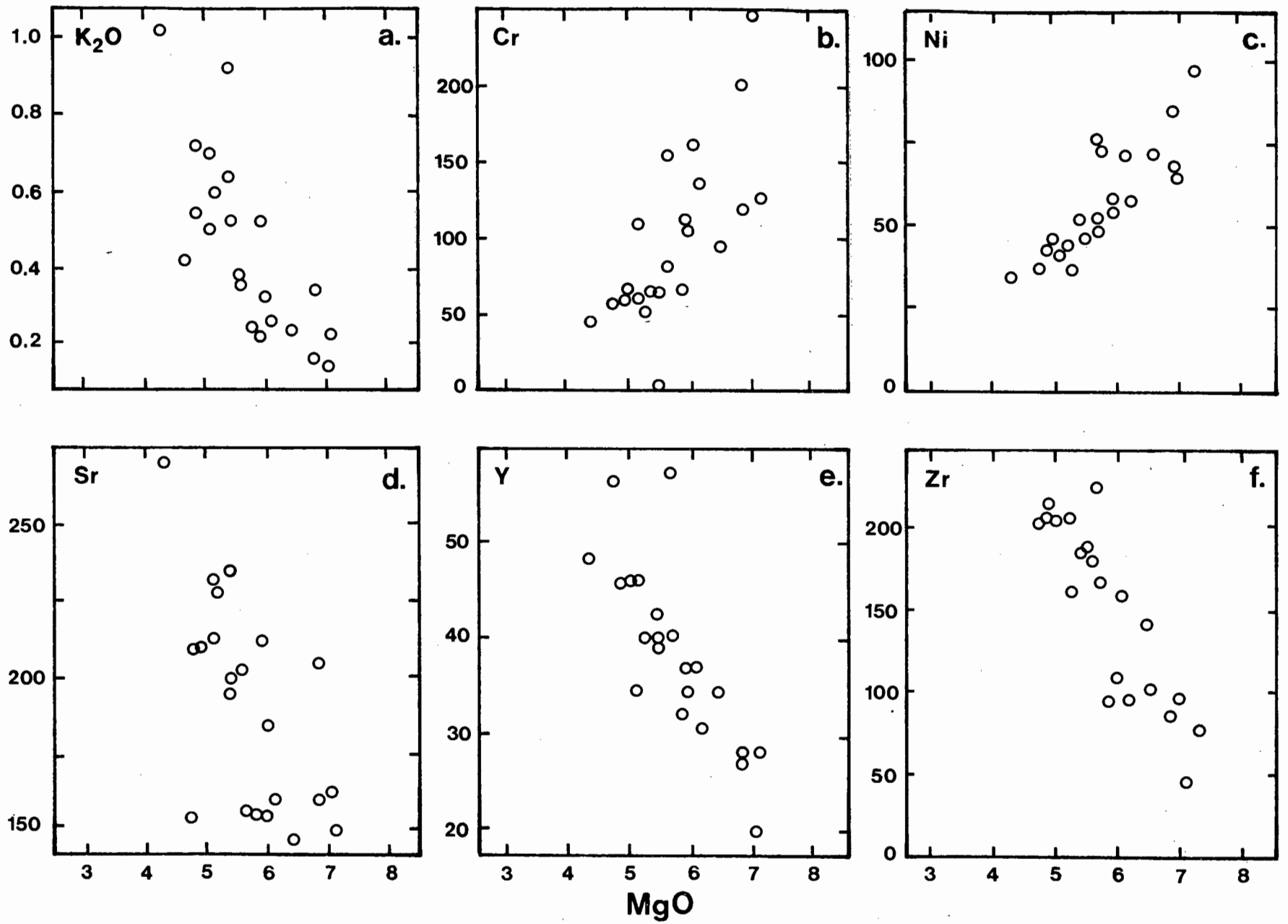
a.
K_2O
1.0
0.8
0.6
0.4
0.2
b.
Cr
200
150
100
50
0
c.
Ni
100
50
0
d.
Sr
250
200
150
e.
Y
50
40
30
20
f.
Zr
200
150
100
50
0
3
4
5
6
7
8
MgO

Fig. 9.4

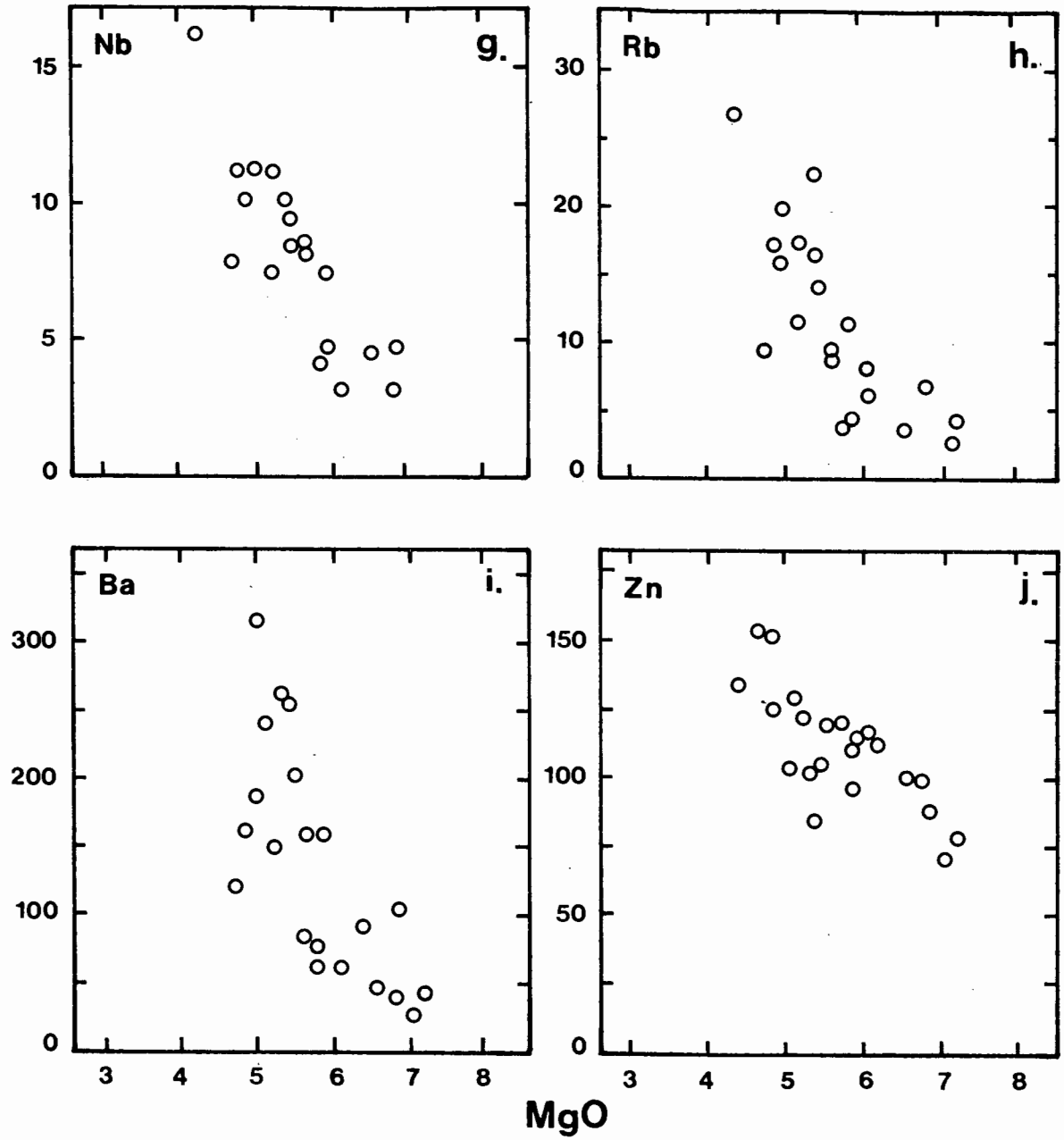
Nb
g.
15
10
5
0
Rb
h.
30
20
10
0
Ba
i.
300
200
100
0
Zn
j.
150
100
50
0
3
4
5
6
7
8
MgO

9.4.2 Major and Trace Element Modelling

The possibility that the Rooi Rand dolerites comprise a consanguineous suite related by low pressure fractional crystallisation has been quantitatively evaluated using the least squares approximation technique of Bryan et al. (1969) and utilising the compositions of observed phenocryst phases (see section 4.6). Two average liquid compositions were estimated from the primitive (RR1) and evolved (RR2) ends of the Rooi Rand variation diagrams and are given in Table 9.6 along with compositions of the phenocryst phases which were used in the mixing calculations. One point is, however, worth mentioning before proceeding with a discussion of the modelling calculations, that is initial-Sr ratios obtained for the Rooi Rand dolerites (Table 10.1) are consistently low (Ave. = .7039, S.D. = .0002) thereby suggesting that crustal contamination, which would probably have led to higher initial ratios in the magmas, played no significant role in the petrogenesis of these volcanics.

A least squares approximation relating the primitive Rooi Rand composition (RR1) to the evolved composition (RR2) is presented together with the input data in Table 9.7. The results indicate that the major element compositions of RR2 can be explained by the removal of about 29% clinopyroxene (En_{50}), 32% plagioclase (An_{69}) and minor amounts of titanomagnetite (~ 3% Us_{56}) and olivine (~ 1%, Fo_{72}) from RR1. The good major element agreement and low standard deviations of the components attest to the consistency of the model. However, it is possible that the F value obtained from this model (0.35) may not be that precise in view of the relatively large fractionation step that has been modelled (7.4 - 4.5% MgO). Compositions of phenocryst phases are likely to change drastically in the liquid compositions over the range 7.4 to 4.5% MgO and as a result F values would be expected to vary in relation to the

TABLE 9.6 Compilation of analyses used in mixing calculations, enrichment factors and mineral data.

	1 RR1	2 RR2	3 E	4 OLIVINE $Fo_{72.59}$	5 CPX 1 $En_{51.01}$	6 ALCPX	7 PLAG 1 $An_{69.08}$	8 PLAG 2 $An_{56.07}$	9 TIMG $Us_{56.42}$
$\%SiO_2$	49.80	51.64		37.46	51.58	48.92	50.93	53.79	.26
TiO_2	1.62	2.78		.05	.69	.01	.07	.10	18.47
Al_2O_3	14.75	12.24		.07	2.92	8.91	30.44	28.35	1.03
FeO	11.82	16.20		24.95	11.35	10.35	.68	.97	79.99
MgO	7.37	4.42		37.07	18.04	16.73	.26	.13	.09
CaO	12.02	8.74		.37	15.24	15.05	14.08	11.59	.13
Na_2O	2.22	2.78		.01	.16	.01	3.48	4.91	.01
K_2O	.30	.80	2.67	.01	.01	.01	.05	.16	.01
P_2O_5	.10	.39	3.90	.01	.01	.01	.01	.01	.01
ppm Rb	5	15	3.0						
Ba	50	200	4.0						
Sr	160	250	1.56						
Y	23	50	2.18						
Sc	39	32	0.82						
Zr	60	230	3.83						
Nb	6	14	2.33						
Ni	80	36	0.45						
Co	55	47	0.85						
Cr	200	20	0.10						
V	275	450	1.64						
Cu	160	410	2.56						
Zn	80	150	1.88						

1. Estimated composition of average primitive Rooi Rand magma.
2. Estimated composition of average evolved Rooi Rand magma.
3. Enrichment factors : Conc. in RR2/conc. in RR1.
4. Olivine; analysis 4, Sample A186, Microfiche Table E3.
5. Clinopyroxene; analysis 7, Sample A186, Microfiche Table E3.
6. Aluminous clinopyroxene; analysis 5, Table 11, Green and Ringwood (1967).
7. Plagioclase; analysis 7, Sample A49, Microfiche Table E3.
8. Plagioclase; analysis 6, Sample A101, Microfiche Table E3.
9. Titanomagnetite; analysis 1, Sample A186, Microfiche Table E3.

TABLE 9.7 Least squares approximation relating average composition of the most primitive and evolved Rooi Rand magmas. Sources of compositions used in the input data are given in Table 9.5.

Input Data

	RR1	OLIVINE	CPX	PLAG	TIMG	RR2
SiO_2	48.80	37.46	51.58	50.93	.26	51.64
TiO_2	1.62	.05	.69	.07	18.47	2.78
Al_2O_3	14.75	.07	2.92	30.44	1.03	12.24
FeO*	11.82	24.94	11.35	.68	79.99	16.20
MgO	7.37	37.07	18.04	.26	.09	4.42
CaO	12.02	.37	15.24	14.08	.13	8.74
Na_2O	2.22	.01	.16	3.48	.01	2.78
K_2O	.30	.01	.01	.05	.01	.80
P_2O_5	.10	.01	.01	.01	.01	.39
		Fo 72.59	Wo 30.99	An 69.08	Us 56.42	
		Fa 27.41	En 51.01	Ab 30.63	Mt 43.58	
			Fs 18.01	Or 0.29		

Least Squares Approximation

	RR1			MIX		
	OBS	CALC	DIFF	COMP	Wt%	S.D.
SiO_2	49.80	49.81	.01	RR2	35.24	.97
TiO_2	1.62	1.72	.10	OLIVINE	1.15	.36
Al_2O_3	14.75	14.76	.01	CPX	29.44	.76
FeO*	11.82	11.80	-.02	PLAG	31.49	.49
MgO	7.37	7.38	.01	TIMG	2.89	.18
CaO	12.02	11.99	-.03			
Na_2O	2.22	2.12	-.10	TOTAL	100.03	1.38
K_sO	.30	.30	.00			
P_2O_5	.10	.14	.04			

Sum of squares of residuals = .02

composition of the fractionating assemblage. However, it is notable that modelling calculations presented by Wood (1978) for a group of Icelandic lavas similar in composition to the Rooi Rand dolerites produce a similar F value (0.36) for an almost equivalent variation in MgO (6.3 - 3.77%).

The adequacy of this model, based on major elements, has been tested by trace element modelling assuming Rayleigh fractionation. Close agreement between the observed trace element content of RR2 and the predicted trace element content calculated using the fractionating assemblage derived from the major element model would provide support for a simple crystal fractionation process whereas poor agreement would imply that a more complex mechanism had caused the geochemical variation observed in the Rooi Rand rocks. Before discussing the results derived from the trace element modelling it should, however, be noted that although the minor and trace element data plotted in Figures 9.4 (aphyric rocks only) show reasonably well developed trends, there is a large amount of scatter within the overall trends. This is particularly true for elements such as K_2O, Sr, Y, Zr, Nb, Rb and Ba and in most cases it is possible to fit two approximately parallel lines to the minor and trace element data. Alteration may account for some of the scatter though the Rooi Rand dykes are generally remarkably fresh. Furthermore, at least Zr and Nb are apparently not affected by weathering processes (Pearce and Cann, 1973) yet both show considerable spread at any particular MgO value. It is therefore possible that a certain degree of chemical heterogeneity (with respect to minor and trace elements) existed in the source area from which the Rooi Rand dykes were formed. Source heterogeneity is also reflected by the spread of Zr/Nb ratios ($\sim$ 15-30 if ratios calculated with Nb approaching the detection limit of $\sim$ 2 ppm are excluded) in the Rooi Rand lavas though on the basis of Sr-isotope data

TABLE 9.8 Predicted and observed trace element content of the average evolved Rooi Rand magma composition RR2 using results of the least squares approximation given in Table 9.7. Distribution coefficients are included in the table.

	RR1	RR2	
	OBS	OBS	CALC
Rb	5	15	14
Ba	50	200	138
Sr	160	250	204
Y	23	50	51
Sc	39	32	34
Zr	60	230	170
Nb	6	14	15
Ni	80[1]	36	34
Co	55	47	49
Cr	200	20	21
V	275	450	443
Cu	160	410	414
Zn	80	150	148

[1] D_{Ol}^{Ni} calculated from the equation of Hart and Davis (1978) using an average MgO Content of 5.90%.

Distribution Coefficients

	OLIVINE	CLINOPYROXENE	PLAGIOCLASE	TITANOMAGNETITE
Rb	0	0	.02[5]	0
Ba	0	0	.05[5]	0
Sr	0	.1[5]	1.5 - 2.4[9]	0
Y	.01[1]	.5[1]	0	.2[1]
Sc	.33[2]	2.4[6]	0	.73[2]
Zr	.01[1]	.1[1]	.01[1]	.1[1]
Nb	.01[1]	.1[1]	.01[1]	2.16[10]
Ni	20.12	2[4,7]	0	12.2[11]
Co	3[3]	2[8]	0	3.4[2]
Cr	.6[4]	5[6]	0	21.1[12]
V	.09[3]	.74[3]	0	5[12]
Cu	.02[2]	.2[3]	.004[2]	.42[2]
Zn	.86[3]	.5[3]	.13[2]	2.6[2]

References: 1 Pearce and Norry (1979) 2 Paster et al. (1974)
3 Bougalt and Hekinian (1974) 4 Lindstrom (1976)
5 Philpotts and Schnetzler (1970) 6 Dale and Henderson (1972)
7 Frey et al. (1978) 8 Lindstrom and Weill (1978)
9 Korringa and Noble (1971) 10 Le Roex (1980)
11 Leeman (1974) 12 Leeman et al. (1978)

it would appear that the source was isotopically homogeneous since as was noted previously initial $^{87}Sr/^{86}Sr$ ratios are remarkably uniform.

Results of the trace element modelling, assuming Rayleigh fractionaction of an assemblage consisting of 2% olivine, 46% clinopyroxene, 48% plagioclase and 4% titanomagnetite, are presented in Table 9.8. Distribution coefficients used in the calculations are also listed in Table 9.8; the value for D_{Ol}^{Ni} was calculated from the expression of Hart and Davis (1978), $D_{Ol}^{Ni} = 124/MgO - 0.90$, using the average MgO content of RR1 and RR2. On the whole the predicted and observed trace element concentractions show a good match though three important elements, viz. Ba, Sr and Zr, are notably discrepant. In the case of these three elements the observed concentrations are substantially greater than the predicted values even if some allowance is made for the scatter shown by the plotted data. It is therefore not possible to obtain a satisfactory major and trace element fit relating RR1 to RR2 using observed phenocryst and microphenocryst phases and assuming simple low-pressure crystal fractionation.

A point that has not been referred to up until this stage is that amongst the Rooi Rand dolerites studied, clinopyroxene and titanomagnetite phenocrysts and microphenocrysts are notably scarce, whereas olivine phenocrysts were found in only one dyke. Nevertheless the major element mixing model presented in Table 9.7 shows that clinopyroxene played a major role in the petrogenesis of the Rooi Rand suite thereby suggesting that the fractionation event which gave rise to the observed range of Rooi Rand magmas may have occurred at relatively high pressures and that the solid phases involved were subsequently removed or resorbed. Furthermore though the least squares approximation presented in Table 9.7 yields an adequate major element fit, the rather large enrichment factor for Sr (1.56; calculated as Sr in RR2/Sr in RR1, see Table 9.6) suggests

that fractionation of a solid assemblage containing 48% plagioclase may not be realistic. A second series of calculations were therefore carried out using analyses of aluminous pyroxenes from the literature to see whether these could also generate a suitable major element model and if so, what the consequences were for the amount of plagioclase required in the solid assemblage.

The results of a model with an aluminous pyroxene is presented in Table 9.9. As in the previous case a good fit was obtained between the major element data though it was found that F values could vary quite notably with variation in the compositions of the aluminous pyroxenes used in the calculations. However, by selecting an aluminous pyroxene with Fe/Mg ratio approaching that of the clinopyroxene used in the least squares model presented in Table 9.7 and a slightly less aluminous plagioclase it was found that an F value of 0.35 could be obtained for the mixing calculation which is identical to the F value obtained in the modelling calculations presented previously (Table 9.7). The only difference between the two sets of major element modelling calculations presented in Table 9.7 and 9.8 is that olivine is not present as a fractionating phase when the aluminous pyroxene is used. However, this is probably due to the greater proportion of pyroxene in the extract assemblage obtained in the major element model presented in Table 9.9.

Results of trace element modelling assuming Rayleigh fractionation and using the proportions of fractionating phases obtained from the above model (Table 9.9) are shown in Table 9.10. From the results presented in this table it is apparent that Sr shows a better, but far from adequate match to the observed value whereas Ba and Zr again show very poor agreement between observed and calculated data. Elements such as Ni also show slightly less satisfactory agreement in Table 9.10 whereas it was found

crystallisation and accumulation of phenocrysts were the only processes operative during the evolution of Rooi Rand magmas. This is borne out by the fact that the behaviour of two critical elements (Zr, Ba) cannot be explained satisfactorily by the models presented above. However, it would appear that fractionation crystallisation at reasonably high pressures may have been one process operative during the evolution of the Rooi Rand dykes since this mechanism is capable of producing a greater enrichment in Sr and thus a more precise fit to the observed data.

It is, however, necessary to propose more complex relationships to explain the behaviour of Ba and Zr, and possibly Sr as well. Derivation from a source area that is heterogeneous with respect to these elements may provide one solution to the problem. It was noted previously that there is considerable scatter in much of the trace element data and Zr/Nb ratios vary considerably. The possibility must therefore exist that the Rooi Rand dykes were formed from a series of magmas which had similar major element compositions but were heterogeneous with respect to trace elements particularly, Zr and Ba. However, in this case there remains the additional assumption that magmas showing the greatest enrichment in these two elements also underwent the greatest degree of fractionation in order to produce the relatively well constrained trends apparent in the rocks which makes the plausibility of such a process somewhat doubtful.

An alternative solution is to assume that (i) Ba behaved as an incompatible element along with Zr during fractionation of the Rooi Rand magmas and (ii) decoupling of the major and trace elements occured during the fractionation event. Only Zr is likely to behave as a truly incompatible element during the petrogenesis of the Rooi Rand dykes since Nb will be

incorporated into titanomagnetite. Whether Ba may act as an incompatible element is certainly questionable. However, D^{Ba}_{Plag} values of as low as 0.054 have been obtained in basaltic systems (Philpotts and Schnetzler, 1970) whereas Le Roex (1980) found that Ba behaved as an incompatible element during the petrogenesis of some oceanic basalts. Apparent decoupling of major and trace elements can be achieved to a certain extent by small variations in the degree of partial melting (eg. see Langmuir et al., 1977) or by fractional crystallisation within a magma chamber which is periodically refilled by new batches of magma from depth and which then mix with existing magma (eg. O'Hara, 1977; Usselman and Hodge, 1978; Donaldson and Brown, 1977; Dungan and Rhodes, 1978).

Usselman and Hodge (1978) have outlined a model for thermal control of open system low-pressure fractionation which may be applicable to the Rooi Rand volcanics. They have shown that periodic replenishment by additional parental liquid can result in a steady thermal fractionation state being achieved in a magma chamber. In this situation a fractionating and mixing magma chamber may remain active for an indefinite period of time and maintain a constant temperature interval bracketing a cotectic boundary. Such a system would result in the buffering of the major and compatible trace elements (whose bulk D = $\pm$1.0) in the liquid, but would result in a decoupling and apparent excessive enrichment in incompatible elements in magmas which were tapped at successive stages. This may therefore be one way of causing the excessive enrichment in Zr noted in the Rooi Rand rocks, and possibly also Ba if it so happened to behave as an incompatible element.

An adequate solution to the problems presented by the Rooi Rand intrusives is at present wanting though it may be inferred that factors

such as source area heterogeneity and possible open system crystal fractionation may have been instrumental in accounting for the geochemical relationships shown by the dykes. Added problems are presented by the degree of uncertainty attached to the values of many distribution coefficients and the possibility that the estimates of F values derived from the modelling calculations in Tables 9.6 and 9.8 may not be all that reliable. Bearing these points in mind it is, however, possible to conclude that fractionation of olivine + clinopyroxene + plagioclase, possibly at relatively high pressures is perfectly adequate to account for the major element variation in the Rooi Rand suite as well as most of the minor and trace element variations.

9.5 Southern Lebombo Lavas and Dykes (Includes Swaziland low-MgO lavas)

The southern Lebombo lavas consist of porphyritic and sparsely porphyritic or aphyric lava flows and form the country rock to the Rooi Rand dykes. The dykes cross-cut the lavas and also consist of aphyric and porphyritic rocks. The lavas and dykes are compositionally much more diverse than the Rooi Rand intrusives, a feature that is in part reflected by the considerable variations in element abundances in representative analyses given in Table 9.3 (analyses 4- 6) and the generally lower correlation coefficients shown by the lavas (Table 9.11) in comparison to the Rooi Rand intrusives. However, the compositional diversity of these volcanics, relative to the Rooi Rand intrusives is best displayed on major element variation diagrams presented in Figures 9.5 a-f and minor and trace element plots presented in Figures 9.6 a-j. Porphyritic lavas and dykes are on average enriched in Al_2O_3 relative to the aphyric volcanics (see Fig. 9.5c) and are thus assumed to have evolved by plagioclase addition to aphyric magmas. Compared with the Rooi Rand dolerites the lava and dyke trends, even for aphyric rocks, are highly scattered

though it is noticeable that for many elements (eg. SiO_2, TiO_2, Al_2O_3, Fe_2O_3, Sc, V, Zn and Cu as shown in Figures 9.5 a-f, 9.6 a-j) the Rooi Rand trends form the edge of the field occupied by the southern Lebombo lavas and intrusive rocks. The scattering seen on the major element plots is also evident in many minor and trace element relationships, notably in very low correlation coefficients for TiO_2, Sr, and Cu when they are related to K_2O, Rb, P, Zr Y and Zn (Table 9.11).

Discussion

Because of the scattered nature of most major element relationships detailed numerical modelling has not been carried out for the southern Lebombo lavas and dykes. However, because of the obvious way in which the Rooi Rand trends form a limiting edge to the compositional fields of the lavas it has been assumed for the purpose of this discussion that the lavas and dykes may have evolved initially by fractionation processes similar to those suggested for the Rooi Rand magmas and that the range of magmas so produced was then acted on by one or more subsequent processes of a different type to produce the scattered relationships observed.

In general the 'processes' which acted on the Rooi Rand type magma have, in the case of the major elements led to depletion of TiO_2, (Fig. 9.5b), Fe_2O_3 (Fig. 9.5d) and Mn (not shown), enrichment of SiO_2 (Fig. 9.5a) and K_2O (Fig. 9.6a), and a slight increase in Al_2O_3 at any given MgO level for the aphyric rocks (Fig. 9.5c). Similarly, for the trace elements the 'processes' must have led to enrichment of Rb, Sr and Ba (Figs. 9.6 c,d,e), and depletion of V, Zn, Cu (Figs, 9.6 f,g,h) and Co (not shown). In addition, any subsequent processes acting on Rooi Rand type magmas must account for the variable and generally high initial Sr

TABLE 9.11 Selection of interelement correlation coefficients for aphyric lavas of the southern Lebombo and Swaziland.

	K	Rb	Ba	Sr	Nb	Zr	P	Ti	Y	Zn	Cu
Rb	+.78										
Ba	+.47	+.45									
Sr	+.13	+.12	+.76								
Nb	+.50	+.44	+.27	-.03							
Zr	+.63	+.52	+.37	+.02	+.83						
P	+.39	+.32	+.46	+.16	+.59	+.78					
Ti	+.03	-.03	-.12	-.25	+.54	+.68	+.48				
Y	+.29	+.16	-.02	-.26	+.74	+.83	+.57	+.88			
Zn	+.15	+.15	-.08	-.27	+.64	+.67	+.52	+.83	+.84		
Cu	+.09	-.02	-.11	-.28	+.61	+.57	+.42	+.76	+.80	+.66	
Si	+.71	+.66	+.34	+.24	+.36	+.39	+.08	-.21	+.04	+.01	-.25
Fe	-.26	-.33	-.23	-.39	+.21	+.39	+.40	+.83	+.69	+.66	+.67
Na	+.29	+.37	+.01	-.05	+.39	+.25	+.14	+.06	+.27	+.14	+.25
Al	+.03	+.03	+.20	+.27	-.36	-.50	-.32	-.68	-.63	-.65	-.52
Ca	-.75	-.65	-.20	-.03	-.62	-.72	-.38	-.31	-.52	-.45	-.18
Mg	-.64	-.49	-.36	-.04	-.63	-.70	-.46	-.35	-.57	-.39	-.31
Ni	-.37	-.25	-.33	-.03	-.26	-.37	-.34	-.17	-.33	-.04	-.23
Cr	-.41	-.25	-.21	+.14	-.35	-.47	-.38	-.31	-.46	-.25	-.29
Co	-.65	-.56	-.28	-.20	-.54	-.56	-.36	-.09	-.35	-.15	-.07
Sc	-.26	-.33	-.20	-.70	+.39	-.03	+.05	+.19	+.23	-.05	+.42

Confidence limits: 1% - .449, 5% - .349.

Figs. 9.5 and 9.6 Variation diagrams for major, minor and trace elements in the southern Lebombo low-MgO lavas and dykes and Swaziland low-MgO lavas. Porphyritic rocks are shown as solid symbols with aphyric and sparsely porphyritic rocks as open symbols. The field of Rooi Rand aphyric rocks are indicated on the diagrams by dashed lines.

O - Swaziland and southern Lebombo lavas

Δ - Southern-Lebombo dykes

(Data from Microfiche Tables F1, F2, F3, F7, Appendix F)

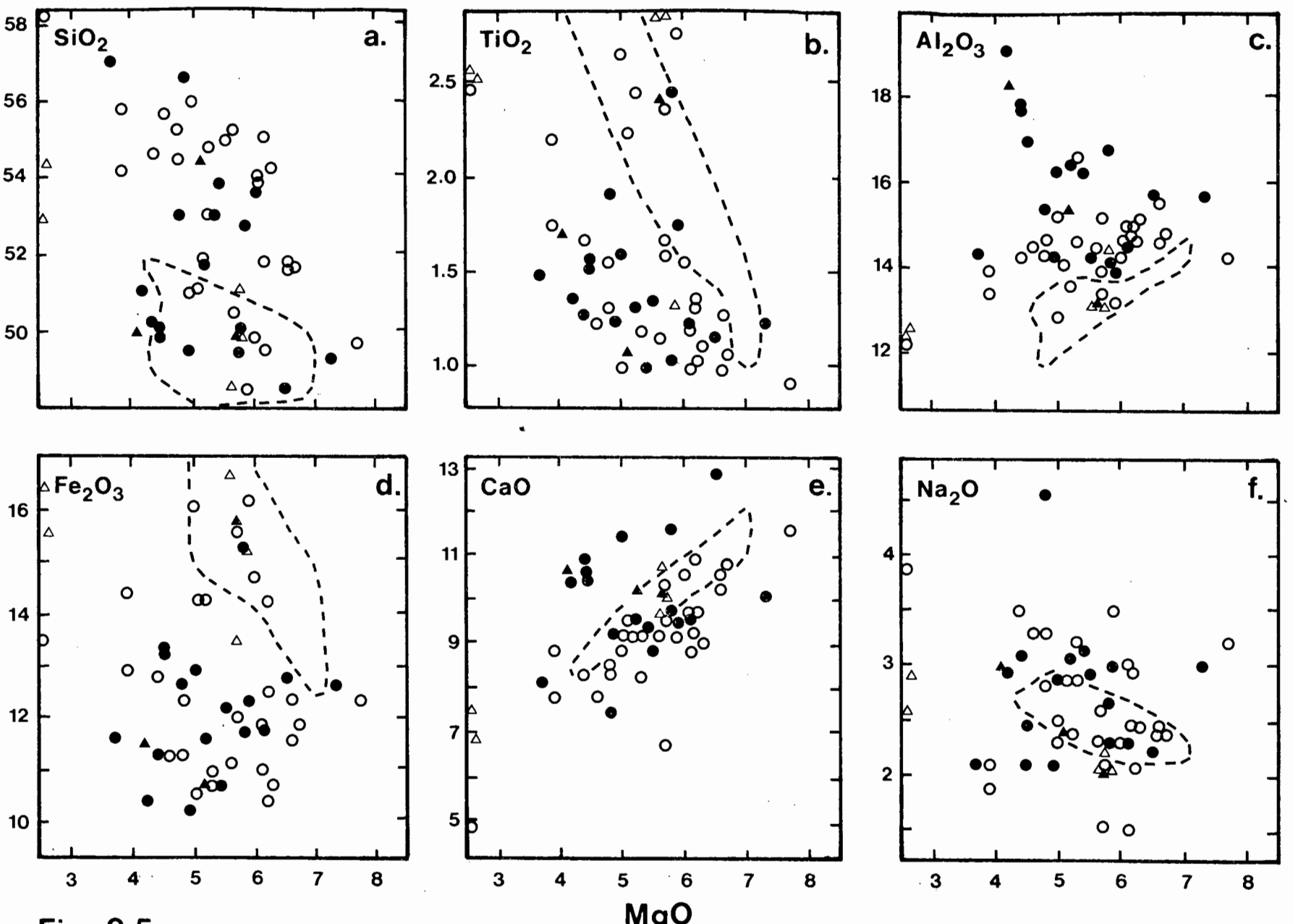

Fig. 9.5

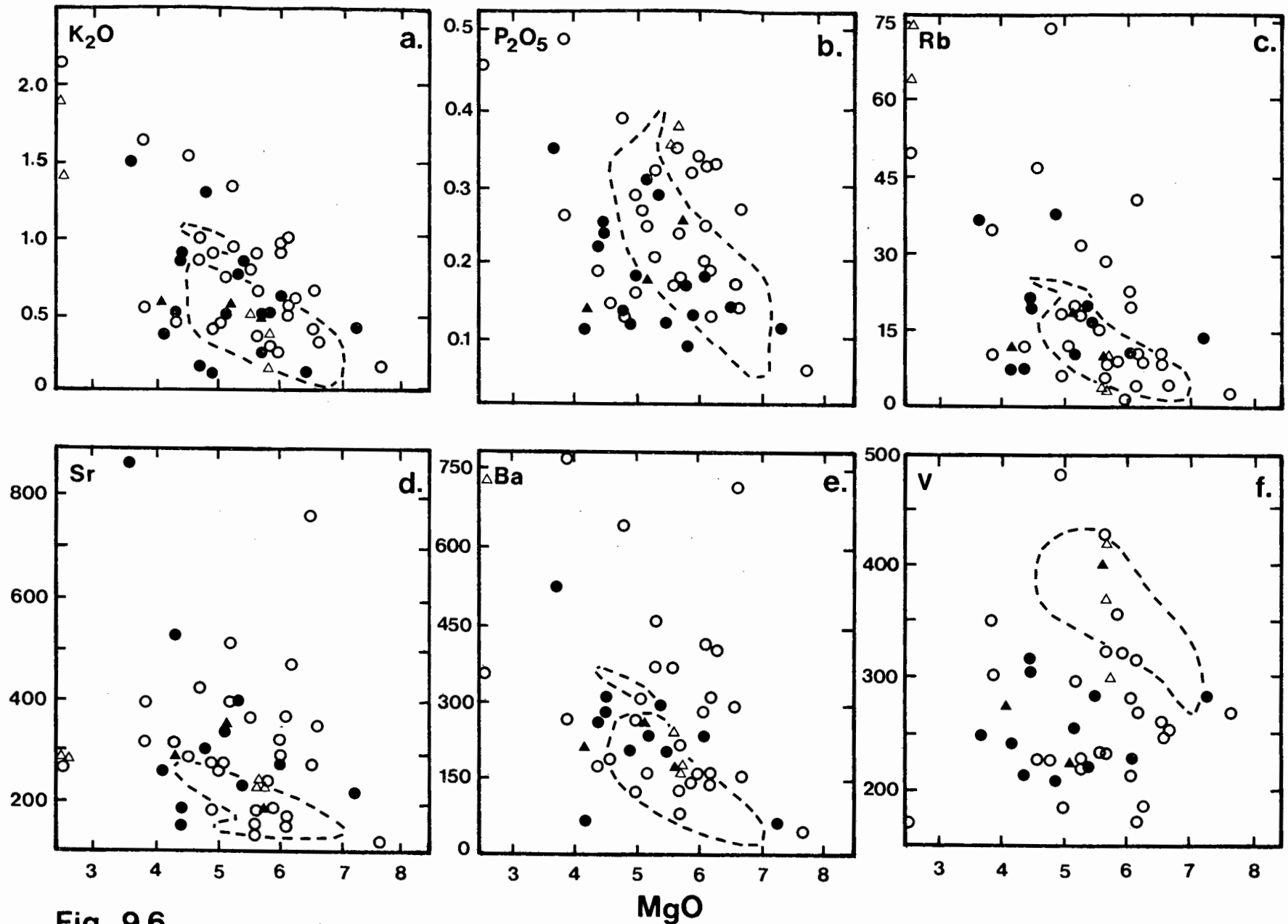

Fig. 9.6

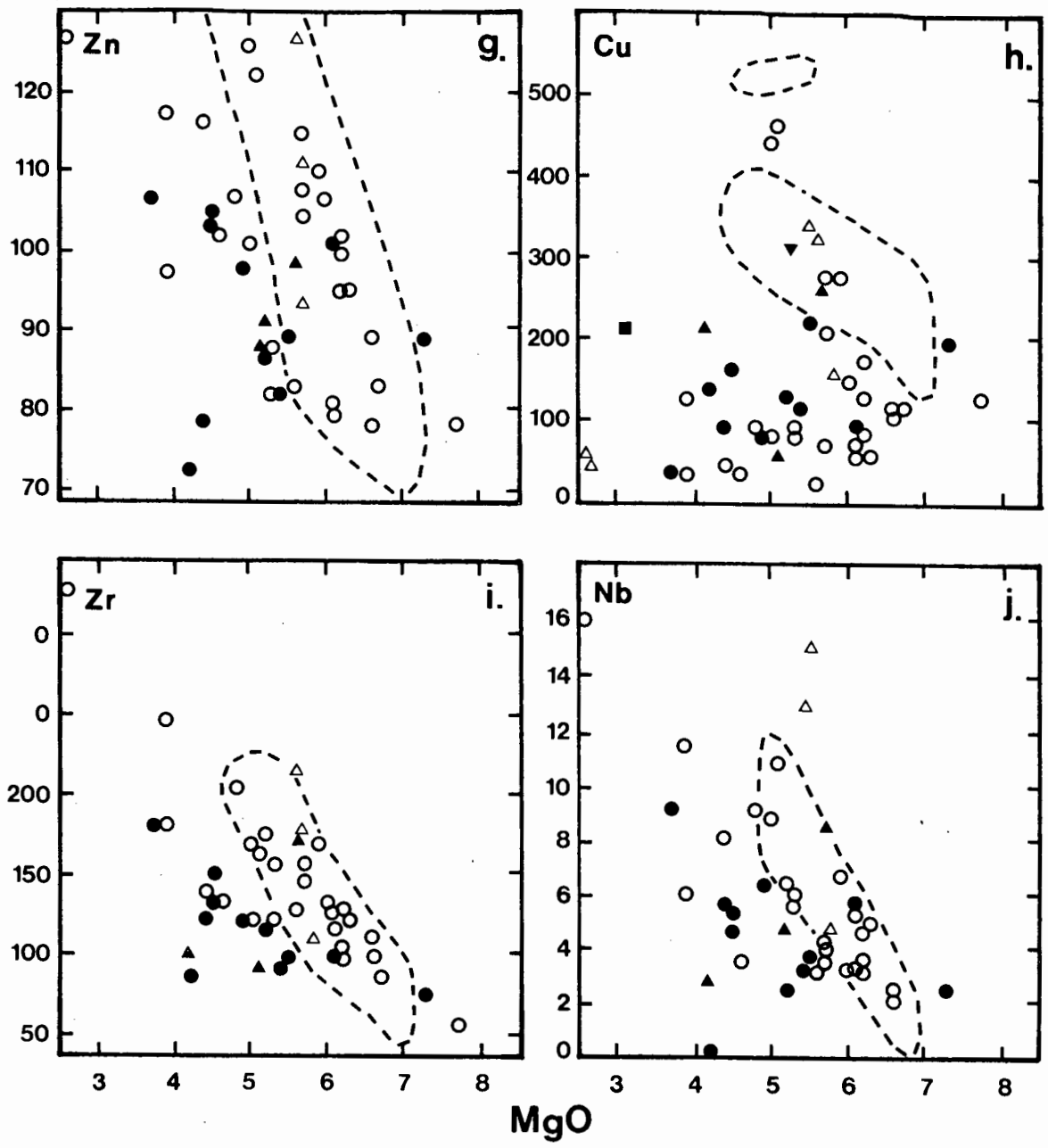
Zn
g.
120
110
100
90
80
70
Cu
h.
500
400
300
200
100
0
Zr
i.
0
0
200
150
100
50
Nb
j.
16
14
12
10
8
6
4
2
0
3
4
5
6
7
8
MgO

isotope ratios encountered in the lavas and normal dykes (see Table 10.1, Chapter 10). Some elements, notably Na_2O (Fig. 9.5f) and P_2O_5 (Fig. 9.6b) appear to show an increased scatter on MgO plots without any obvious enrichment or depletion trend suggesting that these elements were not affected by subsequent processes of alternatively have been redistributed by alteration.

The data outlined above suggest that one of the subsequent processes which may have caused the chemical variations apparent in the southern Lebombo lavas involved contamination with material rich in radiogenic Sr and poor in Fe relative to the dolerites. Furthermore, the enrichment of the lavas in SiO_2, K_2O, Rb and Ba, and the simultaneous depletion in TiO_2, V and Co indicates that the contaminant may have been granitic. However, this hypothesis does not account for the enrichment in Sr (Fig. 9.6d) since granites are not normally enriched in this element relative to the Rooi Rand dolerites. The extreme depletion in Cu also appears to be inconsistent with the granite contamination hypothesis and it is thus suggested that separation of a sulphide phase must also be taken into account. Finally some degree of alteration cannot be ignored and it is possible that this factor accounts for the extreme fluctuations in Na_2O.

9.5.1 Crustal Contamination

Since it has been suggested that crustal contamination may have been responsible for the scatter observed in the geochemical data for the southern Lebombo lavas and dykes a number of analyses of granitic material have been assembled in Table 9.12. Data presented in this table includes average compositions of granitic and rhyolitic rocks, a number of average analyses of Swaziland Pre-Karoo granitoid rocks, and the average compositions obtained for two sets of Lebombo rhyolites. Since the granitoid basement

TABLE 9.12 Analyses of granitic and rhyolitic rocks for consideration as possible contaminants during the petrogenesis of the southern Lebombo and Swaziland low-MgO lavas and dykes.

	Average granites and rhyolite				Average Karoo rhyolites		Pre-Karoo granitic rocks from the Swaziland Basement Complex				
	1	2	3	4	5	6	7	8	9	10	11
% SiO_2	74.23	67.17	71.30	72.82	69.82	70.68	70.80	70.33	75.20	70.40	69.50
TiO_2	.57	.20	.31	.28	.91	.50	.30	.46	.20	.30	.32
Al_2O_3	15.49	13.60	14.32	13.27	12.14	12.65	14.47	14.03	12.87	14.60	14.78
Fe_2O_3	4.23	2.03	3.01	2.70	6.81	.34	2.25	2.57	1.80	2.49	2.78
MnO	.07	.05	.05	.06	.08	.10					
MgO	1.56	.27	.71	.39	.47	.35	.81	.63	.24	1.44	1.32
CaO	3.54	.71	1.84	1.14	2.33	1.47	2.03	2.04	.85	3.55	2.97
Na_2O	3.83	3.48	3.68	3.55	3.74	3.16	4.83	3.57	3.10	4.45	5.64
K_2O	3.04	5.06	4.07	4.30	3.55	4.61	3.35	5.18	5.21	1.50	1.04
P_2O_5	.21	.18	.12	.07	.18	.14					
ppm Rb	170	110			96	130	88	231	278	68	51
Ba	840	420			565	1452	746	1154	371	183	375
Sr	100	440			181	153	536	306	60	233	537
Zr	175	140			293	1084					
Nb	21	20			14	84					
Cr	4	22				5	7	6	<6	22	18
V	44	88				3					
Ni	5	15				1					
Co	1	7				1	5	7	2	9	10
Zn	39	60				135					
Cu	10	30				9					
Y	40	35				121					

KEY TO TABLE 9.12

1: Average high-calcium granite (Turekian and Wedepohl, 1961).

2: Average low-calcium granite (Turekian and Wedepohl, 1961).

3: Average granite (Le Maitre, 1976).

4: Average rhyolite (Le Maitre, 1976).

5: Average Mkutshane rhyolite, Swaziland (2 samples for major elements, 9 samples for trace elements: See Microfiche Table F9; Appendix F).

6: Average Jozini Rhyolite, southern Lebombo (49 samples, see Microfiche Tables F5, F6; Appendix F).

7, 8, 9: Average of Dalmein, Mpageni and Sicunnsa types of shield forming batholiths from Swaziland.

10: Average of Ancient Gneiss Complex, Swaziland.

11: Averate of Tonalite Diapirs, Swaziland.

(7 - 11 from Condie and Hunter, 1976).

Ba (Fig. 9.7c) and K_2O (Fig. 9.7d) show similar relationships with respect to the amount of contamination that is required to cause the observed scatter in the aphyric low-MgO lavas and dykes. The relationship between Ba and MgO (Fig. 9.7c) is illustrated on the assumption that the contaminant contained approximately 1100 ppm Ba. However, concentrations of Ba in granitic melts are widely variable (see Table 9.12) so this relationship should be treated with some caution.

Relationships shown by Fe_2O_3 (Fig. 9.7e), SiO_2 (Fig. 9.7f) and Rb (Fig. 9.7g) are also consistent with the results derived from Figures 9.7 a-d, indicating that about 30% of added contaminant will account for the compositions of the more extreme aphyric rocks. One point to note, however, is that a large number of the lavas and dykes lie within the Rooi Rand fields on plots of Ba, K_2O and Rb versus MgO. This, taken in conjunction with the scattered and sometimes very low Na_2O contents suggests that the alkali metals in these rocks may have been irregularly mobilised and depleted during alteration processes. The Rooi Rand dolerites are, by comparison, compact and fresh rocks which seem to have largely escaped this effect.

The behaviour of other elements in the aphyric lavas (excluding Cu and Sr) is broadly in accord with the granitic contamination hypothesis though it is not possible to draw quantitative conclusions from their behaviour. The slight enrichment in Al_2O_3 at a given MgO level (see Fig. 9.5c) can largely be explained by the addition of a contaminant low in MgO and with about the same Al_2O_3 content as the most basic Rooi Rand liquids. The behaviour of strongly compatible elements such as CaO (Fig. 9.5e) Ni and Cr is however, uninformative. These elements do not shown gross departures from the Rooi Rand trend but contamination by granite

Fig. 9.7 Contamination modelling for the low-MgO volcanics of Swaziland and the southern Lebombo (symbols as in Figures 9.5 and 9.6). Assumed compositional characteristics of the contaminant are as follows:

SiO_2 ~ 70%; MgO = 0.5-1%; Fe_2O_3 = 2-3%;

TiO_2 = 0.3-0.5%; K_2O = 3.5-4%; V = 0-75 ppm;

Rb = 90-100 ppm; Sr ~ 540 ppm; Ba ~ 1100 ppm.

(Data from Table 9.12).

(Data from Microfiche Table F1, F2, F3, F7, Appendix F)

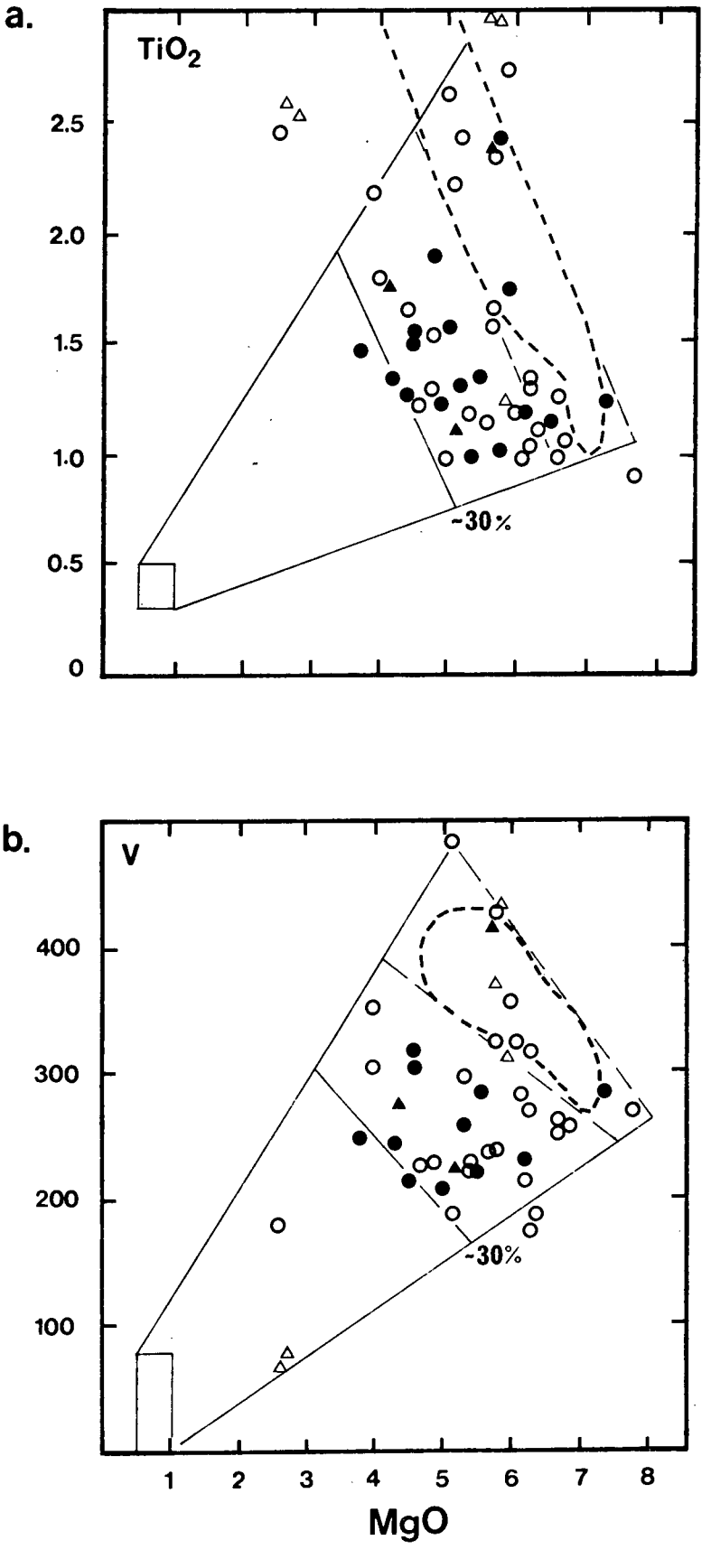

Fig. 9.7

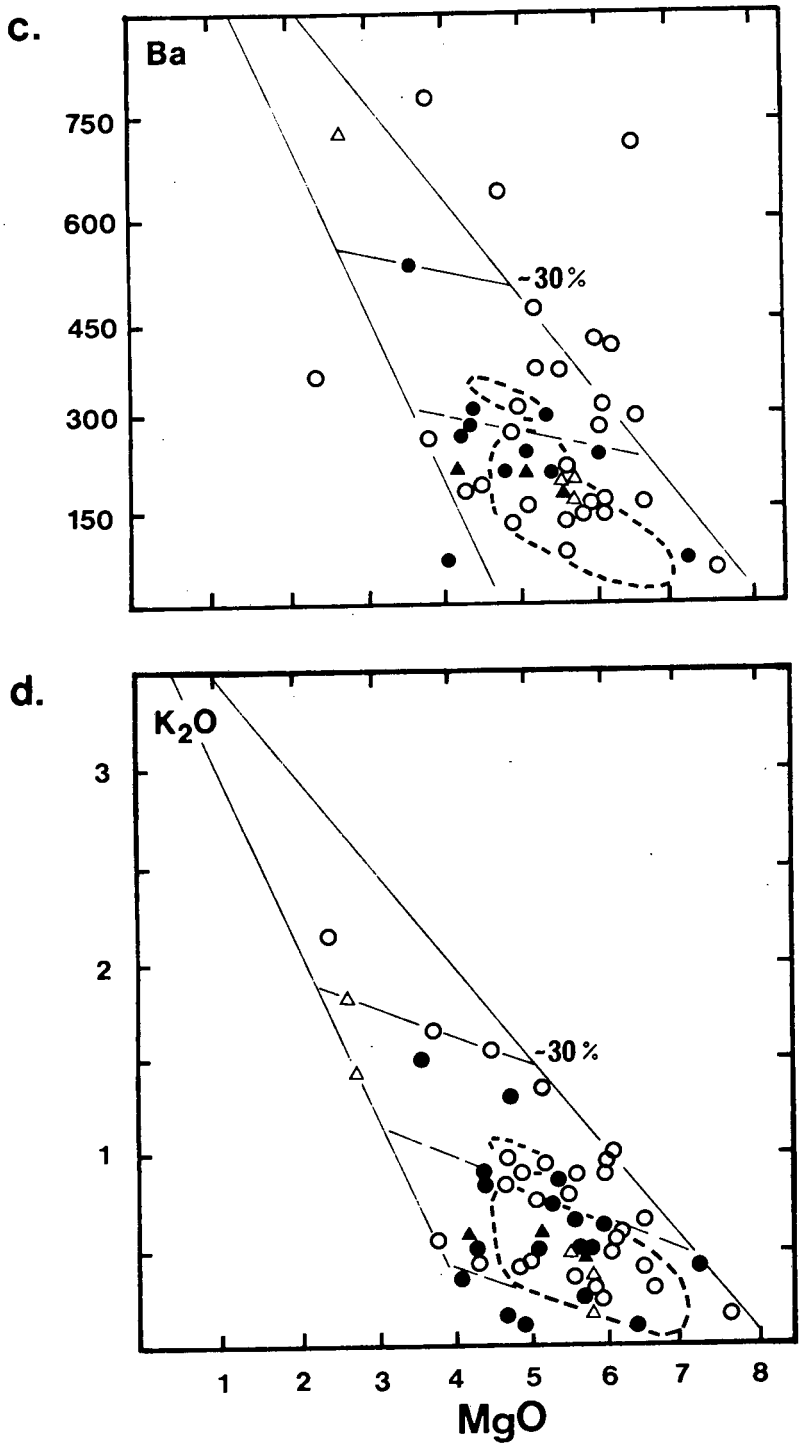
c.
Ba
750
600
450
300
150
~30%
d.
K2O
3
2
1
~30%
1
2
3
4
5
6
7
8
MgO

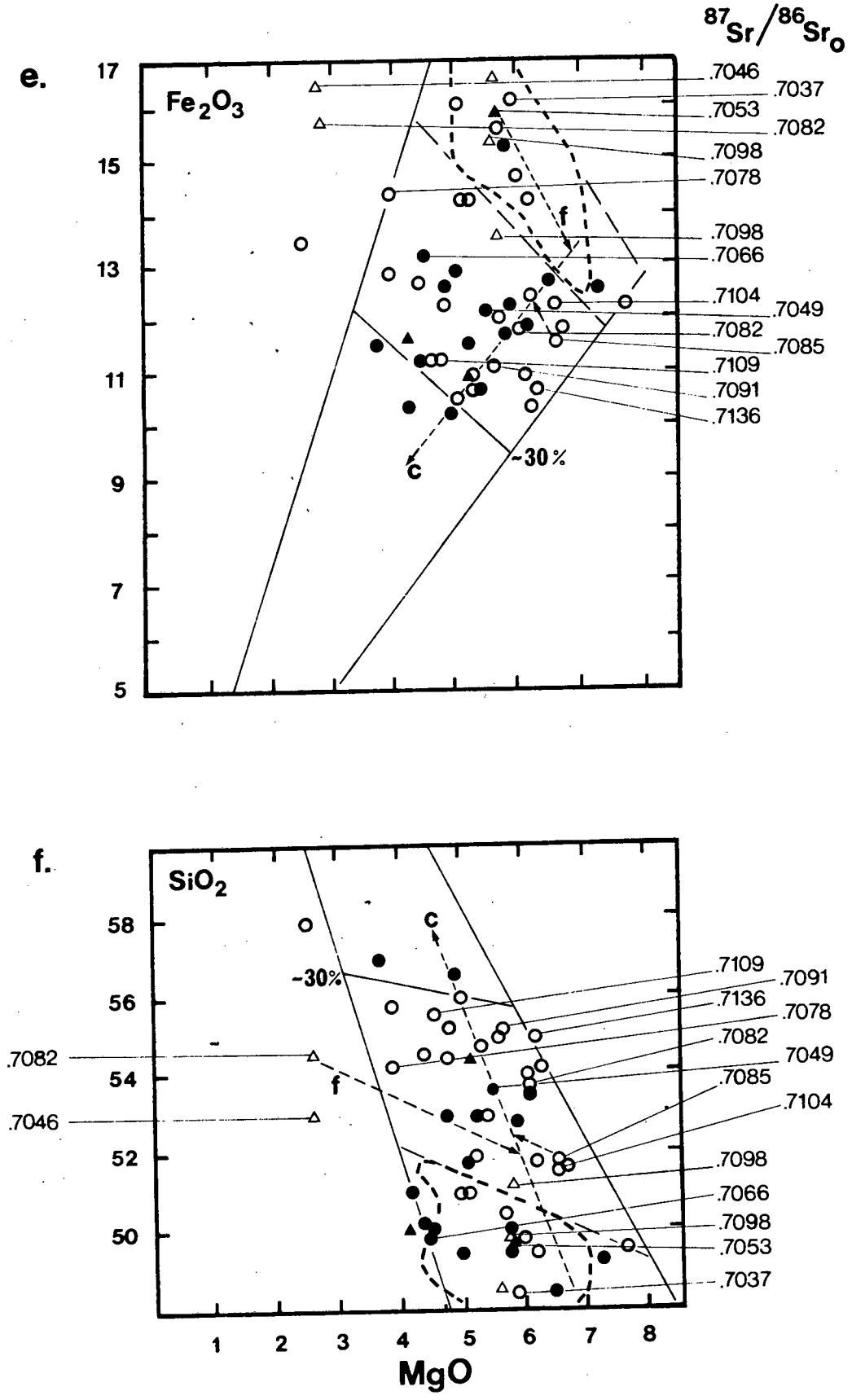
e.
$^{87}Sr/^{86}Sr_o$
Fe_2O_3
17
15
13
11
9
7
5
.7046
.7037
.7053
.7082
.7098
.7078
.7098
.7066
.7104
.7049
.7082
.7085
.7109
.7091
.7136
f
c
~30%
f.
SiO_2
58
56
54
52
50
.7082
.7046
c
~30%
f
.7109
.7091
.7136
.7078
.7082
7049
.7085
.7104
.7098
.7066
.7098
.7053
.7037
1
2
3
4
5
6
7
8
MgO

contamination process as outlined on the basis of major and trace elements.

The Sr data suggest that it is possible that the contaminant may have been tonalitic rather than granitic. However, even though the contamination diagram for Sr constructed in Figure 9.7h is based on a tonalitic composition similar to that obtained for the tonalite diapirs of the Swaziland basement complex (Sr = 537 ppm, average analysis 11, Table 9.12) it does not account for the scatter and enrichment in Sr shown by the southern Lebombo lavas and dykes. Instead it is apparent from Figure 9.7h that a contaminant with in excess of 1 000 ppm Sr would be necessary to account for most of the spread in the plotted data. If however, the average figure of 30% contamination derived from the other major and trace element diagrams (Figs. 9.7 a-g) is used then incorporation of 30% of tonalite into a magma with an original Sr abundance of about 190 ppm (average of Rooi Rand aphyric dykes = 191 ppm) would still be incapable of producing the most Sr enriched lavas and normal dykes. Instead, approximately 50% contamination of a tonalite with more than 1 000 ppm is required to account for the enriched lavas and normal dykes, at which point it is unlikely that the original parental magmas would have retained their basaltic chemistry. Furthermore, tonalites with Sr contents in excess of 1 000 ppm would, on the basis of a detailed literature study, appear to be rather atypical of the basement rocks of Swaziland and other areas adjoining the Lebombo eg. northern Natal.

The second point mitigating against the process of simple crustal contamination stems from the initial-Sr ratio variations shown by the southern Lebombo lavas and dykes. In general it is assumed, and has been shown (eg. Faure et al., 1972, 1974), that the initial-Sr ratio of supposedly contaminated dykes or lavas generally increases as greater amounts of

granitic contaminant are added to the original parental magma composition. The southern Lebombo low-MgO volcanics do not, however, shown any systematic increase in initial ratio with apparently increasing contamination levels. Conversely it has been found by superimposing the initial Sr ratios on the contamination models constructed in Figures 9.7 f and g that there are lavas and dykes with ratios as low as .7059 in the part of the diagram which, on the basis of the major element data modelling would appear to be highly contaminated; likewise there are rocks with exceptionally high initial-Sr ratios in the uncontaminated sector of the diagrams. As a further test of the variation shown by the initial ratios, the plotted data for which initial-Sr ratios are known have been back or forward projected to correct for fractionation, on the simplified assumption that the postulated parental Rooi Rand-type magmas may have been contaminated and that gabbroic fractionation then acted on the secondary magmas. The correction procedure applied to the data is indicated on Figures 9.7 e and f where trend 'c' is considered to represent the possible contamination vector whereas the lines 'f' projected onto this line are considered to be the overall fractionation vector, assuming gabbroic-type fractionation. Results of 'fractionation corrected' initial-Sr ratio variations are shown in Table 9.13 and indicate that even allowing for fractionation, there is still no systematic variation in initial-Sr ratio in relation to increasing contamination.

On the basis of data and arguments presented above, it would therefore appear that Sr and Sr-iostope relationships are not entirely compatible with a crustal contamination process thereby suggesting that alternative processes should be considered. However, the remaining major and trace element data suggest that crustal contamination did at least play a part in the petrogenesis of the southern Lebombo lavas and dykes (eg. see Figs.

TABLE 9.13 Initial-Sr ratio variations in the southern Lebombo lavas and normal dykes corrected for gabbro fractionation.

	INITIAL SR-RATIOS	
	(1)	(2)
INCREASING CONTAMINATION ↑	.71092	.71361*
	.70914	.70914
	.71361*	.71092
	.70822	.70816
	.70486	.70486
	.70664	.70779
	.70779	.70822
	.70816	.70850
	.70461	.71036
	.70850	.70950
	.70975	.70461
	.71035	.70983
	.70983	.70534
	.70534	.70664
	.70375	.70374

ROOI RAND TYPE MAGMA
AVERAGE R_o = .7039

(1) Data from Fe_2O_3 versus MgO variation diagram.

(2) Data from SiO_2 versus MgO variation diagram.

* Visibly contaminated rock. Sample contains small quartzo-feldspathic xenocrysts.

Initial ratios are calculated for 190 my.

9.7 a-h) and in this respect it is interesting to note that the lava with the highest initial-Sr ratio (sample L348, R_o = .71361) displays petrographic evidence of having undergone large scale bulk contamination. Small quartzo feldspathic xenocrysts were found in this sample and its particularly high initial-Sr ratio may therefore be a function of contamination only.

9.5.2 An Alternative Hypothesis: Advanced Crystal Fractionation

If a range of magmas similar to the more basic members of the Rooi Rand suite were subjected to continuing down-temperature crystal fractionation most of the compositional changes ascribed above to contamination by granitic material could unquestionably be reproduced at least qualitatively. Silica-oversaturated basaltic magmas ultimately differentiate towards a granitic residium. The condition which must be satisfied before this fractionation trend is attained is that the elements which are incomaptible in primitive basaltic magmas must become compatible. Amongst the major elements Fe and Ti must be removed in large quantities, which almost inevitably requires the participation of an Fe-Ti oxide in order to reach the relatively low concentrations characteristic of granite. Similarly, the rapid enrichment of elements such as P, Zr and Nb, which is characteristic of primitive basaltic fractionation, must be checked or reversed by the fractionation of phases such as apatite, zircon, and Fe-Ti oxides. This can perhaps be inferred by reference to Figure 9.5 where it can be seen that unlike Rb, Ba and Sr which are enriched relative to the Rooi Rand trend, Zr, Nb and P_2O_5 are in general not enriched relative to the Rooi Rand field.

In basaltic suites in which the above conditions are fulfilled it is thus extremely difficult to distinguish advanced fractionation crystallisation

trends from trends produced by granitic contamination, especially when the precise composition of the contaminant is unknown. However, for reasons listed below, it does not seem likely that advanced crystal fractionation can account for the geochemical relationships observed in the southern Lebombo lavas and dykes as plausibly as a granite contamination hypothesis though these arguments do not necessarily disprove the participation of crystal fractionation to a limited extent. Indeed the heat losses necessitated by the fusion of country rocks during the contamination process will almost certainly cause additional crystallisation and possibly fractionation. Nevertheless the arguments against this process are: (i) the fractionation crystallisation hypothesis requires that a substantial range of Rooi Rand magma compositions all fractionate additional phases, principally Fe-Ti oxides, irrespective of their initial compositions. This implies that phase relations are controlled by substantial fluctuations in pressure and/or fO_2. If the system is open to water it is not improbable that the Fe-Ti oxides could begin to crystallise from magmas showing quite large variations in Fe and Ti contents. To induce the minor phases, apatite and zircon to crystallise similarly from magmas with large variations in P and Zr contents would seem to require the liquidus fields of these minerals to be highly pressure-sensitive. The above processes cannot be disproved with the present data but the contamination hypothesis provides a simpler explanation for most of the relationships shown by the lavas and dykes; (ii) phenocryst phases observed in the southern Lebombo lavas and dykes are plagioclase, with occasional clinopyroxene and olivine as in the Rooi Rand. Opaque phases, apatite and zircon are not seen. This does not disprove the participation of such phases in a fractionation event, as illustrated by the scarceness of clinopyroxene phenocrysts in the Rooi Rand dolerites despite their evident importance as shown by fractional

crystallisation modelling (see section 9.4.2). This is, however, one more piece of circumstantial evidence which suggests that the advanced crystal fractionation model is inadequate to account for the geochemical variation in the southern Lebombo lavas and dykes.

9.5.3 Other Alternative Hypotheses

In view of the problems encountered with both the contamination and advanced fractionation models it seems clear that other alternatives should also be considered. Since formulation of additional hypotheses requires a more detailed consideration of the isotopic data, they are deferred to the following chapter.

9.6 Central and Northern Lebombo Low-MgO Volcanics

Broadly speaking the low-MgO basalts found north of Swaziland may be sub-divided into those lavas which are either aphyric or sparsely porphyritic and those lavas which are more strongly porphyritic. With the exception of rocks from the Komati River, the first group are generally found towards the base of the olivine-poor lava succession and consist predominantly of high-K lavas, viz. shoshonites, absarokites and high-K tholeiitic andesites (collectively referred to as the shoshonitic suite). In contrast porphyritic rocks are generally found higher in the succession and are less enriched in K though interdigitation of both low- and high-K lavas occurs in the field. Dyke rocks which show similar chemical relationships to the extrusive rocks are also found in the central and northern areas of the Lebombo.

Basalts collected from the Komati River (southern end of the central Lebombo, see Fig. 3.1) do not conform with the general relationships noted above. These rocks may be either aphyric or porphyritic and are depleted in K_2O and incompatible elements relative to the other central and northern Lebombo low-MgO basalts. This relationship is apparent from the average

Fig. 9.8 Variation diagrams for major elements in the central and northern Lebombo low-MgO lavas and dykes. Porphyritic rocks are represented by solid symbols. (Komati rocks represent the most southerly samples whereas those from Olifants represent the northernmost samples, (see Fig. 3.1).

□ - Komati River lavas

O - Sabie River lavas and dykes

△ - Olifants River lavas

(Data from Microfiche Tables F14, F15, F18, Appendix F)

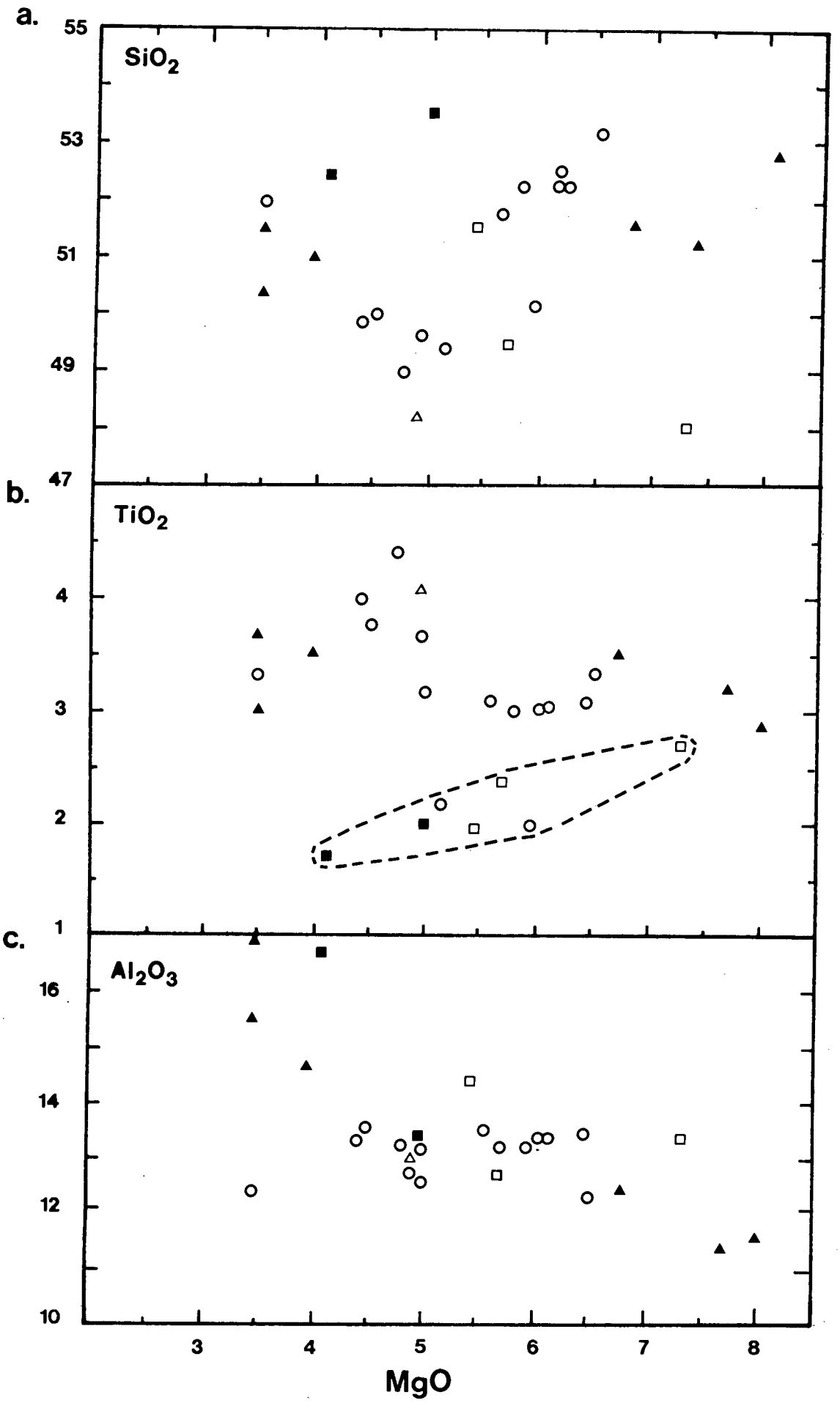
a.
SiO_2
55
53
51
49
47
b.
TiO_2
4
3
2
1
c.
Al_2O_3
16
14
12
10
3
4
5
6
7
8
MgO

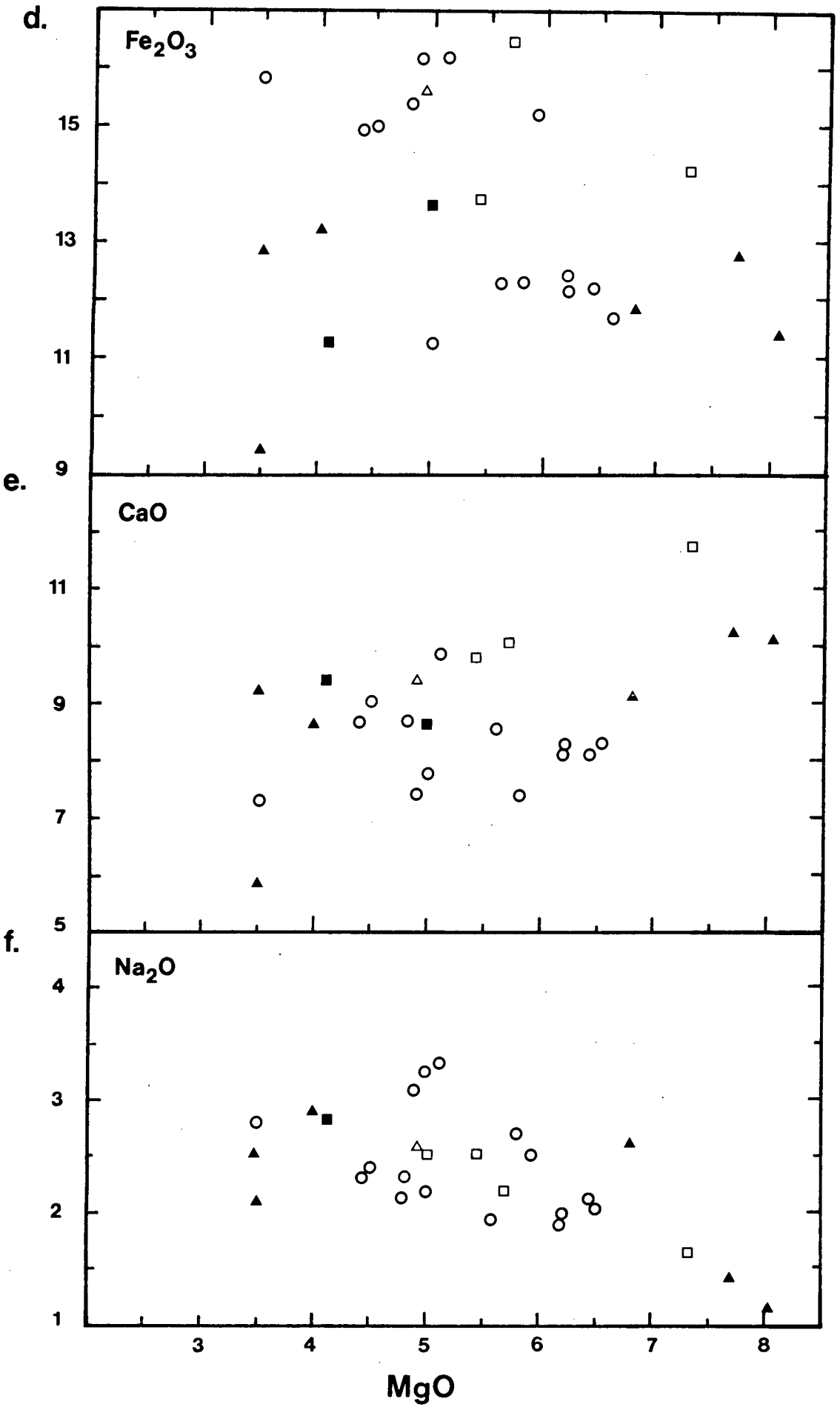
d.
Fe_2O_3
15
13
11
9
e.
CaO
11
9
7
5
f.
Na_2O
4
3
2
1
3
4
5
6
7
8
MgO

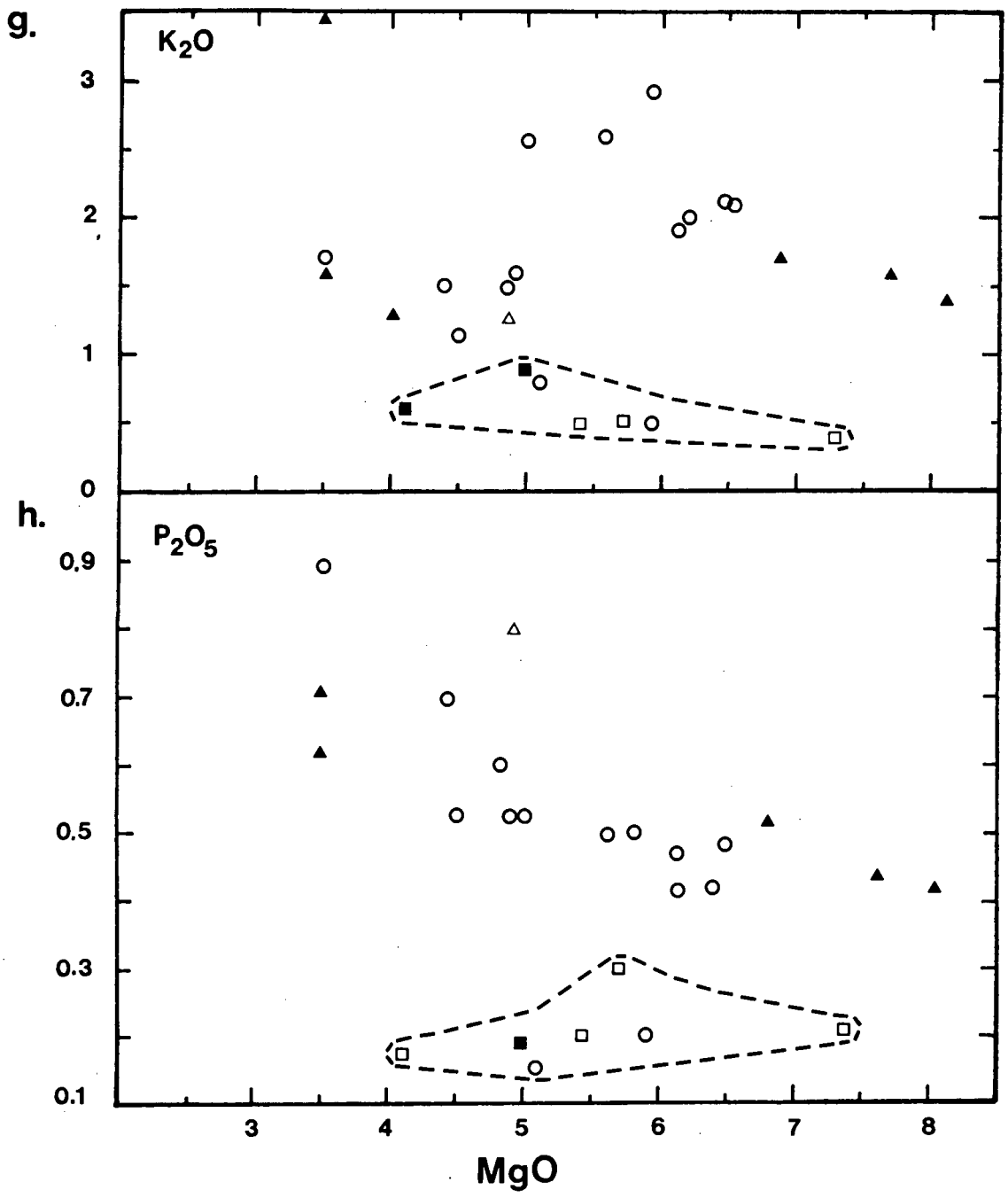
g.
K_2O
3
2
1
0
h.
P_2O_5
0.9
0.7
0.5
0.3
0.1
3
4
5
6
7
8
MgO

analyses listed in Table 9.4 and is also seen on the variation diagrams presented in Figures 9.8 and 9.9. Two samples from the Sabie River show similar relationships (ie. low contents of K_2O, P_2O_5 etc.) to the Komati lavas and where possible the approximate fields that these lavas define on the MgO variation diagrams (Figs. 9.8, 9.9) have been delimited by dotted lines. These low-K rocks are also excluded from the following arguments and will be discussed at the end of this section.

Major and trace elements for the low-MgO lavas and dykes from the central and northern Lebombo (ie. Sabie and Olifants River sections) show exceptionally poor variation trends when plotted against MgO (Figs. 9.8, 9.9) or any other index or fractionation and in many cases it is impossible to ascertain the overall fractionation trends. Al_2O_3, CaO and Na_2O do, however, show indistinct trends when plotted against MgO which suggest that gabbroic type fractionation can be discounted to explain the petrogenesis of these lavas and dykes. This is borne out by the relatively flat trends shown by Al_2O_3 and CaO and increasing Na_2O when plotted against MgO. In contrast gabbroic-type fractionation (e.g. Rooi Rand magmas) would normally lead to strong depletion of Al_2O_3 and CaO, and enrichment of Na_2O with increasing differentiation.

Geochemical relationships shown by K_2O and some of the trace elements are more informative with respect to the petrogenesis of the central and northern Lebombo low-MgO volcanics. On a plot of K_2O versus MgO it would appear that the data define indistinct patterns of enrichment as MgO decreases with a suggestion of two semi-parallel trends. With the exception of those rocks from the Komati River and two rocks from the Sabie River, a plot of P_2O_5 versus MgO also shows a trend of enrichment with increasing differentiation. Similarly Rb, Ba, Sr and Nb show overall trends of enrichment with decreasing MgO.

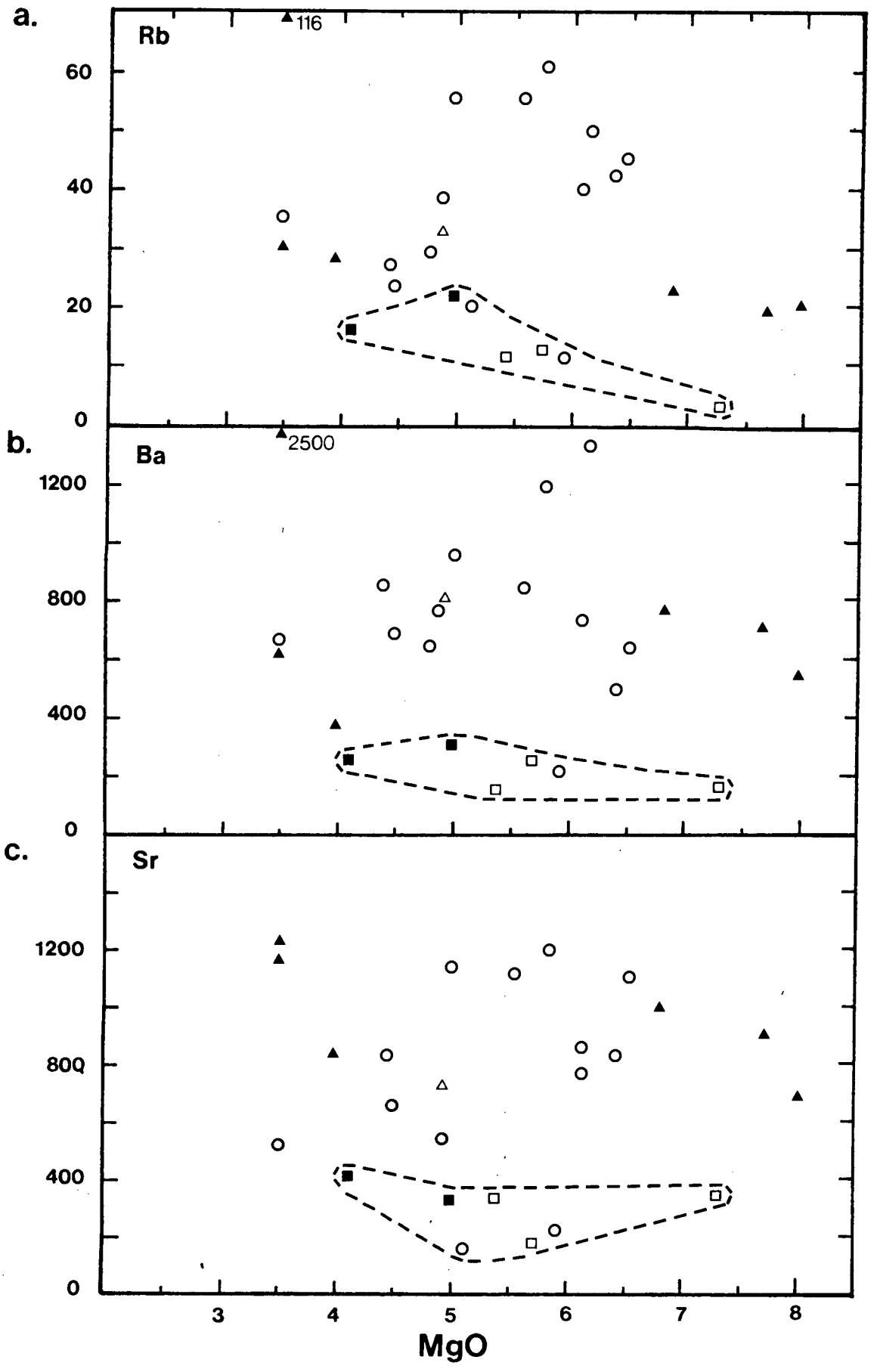

Fig. 9.9 Trace element variation diagrams for the central and northern Lebombo low-MgO lavas and dykes. (Symbols as in Figure 9.8.)

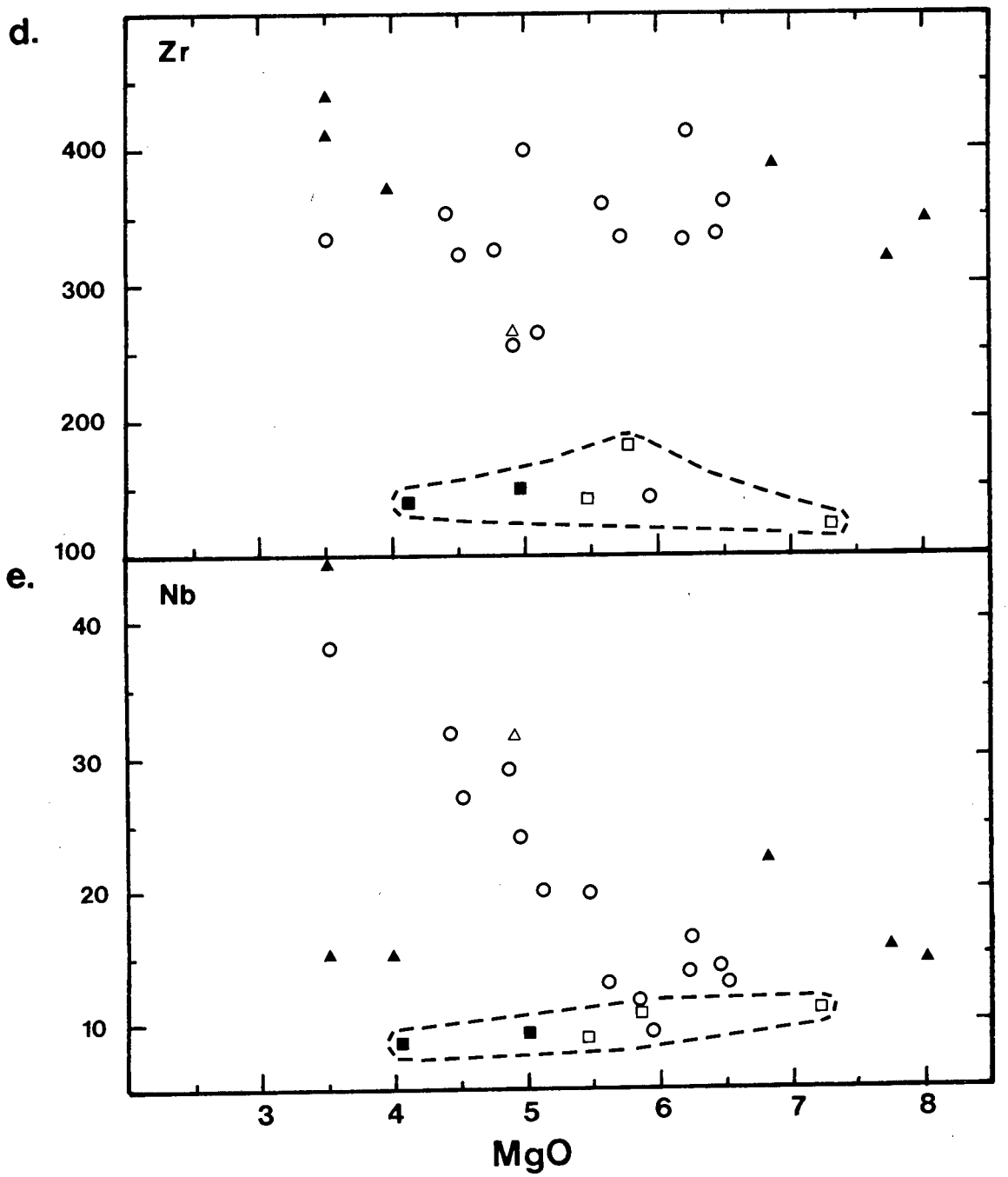
d.
Zr
400
300
200
100
e.
Nb
40
30
20
10
3
4
5
6
7
8
MgO

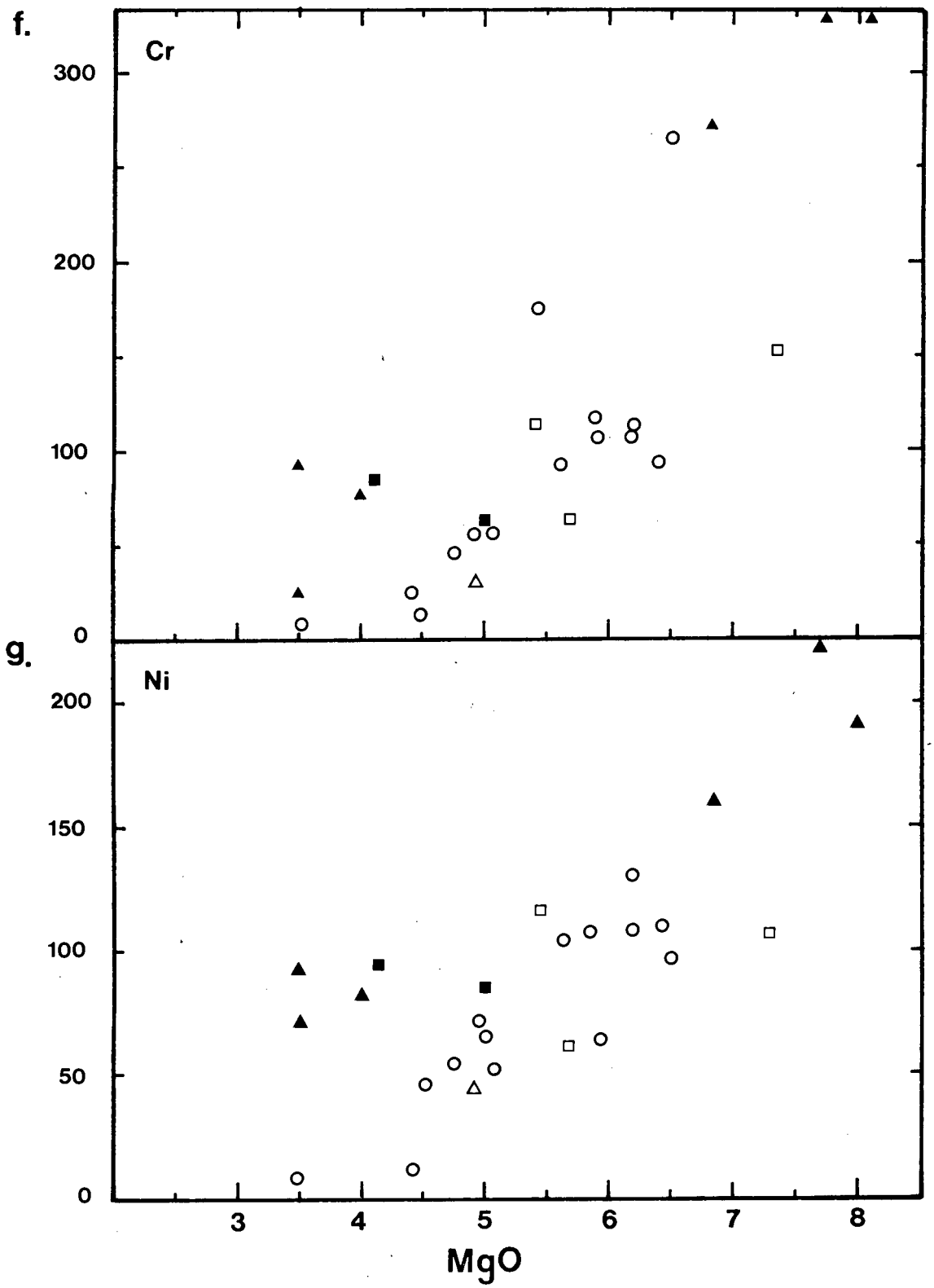
f.
Cr
300
200
100
0
g.
Ni
200
150
100
50
0
3
4
5
6
7
8
MgO

Realistic major element modelling of the central and northern Lebombo low-MgO rocks is not really feasible due to the absence of phenocrysts or microphenocryst phases and the difficulty of deriving suitable average compositions from plots such as SiO_2 and Fe_2O_3 versus MgO (see Figs. 9.8 a,d). Furthermore, the considerable spread in Zr/Nb (9-31) and other inter-incompatible element ratios (e.g. K/Rb = 302-681; K/Zr = 25-102) mitigates against the lavas and dykes being part of the consanguinous volcanic suite. However, a semi-quantitative model was tested on the assumption that crystal fractionation may have taken place at reasonably high pressures and that phenocryst phases were subsequently resorbed or removed. It was found that reasonable mixes could be obtained whereby the more primitive shoshonitic lavas (MgO ~ 7.5%) could be related to the evolved compositions (MgO ~ 3.5%) by fractionation of olivine, clinopyroxene and minor amounts of titano-magnetite. Clinopyroxene was found to dominate all the calculations and on the basis of the semi-quantitative models it would appear that it is unnecessary to invoke plagioclase fractionation for these rocks (ie. as far as major elements are concerned) though good mixes generally required a fairly aluminous clinopyroxene. Fractionation of an assemblage consisting primarily of olivine and clinopyroxene is also compatible with the apparent trend of increasing Sr (Fig. 9.9c) since the presence of plagioclase in the extract would have led to lower degrees of enrichment in Sr (D^{Sr}_{Plag} = 1.5-2.4; see Table 9.8) with increasing differentiation and may even have caused a depletion in Sr if large amounts of plagioclase were involved.

That plagioclase did not play a major role in the petrogenesis of the shoshonitic suite is supported by the absence of a europium anomaly in REE patterns obtained for these rocks (Duncan, unpubl. data). Possible reasons for the apparent absence of plagioclase have been discussed by Cox et al.

(1980) and they propose that the high levels of K_2O characteristic of these rocks may be responsible for suppressing the crystallisation of plagioclase at 1 atmosphere. This relationship has been demonstrated by calculating mineral liquidus temperatures for a cotectic basalt spiked with varying proportions of K_2O or K_2O rich minerals. A summary of the results obtained is presented in Table 9.14. The data show that the plagioclase liquidus temperature is strongly depressed in the spiked compositions with the highest K_2O content whereas with lesser amounts of K_2O the liquidus temperatures approach those of the starting composition. Consequently it is highly probable that the high levels of K_2O characteristic of the shoshonitic suite played an important role in the petrogenesis of these rocks.

Removal of an extract consisting predominantly of olivine and clinopyroxene, coupled with the apparent strong enrichment levels shown by the incompatible elements (with falling MgO) raises the possibility that rocks of the shoshonitic suite may have formed from magmas similar in composition to evolved picrite basalts with relatively low levels of KAR elements. It is quite possible that magmas formed in the last stages of the picritic event became isolated in the crustal regime due to factors such as decreased rates of crustal dilation and diminished thermal energy. These magmas, with their lower levels of MgO and KAR elements would then have been able to undergo low to intermediate pressure fractionation of olivine and clinopryroxene thereby giving rise to a series of low-MgO lavas which would have been relatively enriched in incompatible elements. The proposed mechanism is shown schematically in Figure 9.10. Furthermore, since olivine ($D^{Zr}_{Ol} = 0.01$; $D^{Nb}_{Ol} = 0.01$) and clinopyroxene ($D^{Zr}_{cpx} = 0.1$; $D^{Nb}_{cpx} = 0.1$) are incapable of causing significant changes in the Zr/Nb ratios (see Le Roex, 1980), the considerable spread in Zr/Nb ratios noted in the high-K olivine-

TABLE 9.14 Mineral liquidus temperature calculations

1. Starting composition - Swaziland basalt RC96

K_2O = 0.70%

Temperatures : Fo - 1161°C
En - 1162°
Di - 1166°
Pl - 1162°

2. RC96 + Sanidine

K_2O = 2.66%

Temperatures : Fo - 1135°C
En - 1129°
Di - 1157°
Pl - 1128°

3. RC96 + Leucite

K_2O = 3.13%

Temperatures : Fo - 1170°C
En - 1128°
Di - 1172°
Pl - 1120°

4. RC96 + K_2O

K_2O = 3.36%

Temperatures : Fo - 1176°C
En - 1117°
Di - 1177°
Pl - 1087°

NOTE: Results presented in this table were derived from a Liquidus Temperature Computer Program (XTALS) written by Dr A.R. Duncan of the Department of Geochemistry, U.C.T. The program uses Nathan and Van Kirk (1978) distribution coefficients and liquidus mineral data to calculate the temperatures of the liquidus mineral assemblage in equilibrium with a particular magma composition.

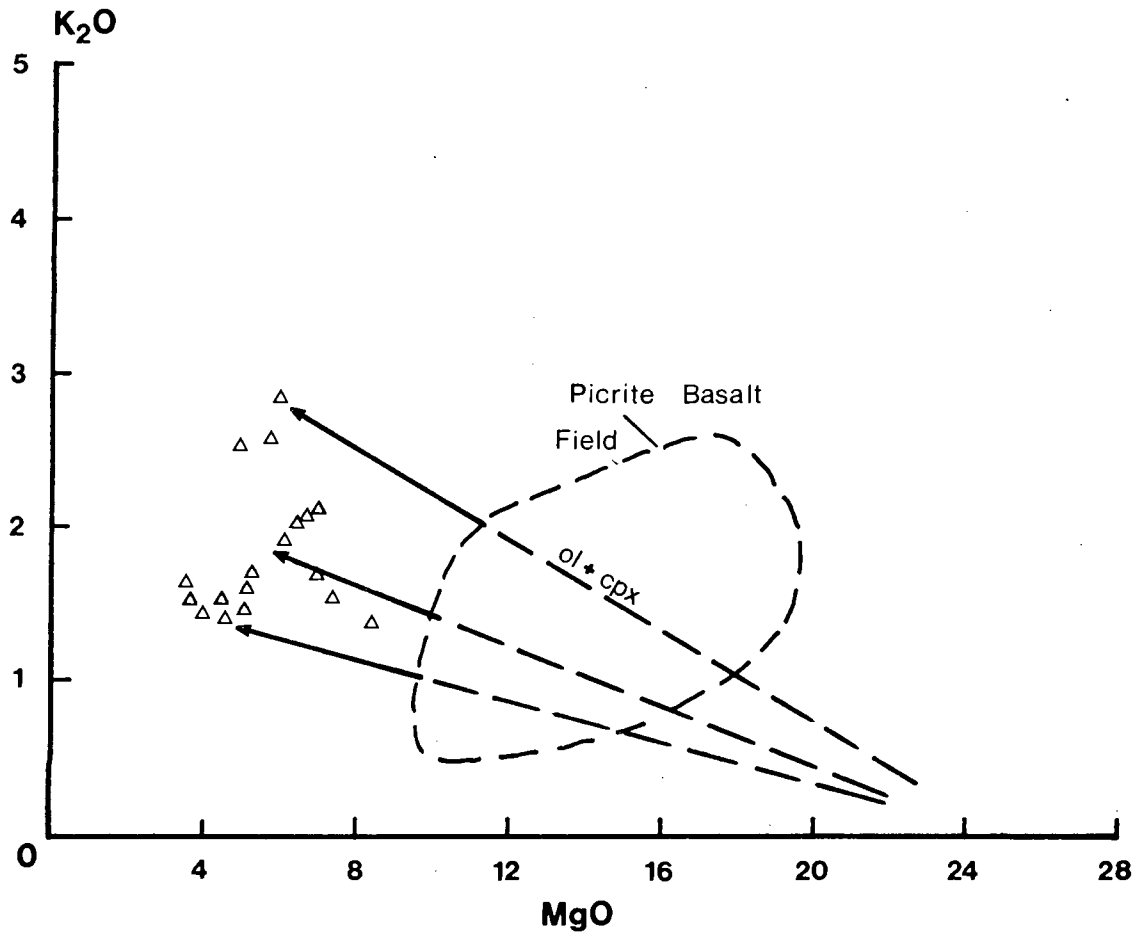

Fig. 9.10 Simplified diagram showing how crystal fractionation of an extract consisting of olivine and clinopyroxene from KAR element rich magmas of similar composition to the evolved picrite basalts could account for the petrogenesis of the low-MgO shoshonitic suite.

poor lavas and dykes would reflect a primary feature of the source magmas. It was shown in a previous chapter that the picrite basalts are characterised by a large range in Zr/Nb ratios (10-34) and it is perhaps not fortuitous that both the shoshonitic suite and picritic rocks show a similar range in Zr/Nb ratios.

Crystal fractionation of olivine and clinopyroxene from magmas enriched in KAR elements clearly provides a plausible mechanism to account for the geochemical relationships noted in the central and northern Lebombo low-MgO volcanics. In this respect it is also interesting to note that analyses of plagioclase phenocrysts from a high-K tholeiitic andesite (sample KA52b) show that the feldspars are enriched in the orthoclase component and plot on trends which are colinear with feldspar compositions obtained from the picrite basalts (see Fig. 9.2). Furthermore, many of the high-K lavas and dykes found in the central and northern Lebombo contain small clusters of clinopyroxene (Plate 9.1F) similar to those found in the evolved picrite basalts (see Plate 8.4A and section 8.2.3). Lastly, the fact that rocks of the shoshonitic suite are generally conformable and occasionally interdigitated with evolved picrite basalts supports a comagmatic crystal fractionation model.

Crustal contamination may have played a role in the petrogenesis of these lavas and dykes though to a much lesser extent than was the case in the southern Lebombo. For example the scatter in plots of SiO_2 and TiO_2 may reflect small amounts of granitic contamination acting on more basic magmas. Other factors do, however, mitigate against extensive crustal contamination. Firstly, initial Sr-ratios, though showing some spread (.704 - .707) are relatively low and it will be argued in the following chapter that the variation in initial ratios shown by these

rocks is more likely to reflect mantle heterogeneity than crustal contamination. Secondly, low MgO lavas from the northern Lebombo generally crop out above the picrite basalts. Consequently it would be expected that crustal contamination would have been most prevalent early in the history of the volcanic cycle, ie. during the early stages of picritic volcanism, whereas subsequent lavas would have been extruded through feeder channels lined with early formed basaltic material. These basaltic linings would act as buffers against subsequent crustal contamination. However, the presence of linings consisting of solidified picritic magma rich in KAR elements raises the possibility that the low-MgO lavas may have been contaminated by material rich in KAR elements thereby accounting for some of the enrichment in incompatible elements noted in the shoshonitic suite. Contamination processes cannot therefore be entirely discounted though on the basis of the geochemical, petrographic and outcrop criteria discussed previously it is concluded that the high-K rocks of the shoshonitic suite represent low pressure fractionation products of picrite basalt magmas.

Lavas from the Komati River, along with two samples from the Sabie River succession (for convenience they are all referred to as Komati samples), contrast strongly with the volcanics of the shoshonitic suite. As noted previously these rocks are depleted in incompatible elements relative to the other central and northern Lebombo low-MgO basalts and in general show major and trace element abundances that are more typical of the lavas and dykes from Swaziland and the southern Lebombo. These relationships are particularly clear from the average analyses presented in Table 9.4 and equally well demonstrated by the MgO variation diagrams (Figs. 9.8, 9.9).

Relatively little can be said about the petrogenesis of the Komati samples in terms of the major element chemistry due to the excessive scatter

area though Logan (pers. comm.) has noted minor occurrences of picrite basalts between the Komati and Sabie Rivers. However, it may also be argued that picrite basalts emplaced at the surface in the central Lebombo were overstepped by the low-MgO basalts or that alternatively the magmas which would have formed picrite basalt flows may have been retained in the crustal regime where they underwent low pressure fractionation to form the high-K lavas of the shoshonitic suite.

Arguments such as those presented above neither prove nor disprove a link between the shoshonitic suite and picrite basalts whereas chemical data clearly provide more unequivocal proof for a close link between these two rock suites. It is therefore concluded that the high-K lavas and dykes sampled from the north of the Komati River formed in response to crystal fractionation (clinopyroxene + olivine) from magmas associated with the picrite basalt event. Conversely, by virtue of their much lower incompatible element contents it is concluded that the southern low-MgO lavas and dykes (ie. rocks from the Komati River southwards) were derived from a unique source area(s) which was characterised by relatively low abundances of incompatible elements relative to the source from which the central and northern Lebombo low-MgO volcanics were derived.

9.7 Summary and Conclusions

In conclusion of this section the following points resulting from attempts to interpret the textural, mineralogical and geochemical data of the Lebombo low-MgO volcanics are stressed.

1. It is apparent that considerable petrographic and chemical variation exists in the low-MgO lavas and dykes of the Lebombo. These

variations appear to have developed in response to a series of inter-related and somewhat complex petrogenetic processes.

2. Modelling calculations show that gabbroic fractionation, possibly at relatively high pressures, accounts for most of the geochemical variation shown by the Rooi Rand magmas.

3. Geochemical variations in the Swaziland and southern Lebombo low-MgO lavas and normal dykes can, in most respect , be attributed to crustal contamination of Rooi Rand type magmas though the behaviour of Sr a d initial-Sr ratios are not entirely consistent with a contamination model. Some fractional crystallisation must have occurred during the petrogenesis of these rocks, though it has not been possible to delimit the extent and nature of this fractionation.

4. Relationships shown by Sr and Sr-isotopes present problems with respect to the petrogenesis of the low-MgO lavas from Swaziland and the southern Lebombo since the behaviour of neither of these elements can be explained in terms of simple crustal contamination processes. In view of this, in the following Chapter Sr-isotope and trace element data will be further used to investigate additional processes that may account for the geochemical variations noted in these rocks.

5. Olivine poor volcanics from the central and northern Lebombo, in particular, lavas and dykes from the Sabie and Olifants Rivers are petrographically and chemically distinct from the low-MgO rocks of the Komati River, Swaziland and southern Lebombo. They are characterised by high abundances of incompatible elements and were probably derived from magmas with compositions similar to evolved KAR element enriched picrite basalts by crystal fractionation of clinopyroxene and olivine.

6. Low-MgO volcanics of the Lebombo can be divided into a northern group characterised by high levels of incompatible elements and a southern group with relatively low levels of incompatible elements. The dividing line between the two groups is reasonably well defined by the chemical data and lies between the Komati and Sabie Rivers.

10 Rb-Sr SYSTEMATICS IN RELATION TO THE PETROGENESIS OF THE VOLCANIC ROCKS

10.1 Introduction

Detailed studies of isotope systematics, particularly those associated with the radioactive decay of Rb, U and Sm constitute an important part of any detailed geochemical appraisal of volcanic rock suites. For this reason a large number of the Lebombo samples which were analysed for major and trace elements, were also analysed for their $^{87}Sr/^{86}Sr$ ratios whereas U-Pb and Sm-Nd isotope studies are being carried out by other workers and are still in progress. The Sr-isotope data have been used in conjunction with major and trace element data to place additional constraints on petrogenetic models formulate for the Lebombo volcanics, particularly with respect to the low-MgO volcanics of the southern Lebombo.

Measured and initial (calculated at 190 my) $^{87}Sr/^{86}Sr$ ratios of the Lebombo and Nuanetsi volcanic rocks are listed in Table 10.1 The isotopic data are presented in the form of histograms and conventional Rb-Sr isochron plots in Figures 10.1 and 10.2, 10.3 respectively. Inspection of the diagrams reveals several important facts, viz. (i) the lavas and dykes show a large range in initial $^{87}Sr/^{86}Sr$ ratios (Fig. 10.1); (ii) there is no indication of a 180 my or older isochron relationship (Figs. 10.2 and 10.3) which must be the approximate age of the basalts since the overlying rhyolites yield a Rb-Sr age of about 177 my (see Chapter 6); (iii) though the data define a steep overall trend (Figs. 10.2, 10.3) there is no sign of a 1620 my "mantle isochron" as suggested by Brooks and Hart (1978) on the basis of previous Karoo strontium data, and (iv) some of the data points (Figs. 10.2, 10.3) lie to the left of the 4.6 by reference line, which is suggestive of pre-Karoo Rb depletion in the mantle source area.

TABLE 10.1 Rb and Sr concentrations(ppm),Rb/Sr ratios and atomic ratios for Sabi, Nuanetsi and Lebombo mafic volcanics.
[x] - Analyst or reference.
(y) - 1σ uncertainty

SAMPLE NAME	Rb	Sr	Rb/Sr	87Rb/86Sr	87Sr/86Sr	Io(190my)
A. ZIMBABWE						
1. SABI						
Mashikiri Formation						
NTS7[3]	70	1500	0.047	0.136	.70566(6)	.70529
NTS8[8]	69	1566	0.044	0.127	.70585(5)	.70551
NTS12[8]	63	1663	0.038	0.110	.70540(6)	.70510
2. NUANETSI						
Letaba River Formation						
NB7[7]	68	1027	0.066	0.191	.7074	.7069
N399[8]	19.4	585	0.033	0.095	.70487(5)	.70461
N149[8]	21.5	604	0.036	0.104	.70493(4)	.70465
N187[8]	25.6	613	0.042	0.121	.70599(5)	.70566
N406[8]	24.0	703	0.034	0.098	.70485(4)	.70459
N113[8]	48.0	735	0.065	0.188	.70531(6)	.70480
N126[8]	33.6	787	0.043	0.124	.70528(5)	.70495
N60[8]	36.4	935	0.039	0.113	.70514(4)	.70483
N133[8]	36.0	958	0.038	0.110	.70505(4)	.70475
N135[8]	33.6	970	0.035	0.101	.70548(5)	.70521
N400[8]	42.3	998	0.042	0.121	.70511(7)	.70478
Sabie River Formation						
NB2[7]	34.5	898	0.038	0.110	.7064	.7061
NB3[7]	64	575	0.110	0.318	.7089	.7080
NB4[7]	58	983	0.059	0.170	.7063	.7058
N175[3]	37	703	0.053	0.153	.70617(22)	.70576
N386[3]	50	1028	0.049	0.142	.70609(7)	.70571
Interbedded Basalts						
NB1[7]	62	183	0.339	0.979	.7122	.7096
NB5[7]	12.5	182	0.069	0.199	.7109	.7104
NB6[7]	72	237	0.034	0.875	.7116	.7092
Picritic Intrusives						
NTS17[8]	13.1	742	0.018	0.052	.70545(6)	.70531
N21[8]	45.8	1130	0.041	0.118	.70554(4)	.70522

N22[8]	33.2	842	0.039	0.113	.70544(4)	.70513
N163[8]	12.2	389	0.031	0.090	.70563(7)	.70539

B. LEBOMBO

a. PAFURI AREA

Mashikiri Formation

KP82[3]	28.6	1034	0.028	0.080	.70696(5)	.70675
KP127[3]	62	1337	0.046	0.133	.70723(6)	.70687

Letaba River Formation

KP112[3]	61.0	795	0.077	0.222	.70531(5)	.70471
KP121[3]	45.0	831	0.054	0.156	.70577(4)	.70535

Dolerites

KP89[2]	14.2	898	0.016	0.046	.70488(4)	.70476
KP129[2]					.70541(5)	.70476

b. SHINGWEDZI RIVER AREA

Letaba River Formation

KS3[3]	58.0	842	0.069	0.199	.70507(4)	.70453

Dolerites

KS36[3]	26.0	297	0.088	0.254	.70513(6)	.70444

c. OLIFANTS RIVER AREA

Mashikiri Formation

KA16[3]	38.7	1320	0.029	0.084	.70543(6)	.70520

Letaba River Formation

0169[3]	113	1177	0.096	0.277	.70549(4)	.70475
KA24[3]	29.5	902	0.033	0.095	.70529(4)	.70503

Sabie River Formation

KA112[3]	32	712	0.045	0.130	.70524(4)	.70489

Dolerites

KA31[3]	45	871	0.052	0.150	.70461(5)	.70420
KA52[3]	48	836	0.057	0.165	.70468(5)	.70424
KA52B[3]	50	953	0.053	0.153	.70469(4)	.70427

d. SABIE RIVER AREA

Sabie River Formation

CL110[3]	54	1100	0.049	0.142	.70711(5)	.70672
CL115[3]	24.4	696	0.035	0.101	.70516(6)	.70492
CL120[3]	60	1162	0.052	0.150	.70678(4)	.70638

Dolerites

CL105[3]	28.2	827	0.034	0.099	.70531(5)	.70672

e. SWAZILAND

Sabie River Formation

LB2[7]	5.0	225	0.022	0.150	.7046	.7044
EH8[3]	18.5	265	0.070	0.202	.70734(4)	.70679

Dolerites (Rooi Rand)

RC110[4]	13.3	298	0.045	0.130	.70446(4)	.70411
RC120[4]	15.5	213	0.073	0.211	.70425(6)	.70368
RC121[4]	4.1	198	0.021	0.061	.70409(4)	.70393

f. SOUTHERN LEBOMBO

Sabie River Formation

L12[1]	6.7	727	0.009	0.026	.71043(3)	.71036
L18[1]	10.7	273	0.037	0.107	.70879(8)	.70850
L29[1]	19.1	302	0.063	0.182	.70865(5)	.70816
L32[1]	10.9	256	0.043	0.124	.70784(6)	.70751
L36[1]	14.9	352	0.042	0.121	.70947(4)	.70914
L57[1]	34	378	0.090	0.260	.70849(6)	.70779
S45[1]	75	417	0.175	0.506	.71229(6)	.71092
L285[3]	16.5	222	0.074	0.214	.70549(4)	.70486
L348[3]	41.0	166	0.247	0.715	.71536(4)	.71361
L505c[1]	19.4	172	0.113	0.326	.70752(2)	.70664
J3[1]	8.8	235	0.038	0.110	.70404(4)	.70374
LB3[7]	23	446	0.052	0.150	.7066	.7062

Dolerites

L94[1]	9.9	228	0.034	0.098	.71001(5)	.70975
L249a[1]	9.7	188	0.052	0.150	.70574(4)	.70534
L503[1]	9.1	234	0.036	0.104	.71011(3)	.70983
L508[1]	74	276	0.268	0.774	.71031(3)	.70822
J55[3]	66	288	0.229	0.661	.70653(4)	.70461

Rooi Rand Dolerites

L496b[1]	21.8	232	0.094	0.271	.70466(8)	.70393
A21[2]	7.7	199	0.039	0.113	.70403(4)	.70372
A22[2]	8.3	158	0.053	0.153	.70428(6)	.70384
A114[2]	11.3	213	0.053	0.153	.70429(6)	.70387
A117[2]	26.3	267	0.099	0.286	.70510(6)	.70432
A129[2]	4.8	150	0.032	0.092	.70421(4)	.70396
A135[2]	6.3	213	0.030	0.087	.70373(4)	.70350
A186[2]	4.3	161	0.027	0.078	.70387(4)	.70366

REFERENCES: [1] Allsopp,H.L. (unpubl. data)
[2] Armstrong,R.A. (unpubl. data)
[3] Bristow,J.W. (unpubl. data)
[4] Cleverly,R.W. (1977)
[7] Manton,W. (1968)
[8] Norry,M.J. (1977)

The range in initial ratios found in the Lebombo and Nuanetsi volcanics is worthy of further comment at this point. Inspection of Figure 10.1 reveals that variation in initial ratios is relatively small in the nephelinites, greater in the picrite-basalts and largest in the low-magnesian rocks, particularly those from the southern Lebombo. The large range of initial ratios found in the Lebombo and Nuanetsi lavas and dykes and Karoo as a whole (see Erlank et al., 1980), is a common feature of continental volcanics, though the range shown by the Lebombo and Nuanetsi rocks appears to be substantially greater than noted elsewhere (Table 10.2). The largest range found in basaltic rocks outside the Karoo is shown by the King Hill lavas (0.7104 - 0.7176; Leeman, 1977) from the Snake River Plain - Yellowstone area though it is still considerably less than that found in the eastern Karoo rocks. Extremely high initial $^{87}Sr/^{86}Sr$ ratios are found in Kirkpatrick basalts (Faure et al., 1974), Ferrar dolerites (Compston et al., 1968) and Tasmanian dolerites (Heier et al., 1965) which are only slightly younger than the Karoo volcanics. However, Sr-isotope ratios from Tasmania and Antarctica are uniformly high and show relatively little variation (Table 10.2).

Geochemical relationships similar to those shown by the Lebombo volcanics have in the past most commonly been explained in terms of crustal contamination eg. Bell and Powell (1969), Hurley et al. (1966) and Faure et al. (1972, 1974, 1979), though it has frequently been exceedingly difficult to substantiate such a mechanism in relation to other aspects of the chemistry of the rock suites concerned (e.g. see Appleton, 1972; Brooks et al., 1976a). In view of the extreme thickness of crustal material continental volcanics must pass through before reaching the surface, some contamination seems inevitable, though un-equivocal proof of such a process is probably only provided by a detailed

TABLE 10.2 Initial $^{87}Sr/^{86}Sr$ ratios in representative continental tholeiitic volcanics.

NAME AND LOCALITY	AGE my	$^{87}Sr/^{86}Sr_o$ *	NO.OF SAMPLES	REF.
Snake River Plain - Yellowstone				
Craters of the Moon Lavas	Recent	.7075 - .7120	21	1
King Hill lavas		.7104 - .7176	15	1
Columbia River				
Lower Yakima	~ 15	.7052	11	2
Middle Yakima	~ 15	.7053	5	2
Upper Yakima	8 - 14	.7069 - .7092	8	2
Antarctica				
Queen Maude Land Basalts	~ 170	.7027 - .7055	13	3
Kirkpatrick Basalts	~ 170	.7094 - .7144	22	4
Ferrar Dolerites	~ 170	.7089 - .7142	22	5
Tasmania				
Dolerites	~ 165	.7107 - .7124	7	6
Karoo				
Central Area lavas & dykes	~ 190	.7040 - .7097	43	7
Nuanetsi & Lebombo dykes & lavas	~ 190	.7035 - .7136	68	7

* Initial ratios calculated for ages indicated.

References

1. Leeman (1977)
2. McDougall (1976)
3. Faure et al. (1979)
4. Faure et al. (1974)
5. Compston et al. (1968)
6. Heier et al. (1965)
7. This study

assessment of two or more isotopic systems. For example, Turri and Taylor (1976) have shown that highly potassic volcanics from Central Italy are frequently accompanied by both higher $^{18}\delta_0$ and $^{87}Sr/^{86}Sr$ ratios, which strongly supports crustal contamination in this case.

Brooks and co-workers (Brooks et al., 1976 b,c; Brooks and Hart, 1978) have adopted a different approach to the problem of high and variable $^{87}Sr/^{86}Sr$ ratios. They suggest that many volcanic rock suites show crude correlations between Rb/Sr and initial $^{87}Sr/^{86}Sr$ and define pseudo- or mantle-isochrons with apparent ages in excess of the eruptive age of the rocks. It is their contention that the pseudo-isochrons are inherited from the mantle and reflect periods during which local or large scale (world wide) chemical heterogeneity (enrichment and/or depletion) developed in response to mantle processes, e.g. major mantle fractionation events. Consequently Brooks and co-workers have argued that high and variable initial-Sr isotope ratios such as those found in the Karoo are the result of long standing chemical heterogeneities in the mantle (e.g. see Brooks and Hart, 1978).

The main problem with a heterogeneous mantle model as proposed by Brooks and co-workers is whether the chemical and isotopic inhomogeneities caused by mantle processes could be effectively removed by convection and diffusion. Some authors (Armstrong, 1968; O'Nions and Pankhurst, 1974) have previously assumed that mantle convection and diffusion will homogenise an inhomogeneous mantle. Conversely, other authors (Dickenson and Luth, 1971; Ringwood, 1974) dispute this because they regard the mantle residue left after the removal of a partial melt as a refractory solid incapable of equilibration with undepleted mantle in view of the slow rates of solid-state diffusion in silicates. Conclusions reached by Jordan (1978) with respect to remixing of depleted and undepleted mantle

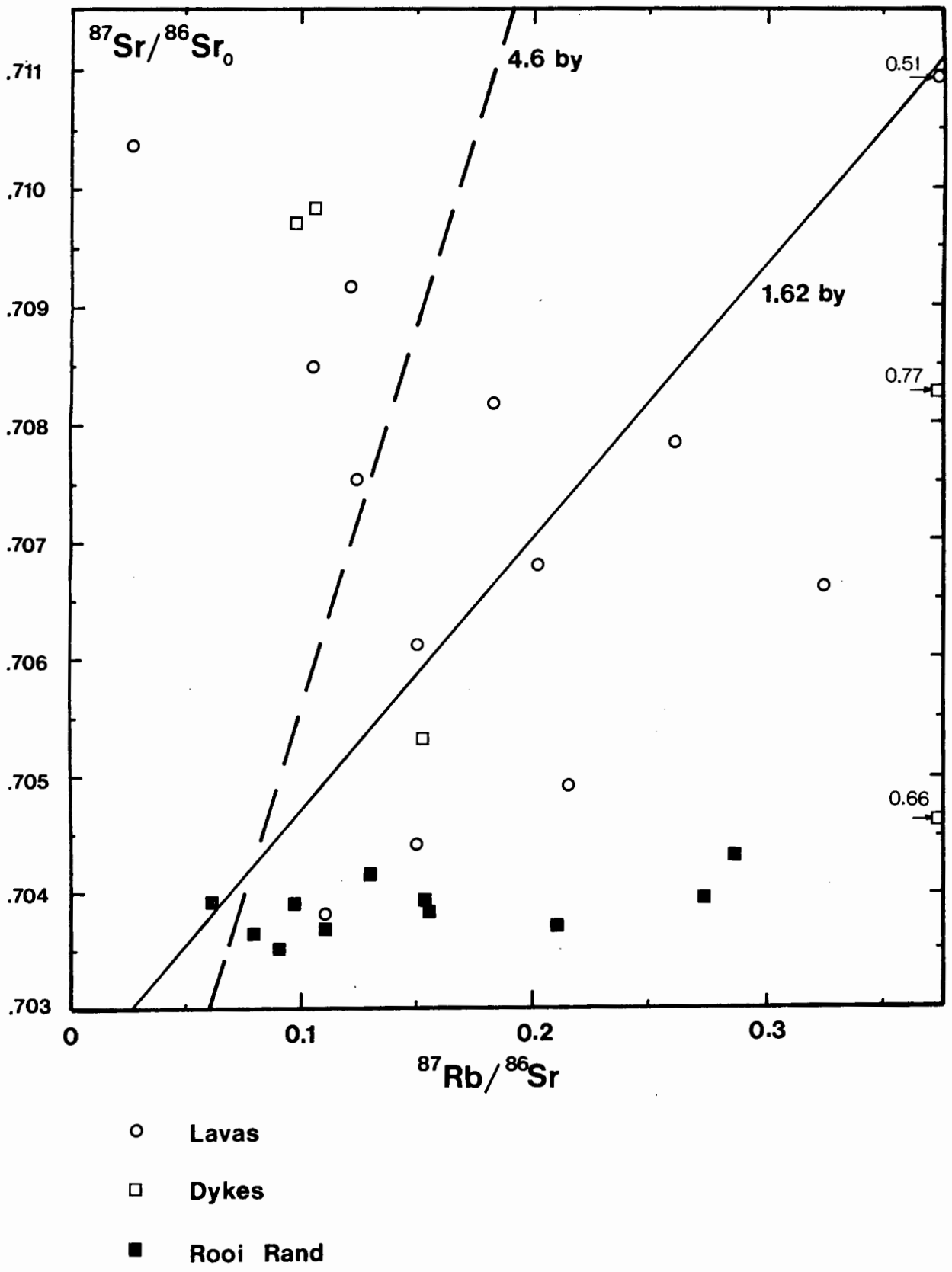

Fig. 10.2 Plot of $^{87}Sr/^{86}Sr_o$ versus $^{87}Rb/^{86}Sr$ for the southern Lebombo and Swaziland low-MgO lavas and dykes.

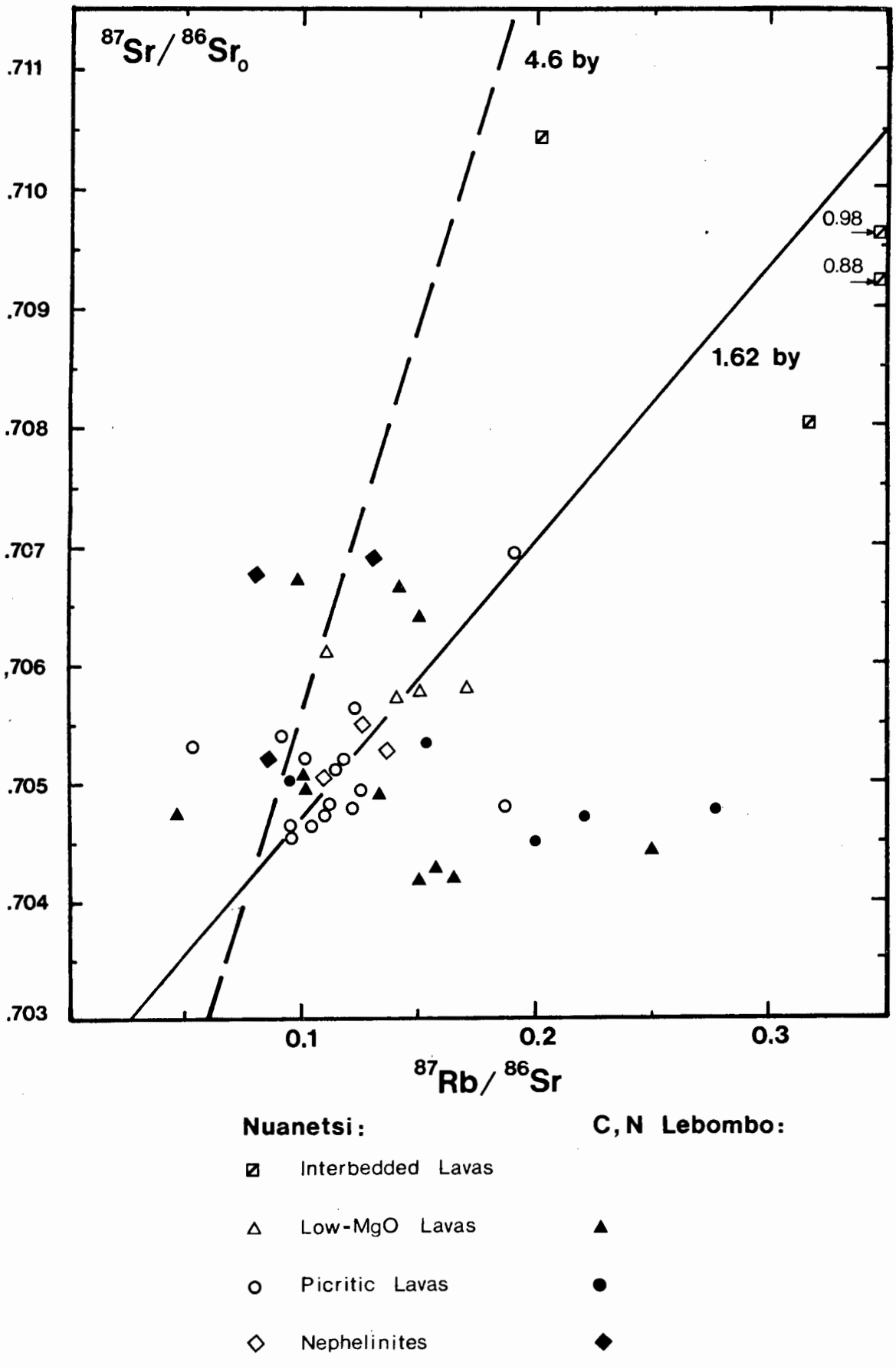

Fig. 10.3 Plot of $^{87}Sr/^{86}Sr_o$ versus $^{87}Rb/^{86}Sr$ for the central and northern Lebombo and Nuanetsi mafic volcanics.

in continental environments support the views of Dickenson and Luth (1971) and Ringwood (1974). Jordan (1978) considers basaltic depletion to be an irreversible process which leads to the formation of depleted mantle zones which become locked into the base of the crust and effectively isolated from further disruption by mantle processes.

Nevertheless, both convection and diffusion should be able to achieve some remixing in a partially molten magma, the effects of which have been investigated by Hofmann (1974, 1975), Hofmann and Magaritz (1977), Hofmann and Hart (1978) and others. Though rates of convection are poorly known Hofmann and Magaritz (1977) have suggested that for a cell diameter of at least 500 km, the time for overturn is of the order of 10^8yr whereas experimental studies (Hofmann and Magaritz, 1977) suggest that characteristic diffusion distances exceed 1 km for only very long times of 10^9 years or more, e.g. for diffusivity of Sr in basalt melt distances of 5.6 cm, 56 m and 1.8 km in 1, 10^6 and 10^9 years were obtained by Hofmann and Magaritz (1977). Thus it would appear that if convection is to homogenise heterogeneous mantle source areas it will take some considerable time unless the convection cells are very small. Similarly, the experimental diffusion data (Hofmann and Magaritz, 1977) suggest that equilibration of a partially molten mantle by diffusion will only be effective on a small (centimetre) scale and that large scale mantle heterogeneities may persist for lengthy time periods.

Recent isotopic studies, particularly those incorporating Nd and Sr isotope data (e.g. Carlson et al., 1978; Carter et al., 1978; De Paolo, 1979; Hawkesworth et al., 1979 a,b; Hawkesworth and Vollmer, 1979; Zindler et al., 1979) have provided a considerable volume of new evidence for the existence of heterogeneity in the mantle. Furthermore, it has been shown that a pseudoisochron model as proposed by Brooks and co-workers is not necessarily applicable (Hawkesworth and Vollmer, 1979) and

instead the concept of mantle metasomatism has been developed to account for mantle heterogeneity, particularly for enriched mantle (Lloyd and Bailey, 1975; Erlank et al., 1980). Perhaps, most significant, however, is that replacement minerals, e.g. phlogopite, K-richterite and opaque oxides, which possibly represent the product of metasomatic events that created heterogeneity in the mantle, have been found in mantle peridotites (Erlank, 1973, 1976; Aoki, 1975; Harte et al., 1975; Dawson and Smith, 1977; Erlank and Rickard, 1977).

The origin of high and variable Sr-isotope ratios in continental basalts therefore involves two possible end member models, viz, crustal contamination or mantle heterogeneity. In reality there are probably a whole spectrum of interpretations, including wall-rock reaction, zone-refining, magma mixing and disequilibrium melting which lie between these two models. Furthermore, since many of the above processes are undoubtedly closely related it is often impossible to invoke one single mechanism to explain the characteristics of a specific set of data.

In the ensuing discussion processes which may account for the origin of the high and variable $^{87}Sr/^{86}Sr_o$ ratios in the Lebombo and Nuanetsi volcanics and unusual major and trace element characteristics of the low-MgO southern Lebombo volcanics are discussed. As far as possible the processes are considered independantly with respect to the three main groups of rocks viz. (i) basic lavas and dykes of the southern Lebombo, (ii) low MgO volcanics of the central and northern Lebombo and Nuanetsi, and (iii) nephelinitic and picritic volcanics of the northern Lebombo, Nuanetsi and Sabi areas. Particular emphasis has been placed on the lavas and dykes of the southern Lebombo (including Swaziland) since these rocks clearly display the greatest range in initial ratios (Fig. 10.3), and on the basis of their geochemical relationships (Chapter 9) appear to have

undergone a complex petrogenetic history. In contrast most of the lavas and dykes from the central and northern Lebombo, Nuanetsi and Sabi areas appear to have behaved in a relatively coherent fashion insofar as the initial-Sr ratios of these rocks are generally low and less variable than is the case in the southern Lebombo rocks.

10.2 Southern Lebombo Lavas and Dykes (includes Rooi Rand intrusives)

10.2.1 Secondary Processes

It is possible that secondary alteration and hydrothermal processes may have led to changes in the Sr-isotope ratios of the erupted lavas and dykes by redistribution of Rb and radiogenic ^{87}Sr. Consequently an attempt has been made to assess the effects of these secondary processes prior to discussing the Sr-isotope data in relation to processes such as contamination, mantle heterogeneity, etc.

(i) Hydrothermal Activity

Zeolites and related minerals such as calcite, are commonly found in amygdales and veins in the Lebombo basalts, particularly the low-MgO lavas. The presence of these minerals indicates that there was probably considerable syn- or post-emplacement hydrothermal activity in the lava pile which may have redistributed mobile elements such as K, Rb and Sr and possibly radiogenic ^{87}Sr.

To assess the possible effects hydrothermal activity may have had on the Sr-isotope chemistry of the lavas and dykes, $^{87}Sr/^{86}Sr$ ratios were measured in (a) zeolite and calcite extracted from a hydrothermal vein and (b) the freshest basalt sample found in proximity to the vein material. The zeolite and calcite were separated by careful crushing and hand picking of the vein material whereas care was taken to ensure that any altered or

vein material was removed from the basalt sample.

Results of the isotopic measurements are presented in Table 10.3 and indicate that the hydrothermal mineralisation responsible for the deposition of calcite and zeolite in the basalts does not appear to be responsible for the high $^{87}Sr/^{86}Sr_0$ ratios in some of the lavas, especially in view of the lower total Sr in the zeolite and calcite relative to the basalt. Furthermore, the similarity of the zeolite and basalt initial ratios implies that zeolisation was syngenetic with basalt formation and/or emplacement.

TABLE 10.3 Sr-isotope ratios of basaltic lava and associated hydrothermal calcite and zeolite. (Ro for 190 my).

SAMPLE	^{87}Rb ppm	^{86}Sr ppm	$^{87}Sr/^{86}Sr$	$^{87}Sr/^{86}Sr_{(o)}$
Calcite	0.036	3.202	.70703 ± 7	.70702
Zeolite	1.040	7.760	.70705 ± 7	.70669
Basalt L505C	5.48	16.62	.70752 ± 12	.70664

(ii) Recent Alteration

Though samples selected for geochemical analysis, and in particular Sr-isotope analysis, were carefully chosen so as to ensure that they were reasonably fresh and free of hydrothermal veining and amygdales, evidence of secondary alteration, e.g. sericitisation of feldspars, was found in even the freshest available material. Recent weathering and redistribution of Rb and/or Sr could effect the Rb/Sr ratios of lavas and dykes and change the value of the initial $^{87}Sr/^{86}Sr$ ratio calculated from the present-day (measured) $^{87}Sr/^{86}Sr$ ratio. Similarly redistribution of radiogenic ^{87}Sr by groundwater may lead to changes in the $^{87}Sr/^{86}Sr$ ratios during alteration such that measured values do not reflect the correct present-day ratios.

To assess the possible effects alteration has had on the Rb/Sr and Sr-isotope ratios, the measured Rb/Sr and initial $^{87}Sr/^{86}Sr$ ratios have been plotted against the total loss on ignition (LOI) (Fig. 10.4) as determined in the southern Lebombo volcanics. Data from the southern Lebombo lavas and dykes have been used since these rocks invariably show the greatest degree of alteration and are characterised by very high Sr-isotope ratios (LOI has been used as an index of alteration since a relatively good correlation was found between increased $CO_2 + H_2O^+$ content and visible alteration effects in the rocks studied - see Chapter 4).

Positive correlation between LOI and Rb/Sr and LOI and $^{87}Sr/^{86}Sr_o$ would imply that alteration had caused an increase in the ratios whereas the reverse would apply for a negative correlation. However, the data in Figures 10.4 a,b are distinctly scattered, though there is a very vague tendency towards a negative correlation, suggesting that the measured ratios in rocks with high LOI's may be marginally lower than the original or 'true' values. Critically, however, there is no positive correlation between the data plotted in Figures 10.4 a and b and it is therefore concluded that the Rb/Sr and initial-Sr ratios have not been greatly affected by recent alteration processes.

Discussion

Data presented above indicates that although the basalts have been subjected to hydrothermal veining and alteration, these processes have caused very little or no change in the measured Rb/Sr and Sr-isotope ratios. Consequently the large range and exceptionally high values observed in the $^{87}Sr/^{86}Sr_o$ data must reflect an inherent feature of the magmas from which the lavas (and dykes) were derived.

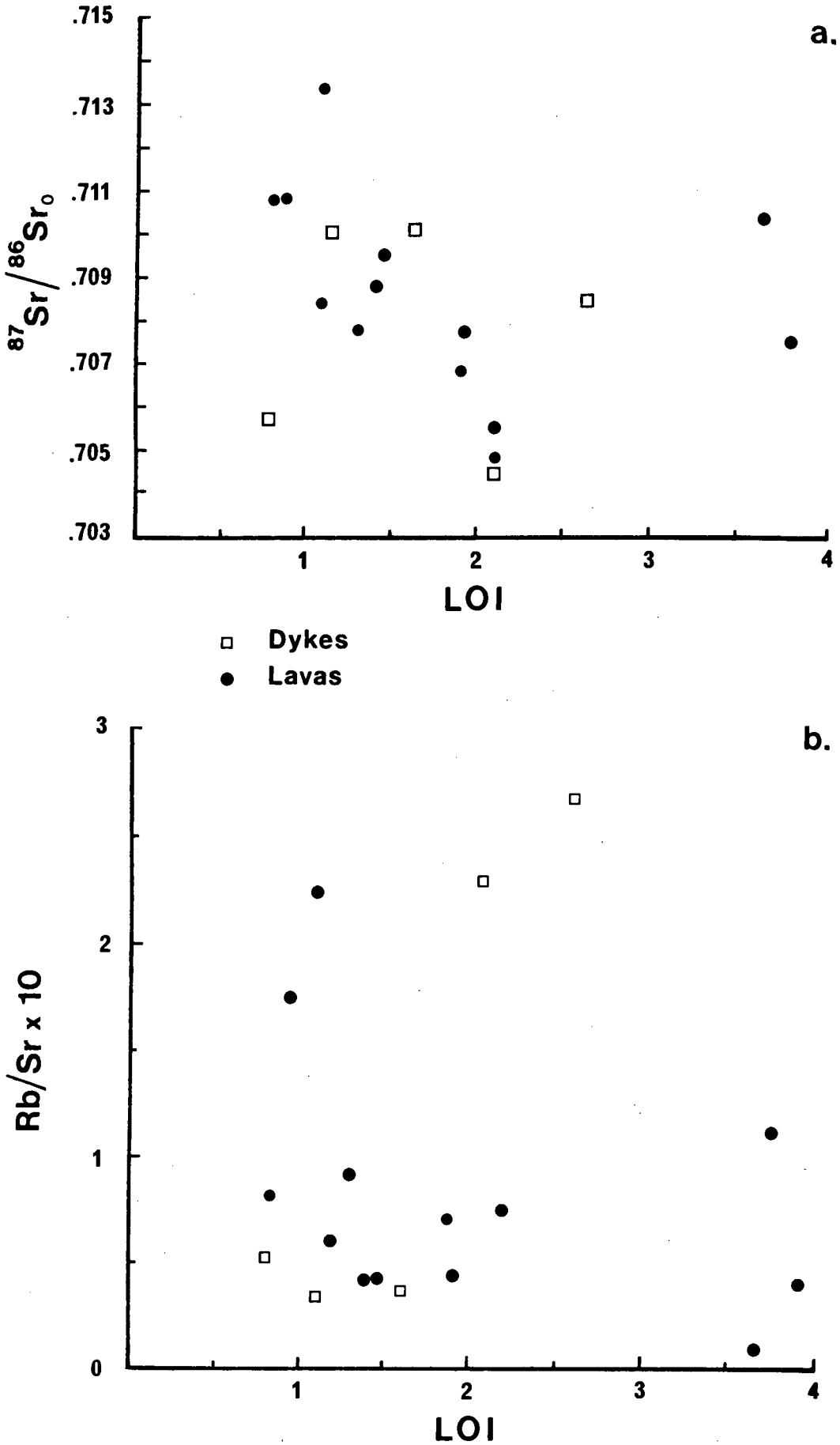

Fig. 10.4 Plots of $^{87}Sr/^{86}Sr_o$ and Rb/Sr versus LOI (Loss on Ignition) for the southern Lebombo low-MgO lavas and dykes.

10.2.2 Crustal Contamination

In Chapter 9 it was shown that crustal contamination of a Rooi Rand-type magma with a granitic type material could account for some of the scatter noted in the major and trace element variation diagrams for the southern Lebombo lavas and normal dykes. However, it was also noted that relationships shown by Sr and Sr-isotope ratios were not altogether compatible with bulk contamination of granite. Similarly it was found that contamination of a Rooi Rand-type magma with an average Swaziland system tonalite would help, but not necessarily resolve the Sr problem. In view of this, an assessment has been made of Sr isotope data, in conjunction with major and trace element data to establish whether (i) additional constraints may be placed on a crustal contamination model or (ii) alternative models may be involved to explain the geochemical variations noted in the southern Lebombo low-MgO volcanics (including Rooi Rand).

The possibility of bulk crustal contamination accounting for some of the variations shown by the southern Lebombo lavas and dykes, has been re-investigated by examining the co-variation between the initial Sr-isotope ratios and elemental abundance, for those elements which are typically either enriched or depleted in the continental crust relative to the underlying mantle. Crustal material, in particular granitic crust, typically has high $^{87}Sr/^{86}Sr$ ratios and SiO_2, K_2O and Rb abundances relative to basaltic rocks. Consequently contamination of a basaltic melt with granitic material should produce positive correlations for the above elements. Conversely, granitic crust generally has lower Sr contents relative to basaltic magmas. Simple two-end member mixing should therefore result in a negative hyperbolic shaped trend on a $^{87}Sr/^{86}Sr_0$ versus Sr diagram (Bell and Powell, 1969), or alternatively the $^{87}Sr/^{86}Sr_0$ versus

1/Sr diagram should show a straight line trend with a positive slope (Faure et al., 1974).

Inspection of the initial Sr-isotope ratio versus element diagrams (Figs. 10.5 a-e) reveals several important features. The Rooi Rand dolerites (including those from Swaziland analysed by Cleverly, 1977) and two basalts plot on almost flat trends; both of the basalts, ie. LB2 and J3, are from the top of the basalt succession. However, the remaining data are strongly scattered and it would appear as though some of the higher ratios could be ascribed to granitic contamination. This is reflected by the poorly developed trend lines of positive slope apparent in subsets of the data on the SiO_2, K_2O, 1/Sr and Rb (?) versus initial Sr-ratio plot, and the negative trend shown by some of the data points on the Sr versus initial ratio plot. The effect of crustal contamination is illustrated schematically by the arrow 'C' on the figures and those rocks which may have been affected by contamination are enclosed in a cross-hatched field on the Sr and 1/Sr versus initial-Sr ratio diagrams.

Mixing lines have been fitted to the samples which appear to be contaminated with granitic crust (Figs. 10.6 a,b) so as to possibly establish the amount of crustal contaminant that would be necessary to account for some of the high ratios. A straight line was fitted to the data on the $^{87}Sr/^{86}Sr_o$ versus 1/Sr plot (Fig. 10.6a) and a general mixing equation similar to that derived by Faure (1977) has been used to fit a hyperbolic curve to the data on a $^{87}Sr/^{86}Sr_o$ versus Sr plot (Fig. 10.6b). By trial and error it was found that the solution which provided the best fit on the $^{87}Sr/^{86}Sr$ versus Sr plot was achieved by mixing a granitic component (C) with $^{87}Sr/^{86}Sr = 0.740$ and Sr = 60 ppm with a basaltic component (A) in which $^{87}Sr/^{86}Sr_o = 0.705$ and Sr = 400 ppm.

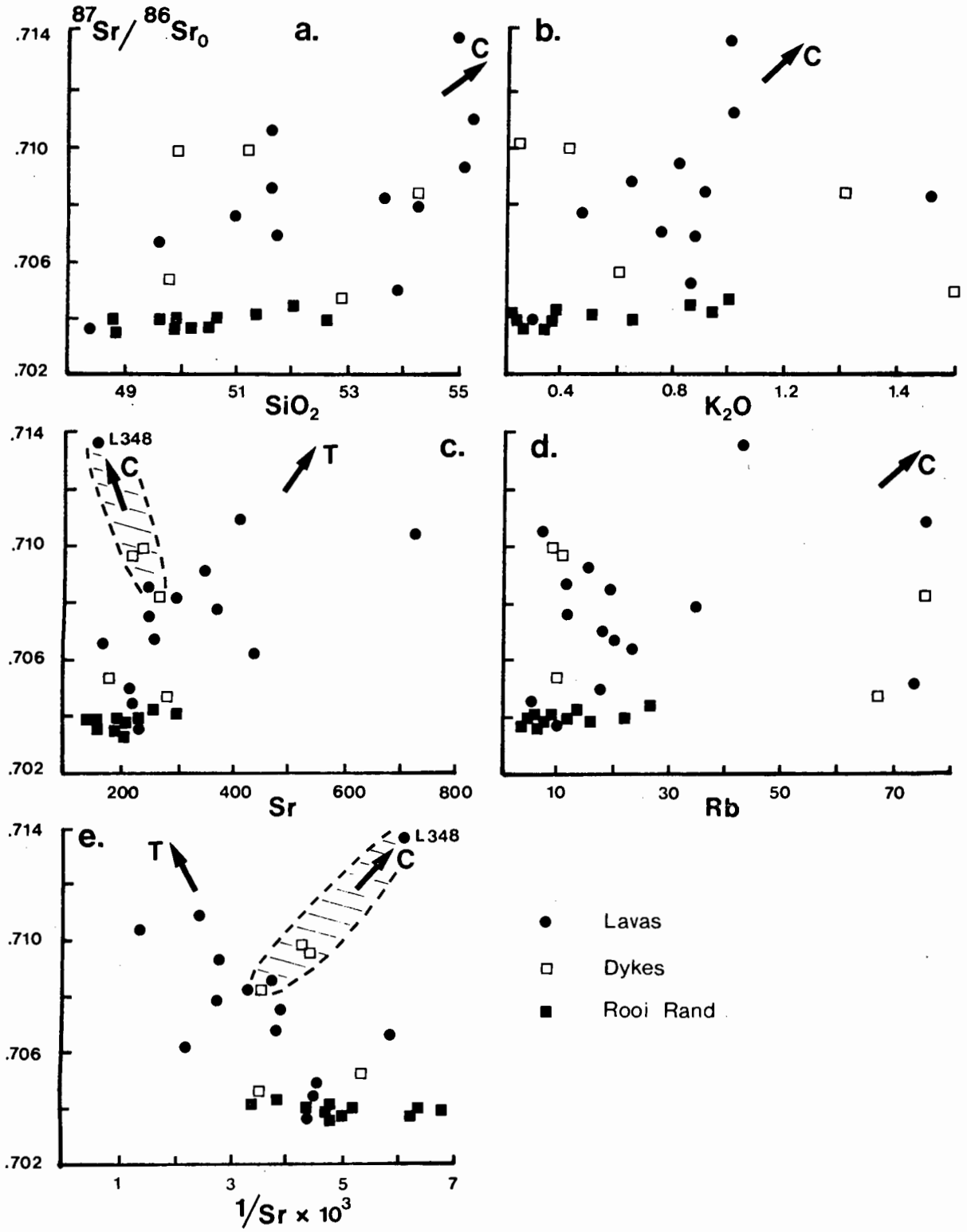

Fig. 10.5 Relations between $^{87}Sr/^{86}Sr_o$ and various major and trace elements for the southern Lebombo and Swaziland low-MgO volcanics. Arrows marked 'C' and 'T' illustrate the probable effects of contaminating lavas or dykes characterised by low initial-Sr isotope ratios with granitic and tonalitic material respectively.

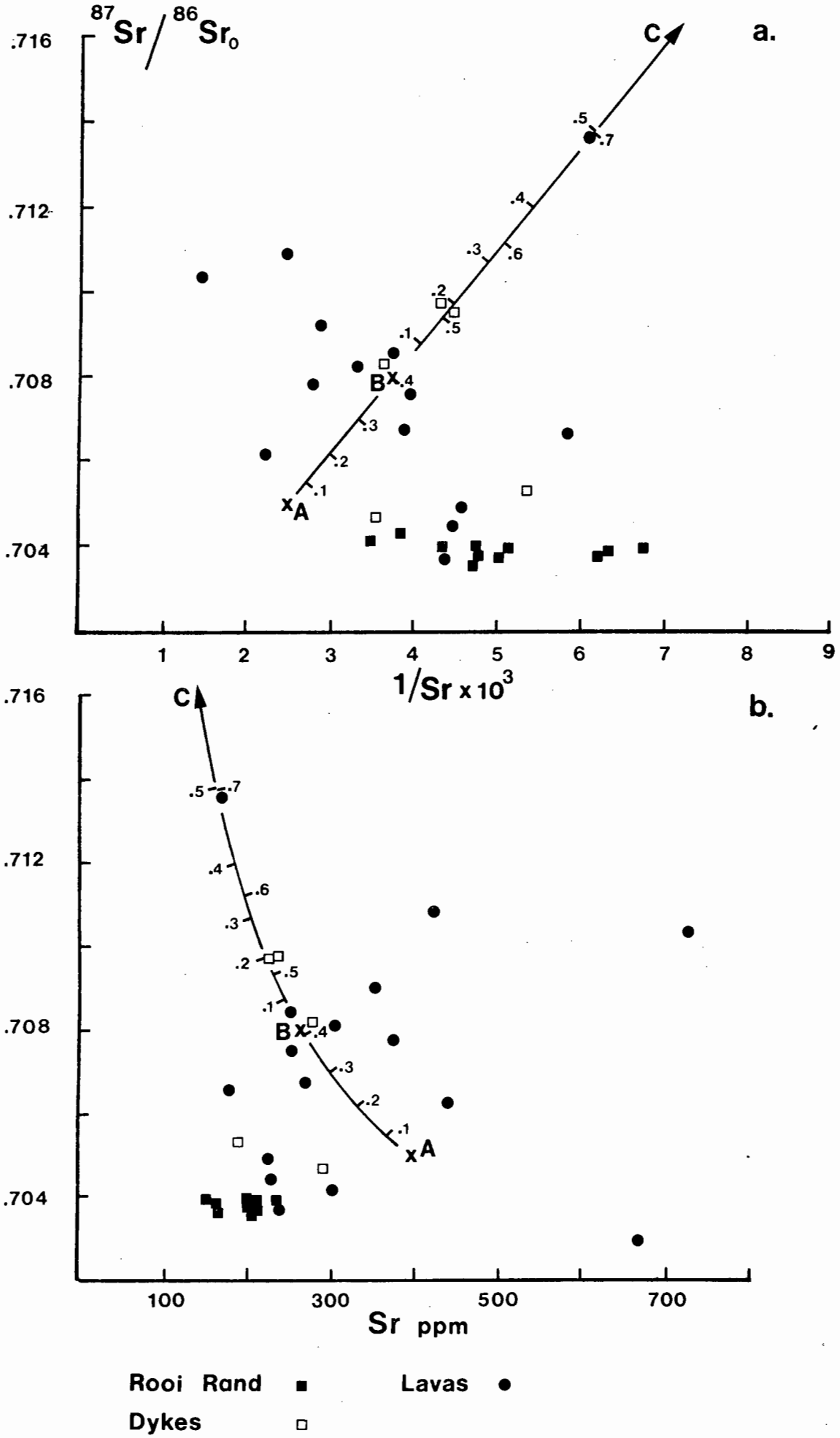

Fig. 10.6 Sr-isotope mixing model for the southern Lebombo and Swaziland low-MgO volcanics assuming the contaminant was of granitic composition. (Symbols as in Fig. 10.5.)

The chemical characteristics of the hypothetical granitic end member imply that it would have had a relatively evolved composition while the Sr content of the basaltic component is rather high. Furthermore, though the selected data provide a reasonable graphical fit it necessitates the incorporation of approximately 70% of the crustal end member into the basaltic melt to produce the basalt with the highest initial-Sr ratio (0.7136, Sample L348). This is most implausible from a major element point of view since in terms of the silica content of sample L348 (SiO_2 = 54.96%; normalised volatile free) it would be necessary to add no more than 25% of a granite with SiO_2 = 70% to a basaltic melt with SiO_2 = 50% to produce the observed silica abundance. In an attempt to overcome this problem a further mixing model was constructed with a hypothetical basaltic end member (B) in which $^{87}Sr/^{86}Sr_0$ = 0.7080 and Sr = 267 ppm. The use of end-member B implies that the contaminated rocks originated from basaltic magmas which already had relatively high $^{87}Sr/^{86}Sr_0$ ratios. In this case approximately 50% of crustal contamination is required to produce the sample with the high initial Sr ratio, which is again in conflict with the SiO_2 abundance of the lava.

Selective contamination involving unequilibrated biotite in lower-crustal granulites may be one method whereby some of the high initial-Sr ratios were produced in the magmas from which the southern Lebombo lavas crystallised. Early formed magmas would be particularly susceptible to contamination of this sort as they moved from their source area through the overlying crustal rocks to the surface. However, with the continued magmatism, the magma pathways would probably have become lined with basaltic material and/or equilibrated with mantle Sr. In general the most radiogenic lavas are located in the lower half of the succession whereas the less radiogenic occur in the upper half such that selective

granitic contamination fits the observed pattern of isotope variation in some of the southern Lebombo lavas. Selective contamination is often cited as a possible means of isotopic enrichment (e.g. see Pankhurst, 1969) though the mechanism is poorly understood. Nevertheless, it would appear to be the most plausible mechanism to account for those granitic southern Lebombo lavas and dolerites which lie on granitic-contamination trends in Figures 10.6 a-b.

However, though there are data plotted in Figures 10.5 a-e which may be ascribed to granitic contamination (selective?) of a basic magma, there are a large number of data points which show trends that appear to be unrelated to contamination of basic magmas with granite. Trends unrelated to granitic contamination are reflected by an envelope of data which shows a positive correlation on the $^{87}Sr/^{86}Sr_0$ versus Sr (Fig. 10.5c) diagram and a negative correlation on the $^{87}Sr/^{86}Sr_0$ versus 1/Sr plot (Fig. 10.5d). Unlike the elements noted above, Rb appears to define a rather crude negative correlation in the lavas and dykes suggesting that they may have suffered Rb depletion.

Since contamination with granitic material is clearly incapable of producing the positive correlation observed between Sr (and possibly some of the other incompatible elements) and $^{87}Sr/^{86}Sr_o$ an additional set of mixing lines based on a tonalitic* type contaminant were fitted to the isotope and trace element data (Figs. 10.7 a,b). Results obtained from contamination modelling with a tonalitic contaminant are critically dependant on the choice of starting compositions, particularly with respect to the tonalite composition (see Figs. 10.7 a,b). The data presented

*Footnote: This choice is influenced by the extensive tonalitic diapirs which form a significant component of the Kaapvaal craton, (see Condie and Hunter, 1976).

graphically in Figure 10.7 show that whereas approximately 60% contamination of a tonalite with low Sr, low initial-Sr (D-D1, Fig. 10.7 a,b) is necessary to produce the most radiogenic lava only 30% is required if a tonalite with 1 000 ppm is used as a contaminant (E-E1, Fig. 10.7 a,b). The initial ratio of the tonalites used in the modelling is perhaps rather low but use of an end member with low Sr, high-initial Sr ratio produces the same overall affect as curve E1 - E2 though the fit of a line involving a high initial ratio is not as good as either D-D1 or E-E1.

Contamination with composition D2 may be acceptable if a selective process similar to that discussed for granitic contamination is accepted. Similarly contamination of Rooi Rand-type magmas with a tonalite characterised by 1 000 ppm cannot be discounted though previous modelling calculations (section 9.5, Fig. 9.7h) suggest that as much as 50% contamination with a tonalite of this composition is necessary to account for the observed spread in Sr in the southern Lebombo lavas and dykes. Nevertheless on the basis of Sr-isotope modelling calculations it is possible to envisage that, excluding granitic contamination, additional correlations noted between initial Sr ratios and the elements plotted in Figures 10.5 a-e may have developed in response to contamination of Rooi Rand type magmas with tonalitic material. Contamination of these magmas with granitic material would then have led to the production of additional scatter in the data and the imposition of the granitic contamination trend (C) apparent in Figure 10.5 a-e. It is apparent, however, that the results obtained above (and in Chapter 9, section 9.5) are entirely model dependant and it is therefore exceedingly difficult to impose tight constraints on any model presented to explain the geochemical relationships of the southern Lebombo low-MgO volcanics in terms of either granitic or tonalitic contamination.

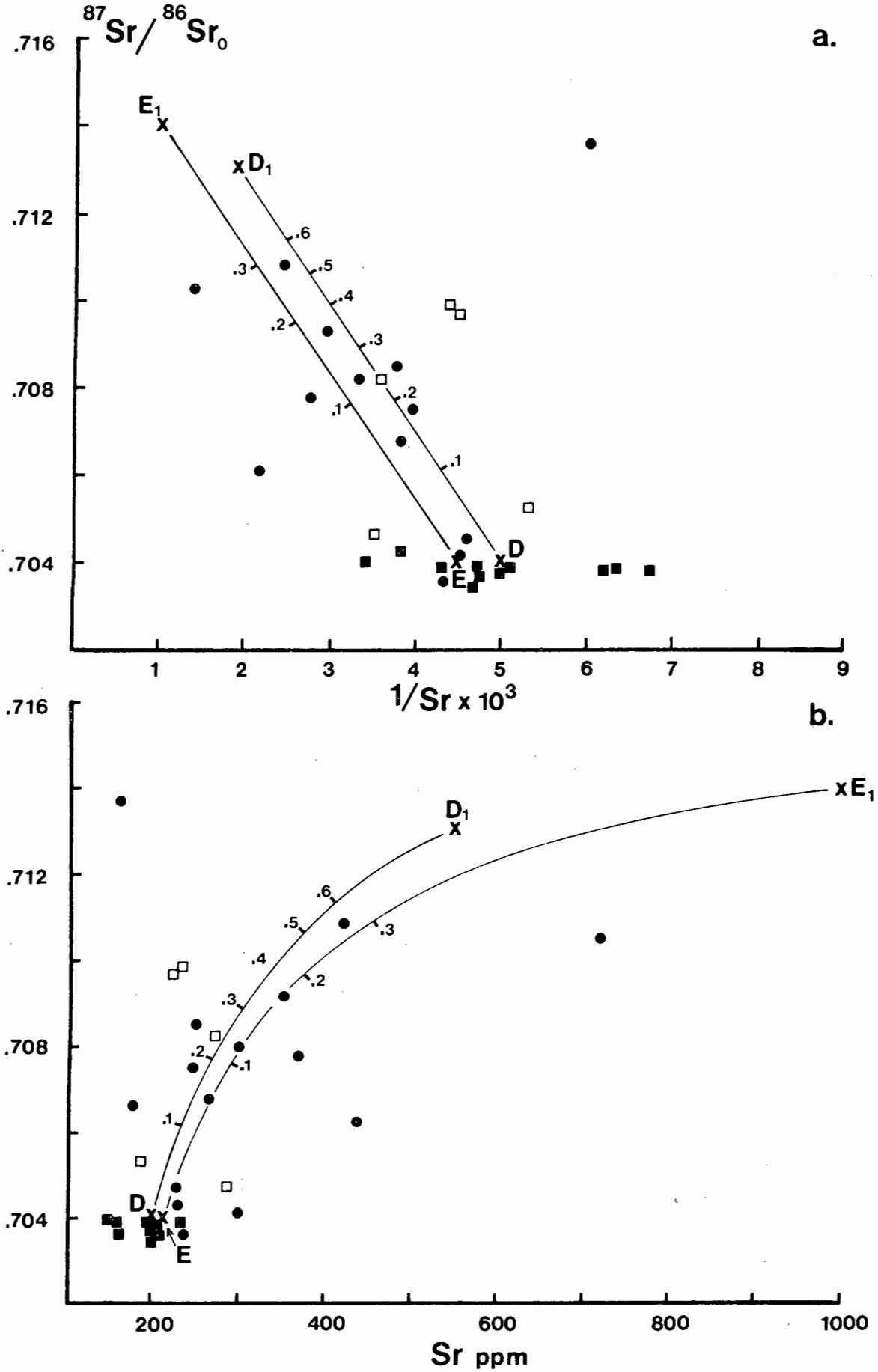

Fig. 10.7 Sr-isotope mixing model for the southern Lebombo and Swaziland low-MgO volcanics assuming the contaminant was of tonalitic composition. (Symbols as in Fig. 10.5.)

Discussion

Data presented in the preceeding section and in Chapter 9, suggest that major and trace element and Sr-isotope variations in the southern Lebombo volcanics are, in the broadest sense, compatible with contamination (selective?) of a Rooi Rand type magma with granitic and tonalitic type contaminants. However, the models presented both here and in Chapter 9 are incapable of unambiguously proving or disproving a crustal-contamination model, particularly when one considers that selective contamination processes are poorly understood and that rocks with in excess of 1 000 ppm Sr do not appear to be that common in the basement outcrops immediately adjoining the Lebombo belt. Coupled with these problems is the fact that no xenoliths of granitic (or tonalitic) rocks have been found in the southern Lebombo lavas and dykes with the exception of sample L348 which contains small quartzo-feldspathic xenocrysts. In addition there is a strong possibility that a differentiating magma (e.g. a Rooi Rand type magma) would have insufficient superheat to assimilate relatively large amounts (e.g. 30%) of crustal material (see Pankhurst, 1969).

Contamination models discussed up until this stage have also assumed the existence of relatively depleted Rooi Rand type magmas prior to the emplacement of the lavas. However, field relationships indicate that the Rooi Rand dykes are younger than the main succession of lavas. It could therefore be argued that the previous assumptions (viz. that the lavas and dykes were derived by contamination of Rooi Rand-type magmas) are invalid and that the lavas and dykes were derived from a source(s) which was both more fertile and radiogenic (with respect to ^{87}Sr) than the source(s) from which the Rooi Rand dykes were derived. With this in mind, and in view of the problems associated with wholesale crustal contamination processes (see above) two additional processes that may account for the

geochemical relationships shown by the southern Lebombo lavas and dykes are considered.

10.2.3 Disequilibrium Melting of a Source Area that is Heterogeneous on a Small Scale ie. Mineral Scale

A model involving disequilibrium melting of an incompatible element enriched source which contains minerals with varying Rb/Sr and $^{87}Sr/^{86}Sr$ ratios, ie. a source which is not isotopically equilibrated before the onset of melting, may possibly account for some of the variation in initial-Sr ratios in the southern Lebombo rocks. In this case the magmas with the highest $^{87}Sr/^{86}Sr$ ratios would be generated by melting of relatively large amounts of the phase with the highest Rb/Sr ratio, e.g. phlogopite (Flower, et al., 1975), whereas magmas with the lowest Sr-isotope ratios would be produced by greater relative melting of phases with lower Rb/Sr values, provided that isotopic equilibration does not take place during melting.

Some of the earliest suggestions of disequilibrium melting associated with basalts were made by Gast et al. (1964) and Peterman et al. (1970) in reference to partial fusion of xenoliths caught in host basalts. Subsequently Harris et al. (1972) used evidence of isotopic disequilibrium in xenoliths to infer that such disequilibrium may persist during partial melting and petrogenesis of basalts. However, isotopic and chemical data derived from mantle xenoliths (e.g. Allsopp et al., 1969; Peterman et al., 1970; Barrett, 1975; Shimizu, 1975; Basu and Murthy, 1976) provides conflicting evidence since some studies appear to indicate equilibration at the time of emplacement, others not. Also, there is a tendency for the more favoured mineral hosts (e.g. diopside, phlogopite, amphibole for Rb, Sr) to be in equilibrium, while minerals which contain only trace amounts of Rb and Sr, may show higher $^{87}Sr/^{86}Sr$ ratios than the former minerals. Furthermore, though disequilibrium within xenoliths and between xenoliths and host basalt or kimberlite is well documented, because the original

spatial relationships between the xenoliths and host magmas are not known, inferences with respect to the precise mechanism of disequilibrium melting in the source region remain questionable.

Recourse to a disequilibrium model to explain the relationships between the Sr-isotope and chemical relationships of the southern Lebombo volcanics is faced with an additional problem. Disequilibrium melting of a source area containing a phase with high $^{87}Sr/^{86}Sr$ and Rb/Sr ratios, e.g. phlogopite, is capable of producing melts with a range of $^{87}Sr/^{86}Sr$ values but meets with considerable difficulty when it comes to trying to explain covariation between Sr-isotope ratio and Sr. The reason for this is that the magmas with the highest ratio would be produced by preferential incorporation into the liquid of a phase with a high Rb/Sr ratio, e.g. phlogopite, whereas the melt with the lowest $^{87}Sr/^{86}Sr$ ratio would be produced by greater relative incorporation of phases, e.g. clinopyroxene, with much lower Rb/Sr ratio (Cox et al., 1976). Consequently it may be argued that the reasonably well developed positive correlation between $^{87}Sr/^{86}Sr$ and Sr-abundance shown by the southern Lebombo volcanics (Fig. 10.5c) is unlikely to reflect disequilibrium melting.

More complex disequilibrium melting models involving phlogopite and aimed at overcoming similar problems in basalts from Iceland and the Reykjanes Ridge have been discussed by O'Nions and Pankhurst (1973), Sigvaldason et al. (1974) and O'Nions et al. (1976). In these models it is proposed that the melts produced by disequilibrium melting partially equilibrate with residual phlogopite, such that melts produced by very small degrees of partial melting have the highest $^{87}Sr/^{86}Sr_0$ ratios and Sr-abundances. Though the models are capable of producing the observed range of $^{87}Sr/^{86}Sr$ in the Icelandic basalts ($0.70291 \pm 4 - 0.70341 \pm 7$) they are incapable of effectively and realistically accounting for the

covariation observed between $^{87}Sr/^{86}Sr$ and Sr. For example, O'Nions et al. (1976) showed that they could produce positive correlation between $^{87}Sr/^{86}Sr$ and Sr for the Icelandic basalts if they assumed that the degree of partial melting involved in the production of the basalts with the highest Sr abundances (~ 300 ppm) decreased to as little as 3-6%. However, since tholeiites are generally thought to represent approximately 20-30% partial melts of their source area (Green, 1971), 3-6% melting is impossibly small for the retention of bulk rock chemistry and consequently there is little geological validity in such a mechanism.

As such, positive correlations between initial-Sr ratios and Sr content appear to be incompatible with disequilibrium melting of a mantle source region. Similarly, essentially linear correlations between initial $^{87}Sr/^{86}Sr$ ratio and K_2O, Ba and Zr are difficult to generate in general by disequilibrium melting models unless small degrees of partial fusion are involved (Cox et al., 1976). In addition there remains the possibility that the extent of melting associated with a magmatic event of the magnitude responsible for the Lebombo and Nuanetsi (and Central Karoo) volcanics may well have led to isotopic homogenisation on a small scale in the source, e.g. mineral or hand specimen scale. In view of the problems associated with creating a positive correlation between initial-Sr ratio and Sr (and other elements) it is therefore concluded that isotopic characteristics of the southern Lebombo volcanics cannot be attributed to disequilibrium melting of a source region which was originally characterised by small scale isotopic heterogeneity.

10.2.4 Melting of a Source that is Heterogeneously Enriched on a Large Scale

The alternative to disequilibrium melting is that involving equilibrium melting of a mantle source that is heterogeneously enriched on a large scale, e.g. 1 km scale. The existence of a chemically heterogeneous

mantle received its first strong 'verification' from the Sr and Pb isotope studies of Faure and Hurley (1963), Hedge and Walthall (1963) and Gast et al. (1964). Subsequent high precision mass spectrometry has provided further evidence for mantle heterogeneity, particularly in oceanic regions (Sun and Hansen, 1975; Hofmann and Hart, 1978; O'Nions et al., 1977). Increased interest has recently been shown in continental volcanics and in the light of recent trace element and Sr-isotope studies, e.g. Erlank et al. (1980), and combined trace element, Nd-isotope, and Sr-isotope studies, e.g. Hawkesworth and Vollmer (1979), it would appear that the subcontinental mantle is also heterogeneous.

In its simplest form this model proposes that 'domains' of the source area with high $^{87}Sr/^{86}Sr$ ratios also have high Sr, Rb, K, Ba and Zr contents whereas other domains with lower Sr-isotope ratios would have correspondingly lower contents of these elements. Essentially linear correlations between Sr-isotope ratios and Sr (and other elements such as K_2O) would then be generated if all the mantle segments underwent more or less the same degree of partial melting.

Positive correlations between Sr-isotope ratios and Sr, as well as other incompatible elements have been noted in volcanic suites from both continental and oceanic environments and in nearly all cases the covariance has been attributed to melting of source regions which are referred to as either heterogeneous or anomolously enriched. Typical examples include the Ross Island basanitoids (Sun and Hansen, 1975), basalts from Iceland and Reykjanes Ridge (O'Nions et al., 1976), a broad spectrum of island arc basanitoid, alkalic, sub-alkalic and calc-alkaline rocks from the Lesser Antilles (Hawkesworth et al., 1979a), and predominantly potassic volcanics from Italy (Cox et al., 1976; Hawkesworth and Vollmer, 1979). Recently Kyle (1980) has also proposed that the very high Sr-isotope

which were either unaffected by enrichment (or depletion) processes or alternatively had been depleted by earlier enrichment and/or melting events.

Melting of a metasomatised, heterogeneously enriched mantle source is also compatible with the temporal variations in intial Sr ratio and Sr content noted in the southern Lebombo lava and intrusive successions. During a magmatic event, volatiles, e.g. H_2O, and incompatible elements contained within metasomatic minerals would tend to promote partial melting such that the earliest melts would be derived from enriched mantle domains (Wood, 1979) and would therefore be the most enriched with respect to Sr, and most radiogenic with respect to Sr-isotope ratios. However, later melts would be derived from less enriched or unenriched ('normal') mantle segments. Consequently it would be expected that those lavas emplaced at the base of the sequence would be characterised by high initial Sr-ratios and Sr (K, Rb, Sr P etc.) abundances whereas lavas higher up the succession would be less radiogenic and less enriched in Sr. In general, the southern Lebombo volcanics fit the above pattern since the lavas with the highest $^{87}Sr/^{86}Sr_o$ ratios and Sr abundances are usually found at the base of the succession whereas initial Sr-ratios and Sr abundances near the top of the lava sequence are generally much lower (e.g. Samples J3, LB2). Similarly, the Rooi Rand dykes which represent the final phase of emplacement are characterised by uniformly low initial-Sr ratios and relatively depleted incompatible element chemistry.

A model involving melting of a heterogeneously enriched mantle source clearly provides an alternate solution to the problems posed by the southern Lebombo volcanics and is presented schematically in Figure 10.8. The main advantage of such a model is that it provides a relatively simple explanation for the depleted chemical nature of the Rooi Rand dykes and at the same time it is possible for granitic contaminants to act on the early

Fig. 10.8 Block diagram illustrating a model whereby the geochemical and isotopic relationships of the southern Lebombo (and Swaziland) low-MgO volcanics may have developed.

I

Transit of volatiles and associated metasomatic fluids through the mantle leads to the formation of heterogeneously enriched domains in the upper mantle and a depleted zone at a greater depth.

During metasomatism there may be continental uplift by thermal and metasomatic expansion in the lithosphere which may ultimately result in crustal fracturing.

Increased Rb/Sr ratios in enriched domains are likely to result in elevated initial-Sr ratios in these segments of the mantle relative to the normal mantle domains. In contrast depleted zones have the lowest Rb/Sr ratios and initial ratios of magmas subsequently derived from this portion of the mantle will be lower than ratios in melts derived from the 'normal' and enriched domains depicted in Stage I.

II

Melting in response to factors such as stress release associated with the fragmentation of eastern Gondwanaland and thermal decomposition of volatile bearing minerals.

Metasomatised domains will in general melt first such that lavas which crystallise from early formed magmas will be both chemically enriched and more radiogenic than subsequent lava flows. There may however, be some interdigitation of 'enriched' and 'normal' flows during the early stages of volcanism. It is also conceivable that the Dokolwayo and Empangeni kimberlites (see section 10.2.5) which are marginally older than the basalts were derived from domains characterised by excessive concentrations of metasomatic minerals and associated volatiles.

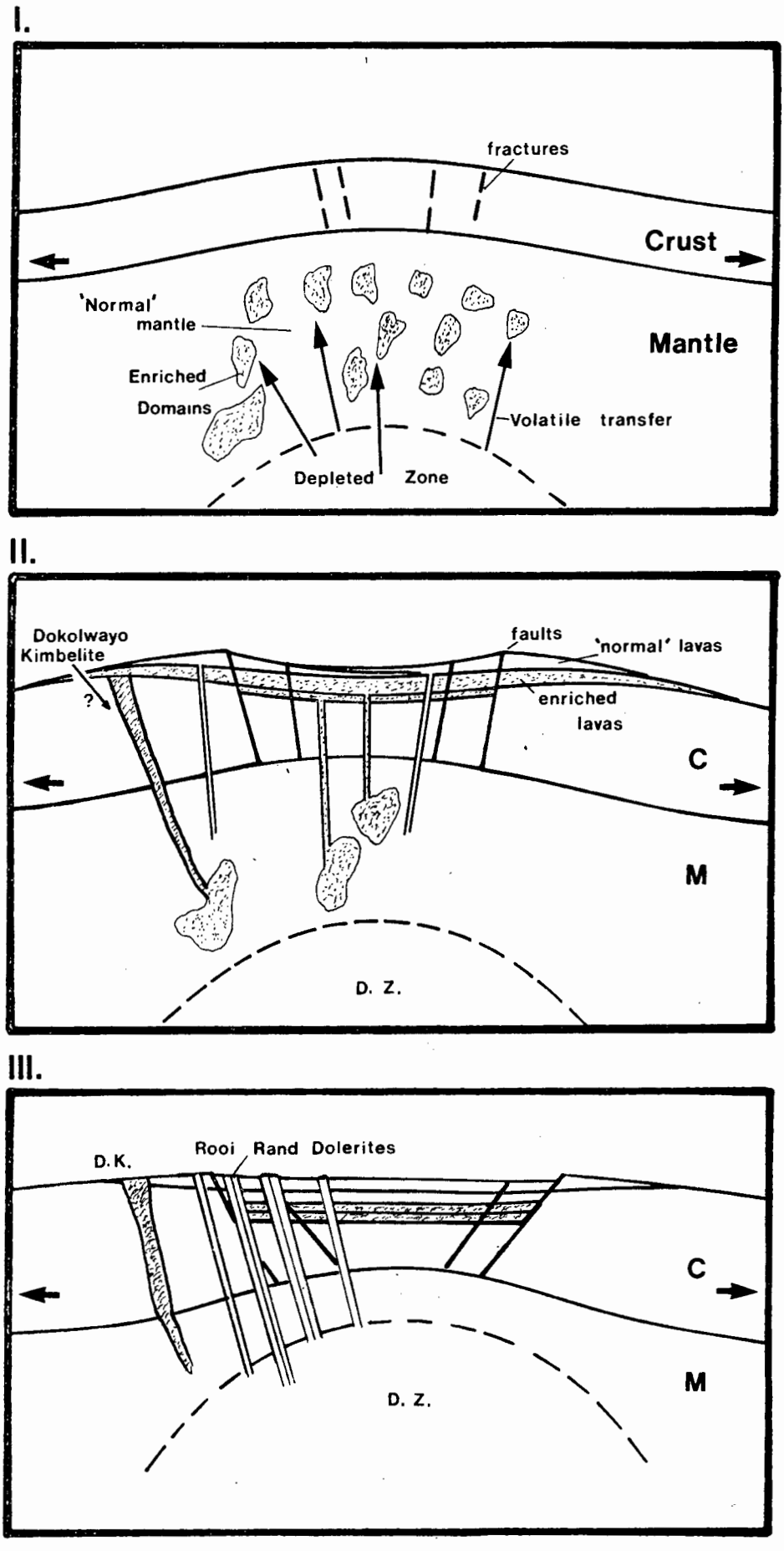
I.
fractures
Crust
'Normal'
mantle
Mantle
Enriched
Domains
Volatile transfer
Depleted Zone
II.
Dokolwayo
Kimbelite
?
faults
'normal' lavas
enriched
lavas
C
M
D. Z.
III.
D.K.
Rooi Rand Dolerites
C
M
D. Z.

Fig. 10.8

Fig. 10.8 continued.

III

Continued continental rifting leads to crustal necking causing an upwarp in the crust/mantle boundary. Assuming that isostatic equilibration was maintained the upwarp in the crust/mantle boundary would have an amplitude about ten times greater than the trough at the surface, ie. a trough 1 km deep at the surface will be reflected by a 10 km upwarp in the crust/mantle boundary below (Betton and Cox, 1979).

During the late stages of southern Lebombo basaltic magmatism melting will therefore take place at greater relative depths, ie. in the depleted zone, such that lavas from the top of the pile, and the cross-cutting Rooi Rand dykes will be characterised by depleted chemical characteristics and low initial Sr ratios.

Contamination Scenario:

Contamination with either crustal or enriched mantle material may effectively alter the chemistry of the magmas formed above and the possible combinations that may develop are listed below. It is envisaged that crustal contamination will be largely restricted to early formed magmas. With continued magmatism, magma pathways through the crust would become lined with basaltic material and/or equilibrated with mantle Sr.

(i)	Enriched magma	(e)	+	crustal material
(ii)	Normal magma	(n)	+	crustal material
(iii)	Normal magma	(n)	+	enriched magma (e)
(iv)	Depleted magma	(d)	+	enriched magma (e)

formed magmas thereby producing the component of granitic contamination noted in Figures 10.5 a-e. Accordingly the contamination scenario that may have led to additional scatter in the geochemical variations noted in the southern Lebombo volcanics is incorporated in the model presented in Figure 10.8.

10.2.5 Possible Causes of Mantle Heterogeneity

Mantle metasomatism (Lloyd and Bailey, 1975; Erlank and Rickard, 1977; Hawkesworth and Vollmer, 1979; Erlank et al., 1980) or veining (Wood, 1979; Wood et al., 1979) have recently become the most commonly referred to processes to explain mantle enrichment (and/or depletion) and hence mantle heterogeneity. (In this thesis 'mantle veining' as described by Wood and co-authors is considered to be synonomous with mantle metasomatism since there is essentially no difference in the end result of either process.) Metasomatism as documented by these workers results in isotopic and incompatible element enrichment in portions of the mantle source area. A fluid phase rich in volatiles, e.g. CO_2, is generally considered to be responsible for the transport of the incompatible elements, LREE etc., during metasomatism (Erlank and Shimizu, 1977; Kyle, 1980; Wood, 1979; Wood et al., 1979).

Petrographic and chemical evidence in support of metasomatism in the southern African subcontinental mantle is displayed by a considerable number of ultramafic nodules collected from kimberlite pipes (Erlank, 1976; Erlank and Rickard, 1977; Erlank, pers. comm.). Geochemical and Sr-isotope studies of the metasomatised nodules provide convincing proof for mantle metasomatism. Erlank and Shimizu (1977) found that initial $^{87}Sr/^{86}Sr$ ratios (calculated at the age of emplacement of the kimberlite pipes in which they occur) of metasomatised nodules are much higher than the initial-Sr ratio of the host kimberlite implying that the event(s) responsible for

metasomatism was in no way related to kimberlite emplacement. On this basis Erlank and Shimizu (1977) infer that the isotopic relationships of the metasomatised nodules, e.g. high $^{87}Sr/^{86}Sr$ ratios, are of mantle origin. In addition, the data obtained by Erlank and Shimizu (1977) show that it is possible to generate high $^{87}Sr/^{86}Sr$ ratios (e.g.~ 0.710) in relatively short times (~ 150 my) whereas previously it has been argued that most mantle heterogeneities were older than about 1.5 by (Brooks, et al., 1976 b,c; Brooks and Hart, 1978; Hofmann and Hart, 1978).

Measurements of Sr contents in diopsides extracted from ultramafic nodules (Erlank and Shimizu, 1977) have a particularly important bearing on the present discussion. Erlank and Shimizu (1977) noted that diopsides from nodules considered to be representative of a metasomatised suite (phlogopite $\pm$ richterite $\pm$ garnet bearing) had much higher Sr contents than diopsides from peridotite nodules containing no primary phlogopite and referred to as "least metasomatised". Sr contents in the latter suite were found to vary between 150 - 220 ppm, whereas abundances in the former suite were found to range from 450 - 1 000 ppm Sr. Concentrations of 450 - 1 000 ppm Sr are unusually high for diopsides and consequently Erlank and Shimizu (1977) proposed that the diopsides acquired their high Sr contents by equilibration with Sr-rich carbonate fluids during a metasomatic process.

Melting of a source region containing metasomatic minerals similar to those described by Erlank and Shimizu (1977), e.g. phlogopite, K-richterite, Sr-rich clinopyroxenes, would undoubtedly account for the isotope and Sr variations in the southern Lebombo lavas. However, there remains the important problem of "scale" since unless metasomatism was reasonably extensive we would be effectively faced with a situation outlined in section 10.2.3 in which unequilibrated minerals existed in the mantle, which though perhaps capable of producing extremely localised isotopic variation,

would probably be incapable of producing regional variations similar to those noted in the southern Lebombo (and the Lebombo as a whole). Petrographic studies of metasomatised mantle peridotites (Erlank, pers. comm.) indicate that the replacement minerals form veins and small pockets. An extensively veined mantle source area would probably provide the optimum environment for the development of the isotopic and chemical relationships similar to those noted in the Lebombo. In the case of the melting of the above source area, though concentrations of incompatible elements, e.g. Sr, would be strongly elevated, major element chemistry would be less strongly affected such that it would still be possible to produce basaltic compositions. Conversely the presence of intensive concentrations of metasomatic minerals on a localised scale would promote alkaline, probably kimberlitic or carbonatitic, volcanism during a magmatic event.

Though no unequivocal proof exists for metasomatism in the mantle underlying the southern Lebombo area, circumstantial evidence does weigh in favour of such a process. Firstly, it has been argued (section 8.7) that the picrite basalts of the northern Lebombo, Nuanetsi and Tuli areas owe their incompatible element enriched nature to metasomatism of the source area. There is physically no reason why metasomatic activity should have been restricted to those parts of the mantle underlying the northern parts of the Lebombo, Nuanetsi and Tuli and it therefore seems reasonable to accept that enrichment processes could have also occurred in the mantle underlying the southern Lebombo. Secondly, localised volatile release from the upper mantle prior to the emplacement of the Swaziland lavas and southern Lebombo lavas and dykes is indicated by the presence of the Dokolwayo kimberlite pipe in Swaziland (see Hawthorne et al., 1979) and a kimberlite-type intrusive body in the Empangeni area (Hawthorne, pers. comm.)

The Dokolwayo pipe intrudes Karoo sediments a few kilometres west of the Swaziland lavas and both field relationships (Hawthorne et al., 1979) and age studies (Allsopp, unpubl. data) indicates that it is only slightly older than the lavas. At present little is known of the Empangeni 'kimberlite' though on the basis of field relationships it too appears to have been emplaced shortly before the lavas. In view of the high levels of volatiles and incompatible elements associated with kimberlites it is generally concluded (e.g. see Boettcher et al., 1979) that they are generated from mantle domains enriched in these components, possibly by metasomatic processes. Furthermore, it is highly probable that the volatiles associated with kimberlites, together with heat supplied by the radioactive decay of elements such as K and Rb, provide the driving force for kimberlite formation. The Dokolwayo and Empangeni kimberlites emplaced as they were slightly prior to the lavas, are therefore considered to represent important evidence for metasomatism in the mantle underlying the southern Lebombo. Hopefully, future mining operations which are planned for the Dokolwayo kimberlite will result in the recovery of mantle xenoliths showing unequivocal evidence of metasomatic enrichment processes which could account for the chemical relationships of the southern Lebombo lavas and dykes.

10.2.6 Effingham Dolerites - An Example of Bulk Granitic Contamination

Of all the Karoo volcanic rocks in the southern Lebombo region, the Effingham dolerites probably display the most evidence for bulk granitic contamination. The dolerites crop out in a narrow belt between the southern end of the Lebombo and Durban (Frankel, 1969; Absolom, 1970) and are considered to be younger than the normal Karoo dolerites (Frankel, 1969) and Lebombo lavas (Bristow, 1976). They are characterised by a distinctly evolved geochemistry in relation to the mafic lavas and dykes

TABLE 10.4 Chemical and isotopic characteristics of Effingham dolerites. Data from Frankel, 1969. Initial-Sr ratio calculated at 190my.

	Rb ppm	Sr ppm	Rb/Sr	$^{87}Rb/^{86}Sr$	$^{87}Sr/^{86}Sr_{(m)}$	$^{87}Sr/^{86}Sr_{(o)}$
Glassy vein	50	680	.074	.214	.7229	.7223
Glassy margin	110	240	.458	1.324	.7199	.7163
Sill centre	100	140	.714	2.065	.7228	.7172
Sill	80	200	.400	1.156	.7153	.7122
Effingham type rock	60	150	.400	1.157	.7206	.7175
Cg dolerite	30	320	.094	0.272	.7124	.7117
Normal Karoo dolerites	20 20	230 240	.087 .083	0.251 0.240	.7075 .7071	.7068 .7065

(Cg - Coarse grained)

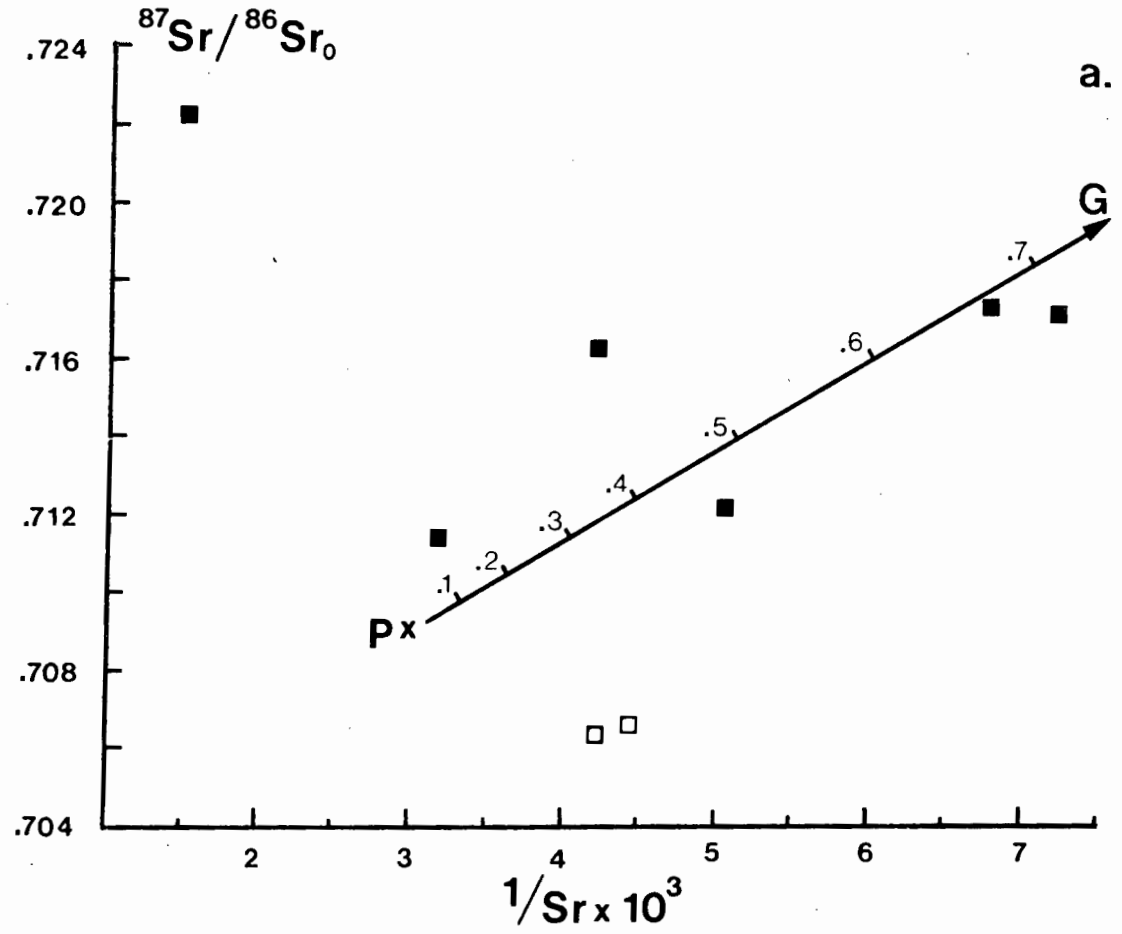

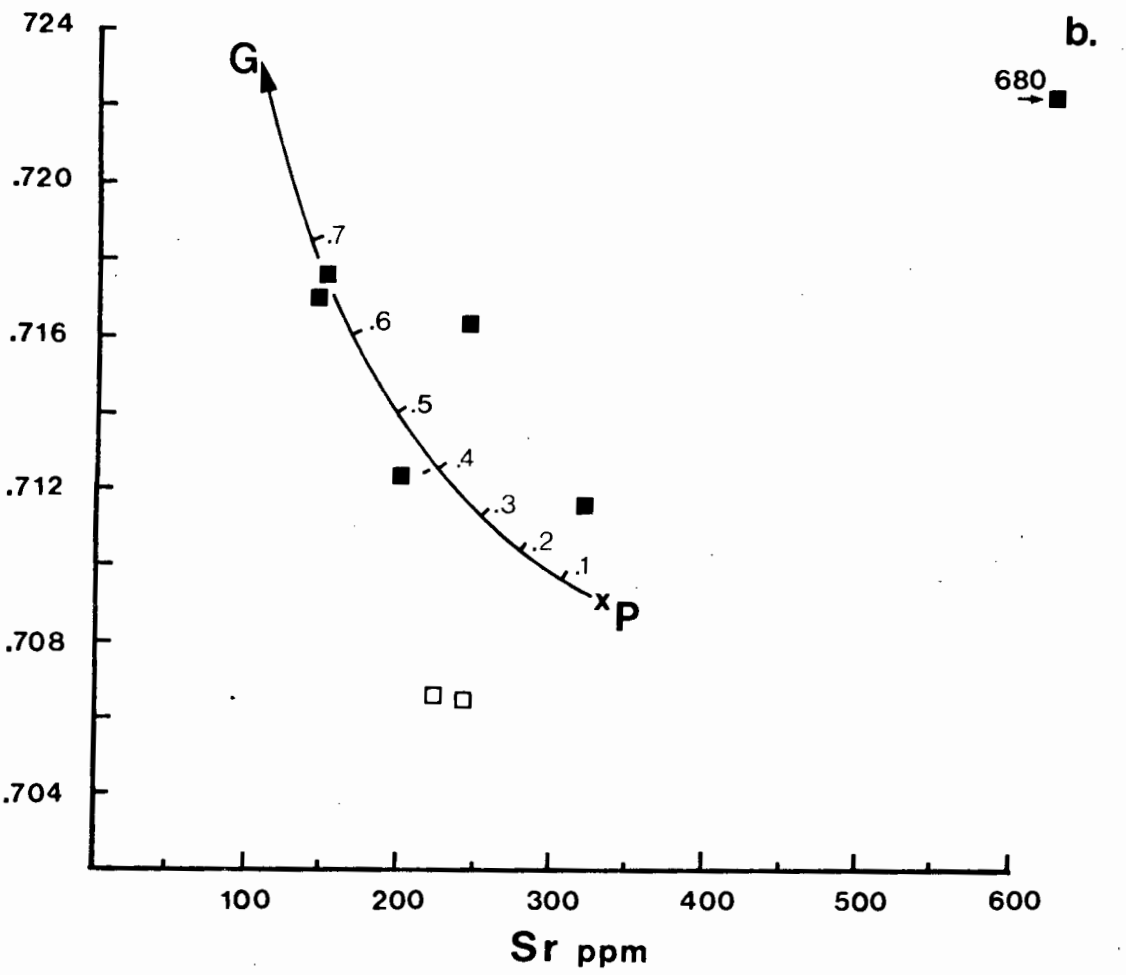

■ Effingham Dolerites □ Normal Dolerites

Fig. 10.9 Sr-isotope mixing model for the Effingham dolerites assuming the contaminant was of granitic composition.

TABLE 10.5 Contamination modelling for Effingham-type dolerites.

	1 A	2 B	3 A+40%B	4 A+50%B	5 A+60%B	6 A+65%B	7 (3)	8 (2)	9 (6)
SiO_2	53.00	74.6	61.64	63.80	65.96	67.04	60.74	63.84	66.39
TiO_2	1.31	.4	1.03	.86	.76	.72	1.85	1.96	1.62
Al_2O_3	14.30	13.6	14.02	13.95	13.88	13.85	15.01	13.59	13.18
Fe_2O_3	12.35	3.6	8.85	7.98	7.10	6.66	10.11	9.03	9.18
MnO	.17	.02	.11	.10	.10	.07	.22	.11	.15
MgO	6.22	.06	3.76	3.14	2.52	2.22	3.18	1.44	1.60
CaO	9.34	1.4	6.16	5.37	4.58	4.18	3.39	4.23	2.21
Na_2O	2.31	2.7	2.47	2.51	2.54	2.56	2.48	2.48	2.64
K_2O	.76	3.8	1.93	2.28	2.58	2.74	2.63	3.04	2.76
P_2O_5	.24	.1	.20	.17	.16	.15	.40	.30	.27
$^{87}Sr/^{86}Sr$	.7090	.740							.7172
Sr (ppm)	366	60							

1. Average of the high $^{87}Sr/^{86}Sr$ lavas and dolerites from south of the Mfolozi River (L12, L18, L29, L32, L36, L57, L94, S45).

2. Representative Precambrian granite from eastern Natal (from Frankel, 1969). The $^{87}Sr/^{86}Sr$ ratio is an assumed value but is within the range of values reported for granitoid rocks from Swaziland (Glikson, 1979) and Sr represents the average of the relatively evolved SiO_2 = 75.2%) Sicunusa type shield forming batholiths in Swaziland (Condie and Hunter, 1976).

3,4,5,6. Compositions derived by the addition of different proportions of granite (B) to the average basic composition (A).

7,8,9. Selected Effingham type dolerites, normalised to 100% volatile free (from Frankel, 1969).

The characteristics of the granitic component are perfectly acceptable though the high Sr-isotopic ratio of the basaltic parent is perhaps surprising. However, the Effingham data points clearly do not lie on a trend with 'normal' and Rooi Rand dolerites (Figs. 10.9 a,b) and inspection of Table 10.5 shows that the Sr content and Sr-isotope ratio of the projected precursor (P) is identical to the average Sr content and Sr-isotope ratio of the most radiogenic southern Lebombo dolerites (A, Table 10.5). This suggests that the Effingham dolerites were formed from an enriched southern Lebombo type magma by the assimilation of crustal material.

The above hypothesis has been tested by mass balance addition of varying proportions of a granitic rock (B) to the average composition (A) of the high $^{87}Sr/^{86}Sr_0$ ratio southern Lebombo volcanics (Table 10.5). Comparisons of the hypothetical compositions to the range of analysed Effingham dolerites reported by Frankel (1969) shows (Table 10.5) that the full range of observed compositions can be generated by crustal contamination, though discrepancies are apparent between some of the observed and calculated values; in particular TiO_2 and Fe_2O_3 show a poor match. More significant though is that both the isotope data and mass balance calculations yield similar results in terms of the proportions of contaminant necessary to produce the most siliceous rock (which also has the highest $^{87}Sr/^{86}Sr_0$ ratio). It would therefore appear that Effingham dolerites may represent enriched southern Lebombo type magmas which were modified due to bulk, rather than selective type, assimilation of crustal material though additional trace element and isotope data are necessary to verify this proposal.

10.3 Central and Northern Lebombo, and Nuanetsi Low-MgO Volcanics

Sr-isotope data for the central and northern Lebombo Low-MgO rocks show drastic changes in comparison to the southern Lebombo data whereas

the Nuanetsi low-MgO rocks show Sr isotope relationships which tend to mirror those found in the southern Lebombo. Initial-Sr isotope ratios for the central and northern Lebombo low-MgO volcanics show a significant though small range which cannot be accounted for by crustal contamination (see Figs. 10.10 a,b). In keeping with the pattern observed in the southern Lebombo, the lowest initial ratios are also found in dolerite dykes and sills cutting the lavas. In Nuanetsi, Sr-isotope ratios measured in the Sabie River basalts are low and show a relatively small range of values. Conversely, the initial-Sr isotope ratios of the Interbedded Basalts show a much greater range in values and are also much higher. Plots of $^{87}Sr/^{86}Sr_o$ versus Sr and $1/Sr$ (Figs. 10.10 a,b) show that whereas the Sabie River lavas appear to be unaffected by contamination, for the interbedded basalts a negative correlation, of crude hyperbolic form suggests the possibility of a mixing process with a crustal component.

Additional Sr-isotope data are needed from the central and northern Lebombo and Nuanetsi low-MgO rocks before the Sr-isotope relationships can be used to substantiate or disprove petrogenetic models proposed on the basis of major and trace element data. Nevertheless on the basis that crustal contamination appears to have played little or no part in the petrogenesis of these rocks (excluding the Nuanetsi Interbedded basalts), it can be inferred that the variation in initial-Sr ratios may well reflect mantle heterogeneity. Furthermore, the range of initial-Sr ratios found in the low-MgO shoshonitic suite is broadly similar to that found in the picritic rocks thereby providing additional evidence for a comagmatic petrogenetic process as proposed in Chapter 9.

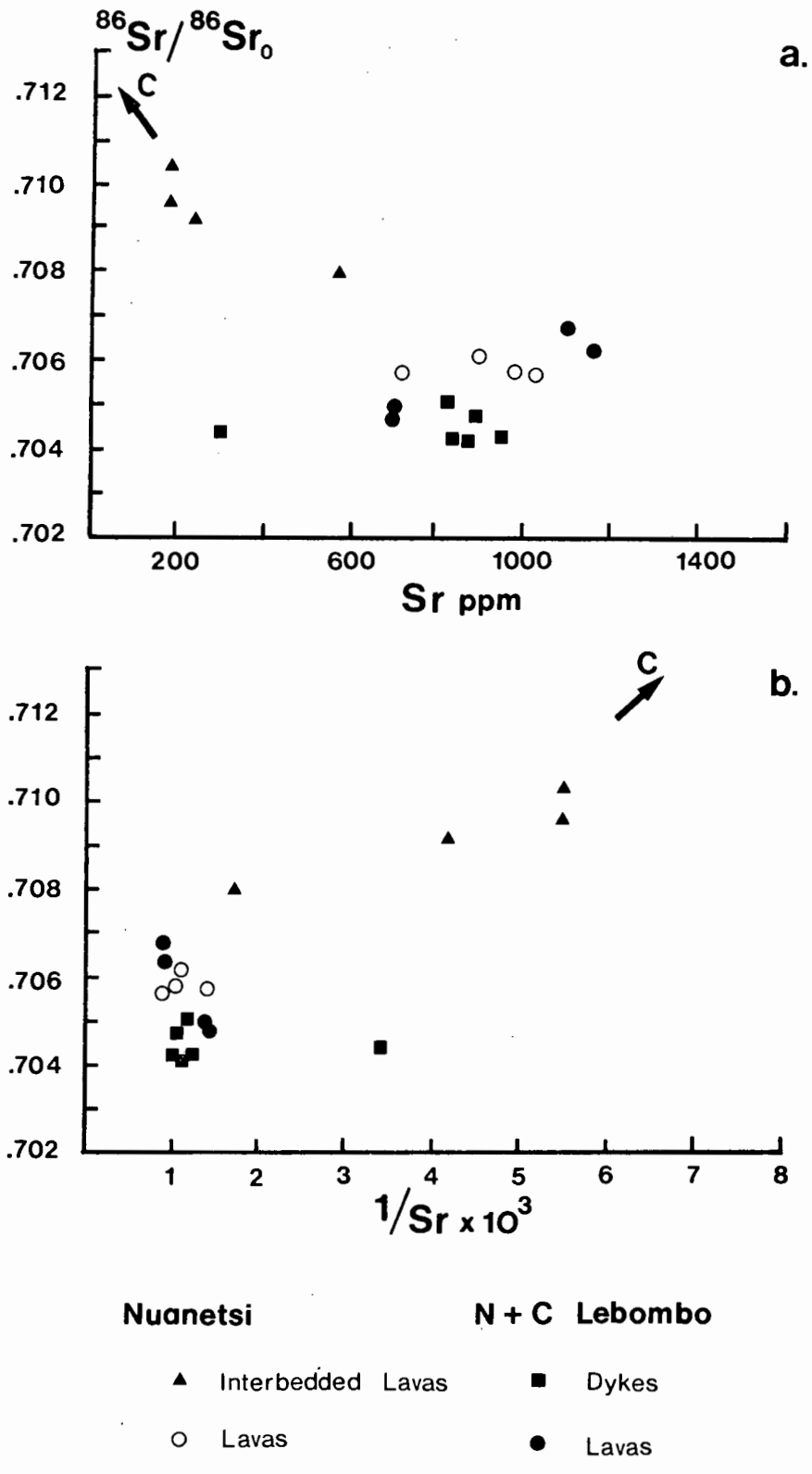

Fig. 10.10 Plot of $^{87}Sr/^{86}Sr_o$ versus Sr and 1/Sr for the central and northern Lebombo and Nuanetsi low-MgO volcanics.

10.4 The Nephelinitic and Picritic Volcanics

The nephelinites, picrite-basalts and picrites show a relatively small, but nevertheless significant range in initial-Sr isotope ratio, and in this respect show a broad similarity with the central and northern Lebombo low-MgO lavas. The role that crustal contamination played in causing the variation in initial ratios has again been investigated by examining the covariation, or absence thereof, between the initial-Sr ratio and the elements SiO_2, K_2O, Sr, Rb and 1/Sr (Figs. 10.11 a-e).

The data plotted in Figures 10.11 a-e indicates that the range in initial Sr isotope ratios cannot be ascribed to crustal contamination unless it was of a highly selective nature. Two nephelinites and a picrite basalt are clearly more radiogenic than the main group of data and may represent lavas affected by a selective contamination process. However, in the case of the nephelinites their SiO_2 undersaturated and high Sr element abundances (Chapter 7) mitigates against excessive crustal contamination, even if it were of a selective nature. Similarly in the case of the picrite basalts the high levels of incompatible element enrichment, coupled with their exceptionally primitive major element chemistry implies that they have been little altered by contamination of crustal material.

Too little isotopic data are available from the nephelinites to be able to place any major constraints on their petrogenesis, though the significant differences between the initial Sr-ratios of the Sabi and northern Lebombo (Pafuri and Olifants River) samples (Table 10.1) suggests that mantle heterogeneity played a role in the genesis of these rocks. In the case of the picrite basalts and picrites considerably more data is available, though unfortunately little is known of the temporal relationships of the samples. Nevertheless, the Sr-isotope data suggests that the picrite rocks were also derived from a heterogeneous source and in this respect

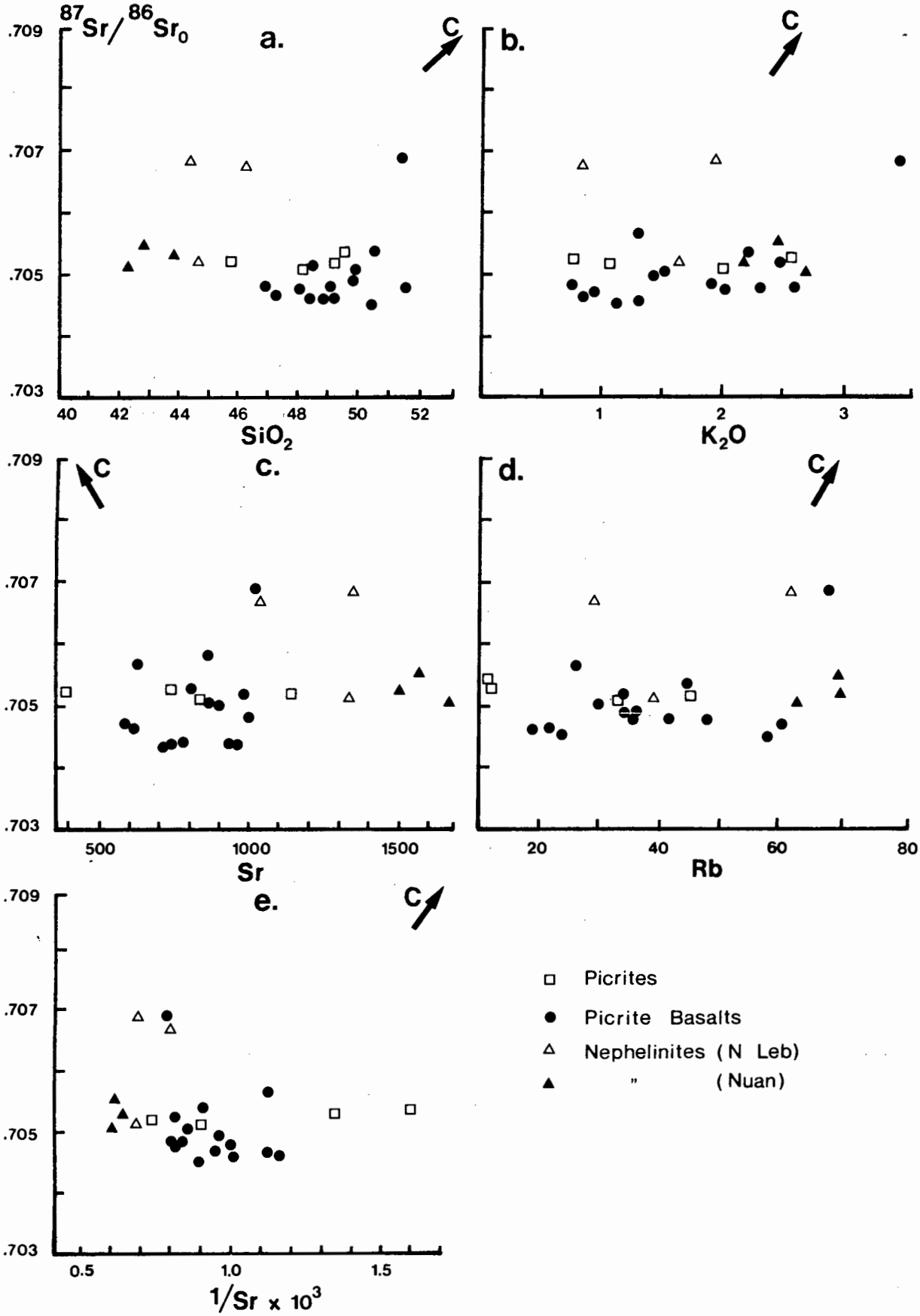

Fig. 10.11 Relations between $^{87}Sr/^{86}Sr_o$ and various major and trace elements for the northern Lebombo (N Leb) and Nuanetsi (Nuan) picrite basalts and nephelinites.

provides additional support for the petrogenetic model presented to account for the unusual geochemical relationships of the picrite basalts (see Chapter 8).

10.5 Relative 'Ages' of the Inferred Heterogeneous Enrichment Events

In concluding this chapter a series of 'age' calculations have been made in an attempt to establish at what stage, relative to the Karoo magmatic event, the inferred mantle enrichment processes which have been discussed in this and previous chapters could have occurred. The general procedure adopted to calculate these ages was to (i) calculate the average initial $^{87}Sr/^{86}Sr$ ratio for the picrite basalts and southern Lebombo lavas and dykes, (ii) assume that the source had a Rb/Sr ratio similar to or less than the average Rb/Sr ratio calculated for the particular rock group, and (iii) back calculate ages assuming that prior to the enrichment events the mantle had a $^{87}Sr/^{86}Sr$ ratio of either .704 or .703 bearing in mind that present day bulk earth ratios for $^{87}Sr/^{86}Sr$ and Rb/Sr have been calculated as .705 and 0.03 respectively (O'Nions et al., 1978).

The average initial-Sr ratio for the picrite basalts is about .705 whereas an average Rb/Sr = 0.05 is obtained from those rocks which have been analysed for their Sr-isotope ratios. Back calculation (using the conventional dating equation) to an initial mantle value of .704 yields an age of about 480 my, or 960 my for an initial ratio of .703. Use of a Rb/Sr similar to that obtained from the picritic rocks (0.05) is considered to be plausible since they appear to have formed by high degrees of partial melting with orthopyroxene and clinopyroxene, neither of which are capable of fractionating Rb/Sr ratios to any large extent, acting as residual phases.

The 'ages' calculated above suggest that the picrite basalts were derived from a source which underwent an enrichment event relatively close to the emplacement of the Karoo lavas. An interesting relationship that

emerges from the above calculations is that if an 'age' of about 480 my is at all realistic then it could be speculated that this mantle enrichment event may have been related to the formation of the metamorphic rocks of the Mozambique Mobile belt which has an age of about 500 my (Clifford, 1970). These rocks flank the eastern margin of the Rhodesian (Zimbabwe) craton and Kaapvaal craton and it is notable that the Lebombo and Sabi volcanics appear to follow the same general trend as the mobile belt or its postulated southern extension (see Cox, 1970; Saggerson and Logan, 1970 and Chapter 11). However, the similarity of ages noted above could be fortuitous and additional studies of U/Pb and Sm/Nd systematics will be needed before possible relationships between mantle events and metamorphic episodes can be established with any degree of certainty.

Considerably older 'ages' of mantle enrichment have been obtained from the southern Lebombo volcanics relative to those obtained for enrichment in the source from which the picritic rocks were derived. If southern Lebombo rocks which appear to lie on granitic contamination trends (e.g. Fig. 10.5) are ignored then the remaining radiogenic samples (ie. samples with $^{87}Sr/^{86}Sr_o > .705$) have an average initial-Sr ratio of about .708 and a Rb/Sr ratio of approximately 0.06. Back calculation to initial mantle values of .704 and .703 yields ages of about 1200 my and 2000 my resepctively However, the average Rb/Sr ratio calculated for the low-MgO volcanics is unlikely to be representative of the source since these rocks have probably undergone a certain amount of plagioclase fractionation. Consequently, if it is assumed that the source had a Rb/Sr ratio of 0.04 even older ages of about 2400 my and 3000 my (back calculated to .704 and .703 respectively) are obtained whereas use of the average Rb/Sr ratio obtained for the picrite basalts and back calculation to an initial-Sr ratio of .704 yields an age of about 1900 my.

Due to the uncertainty associated with the Rb/Sr and initial-Sr ratios in the mantle prior to the inferred enrichment events the data presented above are unlikely to reflect a realistic estimate of the time at which enrichment events may have taken place in the mantle underlying the Lebombo. More important however, is that on the basis of assumptions made above it is possible to conclude that two apparently unrelated enrichment events appear to have occurred in the mantle source regions from which the Lebombo volcanics were derived. In the central and northern Lebombo picritic and related shoshonitic rocks appear to have been derived from a source that underwent an enrichment in KAR elements relatively close to the Karoo magmatic event. In contrast data obtained from the low-MgO lavas and dykes of the southern Lebombo suggest that these rocks were derived from a mantle source which had undergone a considerably older enrichment event. Chemically this latter event also contrasted strongly with the KAR element enrichment processes since with the exception of Sr the southern Lebombo volcanics are clearly unenriched in incompatible elements relative to the northern volcanics.

A final point which should be made in this chapter is that no matter how old the inferred mantle enrichment processes might be, one problem remains with respect to the interpretation of the Sr-isotope data obtained for the Lebombo volcanics. This problem is reflected by the large number of lavas and dykes which lie to the left of the geochron in Figures 10.2 and 10.3 thereby implying that they were derived from a source which had insufficient Rb to generate their radiogenic ^{87}Sr within the age of the earth. Since it has been shown (section 10.2.1) that alteration has had no apparent effect on either the Rb/Sr or $^{87}Sr/^{86}Sr$ ratios of the analysed rocks the simplest explanation which can be offered to account for volcanics with Sr-isotope ratios lying to the left of the geochron is that they were

derived from a source region which underwent recent pre-Karoo Rb depletion. Apart from more speculative models involving for example enrichment in ^{87}Sr coupled with depletion in Rb, no simpler explanation can be offered at this stage though it is hoped that on-going U/Pb and Sm/Nd studies will provide a solution to the above problem.

10.6 Summary and Conclusions

The above detailed study of the strontium isotope and trace element geochemistry of the Lebombo volcanics results in the following conclusions.

1. Granitic contamination was instrumental in causing some of the scatter noted in major and trace element variation diagrams and high initial-Sr ratios found in the Lebombo volcanics, particularly with respect to the southern Lebombo basaltic lavas and dykes.

2. Though some of the results obtained for the southern Lebombo volcanics imply that contamination was of a selective nature, data for the Effingham dolerites suggests that bulk granitic contamination also played a role in the petrogenesis of southern Lebombo low-MgO intrusives.

3. Contamination of a basic, Rooi Rand-type magma with a tonalitic contaminant may account for the positive correlations found between the initial-Sr ratio and Sr (and other elements) in the southern Lebombo volcanics though on the basis of the present data it is also possible that melting of a heterogeneous, metasomatically enriched (and depleted) source may explain the geochemical relationships shown by these volcanics.

4. With the exception of the Nuanetsi Interbedded basalts, crustal contamination appears to have had no apparent effect on the petrogenesis of the low-MgO volcanics from the central and northern areas of the Lebombo, and Nuanetsi. The range of initial-Sr isotope ratios obtained for these latter

rocks is considered to be a function of mantle heterogeneity. Furthermore, the range of Sr-isotope ratios obtained for the shoshonitic rocks is similar to that found in the picritic rocks implying that both suites of lavas could be comagmatic.

5. The source areas from which the nephelinites and picrite basalts were derived were heterogeneous with respect to Sr-isotopes. The Sr-isotope data also suggests that heterogeneous enrichment of the picrite basalt source area took place close to the Karoo magmatic event. In comparison, heterogeneities in the mantle source from which the southern Lebombo low-MgO lavas were derived appear to reflect a considerably older enrichment event.

6. Lastly, and perhaps most important of all, data discussed above show that it is imperative that more than one isotopic system should be examined if tightly constrained models are to be proposed to account for the petrogenesis of continental volcanics such as those found in the Lebombo. Studies of U/Pb and Nd/Sm isotope relationships in the Lebombo volcanics are already in progress and should hopefully be completed before the termination of the Geodynamics Project.

11 STRUCTURAL SETTING AND SYNTHESIS

11.1 Introduction

The Lebombo, Nuanetsi, Sabi and Lupata volcanics are all intimately associated with rifting and/or major monoclinal flexing developed during the breakup of Gondwanaland. Breakup was initiated by the separation of Eastern Gondwanaland (Madagascar, India, Antarctica, Australia) from western Gondwanaland (Africa, South America) and it is possible that tectonic activity which took place in East Africa in the late Carboniferous (Kent 1974) may represent the earliest stages of breakup. In east Africa and Madagascar tectonism was followed by a Permian marine transgression, (Kent, 1972, 1974) and the establishment of open marine conditions in the early Jurassic.

The locus of continental fracturing in East Africa appears to have migrated southwards in the Permo-Triassic period and extensional tectonism in the Zambezi and Limpopo regions during the Ecca are similarly ascribed to the early fracturing of Gondwanaland crust (Cox, 1970). Further south in Natal (South Africa) east-west extensional tectonics are also indicated by the development of graben structures infilled with Ecca and younger sediments e.g. the Nongoma Graben (Whateley, 1979).

The theme of Mesozoic rifting along or to the east of the present day Sabi-Nuanetsi-Lebombo outcrop has been developed by several authors, notably Cox (1970), Flores (1970), Burke and Dewey (1973) and Reeves (1978). Cox et al. (1965) compared the Sabi-Nuanetsi juncture or re-entrant with the Kangerdlugsuaq region of East Greenland and Burke and Dewey (1973) subsequently considered the intersection of the Lebombo and Sabi monoclines with the Limpopo Rift to represent a triple junction and site of mantle plume, a view supported by Rhodes and Bornhorst (1976). The Sabi-Lupata

re-entrant is regarded as another junction of this type, though it has the form of a more complex four-armed structure.

The Limpopo rift and adjacent areas extending westwards and north-westwards from the Sabi-Limpopo re-entrant are characterised by a long history of rifting, sedimentation and volcanism from Precambrian to post-Karoo times (Cox et al., 1965; Jansen, 1975). The Soutpansberg trough which parallels the Limpopo belt but lies slightly to the south is characterised by a thick sequence of meta-sediments and meta-volcanics and has been interpreted as an aulacogen or "failed third arm" of a triple junction by Jansen (1975). More recently Reeves (1978) has also interpreted the Karoo dyke swarm which trends approximately north-east from the Sabi-Lebombo re-entrant through Rhodesia and Botswana (see Cox et al., 1965; Green, 1966; Vail, 1970) as a failed Gondwanaland spreading axis.

Though ascribed to extensional tectonics (Cox, 1970) and described as a monocline (Du Toit, 1929) or faulted monocline (Bristow, 1976) the structural relationships of the Lebombo belt have up until now, been less well understood than those of the adjoining areas. However, in the light of recent studies conducted in the southern Lebombo (Bristow, 1976; Armstrong, 1978), Swaziland (Cleverly, 1977; Betton, 1978) and central and northern Lebombo (this study) it is now possible to present a revised outline of the structural relationships of the area and propose a volcano-tectonic model for the development of the belt.

11.2 Tectonic Reconstruction

In the south detailed mapping and photo-interpretation has shown the Lebombo structure to be a faulted monocline. Strike faulting is well developed along the western flank of the belt and can also be traced in the Sabie River basalts. Detailed mapping of the river sections indicates

that the basic lavas crop out in a series of fault blocks which show an overall steepening in dip to the east. A slight unconformity is present between the Sabie River basalts and Jozini rhyolites and the acid flows dip to the east at relatively shallow angles compared to the underlying basic lavas.

Further north in Swaziland a similar configuration is apparent (see Cleverly, 1977). The Karoo sediments and lowermost Sabie River basalts are strongly faulted and an unconformity is again present between the Sabie River and Jozini Formation. The basic lavas and interbedded rhyolite flows (Twin Ridge Beds) which crop out immediately below the unconformity are again steeply inclined to the east whereas the overlying rhyolites dip at shallower angles and do in fact flatten to the east.

In the central Lebombo strike faulting is far less prevalent and the volcanics dip at relatively shallow angles to the east. Similarly, in the northern Lebombo, faulting is much less common and dip angles are less steep than those in the south. The unconformity between the basic and acid volcanics is also less pronounced and it is notable that the rhyolitic succession is much thinner. Interdigitation of basic and acid volcanics is also more prevalent. The overall trend of the volcanic belt also alters progressively north of Swaziland and becomes east of north though structural elements within the belt retain the same strong north-south lineation noted in Swaziland and the northern Lebombo.

In view of the progressive flattening of the sedimentary and volcanic successions to the north it would appear that the Karoo outcrops found in the central and northern Lebombo form the relatively flat lying westerly shoulder of a monoclinal structure, the main axis of which existed to the east of the present day Lebombo belt. Extrapolation of the inferred

monoclinal axis (Fig. 11.1) from the southern Lebombo and Swaziland northwards supports the view that the main zone of monoclinal warping and faulting took place to the east of the present day outcrop in the central and northern Lebombo.

In the early stages of eastern Gondwanaland rifting the overall structure of the proto-Lebombo rift was in all probability represented by a structure similar to that shown in Fig. 11.2ii. The monocline as seen in the Lebombo today would therefore represent the original westerly margin of a major graben structure which formed during the breakup of eastern Gondwanaland. With continued rifting the margins of the graben would sag inwards becoming more strongly flexed and faulted. The extensional tectonics associated with rifting would also provide channel ways for the emplacement of magmas on both the floor and margins of the graben.

That the Lebombo graben subsequently developed into a sea-floor spreading type environment seems unlikely since there are no indications of ocean-floor type volcanics anywhere in the Lebombo and Zimbabwe areas. However, there is no reason why the Lebombo structure could not have represented a graben structure which developed in response to continental separation with ultimate rifting and sea-floor spreading taking place further to the east. There is the problem of locating the eastern margin of the proposed Lebombo graben though it is probable that it was destroyed as continental rifting continued, with only the stable continental warp (the Lebombo monocline) remaining.

Geophysical studies (Darracott and Kleywegt, 1974) support the above argument. Data obtained by Darracott and Kleywegt (1974) suggest that the Lebombo lavas both extend and flatten to the east. Furthermore, basalts have been encountered in deep drill holes ($\sim$ 4.5 km) beneath the sedimentary

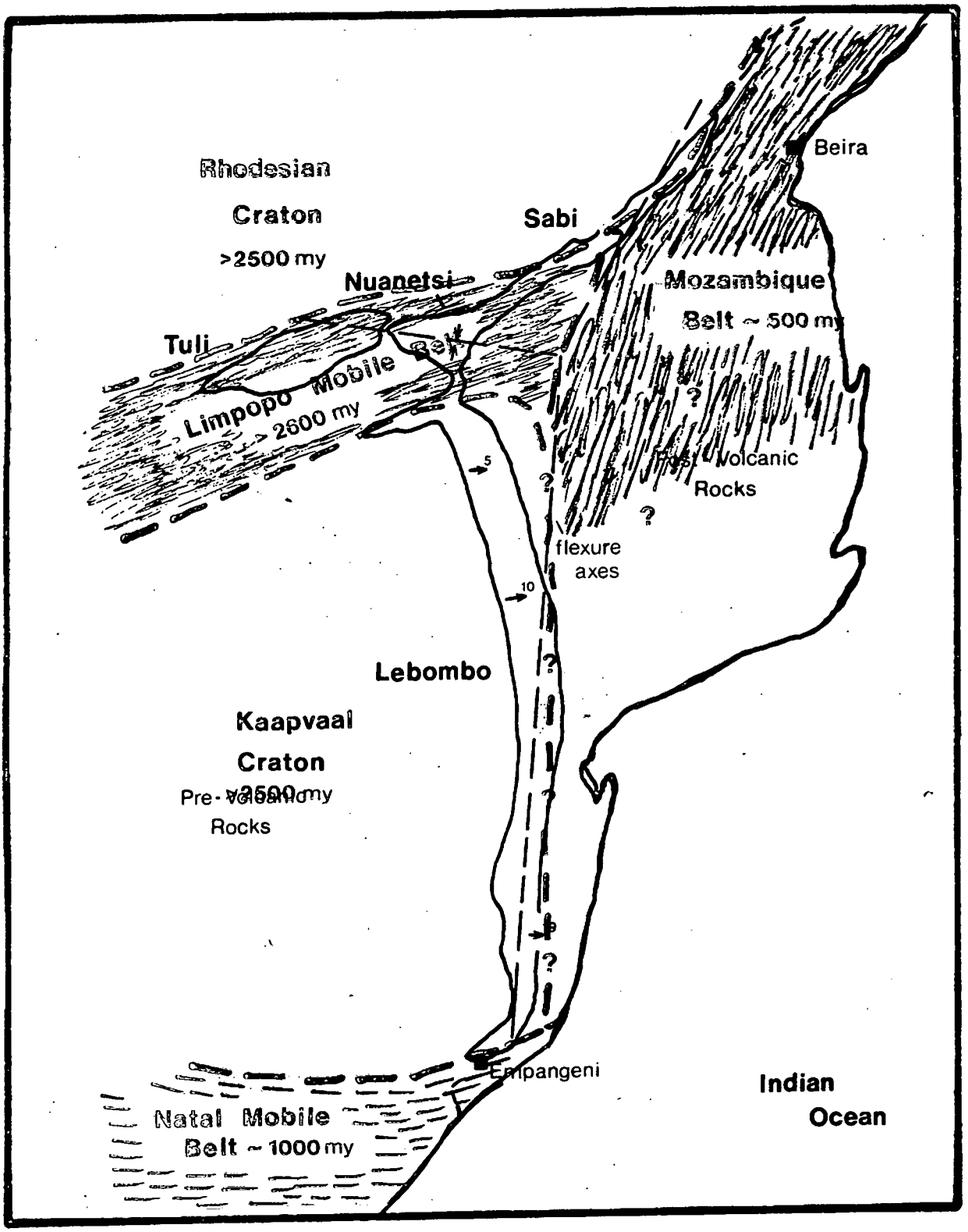

Fig. 11.1 Generalised diagram showing the distribution of the Lebombo, Tuli, Nuanetsi and Sabi volcanics and the inferred trends of the monoclinal and synclinal axes. The overlay indicates the configuration of the orogenic belts and cratonic nuclei with which the Karoo volcanics of eastern Gondwanaland are associated. (Data from Clifford, 1970; Cox, 1970; Saggerson and Logan, 1970; Bristow, 1976). Dip angles in degrees.

day Lebombo belt with the transition to oceanic crust taking place to the east of the present-day coastline. A close analogy is found in the coastal structure of west Greenland in the vicinity of the Svartenhuk Peninsula and Ubenkendt Island where a thick sequence of Tertiary basalts overlying basement rocks dips into the Davies straits but is faulted offshore against a second zone of basement rocks (Clarke and Pederson, 1976).

In conclusion it is therefore proposed that the present day Lebombo marks the faulted and down-warped margin of a Karoo Graben structure that developed in response to the fragmentation of eastern Gondwanaland. The main period of graben formation appears, on the basis of field relationships, to have developed during and subsequent to the emplacement of the lower basaltic succession. Rhyolitic volcanism then commenced towards the final stages of Graben formation and these lavas would have probably been 'ponded' in the Graben in a manner depicted in Figure 11.2. If this is indeed the case, estimates of the volume of rhyolitic material based on outcrop measurements may be very misleading and indicates the need for a detailed geophysical study of the Lebombo structure. An accurate estimate of the volume of rhyolitic material will place important constraints on the petrogenesis of the acid volcanics which on the basis of published (Manton, 1968) and unpublished data (Bristow et al., In prep.) appear to have been derived from a basic source composition.

SYNTHESIS

At this point all that remains is to propose a model, which insofar as possible accounts for the interplay of continental rifting and volcanism in the Lebombo and adjoining areas during the fragmentation of Eastern Gondwanaland. This has been done below. However, at the outset, it should be said that the model presented is undoubtedly complex and in many respects conjectural. Nevertheless the volcanic phenomena of the Lebombo are such that they cannot have formed in response to any other than a series of complex tectono-thermal events and the model is therefore considered to be essentially plausible!

A. PRE-KAROO HISTORY

I. During pre-Karoo times volatile release from the deep mantle led to the transit of fluid phases rich in CO_2 and H_2O and volatile elements such as K, Sr etc. through the upper mantle underlying the Lebombo and south-east regions of Zimbabwe. Migration of these phases along fractures and grain boundaries led to mantle metasomatism and especially the formation of carbonates and alkali-rich silicates, e.g. phlogopite, amphibole and possibly also opaque phases rich in alkali elements similar to those which have been found in metasomatised peridotite nodules (e.g. see Harte et al., 1975; Erlank and Rickard, 1977 and others).

II. The metasomatised mantle zones formed "holding zones" (Bailey, 1977) for phases rich in CO_2, H_2O and volatile elements thereby leading to the formation of enriched mantle domains. Furthermore, depending on both the timing of metasomatism and the composition of the volatiles and resultant metasomatic minerals, initial Sr-isotope ratios may have been elevated by the incorporation of phases characterised by a high Rb/Sr ratio, thereby giving rise to upper mantle zones capable of generating lavas and dykes similar to those found in the southern Lebombo.

An important criterion of the model presented here is that the metasomatism must have occurred in an undepleted mantle, e.g. a mantle which had bulk earth Sr- and Nd-isotopic ratios and which was capable of yielding basaltic melts as far as major elements were concerned. In this respect a notable feature of the pre-Karoo history of eastern Gondwanaland is that in south-eastern Zimbabwe no major basaltic volcanism has taken place since the emplacement of the Umkondo dolerites (age: ~ 1.1 by; Erlank et al., 1980) whereas in the Lebombo zone the last period of basaltic volcanism was marked by the emplacement of the Tsange gabbros (age: ~ 1.5 by; Bristow, unpubl. data). Consequently it is apparent that there were potentially long periods of time during which metasomatic fluids were able to percolate through the upper mantle material. Equally important is that there were no major volcanic events which could have led to the formation of a depleted mantle incapable of generating basaltic melts.

Presumably mantle depletion must have occurred during the formation of the Rhodesian (Zimbabwe) and Kaapvaal cratons (~ 2 500 my; Clifford, 1970). However, the presence of considerable volumes of younger basaltic material (Table 11.1) which crop out within the confines of both cratons implies that the mantle source regions underlying the cratonic regions were periodically replenished in basaltic components by mantle convection or diffusion processes? One additional point of interest that also emerges from a study of the age patterns of volcanism located either on or at the margins of the Kaapvaal and Rhodesian cratons (see Erlank et al., 1980) is that there have been fewer episodes of basaltic volcanism since about 1 500my whereas there was considerable activity in the period 2 000 - 3 000 my. This perhaps suggests that mantle convection and associated basaltic replenishment has been a much slower or less efficient process since about 1.5 by.

TABLE 11.1 Age relations of some Pre-Karoo basaltic volcanics which crop out on the Kaapvaal and Rhodesian (Zimbabwe) cratons. (For a detailed summary of emplacement ages of basic and ultrabasic volcanics in these areas refer to Erlank et al., 1980).

GROUP OR FORMATION	AGE, TECHNIQUE, REFERENCE		
Great Dyke, Zimbabwe	2.51 by;	Rb - Sr	(1)
Ventersdorp lavas, South Africa	ca. 2.2 by;	Rb - Sr	(2)
Bushveld Igneous Complex, South Africa	2.1 - 2.4 by;	Rb - Sr	(1)
Mashonaland Dolerites, Zimbabwe	1.91 by;	Rb - Sr	(3)
Tsange Gabbros, South Africa	ca. 1.5 by;	Rb - Sr	(4)
Umkondo Dolerites, Zimbabwe	ca. 1.1 by;	Rb - Sr	(2)
Karoo Volcanics	ca. 190 my;	K - Ar	(5)

References:
(1) Hamilton (1977)
(2) Erlank et al. (1980)
(3) Compston and McElhinney (1975)
(4) Bristow (unpubl. data)
(5) Fitch and Miller (1971) and others.

B. PROTO RIFT STAGE

I. Horizontal movement of the anisotropic Gondwanaland continental plate in pre-Jurassic times reactivated earlier zones of weakness, leading to fracturing and fissuring, and the channelling of gas release from the deeper mantle. The zones of weakness are typically the most recent orogenic belts, viz. the Mozambique Mobile Belt, Limpopo Mobile Belt and Natal Mobile Belt, which girdle the older cratonic nuclei of Africa, viz. the Rhodesian (Zimbabwe) Craton and Kaapvaal Craton. Stress release along these zones of weakness provided the initial decompression which effectively localised renewed release of volatiles from the mantle.

II. Continental heating by gas fluxing, aided by heat derived from radiogenic metasomatic components, e.g. K^{40}, ultimately led to thermal decomposition of the volatile-bearing metasomatic minerals, thereby propogating melting. Crustal fracturing as a result of updoming of the continental lithosphere and/or Gondwanaland rifting also led to pressure release in the upper mantle thereby further assisting the melting process.

III. Early melts were limited in amount and buffered by the dominant volatile phase still escaping from the deep mantle. In the northern Lebombo and Sabi regions the early volatile phases were dominated by CO_2; high concentrations of CO_2 are reflected by the presence of carbonatites and nephelinite magmas. These melts also formed in a source distinct from the source area from which the overlying picrite basalts were derived.

According to Bailey (1977) carbonatites are the "hallmark of rift volcanism" and it is notable that they are invariably associated with nephelinite magmatism, a classic example being the East African rift system with its numerous nephelinitic volcanoes and attendant carbonatites. There

is continuous CO_2 emission from along much of the East African rift zone and the only active nephelinite volcano, Nyirangongo, maintains an almost continuous emission of CO_2 (Bailey, 1977). Juvenile CO_2 is also considered to be the main heating agent for the geothermal activity along the rift and in some localities in Kenya, CO_2 of high purity is obtained commercially from shallow wells (Bailey, 1977). Evidence of high CO_2 and low H_2O abundances is also provided by the modern alkali carbonatite lavas of Oldonyo Lengai at the south end of the Gregory Rift (Dawson, 1966).

There are therefore, clear indications that the characteristic vapour phase in most cases of proto-rift magmatism is rich in CO_2 and deficient in H_2O. However, it is probable that the CO_2 and H_2O are low temperature, low pressure, near surface expressions of the actual vapour phases present in the magma systems (Bailey, 1977). At greater depths it is likely that the C and H will be present in the form of different species, e.g. CO, CH_4 and H_2 as suggested by high temperature gas collections (Huntingdon, 1973), fluid inclusion studies, and gas composition calculations for alkaline rocks (Mitchell, 1975). Furthermore other gases such as F, Cl and N_2 are undoubtedly present in the mantle.

IV. At this stage initiation of lithosphere separation was achieved. Alternatively the cycle could have failed or stabilised thereby giving rise to a situation similar to that noted in the East African rift systems where the stages of updoming, volatile loss, proto-rift and alkaline volcanism have been achieved without complete crustal separation. It is, however, possible that the East African rift system has yet to reach the final separation stage.

C. GRABEN FORMATION STAGE

I. Following the early period of carbonatitic and nephelinitic volcanism it is envisaged that continental rifting became an irreversible

process and may even have been accelerated by a combination of increased thermal activity along the proto-rift zone, increased rates of mantle convection or other presently unknown processes which may have been responsible for the fragmentation of Gondwanaland in the first place. Decompression associated with the crustal rifting led to greater degrees of melting in the mantle and in view of the small quantities of CO_2 in the mantle it is probable that whatever volatiles were still in existence were depleted in CO_2 and possibly even characterised by relatively high H_2O/CO_2 ratios.

II. Greater degrees of melting in the presence of H_2O rich volatiles led to the formation of silica-saturated magmas thereby explaining the presence of picritic basalts above the nephelinites. Furthermore, the previous enrichment in KAR elements in the source from which the picritic rocks were derived led to these lavas being enriched in incompatible elements. In addition the more enriched nature of the early picrite basalts reflects derivation from a more fertile source whereas the subsequent lavas reflect a progressive depletion of the source by the picritic event.

III. The presence of picritic basalts in the north Lebombo, Nuanetsi and Tuli areas is attributed to the greater amounts of crustal fracturing and dilation in this part of the crust due to the formation of a triple junction-type structure at the northern end of the Lebombo (see Cox, 1970; Reeves, 1978).

In this area of maximum tension picritic magmas were able to reach the surface, whereas further south crustal tension appears to have been less extreme thereby restricting the movement of high density picritic

magmas to the surface. Once picritic magmas were no longer able to reach the surface they remained at depth, allowing the crystallisation of olivine and clinopyroxene. This caused the derivative magmas to evolve to basaltic compositions thereby promoting the necessary decrease in density which allowed the magma to rise to the surface and form the shoshonitic suite which overlies the picrite basalts.

IV. The volcano-tectonic processes outlined up until this point account for the geochemical relationships of the central and northern Lebombo picrite basalts and low-MgO basalts. However, it was shown in previous chapters that the low-MgO volcanics of the southern Lebombo are chemically distinct from those found to the north. They are depleted in incompatible elements but strongly enriched in radiogenic ^{87}Sr relative to the rocks found to the north and on this basis appear to have been derived from a source which contrasted strongly with the mantle composition from which the picritic rocks and related shoshonites were derived.

The Lebombo belt would therefore appear to be unique in that not only does it exhibit a bimodal assemblage of basic and acid lavas but appears to have tapped magmas from two unique mantle sources, one of which apparently suffered an old (> 1 000 my?) enrichment event (southern Lebombo and Swaziland) the other a much younger (< 500 my?) metasomatic enrichment event (central and northern Lebombo). The latter relationship is implied by the Sr-isotope data though in the case of the southern Lebombo event it is possible that the inferred older age is partly or wholly a function of crustal contamination. However, on the basis of the data presented in Chapters 9 and 10 it seems plausible to accept that the radiogenic character of some of the southern Lebombo lavas could well represent an old enrichment event.

The overall volcano-tectonic model outlined above (Fig. 11.2) is applicable to the southern Lebombo with the proviso that the lavas and dykes emplaced during the formation of the southern Lebombo were derived from a unique source area whereas the northern volcanics were derived from a source which differed chemically. Accordingly it may be concluded that large scale lateral heterogeneities existed in the mantle underlying the Lebombo area during the formation of the volcanic belt. However, as is the case in studies of most continental basaltic rocks, well constrained models are difficult to formulate due to the complications posed by the effects of crustal contamination.

D. THE RHYOLITIC STAGE

I. A large portion of the Lebombo basic magmas solidified at the base of the crust because their density was much greater than the overlying sialic material (cf. Baker et al., 1977a). This underplated material became the source of the acid magmas found in the Lebombo (Betton and Cox, 1979).

Continental crust is considerably more rigid than the underlying mantle and so when under stress would yield by necking. Assuming isostatic equilibrium was maintained the upwarp in the crust/mantle boundary would have had amplitude about ten times greater than the trough at the surface such that a trough 1 km deep at the surface would have been reflected by a 10 km upwarp in the crust/mantle boundary below (Betton and Cox, 1979). Basic material underplated onto the base of the crust would have been at a temperature marginally below its solidus and on being uplifted during continued crustal dilation and necking would have eventually melted thereby giving rise to rhyolitic melts. Sr-isotope data support a mechanism whereby the Lebombo rhyolites were derived from a basic source (Manton,

Fig. 11.2 Schematic diagram showing the possible sequence of events that led to the emplacement of the Karoo volcanics in eastern Gondwanaland.

I

(PROTORIFT STAGE)

Initial crustal fracturing is followed by the release of volatiles rich in CO_2 from the mantle. Incipient partial melting occurs. Early melts are buffered by CO_2 and are nephelinitic and carbonatitic in composition.

II

(GRABEN FORMATION STAGE)

Crustal fracturing is followed by crustal dilation or necking. Greater degrees of melting in the presence of H_2O rich volatiles leads to the formation of silica-saturated picritic magmas. With a decrease in thermal energy picritic magmas are prevented from reaching the surface thus remaining at depth where they fractionate olivine and clinopyroxene. Derivative magmas evolve to basaltic compositions thereby promoting the necessary decrease in density thus allowing these magmas to rise to the surface and form the low-MgO lavas which overlie the picritic volcanics. A large portion of the basic magma also solidifies at the base of the crust due to the density contrast with the overlying sialic material.

III

(RHYOLITIC STAGE)

With continued crustal necking underplated material eventually melts (see Betton and Cox, 1979) thereby giving rise to rhyolitic magmas which are emplaced as massive flows above the low-MgO volcanics.

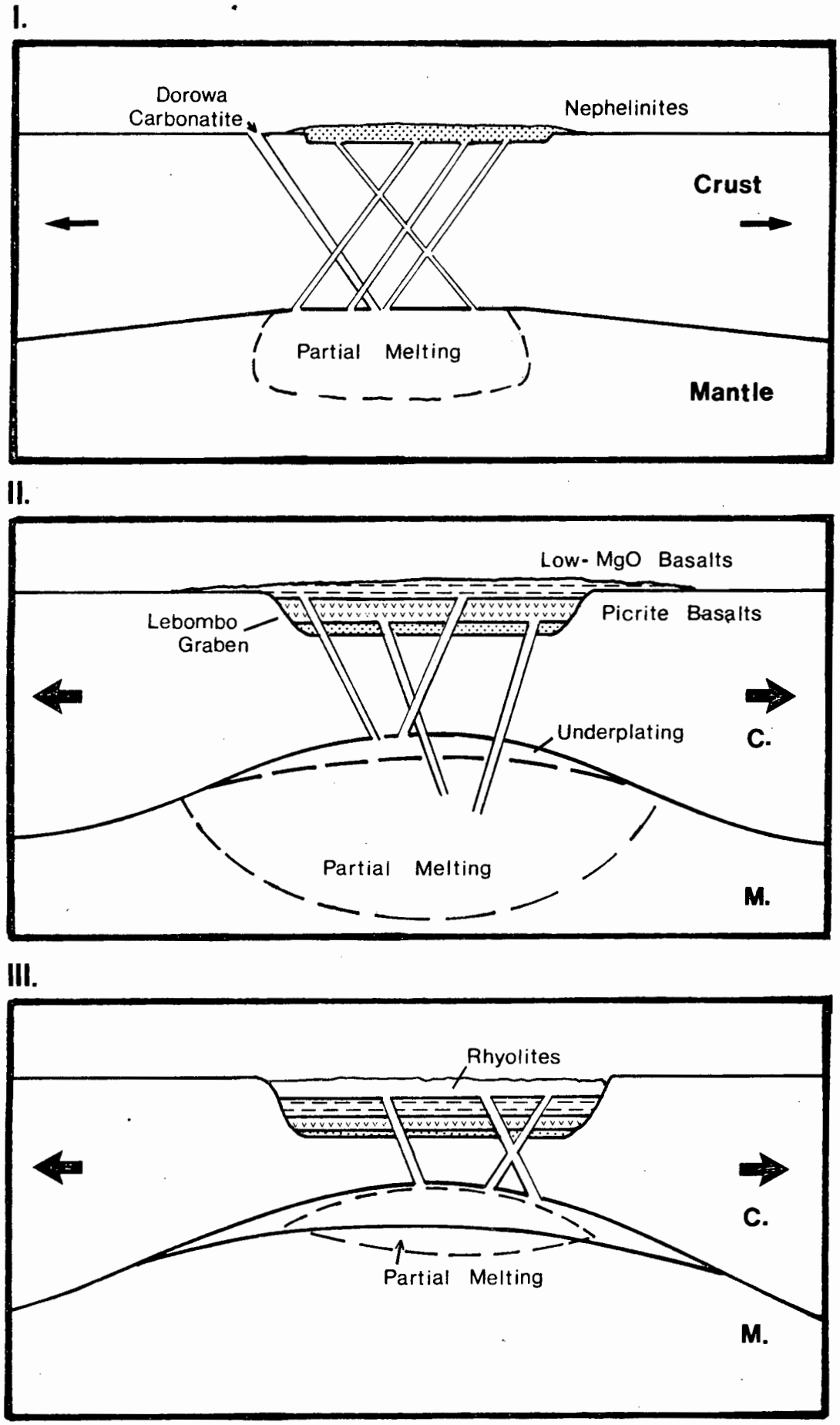
I.
Dorowa
Carbonatite
Nephelinites
Crust
Partial Melting
Mantle
II.
Low- MgO Basalts
Lebombo
Graben
Picrite Basalts
Underplating
C.
Partial Melting
M.
III.
Rhyolites
C.
Partial Melting
M.

Fig. 11.2

1968; Bristow et al., In prep.) and a partial melt of 10 - 12% from a basaltic source similar to that represented by the Rooi Rand dolerites satisfactorily explains most of the major and trace element characteristics of the Karoo rhyolites which overlie the low-MgO lavas of the Sabie River Formation (Betton, 1978).

II. Finally, when crustal separation was completed rhyolitic volcanism would cease and there would be a return to basic magmatism thereby producing the upper basalts found in Mozambique.

****

ACKNOLWEDGEMENTS

This thesis represents the culmination of three and a half years of collaborative work on the Karoo volcanics of southern Africa and I am deeply indebted to all those people who have made this study such a stimulating and rewarding experience.

First and foremost I wish to thank Prof.'s A.J. Erlank and A.R. Duncan for inviting me to Cape Town to continue my earlier studies on the Lebombo volcanics, for providing me with the opportunity to use the vast facilities of the Geochemistry Department and for acting as unstinting supervisors in the course of this study. Many were the pitfalls that they either rescued me from or steered me past and I will always be deeply grateful for their guidance, tuition and encouragement.

Without the analytical expertise of Prof. A.R. Duncan and Dr J.P. Willis, the analytical work presented in this thesis would not have been possible and my knowledge of X-Ray Flourescence techniques would still be negligible. The efforts of, amongst others, Prof. A.R. Duncan and Dr J.P. Willis in initiating me into the lighter side of computing are also gratefully acknowledged. I am also most grateful to Anton Le Roex for his assistance with data reduction, analytical procedures and data interpretation and Dick Rickard for both teaching and assisting me to operate the probe. Likewise my thanks to Dave Reid and Stuart Smith for help and guidance with respect to matters geochemical and Jock Robey, Andy Moore and Sandy Simpson for discussions more topical. Special thanks also to Michele Brauteseth for the considerable amount of time she spent assisting me with the data compilation presented in this thesis and help provided in drafting diagrams and proof reading.

My knowledge of isotope geochemistry also benefited greatly from several trips to the Geochronology Laboratory at the Bernard Price Institute, University of the Witwatersrand, and I am most grateful to Prof. H.L. Allsopp for affording me this opportunity. His guidance and tuition is indeed greatly appreciated as is his ability to cope so pleasantly with 'minor disasters' caused by JWB. He is also thanked for reading many of the earlier drafts of my geochronology and isotope chapters. Likewise my thanks to the remaining staff of the B.P.I. for providing me with unlimited machine time and much help in sample preparation procedures. In particular

I wish to acknowledge the efforts of Rich Armstrong, Trevor Ellworthy, Craig Smith and Dr Hans Welke. Prof. L.O. Nicolaysen is also thanked for permitting me to work at the B.P.I.

Many of the ideas presented in this thesis have been shaped by numerous discussions and working sessions with those famous men of the 'Karoo' Drs K.G. Cox, R.W. Cleverly and P.J. Betton and I am extremely grateful for their help, guidance and penetrating criticism. In particular my thanks to Dr K.G. Cox for assisting me with the interpretation of the geochemical relationships of the southern Lebombo volcanics and Dr R.W. Cleverly for reading many earlier drafts of portions of this thesis. Likewise, I would like to extend my thanks to Prof. E.P. Saggerson for initially affording me the opportunity to work on the Karoo Geodynamics Project and to Rich Armstrong for allowing me to use his Rooi Rand data.

Financial assistance from the C.S.I.R. is gratefully acknowledged, since without their support this thesis would not have been possible. Financial support was made available within Working Group 4, "Geodynamics of Continental and Ocean Rifts, (b) Comparative Geochemical Studies of Ocean and Continental Volcanic Rocks."

My thanks also to: Dr U. deV. Pienaar for allowing me access to the Kruger National Park and the many game rangers and game guards who assisted me during my trips to the Park; the Natal Parks Board for allowing me access to Mkuze and Ndumu Game Reserves; Mr Naas Schutte of the Geological Survey for showing me the more important geological features of the Olifants River area (K.N.P); the Kwazulu Government for allowing me to work in portions of Kwazulu within Zululand; the technical staff of the Department of Geochemistry (UCT) and Department of Geology, University of Natal for assistance with thin and polished section preparation, and Mark Norris-Rogers for assistance both in the field and in sorting and packing rock samples. To all the other unnamed geologists, quarrymen, farmers and willing hands who assisted me in my wanderings through the Lebombo, my thanks.

During my years of study, my parents and brothers have also provided a never ending amount of encouragement and support for which I am eternally grateful. Similarly, I wish to express my sincere thanks to my parents-in-law for their support and encouragement.

Finally, it is impossible to express adequately my appreciation to my wife Marilyn, who for the past years has not only been a constant source of encouragement, but a saviour in times of stress, a typist and a proof reader. Without her help and cheerful support this thesis certainly would not have seen the light of day.

****

Footnote: With apologies to the rock pigeons who once roosted outside my office window. May your nocturnal repose be disturbed no more!

REFERENCES

Absolom,S.A. (1970) Contaminated dolerites of Natal and Zululand Petros,v2,10-15.

Ackerman,P.B., Walker,F. (1960) Vitrification of arkose by Karoo dolerites near Heilbron, O.F.S. Q.J. Geol. Soc. Lond.,v116, 239-254.

Albee,A.L., Ray,L. (1970) Correction factors for electron probe microanalysis of silicates, oxides, carbonates, phosphates and sulfates. Anal. Chem.,v42(12), 1408-1414.

Allsopp,H.L., Ulrych, I.J., Nicolaysen,L.O. (1968) Dating some significant events in the history of the Swaziland system by Rb-Sr isochron methods. Can. J. Earth Sci.,v5, 605-619.

----------, Nicolaysen,L.O., Hahn-Weinheimer,P. (1969) Rb/K ratios and Sr-isotopic compositions of minerals in eclogitic peridotitic rocks. Earth Planet. Sci. Lett.,v5,231-244.

----------, Kostlin,E.O., Welke,H.J., Burger,A.J., Kroner,A., Blignault,H.J. (1979) Rb-Sr and U-Pb geochronology of Late-Precambrian - Early Palaeozoic igneous activity in the Richtersveld (South Africa) and southern South West Africa. Trans. Geol. Soc. S. Afr.,v82(2), 185-204.

Amaral,G., Cordani,U.G., Kawashita,K., Reynolds,J.H. (1966) Potassium-argon dates of basaltic rocks from southern Brazil. Geochim. Cosmochim. Acta.,v30,159-189.

Anderson,W.A. (1901) First report of the geological survey of Natal and Zululand. Surv. Gen. Dept., Natal. Davies and Sons, Pietermaritzburg.

---------- (1904) Second report of the geological survey of Natal and Zululand. Surv. Gen. Dept., Natal. West, Newman and Co.,London.

---------- (1907) Third and final report of the geological survey of Natal and Zululand. Surv. Gen. Dept., Natal. West, Newman and Co.,London.

Aoki,K. (1975) Origin of phlogopite and potassic richterite bearing peridotite xenoliths from South Africa. Contrib. Mineral. Petrol.,v53, 145-156.

--------, Kameyama,E. (1970) High pressure clinopyroxene megacrysts from Itinome-gata volcano. Japanese Assoc. Petrol. Econ. Geol. Jour.,v64, 107-122.

Appelton,J.D. (1972) Petrogenesis of potassium-rich lavas from the Roccamonfina Volcano, Roman Region, Italy. J. Petrol., v13, 425-456.

Armstrong,R.A. (1978) A GEOLOGICAL AND GEOCHEMICAL APPRAISAL OF THE ROOI RAND DYKE SWARM, LEBOMBO. M.Sc. Thesis (unpubl.), Univ. Natal.

Armstrong,R.L. (1968) A model for Sr and Pb isotope evolution in a dynamic earth. Rev. Geophys.,v6, 175-199.

Arndt,N.T. (1977) Partitioning of Ni between olivine and ultrabasic liquids. Carnegie Inst. Wash. Yearb.,v76, 553-557.

Arth,J.G. (1976) Behaviour of trace elements during magmatic processes - a summary of theoretical models and their application. Jl. Res. U.S. Geol. Surv.,v4(1), 41-47.

Assuncao,A.F.T.de, Pinto Coelho,A.V.T., Tavares Rocha,A., (1962) Petrologia das lavas dos Libombos (Mocambique). Estud. Ens. e Doc. (Lisboa),v99, 74pp.

Augistithis,A. (1978) ATLAS OF THE TEXTURAL PATTERNS OF BASALTS AND THEIR GENETIC SIGNIFICANCE. Elsevier Scientific Publ. Co., Amsterdam.

Bailey,D.K. (1974) Continental rifting and alkaline magmatism. In: Sorenson,H. (Ed.), THE ALKALINE ROCKS, 148-159, John Wiley, London.

---------- (1977) Continental rifting and mantle degassing. In: Neuman,E.R., Ramberg,I.B. (Eds.), PETROLOGY AND GEOCHEMISTRY OF CONTINENTAL RIFTS, 1-13, Reidel, Dordrecht.

Baird,A.K. (1961) A pressed specimen die for the Norelco vacuum-path X-ray spectrograph. Norelco Rep.,v8, 108.

Baker,B.H., Goles,G.G., Leeman,N.P., Lindstrom,M.M. (1977) Geochemistry and petrogenesis of a basalt-benmoreite-trachyte suite from the southern part of the Gregory Rift, Kenya. Contrib. Mineral. Petrol.,v64, 303-332.

----------, Crossley,R., Goles,G.G. (1977a) Tectonic and magmatic evolution of the southern part of the Kenya Rift Valley. In: Neuman,E.R., Ramberg,I.B. (Eds.), PETROLOGY AND GEOCHEMISTRY OF CONTINENTAL RIFTS, 29-50, Reidel, Dordrecht.

Barrett,D.R. (1975) The genesis of kimberlites and associated rocks: strontium isotopic evidence. In: Ahrens,L.H., Dawson,J.B., Duncan,A.R., Erlank,A.J. (Eds.), PHYSICS AND CHEMISTRY OF THE EARTH, 9, 637-353, Pargamon, N.Y.

Barton,J.M., Ryan,B., Fripp,R.E.P., Horrocks,P. (1979) Effects of metamorphism on the Rb/Sr and U.Pb systematics of the Singele and Bulai Gneisses, Limpopo Mobile Belt, Southern Africa. Trans. Geol. Soc. S. Afri.,v82(2), 259-270.

Basu,A.R., Murthy,V.R. (1976) Sr-isotope and trace elements in spinel lherzolite xenoliths in basalts, San Quintin, Baja California. EOS.,v57, 355.

---------, ---------- (1977) Kaersutites, suboceanic low-velocity zone, and the origin of mid oceanic ridge basalts. Geology, v5, 365-368.

Bell,K., Powell,J.L. (1969) Strontium isotopic studies of alkali rocks: the potassium-rich lavas of the Byrmiga and Tore-Ankole regions, East and Central Equatorial Africa. J. Petrol.,v10, 536-572.

Bence,A.E., Albee,A.L. (1968) Empirical correction factors for the electron microanalysis of silicates and oxides. J. Geology, v76, 382-403.

Best,M.G. (1974) Mantle-derived amphibole within inclusions in alkalic-basaltic lavas. J. Geophys. Res.,v79, 2107-2113.

Betton,P.J. (1978) GEOCHEMISTRY OF KAROO VOLCANIC ROCKS IN SWAZILAND. D.Phil. Thesis (unpubl.), Univ. Oxford.

---------- (1979) Isotopic evidence for crustal contamination in the Karoo rhyolites of Swaziland. Earth Planet. Sci. Lett.,v45, 263-274.

----------, Cox,K.G. (1979) Production of rhyolites at continental margins: An example from the Lebombo monocline. Geokong. 79, Abstr., 18th Cong. Geol. Soc. S. Afr. 29-31.

Bickle,M.J., Martin,A., Nisbet,E.G. (1975) Basaltic and peridotitic komatiites and stromatolites above a basal un-

conformity in the Belingwe greenstone belt, Rhodesia. Earth Planet. Sci. Lett.,v27, 155-162.
----------, Ford,C.E., Nisbet,E.G. (1977) The petrogenesis of peridotitic komatiites: evidence from high pressure melting experiments. Earth Planet. Sci. Lett.,v37, 97-106.
Binns,R.A., Duggan,M.B., Wilkinson,J.F.G. (1970) High pressure megacrysts in alkaline lavas from northeastern New South Wales. Am. J. Sci.,v269, 132-169.
Bird,M.L. (1971) DISTRIBUTION OF TRACE ELEMENTS IN OLIVINES AND PYROXENES - AN EXPERIMENTAL STUDY. Ph.D. Thesis (unpubl.), Univ. of Missouri, Rolla.
Bloomfield,K. (1961) The age of the Chilwa Alkaline Province. Rec. Geol. Surv. Nyasaland,v1, 95-100.
Boettcher,A.L., Mysen,B.O., Modreski,P.J. (1975) Melting in the mantle: phase relationships in natural and synthetic peridotite - H2O and peridotite - H2O - CO2 with application to kimberlite. In: Ahrens,L.H., Dawson,J.B., Duncan,A.R., Erlank,A.J., (Eds.), PHYSICS AND CHEMISTRY OF THE EARTH,v9, 855-868, Pergamon Press, New York.
----------, O'Neil,J.R., Windom,K.E., Stewart,D.C., Wilshire,H.G. (1979) Metasomatism of the upper mantle and the genesis of kimberlites and alkali basalts. In: Boyd,F.R., Meyer,H.O.A. (Eds.), THE MANTLE SAMPLE, Proceed. Second. Int. Kimb. Conf.,v2, 173-182, A.G.U., Washington.
Botha,E.V.J., Theron,J.C. (1967) New evidence for the early commencement of Stormberg volcanism. Tydskr. Natuurwet., v7, 469-473.
Bougalt,H., Hekinian,R. (1974) Rift valley in the Atlantic Ocean near 36 50' N: Petrology and geochemistry of basaltic rocks. Earth Planet. Sci. Lett.,v24, 249-261.
Bowen,D.J. (1979) The Chishanya carbonatite complex. Geokong. 79, Abstr., 18th Cong. Geol. Soc. S. Afr., 50-51.
Bowen,N.L. (1928) THE EVOLUTION OF THE IGNEOUS ROCKS. Princetown Univ. Press.
----------, Schairer,J.F. (1935) The system MgO-FeO-SiO2. Ibid., Series 5,v29, 151-127.
Bravo,M.S., O'Hara,M.J. (1975) Partial melting of phlogopite-bearing synthetic spinel- and garnet-lherzolites. In: Ahrens,L.H., Dawson,J.B., Duncan,A.R., Erlank,A.J. (Eds.), PHYSICS AND CHEMISTRY OF THE EARTH,9, 845-854. Pergamon, New York.
Bristow,J.W. (1976) THE GEOLOGY AND GEOCHEMISTRY OF THE SOUTHERN LEBOMBO. M.Sc. Thesis (unpubl.) Univ. Natal.
----------, Cleverly,R.W. (1979) Volcanology of the Lebombo rhyolites. Geokong. 79, Abstr., 18th Cong. Geol. Soc. S.Afr., 60-63.
Brooks,C., Hart,S.R., Wendt,I. (1972) Realistic use of two error regression treatments as applied to rubidium-strontium data. Rev. Geophys. Space Phys.,v10, 551-577.
----------, James,D.E., Hart,S.R. (1976a) Ancient lithosphere: its role in young continental volcanism. Science,v93, 1086-1094.
----------, Hart,S.R., Hofmann,A.W., James,D.E. (1976b) Rb-Sr mantle isochrons from oceanic regions. Earth Planet. Sci. Lett., v32, 51-61.

---------, James,D.E., Hart,S.R., Hofmann,A.W. (1976c) Rb-Sr mantle isochrons. Carnegie Inst. Wash. Yearb.,v75,176-207.
---------, Hart,S.R. (1978) Rb-Sr mantle isochrons and variations in the chemistry of Gondwanalands lithosphere. Nature, v271, 220-223.
Brooks,C.K. (1976) The Fe2O3/FeO ratio of basalt analyses: an appeal for a standardized procedure. Bull. Geol. Soc. Denmark, v25, 117-119.
Bruynzeel,D. (1957) A petrographic study of the Waterfall Gorge profile and Insizwa. Ann. Univ. Stellenbosch, v33, 484-535.
Bryan,W.B. (1967) Geology and petrology of Clarion Island, Mexico. Bull. Geol. Soc. Am.,v78, 1461-1476.
---------- (1972) Morphology of quench crystals in submarine basalts. J. Geophys. Res.,v77, 5812-5819.
----------, Finger,L.W., Chayes,F. (1969) Estimate proportions in petrologic mixing equations by least squares approximation. Science, v163, 926-927.
----------, Moore,J.G. (1977) Compositional variations of young basalts in the Mid-Atlantic Ridge rift valley near lat. 36 49'N. Geol. Soc. Am. Bull.,v88, 556-570.
Bultitude,R.J., Green,D.H. (1968) Experimental study at high pressures on the origin of olivine nephelinite and olivine melilite-nephelinite magmas. Earth Planet. Sci. Lett.,v3, 325-337.
----------, ---------- (1971) Experimental study of crystal-liquid relationships at high pressures in olivine nephelinite and basanite compositions. J. Petrol.,v12(1), 121-147.
Bunch,T.E., Keil,K., Olsen,E. (1970) Mineralogy and petrology of silicate inclusions in iron meteorites. Contrib. Mineral. Petrol.,v25, 297-340.
Burger,A.J., Coertze,F.J. (1973) Radiometric age measurements on rocks from southern Africa to the end of 1971. Bull. Geol. Surv. S. Afr.,v58, 46pp.
Burke,K.C., Dewey,J.F. (1973) Plume generated triple junctions: key indicators in applying plate tectonics to old rocks. J. Geol.,v81, 406-433.
Burley,A.J., Evans,R.B., Gillingham,J.M., Masson Smith,D. (1970) Gravity anomolies in Swaziland. Bull. Geol. Surv. Mines Dept. No.7, Swaziland.
Burnham,C.W. (1975) Water and magmas - a mixing model. Geochim. Cosmochim. Acta.,v39, 1077-1084.
Carlson,R.W., MacDougall,J.D., Lugmair,G.W. (1978) Implications for the structure of chemical heterogeneity in the mantle from Nd and Sr isotopic variations. 4th Int. Conf. Geochron. Cosmochron. Isotope Geol., 58-60, USA Geol. Surv. Rep. 78-701.
Carter,S.R., Evensen,N.M., Hamilton,P.J., O'Nions,P.K. (1978) Continental volcanics derived from enriched and depleted source regions: Nd and Sr isotope evidence. Earth Planet. Sci. Lett.,v37, 401-408.
Cawthorn,R.G., (1980) High-Mg Karoo tholeiite and sulphide separation in the Insiswa Intrusion, Transkei. S. Afr. J. Sci. (In Press)
----------, Ford,C.E., Biggar,G.M., Bravo,M.S., Clark,D.F. (1974) Determination of the liquid composition in experimental studies: discrepancies between microprobe analyses and other

methods. Earth Planet. Sci. Lett.,v21, 1-6.
Clarke,D.B. (1970) Tertiary basalts from Baffin Bay: possible primary magma from the mantle. Contr. Mineral. Petrol.,v25, 203-224.
----------, Pederson,A.K. (1976) Tertiary volcanic province of West Greenland. In: Escher,A., Watt,W.S. (Eds.), GEOLOGY OF GREENLAND, 364-385. Geological Survey of Greenland.
----------, O'Hara,M.J. (1979) Nickel, and the existence of high-MgO liquids in nature. Earth Planet. Sci. Lett.,v44, 153-158.
Cleverly,R.W. (1977) THE STRUCTURAL AND MAGMATIC EVOLUTION OF THE LEBOMBO MONOCLINE, SOUTHERN AFRICA, WITH PARTICULAR REFERENCE TO SWAZILAND. D.Phil. Thesis (unpubl.), Univ. Oxford.
---------- (1980) The volcanic geology of the Lebombo monocline in Swaziland. Trans. Geol. Soc. S. Afr.,v82(3), 343-348.
----------, Bristow,J.W. (1979) Revised volcanic stratigraphy of the Lebombo monocline. Trans. Geol. Soc. S.Afr.,v82(2), 227-230.
----------, Betton,P.J. (1979) Petrogenesis of Lebombo rhyolites from Swaziland. Geokong. 79, Abstr., 18th Cong. Geol. Soc. S. Afr., 79-81.
Clifford,T.N. (1970) The structural framework of Africa. In: Clifford,T.N., Gass,I.G. (Eds.), AFRICAN MAGMATISM AND TECTONISM, 1-26, Oliver and Boyd, Edinburgh.
Cohen,E. (1874) Erlanternde Bemerkungen zu der Rontenkarte erner Reise von Lydenburg nach den Goldfelddern und von Lydenburg nach der Delagoa Bai in Oeslichen Suid-Afrika. Jahr. Geogr. Ges., Hamburg, v2, 173-183.
Compston,W.I., McDougall,I., Heier,K.S. (1968) Geochemical comparison of the Mesozoic basaltic rocks of Antartica, South Africa, South America and Tasmania. Geochim. Cosmochim. Acta.,v32, 129-149.
----------, McElhinney,M.W. (1975) The Rb-Sr age of the Mashonaland dolerites of Rhodesia and its significance for paleomagnetic correlation in southern Africa. Precambrian Res.,v2, 303-315.
Condie,K.C., Hunter,D.R. (1976) Trace element geochemistry of Archean granitic rocks from the Barberton region, South Africa. Earth Planet. Sci. Lett.,v29, 389-400.
Coombs,D.S., Wilkinson, J.F.G. (1969) Volcanic lineages and fractionation trends in some undersaturated volcanic rocks and shallow intrusives from the East Otago Volcanic Province (New Zealand). J. Petrol.,v10, 440-501.
Cox,K.G. (1964) Structural evolution of the Masukwe Complex, Nuanetsi Igneous Province, Southern Rhodesia. Trans. Geol. Soc. S.Afr.,v67, 119-127
-------- (1970) Tectonics and vulcanism of the Karoo period, and their bearing on the postulated fragmentation of Gondwanaland. In: Clifford,T.N., Gass,I.D. (Eds.), AFRICAN MAGMATISM AND TECTONICS, 211-236. Oliver and Boyd, Edinburgh.
-------- (1972a) Karoo lavas and associated igneous rocks of southern Africa. Bull. Volc.,v35(4), 867-886.
-------- (1972b) The Karoo volcanic cycle. J. Geol. Soc.,v128. 311-336.
-------- (1978) Komatiites and other high-magnesia lavas: some

problems. Phil. Trans. Roy. Soc. Lond.,v288, 599-609.
--------, Vail,J.R., Monkman,L.J., Johnson,R.L. (1961) The Karoo igneous activity and tectonics in south-east southern Rhodesia. Nature, v190, 40 and 72.
--------, Johnson,R.L., Monkman,L.J., Stillman,C.J., Vail,J.R. (1965) The geology of the Nuanetsi igneous province. Phil. Trans. R. Soc.,v257, 71-218.
--------, Hornung,G. (1966) The petrology of the Karoo basalts of Basutoland. Am. Mines.,v51, 1414-1432.
--------, MacDonald,R., Hornung,G. (1967) Geochemical and petrographic provinces in the Karoo basalts of southern Africa. Am. Miner.,v52, 1451-1474.
--------, Bell,J.D. (1972) A crystal fractionation model for the basaltic rocks of the New Georgia Group, British Solomon Islands. Contrib. Mineral. Petrol.,v37, 1-13.
--------, Jamieson,B.G. (1974) The olivine-rich lavas of Nuanetsi: a study of polybaric magmatic evolution. J. Petrol.,v15, 269-
--------, Hawkesworth,C.J., O'Nions,R.K. (1976) Isotopic evidence for the derivation of some Roman region volcanics from anomalously enriched mantle. Contrib. Mineral. Petrol.,v56, 173-180.
--------, Bristow,J.W., Armstrong,R.A. (1980) The petrography mineralogy and petrogenesis of Karoo Mafic volcanics from the Lebombo, Nuanetsi and Tuli areas of southern Africa. Karoo Geodynamics Proj. Spec. Publ. (In Prep.).
Dale,I.M., Henderson,P. (1972) The partitioning of transition elements in phenocryst-bearing basalts and their implications about melt structure. 24th Int. Geol. Congr., Sect. 10, 105-111.
Darracott,B.W. (1974) On the crustal structure and evolution of south-east Africa and the adjacent Indian Ocean. Earth Planet. Sci. Lett.,v24, 282-290.
----------, Kleywegt,R.J. (1974) The structure of the southern portion of the Lebombo volcanic belt deduced from gravity data. Trans. Geol. Soc. S.Afr.,v77, 301-308.
Dawson,J.B. (1966) Oldonyo Lengai - an active volcano with sodium carbonatite lava flows. In: Tuttle,O.F., Gittens,J. (Eds.), CARBONATITES, 155-168, John Wiley, New York.
----------, Smith,J.V. (1977) The MARID (mica-amphibole-rutile-ilmenite-diopside) suite of xenoliths in kimberlite. Geochim. Cosmochim. Acta.,v41, 309-323.
DeLaeter,J.R., Abercrombie,I.D. (1970) Mass spectrometric isotope dilution analyses of rubidium and strontium in standard rocks. Earth Planet. Sci. Lett.,v9, 327-330
DePaolo,D.J. (1979) Implications of correlated Nd and Sr isotopic variations for the chemical evolution of the crust and mantle. Earth Planet. Sci. Lett.,v43, 201-211.
Dickinson,W.R., Luth,W.C. (1971) A model for plate tectonic evolution of mantle layers. Science, v174, 400-404.
Dingle,R.V., Scrutton,R.A. (1974) Continental breakup and the development of post-Paleozoic sedimentary basins around Africa. Geol. Soc. Am. Bull.,v85, 1467-
----------, Goodlad,S.W., Martin,A.K. (1978) Bathymetry and stratigraphy of the northern Natal valley (SW Indian Ocean):

A preliminary account. Marine Geology, v28, 89-106.
Dixey,F. (1929) The rocks of the Lupata Gorge and the north side of the lower Zambezi. Geol. Mag.,v66, 241-259.
Donaldson,C.H. (1976) An experimental investigation of olivine morphology. Contrib. Mineral. Petrol.,v57, 187-213.
----------, Brown,R.W. (1977) Refractory megacrysts and magnesium-rich melt inclusions within spinel in oceanic tholeiites: indicators of magma mixing and parental magma composition. Earth Planet. Sci. Lett.,v37, 81-89.
Dowsett,J.W., Reid,N.T. (1967) An exploration programme for nickel and copper in differentiated intrusives of East Griqualand and Transkei. Trans. Geol. Soc. S. Afr.,v70, 67-79.
Drever,H.I., Johnston,R. (1957) Crystal growth of forsteritic olivine in magmas and melts. Trans. Roy. Soc. Edinb.,v63, 289-315.
Drysdall,A.R., Weller,R.K. (1966) Karoo sedimentation in northern Rhodesia. Trans. Geol. S.Afr.,v69, 39-69.
Duke,J.M. (1976) Distribution of the period four transition elements among olivine, calcic-clinopyroxene and mafic silicate liquid: experimental results. J. Petrol.,v19, 499-521.
Duncan,A.R., Erlank,A.J. (1979) Regional geochemistry of the Karoo volcanics. Geokong. 79, Abstr., 18th Cong. Geol. Soc. S. Afr., 128-131.
Duncan,R.A., Green,D.H. (1980) Role of multistage melting in the formation of oceanic crust. Geology, v8, 22-26.
Dungan,M.A., Rhodes,J.M. (1978) Residual glasses and melt inclusions in basalts from DSDP legs 45 and 46 : Evidence for magma mixing. Contrib. Mineral. Petrol.,v67, 417-431.
Du Toit,A.L. (1904) Geological survey of Aliwal North, Heschel, Barkly East and Wodehouse. 9th Ann. Rep. Geol. Comm. Colony Cape of Good Hope, 69-100.
---------- (1911) Report on the geological survey of part of the Stormbergen. 16th Ann. Rep. Geol. Comm. Colony Cape of Good Hope, 112-136.
---------- (1929) The volcanic belt of the Lebombo: a region of tension. Trans. Roy. Soc. S. Afr.,v18, 189-218.
---------- (1954) THE GEOLOGY OF SOUTH AFRICA 3rd Edn. Oliver and Boyd, London.
Eales,H.V. (1974) The occurence and geological significance of quartz paramorphs after tridymite in the north-eastern Cape. Trans. Geol. Soc. S. Afr.,v77(1), 37-51.
---------- (1979) Anomalous Karoo spinels along the chromite-titanomagnetite join. S. Afr. J. Sci.,v75, 24-29.
----------, Booth,P.W.K. (1974) The Birds River Gabbro Complex, Dordrecht District. Trans. Geol. Soc. S. Afr.,v77(1), 1-16.
----------, Robey,J. van A. (1976) Differentiation of tholeiitic Karoo magma at Birds River, South Africa. Contrib. Mineral. Petrol.,v56, 101-117.
----------, Marsh,J.S. (1979) High-Mg tholeiitic rocks and their significance in the Karoo Central Province. S. Afr. J. Sci., 400-404.
----------, Snowden,D.V. (1979) Chromiferous spinels of the Elephant's Head dike. Mineralium Deposita, (In Press)

Eggler,D.H. (1974) Effect of CO2 on the melting of peridotite. Carnegie Inst. Wash. Yearb.,v73, 215-223.

---------- (1975) CO2 as a volatile component of the mantle : the system Mg2SiO4-SiO2-H2O-CO2. In Ahrens,L.H., Dawson,J.B., Duncan,A.R., Erlank,A.J. (Eds.), PHYSICS AND CHEMISTRY OF THE EARTH v9, 869-882. Pergamon Press, New York.

---------- (1978) The effect of CO2 upon partial melting of peridotite in the system Na2O-CaO-Al2O3-MgO-SiO2-CO2 to 35kb, with an analysis of melting in a peridotite-H2O-CO2 system. Am. J. Sc.,v278, 305-343.

Elliot,D.H., Watts,D.R. (1974) The nature and origin of volcaniclastic material in some Karoo and Beacon rocks. Trans. Geol. Soc. S. Afr.,v77, 109-111.

Ellis,D. (1976) High pressure cognate inclusions in the newer volcanics of Victoria. Contrib. Mineral. Petrol.,v58. 149-180.

Elthon,D. (1979) High magnesia liquids as the parental magma for ocean floor basalts. Nature, v278, 514-518.

Erlank,A.J. (1973) Kimberlitic potassic richterite and the distribution of potassium in the upper mantle. Int. Kimb. Conf. Abstr., 103-106. Univ. of Cape Town.

---------- (1976) Upper mantle metasomatism as revealed by potassic richterite bearing peridotite xenoliths from kimberlites. EOS,v57, 597.

----------, Hofmeyr,P.K. (1966) K/Rb and K/Cs ratios in Karoo dolerites from South Africa. J. Geophys. Res.,v71,5439-5445.

----------, ---------- (1968) K/Rb ratios in Mesozoic tholeiites from Antarctica, Brazil and India. Earth Planet. Sci. Lett.,v4, 33-38.

----------, Reid,D.L. (1974) Geochemistry, mineralogy and petrology basalts, Leg 25, Deep Sea Drilling Project. In: Simpson,E.S.W.,Schlich,R. (Eds.), INITIAL REPORTS OF THE DEEP SEA DRILLING PROJECT, v25, 543-551, Washington.

----------, Kable,E.J.D. (1976) The significance of incompatible elements in Mid-Atlantic Ridge basalts from 45 N, with particular reference to Zr/Nb. Contrib. Mineral. Petrol., v54, 281-291.

----------, Rickard,R.S. (1977) Potassic richterite bearing peridotites from kimberlite and the evidence they provide for upper mantle metasomatism. Second. Int. Kimb. Conf., Extnd. Abstr.

----------, Shimizu,N. (1977) Strontium and strontium isotope distributions in some kimberlite nodules and minerals. Second Int. Kimb. Conf., Extnd. Abstr.

----------, Allsopp,H.L., Duncan,A.R., Bristow,J.W. (1980) Mantle heterogeneity beneath southern Africa: evidence from the volcanic record. Phil. Trans. Roy. Soc. Lond.,v297, 295-307.

Ewart,A., Taylor,S.R., Capp,A.C. (1968) Trace and minor element geochemistry of the rhyolitic volcanic rocks, Central North Island, New Zealand. Contrib. Mineral. Petrol.,v18, 76-104.

--------, ---------- (1969) Trace element geochemistry of the rhyolite volcanic rocks, Central North Island, New Zealand. Phenocryst data. Contrib. Mineral. Petrol.,v22, 127-146.

Fairburn,H.W., Hurley,P.M. (1971) Evaluation of X-Ray fluorescence and mass spectometric analyses of Rb and Sr in some silicate standards. Geochim. Cosmochim. Acta.,v35, 149-156

Faure,G. (1977) PRINCIPLES OF ISOTOPE GEOLOGY. John Wiley and Sons, New York.

--------, Hurley,P.M. (1963) The isotopic composition of strontium in oceanic and continental basalts: application to the origin of igneous rocks. J. Petrol.,v4, 31-50.

--------, Powell,J.L. (1972) STRONTIUM ISOTOPE GEOLOGY. Springer Verlag.

--------, Hill,R.L. Jones,L.M., Elliot,D.H. (1972) Isotope composition of strontium and silica content of Mesozoic basalt and dolerite from Antartica. In: Adie,R.H. (Ed.), ANTARTIC GEOLOGY AND GEOPHYSICS, 617-624. Oslo, Universiteitsforlaget.

--------, Bowman,J.R., Elliot,D.H., Jones,L.M. (1974) Sr-isotope composition and petrogenesis of the Kirkpatrick basalt, Queen Alexandra range, Antarctica. Contrib. Mineral. Petrol.,v48, 153-169.

--------, ----------, ----------, (1979) The initial 87Sr/86Sr ratios of the Kirwan volcanics of Dronning Maud Land: Comparison with the Kirkpatrick basalt, Transantarctic Mountains. Chem. Geol.,v26, 77-90.

Fitch,F.J., Miller,J.A. (1971) Potassium-argon radioages of Karoo volcanic rocks from Lesotho. Bull. Volc.,v35, 64-84.

Fleck,R.J., Sutter,J.F. Elliot,D.H. (1977) Interpretation of discordant 40Ar/39Ar age-spectra of Mesozoic tholeiites from Antarctica. Geochim. Cosmochim. Acta.,v41, 15-32.

Flores,G. (1964) On the age of the Lupata rocks, lower Zambezi river, Mocambique. Trans. Geol. Soc. S. Afr.,v67, 111-118.

---------- (1970) Suggested origin of the Mozambique Channel. Trans. Geol. Soc. S. Afr.,v73, 1-17.

---------- (1973) The Cretaceous and Tertiary sedimentary basins of Mozambique and Zululand. In: Blant,G. (Ed.), SEDIMENTARY BASINS OF THE AFRICAN COASTS, 81-111, Assoc. Afr. Geol. Surveys, Paris.

Flower,M.F.J., Schmincke,H.-U., Thompson,R.N. (1975) Phlogopite stability and the 87Sr/86Sr step in basalts along the Reykjanes Ridge. Nature,v254, 404-406.

Foland,K.A., Henderson,C.M.B. (1976) Application of age and Sr isotope data to the petrogenesis of the Marangudzi Ring Complex, Rhodesia. Earth Plan. Sc. Lett.,v29, 291-301.

Francis,D.M. (1976) Amphibole pyroxenite xenoliths: cumulate or replacement phenomena from the upper mantle, Nunivak Island, Alaska. Contrib. Mineral. Petrol.,v58, 51-61.

Frankel,J.J. (1950) A note on the vitrification of Karoo sediments by dolerite intrusions. Trans. Roy. Soc. S. Afr.,v32, 287-294.

---------- (1969) The distribution and origin of the Effingham rock type. Mem. Geol. Soc. Am.,v115, 149-173.

Frey,F.A., Green,D.H. (1974) The mineralogy, geochemistry and origin of lherzolite inclusions in Victorian basanites. Geochim. Cosmochim. Acta.,v38, 1023-1059.

---------, Bryan,W.B., Thompson,G. (1974) Atlantic Ocean Floor: Geochemistry and petrology of basalts from Legs 2 and 3 of Deep-Sea Drilling Project. J. Geophys. Res.,v79, 5507-5527.

---------, Prinz,M. (1978) Ultramafic inclusions from San Carlos,

Arizona: Petrologic and geochemical data bearing on their petrogenesis. Earth Planet. Sci. Lett.,v38, 129-176.
----------, Green,D.H., Roy,S.D. (1978) Integrated models of basalt petrogenesis: A study of quartz tholeiites to olivine melilitites from south eastern Australia utilizing geochemical and experimental petrological data. J. Petrol.,v19(3), 463-513.
Frommurze,H.F. (1937) The water-bearing properties of the more important geological formations in the Union of South Africa. Mem. Geol. Surv. S. Afr.,v34.
Gast,P.W. (1968) Trace element fractionation and the origin of tholeiitic and alkaline magma types. Geochim. Cosmochim. Acta.,v32, 1057-1087.
----------, Tilton,G.R., Hedge,C. (1964) Isotopic composition of lead and strontium from Ascension and Gough Islands. Science, v145, 1181-1185.
Gevers,T.W. (1928) The volcanic vents of the western Stormberg. Trans. Geol. Soc. S. Afr.,v31, 43-62.
Gibb,F.G.F., Henderson,C.M.B. (1978) Possible high pressure relics within titaniferous augites in a basic sill. Geol. Mag.,v115(1), 55-62.
Gidkeshaug,A., Creer,K.M., Mitchell,J.G. (1975) Paleomagnetism and K-Ar ages of the South-West African basalts and their bearing on the time of initial rifting of the South Atlantic Ocean. Geophys. J. R. Astr. Soc.,v42, 1-20.
Glassley,W.E., Piper,D.Z. (1978) Cobalt and scandium partitioning versus iron content for crystalline phases in ultramafic nodules. Earth Planet. Sci. Lett.,v39, 173-178.
Glikson,A.Y. (1979) Early Precambrian Tonalite-Trondhjemite sialic nuclei. Earth Sci. Rev.,v15, 1-73.
Gough,D.I., Brock,A., Jones,D.L., Opdyke,N.D. (1964) The palaeomagnetism of the ring complexes at Marangduzi and the Mateke Hills. J. Geophys. Res.,v69, 2499-2507.
Green,D. (1966) The Karoo system in Bechuanaland. Bull. Geol. Surv. Bechuanaland, v2.
Green,D.H. (1971) Composition of basaltic magmas as indicators of conditions of origin: application to ocean volcanism. Phil. Trans. Roy. Soc. Lond.,v268, 707-725.
----------, Ringwood,A.E. (1967) The genesis of basaltic magmas. Contrib. Mineral. Petrol.,v15, 455-465.
----------, Nicholls,I.A., Viljoen,M., Viljoen,R. (1975) Experimental demonstration of the existence of peridotite liquids in earths Archean magmatism. Geology, v3, 11-14.
Green,H.W. (1972) A CO2 charged asthenosphere. Nature, v238, 2-5.
Greenland,P.L. (1970) An equation for trace element distribution during magmatic crystallization. Am. Mineral.,v55, 455-465.
Hakli,T.A., Wright,T.L. (1967) The fractionation of Ni between olivine and augite as a geothermometer. Geochim. Cosmochim. Acta.,v31, 877-844.
Hamilton,J. (1977) Isotope and trace element studies of the Great Dyke and Bushveld Mafic Phase and their relation to early Proterozoic magma genesis in southern Africa. J. Petrol.,v18, 24-52.
Harris,P.G., Hutchinson,R., Paul,D.K. (1972) Plutonic xenoliths

and their relation to the upper mantle. Phil. Trans. Roy. Soc. Lond.,A,v271, 313-323.
Hart,S.R., Brooks,C. (1974) Clinopyroxene-matrix partitioning of K,Rb,Cs,Sr,Ba. Geochim. Cosmochim. Acta.,v38. , 1799-1806.
----------, Davis,K.E. (1978) Nickel partitioning between olivine and silicate melt. Earth Planet. Sci. Lett.,v40, 203-219.
Harte,B., Gurney,J.J. (1975) Ore mineral and phlogopite mineralization within ultramafic nodules from the Matsoku kimberlite pipe, Lesotho. Carnegie Inst. Wash. Yb.,v74, 528-536.
---------, Cox,K.G., Gurney,J.J. (1975) Petrology and geological history of upper mantle xenoliths from the Matsoku kimberlite pipe. In: Ahrens,L.H., Dawson,J.B., Duncan,A.R., Erlank, A.J.,(Eds.) PHYSICS AND CHEMISTRY OF THE EARTH 9, 477-506. Pergamon Press.
Hawkesworth,C.J., Vollmer,R. (1979) Crustal contamination versus enriched mantle: 143Nd/144Nd and 87Sr/86Sr evidence from the Italian volcanics. Contrib. Mineral. Petrol.,v69, 151-165.
----------, O'Nions,R.K., Arculus,R.J. (1979a) Nd and Sr isotope geochemistry of island and volcanics, Granada, Lesser Autilles. Earth Planet. Sci. Lett.,v45, 237-248.
----------, Norry,M.J., Roddick,J.C., Vollmer,R. (1979b) 143Nd/144Nd and 87Sr/86Sr ratios from the Azores and their significance in LIL-element enriched mantle. Nature, v280, 28-31.
Hawthorne,J.B., Carrington,A.J., Clement,C.R., Skinner,E.W. (1979) Geology of the Dokolwayo Kimberlite and associated paleo-alluvial diamond deposits. In: Boyd,F.R., Meyer,H.O.A.,(Eds.), KIMBERLITES DIATREMES AND DIAMONDS, Proceed. Second. Int. Kimb. Conf.,v1, 59-70. A.G.U., Washington.
Hazzard,J.C., Morris,A.E.L., Wissler,S.G. (1971) Petroleum developments in central and southern Africa in 1970. Am. Assoc. Pet. Geol., Bull.,v55, 1559-1602.
Hedge,C.E., Walthall,F.G. (1963) Radiogenic strontium-87 as an index of geologic processes. Science, 140, 1214-1217.
Heier,K.S., Compston,W., McDougall,I. (1965) Thorium and uranium concentrations and the isotopic composition of strontium in the differentiated Tasmanian dolerites. Geochim. Cosmochim. Acta, v29, 643-659.
Heinrich,K.F.J. (1966) X-Ray absorption uncertainty. In: McKinley,T.D., Heinrich,K.F.J., Wittry,D.B. (Eds.), THE ELECTRON MICROPROBE, 269-377, Wiley and Sons, London.
Henderson,J.McC. (1909) Notes on some rocks in the volcanic series of the Karoo System in the Lebombo Mountains. Trans Geol. Soc. S. Afr.,v12, 24-31.
Henderson,P. (1977) Effect of silicate melt structure on mineral melt partitioning. Can. Mineral.,v15, 202.
Himmelberg,G.R.,Loney,R.A. (1971) Petrology of the Vulcan Peak alpine-type peridotite, S.W. Oregan. Bull. Geol. Soc. Am., v84, 1585-1600.
Hodgson,F.D.I., Botha,B.J.V. (1974) The Doros Complex, South West Africa. Neues Jb. Miner.,v9, 398-418.
Hofmann,A.W. (1974) Strontium diffusion in a basalt melt and implications for Sr-isotope geochemistry and geochronology. Carnegie. Inst. Wash. Yearb.,v73, 935-941.
---------- (1975) Diffusion of Ca and Sr in a basalt melt.

Carnegie. Inst. Wash. Yearb.,v75, 259-262.
----------, Magaritz,M. (1977) Diffusion of Ca,Sr,Ba and Co in a basalt melt: Implications for the geochemistry of the mantle. J. Geophys. Res.,v82, No.33, 5432-5440.
----------, Hart,S.R. (1978) An assessment of local and regional isotopic equilibrium in the mantle. Earth Planet. Sci. Lett.,v38, 44-62.
Ho Tun,E. (1979) Volcaniclastic material in Lower Beaufort Group Karoo rocks. Geokong. 79, Abstr., 18th Cong. Geol. Soc. S. Afr., 197-199.
Huntingdon,A.T. (1973) The collection and analysis of volcanic gas from Mount Etna. Phil. Trans. Roy. Soc. Lond.,v274, 119-128.
Hurley,P.M., Fairbairn,H.W., Pinson,W.H. (1966) Rb-Sr isotope evidence in the origin of potash-rich lavas from western Italy. Earth Planet. Sci. Lett.,v5, 301-306.
Hutchinson,R., Dawson,J.B. (1970) Rb,Sr and 87Sr/86Sr in ultra-basic xenoliths and host rocks, Lashine Volcano, Tanzania. Earth Planet. Sci. Lett.,v9, 87-92.
Irvine,T.N., Kushiro,I. (1976) Partitioning of Ni and Mg between olivine and silicate liquids. Carnegie Inst. Wash. Yearb.,v75, 668-675.
Irving,A.J. (1971) GEOCHEMICAL AND HIGH PRESSURE EXPERIMENTAL STUDIES OF XENOLITHS, MEGACRYSTS AND BASALT FROM SOUTHEASTERN AUSTRALIA. Ph.D. Thesis (unpubl.), Australian Nat. Univ.
Ito,K., Kennedy,G.C. (1968) Melting and phase relations in the plane tholeiite lherzolite-nepheline basanite to 40 kilobars, with geological implications. Contrib. Mineral. Petrol.,v19, 177-211.
Jacobsen,J.B.E., McCarthy,T.S. (1975) Possible late Karoo carbonatite and basalt intrusions at Messina, Transvaal. Trans. Geol. Soc. S. Afr.,v78, 153-159.
----------, Rex,D.C., Sevenster,W.J. (1975) K-Ar ages of some mafic dykes from the Messina district, Transvaal. Trans. Geol. Soc. S. Afr.,v78, 359-360.
Jakobsson,P., Jonsson,J., Shido,F. (1978) Petrology of the Western Reykjanes Peninsula, Iceland. J. Petrol.,v19, 669-705.
Jamieson,B.G. (1966) Evidence of the evolution of basaltic magma at elevated pressures. Nature, v212, 243-246.
---------- (1969) THE PETROLOGY OF OLIVINE-RICH BASALTIC ROCKS, NUANETSI, RHODESIA. Ph.D. Thesis (unpubl.), Univ. Edinburgh.
---------- (1970) Phase relations in some tholeiitic lavas illustrated by the system R2O3-XO-YO-ZO2. Min.Mag.,v37 537-554.
----------, Clarke,D.B. (1970) Potassium and associated elements in tholeiitic basalts. J. Petrol.,v11(2), 183-204.
Jansen,H. (1975) The Soutpansberg trough (Northern Transvaal) - an aulacogen. Trans. Geol. Soc. S. Afri.,v78, 129-136.
Jaritz,W., Kreuzer,H., Muller,P., Harre,W. (1977) Die vulkanitserien im kustengebiet von Nordmocambique. Geol. Jb.,v26., 147-165.
Johnson,R.L. (1961) The geology of the Dorowa and Shawa carbon-

atite complexes, southern Rhodesia. Trans. Geol. Soc. S. Afr.,v64, 101-146.
---------- (1966) The Shawa and Dorowa carbonatite complexes, Rhodesia. In: Tuttle,O.F., Gittens,J. (Eds.), CARBONATITES. 205-224, John Wiley and Sons, London.
Joplin,G.A. (1968) The shoshonite association: a review. J. Geol. Soc. Aust.,v15(2), 275-294.
Jordan,T.H. (1978) Composition and development of the continental tectosphere. Nature,v274, 544-548.
Kent,P.E. (1972) Mesozoic history of the east coast of Africa. Nature, v238, 147-148.
---------- (1974) Continental margin of East Africa - a Region of vertical movement. In: Burk,C.A., Drake,C.L. (Eds.), THE GEOLOGY OF CONTINENTAL MARGINS, 313-320. Springer, New York.
Kesson,S.E. (1973) The primary geochemistry of the Manaro alkaline volcanics, southeastern Australia - Evidence for upper mantle heterogeneity. Contrib. Mineral. Petrol.,v42, 93-108.
----------, Price,R.C. (1972) The major and trace element chemistry of kaersutite and its bearing on the petrogenesis of alkaline rocks. Contrib. Mineral. Petrol.,v35, 110-124.
King,B.C. (1965) Petrogenesis of the alkaline igneous rock suites of the volcanic and intrusive centres of E.Uganda. Jl. Petrol.,v6, 67-100.
Knutson,J., Green,T.H. (1975) Experimental duplication of a high-pressure megacryst/cummulate assemblage in a near saturated Hawaiite. Contrib. Mineral. Petrol.,v52, 121-132.
Korn,H., Martin,H. (1954) The Messum igneous complex in South West Africa. Trans. Geol. Soc. S. Afr.,v57, 83-124.
Korringa,M.K., Noble,D.C. (1971) Distribution of Sr between natural feldspar and igneous melt. Earth Planet. Sci. Lett., v11, 147-151.
Kramers,J.D. (1977) Lead and Strontium isotopes in Cretaceous kimberlites and mantle derived xenoliths from southern Africa. Earth Planet. Sci. Lett.,v34, 419-413.
---------- (1979) Lead, uranium, strontium, potassium and rubidium in inclusion-bearing diamonds and mantle-derived xenoliths from southern Africa. Earth Planet. Sci. Lett., v42, 58-70.
Kretz,R. (1961) Some applications of thermodynamics to co-existing minerals of variable composition: orthopyroxene-clinopyroxene and orthopyroxene-garnet. J. Geol.,v69, 361-387.
-------- (1963) Distribution of magnesium and iron between orthopyroxene and calcic pyroxene in natural assemblages. J. Geol.,v71, 773-785.
Krishnamurthy,P., Cox,K.G. (1977) Picrite basalts and related lavas from the Deccan Traps of Western India. Contrib. Mineral. Petrol.,v62, 53-75.
Kushiro,I. (1972) Effect of water on the compositions of magmas formed at high pressures. J. Petrol.,v13, 311-334.
---------- (1973) Partial melting of garnet lherzolites from Kimberlite at high pressures. In: Nixon,P. (Ed.), LESOTHO KIMBERLITES, 294-299.
----------, Erlank,A.J. (1970) Potassium contents of synthetic pyroxenes at high temperatures and pressures. Carnegie Inst.

Wash. Yb.,v68, 233-236.
Kyle,P.R. (1980) Development of heterogeneities in the sub-continental mantle: Evidence from the Ferrar Group, Antarctica. Contrib. Mineral. Petrol.,v73(1), 89-104.
Kynaston,H. (1907) The geology in the neighbourhood of Komati Poort. Trans. Geol. Soc. S. Afr.,v9, 19-31.
Langmuir,C.H., Bender,J.F., Bence,A.E., Hanson,G.N. (1977) Petrogenesis of basalts from the FAMOUS area: Mid-Atlantic Ridge. Earth Planet. Sci. Lett.,v36, 133-156.
Leeman,W.P. (1974) EXPERIMENTAL DETERMINATION OF PARTITIONING OF DIVALENT CATIONS BETWEEN OLIVINE AND BASALTIC LIQUID. Ph.D. Thesis, P.II (unpubl.) Univ. Oregon.
---------- (1977) Comparison of Rb/Sr, U/Pb and rare earth characteristics of sub-continental and sub-oceanic mantle regions. In: Dick,H.J.B. (Ed.) MAGMA GENESIS, 149-168. Oregon Dept. Geol. Mineral. Indst. Bull.96.
----------, Lindstrom,D.J. (1978) Partitioning of Ni2+ between basaltic and synthetic melts and olivines - an experimental study. Geochim. Cosmochim. Acta, v42, 801-816.
----------, Ma,M.-S., Murali,A.V., Schmitt,R.A. (1978) Emperical estimation of magnetite/liquid distribution coefficients for some transition elements. Contrib. Mineral. Petrol.,v65, 269-272.
Le Maitre,R.W. (1976) The chemical variability of some common igneous rocks. J. Petrol.,v17(4), 589-598.
Le Roex,A.P (1980) GEOCHEMISTRY AND MINERALOGY OF SELECTED ATLANTIC OCEAN BASALTS. Ph.D. Thesis (unpubl.) Univ. of Cape Town.
----------, Reid,D.L. (1978) Geochemistry of Karoo dolerite sills in the Calvinia District, Western Cape Province, South Africa. Contrib. Mineral. Petrol.,v66, 351-360.
Lightfoot,B. (1938) Notes on the south-eastern part of southern Rhodesia. Trans. Geol. Soc. S. Afr.,v41, 193-198.
Lindstrom,D.J. (1976) EXPERIMENTAL STUDY OF THE PARTITIONING OF THE TRANSITION METALS BETWEEN CLINOPYROXENE AND COEXISTING SILICATE LIQUIDS. Ph.D. Thesis (unpubl.) Univ. Oregon.
----------, Weill,D.F. (1978) Partitioning of transition metals between diopside and coexisting silicate liquids I: Nickel, cobalt and manganese. Geochim. Cosmochim. Acta., v42, 817-831.
Linning,K. (1968) DIE STOLLINGSKOMPLEKS KAAP KRUIS, SUIDWES-AFRIKA. M.Sc. Thesis (unpubl.), Univ. of Pretoria.
Lloyd,F.E., Bailey,D.K. (1975) Light element metasomatism of the continental mantle: the evidence and the consequences. In: Ahrens,L.H., Dawson,J.B., Duncan,A.R. Erlank,A.J., (Eds.), PHYSICS AND CHEMISTRY OF THE EARTH,9, 389-416. Pergamon, N.Y.
Lock,B.E., Paverd,A.L., Broderick,T.J. (1974) Stratigraphy of the Karoo volcanic rocks of the Barclay East district. Trans. Geol. Soc. S. Afr.,v77, 117-130.
Lombaard,B.V. (1952) Karoo dolerites and lavas. Trans. Geol. Soc. S. Afr.,v55, 175-198.
Longhi,J., Walker,D., Hays,J.F. (1978) The distribution of Fe and Mg between olivine and linear basaltic liquids. Geochim. Cosmochim. Acta.,v42, 1545-1558.
Maaloe,S. (1979) Compositional range of primary tholeiitic magmas

evaluated from major element trends. Lithos, v12, 59-72.
MacDonald,R. (1967) Geochemical and petrographic provinces of Karoo basalts. Proc. Geol. Soc. Lond.,v1637, 44-45.
Mackenzie,D.E., Chappell,B.W. (1972) Shoshonitic and calc-alkaline lavas from the Highlands of Papua New Guinea. Contr. Mineral. Petrol.,v35, 50-62.
Manson,V. (1967) Geochemistry of basaltic rocks: Major elements. In: Hess,H.H., Poldervaart,A. (Eds.), BASALTS,v1, 215-270, Interscience Publishers, New York.
Manton,W.I. (1968) The origin of associated basic and acid rocks in the Lebombo-Nuanetsi igneous province, southern Africa, as implied by strontium isotopes. J. Petrol.,v9, 23-39.
---------- (1973) Whole rock Th-Pb age for the Masukwe and Dembe-Divula Complexes, Rhodesia. Earth Planet. Sci. Lett., v19, 83-89.
----------, Tatsumoto,M. (1971) Some Pb and Sr isotopic measurements on eclogites from the Roberts Victor Mine, South Africa. Earth Planet. Sci. Lett.,v10, 217-226.
Marsh,J.S. (1975) The Luderitz alkaline province, South West Africa I: Descriptive petrology of the Granitberg toyaite complex. Trans. Geol. Soc. S. Afr.,v78, 215-224.
---------- (1976) The Luderitz alkaline province, South West Africa, II: The Pomona and Drachenberg syenite complexes. Trans. Geol. Soc. S. Afr.,v79, 168-176.
----------, Erlank,A.J., Duncan,A.R., Miller,R.McG. (1978) Igneous activity accompanying separation of Africa from South America: the magmatic record of a successful Mesozoic record. Int. Symp. Rio. Grande Rift, Progm. Abstr., 56-59, Sante Fe.
Martini,J.E.J. (1974) On the presence of ash beds and volcanic fragments in the graywackes of the Karoo system in the southern Cape Province, South Africa. Trans. Geol. Soc. S. Afr.,v77, 113-116.
Maske,S. (1966) The petrography of the Ingeli Mountain Range. Ann. Univ. Stellenbosch, v41, 1-109.
Mathias,M. (1956) The petrology of the Messum igneous complex, South West Africa. Trans. Geol. Soc. S. Afr.v59, 23-56.
---------- (1957) The geochemistry of the Messum igneous complex, South West Africa. Geochim. Cosmochim. Acta.,v12, 29-46.
McDougall,I. (1963) Potassium-Argon age measurements on dolerites from Antarctica and South Africa. J. Geophys. Res.,v68(5), 1535-1545.
---------- (1976) Geochemistry and origin of basalts of the Columbia River Group, Oregon and Washington. Geol. Soc. Am. Bull.,v87, 777-792.
Medaris,L.G. (1969) Partitioning of Fe2+ and Mg2+ between coexisting synthetic olivine and orthopyroxene. Ibid.,v267, 945-968.
Meijs,L. (1960) Dolerite dykes in Basutoland. Pius XI Papers, No. 1, 54p. Roma, Basutoland.
Mennel,F.P. (1930) Reference in Lightfoot,B. (1938) Trans. Geol. Soc. S. Afr.,v41, 193-198.
---------- (1938) The igneous rocks of the Sabi basin, S.E. Mashonaland. Proceed. Rhod. Sci. Ass.,v36, 9-19.

Menzies,M. (1977) Residual Alpine lherzolites and harzburgites: geochemical and isotopic constraints on their origin. In: Dick,H.J.B.,(Ed.) MAGMA GENESIS, 129-147. State of Oregon, Dept. Geol. Min. Ind., Bull,96.

Mitchell,A.A. (1979) PETROLOGY AND GEOCHEMISTRY OF KAROO BASALTS AND DOLERITES OF THE MOLTENO AREA. M.Sc. Thesis (unpubl.), Univ. of Rhodes.

Mitchell,R.H. (1975) Theoretical aspects of gaseous and isotopic equilibria in the system C-H-O-S with application to kimberlites. Phys. Chem. Earth.,v9, 903-915.

---------- Crockett,J.H. (1971) The isotopic composition of strontium in some South African kimberlites. Contrib. Mineral. Petrol.,v30, 277-290.

----------, Brunfelt,A.O., Nixon,P.H. (1973) Trace elements in magnesian ilmenites from Lesotho kimberlites. In: Nixon, P.H. (Ed.), LESOTHO KIMBERLITES, 230-235, Lesotho National Development Corporation.

----------, ----------, (1975) Rare earth element geochemistry of kimberlite. In: Ahrens,L.H., Dawson,J.B., Duncan, A.R., Erlank,A.J. (Eds.) PHYSICS AND CHEMISTRY OF THE EARTH, v9, 671-686, Pergamon Press.

Molengraaf,G.A.F. (1898) Report of the State Geologist of the South African Republic for the year 1897. Trans. Geol. Soc. S. Afr.,v4, 119-147.

Moller,P., Morteani,G., Schley,F. (1980) Discussion of REE distribution patterns of carbonatites and alkalic rocks. Lithos,v13, 171-179.

Monkman,L.J. (1961) THE GEOLOGY OF THE MAOSE-MALIBANGWE RIVER BASINS, WITH SPECIAL REFERENCE TO THE STORMBERG VULCANICITY OF SOUTHERN RHODESIA. Ph.D. Thesis (unpubl.), Univ. Leeds.

Moore,A.C. (1965) The North Gap Dyke of the Transkei. Trans. Geol. Soc. S. Afr.,v68, 89-120.

Mountain,E.D. (1960) Felsic material in Karoo dolerites. Trans. Geol. Soc. S. Afr.,v63, 137-151.

Mueller,R.F. (1960) Compositional characteristics of equilibrium relations in mineral assemblages of a metamorphosed iron formation. Am. J. Sci.,v258, 449-497.

---------- (1961) Analysis of relations among Mg,Fe and Mn in certain metamorphic minerals. Geochim. Cosmochim. Acta., v28, 189-207.

Mysen,B.O. (1975) Partitioning of iron and magnesium between crystals and partial melts in peridotite upper mantle. Contrib. Mineral. Petrol.,v52, 69-76.

---------- (1976a) Partitioning of samarium and nickel between olivine, orthopyroxene and liquid: Preliminary data at 20kbar and 1205C. Earth Planet. Sci. Lett.,v31, 1-7.

---------- (1976b) Nickel partitioning between upper mantle crystals and partial melts as a function of pressure, temperature and nickel concentration. Carnegie Inst. Wash. Yearb.,v75, 662-668.

---------- (1978) Experimental determination of nickel partition coefficients between liquid, pargasite and garnet peridotite minerals and concentration limits of behaviour according to Henry's law at high pressure and temperature. Am. J. Sci., v278, 217-243.

----------, Boettcher,A.L. (1975a) Melting of a hydrous mantle:I. Phase relations of natural peridotite at high pressures and temperatures with controlled activities of water, carbon dioxide and hydrogen. J. Petrol.,v16(3), 520-548.
----------, ---------- (1975b) Melting of a hydrous mantle:II. Geochemistry of crystals and liquids formed by anatexis of mantle peridotite at high pressures and high temperatures as a function of controlled activities of water, hydrogen and carbon dioxide. J. Petrol.,v16(3), 549-593.
----------, Eggler,D.H., Seitz,M.G., Holloway,J.R. (1976) Carbon dioxide in silicate melts and crystals. Part I. Solubility measurements. Am. J. Sci.,v276, 455-479.
----------, Kushiro,I. (1979) Pressure dependance of nickel partitioning between forsterite and aluminous silicate melts. Earth Planet. Sci. Lett.,v42, 383-388.
Nathan,H.D., van Kirk,C.K. (1978) A model of magmatic crystallisation. J. Petrol.,v19(1), 66-94.
Nesbitt,R.W. (1971) Skeletal crystal forms in the ultramafic rocks of the Yilgarn Block, Western Australia : evidence for an Archaean Ultramafic liquid. Spec. Publ. Geol. Soc. Australia, v3, 331-350.
----------, Mastins,H., Stolz,G.W., Bruce,D.R. (1976) Matrix corrections in trace-element analyses by XRF : An extension of the Compton scattering technique to long wavelengths. Chem. Geol.,v18, 203-213.
Neuman,E.R. (1976) Two refinements for the calculation of structural formulae for pyroxenes and amphiboles. Nor. Geol. Tidskrf.,v56, 1-6.
Nicolaysen,L.O., Burger, A.J., Johnson,R.L. (1962) The age of Shawa Carbonatite complex. Trans. Geol. Soc. S. Afr., v65, 293-294.
Nisbet,E.G., Bickle,M.J., Martin,A. (1977) The mafic and ultramafic lavas of the Belingwe Greenstone belt, Rhodesia. J. Petrol.,v18,521-566.
Nockolds,S.R., Allen,R. (1956) The geochemistry of some igneous rock series - III. Geochim. Cosmochim. Acta.,v9, 34-77.
Norrish,K., Chappell,B. (1967) X-ray flourescence spectrography. In: Zussman,J. (Ed.), PHYSICAL METHODS IN DETERMINATIVE MINERALOGY. Academic Press.
----------, Hutton,J.T. (1969) An accurate X-ray spectrographic method for the analysis of a wide range of geological samples. Geochim. Cosmochim. Acta.,v33, 431-453.
Norry,M.J. (1977) GEOCHEMICAL STUDIES OF VOLCANICS FROM THE KAROO, MAURITIUS AND THE ADEN VOLCANO. D.Phil. Thesis (unpubl.), Univ. Oxford.
O'Hara,M.J. (1963) Distribution of iron between coexisting olivines and calcium-poor pyroxenes in peridotite, gabbros and other magnesian environments. Am. J. Sci.,v261, 32-46.
---------- (1965) Primary magmas and the origin of basalts. Scott. J. Geol.,v1, 19-40.
---------- (1968a) The bearing of phase equilibria studies in synthetic and natural systems on the origin and evolution of basic and ultrabasic rocks. Earth Sci. Rev.,v4, 69-133.
---------- (1968b) Are ocean floor basalts primary magma? Nature, v220, 683-686.

---------- (1973) Non-primary magmas and dubious mantle plume beneath Iceland. Nature, v243, 507-508.
---------- (1977) Geochemical evolution during fractional crystallisation of a periodically refilled magma chamber. Nature, v2266, 503-507.
----------, Mercy,E.L.P. (1963) Petrology and petrogenesis of some garnetiferous peridotites. Trans. Roy. Soc. Edinb., v65, 251-314.
O'Nions,R.K., Clarke,D.B. (1972) Comparative trace element geochemistry of Tertiary basalts from Baffin Bay. Earth Planet. Sci. Lett.,v15, 436-446.
----------, Pankhurst,R.J. (1973) Secular variation on the Sr-isotope composition of Icelandic volcanic rocks. Earth Planet. Sci. Lett.,v21, 13-21.
----------, ---------- (1974) Petrogenetic significance of isotope and trace element variation in volcanic rocks from the Mid-Atlantic. J. Petrol.,v15, 603-634.
----------, ----------, Gronvold,K. (1976) Nature and development of basalt magma sources beneath Iceland and the Reykjanes Ridge. J. Petrol.,v17(2), 315-338.
----------, Hamilton,P.J., Evensen,N.M. (1977) Variation in 143Nd/144Nd and 87Sr/86Sr ratios in oceanic islands. Earth Planet. Sci. Lett.,v34, 13-22.
----------, Evenson,N.M., Hamilton,P.J., Carter,S.R. (1978) Melting of the mantle past and present: isotope and trace element evidence. Phil. Trans. R. Soc. Lond.,v258, 547-559.
Pankhurst,R.J. (1969) Strontium isotope studies related to petrogenesis in the Caledonian basic igneous province of northeast Scotland. J. Petrol.,v10, 115-143.
----------, O'Nions,R.K. (1973) Determination of Rb/Sr and 87Sr/86Sr ratios of some standard rocks and the evaluation of X-Ray fluorescence spectrometry in Rb-Sr geochemistry. Chem. Geol.,v12, 127-136.
Paster,T.P., Schauwecker,D.S., Haskin,L.A. (1974) The behavior of some trace elements during solidification of the Skaergaard layered series. Geochim. Cosmochim. Acta.,v38, 1549-1577.
Patchett,P.J. (1980) Thermal effects of basalt on continental crust and crustal contamination of magmas. Nature, v283, 559-561.
Pearce,J.A., Cann,J.R. (1973) Tectonic setting of basic volcanic rocks determined using trace element analysis. Earth Planet. Sci. Lett.,v19, 290-300.
----------, Norry,M.J. (1979) Petrogenetic implication of Ti, Zr,Y, and Nb variations in volcanic rocks. Contrib. Mineral. Petrol.,v69, 33-47.
Peccerillo,A., Taylor,S.R., (1976) Geochemistry of upper Cretaceous volcanic rocks from the Pontic Chain, Northern Turkey. Bull. Volc.v39(4), 557-569.
Pemberton,J. (1978) THE GEOCHEMISTRY AND PETROLOGY OF KAROO BASALTS OF THE BARKLY EAST AREA, NORTH-EASTERN CAPE. M.Sc Thesis (unpubl.), Univ. of Rhodes.
Peterman,Z.E., Carmichael,I.S.E., Smith,A.L. (1970) Strontium isotopes in quarternary basalts of southwestern California. Earth Planet. Sci. Lett.,v7, 381-384.

Philpotts,J.A., Schnetzler,C.C. (1970) Phenocryst-matrix partitioning coefficients for K, Rb, Sr, and Ba, with application to anorthosite and basalt genesis. Geochim. Cosmochim. Acta.,v34, 307-322.

Poldervaart,A. (1952) Karoo dolerites and basalts in the eastern part of the Bechuanaland Protectorate. Trans. Geol. Sol. S. Afr.,v55, 125-130.

Prins,P. (1978) THE GEOCHEMICAL EVOLUTION OF THE ALKALINE AND CARBONATITE COMPLEXES OF THE DAMARALAND IGNEOUS PROVINCE, SOUTH WEST AFRICA. Ph.D. Thesis (unpubl.), Univ. Stellenbosch.

Prior,G.T. (1910) Petrographic notes on the dolerites and rhyolites of Natal and Zululand. Ann. Natal Mus.,v2, 141-157.

Pyke,D.R., Naldrett,A.J., Eckstrand,O.R. (1973) Archean ultramafic flows in Munro Township, Ontario. Bull. Geol. Soc. Am.,v84, 955-977.

Ramberg,H., De Vore,G.W. (1951) Distribution of Fe++ and Mg++ in coexisting olivines and pyroxenes. J. Geol.,v59, 193-210.

Reeves,C.V. (1978) A failed Gondwana spreading axis in southern Africa. Nature, v273, 222-223.

Reid,A.M., Donaldson,C.H., Brown,R.W., Ridley,W.I., Dawson,J.B. (1975a) Mineral chemistry of peridotite xenoliths from the Lashaine Volcano, Tanzania. In: Ahrens,L.H., Dawson,J.B., Duncan,A.R., Erlank,A.J. (Eds.), PHYSICS AND CHEMISTRY OF THE EARTH,v9, 525-544, Pergamon Press.

----------, ----------, Dawson,J.B., Brown,R.W., Ridley,W.I. (1975b) The Igwisi Hills extrusive 'kimberlite'. In: Ahrens, L.H., Dawson,J.B., Duncan,A.R., Erlank,A.J. (Eds.), PHYSICS AND CHEMISTRY OF THE EARTH,v9, 199-218, Pergamon Press.

Reid,D.L. (1977) GEOCHEMISTRY OF PRECAMBRIAN IGNEOUS ROCKS IN THE LOWER ORANGE RIVER REGION. Univ. Cape Town, Precamb. Res. Unit Bull.,v22, 394p.

Reynolds,R.C. (1963) Matrix correction in X-ray analysis. Am. Mineral.,v48, 1113-1143.

---------- (1967) Estimation of mass absorption coefficients by Compton scattering : Improvements and extensions of the method. Am. Mineral.,v52, 1493-1502.

Rhodes,R.C. (1972) Structural geometry of subvolcanic ring complexes as related to pre-Cenozoic motions of continental plates. Tectonophysics, v12, 111-117.

----------, Krohn,D.R. (1972) Tectonic control over regional geochemical variation in the Karoo basaltic province of southern Africa. Trans. Geol. Soc. S. Afr.,v75, 11-21.

----------, Bornhorst,R.J. (1976) Petrologic provinces in Jurassic tholeiites of Gondwanaland. Geol. Rundsch.,v65, 930-938.

Richardson,S.H. (1980) Chemical variation induced by flowage differentiation in an extensive Karoo dolerite sheet, southern Namibia. Geochim. Cosmochim. Acta.,v43, 1433-1441.

Ridley,W.I., Dawson,J.B. (1975) Lithopile trace element data bearing on the origin of peridotite xenoliths, aukaramite and carbonatite from Lashaine volcano, N. Tanzania. In: Ahrens,L.H., Dawson,J.B., Duncan,A.R., Erlank,A.J. (Eds.) PHYSICS AND CHEMISTRY OF THE EARTH, 9, 559-570. Pergamon, N.Y.

Ringwood,A.E. (1974) The petrological evolution of island arc systems. J. Geol. Soc. Lond.,v130, 183-204.
Robey,J. van A. (1976) ASPECTS OF THE GEOCHEMISTRY OF THE KAROO DOLERITES AND BASALTS OF THE NORTH EASTERN CAPE PROVINCE, SOUTH AFRICA. M.Sc. Thesis (Unpubl.), Univ. of Rhodes.
Roeder,E. (1965) Liquid CO2 inclusions in olivine-bearing nodules from basalts. Am. Mineral.,v36, 282-286.
Roeder,P.L. (1974) Activity of iron and olivine solubility in basaltic liquids. Earth Planet. Sci. Lett.,v23, 397-410.
----------, Emslie,R.F. (1970) Olivine-liquid equilibrium. Contrib. Mineral. Petrol.,v29, 275-289.
Rogers,A.W. (1925) Notes on the north-eastern part of the Zoutpansberg District. Trans. Geol. Soc. S. Afr.,v28, 33-53.
Rumble,K.C. (1979) THE GEOCHEMISTRY AND PETROLOGY OF THE KAROO ANDESITES AND ASSOCIATED BASALTS OF THE NORTH EASTERN CAPE PROVINCE. M.Sc. Thesis (unpubl.), Univ. Rhodes.
Ryan,P.J. (1968) Some conclusions drawn from a basin analysis of the Ecca Series in the Karoo basin. Palaeont. Afr., v11, 133-134.
Saggerson,E.P., Logan,C.T. (1970) Distribution controls of layered and differentiated mafic intrusions in the Lebombo volcanic sub-province. Geol. Soc. S. Afr., Spec. Publn.,v1, 721-733.
Sato,H. (1977) Nickel content of basaltic magma : identification of primary magmas and a measure of the degree of olivine fractionation. Lithos, v10, 113-120.
Sauvan,P., Esquevin,J., Chennaux,G. (1975) Transformations induites par des intrusions doleritiques dans une Serie Argileuse : L'ecca de Bergville (Afrique Du Sud). Bull. Centre. Rech. Pau - SNPA, v9(2), 261-351.
Scholtz,D.L. (1937) The magmatic nickeliferous ore deposits of East Griqualand and Pondoland. Trans. Geol. Soc. S. Afr., v39, 81-210.
Scrutton,R.A. (1976) Continental breakup and deep crustal structure at the margins of southern Africa. In: De Almeida, F.F.M. (Ed.), CONTINENTAL MARGINS OF ATLANTIC TYPE. Ann. Brazil. Acad. Sci.,v48, 169-177.
Shee,S.R. (1978) THE MINERAL CHEMISTRY OF XENOLITHS FROM THE ORAPA KIMBERLITE PIPE, BOTSWANA. M.Sc. Thesis (unpubl.), Univ. of Cape Town..
Shimizu,N. (1975) Geochemistry of ultramafic inclusions from Salt Lake Crater, Hawaii and from southern African kimberlites. In: Ahrens,L.H., Dawson,J.B., Duncan,A.R., Erlank,A.J. (Eds.), PHYSICS AND CHEMISTRY OF THE EARTH, 9, 655-670. Pergamon, N.Y.
Siedner,G., Mitchell,J.G. (1968) K-Ar determinations on basaltic rocks from South West Africa and their bearing on continental drift. Earth Planet. Sci. Lett.,v4, 451-458.
----------, ---------- (1976) Episodic Mesozoic volcanism in Namibia and Brazil : A K-Ar isochron study bearing on the opening of the South Atlantic. Earth Planet. Sci. Lett.,v30, 292-302.
Sigvaldason,G.E., Steinthorsson,N., Imsland,P. (1974) Compositional variation in recent Icelandic tholeiites and the Kverkfjoll hot spot. Nature, v251, 579-582.

Smith,H.S., Erlank,A.J., Duncan,A.R. Geochemistry of some ultramafic komatiite lava flows from Barberton Mountain Land, South Africa. Precambrian Res. (In press).

Stanton,R.L., Bell,J.D. (1969) Volcanic and associated rocks of the New Georgia Group, British Solomon Island Protectorate. Overseas Geol., Mineral Resources, v10, 113-145.

Steiger,R.H., Jager,E. (1977) Subcommission on geochronology : Convention on the use of decay constants in geo- and cosmochronology. Earth Planet. Sci. Lett.,v36, 359-362.

Stillman,C.J. (1959) THE GEOLOGY OF THE NORTHERN RING COMPLEX OF THE MATEKE HILLS, SOUTHERN RHODESIA. Ph.D. Thesis (unpubl.), Univ. Leeds.

Stockley,G.M. (1947) REPORT ON THE GEOLOGY OF BASUTOLAND. Basutoland Govt. Printer, Maseru.

Stratten,T. (1965) THE PYROCLASTIC AND ASSOCIATED IGNEOUS ROCKS OF THE LEBOMBO MOUNTAIN RANGE, SOUTH OF THE GREAT USUTU RIVER, ZULULAND. M.Sc. Thesis (unpubl.), Univ. Potchefstroom.

---------- (1970) Late Karoo igneous rocks of the southern Lebombo Mountain Range. In: Haughton,S.H. (Ed.), PROCEED. AND PAPERS, 2ND GONDWANA SYMP., 441-445, C.S.I.R., S.A.

Sun,S.S., Hanson,G.N. (1975) Origin of Ross Island basanitoids and limitations upon the heterogeneity of mantle sources for alkali basalts and nephelinites. Contrib. Mineral, Petrol.,v52, 77-106.

Swift,W.H., White,W.C., Worst.B.G., (1953) The geology of the Lower Sabi coalfield. Bull. Geol. Surv. S. Rhod.,v40, 96p.

---------- (1962) The geology of the Middle Sabi Valley. Bull. Geol. Surv. S. Rhod.,v52, 30pp.

Takahashi,E. (1978) Partitioning of Ni2+, Co2+, Fe2+, Mn2+ and Mg2+ between olivine and silicate melts: compositional dependance of partition coefficients. Geochem. Cosmochim. Acta.,v42, 1829-1844.

Taverner-Smith,R. (1979) Prograding Middle Ecca coastal associations from the the Effingham Quarries near Durban. Geokong. 79, Abstr., 18th Cong. Geol. Soc. S. Afr., 61-68.

Taylor,S.R. (1965) Geochemical analysis by spark source mass spectrography. Geochem. Cosmochim. Acta.,v29(12), 1243-1261.

---------- (1971) Geochemical application of spark source mass spectrography II. Photoplate data processing. Geochim. Cosmochim. Acta.,v35(11), 1187-1196.

----------, Gorton,M.P. (1977) Geochemical application of spark source mass spectrography III. Element sensitivity, precision and accuracy. Geochim. Cosmochim. Acta.,v41, 1375-1380.

Thompson,R.H. (1974) Some high-pressure pyroxenes. Mineral. Mag., v39, 768-787.

Thompson,R.N. (1972) The 1-atmosphere melting patterns of some basaltic volcanic series. Am. J. Sci.,v272, 901-932.

---------- (1975) Primary basalts and magma genesis, II. Snake River Plain, Idaho. Contrib. Mineral. Petrol.,v52, 213-232.

----------, Flower,M.F.J. (1971) One-atmosphere melting and crystallisation relations of lavas from Anjouan, Comores Archipelago, Western Indian Ocean. Earth Planet. Sci. Lett.,

v12, 97-107.
Turekian,K.K., Wedepohl,K.H. (1961) Distribution of the elements in some major units of the earths crust. Geol. Soc. Am. Bull.,v72, 175-192.
Turri,B., Taylor,H.P. (1976) Oxygen isotope studies of potassic volcanic rocks of the Roman Province, Central Italy. Contrib. Mineral. Petrol.,v55, 1-31.
Tyndale-Biscoe,R.M. (1949) Notes on a geological reconnaisance of the country east of Beitbridge, Southern Rhodesia. Trans. Geol. Soc. S. Afr.,v52, 403-413.
---------- (1956) Report on a visit to Nuanetsi Ranch. August 1956. Rep. Geol. Surv., S. Rhod. (unpubl.).
Urie,J.G., Hunter,D.R. (1963) The geology of the Stormberg volcanics. Bull. Geol. Surv. Swaziland, v3, 28-44.
Usselman,T.M., Hodge,D.S. (1978) Thermal control of low-pressure fractionation processes. J. Volcan. Geotherm. Res.,v4, 265-281.
Vail,J.R. (1962) Late Karoo intrusion breccias from the Nuanetsi district of southern Rhodesia with special reference to the granite complex of Demba-Divula. Trans. Geol. Soc. S. Afri., v65(2), 139-152.
---------- (1966) E structure e geocronologia da parte oriental de Africa central, com referencias a Mocambique. Bol. Serv. Geol. Minas, Mocambique, v33, 13-31.
---------- (1970) Tectonic control of dykes and related irruptive rocks in Eastern Africa. In: Clifford,T.N., Gass,I.G. (Eds.) AFRICAN MAGMATISM AND TECTONICS, 337-354, Oliver and Boyd, Edinburgh.
----------, Hornung,G., Cox,K.G. (1969) Karoo basalts of the Tuli Syncline, Rhodesia. Bull. Volc.,v33, 398-418.
Van der Schijf,H.P. (1968) Die topographie, geologie end grond-soorte van die Krugerwildtuin met verwysing na plantgemeen-skappe wat op die verskillende grondsorte voorkom. Tydskrif vir Natuurwet.,v8, 32-50.
Van Eeden,O.R., Visser,H.N., Van Zyl.,J.S., Coertze,F.J., Wessels,J.T. (1955) The gology of the eastern Soutpansberg and the Lowveld to the north. Geol. Surv. S.A., Expl. Sheet 42, (Soutpansberg).
Van Niekerk,C.B. (1968) THE SUITABILITY OF EXTRUSIVE ROCKS FOR U-PB RADIOMETRIC DATING. Ph.D. Thesis (unpubl.), Univ. of Cape Town.
Varne,R. (1968) The petrology of Moroto Mountain, Eastern Uganda, and the origin of nephelinites. J. Petrol.,v9, 169-190.
---------, Graham,A.L. (1971) Rare earth abundances in hornblende and clinopyroxene of a hornblende lherzolite xenolith : implications for upper mantle processes. Earth Planet. Sci. Lett.,v13, 11-18.
Verwoerd,W.J. (1966) Fenitization of basic igneous rocks. In: Tuttle,O.F., Gittens,J. (Eds.), CARBONATITES, 295-308. Inter-Science Publishers.
---------- (1967) The carbonatites of South Africa and South West Africa. Geol. Surv. S. Afr., Handbook 6., 452p.
Viljoen,M.J., Viljoen,R.P. (1969) Evidence for the existence of a mobile extrusive peridotite magma from the Komati Formation of the Onverwacht Group. Spec. Publ. Geol. Soc. S. Afr.,

v2, 87-112.
Von Knorring,O., Cox,K.G. (1961) Kennedyite, a new mineral of the pseudobrookite series. Mineral. Mag.,v32, 676-682.
Wachendorf,H. (1971) Die rhyolithe und basalte der Lebombos im Hinterland van Lourenco Margues (Mocambique). Getekt. Forsch.,v40, 1-86.
---------- (1973) The rhyolitic flows of the Lebombos. (SE-Africa) Bull. Volc.,v37(4), 515-529.
Walker,F., Poldervaart,A. (1949), Karoo dolerites of the Union of South Africa. Bull. Geol. Soc. Am.,v60, 591-706.
Wass,S.Y. (1979) Multiple origins of clinopyroxene in alkali basaltic rocks. Lithos, v12, 115-132.
Weaver,S.D., Sceal,J.S.C., Gibson,I.L. (1972) Trace element data relevant to the origin of trachytic and pantelleritic lavas in the East African rift system. Contrib. Mineral. Petrol., v36, 181-194.
Wedepohl,K.H., Muramatsu,Y. (1979) The chemical composition of Kimberlites compared with the average composition of three basaltic magma types. In: Boyd,F.R., Meyer,H.O.A. (Eds.) KIMBERLITES, DIATREMES AND DIAMONDS, Proceed., Second Int. Kimb. Conf.,vI, 300-312, A.G.U., Washington.
Whateley,M.K.G. (1979) Deltaic and fluvial deposits of the Ecca Group (late Carboniferous - Permian) Nongoma Graben, Zululand. Geokong. 79, Abstr., 18th Cong. Geol. Soc. S. Afr., P2, 71-76.
Wilkinson,J.F.G., Binns,R.A. (1977) Relatively iron-rich lherzolite xenoliths of the Cr-diopside suite: A guide to the primary nature of anorogenic tholeiitic andesite magmas. Contrib. Mineral. Petrol.,v65, 199-212.
Willis,J.P. Ahrens,L.H., Danchin,R.V., Erlank,A.J., Gurney,J.J., Hofmeyer,P.K., McCarthy,T.S., Orren,M.J. (1971) Some inter-element relationships between lunar rocks and fines and strong meteorites. In: Levinson,A.A.,(Ed.), PROC. SECOND LUNAR SCI. CONF., M.I.T. Press, 1123-1138.
----------, Erlank,A.J., Gurney,J.J., Theil,R.H., Ahrens,L.H. (1972) Major, minor and trace element data for some Apollo 11, 12, 14 and 15 samples. In: Heymann,L.D.,(Ed.), PROC. THIRD LUNAR SCI. CONF., M.I.T. Press, 1269-1273.
Wilson-Moore,A. (1897) Some observations of the Geology of the Sabie Valley. Trans. Geol. Soc. S. Afr.,v2, 131-140.
Wood,D.A. (1978) Major and trace element variations in the Tertiary lavas of Eastern Iceland and their significance with respect fo the Iceland geochemical anomally. J. Petrol., v19(3), 393-436.
---------- (1979) A variably veined suboceanic upper mantle - Genetic significance for mid-oceanic ridge basalts from geochemical evidence. Geology, v7, 499-503.
----------, Joron,J.-L., Treul,M., Norrey,M., Tarney,J. (1979) Elemental and Sr isotope variations in basic lavas from Iceland and the surrounding ocean floor. Contrib. Mineral. Petrol.,v70, 319-339.
Wooley,A.R., Garson,M.S. (1970) Petrochemical and tectonic relationship of the Malawi carbonatite - alkaline province and the Lupata-Lebombo volcanics. In: Clifford,T.M., Gass, I.G. (Eds.), AFRICAN MAGMATISM AND TECTONISM, 237-262,

Oliver and Boyd, Edinburgh.
----------, Bevan,J.G., Elliot,C.J. (1979) The Karoo dolerites of southern Malawi and their regional implications. Mineral. Mag.,v43, 487-495.
Worst,B.G. (1962) The geology of the Mwanesi Ridge and the adjoining country. Bull. Geol. Surv. S. Rhodesia, v54, 15pp.
Wright,J.B. (1967) Contributions to the volcanic succession and petrology of the Auckland Island II. Upper parts of the Ross Volcano. Trans. Roy. Soc. New Zealand, v5, 71-87.
Wyllie,P.J., Cox,K.G., Biggar,G.M. (1962) The habit of apatite in synthetic systems and igneous rocks. J. Petrol.,v3(2), 238-243.
----------, Huang,W.L. (1975) Influence of mantle CO2 in the generation of carbonatites and kimberlites. Nature, v257, 297-299.
York,D. (1966) Least squares fitting of a straight line. Can. J. Phys.,v44, 1079-1086.
Young,R.B. (1920) The rocks of a portion of Portuguese East Africa. Trans. Geol. Soc. S. Afr.,v23, 98-113.
Zindler,A., Hart,S.R., Frey,F.A., Jakobsson,S.P. (1979) Nd and Sr isotope ratios and rare earth element abundance in Reykjanes Peninsula basalts: Evidence for mantle heterogeneity beneath Iceland. Earth Planet. Sci. Lett.,v45, 249-262.

APPENDICES

APPENDIX A

ANALYTICAL AND COMPUTATIONAL TECHNIQUES

A1 WHOLE ROCK ANALYSIS

A1a Introduction

X-Ray Fluorescence (XRF) techniques were used for the analysis of major and trace elements in the Department of Geochemistry, University of Cape Town (UCT). The analytical methods applied in the UCT laboratory are outlined briefly below.

A1b Major Elements

Major elements, with the exception of Na, were analysed for using the lithium tetraborate fusion method of Norrish and Hutton (1969). Na was analysed for using pressed powder briquettes, prepared using the method of Baird (1961). The operating conditions used are summarised in Table A1a. They have been described briefly by Willis et al. (1971, 1972).

International rock standards were used for calibration and these included USGS standards, NIM standards, CAAS standards and JB-I and JG-I. Estimates of the precision, detection limits and accuracy of the data (as derived from the average absolute error on the standard calibration curves) are listed in Table A1b.

A1c Trace Elements

Trace elements, with the exception of the rare earth elements (REE), were analysed by XRF using pressed powder briquettes. Standard sets similar to those used for major element analyses were used for trace element calibration. Full corrections were made for dead-time, instrumental drift, background, tube line interferences and spectral line interferences. Matrix effects were corrected utilising the appropriate primary and secondary mass

absorption coefficients.

Mass absorption coefficients were calculated from major element analyses using Heinrich's (1968) values. Alternatively, for the elements Sr, Rb, Zr, Y, Nb, Zn, Cu and Ni the mass absorption coefficient determined at the Rb wavelength by either direct measurement (Norrish and Chappell, 1967) or the Compton peak method (Reynolds, 1963) was used. Background corrections were made by calculating background correction factors from specially prepared SiO_2 and SiO_2 + Fe_2O_3(SiFe) blanks. Similarly, tube peak interferences were monitored and corrected for by running SiO_2 blanks. Spectral line interferences, viz. analyte peak cross-tailing and peak on peak interferences, were corrected for by calculating interference correction factors from specially prepared interference standards. Iterative correction procedures were applied in the case of cross-tailing interferences. Instrumental settings and correction procedures used for trace element analyses are summarised in Tables A1c and A1d. Estimates of the uncertainties in the data due to counting statistics are given in Table A1e.

REE data were obtained for a suite of specially selected samples by Dr A.R. Duncan using an AEK MS-7 Spark-Source Mass Spectrograph at the Australian National University (ANU), Canberra. The analytical procedures applied at ANU and the associated errors have been described by Taylor (1965, 1971) and Taylor and Gorton (1977).

	Fe	Mn	Ti	Ca	K	P	Sc	Al	Mg	Na
Tube	W		Cr							
kV	60		50							
mA	50									
Counter	Fl									
Collimator	Fi		C	Fi		C			Fi	C
Crystal	LiF(220)		LiF(200)			GE	PET		TLAP	....
Counting Time on Peak (secs)	10	40	10	10	20	100	100	100	200	200

TABLE A1a. Major Element analytical conditions.

Abbreviations: Fl - Flow; Sct - Scintillation;
Fi - Fine; C - Coarse

OXIDE	PERCENTAGE	PRECISION	ACCURACY	DETECT. LIMIT
Fe_2O_3	9.0	0.038	0.064	0.014
MnO	0.15	0.008	0.003	0.008
TiO_2	1.0	0.008	0.008	0.005
CaO	12.0	0.028	0.030	0.008
K_2O	0.20	0.002	0.022	0.002
P_2O_5	0.20	0.012	0.018	0.011
SiO_2	50.0	0.140	0.264	0.036
Al_2O_3	15.0	0.080	0.079	0.022
MgO	8.0	0.148	0.086	0.072
Na_2O	2.5	0.032	0.067	0.080
Cr_2O_3	0.5	0.008	0.012	0.007
NiO	0.3	0.008	0.005	0.006

TABLE A1b. Estimates of precision, detection limits and average absolute error (accuracy) on the calibration curves for major element oxides using XRF techniques. Precision is expressed as an absolute error (2σ) on the given percentage oxide.

	1			2				
	SrKα	RbKα	m.a.c. at Rbλ	SrKα	RbKα	ZrKα	YKα	NbKα
Tube	Mo			W				
kV	60			60				
mA	50			50				
Counter	Sct			Sct				
Collimator	Fi			Fi				
Crystal	LiF (220)			Lif (220)				
Counter Time on Peak (sec)	2 x 200 ..... Preset Counts			2 x 200				
Vacuum	No			No				
Interference Corrections								
a. Tube								
b. Cross Tailing		(1) RbKα/ULα			(1) RbKα/ULα			
c. Peak on Peak	(2) RbKα	(3) SrKα		(2) RbKα		(6) ThLα (7) SrKβ	(3) RbKα	(4) YKβ (5) UKβ
Blanks used	SiO_2, SiFe			SiO_2, SiFe				
Interference Standards used	U, Rb, Sr			U, Rb, Sr, Th, Y				
M.A.C.	Rb			Rb				

TABLE Alc. Analytical conditions for Trace Elements, Sr, Rb, Zr, Y, Nb.

(Abbreviations as in Table Ala.)

	3		4			5		
	BaL_α	ScK_α	ZnK_α	CuK_α	NiK_α	CoK_α	CrK_α	VK_α
Tube	Cr		Au			W		
kV	50		60			60		
mA	50		50			50		
Counter	Fl		Sct			Fl		
Collimator	Fi		Fi			Fi		
Crystal	LiF (220)		LiF (220)			LiF (220)		
Counting Time on Peak (Sec)	2 x 100		2 x 100			2 x 100		
Vacuum	Vac		Vac			Vac		
Interference corrections:								
a. Tube			(1) AuL_β					
b. Cross Tailing	(2) ScK_β							
c. Peak on Peak	(3) TiK_α						(2) VK_β	(3) TiK_β
d. Peak on Background	(1) CaK_β					(1) FeK_β		
Blanks used	SiO_2, SiFe							
Interference Standards used	Ca, Ti, Sc					SiFe, Ti, V		
M.A.C.	Calculated		Calculated			Calculated		

TABLE A1d. Analytical conditions for Trace Elements Ba, Sc, Zn, Cu, Ni, Co, Cr, and V

(Abbreviations as in Table A1a)

Element	Conc. range	SD (2σ)	D.L.
Zr	40 - 400	0.9 - 1.4	1.4
Nb	4 - 150	1.0 - 1.2	1.8
Y	20 - 40	0.8 - 1.0	1.3
Rb	2.5 - 90	0.8 - 1.1	1.5
Ba	10 - 800	2.1 - 6.0	3.7
Sr	80 800	1.0 - 1.7	1.5
Co	18 - 100	1.9 - 2.5	4.5
Cr	25 - 350	1.5 - 2.1	2.2
Ni	10 - 208	2.5 - 3.7	4.0
V	50 - 350	2.4 - 3.7	5.5
Zn	8 - 150	0.9 - 1.7	1.4
Cu	5 - 90	1.8 - 2.1	2.9
Sc	25 - 40	1.0 - 1.2	1.2
Ga	15 - 20	0.38 - 0.46	0.45

TABLE Ale. Counting errors and detection limits for trace elements (ppm) analysed by XRF techniques. (Detection limit is given at the 99% confidence level, and counting error at the 95% confidence level).

A2 ELECTRON MICROPROBE ANALYSES

A2a Introduction

Compositions of minerals and quench glass were determined with an electron microprobe (EMP). The instrument used was a Cambridge Microscan 5 Microanalyser. Data reduction was completed in an on-line mode using a mini-computer. Samples were prepared as double polished sections on glass slides and were carbon coated.

A2b Major Elements

Operating conditions were as follows :

Beam Current	-	1500 nA
Accelerating Voltage	-	15 kV
Analysing Crystals	-	Quartz (Fe, Mn, Ca, Ti, Cr, K); RAP (Si, Al, Mg, Na)
Detectors	-	Flow-counters with Ar/CO_2 gas mixture.

A narrow (0.25μ) focussed beam was used for most elements, except when analysing feldspars, quench glass and hydrous minerals, when a de-focussed (10 - 30μ) beam was used. Calibration was achieved using natural (eg. Kakanui pyrope, Kakanui hornblende, Stillwater chromite and Marjalahti olivine) and synthetic (pure diopside glass, anorthitic glass and rutile) mineral standards. Raw counts were corrected for dead time and background and standardisation was undertaken at the beginning of each analytical run. Nominal concentrations were calculated from the K-factors (cps/%) derived during the standardisation process. The nominal concentrations were subsequently corrected using the method of Bence and Albee (1968) with the appropriate alpha-factors (Chodos, pers.comm.). For routine analyses of those minerals whose oxides should sum close to 100 percent, analyses were generally only accepted if totals were between 99 - 101 percent. The

stability of the EMP and the analytical procedures used were such that analytical totals seldom fell outside this range.

All iron has been expressed as FeO and no attempt has been made to calculate Fe_2O_3 for pyroxenes and amphiboles. Ferric iron in Fe-Ti oxides has been estimated from microprobe data (Fe determined as FeO) by assuming stoichiometry and charge balance. The method used is based on the procedures discussed by Neumann (1976) and expresses ferric iron as equivalent to the difference between the ideal charge based on stoichiometry and the calculated charge (Le Roex, 1980). End member components of titanomagnetite (ilmenite, geikelite and hematite) and ilmenite (ulvospinel and magnetite) were then calculated by using the proportion of ferric iron obtained by the above method.

Simplified molecular formulae (see below) have been used to calculate the end-member compositions; minor componenets are generally present in only very small amounts and were therefore ignored. For ilmenite, end member compositions were calculated as follows :

$$\text{Il (mol\%)} = (\text{Ti} - \text{Mg} / \tfrac{1}{2}\text{Fe}^{3+} + \text{Ti}) * 100$$
$$\text{Gk (mol\%)} = (\text{Mg} / \tfrac{1}{2}\text{Fe}^{3+} + \text{Ti}) * 100$$
$$\text{Hm (mol\%)} = (\tfrac{1}{2}\text{Fe}^{3+} / \tfrac{1}{2}\text{Fe}^{3+} + \text{Ti}) * 100$$

Titanomagnetite end-member compositions were calculated as follows :

$$\text{Us (mol\%)} = (\text{Ti} / \tfrac{1}{2}\text{Fe}^{3} + \text{Ti}) * 100$$
$$\text{Mt (mol\%)} = (\tfrac{1}{2}\text{Fe}^{3+} / \tfrac{1}{4}\text{Fe}^{3+} + \text{Ti}) * 100$$

The precision of the EMP technique has been discussed in detail by Reid (1977). It is illustrated in Table A2a, where the standard deviation about the mean of 10 analyses of the same spot is compared with the uncertainty due to counting statistics. Data incorporated in Table A2a is

from Reid (1977) (SiO_2 - K_2O; pargasitic hornblende) and Shee (1978) (MnO and Cr_2O_3; garnet megacryst-analyst P.C. Cardoso).

The absolute accuracy of the technique is difficult to establish because it is possible that natural mineral standards are inhomogeneous on the micron scale. Nevertheless, Reid (1977) notes that good agreement was achieved when analysing one natural mineral standard against another using element abundance data obtained by a different technique (eg. XRF data provided by B.W. Chappell, ANU). Furthermore, Le Roex (1980) found that there was excellent agreement between average EMP data for individual grains and XRF data for high purity mineral separates.

A2c Trace Elements : Nickel

Nickel was analysed in selected olivines using the following operating conditions:

Beam Current	-	1000 nA
Accelerating Voltage	-	25 kV
Analysing Crystal	-	Lif (200)
Detector	-	Sealed counter
PHA	-	E = 1.8V (threshold) ΔE= 1.7V (window)

Standardisation was achieved using a natural olivine (NiO = 0.35%) from a kimberlite nodule. Counting times of 150 sec. on the peak and 100 sec. at the background position were used. These times gave an estimated relative precision (based on counting statistics) of $\pm$ 3.36% on 0.23% NiO ($\pm$ 78 ppm on 2300 ppm NiO) and a detection limit of 0.011% (110 ppm) NiO, at the 95% and 99% confidence levels respectively.

OXIDE	$\bar{X}$	S.D.	ERROR	D.L.
SiO_2	41.97	0.08	0.08	0.06
TiO_2	3.92	0.08	0.10	0.07
Al_2O_3	13.51	0.06	0.06	0.04
Cr_2O_3	0.78	0.02	0.02	0.03
FeO	6.82	0.15	0.16	0.10
MnO	0.26	0.01	0.01	0.03
MgO	16.34	0.07	0.10	0.05
CaO	12.10	0.07	0.08	0.05
Na_2O	2.71	0.12	0.14	0.09
K_2O	1.18	0.06	0.10	0.07

TABLE A2a. Estimate of the precision of electron microprobe analyses for major elements.
(All quantities are expressed as oxide weight percent).

$\bar{X}$ = Mean of 10 replicate analyses of the same spot within a pargasitic hornblende (Reid, 1977). Cr_2O_3 and MnO data represents the mean of 12 replicate analyses of a garnet megacryst (Shee,1978).

SD = Standard deviation about the mean.

ERROR = 2σ error (95% confidence level) due to counting statistics.

DL = Theoretical detection limit (99% confidence level).

TABLE A4a. Sample preparation for Sr and Rb analysis by mass spectrometry

1. Weigh clean teflon beaker. Add Rb and Sr spike separately to beaker and dry down; weigh before and after drying each spike.
2. Add rock powder (-300 mesh) and weigh.
3. Add 5 ml HF + 1ml $HCLO_4$. Cover and heat.
4. Check that dissolution is complete, if not repeat step 3.
5. Following complete dissolution uncover and take to complete dryness (charred).
6. Add 10 mls 6N HCL to residue.
7. Dry down slowly.
8. Add 2 mls 2.59N HCL. (Cover and warm until dissolved.) Allow solution to cool completely (process may be accelerated by placing beakers on an ice-pack).
9. Centrifuge in small, ultraclean test tube (10m).

10a. Solution: pass through large iron-exchange column. Elute with ∿66 ml 2.59 HCL then further 18 ml and collect.

10b. Residue: store for Rb analysis.

11. Solution: evaporate to dryness.
12. Residue: redissolve in 2 ml 2.59N HCL
13. Solution: pass through small ion-exchange column. Elute with 5 ml 2.59N HCL then further 4 ml and collect.
14. Solution: evaporate to dryness.
15. Residue: Add 2-3 drops 2%HNO_3, transfer to planchete and dry down. Store until loaded on to filament for analysis.

Powell, 1972), assuming a $^{88}Sr/^{86}Sr$ ratio of 8.375, was used in this study. Furthermore, a $^{85}Rb/^{87}Rb$ correction factor of 2.6 was applied to triple filament runs.

A4e Rb and Sr Analyses

XRF methods were used to determine Rb and Sr in most of the basalt, rhyolite and dolerite samples unless concentrations were particularly low, ie. <5ppm, in which case Rb and Sr abundances were determined by isotope dilution (ID). Data determined by XRF analysis represents the average of duplicate or triplicate analysis. Analyses were rejected unless duplication was better than 1% relative and precision as monitored during the course of the study was found to be better than 1.5% relative.

In view of the close agreement between the adopted Rb and Sr abundances in the USGS standards used for setting up the calibration curves with those obtained by other laboratories (Table A4c), the XRF data are considered to be satisfactory. Cross checks of the XRF data were made by ID analysis. Results of the XRF and ID analyses are given in Table A4d and the close agreement implies that the XRF data represents reasonably accurate estimates of the true concentrations.

A4f Standards and Blanks

Accuracy of the $^{87}Sr/^{86}Sr$ ratios were checked periodically by running the American National Bureau of Standards (NBS) SRM 987 $SrCO_3$ standard. The NBS report a $^{87}Sr/^{86}Sr$ ratio = 0.71014 $\pm$ 20 for this standard. However, measurements of the Sr-isotope ratio in the BPI laboratory consistently yields slightly higher values than that reported by the NBS. A value of 0.71023 $\pm$ 6 has therefore been adopted for the SRM 987 standard at the BPI. Standard data obtained during the present study (Table A4e correspond closely to the adopted value of 0.71023 indicating that

TABLE A4b(iii). Details of data collection

Run	Block Sequence	Number of Blocks	Integration Time	Delay
$^{\Theta}$Natural Sr	B-85-86-87-88-B-B	80 - 100	4 sec	5.0 sec
$^{\Theta}$Spiked Sr	B-88-86-84-86-88-B	20	4 sec	5.0 sec
$^{\Theta\Theta}$Spiked Rb	B-85-87-B	40		

$^{\Theta}$ VG Micromass 30
$^{\Theta\Theta}$ DTM-BPI

TABLE A4c. Rb and Sr abundance data for USGS rock standards used to set up calibration curves during XRF analysis.

Standard	Element/ Ratio	USGS	UCT	ID (1)	ID (2)	ID+XRF (3)
G-1	Rb	220	210	213		
	Sr	250	249	253		
	Rb/Sr	0.880	0.843	0.840		
W-1	Rb	22	21.4			
	Sr	180	188			
	Rb/Sr	0.122	0.114			
G-2	Rb	174	168	169	168	169
	Sr	481	479	476	475	478
	Rb/Sr	0.362	0.351	0.355	0.353	0.354
GSP-1	Rb	252	252	255	255	250
	Sr	237	235	233	233	235
	Rb/Sr	1.063	1.072	1.093	1.091	1.064
AGV-1	Rb	69.0	67.0	67.1	66.6	67.0
	Sr	664	657	662	657	659
	Rb/Sr	0.104	0.102	0.101	0.101	0.102
BCR-1	Rb	48.4	46.7	47.3	46.9	48.2
	Sr	336	328	332	332	332
	Rb/Sr	0.144	0.142	0.142	0.142	0.145

USGS - Fairburn and Hurley (1971)

UCT - Values adopted during the present study

ID(1) - Pankhurst and O'Nions (1973)

ID(2) - De Laeter and Abercombie (1970)

ID+XRF(3) - Fairburn and Hurley (1971)

TABLE A4d. Comparison of Rb and Sr data obtained by XRF (UCT) and ID (BPI) analytical methods. Differences (Δ %) are expressed as percentages of the ID data.

SAMPLE	Rb		Sr		Rb/Sr		Δ %
	XRF	ID	XRF	ID	XRF	ID	
RC74	144	143.6	105	106.1	1.371	1.353	-1.33
RC128	88	87.8	245	245.1	0.359	0.358	-0.33
KA84	134	133.1	212	213.0	0.632	0.625	-1.12
*L335	121	120.3					
*J11	131	128.1					
*78/5	258	260.2					
*E1/1	114	115.5	181	180.8	0.630	0.639	+1.41
*E4/2	49	48.6	699	692.0	0.069	0.070	+1.41
*E2/4	15	14.8	986	973.9	0.015	0.015	-
*E3/1	44	45.8	567	563	0.078	0.081	+3.70

* - ID data from H.L. Allsopp, BPI.

TABLE A4e. Values obtained for the SRM 987 $SrCO_3$ standard at the BPI.

Adopted Value (BPI) : 0.71023 ± 5

DATE	MEASURED $^{87}Sr/^{86}Sr$ RATIO	ANALYST
01.10.78	.71023 ± 3	CBS
02.10.78	.71024 ± 6	CBS
26.01.79	.71022 ± 3	JWB
20.06.79	.71023 ± 12	HLA
04.10.79	.71022 ± 6	CBS
11.01.80	.71023 ± 3	CBS

Abbreviations: HLA - H.L. Allsopp,
JWB - J.W. Bristow,
CBS - C.B. Smith

accuracy was satisfactory. Adjustment of Sr-isotope ratios determined for unknowns was therefore unnecessary.

In the case of ID analyses (Rb and Sr), accuracy of the spike parameters were checked by running the NBS SRM 607 potassium feldspar standard. Values obtained for the standard are listed in Table A4f. Agreement between the measured and NBS values is excellent with differences rarely exceeding 1% relative to the NBS data. Accuracy of the Rb and Sr ID data is therefore considered to be better than $\pm$ 1%.

Blank levels were checked during the course of the work and under normal analytical conditions, ie. complete processing (Table A4a), using single distilled reagents were less than 20ng. Blank corrections were therefore unnecessary for the majority of samples. In the case of samples characterised by low concentrations (<5ppm) of Rb and Sr, eg. Kuleni rhyolites, care was taken to ensure that a very low blank level was attained during the analytical procedure. Low blank levels were achieved by using double distilled reagents in the dissolution and column pre-conditioning and elution stages. Contamination of natural Sr runs with spiked material was avoided by using separate sets of either "spike" or "natural" run ion-exchange columns and teflon beakers during the dissolution and chemical processing stages.

A4g Estimates of Uncertainty

The errors or uncertainties included in the tables of Sr-isotope data are determined from the data collected during each analytical run and are reported as one standard error of the mean. The errors cited depend mainly on the stability during the analytical run and consequently the more stable the run, the lower the uncertainty. Runs with high uncertainties were generally discarded and rerun.

Overall precision of the isotope data has been determined from the analytical runs completed at the BPI by calculating the average absolute error for the entire data set : absolute precision = $\pm$ 0.00006, N =85. Precision as determined from duplicate analyses (Table A4g) is marginally lower ($\pm$ 0.00005; expressed as the average of the differences) though it may not represent a true value in view of the small number of duplicate analyses.

Accuracy of the $^{87}Sr/^{86}Sr$ ratios can be gauged by inspecting the data obtained for the SRM 987 $SrCO_3$ standard and duplicate analyses (Tables A4e and A4g respectively). In both cases differences are generally within the limits of precision ($\pm$ 0.00006) and the absolute error in the $^{87}Sr/^{86}Sr$ ratio is therefore considered to be equivalent to the overall precision of 0.00006.

The main uncertainty in the $^{87}Rb/^{86}Sr$ ratio is dependant on the uncertainty in the Rb/Sr ratio as determined by XRF analyses. The only other measurement involved in the calculation of $^{87}Rb/^{86}Sr$ ratio is the $^{87}Sr/^{86}Sr$ ratio which is far more precisely known. The uncertainty in the Rb/Sr ratio is a function of the analytical precision and quality of the standard calibration. As noted above replicate XRF analyses yield a precision of better than 1.5%, for Rb/Sr ratio values of 0.1 to 8.0 and adopted standard data values are within 1-2% of the values obtained in other laboratories (Table A4c). Similarly, comparisons of ID and XRF data (Table A4d) show that differences in Rb/Sr ratio seldom exceed 1.5%. Since the range observed in Rb/Sr ratios for the majority of analysed samples is not extreme (0.1 - 8.0) a blanket error of 1.5% has been applied to $^{87}Rb/^{86}Sr$ ratios (cf. Brookes et al., 1972).

TABLE A4f. Values obtained for SRM 607 potassium feldspar standard at the BPI.

NBS : Rb = 523.90 ± 1.01

Sr = 65.48 ± 0.32

$^{87}Sr/^{86}Sr$ = 1.20039 ± 0.0002

DATE	Rb	Sr	$^{87}Sr/^{86}Sr$	±	ANALYST
24.06.75	521.9	65.223			HLA
10.08.75	524.8	66.305			HLA
01.06.77	518.4	65.715	1.2011	0.0008	HLA
30.06.77	519.8	65.683	1.1999	0.0002	HLA
07.01.80	518.6	65.495	1.2005	0.0002	TPE
07.01.80	516.5	65.450	1.2005	0.0001	TPE
24.01.80	522.2	65.745	1.19939	0.00007	EB
03.03.80	520.4	65.608	1.19998	0.0001	RAA
06.04.80	521.7	65.585	1.20095	0.0001	HLA

Abbreviations: HLA - H.L. Allsopp, RAA - R.A. Armstrong,
EB - E.B. Barton, TPE - T.P. Ellworthy)

TABLE A4g. Duplicate $^{87}Sr/^{86}Sr$ analyses of selected samples

SAMPLE	A	B	Δ	COMBINED MEAN
L18	.70879 ± 8	.70884 ± 10	.00005	.70881 ± 2
L505c	.70752 ± 6	.70752 ± 10	-	.70752 ± 2
L505 zeolite	.70706 ± 10	.70705 ± 7	.00001	.70705 ± 2
J55	.70651 ± 8	.70656 ± 9	.00005	.70653 ± 2
RC128	.70711 ± 8	.70698 ± 8	.00012	.70705 ± 2
CL115	.70511 ± 6	.70519 ± 4	.00008	.70516 ± 1
KA6B	.70926 ± 8	.70930 ± 9	.00004	.70928 ± 2
NTS7	.70566 ± 6	.70569 ± 4	.00003	.70568 ± 1
KS63	.71642 ± 9	.71642 ± 6	-	.71642 ± 2
DBM11	.70608 ± 8	.70596 ± 8	.00012	.70602 ± 2
		Average = 0.00005		

The following equation was used to calculate $^{87}Rb/^{86}Sr$ (atomic) ratios from Rb/Sr (ppm) ratios:

$$(^{87}Rb/^{86}Sr)_{atomic} = (Rb/Sr)ppm \times (2.693 + .2830 \times {}^{87}Sr/^{86}Sr_{atomic})$$

A4h Interlaboratory Checks

Sr-isotope and Rb-Sr analyses completed in the Isotope laboratory, Department of Geology and Mineralogy, University of Oxford (OX) by Cleverly (1977), Norry (1977) and Erlank (unpubl. data) have been used in this thesis (Chapters 6 and 10). Inter-laboratory checks of Rb, Sr and $^{87}Sr/^{86}Sr$ data were conducted to ensure that data obtained from both sources were directly comparable. Inspection of Tables A4h (i) and (ii) show that there is good agreement between the data obtained from the independant laboratories and that adjustment of one or other data sets was unnecessary.

A4i Regression Treatment

Best fit straight lines were fitted to the Rb-Sr isotope data using the regression model of York (1966). Errors used in the computational procedure are those derived from the analytical data : $\pm$ 0.00006 (1σ) for the $^{87}Sr/^{86}Sr$ ratio and 1.5% for the $^{87}Rb/^{86}Sr$ ratio (section A 4g). The values have been adopted as blanket errors in the regression treatment with the exception that where the 1σ uncertainty for the $^{87}Sr/^{86}Sr$ ratio exceeds $\pm$ 0.00006 the higher (measured) value has been used as the error parameter.

The degree of scatter about the regression lines has been estimated by calculating the MSUM (Brookes et al., 1972). Classification of the regression lines as an errochron or isochron is based on a comparison of the MSUM and F values as outlined in Chapter 6 .

TABLE A4h(i). Comparison of Rb and Sr data obtained at UCT and Oxford. Differences are expressed as percentages of the Oxford data.

SAMPLE	Rb		Sr		Rb/Sr		Δ %
	UCT	OX	UCT	OX	UCT	OX	
RC36	122	127	187	193	0.652	0.658	+ .91
RC40	117	117	174	174	0.672	0.672	-
RC55	128	128	138	136	0.928	0.941	+1.38
RC62	126	125	222	219	0.568	0.571	+0.53
RC66	121	121	168	168	0.720	0.720	-
RC73	239	235	35	34	6.829	6.912	+1.20
RC74	144	143	105	102	1.390	1.402	+0.86
RC119	124	122	133	129	0.932	0.946	+1.48
RC128	88	88	245	244	0.359	0.361	-0.55
RC131	141	144	123	124	1.146	1.161	+0.932
SK138	144	143	198	191	0.732	0.749	+2.27
SK153	126	125	133	131	0.947	0.954	+0.73

TABLE A4h(ii). Comparison of $^{87}Sr/^{86}Sr$ data obtained at the BPI and Oxford.

SAMPLE	$^{87}Sr/^{86}Sr$ BPI	$^{87}Sr/^{86}Sr$ OX
RC74	.71469 ± 8	.71457 ± 10
RC131	.71270 9	.71276 8

APPENDIX B

REVISED VOLCANIC STRATIGRAPHY OF THE LEBOMBO MONOCLINE

R.W. Cleverly and J.W. Bristow

Trans. Geol. Soc. S.Afr., 82 (1979), 227-230

REVISED VOLCANIC STRATIGRAPHY OF THE LEBOMBO MONOCLINE

by

R. W. CLEVERLY and J. W. BRISTOW

ABSTRACT

New volcano-stratigraphic nomenclature is proposed for the Jurassic volcanics of the Lebombo Monocline. Nomenclature is based on field criteria since all major rock types are characterised by distinctive lithologies and can be mapped as individual units. "Lebombo Group" is redefined to include all the basic and acid volcanics of the monocline. Brief descriptions of the main extrusive and intrusive rock types are presented.

CONTENTS

I. INTRODUCTION

As a result of recent work conducted on the tectonic, structural and magmatic aspects of the volcanic rocks of the Lebombo Monocline, we feel that some revision and formalisation of current nomenclature is required to bring the volcanic nomenclature into line with the proposed recommendations of the South African Committee for Stratigraphy.

The Lebombo Monocline consists of a large thickness of Karoo basalts and rhyolites,* warped downwards to the east along the margin of the Karoo volcanic province. There is a broad twofold subdivision with a lower basalt unit, being more easily weathered, forming the lowveld and an upper rhyolite unit forming the Lebombo mountain range.

No dates have yet been obtained on the Lebombo basalts though intrusive dolerites within the basalt have been dated at 188 ± 5 m.y. (Cleverly, 1977; K-Ar) and the overlying rhyolites at 190 ± 7 m.y. (Manton, 1968; Cleverly, 1977; Rb-Sr). Syenites intrusive into the Bumbeni Complex have been dated at 138 ± 3 and 141 ± 2 m.y. by Miller (Burger and Coertze, 1973; Ar-Ar). All the volcanics thus appear to be Early-Middle Jurassic in age.

II. STRATIGRAPHY

The volcanics of the Karoo Supergroup within South Africa have previously been divided into the Drakensberg Group, containing all the basic volcanics, and the Lebombo Group, comprising the rhyolites present in the Lebombo (Stratten, 1970). (Stratten (op. cit.) used the terms "Drakensberg Stage" and "Lebombo Stage"; these have been given Group rankings in accordance with the new stratigraphic nomenclature.)

Recent geochemical data (Manton, 1968; Bristow, 1976; Cleverly, 1977; and unpublished data) suggest that the basalts of the Lebombo are chemically as well as geographically distinct from those of the Drakensberg, and apparently consanguineous with the rhyolites. It seems logical, therefore, to redefine the Lebombo Group to include the basic as well as the acid volcanics present in the Lebombo monocline. Though isotopic age determinations on the Drakensberg and Lebombo volcanics (Manton, 1968; Fitch and Miller, 1971; Cleverly, 1977; and unpublished data) produce ages for the volcanics of both groups which are within error (190 ± 7 m.y.), detailed correlation of the two groups is not possible at this stage. Apart from the work of Stratten (1970), no detailed nomenclature of the volcanics has been published although a number of unpublished reports and theses have been produced (Stratten, 1965; Bristow, 1976; Cleverly 1977; reports of the South African Committee for Stratigraphy and Geological Survey), and this is an attempt to provide a uniform, consistent and useful nomenclature for the Lebombo volcanics. The nomenclature outlined below is entirely based on field characteristics; each formation has a distinctive lithology which enables it to be distinguished from its neighbours and mapped as a unit.

The Lebombo Group is divisible into a number of formations (Table I) which are now discussed individually. Their areal distribution is shown on Fig. 1.

A. Mashikiri Nephelinite
(New Subdivision)

The Mashikiri Nephelinite Formation crops out as a thin sequence (maximum thickness 170 metres) of alkaline (nephelinite) lava flows overlying the Karoo Sediments in the northern part of the Kruger National Park and in the Soutpansberg south of the Limpopo. It is best exposed between Klopperfontein Dam and Mashikiri on the road from Punda Milia to Pafuri, and this is considered to be the type-section. It is clearly distinguished from the overlying olivine-rich lavas of the Letaba Basalt Formation by the presence of stellate glomeroporphyritic aggregates of clinopyroxene and rare nepheline crystals and biotite flakes.

* The terms "basalt(s)" and "rhyolite(s)" are used only in the broadest sense to signify basic and acid volcanic rocks respectively. The geochemistry and volcanology of these rocks will be described in subsequent papers.

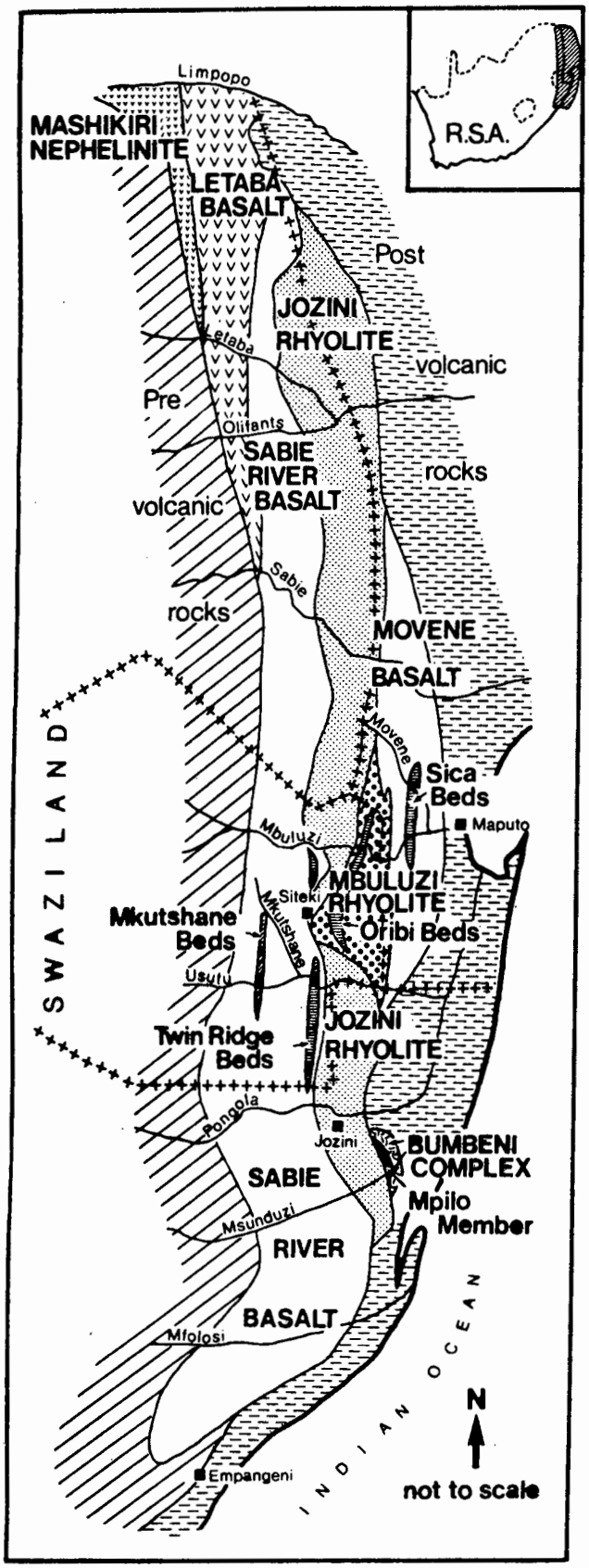

Figure 1
Geological sketch map of the Lebombo showing the various stratigraphic subdivisions discussed in the text.

B. Letaba Basalt
(New Subdivision)

Olivine-rich lavas of the Letaba Basalt Formation crop out extensively in the northern Lebombo with the Sabie River representing the approximate southerly limit of outcrop. Some olivine-poor flows are found within the formation and occasional interdigitated alkali-basalts and shoshonites occur. The exposures along the Letaba River represent the type-section. The maximum thickness of approximately 5 500 metres is reached in the central portion of the outcrop.

TABLE I
Subdivision of the Lebombo Group

Formation	Member	Bed	Lithology
Movene Basalt			Basalts
		Sica	Rhyolites
Bumbeni Complex			Acid extrusives and intrusives
	Mpilo		Trachy-basalt and Trachy-andesite
Mbuluzi Rhyolite			Quartz-phyric rhyolites
		Oribi	Quartz-rich rhyolites
Jozini Rhyolite			Rhyolites (not quartzphyric)
Sabie River Basalt			Basalts
		Twin Ridge	Rhyolites
		Mkutshane	Rhyolites
Letaba Basalt			Olivine-rich basalts
Mashikiri Nephelinite			Nephelinites, alkali basalts

C. Sabie River Basalt
(formerly Drakensberg Stage Basalt)

The Sabie River Basalt Formation is the major basaltic unit within the Lebombo Group, overlying the more basic lavas of the Letaba and Mashikiri formations. It reaches a maximum thickness of approximately 5 km along the southern Swaziland border and forms the lowveld of the eastern Transvaal, Swaziland and northern Zululand. The type-section is along the Sabie River in the south of the Kruger National Park and excellent exposures are also found along the Mfolozi River in Zululand.

The rocks of the Sabie River Formation are dark, fine-grained, generally aphyric basalts although olivine- and plagioclase-phyric varieties are also found. There are significant areal compositional differences within this formation which may lead to further subdivisions on chemical grounds.

1. Mkutshane Beds

These are a number of thin rhyolite flows interbedded in the lower half of the Sabie River Basalt. They crop out only in the central part of the Swaziland outcrop and are best exposed in and around the Mkutshane River. The rocks are fine-grained plagioclase-phyric rhyolites and are distinct from the main group of rhyolites on trace element and isotopic grounds.

2. Twin Ridge Beds

At the top of the Sabie River Basalt sequence are a number of thin interbedded rhyolites called the Twin Ridge Beds. The rhyolites are similar in composition and petrography to the overlying Jozini Rhyolite and are traceable for most of the length of Swaziland. They are best exposed on the Twin Ridge Estate, 5 km south-east of Big Bend, Swaziland.

D. Jozini Rhyolite
(formerly Lebombo Stage Rhyolite)

The Jozini Rhyolite Formation is a thick unit of rhyolite flows which overlies the Sabie River Basalt. It forms the high ground of the Lebombo mountain range and can be traced virtually the full length of the Lebombo reaching a maximum thickness of approximately 5 000 metres in northern Zululand. The rhyolites of the Jozini Formation are generally reddish and plagioclase-phyric. The road and canal cuttings in the vicinity of Jozini town and dam form the type-section.

E. Mbuluzi Rhyolite
(New Subdivision)

The Mbuluzi Rhyolite Formation overlies the Jozini Rhyolite, being clearly distinguished by the presence of quartz phenocrysts. It forms the upper part of the rhyolite outcrop in Swaziland and has been mapped south of the

Usutu River on the eastern side of the Lebombo range. It reaches a maximum thickness of 5 000 metres to the east of Siteki, Swaziland.

The typical rhyolite of the Mbuluzi Formation is grey and fine-grained and contains phenocrysts of white feldspar and quartz. The type-section is that exposed in railway cutttings along the Mbuluzi River.

1. Oribi Beds

The Oribi Beds crop out towards the base of the Mbuluzi Rhyolite, being characterised by particularly abundant quartz phenocrysts. They form positive topographic features, especially in the vicinity of the farm Oribi, 11 km north of Siteki, Swaziland. They are generally about 250 metres in thickness.

F. Bumbeni Complex

The Bumbeni Complex contains a variable suite of rocks that includes rhyolitic lavas, and both ash-fall and ash-flow tuffs, and has a basaltic unit, the Mpilo Member, at its base. The Complex overlies the Jozini Rhyolite Formation and is confined to a small area at the southern end of its outcrop, extending from the southern portion of the Mkuze Game Reserve southwards beyond the Msunduzi River. It reaches a total thickness of approximately 225 metres in the vicinity of the Msunduzi River.

1. Mpilo Member

The Mpilo Member is found at the base of the Bumbeni Complex, overlying disconformably the rhyolites of the Jozini Formation. It contains a thin sequence (maximum thickness 50 metres) of trachybasaltic and trachyandesitic lavas, and is best exposed on the lower flanks of Mpilo Hill north of the Msunduzi River.

G. Movene Basalt

(formerly Lebombo Upper Basalt)

The last formation of the Lebombo Group only crops out in Moçambique. It has been fully described by Assuncao *et al.* (1962) and by Wachendorf (1971, 1973). The following description is mainly from the work of Wachendorf; the names have been proposed for the sake of uniform nomenclature. The Movene Basalt Formation crops out towards the middle of the Lebombo monocline, on the Moçambique side, reaching a maximum thickness of approximately 2 000 metres (Wachendorf, 1971). Small outcrops have been found south of the Usutu River in South Africa. Most of the rocks appear to be similar to the Sabie River Formation though nepheline-normative varieties seem to be common (Assuncao *et al.*, 1962). The formation has been named after the Movene River which dissects the outcrop.

1. Sica Beds (formerly Little Lebombo Rhyolite)

A group of rhyolite flows, the Sica Beds, interbedded with the Movene Basalt give rise to the low hill of the Little Lebombo. The best exposures appear to be along the railway line in the vicinity of Sica Hill.

There are very few data available from the exposures in Moçambique; until the localities become accessible we are unable to confirm the possible relationship between the Movene Basalt Formation and the rocks of the Bumbeni Complex.

H. Intrusive Rocks

A brief discussion of the various intrusive rocks is included here. They have not been included in the various formations since they constitute individually mappable units.

1. Rooirand Dyke Swarm

A major dolerite dyke swarm, giving rise to the Rooirand range of hills, intrudes the lower part of the Sabie River Basalt Formation and the underlying sediments in Zululand and southern Swaziland.

2. Komatipoort Complex

The Komatipoort Complex is an elongated layered gabbro body exposed in and around Komatipoort. It has been described by Saggerson and Logan (1970).

3. Granophyres

A number of granophyre intrusions are present in the Lebombo from Swaziland northwards. They are intruded close to the contact between the Jozini Rhyolite and the Sabie River Basalt, forming rounded hills. The largest bodies are found at Siteki in Swaziland, Mananga on the north Swaziland border, and Muntshe Ridge in the Kruger National Park.

4. Bumbeni Complex Syenites

Syenitic intrusions in the form of small elongate plutons intrude the central portion of the Bumbeni Complex. They have been described by Van Wyk (1963), Stratten (1965) and Bristow (1976).

5. Kuleni Rhyolite Domes and Dykes

Intensely contorted quartz-phyric rhyolite lava domes and dykes crop out south of the Msunduzi River in the Kuleni area. The lava domes are interdigitated with the massive flows of the Jozini Formation whereas the dykes show cross-cutting relationships. The larger domes, e.g. Bobbejaanskrans and Mazinza, form prominent sparsely vegetated hillocks, whereas the dykes occur as north–south-trending ridges up to 100 metres wide.

III. CONCLUSION

In an attempt to produce uniformity of stratigraphic nomenclature a lithostratigraphic classification for the volcanic rocks of the Lebombo Monocline has been proposed in accordance with the guidelines of the South African Committee for Stratigraphy. It divides the volcanics into a number of distinct and mappable stratigraphic units and can be applied over the whole length of the Lebombo.

ACKNOWLEDGMENTS

We would like to thank A. R. Duncan for his comments on the manuscript and NERC and CSIR for financial support.

REFERENCES

Assuncao, A. F. T. de, Coelho, A. V. P., and Rocha, A. T. (1962). Petrologia das lavas dos Libombos, Moçambique. *Est. Ens. Doc. Junta Invest. Ultramar*, Lisbon, **99**, 71 pp.

Bristow, J. W. (1976). *The geology and geochemistry of the southern Lebombo*. M.Sc. thesis (unpubl.), Univ. Natal, Durban, 331 pp.

Burger, A. J., and Coertze, F. J. (1973). Radiometric age measurements on rocks from South Africa to the end of 1971. *Bull. geol. Surv. S. Afr.*, **58**, 45 pp.

Cleverly, R. W. (1977). *The structural and magmatic evolution of the Lebombo Monocline, southern Africa, with particular reference to Swaziland*. D.Phil. thesis (unpubl.), Univ. Oxford, 316 pp.

Cox, K. G., Macdonald, R., and Hornung, G. (1967). Geochemical and petrographic provinces in the Karroo basalts of southern Africa. *Amer. Miner.*, **52**, 1451–1474.

Fitch, F. J., and Miller, J. A. (1971). K-Ar radio ages of Karroo volcanic rocks from Lesotho. *Bull. volcan.*, **35**, Ser. 1., 64–84.

Manton, W. I. (1968). The origin of associated basic and acid rocks in the Lebombo–Nuanetsi igneous province, southern Africa, as implied by strontium isotopes. *J. Petrol.*, **9**, 23–29.

Saggerson, E. P., and Logan, C. T. (1970). Distribution controls of layered and differentiated mafic intrusions in the Lebombo volcanic sub-province. *Spec. Publ. geol. Soc. S. Afr.*, **1**, 721–733.

Stratten, T. (1965). *The pyroclastic and associated igneous rocks of the Lebombo Mountain Range, south of the Great Usutu River, Zululand*. M.Sc. thesis (unpubl.), Univ. Potchefstroom, 76 pp.

———— (1970). Late Karroo igneous rocks of the southern Lebombo Mountain Range. *In:* Haughton, S. H., Ed., *Proceed. and Papers, 2nd Gondwana Symp.*, S.A., CSIR Publ., 441–445.

Van Wyk, W. L. (1963). Groundwater studies in northern Natal, Zululand and surrounding areas. *Mem. geol. Surv. S. Afr.*, **52**, 135 pp.

Wachendorf, H. (1971). Die Rhyolithe und Basalte der Lebombos im Hinterland van Lourenço Marques (Moçambique). *Geotekt. Forsch.*, **40**, 1–85.

———— (1973). The rhyolitic lava flows of the Lebombo (S.E. Africa). *Bull. Volcan.*, **37**, 515–529.

R. W. Cleverly,
Department of Geology,
University of Cape Town,
7700 Rondebosch.

J. W. Bristow,
Department of Geochemistry,
University of Cape Town,
7700 Rondebosch.

Accepted for publication by the Society on 7.8.1979.

APPENDIX C

VOLCANOLOGY OF THE LEBOMBO RHYOLITES

J.W. Bristow and R.W. Cleverly

Geokong 79, 18th Cong. Geol. Soc. S. Afr., Abstr. Vol. (1979), 60-63

Volcanology of the Lebombo Rhyolites

J.W. Bristow and R.W. Cleverly

Introduction

Acid extrusives of the Lebombo monocline extend 600 km from Zululand to the north of the Kruger Park.[1] They are characterised by features of both lavas and ignimbrites; this paper attempts to reconcile these two modes of origin.

Description of the Acid Flows

The flows typically form extensive 'sheet-like' units from about 80 - 350 m in thickness and can be traced along strike for up to 50 km.[2 3] Geochemical and petrographic data suggest that some of the thicker flows may be composite.[4] Flows maintain essentially regular and parallel upper and lower surfaces, except where deformed by later tectonic movement. Because of monoclinal flexuring they are only exposed in cross section and no estimate of their lateral extent could be made. Seven major flow units crop out in the Jozini type-section[3] and some thirty flow units have been recognised in Swaziland on the basis of mineralogical and textural features.[2]

The acid flows typically contain a number of zones[2 3 5] which are discussed below (see Fig. 1).

1. Tuffaceous Zone: Massive flow bases are frequently underlain by a tuffaceous zone varying in thickness from a few millimetres to approximately 4 m. The zone is characterised by material of red, sandy appearance with a poorly developed lamination parallel to the flow contacts. Though referred to as 'tuffaceous' these zones probably represent reworked volcaniclastic material (air-fall and ash-flow), weathered products of the underlying flows and sedimentary material from an extraneous source. In thin section the material consists of glass dust, crystal fragments, poorly preserved glass shards and subrounded quartz and feldspar grains; small flakes of mica also occur in several thin sections.

2. Streaky Basal Zone: Immediately overlying the tuffaceous beds is a microcrystalline or glassy rhyolite zone, separated from the underlying tuffaceous horizon by a sharp contact. This zone is characterised by a streaky-banded appearance with pitchstone or glassy rhyolite encountered at the immediate base, gradational upwards into bands or lenses (1-10 mm wide) of dark and light glassy, microcrystalline and devitrified rhyolite. Where banding is prevalent a 'pinch and swell-type' structure is present. In contrast the streaky appearance is characterised by bifurcations, irregularities, and terminations with feathered ends. There is a complete gradation from streaky to banded rhyolite. In Swaziland well developed fiamme are found at the base of the massive flow.[2]

3. Massive Central Zone: The streaky basal zone grades uniformly into the main mass of the flow by gradual fading of the banding into a more massive rock type. The rhyolite of this massive or 'felsitic' zone[6 7] is characterised by a finely mottled appearance and in thin section textures range from felsitic to microgranophyric with phenocrysts of quartz, and feldspar, typically corroded and resorbed, and minor amounts of pyroxene. In comparison phenocrysts in the basal pitchstone bands do not show the same degree of interaction with the mesostasis. Iron staining along

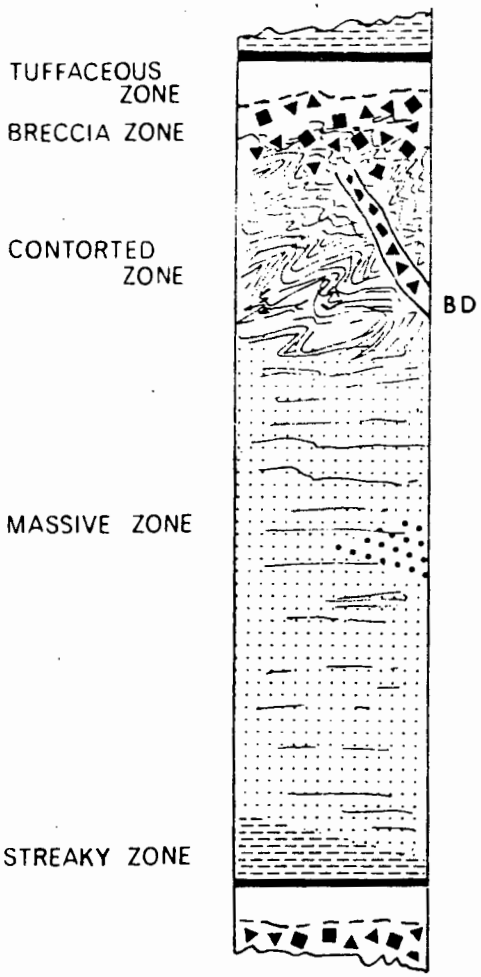

Fig. 1. Idealized section through a typical Lebombo acid-flow
BD - Breccia dyke.

strongly developed planar jointing gives rise to a pseudo-banding in this zone.

The massive zone generally accounts for about 90-95 per cent of each flow.

4. Contorted Zone: The central massive zone is gradational upwards into a flow-banded zone which is invariably highly contorted and folded. The folds have amplitudes ranging from several millimetres to several metres and vary in style from broad open antiforms and synforms to sharp, chevron-like crinkles. Finely developed ptygmatic-like folds are also found and large recumbent-style folding occurs in the cliff faces around the Jozini dam. In general the contorted zone constitutes a small percentage of the entire flow (<10%) but a few flows occur in which flow-folding is prevalent throughout.

5. Breccia Zone: A breccia zone frequently occurs at the top of the rhyolitic flow. The breccias appear to have formed either by flow auto-brecciation, in which case they are gradational into contorted rhyolite, or as pyroclastic flows which may be up to 70 m thick. In the Jozini type section a ramp structure occurs between breccia and contorted rhyolite in a well exposed flow.

Volcanological Interpretation

Previous workers in Swaziland[8] and the southern Lebombo[9] concluded that the acid volcanics were emplaced by a nuee-ardente mechanism and were therefore ash-flows or ignimbrites, whereas rhyolites cropping out in Mozambique were considered to be lavas.[5] More recent detailed mapping and geochemical studies by the authors of this paper have shown that the eruptive mechanism of the Lebombo flows was essentially unique.

The generally accepted mode of emplacement of an ignimbrite involves a glowing, fluidised cloud of hot magmatic particles and pyroclastics (an ash-flow) advancing rapidly over extreme distances away from the eruption site. As the ash-flow slows and gas pressure decreases suspended particles are dropped and if the temperature of the fragments is hot enough welding will occur. With sufficiently high temperatures complete homogenisation may occur, though some ignimbrites are non-welded and the great majority are only partly welded.

Characteristic features of ignimbrites[10 11 12 13] are:

(i) extensive sheet like form and a tendency to form plateaus and jointed cliffs

(ii) presence of fragments and clasts set in a poorly sorted groundmass

(iii) predominance of pyroclastic features

(iv) frequent compositional zoning reflecting an inversion of the fractionation trends of the original magma chamber.

Conversely rhyolite lava[14 15] flows are characterised by:

(i) limited lateral extent and a tendency to form domes or prominent topographical features

(ii) absence of pyroclastic features

(iii) the ubiquitous occurrence of contorted flow banding.

It can be seen from the preceding descriptions that the Lebombo rhyolite flows have many features attributable to either ignimbrites or lavas. Though the extensive sheet-form, sharp flow contacts and rarely preserved eutaxitic features of these rocks are possible indicators of an ash-flow type eruption, criteria such as contorted zones, breccias, absence of compositional zoning and the scarcity of clastic relicts weigh in favour of a lava-flow type eruption. Consequently it has been necessary to examine and formulate alternative eruptive mechanisms for the flows.

Conclusion

To explain the above observations two models can be proposed:

Model 1: If the rhyolites were erupted as abnormally high temperature lavas, they could have attained the mobility to cover large distances and form sheet-like flows similar to those formed by ignimbrites. In view of the tensional regime in which the Lebombo volcanics were erupted[2 3 16] it is postulated that crustal dilation and necking of the upper mantle led to a substantial increase in heat flows at the base of the crust (the likely source region of the rhyolites) thereby generating a series of high temperature magmas. Tensional gaps running the length of the Lebombo would have provided the lava with easy and rapid access to the surface ensuring minimal heat loss and volatile buildup. Lower viscosities due to the increased temperatures would have allowed the lavas to develop a sheet-like form and folds and autobrecciation would have developed in the rapidly cooled flow tops. Small amounts of H_2O and CO_2 might also have assisted in lowering the viscosities of the acid lava, though the general absence of hydrous phases implies that the magmas were relatively dry.

We feel, however, that in view of the extensive sheet-form nature of the flows, they were probably emplaced by an ash-flow type eruption as outlined in the following model:

Model 2: Though there is a distinct scarcity of pyroclastic textures in the Lebombo rhyolites it is possible that the flows were ignimbritic in origin but that most of the primary features of the rocks were destroyed by intense welding, remobilisation and devitrification after emplacement.[10] (It is thought that some of the textural features of zone 2 are the product of compaction and stretching of glass shards and pumice fragments at the base of an ignimbrite.) Alternatively the rocks could have been erupted as degassed ash-flows[17 18] which were never as particulate as classic ash-flow deposits. The size and associated high heat retention capabilities of these flows would have prevented the formation of mineralogical zones[11] and also produced complete homogenisation of the magmatic particles and any foreign clasts. Contorted flow banding resulted from remobilisation

and rheoignimbrite[15 19 20] formation when deposited on a slope, or else formed during primary movement of the degassed material[17 21]. The possible setting up of thermal convection cells within the emplaced flows might also have produced flow banding and would have aided the homogenisation of the flow centre.[20] Large scale flow folds e.g. cliff faces around Jozini dam and exposures in Swaziland, possibly represent primary flow and convective features whereas the numerous smaller flow folds and kink bands of the contorted zone might well have developed in rheoignimbrites and tongues of remobilised lava. Ramp structures[3] are typical of rheoignimbrites[22] and the autobreccias (zone 5) probably developed by fragmentation of the congealing remobilised lava surface.

REFERENCES

[1] Cleverly, R.W. and Bristow, J.W. Trans. Geol. Soc. S. Afr. (In press).
[2] Cleverly, R.W. D. Phil. (Unpubl.) Univ. Oxford (1977).
[3] Bristow, J.W. M.Sc. (Unpubl.) Univ. Natal (1976).
[4] Bristow, J.W. Ph.D. (In prep.)
[5] Wachendorf, H. Bull. Vulcan. 37(4), 515-529 (1973).
[6] Tyndale-Biscoe, R.M. Trans. Geol. Soc. S. Afr. 52, 403-413 (1949).
[7] Monkman, L.J. Ph.D. (Unpubl.) Univ. Leeds (1961)
[8] Urie, J.H. and Hunter, D.R. Bull. Geol. Surv. Swaziland 3, 28-44 (1963).
[9] Stratten, T. M.Sc. (Unpubl). Univ. Potchefstroom (1965).
[10] Ross, C.S. and Smith, R.L. Geol. Soc. Am. Prof. Paper 366 (1961).
[11] Briggs, N.D. N.Z. J., Geol. Geophys. 19, 182-212 (1976).
[12] Rhodes, R.C. Ph.D. (Unpubl.) Univ. New Mexico (1970).
[13] Sparks, R.S.J. and Walker, G.P.L. Nature 241, 62-64 (1973).
[14] Christiansen, R.L. and Lipman, P.W. Geol. Soc. Am. Bull. 77, 671-684 (1966).
[15] Rutten, M.G. and Van Everdingen, R.O. Geol. Mjinb. 40, 49-57 (1961).
[16] Cox, K.G. in African Magmatism and Tectonism, 211-235 (1970).
[17] Schminske, H.U. and Swanson, D.A. Jl. Geol. 75, 641-664 (1967).
[18] Tazieff, H. in Mechanisms of Igneous Intrusion, (1970).
[19] Rittman, A. Volcanoes and their activity (1962).
[20] Cleverly, R.W. Petros 8, 12-14 (1978).
[21] Bristow, J.W. Petros 8, 20-25 (1978).
[22] Lock, B.E. Can. Jl. Earth Sci. 9, 1495-1503 (1972).

J.W. Bristow
Department of Geochemistry
University of Cape Town.

R.W. Cleverly
Department of Geology
University of Cape Town.

Fine grained lava consisting of plagioclase pyroxene apatite and opaque oxide.
Mfolozi River Area: 32 08 45E,28 36 00S

S11e — Basalt: aphyric
Very fine grained lava with an intersertal texture consisting of plagioclase, pyroxene, opaque ore and apatite. Slightly altered.
Mfolozi River Area: 32 10 00E,28 26 05S

S14 — Basalt: sparsely porphyritic
Glomeroporphyritic plagioclase and rare pseudomorphed olivine phenocrysts. Matrix: very fine grained, intersertal texture. Mildly altered.
Mfolozi River Area: 32 07 10E,28 23 20S

S16 — Basalt: sparsely porphyritic
(Similar to S14)
Mfolozi River Area: 32 04 42E,28 23 10S

S20 — Basalt: porphyritic
Glomeroporphyritic plagioclase phenocrysts. Matrix: composed of microphenocrysts of plagioclase and augite intergrown in a subophitic to intersertal texture. Glassy mesostasis is crowded with opaque oxide granules and quench plagioclase microlites. Small chlorite amygdales - olive green with light green cores, occur in the lava.
Mfolozi River Area: 32 07 55E,28 27 50S

S21d — Basalt: aphyric
Medium grained lava composed of rare pseudomorphed olivine microphenocrysts, plagioclase, pyroxene, apatite, opaque oxide and patches of glass. Rock is slightly altered and contains small irregular chloritic amygdales.
Mfolozi River Area: 32 07 48E,28 27 47S

S23a — Basalt: porphyritic
Glomeroporphyritic plagioclase and rare olivine (fresh and pseudomorphed). Matrix: plagioclase pyroxene, apatite, opaque oxide and interstitial glass. Small amygdales as in S21d.
Mfolozi River Area: 32 07 00E,28 28 00S

S45 — Basalt: aphyric
Ultra fine grained lava consisting of plagioclase, pyroxene, apatite and opaque oxide. Intersertal texture.
Mfolozi River Area: 32 03 12E,28 25 40S

S47 — Basalt: aphyric
Coarse grained lava with microphenocrysts of plagioclase and rare pyroxene set in a finer

grained intersertal groundmass of plagioclase and granular pyroxene. Numerous glassy patches occur with opaque-oxide granules and quench feldspars. Small amygdales infilled with chlorite and zeolite are present.
Mfolozi River Area: 32 01 45E,28 24 47S

S49 Basalt: porphyritic
Glomeroporphyritic aggregates of large plagioclase phenocrysts. Rare pseudomorphed olivine microphenocrysts. Matrix: intersertal to subophitic plagioclase, pyroxene and skeletal and equant opaque-oxide. Glassy mesostasis contains granules and quench feldspars. Irregular chlorite amygdales with zeolite cores.
Mfolozi River Area: 32 01 45E,28 26 35S

S51 Basalt: aphyric
(Similar to S45)
Mfolozi River Area: 32 02 48E,28 23 45S

S53 Basalt: porphyritic
(similar to L9)
Mfolozi River Area:

L9 Basalt: sparsely porphyritic
Glomeroporphyritic plagioclase microphenocrysts. Matrix: plagioclase, clinopyroxene and opaque-oxide, fine grained intersertal texture.
Mfolozi River Quarry-flow 3: 32 09 45E,28 26 35S

L12 Basalt: sparsely porphyritic
Very fine grained intersertal lava with occasional glomeroporphyritic plagioclase and minor clinopyroxene.
Empangeni Area: 31 50 55E,28 42 20S

L18 Basalt: sparsely porphyritic
(Similar to L12)
Empangeni Area: 31 50 08E,28 41 42S

L29 Basalt: aphyric
Empangeni Area: 31 51 10E,28 41 50S

L32 Basalt: porphyritic
Phenocrystic olivine, partially pseudomorphed by iron-ore, chlorite and minor iddignsite. Plagioclase and pyroxene microphenocrysts lenticular and granular opaque-oxide. This is a coarse-grained, subophitic rock in which there is also a tendency for larger plagioclase phenocrysts to form glomeroporphyritic textures with olivine and pyroxene microphenocrysts. Apatite is a common accessory and occurs predominantly in chloritized and altered patches of inter-

stitial glass.
Dindi, N Empangeni: 31 52 15E,28 37 30S

L36 Basalt: aphyric
(Similar to L12)
Dindi, N Empangeni: 31 52 32E,28 38 05S

L57 Basalt: sparsely porphyritic
(altered)
Kwesi River, N Empangeni: 31 52 45E,28 38 35S

L59 Basalt: porphyritic
Mayuba, N Empangeni

L63 Basalt: aphyric
Fine grained lava consisting of plagioclase pyroxene and opaque oxide. Intersertal to sub-ophitic texture. Glassy residue contains opaque-oxide granules. Slightly altered with numerous small irregular and large spherical, quartz filled amygdales.
Ubizo, N Empangeni: 31 53 20E,28 39 40S

L87 Basalt: sparsely porphyritic
Glomeroporphyritic plagioclase phenocrysts (altered). Matrix: altered plagioclase and pyroxene, opaque-oxide. Glassy residium. Sample is very strongly altered and slightly amygdaloidal.
Specimen from entablature of basalt flow (5m thick) exposed in rail cutting: Empangeni-Vryheid railwayline: 31 54 42E,28 23 40S

L94 Dolerite Dyke: porphyritic
Glomeroporphyritic plagioclase phenocrysts and very rare pseudomorphed olivine microphenocrysts. Matrix: plagioclase and pyroxene skeletal and granular opaque-oxide. Subophitic to intersertal texture. Apatite is an accessory.
3,9m,237,80N.
Ngqwatayi quarry (Empangeni): 31 49 45E, 28 43 00S

L188C Dolerite: porphyritic
Coarse grained dolerite with an abundance of large plagioclase phenocrysts.
Nesane River quarry: 32 12 58E,28 20 20S

L202b Basalt: aphyric
Coarse grained lava with an intersertal texture consisting of plagioclase, clinopyroxene, opaque-oxide, accessory apatite and altered glass. The rock contains numerous small and large amygdales infilled with zeolite, chlorite, epidote and quartz and is strongly altered. Clinopyroxene

and plagioclase in particular, have undergone extensive alteration.
Simbeleni, N of Nesane River: 31 10 15E, 28 13 05S

L229 Basalt: porphyritic
Fine - medium grained lava with large glomero-porphyritic aggregates of clinopyroxene and plagioclase. The aggregates have a distinctly rounded appearance and might represent cognate xenoliths of gabbroic material derived from lower levels of a fractionating magma chamber. The slide also contains a xenolith of very fine grained plagiophyric basalt.
Hluhluwe River: 32 13 50E,28 07 35S

L249a Dolerite Dyke: coarse grained, subophitic dolerite. Plagioclase, augite and opaque oxide (skeletal and granular). Altered glass occurs intersertially and contains abundant accessory apatite.
11,5m,208,45N.
Hluhluwe River quarry: 32 14 45E,28 07 38S

L257b Basalt: porphyritic (slightly metamorphosed)
Fine grained glomeroporphyritic lava. It is intensly altered and has probably suffered low grade thermal metamorphism and deuteric alteration. This has caused the formation of epidote and large apatite needles in most of the amygdales present in the rock. Excessive amounts of chlorite, calcite and quartz, which were probably introduced during deuteric alteration, are also found in the amygdales.
Hluhluwe River: 32 11 45E,28 07 40S

L285 Basalt: porphyritic (slightly metamorphosed)
This lava is similar to L257b in that it also appears to have undergone intense deuteric alteration. Plagioclase phenocrysts are strongly altered and exhibit a sieve texture. and clinopyroxene has been replaced by chlorite.Opaque-oxide and apatite occur as accessories. Irregular crystals of quartz and K-feldspar are present in the slide and may represent xenoliths of granitic base-ment. Amygdales contain the same minerals as found in L257b.
Kwa-Nompondo, W of H.G.R.: 32 10 05E, 28 03 20S

L318 Basalt: aphyric
Ultra fine grained, intersertal lava consisting of plagioclase, clinopyroxene, disseminated opaque-oxide and accessory apatite.It contains small amygdales infilled with quartz and

L441 — Rhyolite JF
Mkuze Game Reserve (Mtshopi): 32 09 55E, 27 38 25S

L462 — Basalt: aphyric
Very fine grained intersertal rock comprised of plagioclase, clinopyroxene, subhedral opaque-oxide and minor apatite. Slightly amygdaloidal but reasonably fresh.
Mkuze River: 32 02 40E,27 36 20S

L467 — Rhyolite JF
Muhlekazi, W of M.G.R.: 32 10 03E,27 43 31S

L469 — Rhyolite JF
Msunduzi River Area: 32 14 00E,27 45 35S

L485a — Dolerite Dyke: sparsely porphyritic
Medium to coarse grained dolerite. Plagioclase, augite and opaque-oxide (skeletal and granular) Subophitic texture.
Columnar jointed: N-S,70W.
Mkuze River: 31.92E,28.62S

L490 — Dolerite Dyke: sparsely porphyritic
(Similar to L485a)
172,71E.
Mkuze River: 31.95E,27.62S

L496b — Dolerite Dyke: sparsely porphyritic
Medium grained, subophitic texture.
N-S,V
Mkuze River: 31.98E,27.60S

L503 — Dolerite Dyke: sparsely porphyritic
Fine to medium grained rock consisting of plagioclase laths, augite, abundant opaque oxide (skeletal and granular) and interstitial glass.
N-S,70-80W. Cross cuts Jozini Formation.
Mkuze-Jozini Road: 32 01 05E,27 30 35S

L505c
L505d — Basalt: porphyritic
Glomeroporphyritic plagioclase microphenocrysts are set in a fine grained intersertal to subophitic matrix. Rare glassy patches are present and accessories include apatite and opaque-oxide.
Specimens from the entablature of basalt flow exposed in the Ngqwatayi quarry, west of Empangeni: 31 49 45E,28 43 00S

L508 — Dolerite Dyke: porphyritic
(Similar to L503 but contains abundant glass with spherulitic structures.)
N-S,V. Cross cuts Jozini Formation.
Ngweni Quarry: 32 17 15E,27 56 00S

J3	Basalt: aphyric Mkuze-Jozini Road: 32 00 47E,27 29 35S
J55	Dolerite: sparsely porphyritic Fine grained rock consisting of microphenocrysts of plagioclase and clinopyroxene, skeletal ore and abundant glass. Similar petrographically to L372b, L503 and L508. Jozini Dam canal cuttings: 32 04 34E,27 25 13S

TABLE 2: ROOI RAND DOLERITES

L485a	Dolerite Dyke: porphyritic Medium to coarse grained dolerite. Plagioclase, augite and opaque-oxide (skeletal and granular) Subophitic texture. Columnar jointed: N-S,70W Mkuze River: 31 55 02E,27 37 00S
L490	Dolerite Dyke: sparsley porphyritic Similar to L485a 172,71E Mkuze River: 31 58 53E,27 30 35S
L496b	Dolerite Dyke: sparsley porphyritic Medium grained, subophitic texture. N-S,V Mkuze River: 31 58 53E,27 35 43E
A1	Dolerite Dyke: aphyric Medium-grained with rare zoned plagioclase microphenocrysts. Groundmass comprised of plagioclase laths and intersertal augite, with subhedral opaque ore, some of which display "comb structures". Minor quartz and biotite. Mkuze River: 31 49 13E,27 32 20S Ref. Armstrong, 1978.
A13	Dolerite Dyke: aphyric Medium-grained, sparsley feldsparphyric with one plagioclase phenocryst displaying an arrangement of glass inclusions. Groundmass texture is intersertal. Granular and skeletal opaque ores. Pseudomorphed olivine. Mkuze River: 31 49 55E,27 29 18S Ref. Armstrong, 1978.
A20	Dolerite Dyke: aphyric Medium-grained, comprised essentially of plagioclase and augite in subophitic texture. Rounded pseudomorphs of olivine.

Pongola River: 31 52 15E,27 26 03S
Ref. Armstrong,1978

A21 Dolerite Dyke: porphyritic
Glomeroporphyritic plagioclase and occasional pyroxene microphenocrysts. Intersertal, fine-grained matrix. Pseudomorphed olivine (?). Sericitization and chloritization of plagioclase and pyroxene phenocrysts.
Pongola River: 31 52 15E,27 26 03S
Ref. Armstrong, 1978.

A22 Dolerite Dyke: aphyric
Comprises very elongate (elongation ratios up to 14.1) plagioclase crystals, together with pyroxene and both granular and skeletal opaque ore.
Pongola River: 31 52 15E,27 26 03S
Ref. Armstrong, 1978.

A24 Dolerite Dyke: porphyritic
Glomeroporphyritic plagioclase, frequently zoned, set in fine-grained matrix comprising acicular plagioclase subophitically related to pyroxene. Scattered opaque ore grains. Accessory apatite.
Pongola River: 31 52 15E,27 26 03S
Ref. Armstrong, 1978.

A28 Dolerite Dyke: porphyritic
Glassy rock with phenocrysts of plagioclase, together with euhedral microphenocrysts of pyroxene and partially and wholly altered olivine. Quenched plagioclase microlites display fluidal textures. Cryptocrystalline opaque ore.
Pongola River: 31 52 15E,27 26 03S
Ref. Armstrong, 1978.

A41 Dolerite Dyke: porphyritic
Feldsparphyric dolerite with subophitic groundmass. Rounded olivine crystals, generally altered along irregular cracks and around edges but with fresh cores. Abundant opaque ore, frequently approaching idiomorphism.
Pongola River: 31 51 46E,27 25 21S
Ref. Armstrong, 1978.

A46 Dolerite Dyke: porphyritic
Medium-grained dolerite, with subophitic groundmass texture. Plagioclase phenocrysts are up to 5.5mm in length. Large pseudomorphed olivine crystals (?).
Pongola River: 31 51 45E,27 25 20S
Ref. Armstrong, 1978.

A49 Dolerite Dyke: porphyritic
Plagioclase phenocrysts display glomeroporphyritic texture. Quenched acicular plagioclase make up the fine groundmass with pyroxene, opaque ore and glass. Although no fresh olivine is present, large 'clots' of penninite may represent pseudomorphed olivine.
Pongola River: 31 51 44E,27 25 19S
Ref. Armstrong, 1978.

A54 Dolerite Dyke: aphyric
Medium-grained dolerite comprising large augite crystals ophitically enclosing plagioclase laths.
Pongola River: 31 50 59E,27 24 27S
Ref. Armstrong, 1978.

A70 Dolerite Dyke: porphyritic
Fine-grained dolerite comprising glomeroporphritic plagioclase in a groundmass of small acicular plagioclase subophitically related to pyroxene. A number of plagioclase phenocrysts contain numerous inclusions of glass and small pyroxene crystals.
Pongola River: 31 50 31E,27 23 46S
Ref. Armstrong, 1978.

A79 Dolerite Dyke: aphyric
Dolerite consisting of small,acicular plagioclase crystals, pyroxene and relatively large subhedral opaque ore crystals. The plagioclase is subophitically enclosed by the pyroxene. Small patches of myrmekitic material.
Pongola River Area: 31 49 57E,27 21 17S
Ref. Armstrong, 1978.

A82 Dolerite Dyke: porphyritic
Glomeroporhyritic plagioclase set in an extremely fine-grained groundmass comprising acicular plagioclase, intersertal pyroxene and granular opaque ore. Possible pseudomorphed microphenocrysts of olivine.
Pongola River Area: 31 49 57E,27 21 17S
Ref. Armstrong, 1978.

A85 Dolerite Dyke: aphyric
Fine- to medium-grained dolerite, comprising a mesh of acicular plagioclase and intersertal pyroxene. A few small pyroxene crystals show a very low +2Vz angle, suggesting the presence of minor pigeonite.
Pongola River Area: 31 49 55E,27 21 19S
Ref. Armstrong, 1978.

A94 Dolerite Dyke: porphyritic

Feldsparphyric. Plagioclase phenocrysts are arranged in glomeroporphyritic aggregates ("crow's foot" texture) in a very fine-grained groundmass of acicular plagioclase and intersertal pyroxene.
Pongola River Area: 31 45 53E,27 20 42S
Ref. Armstrong, 1978.

A96 Dolerite Dyke: aphyric
small acicular plagioclase and intersertal pyroxene. Subhedral opaque ore crystals of variable size.
Pongola River Area: 31 45 53E,27 20 42S
Ref. Armstrong, 1978.

A101 Dolerite Dyke: sparsely porphyritic
Fine-grained dolerite with microphenocrysts of plagioclase and olivine. Groundmass comprises essentially small plagioclase laths subophitically enclosed by pyroxene. Olivine 'armoured' by a reaction rim of undetermined isotropic material. Some pyroxene crystals partially altered around edges to hornblende. Biotite flakes also present.
Pongola River Area: 31 45 49E,27 20 41S
Ref. Armstrong, 1978.

A114 Dolerite Dyke: aphyric
Fine-grained dolerite. Acicular plagioclase and intersertal pyroxene. Flakes of highly pleochloric brown biotite, probably an alteration product after pyroxene.
Pongola River Area: 31 45 43E,27 20 38S
Ref. Armstrong, 1978.

A117 Dolerite Dyke: aphyric
Fine-grained dolerite consisting essentially of acicular plagioclase and intersertal pyroxene Scattered granular opaque ore and accessory quattz. Small crystals of hornblende and biotite appear to be secondary after pyroxene.
Pongola River Area: 31 45 42E,27 20 37S
Ref. Armstrong, 1978.

A129 Dolerite Dyke: sparsely porphyritic
Fine- to medium-grained dolerite. Acicular plagioclase and pyroxene subophitically and ophitically related. Scattered opaque ore. Very small plagioclase and pyroxene crystals occasionally display radial intergrowth.
Hluhluwe River: 32 11 09E,28 08 29S
Ref. Armstrong, 1978.

A135 Dolerite Dyke: porphyritic
Medium-grained dolerite with plagioclase pheno-

Fine- to medium-grained dolerite. Acicular plagioclase and intersertal augite. Granular opaque ore.
Mkuze River: 31 57 22E,27 35 39S
Ref. Armstrong, 1978.

A175 Dolerite Dyke: aphyric
Fine-grained dolerite. Plagioclase, pyroxene and opaque ore. Intersertal.
Mkuze River: 31 53 10E,27 36 36S
Ref. Armstrong, 1978.

A179 Dolerite Dyke: aphyric
Fine-grained rock consisting of plagioclase, rounded intersertal pyroxene and small granular opaque ore. Minor devitrified glass.
Msunduzi River: 32 01 40E,27 49 34
Ref. Armstrong, 1978.

A182 Dolerite Dyke: aphyric
Fine-grained dolerite. Generally intersertal,but the larger pyroxene crystals enclose plagioclase laths subophitically. Accessory biotite.
Msunduzi River: 32 01 05E,27 49 22S
Ref. Armstrong, 1978.

A186 Dolerite Dyke: sparsely porphyritic
Extremely fine-grained dolerite with micro-porphyritic plagioclase, augite and olivine set in a groundmass of plagioclase, pyroxene and opaque ore.
Msunduzi River: 32 01 05E,27 49 22S
Ref. Armstrong, 1978.

A189 Dolerite Dyke: aphyric
Acicular plagioclase and rounded augite crystals in a glassy matrix. Microlites of plagioclase display fluidal textures.
Msunduzi River: 32 01 05E,27 49 22S
Ref. Armstrong, 1978.

TABLE 3: SWAZILAND VOLCANICS

EH8 Basalt: sparsely porphyritic
Fine-medium grained intersertal to subophitic lava. Plagioclase, clinopyroxene, minor apatite and a little interstitial glass constitute the mineral assemblage. (Microprobe data: Betton, 1978).
Ehlane Nature Reserve, Swaziland:

EH9 Basalt: sparsely porphyritic
Medium grained, highly altered rock consisting

of pseudomorphed olivine, altered plagioclase, pyroxene, interstitial mesostasis and patches of chlorite. Clinopyroxene rims are present on the olivine microphenocrysts.
Ehlane Nature Reserve, Swaziland:

S4 Basalt: porphyritic
Phenocrysts: Extremely sparse tabular crystals of basic plagioclase (up to 0.5mm). Groundmass: Very fine grained with plagioclase laths up to 0.15mm, slightly sericitised. Smaller turbid crystals of clinopyroxene visible. The ore is disseminated as fine granules. A small amount of epidote and chlorite is present.
6.25km E of Maloma on Road to Nsoko.
Ref. Cox et.al. 1967.

S5 Basalt: aphyric
Non-porphyritic. Feldspar laths are sericitised and reach 0.3mm. Original pyroxene granules (0.1mm) replaced by tremolite-actinolite. There is some chlorite interstitially and a certain amount of epidote is present. The ore is in equidimensional crystals having the typical skeletal appearance of ilmenite.
0.31km E. of S4.
Ref. Cox et.al. 1967.

S9 Basalt: porphyritic
Phenocrysts: Large (8mm) plagioclases (andesite) replaced partly by veins of chlorite plus small amounts of altered olivine. Groundmass: Coarse sub-ophitic texture with plagioclase laths (oligoclase-andesine) reaching 0.5mm. Clino-pyroxene partly replaced by tremolite. Moderately abundant interstitial chlorite.
Maloma-Nsoko road, 1.09km W. of Lubuli township.
Ref. Cox, et.al. 1967.

S10 Basalt: porphyritic
Phenocrysts: Equidimensional basic plagioclase (2-3mm) partly replaced by chlorite veins, ca. 10 percent. Small amounts of chloritised small olivines (ca 1 percent). Groundmass: Plagioclase somewhat chloritised, clinopyroxene fresh. The ore as in S5.
0.32 km E. of S9.
Ref. Cox, et.al. 1967.

S11 Basalt: porphyritic
Rock almost identical with S10. The olivine is somewhat less abundant.
Lubuli township, Maloma-Nsoko road.
Ref. Cox, et.al. 1967.

S13 Basalt: porphyritic
Phenocrysts: Altered olivine and plagioclase similar to the two specimens above. Groundmass: like the above. The texture is intergranular, occasionally subophitic.
Cecil Mack pass, exactly on Swaziland-Natal boundary.
Ref. Cox, et.al. 1967.

S17 Basalt: porphyritic
Phenocrysts: Large basic plagioclases (10mm. partly replaced by epidote and carbonate), extremely sparsely distributed. Groundmass: Ophitic texture, the augites are relatively large and sparsely distributed, ophitically enclosing euhedral plagioclase laths.
Quarry 200m N. of new bridge, Big Bend.
Ref. Cox, et.al. 1967.

NG25 Basalt: sparsely porphyritic
Fine-medium grained rock consisting of small olivine microphenocrysts, plagioclase, clinopyroxene, opaque-oxide, minor apatite and some interstitial glass. Texture is intersertal to subophitic.
Ndumu Game Reserve.

TABLE 4: CENTRAL LEBOMBO VOLCANICS

TABLE 4a: Sabie and Komati River Area

CL99 Granophyre
Muntshe Ridge: 31 52 57E,25 30 16S

CL100 Basalt: sparsley porphyritic
Fine grained lava consisting of plagioclase laths small equidimensional clinopyroxenes and conspicuous amounts of cloudy and altered mesostasis with apatite and abundant spicules of opaque-oxide. Small nodular clinopyroxene aggregates and irregular green chlorite patches also occur in this slide.
Sabie River: 31 53 35E,25 06 05S

CL102 Dolerite: aphyric
(Similar to CL100)
Sabie River: 31 53 40E,25 06 08S

CL105 Dolerite: aphyric
Fine grained intersertal rock which contains prominent quartz in addition to plagioclase, clinopyroxene, apatite and equidimensional

opaque-oxide.
Sabie River: 31 53 45E,25 06 10S

CL108 Basalt: aphyric
Fine grained lava consisting of plagioclase laths, equidimensional clinopyroxene, spicular ore, apatite, rare K-feldspar and a large amount of altered mesostasis. Also contains rare pseudomorphed olivine microphenocrysts.
Sabie River: 31 53 52E,25 06 12S

CL110 Basalt: aphyric
(Similar to CL100)
Sabie River: 31 53 58E,25 06 15S

CL111 Basalt: sparsley porphyritic
Fine grained lava with microphenocrysts of plagioclase (glomeroporhyritic), rare pseudomorphed olivine, nodular clinopyroxene set in a matrix of microcrystalline feldspar and pyroxene, apatite and spicular opaque-oxide.
Sabie River: 31 54 08E,25 06 15S

CL113 Basalt: aphyric
(Smilar to CL100)
Sabie River: 31 54 12E,25 06 17S

CL115 Basalt: aphyric
Fine grained intersertal rock consisting of clinopyroxene, plagioclase, apatite and equidimensional ore, possibly also a little interstitial quartz.
Sabie River: 31 54 14E,25 06 18S

CL118 Basalt: sparsley porphyritic
Microphenocrysts plagioclase and nodular clinopyroxene set in a very fine grained, altered mesostasis with spicular opaque-oxide and apatite.
Sabie River: 31 54 20E,25 06 26S

CL120 Basalt: sparsley porphyritic
(Similar to CL118 but contains rare microphenocrysts of pseudomorphed olivine).
Sabie River: 31 54 25E,25 06 29S

CL132 Basalt: aphyric
Fine grained lava consisting of abundant plagioclase, and lesser amounts of clinopyroxene, granular and spicular opaque-oxide and apatite, also rare K-feldspar.
Sabie River: 31 55 25E,25 07 16S

CL143 Dolerite: aphyric
Fine-medium grained, subophitic rock, con-

sisting of plagioclase, clinopyroxene, equidimensional opaque oxide, apatite and rare patches of interstitial glass.
Sabie River: 31 56 10E,25 07 21S

CL156 Dolerite: aphyric
Fine - medium grained rock consisting of clinopyroxene, plagioclase, equidimensional opaque-oxide, apatite and rare pseudomorphed olivine microphenocrysts.
Sabie River: 31 57 38E,25 09 45S

CL209 Rhyolite
Porphyritic - glomeroporhyritic: Phenocrysts: plagioclase (with perthitic patches), clinopyroxene (light green), minor amounts of opaque oxide, and rare zircons and apatites. Matrix: very fine grained, with incipient crystallites.
Sabie River: 31 59 45E,25 09 46S

CL267 Basalt: aphyric
(Similar to CL115)
Sabie River:

CL351 Basalt: aphyric
Fine grained lava consisting of plagioclase clinopyroxene, equidimensional ore, apatite and minor amounts of glassy mesostasis.
Gabinja Road:

CL356 Basalt: aphyric
Medium grained lava: clinopyroxene, plagioclase, opaque ore and minor apatite. Subophitic texture.
Komati River: 31 52 57E,25 30 16S

CL360 Basalt: porphyritic
(Similar to CL356)
Komati River: 31 53 30E,25 30 14S

CL372 Basalt: porphyritic
Glomeroporphyritic plagioclase phenocrysts (up to 6.5mm) Matrix fine grained intersertal: clinopyroxene, plagioclase, dispersed opaque-oxide. Small chlorite amygdales.
Komati River: 31 53 48E,25 30 12S

CL376 Basalt: porphyritic
Komati River: 31 54 45E,25 29 40S

CL451 Rhyolite
Ka-Mahlenti: 31 56 47E,25 40 30S

TABLE 5: NORTHERN LEBOMBO VOLCANICS

TABLE 5a: Olifants River Area

KA5	Rhyolite: JF Mozam. Border: 31 44 25E,23 56 05S
KA6b	Rhyolite: JF Porphyritic-glomeroporphyritic. Phenocrysts: altered plagioclase and minor K-feldspar, altered pyroxene, opaque oxide, apatite and zircon. Matrix: microcrystalline to micro-granophyric with dispersed ore and abundant apatite. 20m below KA6a
KA13	Rhyolite Dyke 10m,N-S,V Letaba River, W of confluence: 31 44 43E, 23 58 42S
KA15	Nephelinite Lava Fine grained rock with small olivine phenocrysts (3%) now totally altered and prominent cpx needles set in a matrix which contains abundant isotropic and grey-polarizing material. 0.03m above volcaniclastics - lava contact. Olifants River: 31 34 27E,24 02 03S
KA16	Nephelinite: porphyritic Similar to KA15 0.03m above KA15
KA24	Picrite Basalt: 2P Phenocrysts: olivine, mantled orthopyroxene (15%) and clinopyroxene. Matrix: skeletal opaque ore, olivine microphenocrysts, subhedral and anhedral pyroxene, anhedral plagioclase, apatite and interstitial glass. Ndziyo Track: 31 34 45E,24 61 30S
KA25	Olivine Basalt Minor amounts of olivine and orthopyroxene, clinopyroxene (nodular aggregates and macrophenocrysts) and plagioclase constitute the phenocryst assemblage. The groundmass is microcrystalline to glassy and contains small irregular amygdales in addition to dispersed ore crystallites. Shishwayini Track, Olifants river: 31 36 20E, 24 02 30S
KA29	Picrite Basalt: 2P

Phenocrysts: olivine and clinopyroxene, mostly as nodular aggregates. Matrix: spicular ore anhedral pyroxene, skeletal and lath shaped plagioclase, and interstitial glass with feldspar crystallites and apatite.

KA31 Dolerite Dyke: sparsely porphyritic
Fine grained rock consisting of pyroxene, plagioclase, equidimensional opaque-oxide and abundant cryptocrystalline mesostasis. Quartz and sanidine are prominent interstitial materials, as in apatite.
Dyke contains basement xenoliths.
5m,200,75-80W
Olifants River: 31 37 10E,24 01 33S

KA32 Dolerite Stringer: sparsely porphyritic
0.5m,214,V
Olifants River, 150m E of KA31

KA34 Basalt: porphyritic
Phenocrysts: pseudomorphed olivine (<3%), orthopyroxene, clinopyroxene (rare macrophenocrysts, otherwise mostly nodular) and-plagioclase. The matrix is microcrystalline with clinopyroxene, plagioclase, disseminated opaques and numerous apatite needles. Highly altered, mantled orthopyroxene is also present.
Ndziyo Track: 31 37 55E,24 00 55S

KA35 Dolerite Dyke: porphyritic
20m,208,60-65W
Ndziyo Track: 31 38 05E,24 00 55SS

KA41 Rhyolite Dyke
KA42 Samples from a major rhyolite dyke characterized by strong vertical banding, contorted banding and tremendous brecciation, particularly along the margins where blocks greater than 5m in diameter are encountered.
25m,N-S,V
Kwa-Nwatimhisi:

KA52 Andesitic Dolerite Sill: microporphyritic chill margin.
Consists of microphenocrysts of plagioclase (glomeroporphyritic) clinopyroxene (typically nodular), subhedral opaque oxides and rare olivine pseudomorphs set in a slightly devitrified, glass groundmass.
Olifants River look-out.

KA52b Andesitic Dolerite Sill: microporphyritic
Coarser grained rock than the above. It contains greater amounts of clinopyroxene and olivine

and is characterized by a microcrystalline groundmass consisting of intergrown sanidine, quartz, spicular ore, skeletal pyroxene and abundant apatite. Needles of apatite are common in the plagioclase microphenocrysts.
Sample from approximately 18m below KA52

KA52c — Andesitic Dolerite Sill: microporphyritic
Similar to KA52b though slightly coarser and contains more olivine.
Sample from river-bed directly below KA52
Olifants River Look-Out: 31 40 04E,24 00 58S

KA75 — Rhyolite
Mahalamhala Road: 31 44 33E,23 56 00S

KA76 — Rhyolite
Groundmass is rather strongly altered
Mahalamhala Road: 31 44 34E,23 55 45S

KA78 — Rhyolite
Mahalamhala Road: 31 44 43E,23 55 46

KA82 — Rhyolite
Mahalamhala Road: 31 45 19E,23 54 10S

KA84 — Rhyolite
Microgranophyric groundmass.
Mahalamhala Road: 31 45 30E,23 53 35S

KA87 — Granophyre
Porphyritic - glomeroporphyritic. Pyroxenes and feldspars are pseudomorphed and altered. Groundmass exhibits a well developed granophyric texture.
Mahalamhala Road: 31 45 18E,23 54 13S

KA103 — Basalt: macroporphyritic
An unusual lava with giant plagioclase phenocrysts (up to 5cm) set in a fine grained intersertal matrix. The phenocrysts are arranged in well developed 'birds-foot' textures and appear to be most densely concentrated in the middle of the flow. A series of flows all containing giant feldspars crop out in the Letaba River and show well developed flow features.
Letaba River:

KA111 — Rhyolite
Olifants - Letaba River confluence:

KA112 — Basalt: sparsely porphyritic
Fine grained lava with an intersertal to subophitic texture: slightly amygdaloidal.
Olifants - Letaba River confluence:

KA121 — Rhyolite
Porphyritic - glomeroporphyritic. Phenocrysts: feldspar, pyroxene and minor olivine (all strongly altered or pseudomorphed), apatite and zircon. Matrix: fine grained microcrystalline.
Olifants Rest Camp (near Guest Lodge):

KNP13a
KNP13d — Basaltic Dykes: porphyritic
These dyke-like outcrops consist of highly altered feldspar microphenocrysts set in a murky, oxidized mesostasis. Clinopyroxene might also have been present. They are intensively veined by calcite and chlorite and in addition, patches of both these minerals are found in the groundmass.
Kwa-Nwatimhisi: 31 39 55E,23 59 20S

010b — Rhyolite
Porphyritic - glomeroporphyritic. Phenocrysts: plagioclase, rare K-feldspar, clinopyroxene, pseudomorphed olivine, opaque-oxide, apatite and minor zircon. Matrix: microcrystalline with occasional microgranophyric patches. Reasonably fresh rock through feldspars are rather strongly altered.
Olifants Rest Camp:

011C — Dolerite: sparsley porphyritic
Medium to coarse grained rock consisting of abundant plagioclase and lesser amounts of clinopyroxene, euhedral and subhedral (mostly equant) opaque-oxide and large needles of apatite (up to 1.5mm). Numerous patches and disseminated streaks and bands of chlorite occur in the rock. Some of the larger patches possibly represent pseudomorphed olivines.
Olifants River, below Rest Camp:

013c — Contaminated Dolerite: porphyritic
Olifants River, below Rest Camp:

018 — Dolerite: porphyritic
Coarse grained dolerite similar to 011c. It is slightly more altered than 011c and also contains a few large skeletal opaques.
Olifants River Area:

022 — Andesite Dolerite Sill: porphyritic
Coarse grained gabbroic rock consisting of plagioclase, clinopyroxene, opaque-oxide needles, rare olivine pseudomorphs and apatite.
Olifants River Area:

030 Andesite Dolerite: porphyritic
Coarse grained dolerite similar to sample 022 but contains patches of chlorite and large apatite needles (up to 1.5mm)
Olifants River Area:

031 Andesite Dolerite Sill: porphyritic
Coarse grained gabbroic rock with pseudomorphed olivine, abundant apatite, very large opaque-oxide crystals (up to 0.5mm) and interstitial granophyric material.
Olifants River Area:

068 Basalt: porphyritic
Phenocrysts: plagioclase, clinopyroxene (nodular). Matrix: intersertal, with plagioclase laths, small anhedral clinopyroxenes and equidimensional opaques.
Olifants River Area:

0169 Basalt: porphyritic
Medium to coarse grained lava with phenocrysts of plagioclase. Matrix consists of plagioclase, clinopyroxene, minor apatite, abundant spicular opaque-oxide and some K-feldspar. Rock is altered and contains patches of chlorite as well as chlorite infilled amygdales. Rare pseudomorphs of olivine are also present.
Balule Road,Olifants River:

0183 Basalt: porphyritic
Pyroxene-phyricilava with a groundmass consisting mostly of plagioclase and a fine microcrystalline of glassy mesostasis with much spicular opaque.
Balule Road, Olifants River:

0248 Picrite Basalt: 1P
Coarse to medium grained rock with subhedral and rounded olivine phenocrysts and rare unmantled orthopyroxenes. Matrix: plagioclase, clinopyroxene, opaque ores (includes kennedyite). K-feldspar overgrowths occur on some plagioclase laths.
Olifants River Area:

0287 Picrite Basalt: 3P
Phenocrysts: olivine, mantled orthopyroxene, clinopyroxene and plagioclase. Matrix: glassy with skeletal plagioclase microphenocrysts and skeletal opaque-oxides.
Olifants River Area:

TABLE 5b: Shingwedzi River Area

KS3 — Picrite Basalt: 3P
Phenocrysts: abundant olivine, up to 1mm in diameter, clinopyroxene, often in glomeroporphyritic aggregates of many small crystals, mantled orthopyroxenes and plagioclase microphenocrysts. Groundmass consists of plagioclase laths, clinopyroxene and brown glass with skeletal ore.
Vicinity Shingwedzi River: 31 27 30E,23 06 37S

KS7 — Picrite: probably a dyke
Holocrystalline rock consisting of olivine, clinopyroxene, orthopyroxene and intercumulus plagioclase. Numerous small clinopyroxenes are included in the plagioclase. Lath shaped and skeletal ore (includes kennedyite) and abundant apatite are also apparent.
Probable strike - 168
Track East of Shingwedzi: 31 28 22E,23 06 32S

KS16 — Rhyolite
Mozam. Border

KS19 — Rhyolite
Stream bed alongside road, S of Gondegonde:
31 33 37E,23 11 56S

KS26 — Dolerite Dyke: porphyritic
Fine grained rock consisting of radial and plumose aggregates of plagioclase and pyroxene, skeletal ore and abundant microcrystalline mesostasis.
4m,200,80W
Shingwedzi River: 31 31 35E,23 11 00S

KS35a — Picrite Basalt: 2P
Shingwedzi River:

KS36 — Dolerite Dyke: porphyritic
Fine-grained plagiophyric rock. Also contains rare clinopyroxene phenocrysts. Groundmass consists of clinopyroxene, plagioclase and opaque oxides.
Shingwedzi River:

KS41 — Picrite Basalt: 1P
Phenocrysts: subhedral and rounded olivines (strongly altered around the margins and along cracks). Matrix: Microcystalline with sheaves of feldspar, small equidimensional pyroxene and skeletal laths of opaque oxide. Apatite is common and a few small amygdales are apparent.
Shingwedzi River:

KS47 Picrite Basalt: 2P
Phenocrysts: subhedral and rounded olivine up to 1.5mm and commonly pseudomorphed, abundant orthopyroxene (found as both discrete zoned euhedral and subhedral phenocrysts, and as resorbed, clustered crystals with marginal clinopyroxene overgrowths), and clinopyroxene (nodular aggregates and rare macrophenocrysts, up to 3mm). Matrix: skeletal opaque oxide, acicular plagioclase (up to 0.75mm) and apatite with abundant interstitial glass.
Shingwedzi River: 31 27 30E,23 07 26S

KS53 Picrite: probably a dyke
Holocrystalline rock with abundant rounded olivines (up to 2mm), subhedral clinopyroxene laths (up to 2mm), euhedral and subhedral opaque oxides, including kennedyite, intergranular plagioclase and alkali-feldspar. Apatite needles are also ubiquitous.
Shingwedzi-Punda Milia Road: 31 22 05E, 23 00 50S.

KS56 Dolerite: porphyritic
Shingwedzi River: 31 27 00E,22 52 50S

TABLE 5c: Pafuri Area

KP82 Nephelinite: porphyritic
Seriate textured lava. Contains phenocrysts (1.5-8mm, 5.8%) and microphenocrysts (<0.5mm) of clinopyroxene, pseudomorphed olivine crystals (<0.6mm, 2.3%) and phenocrysts of octahedral opaque-oxide set in a very fine grained matrix. The clinopyroxene phenocrysts are generally pale yellow, free of apatite and show both hour glass and oscillatory zoning. The larger crystals are occasionally cored by irregular, unpigmented crystals. The groundmass consists of abundant isotropic material (analcite?) together with considerable amounts of grey-polarising material (probably nepheline), apatite needles, and diffuse patches of ore. There is also much opaque dust and occasional patches of coarsely crystalline zeolite. A few well formed spherical amygdales infilled with zeolite are also found in the rock.
Mashikiri Type Section: 31 11 35E,22 33 50S.

KP87 Nephelinite: porphyritic
Porphyritic lava with phenocrysts and rare macrophenocrysts of clinopyroxene, olivine

phenocrysts, and titanomagnetite grains set in a fine to medium grained matrix. Aegerine augite, biotite and a sodic amphibole are present as small grains and flakes in the groundmass.
Mashikiri Type section:

KP83 Nephelinite: porphyritic
Mashikiri Type Section: 31 11 05E,22 34 48S.

KP89 Dolerite Dyke: porphyritic
Kloppersfontein Dam Area: 31 09 23E,22 38 03S.

KP92 Nephelinite: porphyritic
Kloppersfontein Dam Area: 31 11 22E,22 37 30S.

KP97 Picrite Basalt: 1P
Masokospan Road: 31 13 20E,22 37 16S.

KP101 Picrite Basalt: 2P
Phenocrysts: subhedral and anhedral olivine, rare mantled orthopyroxene. The olivines tend to be clustered in nodular aggregates with curvolinear internal boundaries. A few olivine megacrysts are also apparent in the rock. They contain patches of trapped melt with small euhedral opaque-oxide crystals. Matrix: glassy with microphenocrysts of clinopyroxene and opaque-oxide granules and spicules. The pyroxenes exhibit a variety of skeletal textures eg. acicular form, clothespeg structure, dove-tailed ends. Small irregular amygdales are present in the groundmass.
Machayipan-Pafuri Road: 31 12 09E,22 31 25S.

KP106 Picrite-Basalt: 1P
Microcrystalline lava which contains olivine phenocrysts and skeletal clinopyroxenes. Many of the olivines are characterized by euhedral and subhedral crystal outlines with well formed reentrants.
Machayipan-Pafuri Road: 31 12 00E,22 30 10S.

KP108 Picrite Basalt: 1P
Olivines occur as euhedral and subhedral phenocrysts, often in clusters. Pyroxene is found as skeletal crystals, along with bladed and spicular opaque-oxides and apatite, in a glassy groundmass.
Pafuri Road: 31 12 05E,22 29 40S.

KP109 Dolerite Dyke: porphyritic
Pafuri Road: 31 12 15E,22 29 35S.

KP111 Picrite Basalt: 1P

Cryptocrystalline lava with abundant euhedral and subhedral olivine phenocrysts (1-1.8mm) Many of the phenocrysts are characterized by re-entrants or contain spherical glass inclusions and a few crystals have a needle-like morphology. A lttle skeletal clinopyroxene is present in the groundmass.
Pafuri Road: 31 13 09E,22 28 55S.

KP112 Picrite-Basalt: 2P
Lava consisting predominanatly of olivine and minor clinopyroxene phenocrysts set in a glassy mesostasis containing skeletal opaques and clinopyroxenes, and apatite needles.
Pafuri Road: 31 13 14E,22 28 48S.

KP121 Picrite Basalt: 2P
Olivine occurs as macrophenocrysts and phenocrysts, as does clinopyroxene. Mantled orthopyroxene is also present.
Circular Drive, Pafuri: 31 25 40E,22 27 01S.

KP127 Nephelinite: porphyritic
Coarse grained, slightly amygdaloidal lava.
Mutale Road: 31 05 35E,22 25 44S.

KP129 Dolerite: porphyritic
Fine grained, feldsparphyric intrusion.
Mutale Road: 31 06 10E,22 25 25S.

KP134 Nephelinite: porphyritic
Phenocrysts: clinopyroxene (32.4%, up to 7mm), altered olivine (3.6%), opaque oxide and apatite which is included in the clinopyroxene. The clinopyroxenes are neutral in colour, have a flattened prismatic habit, and show fine oscillatory zoning. Matrix: contains abundant small nephelines, rarer clinopyroxene prisms and abundant ore. There is some interstitial brown glass. Also quite common is a sodic-amphibole, pleochroic from pale pinkish brown to greyish yellow green. Much less common are flakes of foxy red biotite. Apatite needles are conspicuous and aegerine occurs as rare prisms and overgrowths on the clinopyroxene crystals.
Boundary Road: 31 05 18E,22 25 27S.

KP142 Picrite Basalt: 2P
Banyini Pan: 31 07 29E,22 21 04S.

KP144 Picrite Basalt: 1P
Microcrystalline lava with olivine macrophenocrysts and phenocrysts.
Banyini Pan - Makulekas Road Junction: 31 12 51E, 22 22 54S.

TABLE 6: SABI VOLCANICS

TABLE 6a: Mashikiri Fm. (Nephelinites)

NTS7	Nephelinite: porphyritic N of Bendezi Hill, Lundi River area
NTS8	Nephelinite: porphyritic Sample from above NTS7.
NTS12	Nephelinite: porphyritic Sample from hill south of NTS7 locality.
NTS13	Nephelinite: porphyritic Sample from hill south of NTS7 locality.
NTS15	Olivine nephelinite: porphyritic Sample from hill to south-east of NTS13.
N201	Nephelinite: porphyritic Summit of Bendezi Hill, Lundi River area. Ref. Jamieson, 1969.
N207	Nephelinite: porphyritic Northern slopes of Bendezi Hill. Ref. Jamieson, 1969.
N212	Olivine Nephelinite: porphyritic 1.7km south west of Bendezi Hill. Ref. Jamieson, 1969.
N222	Nephelinite: porphyritic 0.63km west of Chilongas. Ref. Jamieson, 1969.

The alkaline rocks which occur at the base of the volcanic succession in the Bendezi-Chilongas area consist essentially of nepheline and augite. Both minerals are present as groundmass and euhedral phenocryst phases. In N201 and N207 the augite phenocrysts and groundmass crystals are zoned to aegerine-augite. Less common phenocryst phases are olivine (N207 and N212), apatite (N207 and N222) and biotite (N222). The groundmass in the 4 specimens is holocrystalline, consisting mainly of augite laths and interstitial nepheline or its alteration products. The medium grain size of N212 suggests it may be a dyke rock (Jamieson, 1969).

TABLE 7: NUANETSI VOLCANICS

TABLE 7a: Letaba River Fm. (Picrite Basalts)

NB7

Picrite Basalt: 2P
N of Davata Dip.

N1

Picrite Basalt: 2P
Large, anhedral olivine phenocrysts which are rather spongy, microphenocrysts of clinopyroxene and olivine, minute acicular and granular ore in glass. General appearance suggests the rock has undergone slight thermal metamorphism.
Phen.oliv.17 Microph.oliv.7 Microph.cpx.23 Ore.11 Glass.42
0.16km West of Gomakwe Intrusion.
Ref. Jamieson, 1969.

N5

Picrite Basalt: 1P
Subhedral phenocrysts set in a fine-grained, matrix. Thermally metamorphosed. Probably transitional to 2-phenocryst picrite basalt.
Oliv.9 Cpx.6 Ore.3 Matrix.82
0.16km West of Gomakwe intrusion.
Ref. Jamieson, 1969.

N13

Picrite Basalt: 2P
Large phenocrysts (up to 2mm diameter) of olivine (subhedral-euhedral), clinopyroxene (euhedral) and bladed ore in a glassy matrix with a few, small, acicular feldspar and apatite crystals. Considered to be enriched in cumulus olivine.
Phen.oliv.46 Phen.cpx.17
1.6km South-west of Gomakwe intrusion.
Ref. Jamieson, 1969.

N34

Picrite Basalt: 1P
Olivine phenocrysts are subhedral and up to 1.5mm in diameter, tabular to prismatic ore and clinopyroxene microphenocrysts, abundant acicular clinopyroxene crystals (up to 0.5mm long) in a colourless-faint brown glass. Transitional to 2-phenocryst picrite basalt.
Oliv.24 Cpx.25 Ore.5 Matrix.46 Opx.tr.
0.63km North of Beacon.
Ref. Jamieson, 1969.

N35

Picrite Basalt: 1P
Olivine phenocrysts are subhedral and up to

2mm in diameter, abundant microphenocrysts of clinopyroxene, generally displaying delicate skeletal habit. Ore dendritic and skeletal, frequently occurring in the parallel growth habit known as combs, glass colourless-faint brown.
Oliv.25 Cpx.22 Ore.13 Matrix.40
0.63km North of Beacon.
Ref. Jamieson, 1969.

N40 Picrite Basalt: 1P
Olivine phenocrysts are subhedral and up to 2mm in diameter. Clinopyroxene occurs as fine-grained euhedral crystals. Plagioclase laths are subhedral and up to 2.5mm long (often with axial holes) - and polysynthetic twinning is irregular or absent, interstitial glass.
Oliv.19 Cpx.30 Plag.26 Ore.8 Glass.17
Cpx.tr.
1.6km East of Beacon.
Ref. Jamieson, 1969.

N55 Picrite Basalt: 2P
Large euhedral clinopyroxene phenocrysts (up to 2.5mm long) and smaller, rounded olivine phenocrysts, together with prisms and laths of kennedyite. All in a felsic glass groundmass. Transitional to a picrite or 2-phenocryst glassy picrite basalt. One very large orthopyroxene phenocryst (3mm).
Oliv.31 Cpx.27 Ore.3 Matrix.38 Opx.1
0.32km South-east of Gomakwe intrusion.
Ref. Jamieson, 1969.

N60 Picrite Basalt: 2P
A rock very similar to N55. The fresh, euhedral clinopyroxene phenocrysts contrast with the more rounded, smaller olivine phenocrysts, which show some alteration to a red iddingsitic product. Very fine-grained, acicular laths of plagioclase, often with a fluxion orientation, occur in the glassy groundmass. Enrichment in cumulus olivine, and possibly clinopyroxene suspected.
Oliv.39 Cpx.16 Ore.4 Matrix.41
0.95km South of Gomakwe intrusion.
Ref. Jamieson, 1969.

N72 Picrite Basalt: 2P
Large (up to 3mm in diameter) phenocrysts of irregularly shaped olivine. Clinopyroxene phenocrysts much smaller (ca. 0.5mm long) and are prismatic - lathlike. Large single crystals of orthopyroxene and clusters, all with marginal clinopyroxene rims. Glassy

groundmass with abundant small plagioclase laths, many of which are acicular.
Oliv.29 Cpx.22 Ore.4 Plag.+Matrix.43 Opx.2
1.3km North-west of Gomakwe intrusion.
Ref. Jamieson, 1969.

N76 Picrite Basalt: 1P
Relatively abundant orthopyroxene phenocrysts (one of which is 6mm long). They are invariably rimmed by clinopyroxene. One large irregular olivine cyrstal which is 6mm by 3mm, is considered to be an inherited megacryst. The olivine phenocrysts are rounded, up to 1.5mm in diameter, and somewhat altered. These together with the small, euhedral clinopyroxene microphenocrysts and bladed ore crystals, up to 1.5mm long, are set in a glassy matrix along with considerable acicular plagioclase. Transitional to a 1-phenocryst glassy picrite basalt.
Oliv.39 Cpx.17 Ore.4 Matrix.36 Opx.4
0.63km SSW of Gomakwe intrusion.
Ref. Jamieson, 1969.

N79 Picrite Basalt: 2P
Subhedral olivine phenocryst (up to 1mm in diameter) and rare clinopyroxene phenocrysts in a groundmass of granular clinopyroxene and olivine, plagioclase laths, anhedral ore grains and glass. Relatively coarse grained.
Phen.oliv.15 Phen.cpx.tr. Matrix.85
2.5km South-south-east of Gomakwe intrusion.
Ref. Jamieson, 1969.

N84 Picrite Basalt: 1P
Relatively infrequent subhedral-euhedral olivine phenocrysts (up to 1mm in diameter) granular clinopyroxene, skeletal and dendritic which are up to 1.5mm long, all set in a glassy base.
Phen.oliv.7 Matrix.93
2.5km South-east of Gomakwe intrusion.
Ref. Jamieson, 1969.

N88 Picrite Basalt: 1P
A relatively coarse-grained rock with only small patches of interstitial glass and mesostasis, abundant large orthopyroxene phenocrysts (up to 7mm long), all of which are surrounded by clinopyroxene rims, altered olivine microphenocrysts (up to 1mm in diameter), smaller olivine crystals, clino-pyroxene prisms, plagioclase laths and laths of ore constitute the matrix.

Phen.oliv.5 Matrix.74 Opx.21
3.2km South-east of Gomakwe intrusion.
Ref. Jamieson, 1969.

N89 Picrite Basalt: 1P
A rare basalt type containing occasional microphenocrysts of olivine and very sparse orthopyroxene phenocrysts in a groundmass of subhedral-anhedral clinopyroxene, ore and stubby plagioclase laths. A pronounced sub-ophitic relationship between clinopyroxene and plagioclase is a prominent feature. No modal analysis as distinction between microphenocrysts and groundmass crystals is very slight.
3.2km South-east of Gomakwe intrusion.
Ref. Jamieson, 1969.

N91 Picrite Basalt: 2P
Microphenocrysts of euhedral-subhedral olivine and clinopyroxene (always less than 1.5mm maximum dimension), relatively abundant small orthopyroxene phenocrysts with characteristic clinopyroxene rim. Clinopyroxene microphenocrysts tend to form clusters. Groundmass of plagioclase laths, granular clinopyroxene, ore and glass.
Oliv.19 Cpx.23 Ore.8 Plag.26 Glass.21
3.2km South-east of Gomakwe intrusion.
Ref. Jamieson, 1969.

N100 Picrite Basalt: 2P
A thermally matamorphosed assemblage consisting of anhedral, oxidised, olivine phenocryst and a few subhedral clinopyroxene and orthopyroxene phenocrysts all in a dense groundmass with abundant, fine-grained, granular ore.
Oliv.9 Cpx.5 Matrix.84 Opx.2
0.05km South of Gomakwe intrusion.
Ref. Jamieson, 1969.

N102 Picrite Basalt: 3P
Small (less than 1mm) phenocrysts of oxidised olivine, subhedral clinopyroxene and euhedral plagioclase laths in an extremely fine-grained groundmass of grnular ore, felsic material and clinopyroxene. One prominent cluster of orthopyroxene has clearly suffered thermal metamorphism.
Oliv.10 Cpx.9 Plag.1 Matrix.77 Opx.3
0.04km South-east of Gomakwe intrusion.
Ref. Jamieson, 1969.

N105 Picrite Basalt: 2P
Microphenocrysts of euhedral-subhedral olivine

and clinopyroxene and combs of ore in a brown translucent glass. Microphenocrysts are always less than 1mm in diameter and average 0.3mm. Rare orthopyroxene phenocrysts.
Oliv.18 Cpx.29 Ore.9 Glass.44 Opx.tr.
1.3km East-south-east of Beacon.
Ref. Jamieson, 1969.

N113 Picrite Basalt: 2P
Subhedral microphenocrysts of olivine and clinopyroxene, skeletal and dendritic ore and rare orthopyroxene phenocrysts in a matrix of long acicular plagioclase crystals (up to 2mm long) and glass.
Oliv.18 Cpx.25 Ore.6 Matrix.51 Opx.tr.
3.8km North-west of Chikombedzi.
Ref. Jamieson, 1969.

N117 Picrite Basalt: 1P
Large, subhedral olivine phenocrysts (up to 2.5mm in diameter) in a matrix of granular subhedral clinopyroxene, quenched plagioclase crystals, up to 1.5mm long and frequently with axial cavities, ore and glass. Relatively abundant large orthopyroxene phenocrysts with clinopyroxene rims.
Phen.oliv.5 Matrix.89 Opx.6
3.8km North-west of Chikombedzi.
Ref. Jamieson, 1969.

N126 Picrite Basalt: 2P
Subhedral phenocrysts of olivine (up to 1.5mm in diameter) and smaller microphenocrysts of subhedral clinopyroxenes. The rare remnants of orthopyroxene phenocrysts are surrounded by large, euhedral clinopyroxene phenocrysts (up to 6mm long) displaying polysynthetic twinning. Acicular plagioclase crystals in the glassy groundmass are up to 2mm long.
Oliv.19 Cpx.24 Ore.4 Plag.+Glass.52 Opx.1
2.2km South-south-west of Beacon.
Ref. Jamieson, 1969.

N133 Picrite Basalt: 1P
Large phenocrysts (up to 2mm in diameter) of subhedral-rounded olivine. Bladed crystals of kennedyite attain lengths of 2mm. Matrix consists of subhedral clinopyroxene and fine-grained plagioclase laths in interstitial alkali feldspar, rare acicular apatite.
Oliv.34 Cpx.24 Feldspar.39 Apatite.tr. Ore.3.
2.5km South of Beacon.
Ref. Jamieson, 1969.

N135

Picrite Basalt: 1P
Large euhedral phenocrysts of olivine (up to 3mm long).Granular microphenocrysts of olivine and clinopyroxene and combs of ore, reddish-brown glass.
Phen.oliv.22 Microph.oliv.+Microph.cpx.28 Glass.+ore.46 Mesostasis.4
2.5km South of Beacon
Ref. Jamieson, 1969

N149

Picrite Basalt: 2P
Subhedral olivine phenocrysts up to 1.5mm in diameter. Euhedral clinopyroxene phenocrysts display polysynthetic twinning and are associated with the rare orthopyroxene phenocrysts. The groundmass consists of granular clinopyroxene, ore combs, plagioclase laths and interstitial glass.
Oliv.16 Cpx.6 Matrix.78 Opx.tr.
1.9km East of Beacon.
Ref. Jamieson, 1969.

N187

Picrite Basalt: 2P
Clinopyroxene phenocrysts occur as single euhedral crystals up to 1mm long and as aggregates of several crystals which surround the remnant cores of orthopyroxene phenocrysts. Olivine phenocrysts are smaller and generally altered to a green product. The relatively coarse-grained matrix consists of clinopyroxene, ore, plagioclase laths and some interstitial glass.
Oliv.19 Phen.cpx.20 Cpx.11 Plag.33 Glass.9 Ore.5 Opx.3
5km South-south-west of Chitea intrusion.
Ref. Jamieson, 1969.

N190

Picrite Basalt: 1P
Anhedral olivine phenocrysts, many with cavities and amoeboid habit up to 1mm in diameter, very small clinopyroxene microphenocrysts and ore combs in a brown glass.
Oliv.23 Cpx.21 Glass.+Ore.56
6.3km South-west of Chilongas.
Ref. Jamieson, 1969.

N225

Picrite Basalt: 1P
Small, rounded olivine phenocrysts in a groundmass of granular clinopyroxene, olivine (rather altered), plagioclase laths, ore and glass. Almost aphyric.
Phen.oliv.4 Oliv.10 Cpx.36 Matrix.50
2.7km South-east of Chilongas.
Ref. Jamieson, 1969.

N231

Picrite Basalt: 1P
Subhedral olivine phenocrysts, somewhat altered and microphenocrysts of subhedral-anhedral clinopyroxene in matrix of ore combs, acicular plagioclase with a quenched appearance.and There is much brown glass.
Oliv.29 Cpx.17 Matrix.54
6.3km South-east of Chilongas.
Ref. Jamieson, 1969.

N245

Picrite Basalt: 1P
Rare, rounded olivine phenocrysts, up to 1mm in diameter. Even-grained groundmass of granular olivine and clinopyroxene, plagioclase laths, ore and glass, intersertal texture.
Phen.oliv.4 Oliv.11 Cpx.20 Rest.65 Opx.tr.
2.8km East-north-east of Chitea intrusion
Ref. Jamieson, 1969.

N355

Picrite Basalt: 2P
Abundant small phenocrysts of euhedral clinopyroxene and subhedral olivine, maximum phenocryst size 1mm. Clinopyroxene phenocrysts occasionally form clusters. Groundmass of smaller, anhedral olivine and clinopyroxene crystals, plagioclase laths (often with axial cavities) ore and glass.
Oliv.20 Cpx.29 Plag.23 Glass.22 Ore.6 Opx.tr.
Beside railway at base of volcanic succession.
Ref. Jamieson, 1969.

N356

Picrite Basalt: 1P
Large, euhedral olivine megacrysts up to 5mm by 4mm contrast with subhedral olivine phenocrysts which are up to 1mm in diameter. Subhedral microphenocrysts of clinopyroxene and needles of ore, all in clear glass.
Megacryst.oliv.7 Phen.oliv.22 Cpx.17 Glass.48 Ore.6 Cpx.tr.
0.32km East of railway at base of volcanic succession.
Ref. Jamieson, 1969.

N357

Picrite Basalt: 2P
Subhedral phenocrysts of olivine and clinopyroxene in a dense fine-grained groundmass. A thermally metamorphosed sample.
Oliv.14 Cpx.6 Matrix.80
2.5km North-east of railway at base of volcanic succession.
Ref. Jamieson, 1969.

N361

Picrite Basalt: 1P

TABLE 7b: Sabie River Fm. (Low-MgO Basalts)

N175	Basalt: aphyric Very fine grained non-porphyritic lava. Very fresh. Intergranular texure. Apatite-rich. 33 km. NE Chikombedzi. (KGC)
N180	Basalt: aphyric Fine grained non-porphyritic. Some small patches of (?) silicification. 33 km. NE Chikombedzi. (KGC)
N181	Basalt: aphyric Fresh, fairly fine grained. Intergranular but moderate amounts of interstitial glass. Very rare tiny microphenocrysts of plagioclase. 33 km. NE Chikombedzi. (KGC)
N183	Basalt: sparsely porphyritic Very fine grained. Rare microphenocrysts of plagioclase. Green chloritic matrix in part. Siliceous amygdales. 32 km. NE Chikombedzi. (KGC)
N184	Basalt: aphyric Moderately coarse, aphyric, contains devitrified brown glass. Occasional small patches of calcite. 27 km. NE Chikombedzi. (KGC)
N186	Basalt: sparsely porphyritic Pronounced flow structure, fine grained intergranular texture. Abundant microphenocrysts of an opaque phase (ore). Very rare rounded clots of clinopyroxene phenocrysts. 20 km. NE of Chikombedzi. (KGC)
N235	Basalt: sparsely porphyritic Fine grained. Distinct but very rare phenocrysts of plagioclase and clinopyroxene. Occasional interstitial groundmass quartz and occasional hornblende. Very apatite-rich. 47 km. NE Chikombedzi. (KGC)
N236	Basalt: sparsely porphyritic Fairly coarse, a little sericitised and quite chlorite-rich. Sparse microphenocrysts of clinopyroxene and plagioclase with calcite/chlorite pseudopmorphs after probable olivine. 47 km. NE Chikombedzi. (KGC)
N237	Basalt: aphyric Coarse, aphyric, rather sericitised and with

occasional calcite patches. Abundant groundmass quartz.
47km. NE Chikombedzi. (KGC)

N238 Basalt: sparsely porphyritic
Very fine grained and fresh, showing flow structure and rare clinopyroxene microphenocrysts. Interstitial quartz and a little calcite.
47 km. NE Chikombedzi. (KGC)

N243 Basalt: porphyritic
Chikwedziwa type lava.
2.8km E Chitea intrusion.
Ref. Jamieson, 1969.

N246 Basalt: sparsely porphyritic
Fairly fine grained with very small and rare microphenocrysts of clinopyroxene and plagioclase. Siliceous amygdales.
38 km. NE Chikombedzi. (KGC)

N247 Basalt: sparsely porphyritic
Fairly fine grained, fresh, holocrystalline with intergranular texture. About 2% (total) of phenocrysts consisting of small fresh olivines and clots of clinopyroxene.
38 km. NE Chikombedzi. (KGC)

N251 Basalt: aphyric
Fine grained, aphyric, with flow structure. Abundant groundmass quartz. Prominent rather larger and abundant crystals of opaque ore.
38 km. NE Chikombedzi. (KGC)

N285 Basalt: porphyritic
Chikombedzi type lava.
Nuanetsi River, 200m N of causeway.
Ref. Jamieson, 1969.

N306 Basalt: aphyric
Fairly fine grained, aphyric. Interstitial chlorite represents (?) altered glass.
1.5 km. NE Chikombedzi. (KGC)

N335 Basalt: porphyritic
Thermally metamorphosed ankaramitic basalt.
1km WNW Wusaka Pan.
Ref. Jamieson, 1969.

N386 Olivine-rich Basalt: porphyritic
Highly porphyritic rather coarse basalt with approx. 20% altered olivine phenocrysts, 10% fresh clinopyroxene phenocrysts. Groundmass plagioclase is unaltered. Opaque grains in

groundmass are spicular or platy. The rock has a generally altered appearance, probably due to metamorphism by the Main Granophyre.
Gezani Scarp, 26 km. W of Malipati. (KGC)

N390 Basalt: aphyric
Aphyric, rather altered. Abundant small clinopyroxene prisms. Cloudy mesostasis may include a small amount of altered olivine.
Gezani Scarp, 26 km. W of Malipati. (KGC)

N436 Basalt: porphyritic
A porphyritic rock with phenocrysts of plagioclase, augite and completely pseudomorphed olivine (approximate volume % are Pl-6, cpx-3, olivine pseudomorphs-3). There is no sign of an opaque phase or apatite as phenocrysts. Plagioclase phenocrysts are thin plates up to 3mm in diameter, most clinopyroxenes and olivines are ca. 0.5mm. The texture is glomeroporphyritic (frequently plagioclase only, some clots are pl+cpx, a few are pl+cpx+ol). Olivine is veined by a mineral aggregate which is characterized by, sinuous grain boundaries and wavy spherulitic extinction. It appears to be quartz or chalcedony and is accompanied by some grains of calcite. Some large plagioclases are partly melted. The groundmass is very fine-grained and heavily charged with opaque dust. However, fresh plagioclase laths are abundant and fresh clinopyroxene is also visible. There is a vague trachytic texture. The thin section is cut by a vein of (?) quartz (as in the ol).
11.2 km. ENE mouth of Bubye River. (KGC)

N497 Basalt: porphyritic
0.8km N of Marumbe Complex.
Ref. Jamieson, 1969.

NTS4 Hornfelsed Basalt: porphyritic
Contains about 10% plagioclase phenocrysts. Hornfelsed by minor intrusions of granophyre.
4.2 km. S of Chikombedzi. (KGC)

TABLE 7c: Interbedded Basalts

N340 Basalt: porphyritic
0.8km NW of Jordaan's.
Ref. Jamieson, 1969.

N350 Basalt: aphyric
Moderately coarse aphyric basalt. Plagioclase rather sericitised. Occasional interstitial

chlorite.
6.5 km. SSE centre of Dembe Complex. (KGC)

N377 Basalt: aphyric
Fairly fine grained, intergranular. Aphyric. Occasional chlorite pseudomorphs after small olivines. Generally a rather pyroxene-rich rock.
Umvumvu River, 16 km. S of Dembe Complex. (KGC)

NTS28 Basalt: aphyric
Fine grained aphyric with flow structure. Rather prominent quartz, both interstitial and in patches and streaks. Plagioclase and clinopyroxene both cloudy indicating possible thermal metamorphism.
8 km. S of Dembe Complex. (KGC)

NTS56 Basalt: aphyric
A coarse rock with rather large scattered sub-ophitic clinopyroxene and irregular granular aggregates of fine grained olivine. Very obviously two generations of apatite. An unusual type.
3.5 km. NNW of Malipati. (KGC)

TABLE 7d: Picrites

N15 Picrite: 1P
Large, subhedral olivine phenocrysts (up to 3mm in diameter) in a groundmass of olivine, clinopyroxene, skeletal plagioclase laths and interstitial glass. Relatively coarse grained.
Phen.oliv.5 Oliv.14 Cpx.31 Plag.34 Glass.14 Ore.2
1.2m dyke, 1.9km ESE of Beacon.
Ref. Jamieson, 1969.

N26 Picrite: 1P
Olivine phenocrysts subhedral-euhedral, up to 3mm in diameter, rare orthopyroxene phenocrysts, up to 2mm in length and rimmed by clinopyroxene. Clinopyroxene and ore microphenocrysts all in a matrix of glass, fine-grained plagioclase and finely comminuted ore granules. Has suffered slight thermal metamorphism, presumably when the Beacon sill was intruded.
Oliv.21 Cpx.25 Ore.7 Matrix.46 Opx.1
4-5m dyke, Beacon.
Ref. Jamieson, 1969.

N37 Picrite: 2P
Olivine phenocrysts frequently somewhat skeletal (up to 1.5mm in diameter), and prismatic euhedral

clinopyroxene microphenocrysts in a brown glass. Lathlike - bladed ore micropohenocrysts, very rare fine-grained acicular plagioclase. One cluster of orthopyroxene phenocrysts.
Oliv.24 Cpx.26 Ore.+Glass.50 Opx.tr.
2m E-W dyke, 1.6km E of Beacon.
Ref. Jamieson, 1969.

N41 Picrite
Somewhat rounded olivine crystals up to 3mm in in diameter. Clinopyroxene displays more euhedral habit, and is generally less than 1mm long. Ore occurs as bladed crystals which are frequently brown and translucent - probably kennedyite. Felsic groundmass contains alkali feldspar and plagioclase. One large crystal of orthopyroxene with clinopyroxene rim.
Oliv.33 Cpx.25 Ore.5 Plag.22 Alk.felds.14 Opx.tr.
1.6km ENE of Beacon.
Ref. Jamieson, 1969.

N90 Picrite
Mafic holocrystalline rock composed of abundant subhedral olivine (up to 2mm in diameter), clinopyroxene, orthopyroxene and ore, probably kennedyite. Interstitial groundmass of plagioclase laths (up to 1mm long) and anhedral alkali feldspar. The orthopyroxene is not rimmed by clinopyroxene and forms subhedral prismatic crystals up to 3mm long.
Oliv.48 Cpx.15 Opx.4 Ore.2 Feld.31
100m E-W dyke, 3.2km SE of Gomakwe Intrusion.
Ref. Jamieson, 1969.

N95 Picrite
Holocrystalline rock consisting of rounded - subhedral olivine, subhedral clinopyroxene and plagioclase and euhedral kennedyite laths and prisms. Alkali feldspar rare and interstitial. One remnant crystal of orthopyroxene surrounded by a cluster of clinopyroxene prisms was noted.
Oliv.36 Cpx.27 Plag.25 Alk.felds.8 Ore.3 Opx.tr.
3.2km SE of Gomakwe Intrusion.
Ref. Jamieson, 1969.

N160 Picrite: 2P
Probably a sample of a dyke. Subhedral olivine phenocrysts, up to 1.5mm in diameter and euhedral clinopyroxene phenocrysts of similar dimensions. The clinopyroxenes tend to form clusters around the remnant cores of orthopyroxene phenocrysts> Small, euhedral plagioclase laths (up to0.3mm long) in a dark brown-black glass.

Oliv.22 Cpx.18 Plag.14 Glass.46 Opx.tr.
1.3km NW of Gomakwe intrusion.
Ref. Jamieson, 1969.

N163 Picrodolerite
A holocrystalline rock with an average grain-size of 0.3mm. Olivine crystals are subhedral and larger than average. Plagioclase forms stout laths and prisms, some of which are totally enclosed in the relatively abundant orthopyroxene, most of which appears to be in equilibrium with the rest of the assemblage.
Oliv.13 Cpx.28 Opx.15 Plag.35 Alk.felds.3 Ore.5
Chitea intrusion.
Ref. Jamieson, 1969.

N364 Picrodolerite
Coarse-grained, holocrystalline rock consisting of olivine, clinopyroxene, plagioclase, ore and orthopyroxene. The subhedral orthopyroxene crystals lack clinopyroxene rims.
Oliv.18 Cpx.26 Opx.13 Plag.36 Ore.2 Glass.1
4.3km NNE of Chikombedzi.
Ref. Jamieson, 1969.

N519 Picrite: 3P
Consists of subhedral olivine phenocrysts (up to 1mm in diameter), smaller clinopyroxene phenocrysts occuring in clusters, and rare plagioclase phenocrysts (up to 1mm in length). Groundmass of glass, plagioclase laths, clino-pyroxene, and ore combs.
Pheno.oliv.9 Pheno.cpx.1 Pheno.plag.tr.
Rest.90
4m dyke, 3.2km E of Beacon.
Ref. Jamieson, 1969.

TABLE 7e: Beacon Sill

N21 Picrite
Olivine generally large (up to 3mm in diameter), clinopyroxene occurs as euhedral, prismatic crystals up to 0.75mm in diameter. Ore phase is translucent and has a bladed habit - probably kennedyite. Abundant alkali feldspar in felsic matrix.
Oliv.29 Cpx.27 Alk.Felds.+Plag.+Glass.38
Ore.6 Apatite.1
Ref. Jamieson, 1969.

N22 Picrite
Holocrystalline rock with all species except

interstitial alkali feldspar and the ore phase forming subhedral grains ca. 1mm in diameter. A few bladed to prismatic ore crystals are up to 4mm long.
Oliv.38 Cpx.25 Feldspar.35 Ore.2 Apatite.tr.
Ref. Jamieson, 1969.

N23 Picrite
A holocrystalline rock with abundant olivine-rounded, subhedral crystals up to 2mm in diameter and clinopyroxene, the latter occuring as prismatic crystals up to 3mm long. Clino-pyroxene tends to form radiating clusters or rosettes. Plagioclase and alkali feldspar are interstitial. Ore blebs thoroughly opaque and probably titaniferous magnetite - cf. N21 and N22.
Oliv.42 Cpx.32 Alk.Felds.19 Plag.4 Ore.3
Ref. Jamieson, 1969.

N27 Picrite
Large, subhedral olivine crystals (up to 3mm in diamter) euhedral clinopyroxene crystals (also up to 3mm in length) and smaller ore laths and bladed crystals in a fine-grained felsic groundmass. Transitional to a 2-pheno-cryst Picrite Basalt.
Oliv.37 Cpx.21 Ore.4 Matrix.38
Ref. Jamieson, 1969.

TABLE 7f: Bezi Picrites

NTS6
NTS17
NTS18 Picrites
Mineralogically and texturally these picrites are very different from the other relatively coarse-grained picrites. They contain little or no alkali feldspar and have relatively abundant orthopyroxene which appears to have been in equilibrium at the time of final crystallisation. In particular they are characterised by lower contents of K_2O, P_2O_5 Ba, Rb and Zr, and higher CaO than the typical picrites and picrite basalts (Jamieson, 1969).

TABLE 7g: Basic Intrusives

N241 Dolerite
An ophitic dolerite rich in micropegmatite. Contains abundant single crystals of chlorite replacing assumed orthopyroxene, in each case rimmed by fresh clinopyroxene. An extraordinary

rock.
38km NE of Chikombedzi. (KGC)

N411 Dolerite
Moderately coarse intergranular dolerite with abundant fine grained micropegmatite. Plagioclase a little sericitised but otherwise nice and fresh.
Dyke 13km SW of Malipati. (KGC)

N414 Dolerite
Similar to N411 but contains more opaques.
Dyke 11 km WSW of Malipati. (KGC)

N421 Dolerite
Coarse dolerite with slightly sub-ophitic clinopyroxene. Extraordinary mesostasis of fine prismatic euhedra of colourless (?) amphibole with some clinopyroxene, sericite and biotite scraps all set in a matrix of quartz (+ some apatite).
Dyke 6km WSW of Malipati. (KGC)

N423 Dolerite
Coarse gabbroic rock contains moderately abundant pseudomorphs after olivine. Otherwise consists of clinopyroxene, plagioclase, ore, quartz, alkali feldspar and occasional biotite with abundant apatite. Much altered to calcite and sericite.
Dyke 6km WSW of Malipati. (KGC)

N438 Dolerite
Similar to N441 but much more sericitisation of plagioclase.
(?) Dyke 3km W of mouth of Bubye River. (KGC)

N441 Dolerite
Medium grained (0.5 - 1mm) sub-ophitic rock consisting of augite, pigeonite (uniaxial) basic plagioclase, and opaque phase, minor micropegmatite, and rare apatite. Degree of alteration slight - some sericitisation of plagioclase. Augite and probably pigeonite locally altered to chlorite, pale brown-green amphiboles, and (?) biotite.
(?) Dyke 3.5km W of mouth of Bubye River. (KGC)

APPENDICES E AND F

(Microfiche Tables)

In view of the large number of mineral and whole rock analyses obtained in this thesis and compiled from published and unpublished sources, individual analyses are presented in microfiche tables (see pocket inside back cover).

Table numbers are given in the index of each microfiche card and are also listed in Appendices E and F together with appropriate abbreviations and annotations.

APPENDIX E

(Microfiche Table E)

MINERAL ANALYSES OF LEBOMBO VOLCANICS

TABLE E : NORTHERN LEBOMBO NEPHELINITES

TABLE E1a : Nephelinite KP83

TABLE E1b : Nephelinite KP87

TABLE E2 : NORTHERN LEBOMBO PICRITE BASALTS

E2a : Picrite basalt KA24

E2b : Picrite basalt KA29

E2c : Picrite basalt KS3

E2d : Picrite basalt KS47

E2e : Picrite basalt KP98

E2f : Picrite basalt KP101

E2g : Picrite basalt KP108

E2h : Picrite basalt KP111

E2i : Picrite basalt KP112

E2j : Picrite basalt KP121

TABLE E3 : LEBOMBO OLIVINE-POOR VOLCANICS

E3a : Sparsely porphyritic lava EH8 (Betton, 1978)

E3b : Aphyric lava CL100

E3c : Plagioclase-phyric lava CL372

E3d : Andesitic dolerite sill KA52b

E3e : Rooi Rand Dolerite A49 (Armstrong, 1978)

E3f : Rooi Rand Dolerite A101 (Armstrong, 1978)

E3g : Rooi Rand Dolerite A129 (Armstrong, 1978)

E3h : Rooi Rand Dolerite A170 (Armstrong, 1978)

E3i : Rooi Rand Dolerite A186 (Armstrong, 1978)

E3j : Rooi Rand Dolerite A189 (Armstrong, 1978)

APPENDIX F

(Microfiche Table F)

MAJOR AND TRACE ELEMENT DATA COMPILATION

TABLE

F1	(SL,SR)	SOUTHERN LEBOMBO	- Sabie River Formation (South of Hluhluwe)
F2	(SL,SR)	" "	- Sabie River Formation (North of Hluhluwe)
F3	(SL,IN)	" "	- Basic Intrusives
F4	(SL,RRD)	" "	- Rooi Rand Dolerites
F5	(SL,JZ)	" "	- Jozini Formation (Ngweni Area)
F6	(SL,JZ)	" "	- Jozini Formation (Type Section)
F7	(SW,SR)	SWAZILAND	- Sabie River and Movene Formation
F8	(SW,IN)	"	- Basic Intrusives
F9	(SW,MK)	"	- Mkutshane Beds
F10	(SW,TR)	"	- Twin Ridge Beds
F11	(SW,JZ)	"	- Jozini Formation
F12	(SW,MB)	"	- Mbuluzi River Formation
F13	(SW,OB)	"	- Oribi Beds
F14	(CL,SR)	CENTRAL LEBOMBO	- Sabie River Formation (Type Section)
F15	(CL,IN)	" "	- Basic Intrusives
F16	(NL,MS)	NORTHERN LEBOMBO	- Mashikiri Formation
F17	(NL,LB)	" "	- Letaba Formation
F18	(NL,SR)	" "	- Sabie River Formation
F19	(NL,IN)	" "	- Picritic and Low-MgO Intrusives
F20	(CN,AV)	CENTRAL AND NORTHERN LEBOMBO	- Acid Volcanics (Jozini Formation, Olifants Beds, Rhyolite Dykes and Granophyres).
F21	(NU,MS)	NUANETSI	- Mashikiri Formation (Sabi area)
F22	(NU,LB)	"	- Letaba Formation
F23	(NU,SR)	"	- Sabie River Formation
F24	(NU,IN)	"	- Basic Intrusives (Picritic Intrusives, Beacon Sill, Bezi Dyke, low-MgO Intrusives and Chilembeni Intrusion).
F25	(NU,IB)	"	- Interbedded Basalts
F26	(NU,AV)	"	- Nuanetsi Acid Volcanics
F27	(NU,GG)	"	- Granites and Granophyres
F28	(TU,LB)	TULI	- Letaba Formation
F29	(TU,SR)	"	- Sabie River Formation

TABLE F 0 :DETAILS OF CODING AND AREA BOUNDARIES

I. CODING DETAILS

a) COUNTRY CODE b) AREA AND FORMATION OR INTRUSIVE ROCK CODE

ZIMBABWE

Nuanetsi

1107	030 xxx	Mashikiri Formation
	031	Letaba River Formation
	032	Sabie River Formation
	033	Interbedded Basalts
	034	Rhyolites
	035	Picrites
	036	Bezi Dyke
	037	Basic Intrusives
	038	Chilembeni Intrusion
	039	Acid Intrusives

Tuli

	042 xxx	Letaba River Formation
	043	Sabie River Formation
	044	Basic Intrusives

Regional

	100 xxx	Wankie Basic Lavas and Intrusives
	101	Nyamandhlovu Basic Lavas and Intrusives
	102	Featherstone Basic Lavas and Intrusives
	105	Shawa, Dorwa and Chishanya Carbonatite Complexes

SOUTH AFRICA

Northern Lebombo

1101	048 xxx	Mashikiri Formation
	049	Letaba River Formation
	050	Sabie River Formation (general)
	051	
	052	
	053	Olifants Beds
	054	Jozini Formation
	055	Picrites
	056	Basic Intrusives
	057	Granophyres
	058	Acid Intrusives

Central Lebombo

	060 xxx	Letaba Formation
	061	Sabie River Formation
	062	Jozini Formation
	063	Basic Intrusives (general)
	064	Komatipoort Intrusive Complex
	065	Acid Intrusives

a) COUNTRY CODE b) AREA AND FORMATION OR INTRUSIVE ROCK CODE

SWAZILAND

1104	069 xxx	Sabie River Formation
	070	Mkutshane Beds
	071	Twin Ridge Beds
	072	Jozini Formation
	073	Mbuluzi Formation
	074	Oribi Beds
	075	Movene Formation
	076	Basic Intrusives
	077	Acid Intrusives

SOUTH AFRICA

Southern Lebombo

1101	081 xxx	Sabie River Formation
	082	Jozini Formation (general)
	083	Kuleni Rhyolites
	084	Bumbeni Complex (general)
	085	Mpilo Member
	086	Basic Dykes (general)
	087	Rooi Rand dykes
	088	Acid Intrusives
	089	Syenitic Intrusives

c) PETROGRAPHIC TYPE CODE : xxx

001 - 499	-	Aphyric and sparsely porphyritic volcanics
500 - 899	-	Porphyritic volcanics
900 - 999	-	Porphyritic volcanics, >18% MgO.

d) ROCK TYPE CODE

i) Mafic Volcanics

321300*	-	Nephelinites
311330	-	Shoshonites
311320	-	Tholeiitic Andesites, Intermediate -K lineage
311310	-	Tholeiitic Andesites, Low-K lineage
311230	-	Absarokites
311220	-	Basalts, Intermediate-K lineage
311210	-	Basalts, Low-K lineage
311130	-	Picrite Basalts, High-K lineage
311120	-	Picrite Basalts, Intermediate-K lineage
311110	-	Picrite Basalts, Low-K lineage

ii) Acid Volcanics

312400	-	Dacite
312500	-	Rhyodacite
312600	-	Rhyolite

*5 replaces leading 3 for Intrusive Rocks.

iii) Intermediate Volcanics

322400 - Trachybasalts

II. BOUNDARIES OF AREAS

i)	Nuanetsi	- Includes Sabi area
ii)	Tuli	- Area west of Beit Bridge - Fort Victoria Road.
iii)	Northern Lebombo	- Limpopo River north.
iv)	Central Lebombo	- Northern border at 24½°S.
v)	Swaziland	- In north, boundary of country. In south, E - W line coinciding with southern limit of country (icnludes portion of Lebombo which crops out in north-eastern Natal).
iv)	Southern Lebombo	- Area south of extended southern Swaziland boundary.

DATA COMPILATION REFERENCES

53 001

W.H.SWIFT, W.C.WHITE, J.W.WILES AND B.G.WORST (1953): THE GEOLOGY OF THE LOWER SABIE COALFIELD. BULL. GEOL. SURV. S. RHOD.,40,96p.

61 001

R.L.JOHNSON (1961): THE GEOLOGY OF THE DOROWA AND SHAWA CARBONATITE COMPLEXES, SOUTHERN RHODESIA. TRANS. GEOL. SOC. S. AFR., 64,101-145

65 001

K.G.COX, R.L.JOHNSON, L.J.MONKMAN, C.J.STILLMAN, J.R.VAIL, AND D.N.WOOD. THE GEOLOGY OF THE NUANETSI IGNEOUS PROVINCE. PHIL TRANS. R. SOC. LOND.,SER.A,257,71-218.

67 001

K.G.COX, R.MACDONALD, AND G.HORNUNG (1967): GEOCHEMICAL AND PETROGRAPHIC PROVINCES IN THE KAROO BASALTS OF SOUTHERN AFRICA. AM. MIN.,52,1451-1474.

69 001

J.R.VAIL, G.HORNUNG AND K.G.COX (1969): KAROO BASALTS OF THE TULI SYNCLINE. BULL. VOLCAN.,33,398-418.

69T002

B.G.JAMIESON (1969): PETROLOGY OF OLIVINE-RICH BASALTIC ROCKS NUANETSI PROVINCE, RHODESIA. PHD. THESIS, EDINBURGH UNIVERSITY
XRF DATA:- ANALYSED AT GEOLOGY DEPT., UNIVERSITY OF EDINBURGH (B.G.JAMIESON)

70 001

E.P.SAGGERSON AND C.LOGAN (1970): DISTRIBUTION CONTROLS OF LAYERED AND DIFFERENTIATED MAFIC INTRUSIONS IN THE LEBOMBO VOLCANIC SUB-PROVINCE. GEOL. SOC. S. AFR.,SPEC. PUBL. 1,
XRF DATA:- ANALYSED AT THE NATIONAL INST. OF METALLURGY, JOHANNESBURG.

75T001

A.J.ERLANK, A.R.DUNCAN, AND J.W.BRISTOW (1975-1980): SOUTH AFRICAN NATIONAL GEODYNAMICS PROGRAMME: W.G. 4(B) GEOCHEMISTRY OF KAROO VOLCANICS. UNPUBLISHED DATA.

XRF DATA:- ANALYSED AT DEPT. OF GEOCHEMISTRY, UNIVERSITY OF CAPE TOWN (A.R.DUNCAN, J.W.BRISTOW, M.K.BRAUTESETH, Y.C.ABRAHAM)

ISOTOPIC DATA:- ANALYSED AT DEPT. OF GEOLOGY AND MINERALOGY, OXFORD UNIVERSITY, AND AT BERNARD PRICE INST., UNIVERSITY OF THE WITWATERSRAND (A.J.ERLANK, H.L.ALLSOPP, J.W.BRISTOW)

SSMS DATA:- ANALYSED AT RESEARCH SCHOOL OF EARTH SCIENCES, AUSTRALIAN NATIONAL UNIVERSITY (A.R.DUNCAN, J.M.G.SHELLEY, P.E.MUIR)

75T002

B.G.JAMIESON (1969): PETROLOGY OF OLIVINE-RICH BASALTIC ROCKS, NUANETSI PROVINCE, RHODESIA. PHD. THESIS, EDINBURGH UNIVERSITY

XRF DATA:- MAJOR ELEMENTS ANALYSED AT GEOLOGY DEPT., UNIVERSITY OF EDINBURGH (B.G.JAMIESON). TRACE ELEMENTS ANALYSED AT DEPT. OF GEOCHEMISTRY, UNIVERSITY OF CAPE TOWN (A.R.DUNCAN, J.W.BRISTOW, M.K.BRAUTESETH, Y.C.ABRAHAM).

76T003

J.W.BRISTOW (1976): THE GEOLOGY AND GEOCHEMISTRY OF THE SOUTHERN LEBOMBO. M.SC. THESIS, UNIVERSITY OF NATAL (DURBAN).

XRF DATA:- ANALYSED AT DEPT. OF GEOCHEMISTRY, UNIVERSITY OF CAPE TOWN (A.R.DUNCAN, M.K.BRAUTESETH, Y.C. ABRAHAM)

ISOTOPIC DATA:- ANALYSED AT BERNARD PRICE INST., UNIVERSITY OF THE WITWATERSRAND (H.L.ALLSOPP, J.W.BRISTOW)

SSMS DATA:- ANALYSED AT RESEARCH SCHOOL OF EARTH SCIENCES, AUSTRALIAN NATIONAL UNIVERSITY (A.R.DUNCAN, J.M.G.SHELLEY, P.E.MUIR)

77T003

R.W.CLEVERLY (1977): THE STRUCTURAL AND MAGMATIC EVOLUTION OF THE LEBOMBO MONOCLINE, SOUTHERN AFRICA, WITH PARTICULAR REFERENCE TO SWAZILAND. D.PHIL. THESIS, UNIVERSITY OF OXFORD.

XRF DATA:- ANALYSED AT DEPT. OF GEOLOGY AND MINERALOGY, OXFORD UNIVERSITY (R.W.CLEVERLY)

ISOTOPIC DATA:- ANALYSED AT DEPT. OF GEOLOGY AND MINERALOGY, OXFORD UNIVERSITY (R.W.CLEVERLY) AND BERNARD PRICE INST., UNIVERSITY OF THE WITWATERSRAND (J.W.BRISTOW)

SSMS DATA:- ANALYSED AT RESEARCH SCHOOL OF EARTH SCIENCES,

AUSTRALIAN NATIONAL UNIVERSITY (A.R.DUNCAN, J.M.G.SHELLEY, P.E.MUIR)

78T002

R.A.ARMSTRONG (1978): A GEOLOGICAL AND GEOCHEMICAL APPRAISAL THE ROOI RAND DYKE SWARM, LEBOMBO. M.SC. THESIS, UNIVERSITY OF NATAL (DURBAN)

XRF DATA:- ANALYSED AT DEPT. OF GEOCHEMISTRY, UNIVERSITY OF CAPE TOWN (R.A.ARMSTRONG)

ISOTOPIC DATA:- ANALYSED AT BERNARD PRICE INST., UNIVERSITY OF THE WITWATERSRAND (R.A.ARMSTRONG)

SSMS DATA:- ANALYSED AT RESEARCH SCHOOL OF EARTH SCIENCES, AUSTRALIAN NATIONAL UNIVERSITY (A.R.DUNCAN, J.M.G.SHELLEY, P.E.MUIR)

79T003

K.G.COX AND M.PARISH (1979-1980): SOUTH AFRICAN NATIONAL GEODYNAMICS PROGRAMME: W.G. 4(B) GEOCHEMISTRY OF KAROO VOLCANICS. UNPUBLISHED DATA.

XRF DATA:- ANALYSED AT DEPT. OF GEOLOGY AND MINERALOGY, OXFORD UNIVERSITY (K.G.COX, M.PARISH)

79T004

K.G.COX AND I.EVANS (1979-1980): SOUTH AFRICAN NATIONAL GEODYNAMICS PROGRAMME: W.G. 4(B) GEOCHEMISTRY OF KAROO VOLCANICS. UNPUBLISHED DATA.

XRF DATA:- ANALYSED AT DEPT. OF GEOLOGY AND MINERALOGY, OXFORD UNIVERSITY (K.G.COX, I.EVANS)

80T001

J.W.BRISTOW (1980): THE GEOCHRONOLOGY AND GEOCHEMISTRY OF KAROO VOLCANICS IN THE LEBOMBO AND ADJACENT AREAS. PHD. THESIS, UNIVERSITY OF CAPE TOWN.

XRF DATA:- ANALYSED AT DEPT. OF GEOCHEMISTRY, UNIVERSITY OF CAPE TOWN (J.W.BRISTOW, M.K.BRAUTESETH)

ISOTOPIC DATA:- ANALYSED AT BERNARD PRICE INST., UNIVERSITY OF THE WITWATERSRAND (J.W.BRISTOW, H.L.ALLSOPP, R.A.ARMSTRONG)

SSMS DATA:- ANALYSED AT RESEARCH SCHOOL OF EARTH SCIENCES, AUSTRALIAN NATIONAL UNIVERSITY (A.R.DUNCAN, J.M.G.SHELLEY, P.E.MUIR)